University of Southampton
Faculty of Engineering and the Environment

Institute of Sound and Vibration Research

Modelling the cochlear origins of distortion product otoacoustic emissions

Jacqueline Ann Young

A thesis submitted for the degree of
Doctor of Philosophy

2011

UNIVERSITY OF SOUTHAMPTON

ABSTRACT

FACULTY OF ENGINEERING AND THE ENVIRONMENT

INSTITUTE OF SOUND AND VIBRATION RESEARCH

Doctor of Philosophy

MODELLING THE COCHLEAR ORIGINS OF DISTORTION PRODUCT OTOACOUSTIC EMISSIONS

by Jacqueline Ann Young

Distortion product otoacoustic emissions (DPOAEs) arise within the cochlea in response to two stimulus tones (f_1 and f_2) at frequencies such as $2f_1 - f_2$ and $2f_2 - f_1$. Each DPOAE derives from two contributing mechanisms within the cochlea: a distributed distortion source and a reflection source. They are used for hearing screening, but a better understanding of their cochlear origin and transmission could potentially extend their clinical application to facilitate objective hearing loss assessment, differential diagnosis of sensorineural hearing losses and improved auditory rehabilitation using hearing aids.

In this thesis a numerical model of the human cochlea is developed to study the generation of DPOAEs. It is based on a pre-existing active nonlinear model, the micromechanics of which are carefully re-tuned to simulate the response of the human cochlea to single- and two- tone stimulation. Particular attention is paid to the form and position of the nonlinearity within the model to best match experimental results. The model is also reformulated to verify its stability and ensure computational convergence of the iterative frequency domain solution method. Its predictions are validated against estimated time domain simulations and documented experimental DPOAE measurements. Additionally a novel method is developed for decomposing each frequency component of the cochlear response into forward and backward travelling waves, which is applied to investigate the multiple sources of both the $2f_1 - f_2$ and $2f_2 - f_1$ DPOAEs.

The model is used to explain and predict a variety of phenomena observed in experimental DPOAE studies. It also confirms for the $2f_1 - f_2$ emission, that the two source mechanisms are spatially separated and that the only significant reflection contribution is associated with the $2f_1 - f_2$ travelling wave. In contrast, it predicts that the two source mechanisms will overlap in the case of the $2f_2 - f_1$ DPOAE, which can be influenced by reflection of both the primary and $2f_2 - f_1$ travelling waves.

Table of contents

List of figures

List of tables

List of accompanying materials

- A CD containing a PDF version of this thesis, and relevant MATLAB files

Declaration of Authorship

I, Jackie Young, declare that the thesis entitled Modelling the Cochlear Origins of Distortion Product Otoacoustic Emissions and the work presented in the thesis are both my own work, and have been generated by me as the result of my own original research. I confirm that:

• this work was done wholly or mainly while in candidature for a research degree at this University;
• where any part of this thesis has previously been submitted for a degree or any other qualification at this University or any other institution, this has been clearly stated;
• where I have consulted the published work of others, this is always clearly attributed;
• where I have quoted from the work of others, the source is always given. With the exception of such quotations, this thesis is entirely my own work;
• I have acknowledged all main sources of help;
• where the thesis is based on work done by myself jointly with others, I have made clear exactly what was done by others and what I have contributed myself;
• parts of this work have been published under my maiden name as:
How, J. A., S. J. Elliott and B. Lineton (2010). "The influence on predicted harmonic and distortion produce generation of the position of the nonlinearity within cochlear micromechanical models (L)." Journal of the Acoustical Society of America 127(2): 652 − 655.

Acknowledgements

I would like to thank Steve Elliott and Ben Lineton for their wisdom, guidance, and support. I have really enjoyed this research and have been inspired by their enthusiasm. It has been a pleasure to work as part of this team, and to build on their previous work.

I am also very grateful for the support of Jamie and the rest of my family who have been amazingly encouraging.

Symbols

A, B,**C, D**	Matrices used to describe the state space cochlear model
a_0, C_0, K_0	Constants in the Greenwood formula
b	The ratio of frequency to natural frequency in the Kanis & de Boer cochlear model [dimensionless]
b_w	The ratio of the average displacement across the width of the CP to the maximum displacement over the width of the BM
e_0, d_0, δ_{sc},σ_0	Constants used to describe the active mechanism properties of the CP in the Kanis & de Boer model
f_0	The frequency of a single tone stimulus [Hz]
f_1 , f_2	The frequencies of two stimulus tones (f_2>f_1) [Hz]
f_{dp}	Distortion product frequency [Hz]
f_{mean}	The geometric mean frequency [Hz]
f_{Source}	The characteristic frequency corresponding the location of the dominant wave-fixed DP source region
f_x	Characteristic frequency for position x [Hz]
$F(u)$	An arbitrary function
g_{lever}	The BM to IHC lever gain
G	Gain of the cochlear amplifier [dB]
H	Height of the cochlear channels [m]
k	Complex wavenumber of the travelling wave [m^{-1}]
k_0	Wavenumber of the travelling wave at the base of the cochlear model [m^{-1}]
L	Length of the cochlea [m]
L_1, L_2	The levels of two stimulus tones corresponding to f_1 and f_2 [dB SPL]
m_{KB}, k_{KB}, c_{KB}	Mass [kg m^{-2}], stiffness [kg m^{-2} s^{-2}] and damping [kg m^{-2} s^{-1}] of the passive cochlear partition
m_0, δ, s_0, κ	Constants which specify the passive mechanical properties of the CP in the Kanis & de Boer model
$m\omega$	The angular frequency of the m^{th} harmonic component [rad s^{-1}]
n	The n^{th} iterative cycle
N	The total number of elements in a discrete cochlear model
N_t	The number of samples representing the stimulus in the time domain
$p_0^{\pm}$	Coefficient of the WKB forward or backward travelling wave [kg m^{-1} s^{-2}]
p_d	Semi-difference pressure [kg m^{-1} s^{-2}]
p_f	Fluid pressure [kg m^{-1} s^{-2}]

p_{OHC}^{lin}, p_{OHC}^{QL}	The semi-difference pressure output of the OHCs in a linear or quasilinear model [kg m^{-1} s^{-2}]
$p_{OHC,A}^{QL}$	Pressure output of the OHCs in response to stimulation at only the fundamental frequency [kg m^{-1} s^{-2}]
$p_{OHC,B}^{QL}$	Pressure output of the OHCs in response to stimulation at the fundamental and harmonic frequencies [kg m^{-1} s^{-2}]
p_{ref}	Scaling constant used in the quasilinear method which has the dimensions of pressure
Q_1, Q_2	Parameters used to influence sharpness of tuning and CA gain in the cochlear model [dimensionless]
Q_{10dB}	Measure of tuning sharpness [dimensionless]
R_{stapes}	Reflection coefficient for backward travelling waves at the stapes
S	Distributed pressure source [kg m^{-1} s^{-2}]
t_{delay}	Estimated time delay [s]
u_f, v_f	Horizontal and vertical fluid velocities [m s^{-1}]
u_{st}	Stapes velocity [m s^{-1}]
v	Vertical velocity of the cochlear partition [m s^{-1}]
$V(k)$	Inverse Fourier transform of the BM velocity $v(x)$ [m s^{-1}]
$\mathbf{w}(t)$, $\mathbf{u}(t)$, $\mathbf{y}(t)$	State vectors used in the state space cochlear model
x	Distance from the base along the cochlear partition [m]
x_1, x_2	The characteristic places corresponding to f_1 and f_2 [m]
x_A, x_B	The observation locations in the He *et al* experiment
y	An arbitrary system variable used in the WKB derivation
Y_{CP}, Y_{st}	Specific acoustic admittance of the CP and the stapes [kg^{-1} m^2 s^1]
z	Vertical distance above the cochlear partition [m]
$Z^{\pm}$	The impedance of forward or backward travelling waves [kg m^{-2} s^{-1}]
Z_c	Cochlear input impedance [kg m^{-2} s^{-1}]
Z_{char}	The characteristic impedance of the system [kg m^{-2} s^{-1}]
Z_{CP}^{pass}, Z_{CP}^{active}	Specific acoustic impedance of the CP in a linear passive, or active, model [kg m^{-2} s^{-1}]
Z_{OHC}^{lin}, Z_{OHC}^{QL}	The specific acoustic impedance associated with the OHCs in a linear, or quasilinear, model [kg m^{-2} s^{-1}]
Z_1, Z_2, Z_3, Z_4	Specific acoustic impedances in the Neely & Kim cochlear model [kg m^{-2} s^{-1}]
α, β, γ_B, η	Parameters used to define the first order Boltzmann function
γ, γ_{QL}	The OHC gain in a linear, or quasilinear, model [value 0 to1]
Δ	Length of a single element in the discrete cochlear model [m]

Δf	Frequency separation [Hz]
η_k , χ_k	Real and imaginary parts of the wavenumber k [m-^{1}]
λ	The eigenvalue of the state space system matrix **A** [s-^{1}]
$\lambda_{TW,}$ c_{TW}	Wavelength and velocity of the travelling wave [m and m s-^{1}]
ξ	The shear displacement between the TM and the OC [m]
ξ_p	Vertical displacement of the CP [m]
ρ	Density of the cochlear fluids [kg m-^{3}]
σ	The real part of eigenvalue λ [s-^{1}]
ϕ	Phase [radians]
ϕ_{f_1} , ϕ_{f_2}	Phase of the f_1 and f_2 waves [radians]
$\varphi^{\pm}$	WKB basis functions
ω	Angular frequency [rad s^1]
ω_n	The natural angular frequency of the passive CP

Abbreviations

BM	Basilar membrane
CA	Cochlear amplifier
CEOAE	Click evoked otoacoustic emission
CF	Characteristic frequency
CP	Cochlear partition
DP	Distortion product
DPOAE	Distortion product otoacoustic emission
FTC	Frequency tuning curve
HTL	Hearing threshold level
IHC	Inner hair cell
(I)FFT	(Inverse) Fast Fourier transform
MET	Mechano-electric transduction
OAE	Otoacoustic emission
OC	Organ of Corti
OHC	Outer hair cell
SFOAE	Stimulus frequency otoacoustic emission
SNR	Signal to noise ratio
SOAE	Spontaneous otoacoustic emission
SPL	Logarithmic measure of sound pressure level using a reference of 20 μPa
TEOAE	Transient evoked otoacoustic emission
TM	Tectorial membrane
WKB	Wentzel, Kramers and Brillouin

Key definitions

Characteristic place	The location on the cochlear partition corresponding to the peak in the travelling wave envelope in a linear active cochlear model, or a nonlinear model at low stimulus levels
Best place	The location on the cochlear partition corresponding to the peak in the travelling wave envelope in a nonlinear cochlear model. This position will shift closer the base as the stimulus level increases
Upper side band emission	A DPOAE with frequency greater than f_2
Lower side band emission	A DPOAE with frequency less than f_1
Quasilinear system	A system in which the fundamental, or primary, response is not significantly influenced by harmonic or distortion product responses
Baseline model	A cochlear model in which the impedance properties of the cochlear partition vary smoothly with distance from the base
Perturbed model	A cochlear model in which random perturbations have been introduced onto the underlying cochlear partition impedance exhibited by the baseline model

1. Introduction

This thesis is concerned with understanding the generation mechanisms of distortion product otoacoustic emissions (DPOAEs) using numerical models of the cochlea. In this chapter the anatomy and physiology of the mammalian cochlea are briefly reviewed to provide the context for the model. The properties and applications of otoacoustic emissions are then discussed to allow comparison with the model predictions.

The chapter concludes with a list of research questions which have been addressed and a summary of the contributions of the thesis.

1.1 Anatomy of the ear

Figure 1.1a shows the principal structures of the ear. Sound is transmitted from the ear canal through the middle ear, via the tympanic membrane and ossicles, into the cochlea. The cochlea converts an acoustic stimulus into neural electrical signals which are transmitted to the brain via the auditory nerve. In this section the anatomy of the middle ear and cochlea are described so that the chief mechanisms can then be explained.

1.1.1 The middle ear

The middle ear, illustrated in figure 1.1b, consists of three ossicles: the malleus, incus and stapes. These bones transmit vibrations from the tympanic membrane to the oval window of the cochlea, acting collectively as an impedance-matching transformer. The efficient transmission achieved by the middle ear is attributed to three properties (Pickles, 1982): the effective area ratio between the tympanic membrane and the stapes footplate, the effective lever ratio of the malleus and incus bones, and the relative motion of the tympanic membrane and malleus. Overall, the middle ear performance is well modelled by a mass-spring-damper system for stimulus frequencies under 10 kHz (Relkin, 1988). Figure 1.2 shows that the human middle ear provides a maximum gain of approximately 20 dB at 1 kHz and that its response becomes nonlinear for stimulus levels above 140 dB SPL. At these high stimulus levels the middle ear performance becomes nonlinear as reflexes and ligaments act to restrict the stapes motion (Pascal *et al.,* 1998). For the sound levels of interest here however, which are all below 140 dB SPL, the middle ear can be accurately modelled as a linear system.

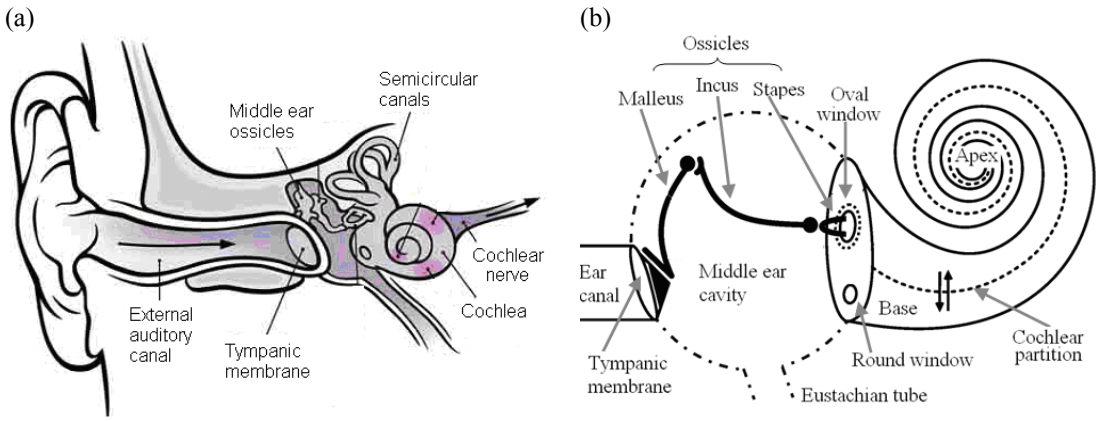

Figure 1.1 Illustrations of (a) the ear overview and (b) the the middle ear.
[From (a) figure 1a of Chittka & Brockmann (2005), open access journal, and (b) figure 1a of Nobili *et al.* (2003) with permission from JARO]

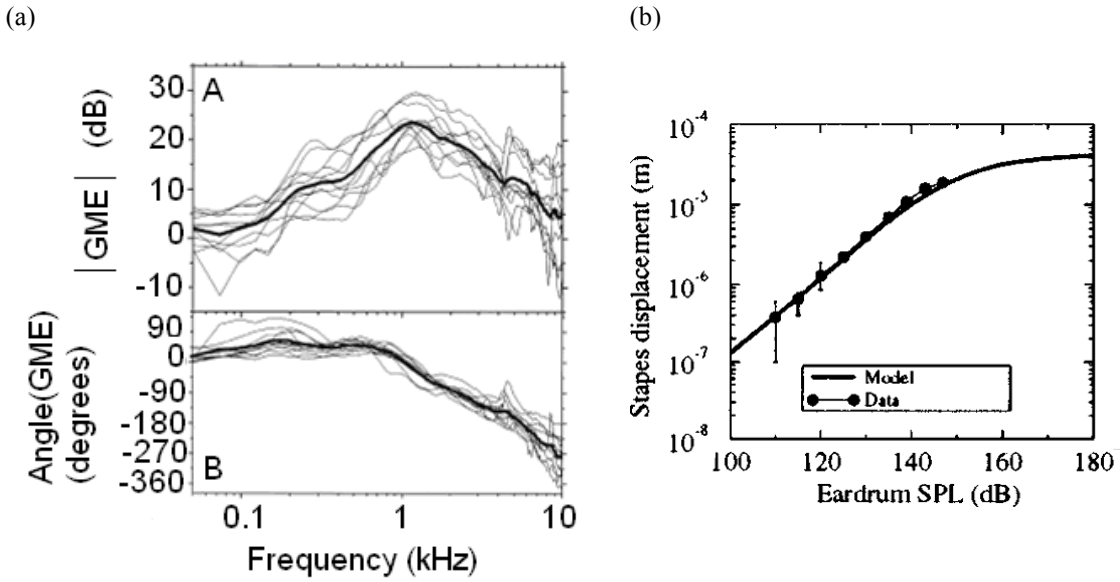

Figure 1.2 The response of the middle ear
(a) The gain of the middle ear (GME), measured as the ratio of the occluded ear canal acoustic pressure to the fluid pressure in the scala vestibuli, in 11 human temporal bones (grey lines) and the average result (black line). (b) Peak-to-peak stapes displacement as a function of sound pressure level (SPL) at the eardrum of a cat using a 315 Hz stimulus. [From (a) figure 2 of Aibara *et al.* (2001) and (b) figure 6 of Pascal *et al.* (1998) with permission from Elsevier and the ASA respectively].

1.1.2 The cochlea

In humans, the snail-shaped cochlea has a length of approximately 3.5 cm and incorporates about 2¾ turns (Gelfand, 1998). Figure 1.3 shows an idealised representation of the uncoiled longitudinal cochlea cross-section. The cochlea is divided length-ways by Reissner's membrane and the cochlear partition (CP) into three longitudinal ducts; the scala vestibuli, the scala media and the scala tympani. Each duct contains fluid, either perilymph or endolymph. These two fluids differ in their chemical composition (Gelfand, 1998), but both have similar density to water (~1000 kg/m^3) (Steele *et al.*, 2000). The CP separates the scala media and the scala tympani. It is composed of the spiral lamina, the basilar membrane (BM), the tectorial membrane, and a collection of cells (the organ of Corti) located between these membranes. Reissner's membrane is often neglected in mechanical cochlear models as it is acoustically transparent and appears to exist only in order to chemically separate the cochlear fluids (Dallos, 1992). The helicotrema, at the apex of the cochlea, provides a fluid link between the scala vestibuli and scala tympani, which limits damage that may be caused by excessive low frequency stimulation (Patuzzi, 1996). The middle ear makes contact with the cochlea via the stapes footplate, which is sealed onto the oval window by an elastic ligament (Dallos, 1992).

Figure 1.4 shows the transverse cross-section of the cochlea. Movement of the cochlear fluids causes relative motion of the BM with respect to the TM. As consequence of this relative motion, the hair cells located within the organ of Corti release neurochemicals to stimulate the auditory neurons (Patuzzi, 1996). There are two categories of cochlear model that differ in their treatment of

the CP (Patuzzi, 1996). In *macromechanical* models, any relative movement between the structures within the CP is neglected so that the partition moves as one unit. The alternative is a *micromechanical* model, in which this relative movement within the CP is not neglected.

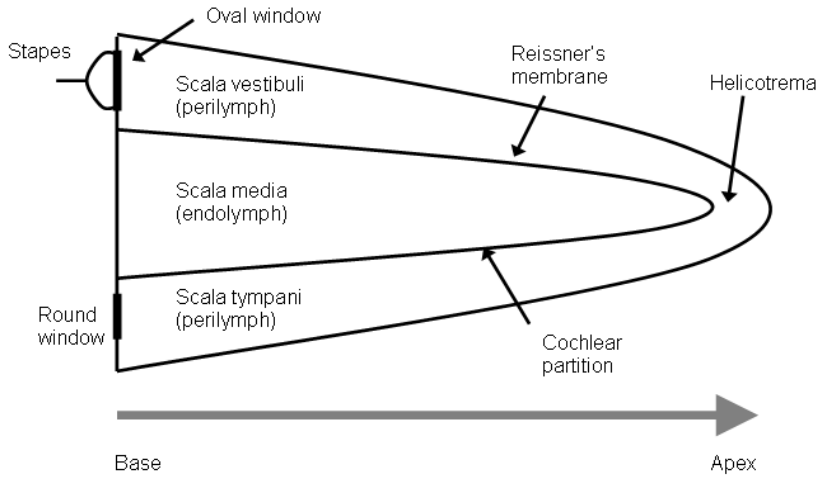

Figure 1.3 Representation of the cochlear ducts
[Based on Patuzzi (1996), figure 4.9]

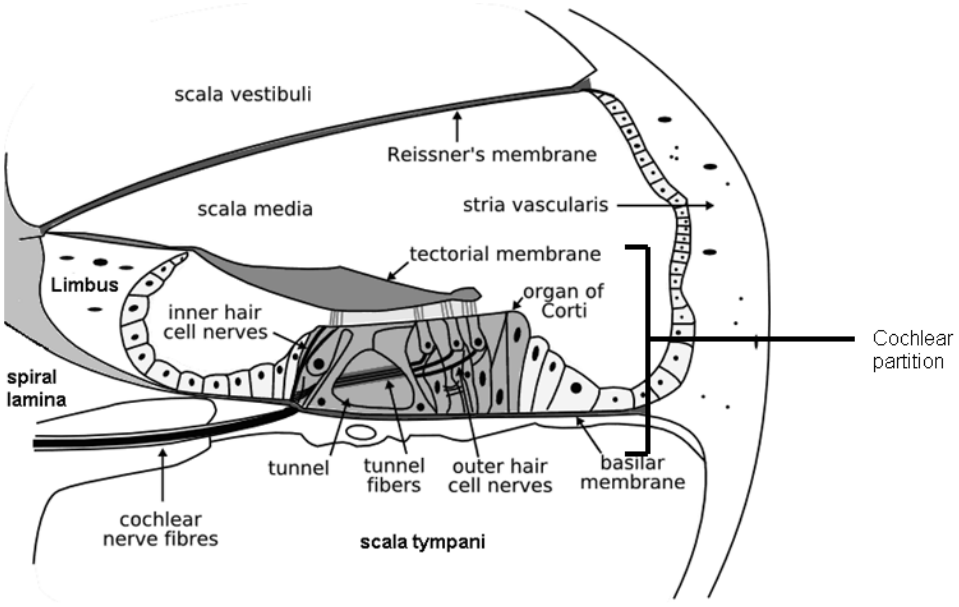

Figure 1.4 Cross-section of the guinea pig cochlea
[From figure 1 of Davis (1953), with permission of Elsevier]

1.1.3 Hair cells

The two types of hair cell located within the organ of Corti are illustrated in figure 1.5. Inner hair cells (IHCs) are thought to act primarily as sensory cells as they synapse directly with the auditory nerve (Nobili *et al.*, 1998). The cell is stimulated when relative motion between the BM and tectorial membrane causes a deflection of its stereocilia. This deflection produces a sound-induced receptor current within each hair cell (Patuzzi, 1996). The receptor current and the associated receptor potential (the change in voltage across the membrane) act to release neurochemicals to stimulate the auditory neurons. As the receptor potential is induced by BM motion, the neurons that are most responsive to a given frequency stimulus will be those that synapse with hair cells located at the characteristic place (defined in section 1.2.1).

Outer hair cells (OHCs) are also stimulated by relative motion between the BM and tectorial membrane. However, these hair cells act to enhance the motion of the BM rather than to stimulate auditory neurons (Ashmore *et al.*, 2002). This positive feedback could be achieved through somatic motility, as the length of the cell varies with changes in receptor potential (Brownell *et al.*, 1985; Dallos, 1992). An alternative positive feedback mechanism is motility of the stereocilia, suggested by observations in amphibians (Martin & Hudspeth, 1999). Several of the OHC processes are nonlinear, as illustrated in figure 1.6. These include the mechano-electric transduction (MET), the electro-mechanical motility, and the gating of mechanical channels (Liberman *et al.*, 2004).

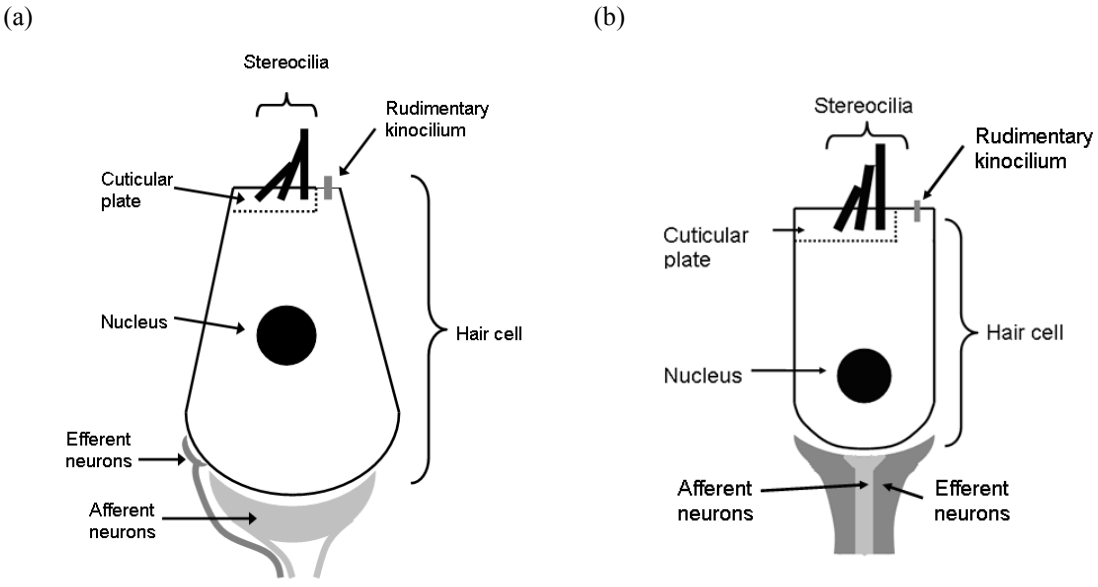

Figure 1.5 Illustrations of (a) an inner hair cell (IHC) and (b) an outer hair cell (OHC)
Details are based on the description given in Gelfand (1998).

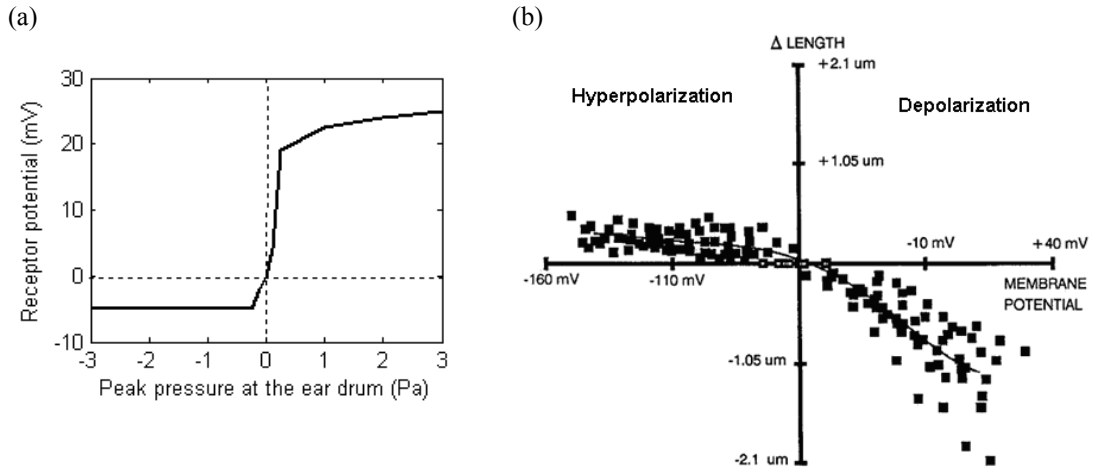

Figure 1.6 Examples of guinea pig OHC input-output functions
(a) mechano-electric transduction [Re-drawn from Dallos, 1996) and (b) electro-mechanical transduction [From figure 3 of Santos-Sacchi (1989), with permission of Elsevier]

1.2 Cochlear mechanics

In this section, the principal processes at work within the cochlea are described. It is these properties that a cochlear model must be able to replicate in order to accurately predict more complex cochlear responses.

1.2.1 The travelling wave

When the stapes vibrates there are two types of wave that can propagate within the cochlea as a result. The first is the 'travelling', or 'slow', wave which propagates along the basilar membrane (BM) at a rate that is slower than the speed of sound in water. The second is the 'compression', or 'fast', wave which travels at approximately the speed of sound in water and fills the entire cochlea almost instantaneously. Dong & Olsen (2008) explain that this compression wave can be viewed simplistically as a uniform background pressure that varies in time with the motion of the stapes. They comment that the two types of wave can be distinguished within the cochlear fluid by the associated spatial pressure variations. For example, the compression wave is associated with a spatially uniform pressure distribution, whilst the travelling wave leads to a spatially varying pressure distribution close to the BM.

The BM travelling wave, first observed by von Békésy (1960), is shown in figure 1.7. This wave propagates along the BM from base to apex, getting larger as it travels due to the exponentially decreasing stiffness of the BM (Patuzzi, 1996). The travelling wave reaches a maximum and then collapses abruptly (Gelfand, 1998). In the region of maximum amplitude the wave speed practically halts and so energy 'piles-up' at this position (Dallos, 1992). The amplitude of the travelling wave at each location along the cochlear partition (CP) is referred to as the travelling wave 'envelope' and is illustrated by the dotted line in figure 1.7. Temporal electrophysiological measurements demonstrate that the travelling wave is responsible for the excitation of hair cells (von Békésy, 1970). In contrast to this, the compression wave is usually neglected in cochlear models as it does not appear to produce significant hair cell excitation, and it is not coupled to the travelling wave (Dong & Olsen, 2008).

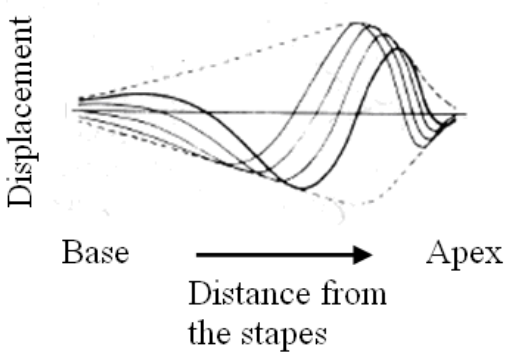

Figure 1.7 The basilar membrane (BM) travelling wave
The solid lines show successive patterns of BM displacement, and the dotted line represents the envelope of the travelling wave, for stimulation at 200 Hz.
[From figure 12/ − 17b of von Békésy (1960), with permission from ASA].

The natural frequency of the cochlear partition (CP) decreases from base to apex, as its mass and stiffness properties vary with distance from the stapes. Therefore, the CP provides frequency discrimination of the sound stimuli as the peak of the travelling wave envelope occurs at a location on the partition where the natural frequency corresponds to the stimulus frequency (de Boer, 1996). This location is near the base for high-frequency stimuli and near the apex for low frequency stimuli (Dallos, 1992). Very low frequency stimuli (~200 Hz) can result in BM displacement patterns that propagate along the entire length of the cochlea. The BM displacement and velocity can reach up to 30 nm and 2 mm/s respectively for an 80 dB SPL stimulus in the Chinchilla cochlea (Robles & Ruggero, 2001). The location at which the travelling wave envelope has the greatest amplitude, for a given stimulus frequency, is often called the 'best' place for that frequency. Similarly the stimulus frequency that produces the maximal BM displacement (or velocity) at a specific location on the cochlear partition is known as the 'best' frequency for that place (e.g. Dong & Olson, 2005). An active process, described in section 1.2.2, is thought to operate within the cochlea. One consequence of this activity near the base, is an increase in the best frequency of about half an octave relative to the passive natural frequency at a specific location (Steele *et al.*, 2006). The best place (or best frequency) in an active cochlea is also known as the 'characteristic' place (or 'characteristic' frequency) (Dallos, 1992). Figure 1.8 shows the amplitude and phase accumulated by the travelling wave as it progresses from the base of the cochlea to the characteristic place. The accumulated phase observed at the characteristic place is fairly constant for a given species, for a range of stimulus frequencies. For example the travelling wave of the squirrel monkey accumulates a phase lag of approximately 12 radians (or about 2 cycles), relative to the stapes motion, en route to its characteristic place irrespectively of the distance between that place and the base.

As the location of the characteristic place is monotonically dependent on frequency, an empirical frequency-position function can be constructed as shown below (Greenwood, 1996; Le Page, 2003) . This can be applied to several species using the parameters given in table 1.1.

$$f_x(x) = C_0 \cdot \left(10^{a_0(1-x/L)} - K_0\right) \qquad \textbf{(1.1)}$$

In this expression, f_x is the characteristic frequency corresponding to location x on the BM, L is the length of the cochlea, and C_0, a_0 and K_0 are all constants which differ between animals. The place-frequency maps obtained from this formula are shown in figure 1.9 for three different species. The cochlear model discussed in Chapter 2, devised by Kanis & de Boer (1993), is based on the human cochlea and is therefore designed to have a place-frequency map similar to the solid line shown in figure 1.9.

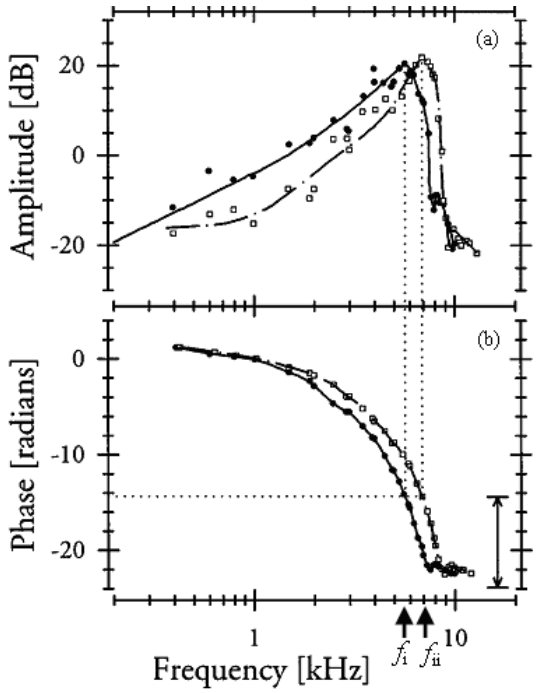

Figure 1.8 The basilar member (BM) response to stimulation at the stapes
The (a) amplitude and (b) phase of the ratio of BM to malleus displacement in the squirrel monkey cochlea. The responses are observed at two different locations, separated by 1.5 mm, where f_i and f_{ii} are the characteristic frequencies of the basal and apical sites respectively.
[From figure 5 of Shera & Guinan (1999), with permission from ASA].

Mammal	C_0 (Hz)	a_0	K_0	L (mm)	f_{base} (kHz)	f_{apex} (Hz)
Elephant	81	1.8	1	60	5.1	0
Cow	52.6	2.1	1	38.3	6.6	0
Human	165.4	2.1	1	35	20.8	0
Macaque	360	2.1	0.85	25.6	45.3	54
Domestic cat	456	2.1	0.8	25	57.4	91
Guinea pig	350	2.1	0.85	18.5	44.1	53
Chinchilla	163.5	2.1	0.85	18.4	20.6	25
Gerbil	398	2.2	0.631	12.1	63.1	147
Mouse	7130	0.99	1	6.8	105.3	0

Table 1.1 The parameters for Greenwood's frequency-position function equation (1.1)
The data is taken from Le Page (2003) and the characteristic frequencies at the base (f_{base}) and at the apex (f_{apex}) are also shown.

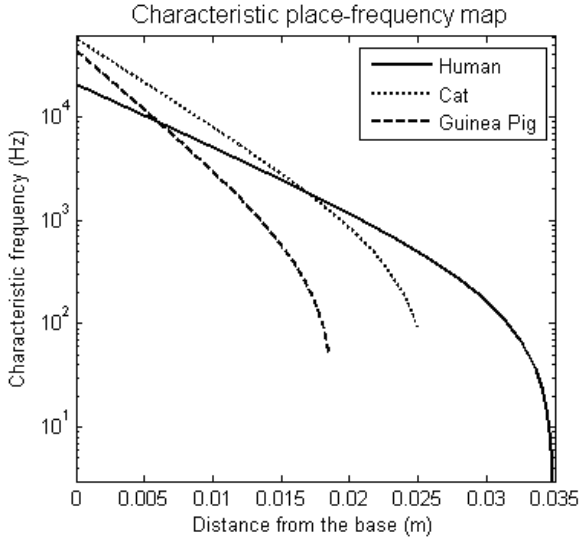

Figure 1.9 The calculated place-frequency maps for humans, cats and guinea pigs
These results were obtained using equation (1.1) and the data from table 1.1.

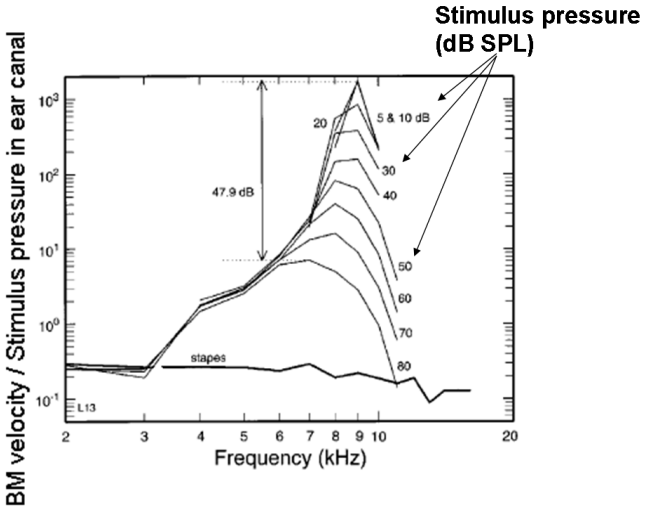

Figure 1.10 The nonlinear frequency response of the BM
The response is observed 3.5 mm from the basal end of the chinchilla cochlea using laser interferometry. The characteristic frequency at this location is approximately 10 kHz. [From figure 10 of Ruggero *et al.* (1997), with permission from the ASA]

1.2.2 The active process

Figure 1.10 shows the variation in BM frequency response with stimulus pressure level observed in the chinchilla cochlea using a laser interferometry (Ruggero *et al.*, 1997). At high stimulus levels, the frequency response is broad, and is comparable to the responses observed in dead or damaged cochlea (Johnstone *et al.*, 1986; Dallos, 1992). This response can be described by a passive cochlear model (e.g. Zwislocki, 1950), in which the CP can only absorb acoustical energy (de Boer, 1995b). At low stimulus levels, the frequency response is sharper as the BM vibrations are enhanced at frequencies close to the characteristic frequency. It is necessary for a model to incorporate a locally active region, just basal to the characteristic place, in order to replicate these low level responses (de Boer & Nuttal, 1999). This active process, or "*cochlear amplifier*" (Davis, 1983), injects energy into the travelling wave which is dissipated elsewhere along the cochlear partition (de Boer, 1995b). The "gain" of the cochlear amplifier usually refers to the 40 − 60 dB increase in the active BM response compared to the passive case (Nobili *et al.*, 1998), evident in figure 1.10. The active process also increases the frequency at which the maximum response occurs at a specific location by about half an octave compared to the passive response (Steele *et al.*, 2006) and sharpens the tuning of the BM frequency response. For example, in a chinchilla cochlea, the Q_{10dB} [1] increases from 1.4 to 5 as the stimulus level reduces from 90 dB SPL to 10 dB SPL (Robles & Ruggero, 2001).

The active process is thought to occur at the level of the BM, as mechanical tuning within the cochlea is as sharp as neural tuning (Khanna & Leonard, 1982; Sellick *et al.*, 1982; Robles *et al.*, 1986), and is associated with the collective action of the OHCs (Davis, 1983). Evidence for the cochlear amplifier originates from 'inverse' solutions in cochlear modelling, where the unknown

[1] Q_{10dB} is equal to the frequency of the response peak divided by the bandwidth 10dB below the peak (Robles & Ruggero, 2001). Therefore higher Q_{10dB} values indicate sharper tuning.

distribution of the CP impedance is obtained from physiological measurements of the cochlear response to single tone stimulation. The resulting impedance is found to exhibit a negative real component over the region just basal to the peak of the travelling wave envelope (Zweig, 1991; de Boer, 1996). The location of this region of negative damping is dependent on the stimulus frequency and indicates that the travelling wave energy increases in this region (Allen & Neely, 1992).

Patuzzi (1996) summarises that there are several other physiological phenomena which are consistent with an active process operating within the cochlea. These include the high metabolic rate of the cochlea, and the loss of neural sensitivity to low level sound following cochlea damage (induced by trauma or drugs). He also points out that it is difficult to explain the origin of otoacoustic emissions (especially spontaneous otoacoustic emissions) with a passive cochlear model.

1.2.3 The response of the cochlear base to single tone stimulation

Most of our knowledge of cochlear mechanics comes from experimental studies of the basal end of small animal cochleae, as the base of the cochlea is easier to access relative to the apex (Robles & Ruggero, 2001). However, there is some evidence that the behaviour of the apical region differs from that of the base (Kiang & Moxon, 1974) and this issue will be addressed in section 1.2.4.

Figure 1.10 illustrates that the response of the BM to single tone stimulation has a nonlinear dependence on stimulus level close to the characteristic frequency, and a more linear dependence at higher and lower frequencies (Ruggero *et al.*, 1997). Figure 1.11 shows an example of the growth of the BM response at the characteristic place, for increasing stimulus level. Pickles (1982) identifies three regions on this graph: linear growth at low stimulus levels up to about 30 dB SPL, compressive nonlinear growth at a rate of approximately 0.2 dB/dB as a consequence of saturation of the action process for inputs between about 30 and 100 dB SPL, and linear growth at high levels where the passive component dominates the active component. It can also be seen from figure 1.11 that the input-output function becomes more linear when the cochlea is damaged.

The nonlinear response of the cochlea is also evident in the harmonic distortion evoked by a single tone stimulus (Cooper, 1998). In addition, nonlinear phenomena such as mutual suppression and distortion products are observable in the cochlear response to two tone stimulation (Robles & Ruggero, 2001). The mechanoelectrical transduction processes in the OHCs, where the stereocilla deflection generates a current, is likely to be the dominant source of this nonlinear behaviour (Ashmore, 2008). The compressive nonlinear behaviour of the cochlea has been successfully modelled using dynamic nonlinear models in the past (Kanis & de Boer, 1993; Harte *et. al*., 2005; van der Heijden, 2004; Ku, 2008).

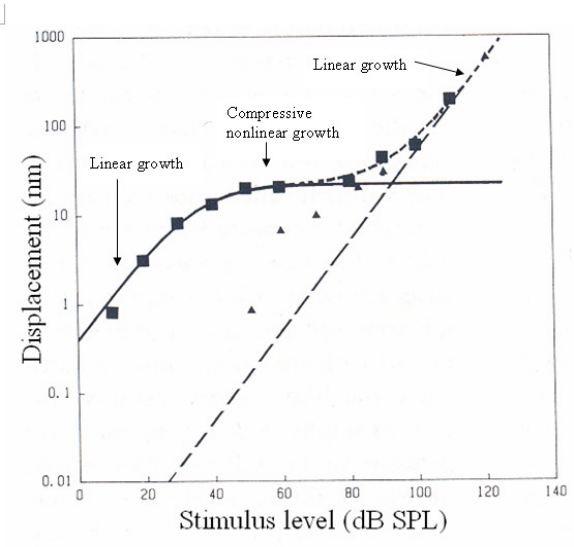

Figure 1.11 Input-output function of the BM response at the characteristic frequency
Responses were measured before (squares) and after (triangles) trauma in the guinea pig cochlea. The solid, dashed and dotted lines represent the growth function that would be expected from a saturated mechanism, a linear mechanism or a combined mechanism respectively.
[From figure 5 of Johnstone *et al.* (1986), with permission from Elsevier]

Another property of the single tone response in the basal region of the cochlea is approximate "scaling symmetry", which means that the amplitude and phase of the travelling wave remain almost unchanged in a co-ordinate system that moves with the envelope of the travelling wave (Shera *et al.*, 2000). For example the phase lag, relative to the stapes motion, of the travelling wave at the characteristic place is nearly constant for all stimulus frequencies as shown in figure 1.8.

1.2.4 The response of the cochlear apex to single tone stimulation

Invasive experimental techniques can obscure the response of the apical region of the cochlea (Cooper & Rhode, 1995). However, evidence from neural measurements suggests that the cochlear processing of sound may differ between the basal and apical regions. For example the sharpness of cochlear nerve tuning decreases as characteristic frequency decreases, as shown in figure 1.12 (Robles & Ruggero, 2001). The form of the low-frequency tail of the neural frequency tuning curve (FTC) also depends on the characteristic frequency of the auditory nerve fibre (Kiang & Moxon, 1974). In addition the phase lag of neural response at the characteristic place reduces as the stimulus frequency decreases, as shown in figure 1.13. This indicates that the approximate scaling symmetry observed in the basal region of the cochlea does not extend throughout the cochlear length. Finally the effect of damage on the neural response appears to differ between basal and apical regions of the cochlea. In the apical region, most of the neural FTC is elevated by cochlear trauma, whilst only the tip of the FTC is affected in the basal region (Johnstone *et al.*, 1986). Also, if the tip of the FTC can be associated with cochlear amplifier (CA) gain, then the influence of drug induced damage suggests that the CA gain is lower in the apical, relative to the basal, region of the cochlea (Gorga *et al.*, 2007).

Differences in the form of the BM frequency response are also evident between the base and the apex, as shown in figure 1.14 (Robles & Ruggero, 2001). The apical BM response is less sharply tuned and exhibits less cochlear amplifier gain compared to the more basal response. In addition,

the frequency of maximum sensitivity is almost independent of stimulus level in the apical region but reduces with stimulus level in the basal region of the cochlea. Studies using masking techniques and otoacoustic emissions in human subjects suggest that the compressive nonlinear growth rate at the characteristic frequency is approximately the same in apical and basal regions, but that the range of stimulus levels over which the nonlinear growth occurs is less in the apex than the base (Lopez-Poveda *et al.*, 2003; Gorga *et al.*, 2007). These studies also provide some evidence that the cochlear gain may be lower at 500 Hz compared to 4000 Hz, but these results could be compromised by the variations in noise level with frequency (Gorga *et al.*, 2007).

Most cochlear models are designed to replicate the responses observed in the basal region of the cochlea, as much more experimental data is available to describe the base compared to apex. However, Shera *et al.* (2000) comment that deviations from the typical basal behaviour start to become evident in human subjects when the characteristic frequency is reduced below 3 kHz, which corresponds to locations which are over 13 mm from the stapes. This imposes a limitation on the usefulness of many current cochlear models as the most important frequencies for speech perception are in the range 0.25 − 8 kHz (Dillon, 2001). Models need to represent the properties of the apical region, based on either basal responses or the limited experimental data available, to optimize their relevance in this regard.

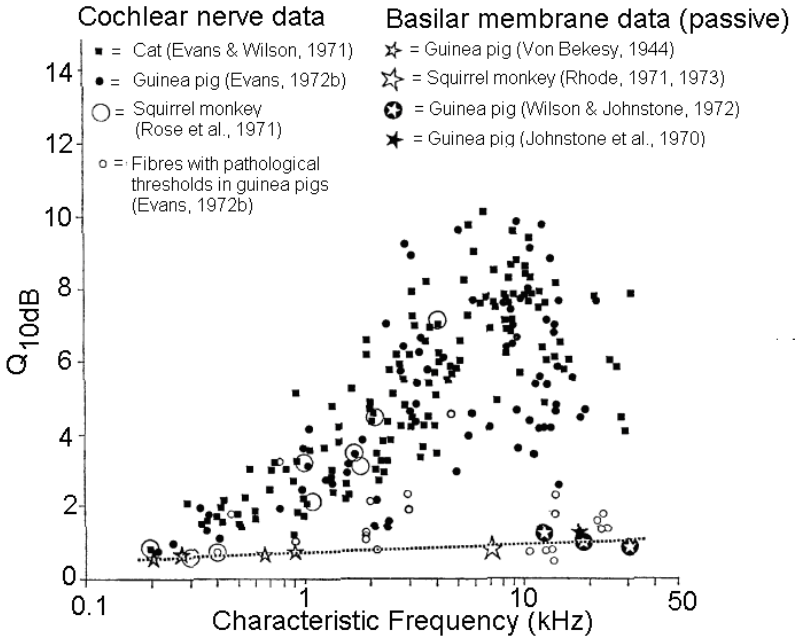

Figure 1.12 The relationship between BM tuning and characteristic frequency.
The sharpness ($Q_{10\,dB}$) of tuning for cochlear nerve and BM threshold responses are shown as a function of characteristic frequency for a range of animals. The data from the BM tuning curves refers to damaged cochlea, where the response is likely to be entirely passive.
[From figure 2 of Evans (1975), with permission from Informa Healthcare]

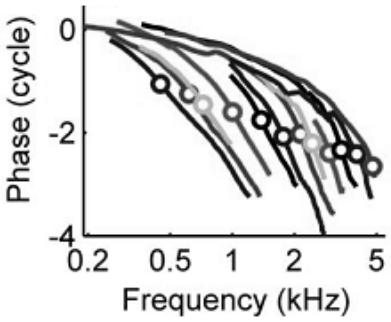

Figure 1.13 Phase of the neural response to stapes stimulation
Responses were observed from nerve fibres at different locations along the BM of the cat cochlea for a range of stimulus frequencies. The circles indicate the characteristic frequency of the nerve fibres.
[From figure 5 of van der Heijden & Joris (2006), with permission from Elsevier]

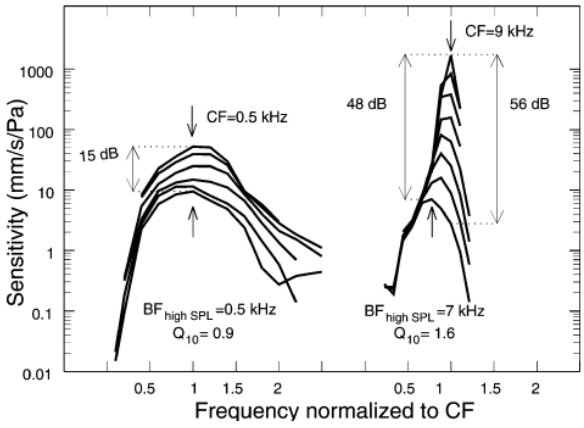

Figure 1.14 The response of the BM at a basal and apical location
The sensitivity (ratio of BM velocity to stimulus pressure) was recorded at the 0.5 and 9 kHz characteristic places in the chinchilla cochlea. The multiple curves correspond to different stimulus levels, and the best frequencies for the high stimulus levels are also indicated.
[From figure 13 of Robles & Ruggero (2001), with permission from Am. Physiol. Soc.]

1.3 Classification of otoacoustic emissions

An otoacoustic emission (OAE) is acoustic energy released by the cochlea and recorded in the external ear canal. OAEs were predicted by Gold (1948), and first detected in the ear canal by Kemp (1978). Traditionally OAEs have been classified using the auditory stimulation that evokes them, as listed below (Probst *et al.*, 1991; Hall, 2000). Example recordings of these emissions are shown in figure 1.15.

(i) Spontaneous otoacoustic emissions (SOAEs) are narrow band that occur without a deliberate stimulus.
(ii) Transient evoked otoacoustic emissions (TEOAEs) occur in response to a brief stimulus, such as a click or tone burst.
(iii) Stimulus frequency otoacoustic emissions (SFOAEs) are elicited by a pure tone stimulus and have the same frequency as that stimulus.
(iv) Distortion product otoacoustic emissions (DPOAEs) which are evoked by two pure tones presented simultaneously in the ear canal. The conventional notation used to describe the stimuli is f_1 and L_1 for the frequency and level of the lower frequency tone, and f_2 and L_2 for the other tone. For any two stimulus tones DPOAEs could theoretically occur at all frequencies equal to nf_1+mf_2, where n and m are integers, but many are too small relative to the background noise to be detected. However, there are several which are large enough to be reliably detected, as described in section 1.5.

Section 1.4.1 describes the sources of OAEs and introduces an alternative classification based on the hypothesised physiological origin of the emission. As DPOAEs are of special interest in this work, the methods for measuring these emissions and an overview of their properties are presented in sections 1.5 and 1.6 respectively.

(a) SOAEs

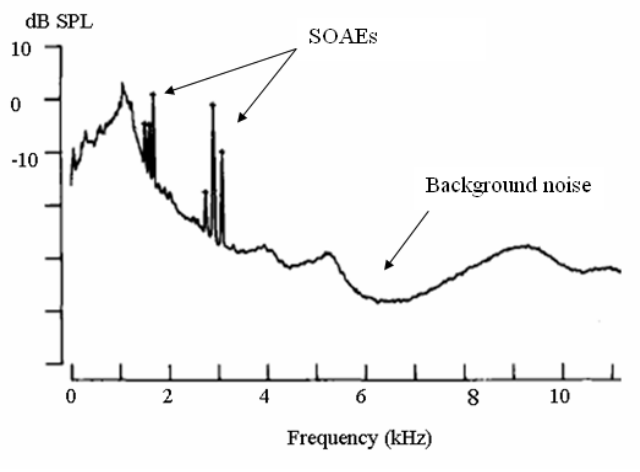

(b) TEOAE

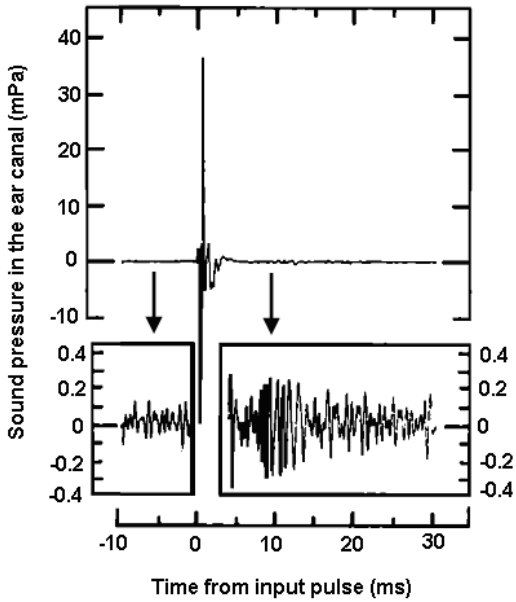

(c) SFOAE

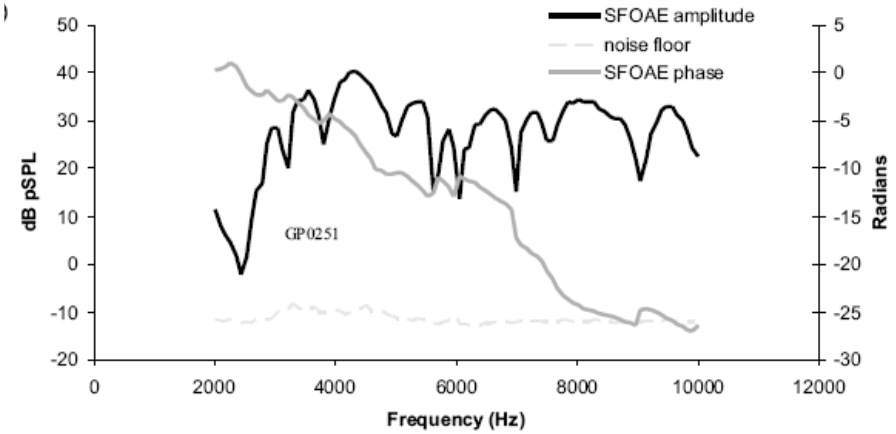

(d) DPOAEs

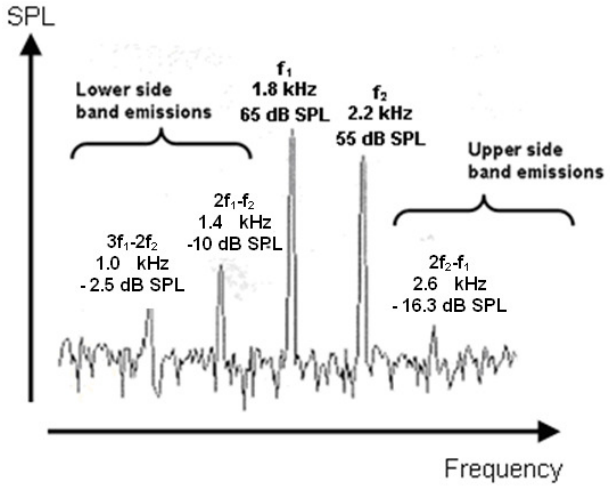

Figure 1.15 Examples of otoacoustic emission (OAE) recordings
(a) Spectrum of SOAEs [Adapted from figure 2 of Lind & Randa, 1992), (b) A TEOAE time history evoked by a click stimulus. The lower boxes highlight the response immediately before and after the click. [From figure 1 of Kemp (1978), with permission from ASA], (c) An SFOAE measured at difference frequencies [From figure 1 of Goodman *et al.* (2003) with permission from Elsevier, and (d) Spectrum of DPOAEs in the presence of two stimulus tones (f_1 and f_2, where $f_1<f_2$). The emissions are classified as "upper" or "lower" side band emissions if their frequency is greater than or less than f_2 respectively. [Adapted from Lonsbury-Martin & Martin (2007), figure 5.1]. All responses are from human ears, apart from (c) which corresponds to a guinea pig ear.

1.4 The sources of otoacoustic emissions

This section gives an overview of the evidence for the cochlear origin of OAEs (section 1.4.1) and describes the cochlear mechanisms by which the emissions are thought to originate and propagate (section 1.4.2). The spotlight is then turned onto DPOAEs with a description of the location and mechanism of their cochlear sources (section 1.4.3). The section ends with a discussion of the possible role of fluid compression waves in the production of DPOAEs.

1.4.1 Cochlear origins

A range of experiments using two different approaches were conducted during the 1980s to confirm that OAEs are generated within the cochlea. First it was established that alternative sources, such as the middle ear or neural mechanisms, were not responsible. For example drug induced paralysis or relaxation of the middle ear muscles produced no systematic changes in the SOAEs recorded from guinea pigs or anesthetised cats (Evans *et al.*, 1981; Guinan & McCue, 1987). Also, the long latencies, frequency dispersion and saturation properties of TEOAEs are difficult to reconcile with a theoretical source located in the middle ear (Probst *et al.*, 1991). In addition, several observations are inconsistent with a neural source: TEOAE detection thresholds are lower than the corresponding psychophysical thresholds (Kemp (1978);Wit & Ritsma, 1979); OAE polarity reverses when stimulus polarity reverses (Kemp, 1978); and the TEOAE amplitude exhibits nonlinear growth with stimulus level (Kemp, 1978). The second approach was to show that cochlear trauma changes OAEs, using hypoxia, ototoxic drugs or acoustic over-exposure. For example, Mills (2002) demonstrated that cochlear damage associated with furosemide injection results in elevated DPOAE thresholds.

The above experiments revealed that OAEs originated from the cochlea, and further work established that the cochlear source is closely associated with the OHCs. For instance, the destruction of OHCs lead to changes in the DPOAE thresholds of bats and chinchilla (Hofstetter *et al.*, 1997; Krossel & Vater, 2000). Also the administration of aminoglycoside antibiotic drugs, which primarily damage OHCs (Forge & Schacht, 2000), reduce TEOAE levels (Stavroulaki *et al.*, 1999) and aspirin can abolish SOAEs and SFOAEs in humans (McFadden & Plattsmier, 1984; Long & Tubis, 1988). In contrast, the destruction of inner hair cells (IHCs) has little effect on DPOAE and TEOAE properties when OHC function is retained (Wake *et al.*, 1996; Hofstetter *et al.*, 1997). Two different source mechanisms for OAE generation are described in the following section but it should be noted that the properties of the travelling wave, which are influenced by the OHCs, are important in both mechanisms.

In summary, OAEs are known to originate within the cochlea and their properties depend on the function of the OHCs.

1.4.2 Source mechanisms

The previous section established that OAEs originate within the cochlea and that their properties depend on the function of the OHCs. Kemp (1986) considered how OAEs relate to travelling waves in the cochlea in order to shed light on the mechanisms underlying their generation. He classified OAEs as either "wave-fixed" or "place-fixed", depending on the relationship between the emission source and the travelling wave envelop as the stimulus frequency is varied. A wave-fixed source is one where the source moves along the cochlear partition as the stimulus frequency is varied, maintaining a constant position relative to the forward travelling wave envelop. In contrast a place-fixed source does not move along the cochlear partition if the stimulus frequency is altered. This leads to a difference in the phase behaviour between wave-fixed and place-fixed sources. For a place-fixed source the phase is related to the phase of the travelling at a fixed location, whilst for a wave-fixed source the phase is related to a point that moves with the travelling wave envelope. Shera & Guinan (1999) built on Kemp's classification to identify two different source mechanisms which can generate OAEs.

(i) Reflection source mechanism

This mechanism involves the linear scattering of a forward travelling wave off pre-existing perturbations in the cochlear mechanics to generate backward travelling waves. Upon reaching the base of the cochlea, these backward travelling waves could vibrate the stapes and be detected in the ear canal as an OAE. Evidence that these reflection sites could exist is based on the observation that the primate cochlea appears disorganised (Wright, 1984) indicating that impedance discontinuities could be distributed throughout its length.

Although the mechanical perturbations are thought to be present along the whole cochlear partition, Zweig & Shera (1995b) suggest that for a single tone stimulus the tall and broad peak of the travelling wave envelope ensures that the wavelets originating from the region of the characteristic place have much larger amplitude than those reflected elsewhere. These reflections must be coherent, so that constructive interference occurs between the reflected wavelets, in order for a backward travelling reflected wave to be generated. Coherent reflections are expected to arise in the cochlea given that the travelling wave envelope has a slowly varying wavelength, λ_{TW}, and that the spacing between some of the randomly distributed impedance irregularities in the vicinity of the characteristic place is equal to an integer multiple of $\lambda_{TW}/2$. Therefore the largest contribution to a reflection source emission, evoked by a single tone stimulus, is thought to originate near the characteristic place of the forward travelling wave.

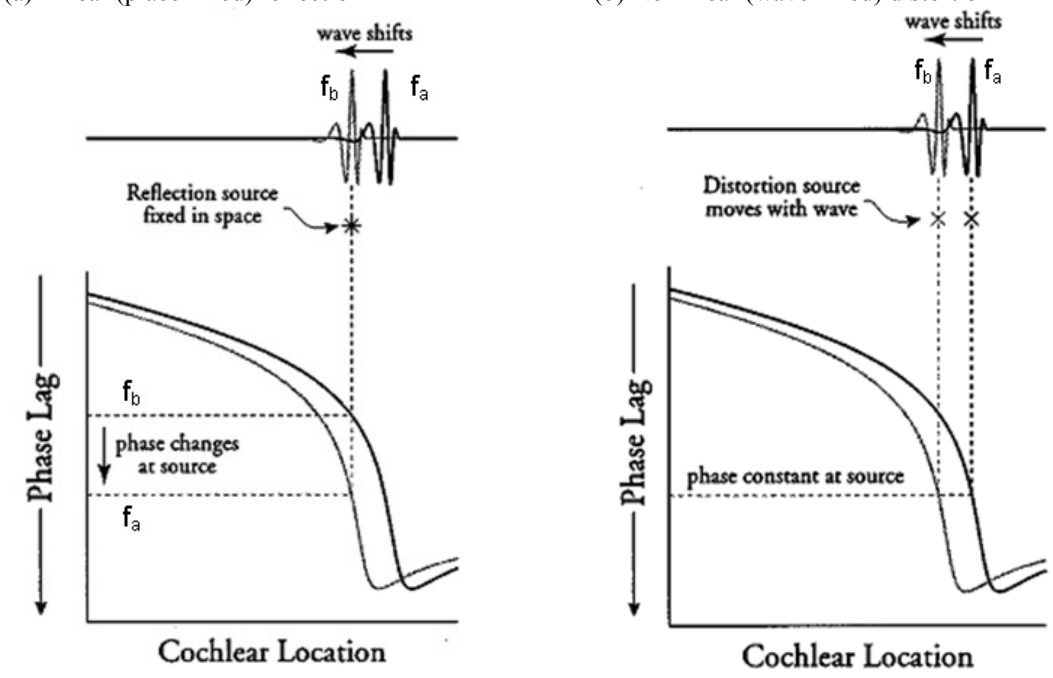

Figure 1.16 Illustration of the influence of stimulus frequency on the phase of emission sources
The change in the source phase for (a) a place-fixed (reflection) source emission and (b) a wave-fixed (distortion) source emission, evoked by a single stimulus tone, is illustrated when the stimulus tone frequency is decreased from f_a to f_b. [From figure 2 of Kalluri & Shera (2001), with permission from ASA]

If the evoked emission arising from a single tone stimulus originates from a reflection source, Shera & Guinan (1999) argue that the phase of the emission should vary rapidly with stimulus frequency, as illustrated in figure 1.16a. This is because the reflection sites are fixed and so the phase of the incident forward travelling wave varies when a small change in stimulus frequency occurs, resulting in a change in emission phase (with respect to the stimulus tone). Therefore, the "reflection" source described by Shera & Guinan is analogous to the "place-fixed" source in Kemp's scheme.

(ii) Distortion source mechanism

This source mechanism is a consequence of the nonlinear response characteristics of the OHCs. When stimulated by two forward travelling waves, evoked by the simultaneous presentation of two pure tones (f_1 and f_2) in the ear canal, the nonlinear output of the OHCs will contain distortion product (DP) components in addition to components at the two primary frequencies. If the DP component is generated in a region of the cochlea which supports travelling waves at the DP frequency then, once generated, the DP travelling wave may propagate both backward towards the stapes to produce an emission in the ear canal, and forward towards the apex and the DP characteristic place (Kim *et al.*, 1980). As a consequence of the scaling symmetry in the cochlea (see section 1.2.3), the phase of a distortion source emission evoked by two pure tone stimuli is not expected to vary very much for small changes in the stimulus frequency provided that f_2/f_1 is

constant (Shera & Guinan, 1999), as illustrated in figure 1.16b. A "distortion" source in Shera & Guinan's scheme corresponds to a "wave-fixed" emission in Kemp's description.

Shera & Guinan (1999) use the different phase properties of the two source mechanisms, to identify the dominant source mechanism responsible for generating different evoked OAEs. For example, figure 1.17 shows that the phase of an SFOAE evoked by a low level stimulus varies rapidly with stimulus frequency which suggests it is generated by a place-fixed (reflection) source mechanism. Conversely the DPOAE shown in figure 1.17 maintains an almost constant phase as the stimulus frequencies are varied with fixed f_2/f_1 ratio, which would be consistent with a wave-fixed (distortion) source generation mechanism. A schematic diagram illustrating Shera & Guinan's theory for the source mechanisms of SFOAEs and DPOAEs is shown in figure 1.18.

Shera & Guinan suggest that OAEs should be classified according to their source mechanism rather than the evoking stimulus, as shown in figure 1.19. Using the unmixing techniques described in section 1.5, they illustrate that DPOAEs are composed of two source contributions: a wave-fixed (distortion) component and a residual place-fixed (reflection) component. In their taxonomy, SOAEs are categorized as predominantly reflection source emissions, as they are thought to arise from multiple reflections within the cochlea (Kemp, 1986) which are stabilized by cochlear nonlinearities (Shera & Guinan, 2008).

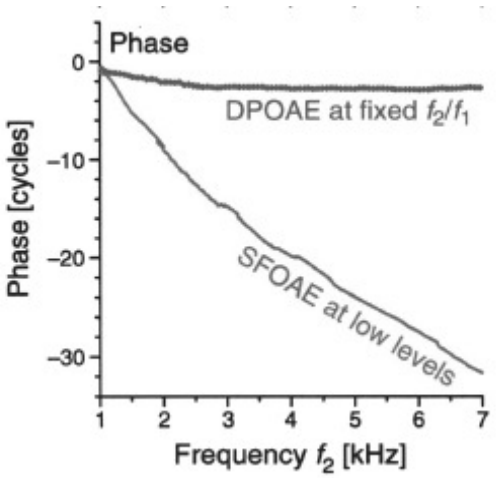

Figure 1.17 The phase variation of an SFOAE and a DPOAE with stimulus frequency
The SFOAE was obtained using a probe level of 40dB SPL. The $2f_1 - f_2$ DPOAE was measured using a swept f_2 and fixed f_2/f_1 ratio (=1.2) with L_1 and L_2 equal to 50 and 40 dB SPL respectively. To obtain a predominantly distortion source DPOAE, it was recorded in the presence of a third stimulus tone ($f_3 \sim 2f_1 - f_2$ and L_3= 55dB SPL) to suppress the reflection component originating from the $2f_1 - f_2$ characteristic place. [From figure 3 of Shera (2004), with permission from Wolters Kulver Health]

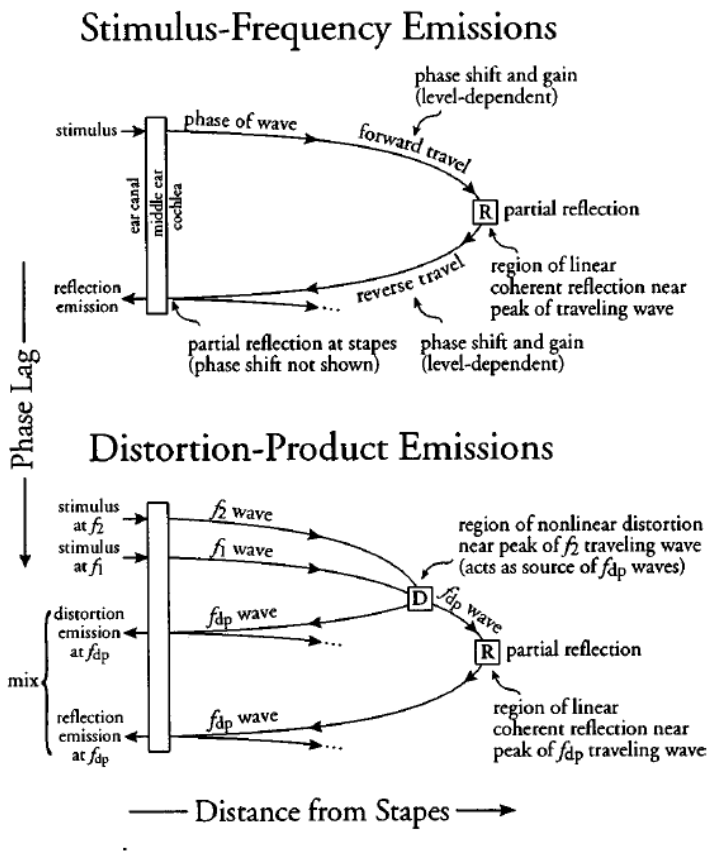

Figure 1.18 Illustration of SFOAE and DPOAE generation mechanisms at low stimulus levels [From Shera & Guinan (1999), figure 12 with permission from ASA].

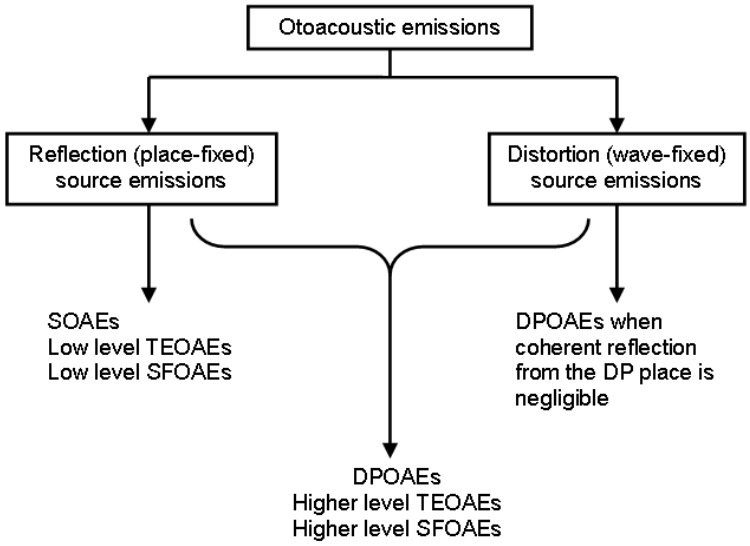

Figure 1.19 Summary of the Shera & Guinan (1999) taxonomy for OAE classification
The taxonomy is based on the source mechanism, rather than the stimulus used to evoke the emission, but in general evoked emissions contain contributions from both reflection (place-fixed) and distortion (wave-fixed) sources at high stimulus levels. [Re-drawn from Shera & Guinan (1999), figure 10]

1.4.3 Location of cochlear sources for DPOAEs

The previous sections presented the evidence for the cochlear origin of OAEs and the two different source mechanisms within the cochlea. This included a description of the two source mechanisms which are thought to contribute to the DPOAE detected in the ear canal: the nonlinear wave-fixed (distortion) source and the linear place-fixed (reflection) source. These two DPOAE sources can be spatially distinct (Brown *et al.*, 1996), and so in this section the evidence for the location of these sources is presented. It should be noted that the mechanism for DP propagation out of the cochlea is controversial, but for now we consider that this propagation occurs via backward travelling waves and defer discussion of the alternative theory until section 1.4.4.

DPs can be categorized by their frequency relative to the stimulus tones (f_1 and f_2, where $f_2 > f_1$). For example the emission frequency is either below or above the stimulus tones, so the DP is referred to as either a 'lower-' or 'upper-' side band emission respectively. As it is likely that the location of the source mechanisms for DP generation depend on its frequency compared to the stimulus tones, we consider the source locations of lower and upper side band emissions separately.

(i) Lower side band distortion products

The characteristic place for a lower side band DP is apical to the best places of both f_1 and f_2. Kim *et al.* (1980) observed that lower side band emissions ($2f_1 - f_2$ and $f_2 - f_1$) appeared to be generated in the region of maximum overlap between the primary travelling waves evoked by the stimulus tones, from their neural recordings in cat cochleae. Their results also suggested that, once generated in this overlap region, the DPs could travel both basally and apically. They observed that the response to the forward travelling DP at its characteristic place was essentially the same as that elicited by a single tone stimulus at the DP frequency presented in the ear canal. An illustration of how these two components arise and could contribute to the total DPOAE recorded in the ear canal is shown in figure 1.20a. In addition to this neural data, measures of the DP component of the pressure in the scala tympani near the BM of the gerbil cochlea by Dong & Olsen (2008) confirm that the amplitude of DP is greatest in the vicinity of the f_2 best place and the CP characteristic place. This is shown in their results, reproduced in figure 1.21a, of the $2f_1 - f_2$ DP amplitude of the scala tympani pressure at the 18 kHz best place. Peaks in the DP amplitude are observed when the DP frequency is equal to either 11 or 18 kHz, as at these frequencies either the DP or f_2 frequency corresponds to the best frequency of the observation site.

(a) A lower side band emission (e.g. $2f_1 - f_2$)

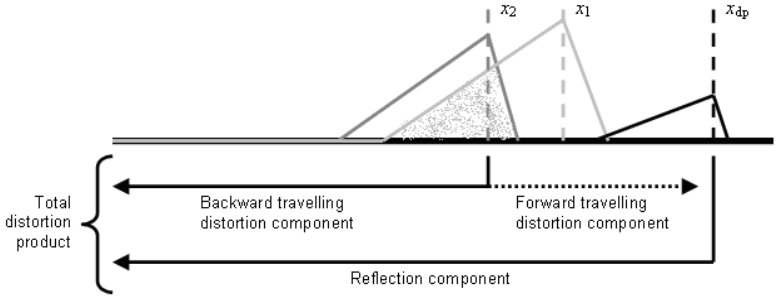

(b) An upper side band emission (e.g. $2f_2 - f_1$)

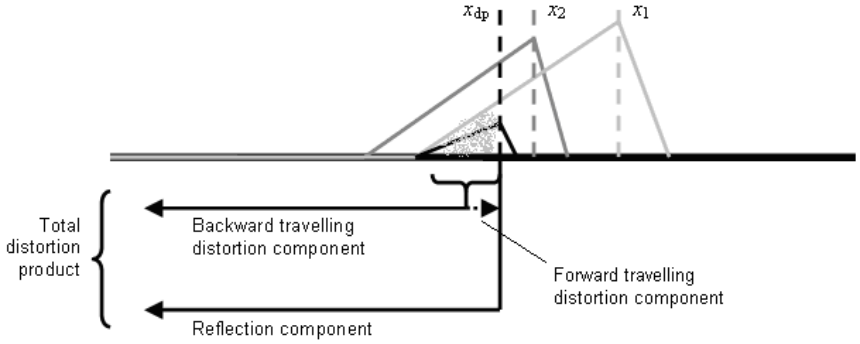

Figure 1.20 Illustrations of the distortion product source mechanisms
(a) a lower side band emission [Re-drawn from Shaffer *et al.* (2003), figure 1] and (b) an upper side band emission. The grey and black lines represent the travelling waves corresponding of the stimulus tones and the DP frequency respectively. The grey shaded area indicates the predicted distortion source mechanism location. DPs corresponding to other frequencies are neglected for clarity.

(a) The $2f_1 - f_2$ DP

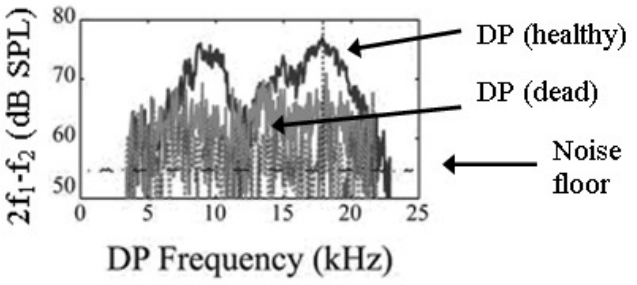

(b) The $2f_2 - f_1$ DP

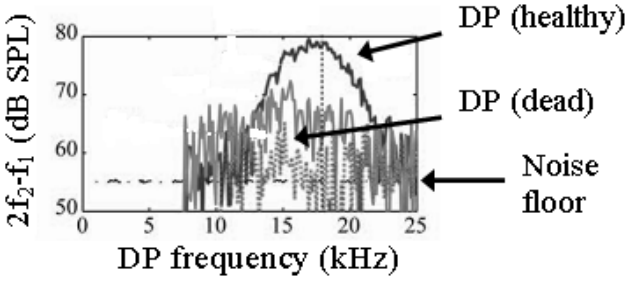

Figure 1.21 The (a) $2f_1 - f_2$ and (b) $2f_2 - f_1$ DP components of the scala tympani pressure
Responses were observed near the BM at the 18 kHz best place in a gerbil cochlea (L_1=L_2=80 dB SPL & f_2/f_1=1.25). The solid black, solid grey and dotted grey lines show measurements from a healthy, damaged and dead cochlea respectively. In (a), f_2 is approximately equal to the best frequency when the $2f_1 - f_2$ = 11 kHz.
[From Dong & Olsen (2008), figure 3, with permission from ASA]

Theory predicts that a DP should arise predominantly from a distortion source mechanism in the vicinity of the f_2 characteristic place, as this is the region of maximum overlap between the primary travelling waves evoked by the stimulus, and a reflection source mechanism located at the DP characteristic place (Shera & Guinan, 1999). Although the results of Dong & Olsen (2008) confirm that DP levels are higher at these two locations, compared to other positions along the cochlea, additional evidence is required to determine the mechanism generating these enhancements and to demonstrate that the DPs elicited in these areas can propagate back towards the stapes with sufficient magnitude to be detected in the ear canal as a DPOAE.

The nature of the source mechanism located in the region of overlap between the two primary travelling waves was investigated by Shaffer *et al.* (2003). They measured the $2f_1 - f_2$ DPOAE in a normal hearing human subjects, and introduced a third tone to suppress any source located at the DP characteristic place. For stimulus levels L_1 and L_2 equal to 60 and 45 dB respectively, and f_2/f_1=1.2, the residual $2f_1 - f_2$ DPOAE had a amplitude between 0 and 10 dB for $2f_1 - f_2$ frequencies between 1.4 and 2.4 kHz when the suppressor was applied. The residual DPOAE displayed almost constant phase as the DP frequency varied, behaviour typical of a DP generated by a wave-fixed (distortion) source mechanism as illustrated in figure 1.17 (Shera, 2004). This is consistent with cochlear modelling predictions that the distortion source of the $2f_1 - f_2$ DP is distributed over a region which is a few millimetres long (van Hengel & Duifhuis, 1999) and located in the vicinity of the f_2 characteristic place (Zhang & Mountain, 2008). Figure 1.22 illustrates the length of the distribution distortion source predicted by Zhang & Mountain (2008) using a one-dimensional model of the gerbil cochlea, for various stimulus frequency ratios and L_1=L_2=60 dB SPL. They predict that the source length increases from about 2.5 mm to 5 mm as the f_2/f_1 ratio decreases from 1.8 to 1.1. The distributed source produces travelling waves which can propagate in both directions, but it is directional (Shera & Guinan, 2008). For example, Shera & Guinan (2007) observed in cat cochleae that although the amplitude of the forward travelling wave generated by this distributed distortion source region exhibited little amplitude fluctuation with changes in f_2/f_1, the amplitude of the backward travelling wave reduced in amplitude significantly for small f_2/f_1 ratios. Therefore a distributed, directional, distortion source of lower side DPs is thought to be located over a small area in the vicinity of the f_2 characteristic place. It is assumed that this finding extends to all other lower side band DPs, in addition to the $2f_1 - f_2$, as range of DP components in the BM velocity are evident at the f_2 site (Robles *et al.*, 1997).

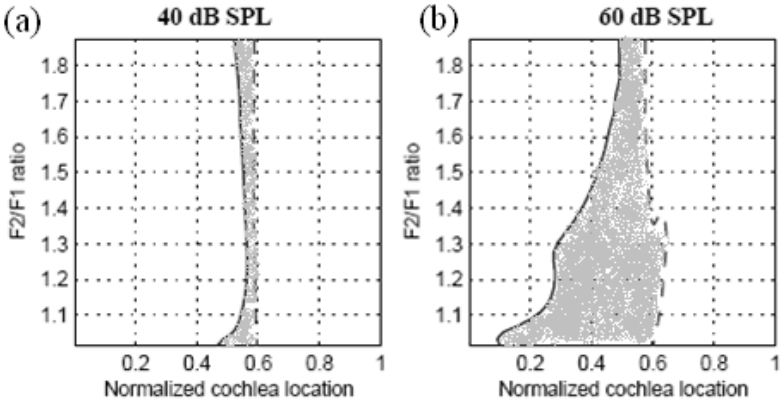

Figure 1.22 Estimated region of $2f_1 - f_2$ DP generation within the gerbil cochlea
The right (dashed) and left (solid) lines indicate the apical and basal boundaries of the region for various f_2/f_1 ratios with f_2=3 kHz. The results are presented for (a) L_1=L_2 = 40dB SPL and (b) L_1=L_2 = 60 dB SPL. The apical boundary for the generation region is defined as the point at which the DP generated between the boundary and the apex is 10 dB below the total DP level. Similarly, the basal boundary is defined as the location at which the DP generated between the base and the boundary is 10 dB below the total DP level. The total length of their cochlear model is 12.1 mm. [From figure 3 of Zhang & Mountain (2008), with permission from the authors and World Scientific].

Once generated in the vicinity of the f_2 best place, the DP travelling wave can propagate forward towards its characteristic place and be perceived by the listener (Goldstein, 1967; Zureck & Sachs, 1979). Shaffer *et al.* (2003) used suppression techniques and observations of phase behaviour to determine that a place-fixed (reflection) mechanism, which generates a backward DP travelling wave, is located at the DP characteristic place. The place-fixed (reflection) source mechanism located at the DP characteristic place requires an incident wave which corresponds to the forward travelling wave generated by the wave-fixed (distortion) source positioned near the f_2 best place. This dependence of the place-fixed source on the wave-fixed source is consistent with suppression experiments which demonstrate a greater $2f_1 - f_2$ DPOAE amplitude reduction when the suppressor tone is presented close to the f_2 frequency (Kummer *et al.*, 1995) than when the suppressor is close to the f_{dp} frequency (Shaffer *et al.*, 2003).

In summary, the two dominant sources of lower side band DPOAEs are thought to correspond to a distortion (wave-fixed) mechanism in the vicinity of the f_2 characteristic place and a reflection (place-fixed) mechanism from the DP characteristic place. The relative magnitude of these components in the ear canal can vary (Brown *et al.*, 1996) and leads to complicated interference effects. This simple picture may be complicated by multiple reflections between the base and the characteristic place (Stover *et al.*, 1996) as indicated in figure 1.18.

(ii) Upper side band distortion products

The characteristic place for an upper side band DP is on the basal side of the f_2 best place. The spatial separation of the DP characteristic place and the f_2 best place is expected to reduce as the stimulus level increases because the f_2 best place shifts closer to the base. Although upper side band DPs have been detected in the BM motion in the vicinity of the f_2 best place (Robles *et al.*, 1997), this is not thought to give rise to a substantial DP travelling wave because this location is beyond the DP characteristic place.

Less information is available regarding the sources of upper side emissions, such as the $2f_2 - f_1$ DP, compared to the literature on the $2f_1 - f_2$ lower side band emission. However, analysis of group delay suggests that there are again at least two source mechanisms at work for upper side band DPOAEs (Prijs *et al.*, 2000). But these sources may not be spatially distinct as they were for the lower side band emissions. For example, the intracochlear measurement of Dong & Olsen (2008), reproduced in figure 1.21b, shows that the only peak in the amplitude of the $2f_2 - f_1$ pressure component occurs when the DP frequency is equal to the best frequency of the observation location. The distortion source for upper-side band DPOAEs is thought to be basal of the f_2 characteristic place as Martin *et al.* (1998) found that suppression of the $2f_2 - f_1$ emission was most effective when using a probe tone with frequency greater than f_2. By extending the principles that are known about lower-side band emission generation, Wilson & Lutman (2006) separate the $2f_2 - f_1$ DPOAE into a distortion (wave-fixed) and reflection (place-fixed) using a time-window technique that exploits the different phase properties of emission components from these sources. As a result of their work, they propose that upper-side band emissions contain contributions from these two source mechanisms. Firstly, there is a distortion source distributed over a region of the cochlea basal to the DP characteristic place, where the primary travelling waves overlap. Secondly there is a reflection source located at the DP characteristic place. The way that these two sources could combine to form a DPOAE is illustrated in figure 1.20b.

1.4.4 Compression waves

It is possible for two types of wave to propagate within the cochlea; a slow BM travelling wave and a fast compression wave. As discussed in section 1.2.1, the forward transmission of sound from the stapes is dominated by the BM travelling wave. Similarly the backward transmission of DPs, from their generation site to the stapes, is commonly believed to occur via BM travelling waves (Kemp, 1980; Kim, 1980 etc). However, this conventional view of the backward transmission of DPs has recently been challenged. For example, Ren (2004) measured the $2f_1 - f_2$ DP component of BM vibration between the base and the f_2 best place in the gerbil cochlea using laser interferometry. He observed that the phase of the BM vibration was consistent with a forward, not a backward, DP travelling wave. He also noted that the stapes vibrated at the DP frequency before the DP

component was observed in BM motion near the base of the cochlea. He concluded that the $2f_1 - f_2$ DP is transmitted from its generation site to the stapes via fluid compression wave, and that the stapes vibration then initiates a forward travelling wave on the BM at the DP frequency. Similar phase behaviour has since been observed in gerbils by He *et al.* (2008) and in guinea pigs by de Boer *et al.* (2008). In addition, Siegel *et al.* (2005) measured high frequency SFOAE latency in chinchilla and found the values were too high to be consistent with backward travelling waves but that the results could be explained by compression waves. As a consequence of these recent experimental findings, there is dispute regarding the dominant mechanism for the reverse propagation of DPs within the cochlea. Some attempts have been made to simulate Ren's results in models without the use of compression waves, and the outcome has been mixed (Vetesnik *et al.*, 2006; de Boer *et al.*, 2008).

The model described in the following chapters does not incorporate fast compression waves, and only allows sound to escape from the cochlea via backward travelling waves. This approach has been taken, despite the controversy, because the following substantial evidence exists to suggest that backward travelling waves are the dominant mechanism by which OAEs are transmitted out of the cochlea.

- Measurements of intracochlear pressure variation in gerbils demonstrates that the travelling wave mechanism dominates the compression wave mechanism (Dong & Olsen, 2008).
- Estimates of reverse, or round-trip, travel times for OAEs are more consistent with backward travelling waves than fast compression waves (Schoohoven *et al.*, 2001; Moleti & Sisto, 2008; Harte *et al.*, 2009).
- Allen-Fahey experiments, where DPOAE levels are observed whilst the f_2/f_1 ratio is varied and the source amplitude is controlled, support the predominance of the travelling wave over the compression wave (Shera *et al.*, 2007).
- A suitable volume source within the cochlear partition would be necessary to generate compression waves, and it is difficult to imagine how the fluid filled organ of Corti could act as such a source. For example, there is no physiological evidence that the OHCs produce a volume change in the CP when stimulated (Ashmore, 2008).

1.5 Measurement of DPOAEs

In this section, an overview of the techniques used for measurement and analysis of DPOAEs is presented, followed by a description of common recording stimulus paradigms. This gives insight into how the properties of the DPOAEs discussed in chapters 4 and 5 have been established experimentally.

1.5.1 Measurement and analysis

Measuring a DPOAE

The equipment shown in figure 1.23 is typically used to measure a DPOAEs. A probe in the ear canal contains a microphone and a receiver. The probe can be secured in the ear canal using a soft plastic tip, but an air tight seal is not required (Hall, 2000). The mixing of the pure tones could be performed electronically, and the result presented through a single receiver, but acoustic mixing where each tone is delivered through a separate transducer is less susceptible to nonlinear interaction artefacts (Probst *et al.*, 1991). Both the recording microphone and the receiver should have a flat frequency response (between 0.3 and 8kHz) and perform linearly over the required range of stimulus levels (Grandori, 1985). The receivers require in situ calibration, prior to DPOAE measurement, using a method such as the two-stage approach described by Knight & Kemp (1999).

DPOAEs can be analysed by either selecting a specific DP frequency (such as $2f_1 - f_2$) and applying a narrow band filtering technique, or by digital analysis using an FFT of the recording in the ear canal (Probst *et al.*, 1991). A single DPOAE is usually identified if it satisfies three criteria: The amplitude exceeds the noise floor by 3 to 6 dB (Martin *et al.*, 1990; Hatzopoulos *et al.*, 2001); the amplitude exceeds a minimal absolute value; and the measurement is repeatable within 5 dB. A minimum absolute value is imposed on the DPOAE level, such as 5 dB SPL (Martin *et al.*, 1990) or approximately 80dB below the primary levels (Lukashkin & Russell, 2005), to ensure rejection of system artefacts.

There are many commercial devices available for measuring DPOAEs, and they differ in terms of their probe shape, noise reduction strategies, and default criteria for DPOAE identification. However, Parthasarathy & Klostermann (2001) demonstrated that across four different devices, the probe fitting, mean test time and mean $2f_1 - f_2$ DPOAE amplitude was not significantly different. Their results suggest that the characteristics of measured DPOAEs do not depend on the device, but that differences in stimulus parameters and identification criteria can significantly affect results.

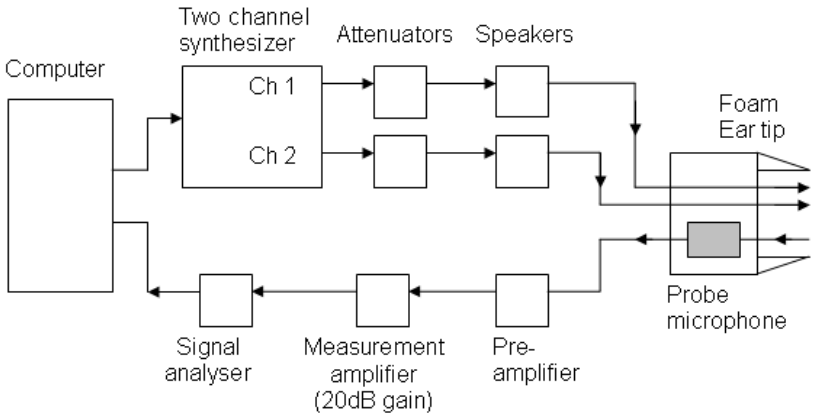

Figure 1.23 Block diagram illustrating the equipment required for DPOAE measurement. [Re-drawn from Martin *et al.* (1990) figure 5].

Separating the DPOAE components from difference source mechanisms

The process of separating the DPOAE into components arising from the two different source mechanisms described in section 1.4.2, is called *unmixing*. The two common approaches to unmixing are described by Kalluri & Shera (2001). First, a third stimulus tone with frequency close to the DP frequency can be used to suppress the contribution to the DPOAE originating from the place-fixed (reflection) source mechanism located near the DP characteristic place. When the suppressor is present, the residual DPOAE is attributed to the wave-fixed (distortion) source mechanism distributed near the f_2 best place. The contribution to the total DPOAE by the place-fixed (reflection) source mechanism is established by subtracting the distortion source component from the total DPOAE recorded in the absence of the suppressor tone. This approach assumes a linear summation between the two components and could be limited by nonlinear effects introduced by the suppressor tone. The second approach exploits the different phase characteristics of the two source mechanisms, as illustrated in figure 1.24. The level of the DPOAE is recorded across a range of DP frequencies, using a fixed f_2/f_1 ratio paradigm. Under these conditions the phase of the wave-fixed (distortion) source component should be approximately constant, whilst the phase of the contribution from the place-fixed (reflection) source should vary rapidly with DP frequency. Once the phase of the DPOAE has been unwrapped relative to the stimulus tones, an inverse fast Fourier transform (IFFT) is performed and a time-windowing technique is then applied to separate the two components. The wave-fixed source component for the $2f_1 - f_2$ emission can be contained in a time window spanning values between 0 and 1 − 2 ms, whilst the place-fixed component extends from 2.25 ms onwards (Knight & Kemp, 2001). It would not be appropriate to conclude from this that the travel time of the DP from the reflection source exceeds that of the distortion source, although this would agree with the spatial separation of the sources, because the 'latency' values arise as a consequence of the different phase characteristics of the source mechanisms not their distance from the stapes.

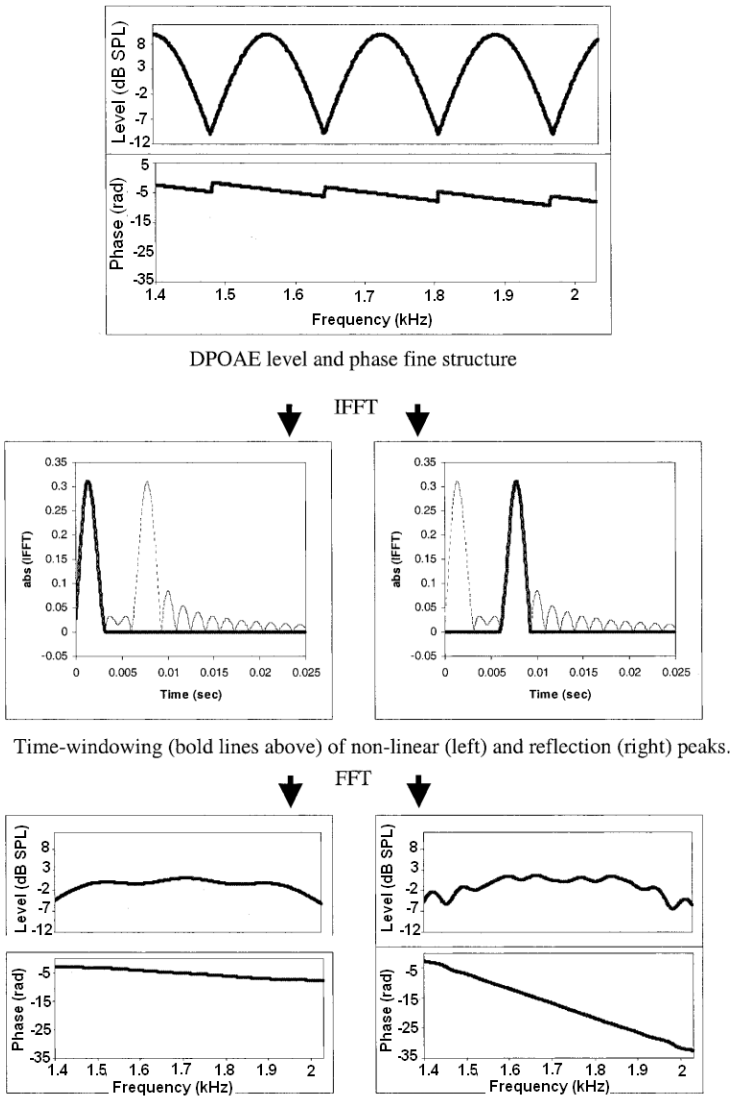

Figure 1.24 An illustration of the inverse fast Fourier transform (IFFT) unmixing method
This approach was used by Kalluri & Shera (2001) to separate the components of the DPOAE that arise from a reflection source and a distortion source. The top graph represents the amplitude and phase of a typical DPOAE recorded using a constant f_2/f_1 ratio. The second row of graphs illustrates the results of the IFFT and time windowing. The bottom graphs illustrate the amplitude and phase of the unmixed distortion source component (left) and reflection source component (right). [From figure 6 of Shaffer *et al.* (2003) with permission from Wolters Kulver Health]

1.5.2 Recording and reporting paradigms

There are several common approaches to recording and reporting DPOAE observations, and these methods are discussed below. Examples can be found in the following section, alongside the description of DPOAE properties.

(i) An amplitude spectrum is a record of the DP frequencies and their amplitudes, which are evoked by a single stimulus tone pair.
(ii) DPgrams illustrate the amplitude of a single DPOAE (such as the $2f_1 - f_2$) as a function of frequency. Usually L_1 and L_2 are kept constant during these measurements, as is f_2/f_1.
(iii) Input-output (I/O) functions or **growth functions** consist of DPOAE amplitude plotted as a function of stimulus level. The stimulus frequencies are fixed during these measurements, and the stimulus levels are related by a simple formula. Some studies use a fixed level difference ($L_1 - L_2$) [Mills, 2002), whilst others use a "scissor paradigm" (Janssen & Muller, 2008). The scissor paradigm was designed so that the responses to both primary tones would grow at an equal rate at the f_2 characteristic place, and therefore preserve the degree of overlap between the primary travelling wave envelopes. In order to achieve this $L_1=0.4L_2+39$dB, so that L_1 increases at a slower rate than L_2 to compensate for the greater degree of compression exhibited by the f_2 response at the f_2 characteristic place (Kummer *et al.*, 1998).
(iv) Frequency-ratio functions are constructed by plotting the emission amplitude (and phase) as a function of the stimulus frequency ratio (f_2/f_1). L_1 and L_2 are kept constant during these measurements (Lukashkin & Russell, 2001), along with either f_2, f_1 or f_{dp} (Mills, 2002).
(v) Contour maps of DPOAE amplitude represent the dependence of the emission on two different stimulus parameters simultaneously. As DPOAE amplitude (and phase) is dependent on 4 variables (f_2, f_1, L_1, & L_2), contour plots can be viewed as a slice through a 4 − dimensional space (Mills, 2002).
(vi) DPOAE suppression tuning curves are plotted by introducing a third stimulus tone f_3 (in addition to f_1 and f_2) which acts to suppress on of the emission sources. Therefore the suppressor tone usually has a frequency close to either f_2 or f_{dp}.

1.6 Properties of DPOAEs

A cochlear model must replicate the known properties of DPOAEs in order to provide insight into their generation mechanisms and make valid predictions for future experiments. For this reason, a brief overview of these properties is given in this section, but further details can be found in chapters 4 and 5.

1.6.1 Characteristics of human DPOAEs

Amplitude

In mammals, the largest DPOAE is the $2f_1 - f_2$ emission, with an amplitude of 5 − 15 dB SPL or 50 − 60 dB below the stimuli for moderate stimulus levels (Lonsbury-Martin & Martin, 2008). The $2f_1 - f_2$ DPOAE can be up to 20 dB greater than $2f_2 - f_1$ (Knight & Kemp, 1999). For an individual ear, the amplitude of different order DPOAEs are related such that an ear with a high level $2f_1 - f_2$ DP is also expected to exhibit a high amplitude $2f_2 - f_1$ emission (Wilson & Lutman, 2006). For an individual subject, amplitude measures are usually repeatable within 3 dB for the $2f_1 - f_2$ DPOAE, even if the recordings are separated by an interval of several weeks (Franklin *et al.*, 1992; Roede *et al.*, 1993; Zhao & Stephens, 1999; Wagner *et al.*, 2008). In addition the amplitude of the $2f_1 - f_2$ DPOAE has little dependence on stimulus frequency. For example, the average $2f_1 - f_2$ DPOAE amplitude recorded from a group of 20 subjects varies by less than about 15 dB as f_2 increases from 1 to 8 kHz (Mills *et al.*, 2007).

Fine structure

If small frequency intervals are used to record DPOAE amplitude for a range of stimulus frequencies using a fixed f_2/f_1 ratio, from an individual subject, then a fine structure becomes evident. In humans, the difference in amplitude between the $2f_1 - f_2$ fine structure peaks and troughs can be to up 20dB (He & Schmiedt, 1993). If peaks in the fine structure occur at DP frequencies of f_a and f_b, then in humans it is usually found that $(f_a - f_b)/\sqrt{f_a f_b} \approx 1/15$ (Zweig & Shera, 1995b; Dhar & Abdala, 2007). The peaks and troughs can occur at the same emission frequencies for both the $2f_1 - f_2$ and $2f_2 - f_1$ DPOAEs (Knight & Kemp, 1999). This DPOAE fine structure is thought to be associated with the fine structure observed in other cochlear measures: SFOAE amplitude, pure tone audiograms recorded using small frequency intervals and the frequency spacing of SOAEs (Zweig & Shera, 1995a).

Growth functions

The DPOAE growth rate with increasing stimulus level is dependent on the stimulus parameters (Knight & Kemp, 1999; Rhode, 2007; Mills, 2002). For example, using the scissor stimulus paradigm and f_2/f_1=1.2, Kummer *et al.* (1998) observed that the $2f_1 - f_2$ DPOAE growth rate reduced from 1 dB/dB to 0.2 dB/dB when L_2 increased above 40 dB SPL. At higher stimulus levels (e.g. L_2 > 80 dB SPL), the growth rate increases above that observed for moderate stimulus levels (Dorn *et al.*, 2001). DPOAE amplitude does not always increase uniformly with stimulus level, and deviations from monotonic growth are called "notches" (He & Schmiedt, 1993). These notches occur more commonly in rodents than in humans and Kummer *et al.* (1998) found notches exceeding 2 dB in only 3% of human DPOAE growth functions. In humans, the notches are thought to arise as a consequence of "the mixing of the DPOAE source components in the ear canal" which also produces fine structure in DP-grams (He & Schmiedt, 1993; Mauermann *et al.*, 1999).

Frequency and level differences

The amplitude of lower side band emissions, such as the $2f_1 - f_2$ DPOAE, can be optimised using an f_2/f_1 ratio between 1.2 and 1.32 for stimulus levels between 65 and 75 dB SPL (Knight & Kemp, 1999). The amplitude of the emission falls off when the f_2/f_1 ratio is moved away from the optimal value. The reason for this amplitude dependence of lower side band emissions on the f_2/f_1 ratio is discussed in section 4.1.6. In addition, there is an optimal level difference ($L_1 - L_2$) which maximises the amplitude of both the upper and lower side band DPOAEs. In human subjects the optimal level difference, which elicits the greatest $2f_1 - f_2$ DPOAE amplitude, depends on f_2/f_1 and decreases from 10 dB to 5 dB when f_2/f_1 becomes very small (Knight & Kemp, 1999). For the $2f_2 - f_1$ DPOAE, the optimal level difference is about 0 or − 5 dB (Fitzgerald & Prieve, 2005). The origin of the optimal level difference is investigated in section 4.1.5.

1.6.2 Comparison of OAEs between mammals

Much of the information on DPOAEs that has been acquired through invasive physiological measurements relates to rodent cochleae. Therefore it is important to appreciate some the differences between the OAE properties of humans and other mammals.

Laboratory animals typically have hearing that extends one or two octaves beyond that of humans, as shown in figure 1.9. There is some evidence that laboratory animals may have broader auditory filters compared to humans (Shera *et al.*, 2002), although this has been disputed (Ruggero & Temchin, 2005). The f_2/f_1 ratio which optimizes the $2f_1 - f_2$ in animals such as rabbits, mice, guinea pigs and gerbils is generally higher than that observed in humans for the same stimulus paradigms,

possibly as a consequence of the difference in place-frequency maps (Lonsbury-Martin & Martin, 2008). In addition there is speculation that the cochleae of rodents are smoother than primate cochleae (Withnell *et al.*, 2003). This would be expected to reduce the place-fixed (reflection) component of DPs, reduce the fine structure amplitude of DPOAEs, and reduce the amplitude of other place-fixed (reflection) source emissions such as SOAEs, SFOAEs and TEOAEs. Physiological evidence supporting this hypothesis includes a lack of fine structure in DPOAEs recorded from rabbits and rodents (Whitehead, 1998), and reduced prevalence of SOAEs and TEOAEs in rabbits and rodents compared to primates (Lonsbury-Martin & Martin, 2008).

In general DPOAE amplitudes are larger, by approximately 25 to 30 dB, in rabbit and rodent ears compared to human or monkey ears at moderate stimulus levels when testing within the best hearing range of each species (Lonsbury-Martin & Martin, 2008). Notches can be found in the DPOAE growth functions of all mammals for some, but not all, stimulus paradigms. For example, Lonsbury-Martin & Martin (2008) report that notches can only be found between stimulus levels of 55 and 70 dB SPL in rabbits and guinea pigs, but they occur over a wider range of stimulus levels in primate ears. In rabbits, a notch can be replicated across all subjects using the same stimulus parameters. This is not the case for primates, where the stimulus parameters which correspond to a notch in the DPOAE growth function differ between individuals. Whitehead (1998) comments that the origin of notches in DPOAE growth functions may differ between small laboratory mammals and humans. There is some evidence to suggest that notches in human DPOAE growth functions are associated with fine structure (He & Schmiedt, 1993), whilst two different suggestions have been made for the origin of notches in the DPOAE growth functions of small mammals. Firstly, Whitehead (1995b) proposes that notches arise as a consequence of two different and distinct distortion generation mechanisms operating at high and low stimulus levels, which differ in their physiological vulnerability. The alternative suggestion of Mills (2002) is that the notches could arise from a single, distributed, distortion source mechanism.

In summary these differences suggest that care should be taken inferring human DPOAE characteristics from measurements made in the ears of other mammals.

1.7 Applications of DPOAEs

In this section the clinical applications of OAEs are discussed, along with the current limitations of these applications and possible future developments. We also consider two different methods that have been suggested for estimating the gain of the cochlear amplifier using DPOAE measurements: DPOAE suppression tuning curves and Allen-Fahey type experiments.

1.7.1 Clinical applications

Hearing screening

In the UK, TEOAEs are used for universal neonatal hearing screening, based on the observation that they occur in all normal hearing ears (Kapadia & Lutman, 1997) and are generally not observed if the subject has a sensorineural hearing loss greater than 40 − 45 dB HL (Hall, 2000). DPOAEs are also frequently used to screen for hearing loss. Based on a study of 7179 infants, Norton *et al.* (2000) suggest that DPOAEs can be used to identify a hearing loss where the threshold exceeds 30 dB HL, provided appropriate stimulus parameters are used (e.g. f_2/f_1=1.22, L_1=65 dB SPL and L_2=50dB SPL).

Hearing loss estimation

There have been several attempts to use DPOAEs to not only screen for hearing loss, but to establish the hearing threshold levels (HTLs) for subjects with mild hearing loss. If this application were to be successful it would provide a valuable objective method of hearing testing and a tool for differential diagnosis between types of sensorineural hearing loss. This would be particularly helpful for assessment in cases of suspected non-organic hearing loss, or for patients who are unable to perform conventional behavioural tests such as pure tone audiometry. Improved differential diagnosis of sensorineural hearing loss may also contribute to an improved auditory rehabilitation process and hearing aid fitting strategies.

Attempts to estimate HTLs from DPOAE measurements mainly try to establish a link between HTLs and either the emission threshold levels (e.g.Dorn *et al.*, 2001) or the emission growth function (Dorn *et al.*, 2001; Boege & Janssen, 2002). Each of these methods is usually limited to frequencies where f_2 is greater than 1 kHz, since low frequency DPOAEs can be difficult to record (Gorga *et al.*, 1994). In addition the definition of the emission threshold is usually dependent on the noise floor of the study (Dorn *et al.*, 2001). Some studies find high correlation (0.77 to 0.86) between $2f_1 - f_2$ DPOAE thresholds, defined as the stimulus level at which the emission exceeds the experimental noise floor, and HTLs for mild to moderate hearing losses (Dorn *et al.*, 2001). However, this is not replicated in other work (Gaskill & Brown, 1993). This discrepancy could be

due to the different stimulus paradigms, or the influence of DPOAE fine structure (Shaffer *et al.*, 2003), but a lack of consistent correlation means that DPOAE thresholds are not used routinely in clinics for estimating HTLs. The gradient of the DPOAE growth function is also affected by hearing loss as it tends to increase as hearing loss increases (Dorn *et al.*, 2001). However, it has not yet been determined if growth functions can be used to reliably determine the extent of a hearing loss.

Other clinical applications

Although it is not yet possible to use DPOAE growth functions to reliably predict hearing threshold levels in subjects with hearing loss, there is evidence that DPOAE growth functions closely resemble psychoacoustic loudness growth curves (Janssen & Muller, 2008). Therefore it may be possible to use DPOAE growth functions for prescribing hearing aid settings in the future. However, the application of DPOAEs to hearing aid rehabilitation is limited by intersubject variation which makes it difficult to predict loudness growth directly from an individual DPOAE input-output function (Neely *et al.*, 2003a). In addition otoacoustic emissions can be used to monitor the effect of drug treatments which are known to have ototoxic properties (Hall, 2005).

The routine clinical application of OAEs is currently limited to the screening of neonates (and other patient groups where objective testing is required) and the test battery for non-organic hearing loss. However, these applications could be vastly extended if more reliable methods for predicting hearing threshold levels and growth functions from OAEs were available.

1.7.2 Suppression tuning curves

Various attempts have been made to use DPOAEs as a non-invasive tool for investigation of the cochlear amplifier (CA). As these investigations generally attempt to quantify the CA gain, they are closely related to studies seeking a relationship between DPOAE measures and hearing loss. However, large inter-subject variability makes it difficult to conclude CA properties for an individual on the basis of DPOAE measures (Neely *et al.*, 2003b).

DPOAE suppression tuning curves can be obtained for a variety of stimulus levels. Examples are shown in figure 1.25, where the level of the suppressor is set to reduce the $2f_1 - f_2$ DPOAE amplitude by 3 dB. When using a suppressor frequency close to f_2, Gorga *et al.* (2003) associate changes in the tip-to-tail difference of DPOAE suppression tuning curves with changes in CA gain. However, they advise that the absolute value of the tip-to-tail difference might not be a direct measure of CA gain for a specific stimulus level. On this basis figure 1.25 indicates that the CA gain reduces by 20 dB as the stimulus level (L_2) increases from 20 to 60 dB SPL.

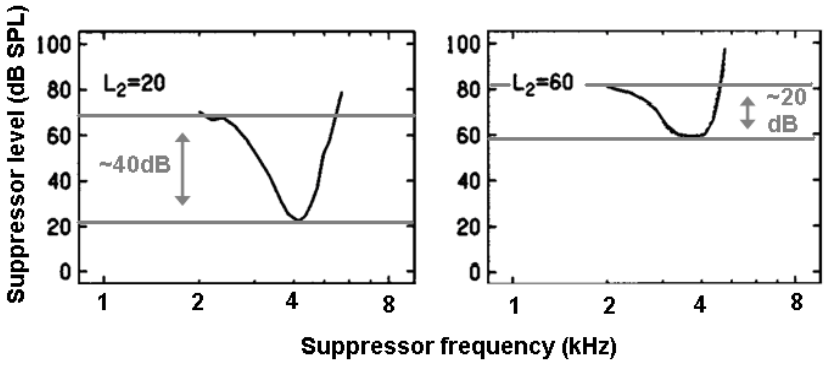

Figure 1.25 Examples of $2f_1 - f_2$ DPOAE suppression tuning curves
Responses are shown for a human subject with normal hearing threshold levels. The value of L_2 is shown in each graph, and L_1=0.4L_2+39dB. The stimulus frequencies were f_2=4 kHz and f_2/f_1=1.22. The grey lines and arrows indicate the tip-to-tail difference for each tuning curve. [From figure 7 of Gorga *et al.* (2003),with permission from ASA]

Some studies have focused on other aspects of the tuning curves, such as Mills (1998) who determined a relationship between the low frequency slope of the curve and the CA gain in gerbils. Overall, these investigations suggest that it may be possible to establish a relationship between DPOAE suppression tuning curves and CA gain in humans, although further work is needed to achieve this.

1.7.3 Allen-Fahey type experiments

Allen & Fahey (1992) proposed a method for measuring the gain of the cochlear amplifier (CA) using simultaneous measures of the $2f_1 - f_2$ DP in the ear canal and at its characteristic place. Their experiment has since been repeated by several research groups, with various modifications (de Boer *et al.*, 2005; Shera & Guinan, 2007). In this section the principle of the experiment and interpretation of the results are described.

The principle of the experiment

The Allen-Fahey experiment assumes that the $2f_1 - f_2$ DPOAE originates entirely from the distortion source mechanism located at the f_2 best place. Once generated at this site, the DP is expected to propagate both backwards towards the stapes and forward towards its own characteristic place. The CA is expected to amplify forward travelling DP wave over a region just basal to the DP characteristic place. During the experiment, the stimulus frequency ratio is gradually reduced whilst the DP frequency is held constant. For each DP frequency, the levels of the primary tones (L_1 and L_2) are adjusted so that the amplitude of the DP vibration at its characteristic place is constant for all f_2/f_1 values, and the level of the $2f_1 - f_2$ DPOAE in the ear canal is monitored. When f_2/f_1 is much greater than one, the f_2 best place should be basal to the

region over which the CA acts on the $2f_1 - f_2$ DP forward travelling wave. Figure 1.26a illustrates that in this case the DP forward travelling wave is expected to be amplified by the CA en route to its characteristic place. When f_2/f_1 is very close to one, the f_2 best place shifts to the apical side of the region over which the CA acts on the DP travelling wave. For this reason, Figure 1.26b shows that in this case the $2f_1 - f_2$ DP forward travelling wave is not expected to be amplified by the CA en route to its characteristic place. If the CA provides a gain, G, to the DP travelling wave then the DPOAE is expected to be a factor of G^2 smaller for the first paradigm ($f_2/f_1 > 1$) compared to the second paradigm ($f_2/f_1 \sim 1$), as illustrated in figure 1.26.

The original Allen-Fahey experiment was performed in cats, and the neural response at the DP characteristic place was monitored invasively. The experiment was repeated in guinea pigs by de Boer *et al.* (2005) who used laser interferometry to measure the BM motion, instead of the neural response, at the DP characteristic place. Shera & Guinan (2007) developed a non-invasive method for monitoring the BM response at the DP characteristic place using a third stimulus tone, which they used to repeat the Allen-Fahey experiment in cats.

(a)

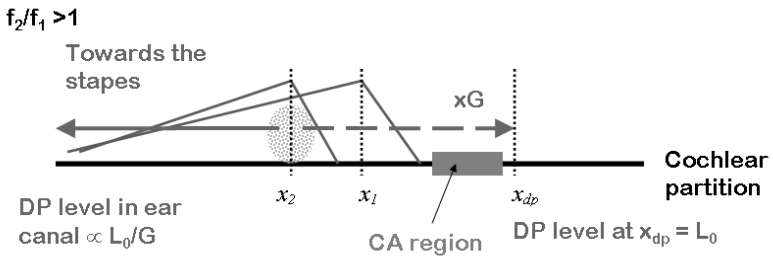

(b)

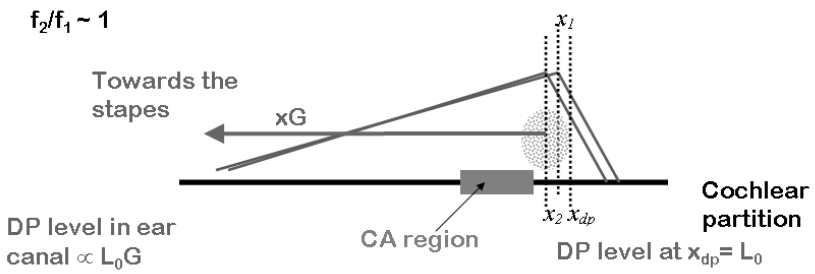

Figure 1.26 The Allen & Fahey (1992) stimulus paradigm During the experiment the f_2/f_1 ratio is reduced from (a) high to (b) low for a fixed $2f_1 - f_2$ DP frequency. The DP amplitude at its characteristic place (x_{dp}) is kept constant at L_0. The characteristic places for f_1 and f_2 are denoted by x_1 and x_2 respectively. The CA region provides a gain G to the DP travelling wave, in both directions.

Interpreting the result

Allen & Fahey (1992) summarise that, based on the principles described above, the *maximum* value of the CA gain (G) observed in their experiment is 10dB. Replications of their experiment found similar results (de Boer *et al.*, 2005; Shera & Guinan, 2007). As this estimated gain is much less than the 30 or 40 dB expected, they conclude that the simplest explanation is that there is no cochlear amplifier. However, other groups (de Boer *et al.*, 2005; Shera & Guinan, 2007) suggest that the result indicates a flaw in the method rather than evidence against the existence of the CA. Based on the assumption that there is a CA, and the experiment fails to demonstrate this, the following explanations have been offered to account for the null result:

- There may be wave interference occurring between the DP and the primaries, or DPs at other frequencies (de Boer *et al.*, 2005)
- The directionality of the distortion source (wave-fixed) mechanism may change with f_2/f_1 ratio (Shera & Guinan, 2007), as a result of the distributed nature of the source region (Neely & Liu, 2008), which would invalidate the underlying assumptions of the method
- There may be some suppression of the DP for small f_2/f_1 ratios (Shera & Guinan, 2007)
- The contribution of the reflection source (place-fixed) mechanism is neglected
- DPs travel out of the cochlea via fluid compression waves, not reverse travelling waves, and therefore the principle of the method is flawed (Ren & Nuttal, 2006)

The diversity of these explanations indicates that the assumptions on which the Allen-Fahey experiment was based are over simplified and that there is a need for an increased understanding of the detailed mechanisms involved in the generation and propagation of DPs within the cochlea. The explanations of the Allen-Fahey results will be further discussed using the results of the cochlear model in section 5.2.1.

1.8 Modelling efforts of cochlear responses and OAEs

1.8.1 Historical overview

Models of cochlear mechanics are constructed to replicate basic physiological properties, such as the fundamental and harmonic cochlear responses to a single tone stimulus, and then applied to interpret more complex observations and develop valid experimental hypotheses. For example, cochlear modelling was used by Helmholtz (1877) to explore perception of tones and by Gold (1948) to interpret the sharp tuning observed in the cochlea and predict otoacoustic emissions. More recently models have been used to demonstrate that a cochlear amplifier mechanism is necessary to explain the sharply tuned response of the BM to single tone stimulation (de Boer, 1995a).

Many different types of cochlear model have been proposed including hardware models, constructed either from plastic and metal materials or electrical networks (Zwicker, 1986; White & Grosh, 2005; Wittbrodt *et al.*, 2006), and abstract mechanical models solved by computer (Neely & Kim, 1986; Kanis & de Boer, 1993; Kolston & Ashmore, 1996; Elliott *et al.*, 2007; Gan *et al.*, 2007). The abstract models, where the cochlea is divided into longitudinal elements, have varying numbers of degrees of freedom ranging from 2 to over 10^4 per slice (Neely & Kim, 1986; Baumgart *et al.*, 2008).

Early cochlear models were designed to simulate only the amplitude and phase of linear, passive response of the cochlea to single tone stimulation (e.g. Zwislocki, 1950; Schroeder, 1973; Zweig *et al.*, 1976; Steele & Taber, 1979; Allen, 1980; de Boer, 1980). Models then progressed to incorporate an active process (de Boer, 1983; Neely & Kim, 1986; Mammano & Nobili, 1993; Geisler & Sang, 1995 etc) and nonlinearity. The nonlinear models were either solved in the time domain (e.g.Hall, 1974; Kim *et al.*, 1980; Mauermann *et al.*, 1999; van Hengel & Duifhuis, 1999), or in the frequency domain using iterative or perturbation techniques (Kanis & de Boer, 1993; Chadwick, 1998; Talmadge *et al.*, 1998; Lim & Steele, 2002; Talmadge *et al.*, 2004 etc).

1.8.2 Modelling of DPOAEs

We intend to use a one-dimensional active nonlinear cochlear model to investigate the principal mechanisms of DPOAE generation. Such models have been used successfully in the past to simulate DPOAEs (e.g. Kanis & de Boer, 1997; van Hengel & Duifhuis, 1999; Neely & Liu, 2008). However, a consequence of selecting such a simple model is that the predicted responses in the vicinity of the peak of the travelling wave envelope may be less accurate than the responses of two- or three- dimensional models. This limitation may influence the amplitude of the predicted place-fixed (reflection) DPOAE component to a small extent (Shera *et al.*, 2005).

Several studies have used cochlear modelling to predict properties of intracochlear DPs and DPOAEs. Although these results are consistent with experimental measurements they are frequently limited to a small range of stimulus parameters or DP frequencies. For example, Kanis & de Boer (1997) use a one-dimensional model to predict the dependence of the $2f_1 - f_2$ DP on the f_2/f_1 ratio, but do not extend the work to investigate the effect of this ratio on other DPs or to probe the properties of the generation region. Other studies apply models to predict a few isolated features of DPOAEs, such as the frequency spectrum in the ear canal (Moleti *et al.*, 2009) and fine structure (Talmadge *et al.*, 1998; Shera *et al.*, 2000). Talmadge *et al.* (1998) use their one dimensional model of the human cochlea, which incorporates inhomogeneities in the impedance of the model to act as sites of reflection, to estimate the forward and backward travelling waves for a variety of DPs. This approach provides a useful tool for investigating the source of DP components within the cochlea, but their method is limited to low stimulus levels and small stimulus frequency ratios as they deliberately neglect the nonlinear effects of self- or mutual- suppression of the primary tones to simplify the calculations.

Vetesnik *et al.* (2006) use a two-dimensional cochlear model, based on that proposed by Mammano & Nobili (1993), to simulate a variety of DPOAE properties including spatial distributions and dependence on the f_2/f_1 ratio for both the $2f_1 - f_2$ and $2f_2 - f_1$ DPs. They also predict the growth of these DPs for a range of cochlear amplifier gain values. However, their model produces only the wave-fixed (distortion) component of the DPOAE and the place-fixed (reflection) component is neglected. In addition they rely on the maxima in the spatial distribution of BM displacement at $2f_1 - f_2$ and $2f_2 - f_1$ to infer the source location of these DPs. Although their results are consistent with two source contributions from the vicinity of the f_2 best place and DP characteristic place, they do not provide evidence that the DPs generated at these locations are effectively transmitted out of the cochlear model.

It is rare for the harmonic response evoked by a pure tone stimulus to be examined along with the production of the DPs in a single cochlear model. Nonetheless in cases where both types of distortion are described, such as the work of Lim & Steele (2002), the predicted harmonic response

provides useful additional evidence when assessing the validity of the model against experimental data. However, the Lim & Steele (2002) results are restricted to a small range of stimulus parameters making extensive verification of their model difficult.

In summary, although many cochlear models have been developed to simulate DP generation within the cochlea, so far none has given a comprehensive overview of a range of predicted DPOAE properties and their generation mechanisms whilst incorporating both wave-fixed and place-fixed components. In addition, it would be useful to be aware of the harmonic responses to single tone stimulation in such a model to determine if these were also consistent with physiological studies.

1.9 Research questions and contributions

The aim of this thesis is to develop a cochlear model to investigate the mechanisms involved in the production of DPOAEs. There are three stages to the work: chapters 2 and 3 describe the development and validation of the model; chapters 4, 5 and 6 illustrate the application of the model to answer some specific questions; and finally chapter 7 provides a discussion of the strengths and the limitations of the model and suggests some ideas for future work.

The model is verified in the first part of this thesis by comparing its predictions of the cochlear response with physiological measurements and the estimates of other cochlear models. This includes a comparison between our quasilinear frequency domain model and a state space time domain model. The aspects of the cochlear response used for the verification process were the fundamental and harmonic responses of the BM to single tone stimulation and the mutual suppression that occurs in the BM response to two tone stimulation. We also made some preliminary estimates of the $2f_1 - f_2$ DP properties predicted by the model before proceeding to study the $2f_1 - f_2$ and $2f_2 - f_1$ DPOAEs in more depth.

In chapters 4, 5 and 6 the model is applied to investigate the following research questions:

- What are the strengths and weaknesses of the model regarding $2f_1 - f_2$ and $2f_2 - f_1$ DPOAE prediction?
- What explanation does the model provide for the dependence of the $2f_1 - f_2$ and $2f_2 - f_1$ DPOAE amplitudes on the stimulus parameters?
- What causes notches in the growth of the $2f_1 - f_2$ DPOAE amplitude predicted by the model?
- What is the origin of DPOAE fine structure in our model?
- What forward and backward DP travelling waves are generated within the model in response to two tone stimulation?
- What explanation does our cochlear model, which contains a cochlear amplifier, offer for the outcome of the Allen & Fahey experiment?
- Can the model provide insight into the results of Ren and colleagues who are unable to detect backward travelling waves on the BM at DP frequencies?
- What is the source mechanism for the $2f_2 - f_1$ DPOAE suggested by our model? Can these upper sideband emissions be simulated by a cochlear model that does not incorporate fluid compression waves?

Overall, the most important contributions of the thesis may be summarised as follows:

(i) Reformulation of the Kanis & de Boer (1993) quasilinear model of the cochlea to ensure computational convergence of the iterative process and to verify stability of the model. The solution is also decomposed into forward and backward travelling wave components to facilitate interpretation of the results.

(ii) The fine tuning of the micromechanical parameters in the cochlear model is extended to improve the agreement between experimental responses of the cochlea to single and two tone stimuli and those predicted by the model. The effect of the position of the nonlinearity within the micromechanical feedback loop has also been clarified (How *et al.*, 2010).

(iii) A comprehensive comparison of experimental results and the simulated properties of the $2f_1 - f_2$ and $2f_2 - f_1$ DPOAEs predicted by the baseline and perturbed model. This allows many of the DPOAE characteristics to be explained but also determines which features of these emissions cannot be understood in such a simple model. This review also serves to establish which characteristics of the emissions are most sensitive to flaws in the tuning of the cochlear micromechanical model and could therefore be useful in tuning the parameters further.

(iv) Confirmation of the origin of the optimal stimulus level difference characteristic exhibited by both $2f_1 - f_2$ and $2f_2 - f_1$ in a coupled cochlear model.

(v) The identification and explanation of predicted notches in the wave-fixed component of the $2f_1 - f_2$ DPOAE growth function in the cochlear model.

(vi) Clarification of the limitations of the Allen-Fahey experiment.

(vii) Development of tools for assessing the directionality of wave-fixed DP sources within the cochlear model.

(viii) Suggestions regarding the source mechanism for the $2f_2 - f_1$ DPOAE.

2. The Kanis & de Boer micromechanical model

Kanis & de Boer (1993) developed a model to replicate the nonlinear behaviour of the cochlea. Their motivation was to provide insight into the mechanisms of cochlear nonlinearity which cannot be obtained easily through the use of more complex models (Kanis, 1995). They also proposed a "quasilinear" iterative method, to estimate the response of the model in the frequency domain, which can be used to evaluate the DPs predicted by the model (Kanis, 1995; Kanis & de Boer, 1997).

In this chapter the Kanis & de Boer model is described along with their quasilinear method for predicting its response. We start by reviewing the cochlear wave equation, and the associated solution methods in section 2.1. We then describe their linear micromechanical model (section 2.2). We go on to propose a method for decomposing the predicted travelling wave into forward and backward propagating components (section 2.3) and illustrate the features of this method using the results of the linear model. In section 2.4, nonlinearity is introduced into the micromechanical model and the quasilinear method is reviewed. Finally, we present the state space formulation of the Kanis & de Boer cochlear model and use it to verify the stability of the model, which is required for the quasilinear method to be valid. The state space model also provides a convenient method of performing time domain simulations, whose steady state response can be compared with those of the quasilinear method (section 2.5).

2.1 The wave equation

2.1.1 The one-dimensional wave equation

Figure 2.1 shows a two-dimensional representation of the cochlea (Zweig *et al.*, 1976; Steele & Taber, 1979). The cochlear partition (CP), the vertical CP velocity (v), the height of the channels (H), length of the cochlea (L), the stapes velocity (u_{st}), the horizontal and vertical fluid velocities (u_f and v_f respectively), and the fluid pressure (p_f) are all shown. The three dimensions of the cochlea have been reduced to two by neglecting radial motion and averaging the CP properties, such as its mass, across its width. This model also assumes that the cochlea is straight with channels of constant height, that the walls are rigid and that there are no fluid ducts, that Reissner's membrane can be neglected so that there are only two significant channels, that the two channels are symmetric, that the cochlear fluids are incompressible and that there is no significant structural longitudinal coupling along the CP. The appropriateness and consequences of some of these assumptions are discussed in appendix A.1.

For a passive linear model such as this, the wave equation (2.1) describes its response to sinusoidal stimulation in the presence of an internal distributed pressure source $S(x,\omega)$, and is derived in appendix A. In this equation ω, ρ, and Z_{CP}^{pass} denote the angular frequency of the stimulus, the density of the cochlear fluids, and the impedance of the cochlear partition respectively. The semi-difference pressure, p_d, is introduced to simplify the notation (Peterson & Bogert, 1950) and is defined in terms of the fluid pressure above and below the CP in (2.2). The CP impedance is defined in (2.3).

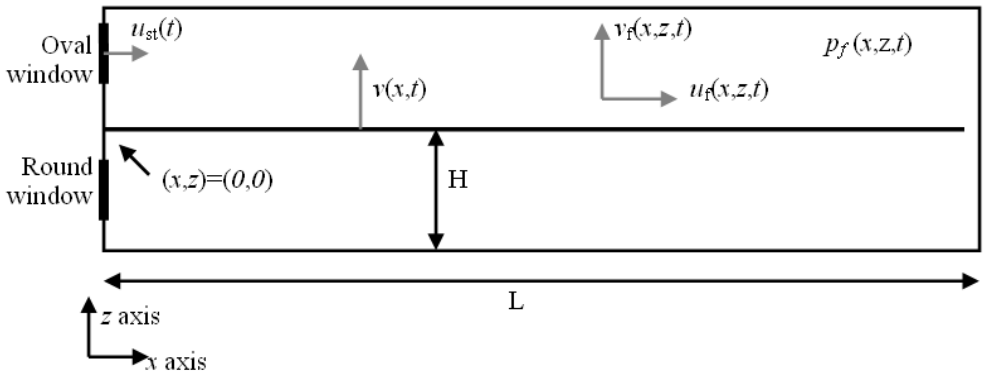

Figure 2.1 A two-dimensional illustration of the cochlea
The cochlear partition (CP), the vertical CP velocity (v), the height of the channels (H), length of the cochlea (L), the stapes velocity (u_{st}), the horizontal and vertical fluid velocities (u_f and v_f respectively), and the fluid pressure (p_f) are all shown.

$$\frac{\partial^2 p_d(x,\omega)}{dx^2} + \frac{-2i\omega\rho}{H \cdot Z_{CP}^{pass}(x,\omega)} \cdot p_d(x,\omega) = \frac{1}{2} \cdot \frac{2i\omega\rho}{H \cdot Z_{CP}^{pass}(x,\omega)} S(x,\omega) \tag{2.1}$$

where $$p_d(x,z,t) \equiv \tfrac{1}{2}\left(p_f(x,z,t) - p_f(x,-z,t) \right) \tag{2.2}$$

and $$Z_{CP}^{pass}(x,\omega) \equiv \frac{-2p_d(x,\omega)}{v(x,\omega)} \tag{2.3}$$

This wave equation is one dimensional, as all of the variables depend on only one spatial co-ordinate, *x*. This is a consequence of the long-wave approximation which states that the wavelength of the travelling wave is much greater than the height of the cochlear channel, as discussed in appendix A3. There are two boundary conditions of the model: conservation of horizontal momentum at the base (2.4) and no semi-difference pressure at the helicotrema (2.5).

$$\left.\frac{\partial p_d(x,\omega)}{\partial x}\right|_{x=0} = -i\omega\rho u_{st} \tag{2.4}$$

$$p_d(L,\omega) = 0 \tag{2.5}$$

2.1.2 Overview of solution methods

There are two common approaches to solving the linear wave equation (2.1) in the frequency domain, for a known CP impedance, in the absence of an internal distributed source: The finite difference method and the WKB approach.

The finite difference method uses a lumped-parameter formulation, where the length of the cochlea is represented by N discrete elements as shown in figure 2.2. Elements 2 to N-1 correspond to sections of the cochlear partition, and their dynamics are described by the CP impedance. The first and last elements represent models of the middle ear dynamics and helicotrema. Appendix B1 describes how this framework allows the wave equation (2.1) to be written in matrix form and solved using computer software such as MATLAB. It also illustrates that it provides an accurate representation of the distributed system provided N ≥ 500. For this reason we generally use 500 elements to represent the length of the cochlear partition. However, in early work we took a more cautious approach and used 1000 elements rather than 500.

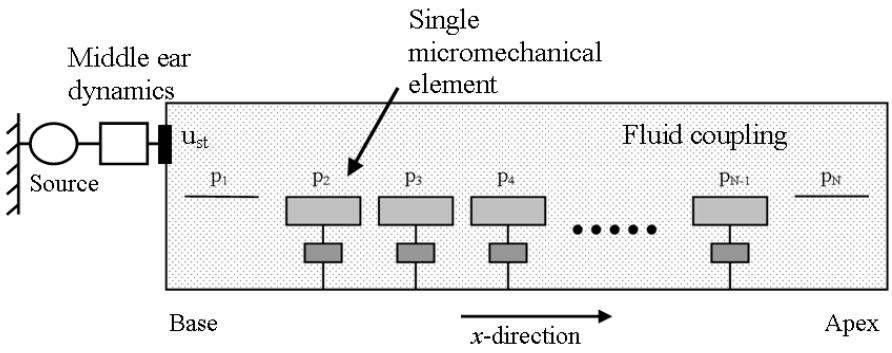

Figure 2.2 The one-dimensional lumped-parameter model of the cochlea
Elements 2 to N-1 represent micromechanical models of the cochlear partition. Elements 1 and N correspond to models of the middle ear dynamics and helicotrema respectively. [Based on Elliott *et al.* (2007), figure 4]

The WKB solution for the wave equation (2.1) is derived in appendix B.2.1. To summarise, this method approximates the total pressure distribution (2.6) by a linear sum of two basis functions (2.7). The constants p_0^+ and p_0^- are determined by the boundary conditions, and k_0 is chosen to normalise the basis functions at the base of the model.

$$p_d(x) = p_0^+ \varphi^+(x,\omega) + p_0^- \varphi^-(x,\omega) \tag{2.6}$$

$$\varphi^+(x,\omega) = \sqrt{\frac{k_0}{k(x,\omega)}} \exp\left(-i\int k(x,\omega)dx\right) \text{ and } \varphi^-(x,\omega) = \sqrt{\frac{k_0}{k(x,\omega)}} \exp\left(+i\int k(x,\omega)dx\right) \tag{2.7}$$

where the wavenumber, k, is complex

$$k^2(x) = \frac{-2i\omega\rho}{H(x)\cdot Z_{CP}(x)} \tag{2.8}$$

The basis functions φ^+ and φ^- are interpreted as travelling waves propagating forward and backward respectively, as discussed in appendix B.2.2. The wavelength of these travelling waves is inversely proportional to the real part of $k(x)$, whilst the imaginary component of $k(x)$ describes the exponential growth rate of the travelling wave amplitude. The WKB solution is derived based on the assumption that there is little variation in $k(x)$ over the distance of one spatial wavelength, as expressed in (2.9). This is equivalent to the condition that there are no substantial reflections in the cochlear model. This condition is generally satisfied through the cochlear model (appendix D.1), and the WKB solutions obtained using (2.6) and (2.7) are consistent with those obtained using the finite difference approach (appendix B.2.3). It is also possible to apply the WKB solution to linear models containing internal sources or sources of reflection as described in appendix B.2.4.

$$\left|\frac{1}{k^2(x)}\frac{dk(x)}{dx}\right| << 1 \tag{2.9}$$

Finally it is necessary to use models of the stapes, middle ear and ear canal if the solution to the wave equation is to be used to predict DPOAEs. The stapes model is necessary for the application of the basal boundary condition in the cochlear mechanics. The middle ear and ear canal also need to be incorporated if stimuli are to be presented in the ear canal, and if sound is to be transmitted in and out of the cochlear model. These details are discussed in appendix C. In general, the stapes is represented by a simple mass-spring-damper model. However under some circumstances it is useful to substitute an alternative stapes representation, to minimise reflections at the basal boundary, so in these cases the use of this alternative boundary condition will be noted as required.

2.2 The micromechanical model

The wave equation (2.1) applies to all linear cochlear models of the type illustrated in figure 2.1, whatever the impedance of the cochlear partition, $Z_{CP}(x,\omega)$. Many different models for the cochlear partition (CP) have been proposed in the literature. They differ in their descriptions of the CP dynamics and therefore have different expressions for $Z_{CP}(x,\omega)$. *Macro*mechanical models neglect any motion within the CP, whilst *micro*mechanical models incorporate relative motion between structural components of the CP such as the basilar membrane (BM) and tectorial membrane (Patuzzi, 1996).

In this section the linear active micromechanical model introduced by Kanis & de Boer (1993) is described and the responses illustrated. Their model is designed to replicate the response of the human cochlea. A discussion of other micromechanical models is deferred until chapter 3.

2.2.1 The impedance

Figure 2.3 illustrates a single element of the linear Kanis & de Boer cochlear model. The passive version of the model is effectively macromechanical, because the CP moves as a single unit of mass, m_{KB}, with stiffness, k_{KB}, and damping, c_{KB}. The upward displacement of the CP is denoted by ξ_p, and its upward velocity as v. The passive CP impedance, Z_{CP}^{pass}, is defined in (2.10) in terms of the semi-difference pressure and vertical CP velocity. It can be expressed as a function of the CP properties as shown in (2.11).

$$Z_{CP}^{pass}(x,\omega) = \frac{-2p_d(x,\omega)}{v(x,\omega)} \tag{2.10}$$

$$Z_{CP}^{pass}(x,\omega) = i\omega m_{KB}(x) + c_{KB}(x) + \frac{k_{KB}(x)}{i\omega} \tag{2.11}$$

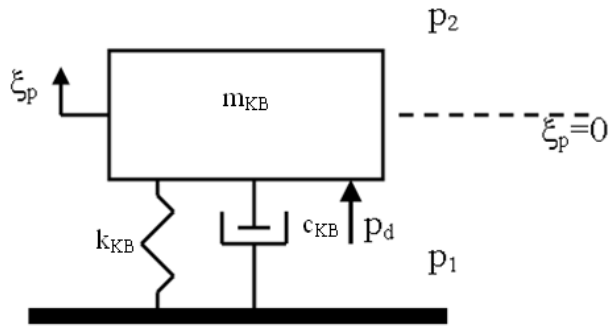

Figure 2.3 A representation of a single element in the Kanis & de Boer cochlear model
The vertical displacement of the CP (ξ_p), the CP mass (m_{KB}), stiffness (k_{KB}) and damping (c_{KB}) are all shown. The fluid pressure below and above the CP (p_1 and p_2) is related to the semi-difference pressure $p_d = \frac{1}{2}(p_2 - p_1)$.

Kanis & de Boer suggest a distribution of the CP properties along the cochlea as described in (2.12) to (2.14), where $m_0 = 0.5$ kgm^{-2}, $\delta = 0.4$, $s_0 = 10^{10}$ kgm^{-2}s^{-2} and $\kappa = 300$ m^{-1}. They set the height H equal to 1 mm and generally only consider the basal 0.01 m of the cochlea, but the model can be extended to 0.035 m. The CP mass is constant throughout the cochlea, but the damping and stiffness vary exponentially. The value of the exponential growth factor, κ, was chosen so that the stiffness variation was consistent with that observed in human cadaver cochleae (de Boer, 1980). For this passive model the natural frequency, ω_n, is a function of distance from the base (2.15), and the width of the resonance peak is inversely proportional to the constant damping parameter δ (de Boer, 1996).

$$m_{KB}(x) = m_0 \tag{2.12}$$

$$c_{KB}(x) = \delta\sqrt{m_0 s_0}\cdot e^{-\kappa x/2} \tag{2.13}$$

$$k_{KB}(x) = s_o e^{-\kappa x} \tag{2.14}$$

$$\omega_n = \sqrt{\frac{s_0}{m_0}}\cdot e^{-\kappa x/2} \tag{2.15}$$

Kanis & de Boer also develop an active micromechanical cochlear model, based on the passive model described above, by incorporating an impedance associated with the OHCs, Z_{OHC}^{lin}. This impedance is defined in terms of the OHC output pressure, p_{OHC}^{lin}, and the CP velocity in (2.16). Its form appears to be an algebraic approximation to the impedance that provides realistic solutions rather than being based on a specific dynamic model of the CP. The superscript *lin*, emphasises the linear nature of these variables. The impedance Z_{OHC}^{lin} is related to the parameters of the model as shown in (2.18), where the constants e_0 (4.28×10^{-5} kgm^{2}s) and d_0 (1404 kgs^{-1}) are associated with the OHCs, δ_{sc} (0 .4) is a dimensionless damping parameter, and σ_0 (0.7) is a dimensionless parameter that shifts the frequency of the OHC resonance relative to the BM resonance. The variables $\omega_n(x)$, and b(x,ω) are defined in (2.15) and (2.19). The total active CP impedance, Z_{CP}^{active}, is the linear sum of the two impedance components as shown in (2.17). These components are both specific acoustic impedances with the dimensions of mass per unit area per unit time.

$$Z_{OHC}^{lin}(x,\omega) = \frac{p_{OHC}^{lin}(x,\omega)}{v(x,\omega)} \tag{2.16}$$

$$Z_{CP}^{active}(x,\omega) = Z_{CP}^{pass}(x,\omega) - Z_{OHC}^{lin}(x,\omega) \tag{2.17}$$

where

$$Z_{OHC}^{lin}(x,\omega) = e_o\omega_n(x)\cdot d_0\left\{\frac{1+ib(x,\omega)}{\delta_{sc}+i\left[b(x,\omega)-\dfrac{\sigma_0^2}{b(x,\omega)}\right]}\right\} \tag{2.18}$$

$$b(x,\omega) = \frac{\omega}{\omega_n} \tag{2.19}$$

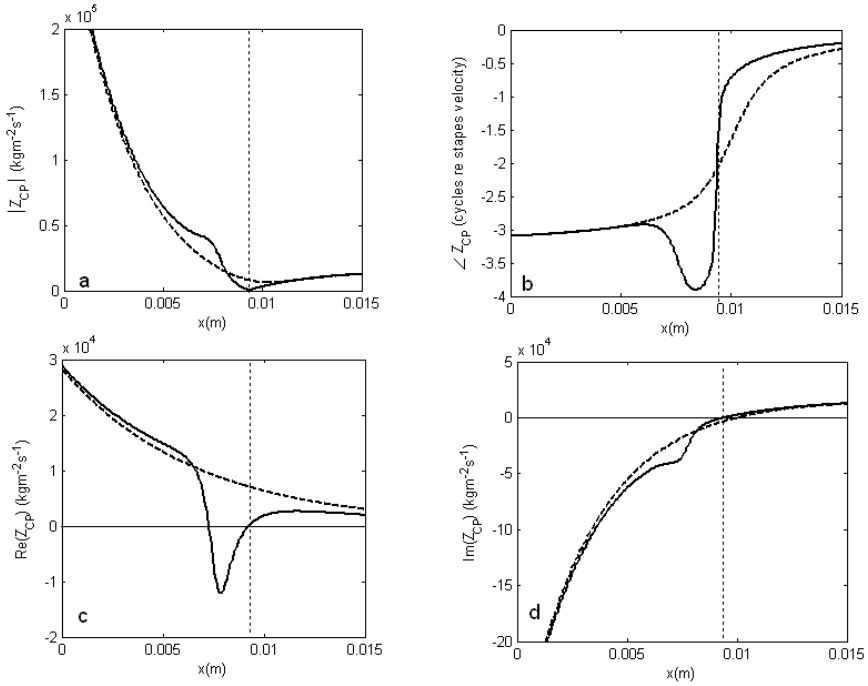

Figure 2.4 The CP impedance of the linear Kanis & de Boer cochlear model
The (a) magnitude, (b) phase, (c) real part and (d) imaginary part of the predicted CP impedance are shown for the active (solid line) and passive (dashed line) linear model, following a 5 kHz stapes stimulus. The model length is 0.035 m, but only the first 0.015 m is shown here for clarity. The 5 kHz characteristic place is illustrated by the thin dotted vertical lines.

Figure 2.4 shows the CP impedance distribution along the cochlea when the model is stimulated at 5 kHz. The real part of the active impedance is negative in the region immediately basal to the characteristic place, indicating that the OHCs are injecting energy into the travelling wave over this region.

2.2.2 Response of the linear model

The pressure and velocity distribution along the Kanis & de Boer cochlear model, evoked by a single tone stimulus applied to the stapes, is shown in figure 2.5. These responses were estimated with the finite difference method, using N=1000. Note that only the first 15 mm of the full 35 mm length is shown. Comparing the maximum CP velocity for the passive and active cases indicates that the cochlear amplifier (CA) gain of the active model is about 38 dB. The response of the active model also peaks about 2.5 mm further along the cochlea than the response of the passive model, corresponding to a shift in the best frequency at a single position of approximately ½ an octave. In addition to increasing the maximum amplitude of the travelling wave, the CA acts to increase the rate of spatial variation of the phase of p_d and v in the vicinity of the best place. The velocity phase lag, relative to the stapes motion, accumulated by the travelling wave when it reaches the best place is approximately 2 cycles in figure 2.5d. This is consistent with the 1.5 − 2.5 cycles of phase

accumulation at the best place measured in the base of mammalian cochlea (Robles & Ruggero, 2001).

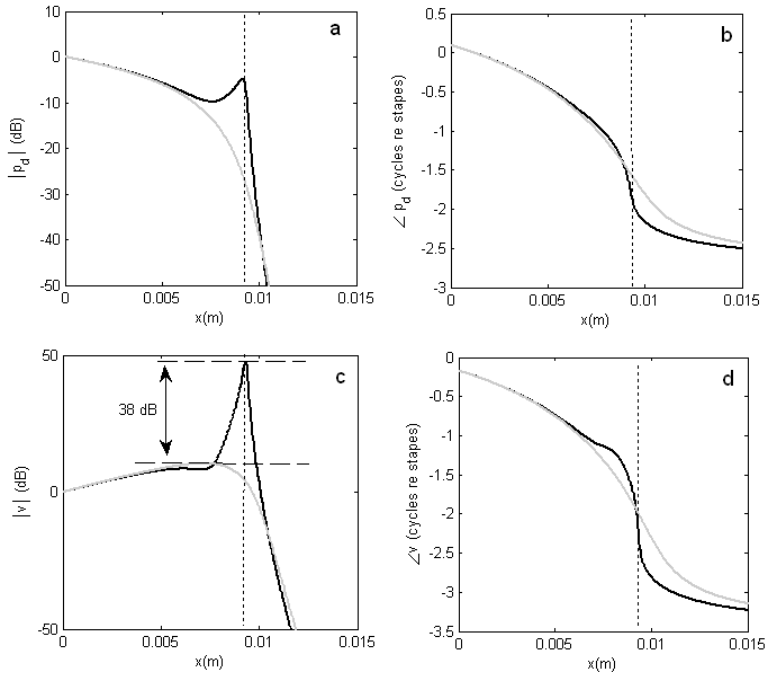

Figure 2.5 The response of the linear active Kanis & de Boer cochlear model
The amplitude and phase of the semi-difference pressure (a and b) and the CP velocity (c and d) evoked by a 5 kHz stimulus are shown. Responses of the linear active (black lines) and passive (grey lines) models were obtained using the finite difference method. Results are given in units of dB relative to the semi-difference pressure at the base or stapes velocity in plots a and c respectively. The 5 kHz characteristic place in the active model is denoted by the thin dotted vertical lines.

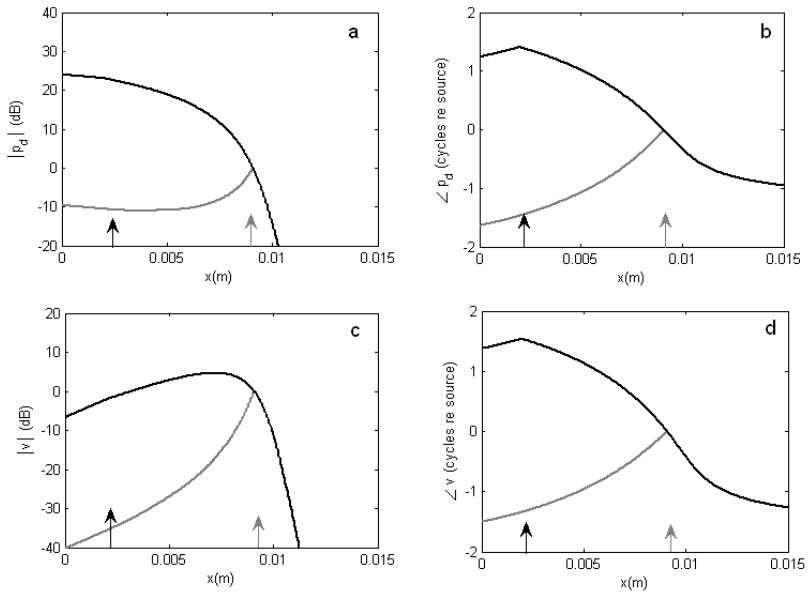

Figure 2.6 The response of the passive linear model to an internal stimulus
The magnitude and phase of the semi-difference pressure (a and b) and the CP velocity (c and d) evoked by an internal 5 kHz source in the passive linear Kanis & de Boer cochlear model are shown. The source is located at either 2mm (black arrow) or 9mm (grey arrow) from the base. The responses to the 2mm and 9mm sources are drawn in black and grey respectively, and were obtained using the finite difference method and the basal boundary condition was modified to minimise reflections, as described in appendix C.2. The results are given in units of dB relative to the semi-difference pressure or the vertical CP velocity at the 9 mm source location in plots a and c respectively.

The response of the passive linear Kanis & de Boer cochlear model to an internal point source at 5 kHz is shown in figure 2.6. In this case the phase of the response falls off in both directions away from the source and illustrates how a DP might propagate out of the cochlea. This reverse propagation within the cochlea is discussed in more detail with regarding to forward and backward travelling waves in section 2.3.

The expression for the total linear CP impedance given in (2.17) can be modified to include a parameter $\gamma(x)$ which takes a value between 0 and 1 at every location (Neely & Kim, 1986).

$$Z_{CP}^{active}(x,\omega) = Z_{CP}^{pass}(x,\omega) - \gamma(x) \cdot Z_{OHC}^{lin}(x,\omega) \tag{2.20}$$

We shall refer to $\gamma(x)$ as the OHC gain, to distinguish it from the CA gain which usually takes a value of 30 − 40 dB (section 1.3.2.). In a fully active linear model, $\gamma = 1$ throughout the model. In a completely passive model, where the action of the OHCs is neglected, $\gamma = 0$ everywhere. Gradual reduction of γ from 1 to 0 can be used to simulate the effect of a nonlinear function in the cochlear model, which would act to reduce the OHC gain as the stimulus level increases, as shown in figure 2.7.

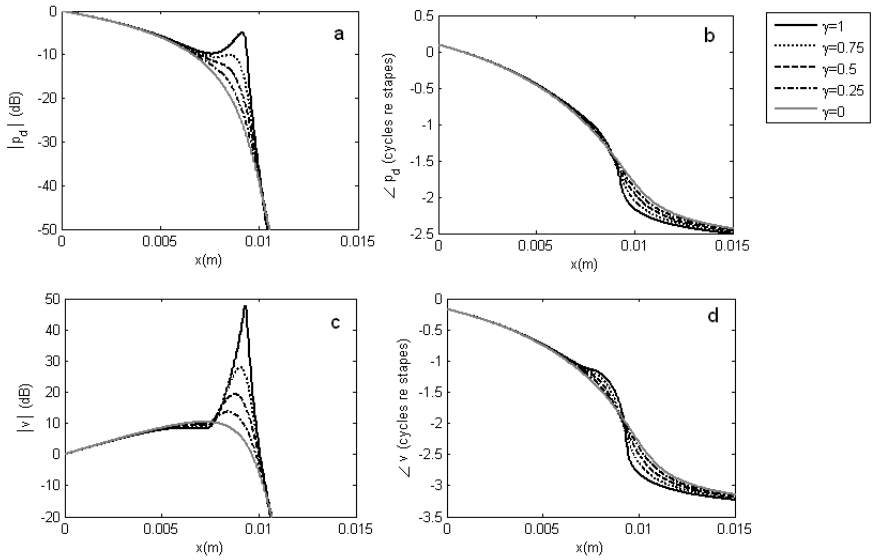

Figure 2.7 The influence of OHC gain, γ, on the response of the linear active model
The (a) amplitude and (b) phase of the semi-difference pressure, and the (c) amplitude and (d) phase of the CP velocity, evoked by a 5 kHz in the linear active Kanis & de Boer model are shown. In each case γ is constant throughout the model, at the value indicated in the key. The results are given in units of dB relative to the semi-difference pressure and vertical CP velocity at the base of the cochlear model in plots a and c respectively.

2.3 Forward and backward travelling wave decomposition

The finite difference method can be used to determine the distribution of the semi-difference pressure, $p_d(x,\omega)$, but it does not explicitly reveal the direction of the travelling wave. In this section a method is presented for decomposing the finite difference solution p_d into forward and backward travelling components. This provides a useful tool when examining models with internal sources or sources of reflection in chapters 4, 5 and 6.

The mathematical steps described below are similar to those presented by Talmadge *et al.* (1998), but the application is different. For example, Talmadge *et al.*construct the distribution of the total semi-difference pressure arising in the cochlear model from the forward and backward travelling wave components predicted by the WKB method. In contrast, we use the finite difference method to estimate the total semi-difference pressure, and then decompose it into forward and backward travelling waves using the WKB approach. Both approaches to evaluating the forward and backward travelling wave components invoke the same assumptions, such as the validity of the WKB approximation described in section 2.1.2. They are also both subject to a similar degree of numerical error (appendix B.2.3). However we choose to use the decomposition method as it allows a more straight forward evaluation of the total semi-difference pressure, which is not dependent on the WKB approximation, compared to the approach of Talmadge *et al.* We also develop a strategy for analysing the validity of the decomposition process (section 2.3.2).

2.3.1 The decomposition method

The decomposition process divides the total finite difference solution, p_d, into the forward (+) and backward (−) travelling components suggested by the WKB solution as shown in (2.21) − (2.23). This is the reverse of the usual application of the WKB method, which seeks to determine $p_d(x)$ from $p_d^+(x)$ and $p_d^-(x)$, where:

$$p_d(x) = p_d^+(x) + p_d^-(x), \tag{2.21}$$

$$p_d^+(x) = p_0^+(x)\frac{\sqrt{k_0}}{\sqrt{k(x)}} \cdot \exp\left(-i\int_0^x k(x')\,dx'\right), \tag{2.22}$$

$$\text{and} \quad p_d^-(x) = p_0^-(x)\frac{\sqrt{k_0}}{\sqrt{k(x)}} \cdot \exp\left(+i\int_0^x k(x')\,dx'\right). \tag{2.23}$$

In these expressions, k_0 a constant which denotes the wavenumber at the base of the model and is included so that the basis functions are normalised at $x = 0$, as described in appendix B.2.2. Also, the coefficients $p_0^+(x)$ and $p_0^-(x)$ should be constant provided that there are no internal sources

present in the cochlear model. These coefficients, p_0^+ and p_0^- correspond to the amplitude of the forward and backward travelling waves at the base of the cochlear model respectively. It should be noted that, in general, the amplitudes of the forward and backward travelling waves are given by the absolute values of $p_0^+\sqrt{k_0/k(x)}$ and $p_0^-\sqrt{k_0/k(x)}$ respectively, and so the coefficients p_0^+ and p_0^- are not synonymous with the travelling wave amplitudes at any location other than the base of the cochlear model.

The decomposition is achieved using both the computed semi-difference pressure $p_d(x)$ and the computed longitudinal fluid velocity, $u_f(x)$; which was evaluated using the finite difference approximation for dp_d/dx. The decomposition formula can be obtained by differentiating the $p_d^{\pm}(x)$ functions with respect to x (2.24), and substituting the result into the equation for conserving longitudinal momentum (2.25) to obtain (2.26).

$$\begin{aligned}
\frac{dp_d^+(x)}{dx} &= p_0^+\sqrt{k_0}\left\{\begin{array}{l} -\frac{1}{2}\left[k(x)\right]^{-3/2}\cdot\frac{dk(x)}{dx}\cdot\exp\left(-i\phi(x)\right) \\ +\left[k(x)\right]^{-1/2}\cdot\left(-i\frac{d\phi(x)}{dx}\right)\cdot\exp(-i\phi(x))\end{array}\right\} \\
&= -p_d^+(x)\cdot\left\{\frac{1}{2k(x)}\cdot\frac{dk(x)}{dx}+ik(x)\right\} \\
\frac{dp_d^-(x)}{dx} &= p_0^-\sqrt{k_0}\left\{\begin{array}{l} -\frac{1}{2}\left[k(x)\right]^{-3/2}\cdot\frac{dk(x)}{dx}\cdot\exp\left(+i\phi(x)\right) \\ +\left[k(x)\right]^{-1/2}\cdot\left(+i\frac{d\phi(x)}{dx}\right)\cdot\exp(+i\phi(x))\end{array}\right\} \\
&= p_d^-(x)\cdot\left\{\frac{-1}{2k(x)}\cdot\frac{dk(x)}{dx}+ik(x)\right\}
\end{aligned} \qquad (2.24)$$

where $\phi(x)=\int_0^x k(x')dx'$

$$-i\rho\omega u_f(x)=\frac{dp_d(x)}{dx}=\frac{dp_d^+(x)}{dx}+\frac{dp_d^-(x)}{dx} \qquad (2.25)$$

$$-i\rho\omega u_f(x)=-\frac{1}{2k(x)}\frac{dk(x)}{dx}\left\{p_d^+(x)+p_d^-(x)\right\}-ik(x)\left\{p_d^+(x)-p_d^-(x)\right\} \qquad (2.26)$$

Combining (2.21) and (2.26) gives

$$p_d^+(x)=\frac{1}{2ik(x)}\left\{\rho i\omega u(x)-p_d(x)\cdot\left(\frac{dk(x)}{dx}\cdot\frac{1}{2k(x)}-ik(x)\right)\right\} \qquad (2.27)$$

$$p_d^-(x)=\frac{1}{2ik(x)}\left\{-\rho i\omega u(x)+p_d(x)\cdot\left(\frac{dk(x)}{dx}\cdot\frac{1}{2k(x)}+ik(x)\right)\right\} \qquad (2.28)$$

which can also be written as shown below. If the WKB approximation is valid, then the term labelled $q(x)$ in (2.29) should be small compared to 1 and the method reduces to wave decomposition in a uniform system.

$$p_d^{\pm}(x) = \frac{1}{2}\left\{ \mp \frac{\rho\omega u_f(x)}{k(x)} + p_d(x) \cdot \left(1 \mp \underbrace{\frac{dk(x)}{dx} \cdot \frac{1}{2ik^2(x)}}_{q(x)} \right) \right\} \tag{2.29}$$

In the following section the validity of the decomposition method is investigated. When the results of the decomposition process are valid, the amplitude of the predicted forward and backward travelling wave components typically alter by less than 1 dB if the $q(x)$ term is neglected. However, it is retained in all following simulations as it can significantly modify the amplitude of any erroneous predictions.

2.3.2 Accuracy and validity of the decomposition method

The accuracy of the decomposition procedure is limited by any numerical errors in the total semi-difference pressure or fluid velocity estimated by the finite difference method, and the validity of the WKB approximation. A consequence of these limitations is that small, but finite, erroneous travelling wave components may be predicted in scenarios where they have no physical origin. Consider, for example, the semi-difference pressure evoked by a stapes stimulus applied to a linear cochlear model in which there are no significant sites of reflection (appendix D.1). In this case the decomposition method would ideally predict that the total semi-difference pressure, $p_d(x)$, corresponds exactly to the forward travelling wave, $p^+(x)$. However in practice, as a result of errors associated with the numerical calculations and WKB approximation, the decomposition method would predict that the total semi-difference pressure is equal to the sum of the estimated forward travelling wave, $p_{est}^+(x)$, and an error term, $\varepsilon(x)$, as shown below.

$$p_d(x) = p_{est}^+(x) + \varepsilon(x) \tag{2.30}$$

As a consequence of the use of expression (2.21) in the decomposition method, any error $\varepsilon(x)$ in the estimated forward travelling wave is incorporated into the estimated backward travelling wave. For this reason, the decomposition method will predict a small erroneous estimated backward travelling wave, $p_{est}^-(x)$, even in this scenario where such a wave has no physical origin. In this section two approaches are presented which can be used to discriminate between erroneous predictions of the decomposition method and valid forward and backward travelling wave estimates which offer insight into the propagation direction of waves within the cochlear model.

The first approach estimates the amplitude of the error term $\varepsilon(x)$, and uses this to form an "error floor". Only the estimated forward or backward travelling wave components with amplitudes above this error floor will be considered valid predictions of the decomposition procedure. As errors associated with the WKB approximation are difficult to quantify, we assume that the amplitude of $\varepsilon(x)$ is similar to the scale of numerical errors in the finite difference method, approximately 0.5 dB (appendix B.1). This leads to an estimated error floor at -24.5 dB relative to $p_d(x)$, neglecting any inaccuracies the WKB approximation. The usefulness of this error floor can be demonstrated from considering the decomposition of the semi-difference pressure in the active linear 'baseline' cochlear model, in which the impedance properties of the cochlear partition vary smoothly with distance from the base and no significant reflection of forward travelling waves should occur (appendix D.1). Figure 2.8 shows the total semi-difference pressure evoked by a 5 kHz stimulus applied at the stapes. It also shows the forward and backward travelling waves predicted by the decomposition method, and the error floor is included for reference. The estimated forward travelling wave amplitude is above the error floor and within 0.3 dB of the total $p_d(x)$ distribution throughout the region between the stapes and the 5 kHz characteristic place. In contrast the estimated backward travelling wave amplitude is below the error floor, which indicates it is an erroneous prediction and can be neglected. The phase behaviour of the erroneous predicted 'backward' travelling wave (figure 2.8b) also indicates that this component is an artefact as its phase decreases with increasing x, which is typical of a forward, not backward, travelling wave as indicated in (2.22) and (2.23). Therefore, taking into account the error floor, the decomposition process suggests that a 5 kHz stapes stimulus will evoke only a forward travelling wave, and no significant backward travelling wave, in a linear active baseline cochlear model.

Another approach is to identify valid decomposition estimates from the behaviour of the travelling wave coefficients $p_0^{\pm}(x)$. In a model containing no internal sources, or sites of reflection, these coefficients should be constant along the CP. In cases where internal sources, or sites of reflection are present, then fluctuations should occur in the amplitude of both coefficients. However, if the error $\varepsilon(x)$ dominates either the estimated forward or backward travelling wave component predicted by the decomposition method, it will cause fluctuations in the amplitude of either the $p_0^{+}(x)$ or $p_0^{-}(x)$ distribution respectively. These erroneous fluctuations cannot be attributed to internal sources or sites of reflection as they usually are only evident at significant levels in one of the travelling coefficients and not the other. For example, figure 2.8c shows that the $p_0^{+}(x)$ coefficient is essentially uniformly distributed between the base and the characteristic place as its amplitude varies by less than 0.1 dB over this region. In contrast, the $p_0^{-}(x)$ coefficient amplitude fluctuates in excess of 36 dB between the base and the 5 kHz characteristic place. This variation in the amplitude $p_0^{-}(x)$, combined with the observed absence of substantial fluctuations in the

$p_0^+(x)$ coefficient, suggests that the prediction of the estimated backward travelling wave is dominated by the error $\varepsilon(x)$ and should be neglected. This approach is subjective, as is it not apparent what level of fluctuation in the amplitude of the $p_0^{\pm}(x)$ coefficients should be considered indicative of an error. We arbitrarily use a value of 10 dB to determine whether amplitude variations on of the travelling wave coefficients should indicate caution in interpreting the result. Overall, this approach yields the same conclusion as the error floor analysis: taking into account numerical errors and inaccuracies in the WKB approximation, the decomposition process predicts that a 5 kHz stapes stimulus will evoke only a forward travelling wave, and no significant backward travelling wave, in a linear active baseline cochlear model.

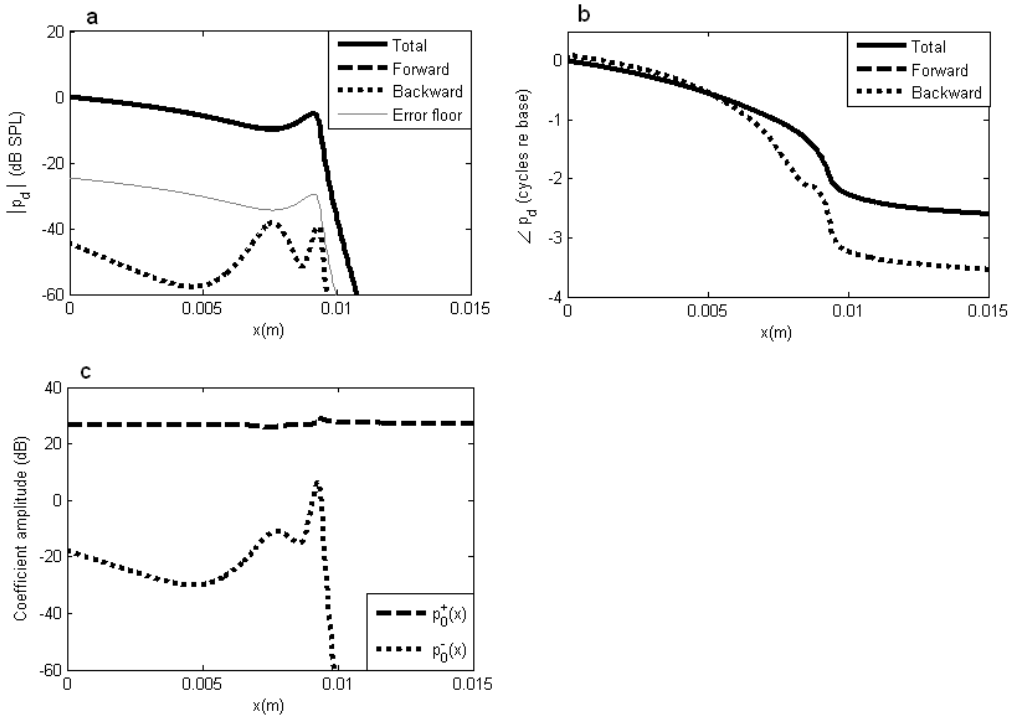

Figure 2.8 The estimated forward and backward travelling waves in a baseline cochlear model
The (a) amplitude and (b) phase of the total semi-difference pressure, and the forward and backward travelling components, evoked by a 5 kHz stapes stimulus in the linear active Kanis & de Boer cochlear model are shown. As the model is 'baseline', no irregularities have been deliberately imposed on the CP impedance. Results were evaluated using the finite difference method, and decomposition process, with N=1000. The 'error floor' is shown in (a) for reference. (c) The amplitude of the coefficients for the forward and backward travelling waves. In plots a and b, the amplitudes are given in dB relative to the value of p_d at the base of the model.

2.3.3 Application to internal sources

Figure 2.9I shows the forward and backward travelling components of the semi-difference pressure evoked by an internal sinusoidal point source located between the base and the characteristic place in the linear active Kanis & de Boer model. In order to allow a simple interpretation of the results, the basal boundary condition is adjusted to minimise reflections by setting the stapes impedance equal to the impedance for a backward travelling wave at the base of the CP (appendix C.2). Figure 2.9Ic illustrates that at the location of the internal point source, both the $p_0^+(x)$ or $p_0^-(x)$ coefficients exhibit a sharp change in amplitude. However, on the basal side of the source location p_0^- is essentially constant (less than 1 dB amplitude variation) whilst the p_0^+ coefficient level fluctuates considerably (in excess of 40 dB). In this basal region, only the amplitude of the estimated backward travelling wave component exceeds the error floor of the decomposition method. In contrast, on the apical side of the source location, p_0^+ is almost uniform (less than 2 dB level variation) whilst the p_0^- coefficient exhibits substantial amplitude variation exceeding 50 dB. In this apical region, only the amplitude of the estimated forward travelling wave component exceeds the error floor of the decomposition method. Collectively, these observations suggest that both the estimated forward travelling wave in the basal region, and the estimated backward travelling wave in the apical region, should be neglected because they are dominated by errors associated with numerical inaccuracies and the limitations of the WKB approximation. Therefore, taking into account numerical errors and inaccuracies in the WKB approximation, the decomposition procedure predicts that an internal sinusoidal point source located between the base and the characteristic place will evoke a backward travelling wave which propagates from the source to the stapes and a forward travelling wave which propagates from the source to the characteristic place.

In figure 2.9II the basal boundary condition has been altered so that there is approximately complete reflection of the backward travelling wave at $x = 0$. The response to the internal sinusoidal point source on the apical side of the source region is essentially unchanged by the reflective basal boundary condition. However, the introduction of reflection off the stapes does influence the predicted response between the base and the source location. In this region, when the reflecting basal boundary condition is imposed, both the $p_0^+(x)$ or $p_0^-(x)$ coefficients exhibit almost constant amplitude which varies by less than 1 dB and the amplitudes of the both the estimated forward and backward travelling wave components exceed the error floor. Therefore, taking into account numerical errors and inaccuracies in the WKB approximation, the decomposition procedure indicates that an internal sinusoidal point source located between the base and the characteristic place will give rise to a backward travelling wave which propagates towards

the base and can be reflected at the stapes to generate a forward wave which travels into the cochlear model from the base.

(I)

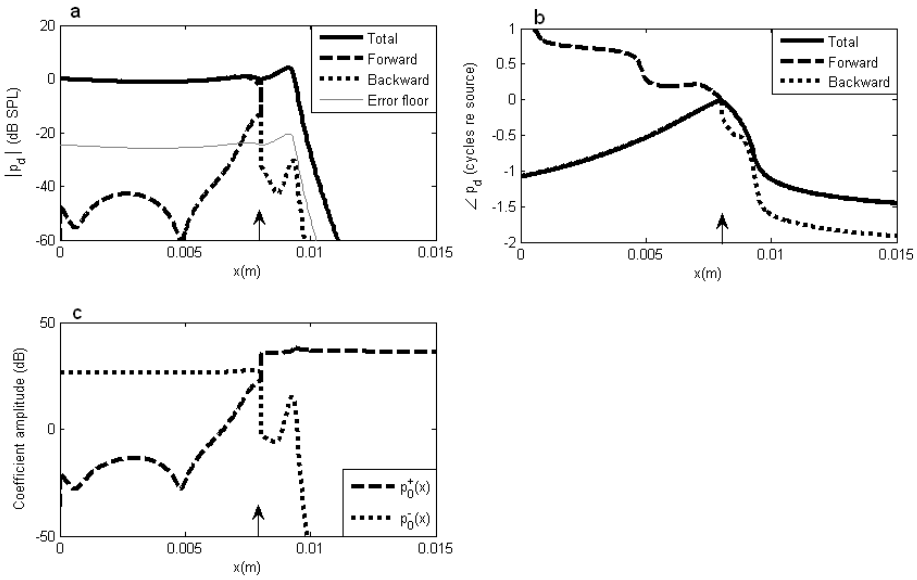

(II)

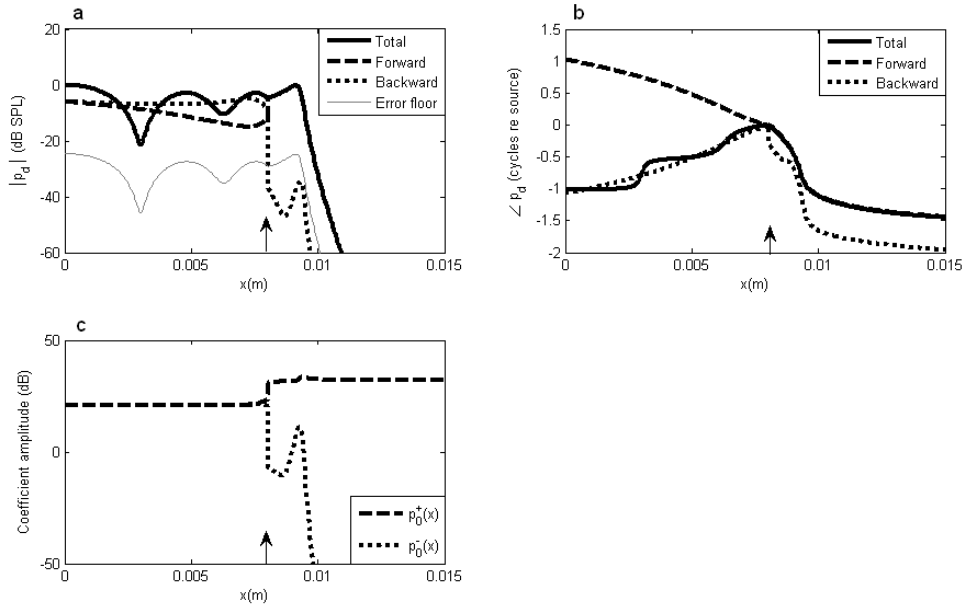

Figure 2.9 The estimated forward and backward travelling waves evoked by an internal source
Plots (a) and (b) show the amplitude and phase of the total semi-difference pressure, and the forward and backward travelling components, evoked in the linear active Kanis & de Boer model by a 5 kHz *internal point source* located at a distance of 8 mm from the stapes (black arrows). Also (c) shows the amplitude of the coefficients for the forward and backward travelling waves. Results evaluated using the finite difference method, and decomposition process, with N=1000 and a boundary condition at the stapes such that either (I) there is no reflection of backward travelling waves or (II) there is complete reflection of the backward travelling wave.

2.3.4 Application to sites of reflection

In chapter 4, impedance irregularities are deliberately introduced into the active micromechanics of the cochlear model to act as sources of reflection. These perturbations could arise from either the active mechanics, perhaps from differences in the force exerted by neighbouring OHCs (Zweig & Shera, 1995a) or the passive mechanics, possibly from spatial variations in the BM radial fibres (Shera & Guinan, 2008).The response of a linear model is determined by the total CP impedance, which is a linear combination of the passive and active impedances (2.20), and so the qualitative change in the response should be the same, whether a perturbation is introduced into the active or the passive mechanics. The same should be true of the quasilinear model, described in chapter 3, at low stimulus levels. We choose to introduce irregularities into the active mechanics, rather than the passive mechanics, of the cochlear model.

Reflections can be generated from perturbations imposed on the CP impedance via the OHC gain parameter $\gamma(x)$. This variable was introduced in (2.20) and takes a value between 0 and 1 (Elliott *et al.*, 2007; Ku *et al.*, 2008). Figure 2.10 shows an example of the effect of a step-down change in $\gamma(x)$, from 1 to 0.95, in the linear active model at the characteristic place. The model is stimulated at the stapes by a 5 kHz tone, and the step-down change in $\gamma(x)$ is positioned 9 mm from the base. In the basal region, between the stapes and the internal reflection site, both the $p_0^+(x)$ or $p_0^-(x)$ coefficients exhibit almost constant amplitude (variations of less than 2 dB) and the amplitudes of the both the estimated forward and backward travelling wave components exceed the error floor. These observations suggest that, on the basal side of the reflection site, neither the estimated forward or backward travelling waves are significantly influenced by errors associated with numerical inaccuracies and the limitations of the WKB approximation. Section 2.3.2 established that, in the absence of an internal reflection site, the stapes stimulus evoked only a forward travelling wave. Introduction of the reflection site into the cochlear model has little influence on the apical side of the site. However, in the basal region of the model, the decomposition procedure suggests that the internal reflection site gives rise to a backward travelling wave which was not evident before the reflection site was introduced.

The amplitude of the backward travelling wave is dependent on both the location, and the scale of the perturbation. For example, if the step-down change in $\gamma(x)$ is reduced from 5% to 1%, the amplitude of the backward travelling wave observed at the base of the model decreases by approximately 10 dB. In addition, if the backward travelling wave generated by a fixed internal reflection site is estimated for a range of excitation frequencies, as shown in figure 2.11, then the amplitude of the reflected wave is greatest when the stimulus frequency corresponds to the characteristic frequency of the reflection site.

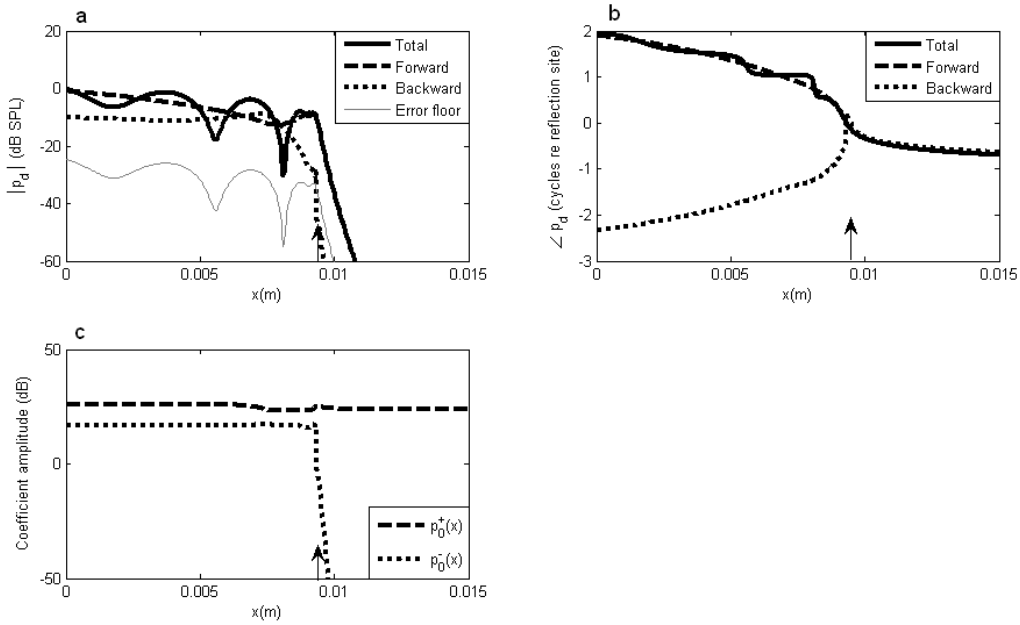

Figure 2.10 The estimated forward and backward travelling waves in a perturbed cochlear model
Plots (a) and (b) show the amplitude and phase of the total semi-difference pressure, and the forward and backward travelling components, in the linear active Kanis & de Boer model stimulated by a 5 kHz tone at the stapes. Also, (c) shows the amplitude of the coefficients for the forward and backward travelling waves. This perturbed model contains a 5% step-down change in the distribution of $\gamma(x)$ at 9 mm from the stapes as indicated by the black arrows. The results were obtained using a reflectionless boundary condition at the base, and N=1000.

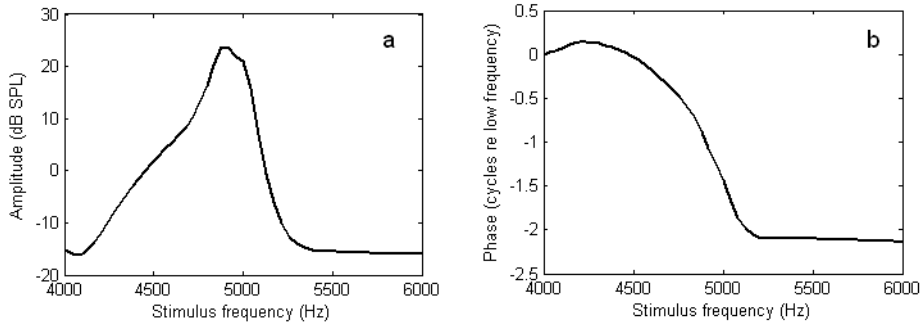

Figure 2.11 The influence of stimulus frequency on the reflected waves generated by a place-fixed impedance irregularity in a perturbed cochlear model
Plots (a) and (b) show the amplitude and phase of the backward travelling wave at the base of the linear Kanis & de Boer model as a function of stimulus frequency when a step-down change in $\gamma(x)$, from 1 to 0.95, is imposed at the 5 kHz characteristic place. The results were obtained using a reflectionless basal boundary condition, a stapes stimulus level of 10^{-8}m/s, and N=1000.

2.4 The quasilinear method

So far we have described a linear cochlear model in which none of the parameters depend on the stimulus level. However, Kanis & de Boer incorporate a nonlinear function into their active cochlear model, in order to replicate the nonlinear response of the cochlea to stimulation. They also develop a 'quasilinear' method for predicting the steady state response of this model, in the frequency domain, as described in this section.

2.4.1 The nonlinearity

The linear active variant of the Kanis & de Boer model can be described by the feedback diagram shown in figure 2.12a (Neely, 1985), where p_{OHC}^{lin} is the linear pressure arising from the active outer hair cells (OHCs) and is assumed to act in the same way on the basilar membrane (BM) as the transmembrane pressure difference, p_d. In this diagram, the impedances Z_{pass} and Z_{OHC}^{lin} are defined in equations (2.10) and (2.16) respectively.

Kanis & de Boer implicitly introduce a nonlinearity into the micromechanical feedback loop, as shown in figure 2.12b. This is assumed to be a hyperbolic tangent nonlinearity, which modifies the pressure output of the OHCs such that

$$p_{OHC}^{QL}(x,t) = p_{ref} \tanh[p_{OHC}^{lin}(x,t) / p_{ref}] \tag{2.31}$$

In the above expression the scaling constant p_{ref} has the units of the pressure and is assigned a value of 2 by Kanis & de Boer (1993).

(a) The linear micromechanical model

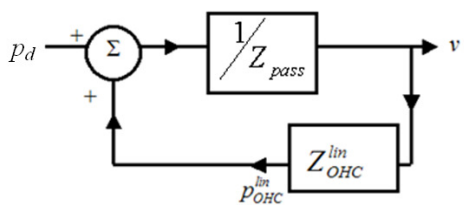

(b) The nonlinear micromechanical model

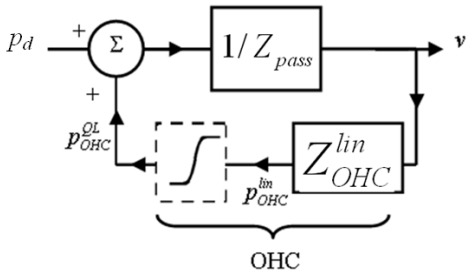

$$Z_{CP}^{active} \equiv \frac{p_d}{v} = \frac{1 - Z_{OHC}^{lin}/Z_{pass}}{1/Z_{pass}} = Z_{pass} - Z_{OHC}^{lin}$$

Figure 2.12 Representations of a single (a) linear and (b) nonlinear micromechanical element
Kanis & de Boer modify their (a) linear model by inserting a nonlinear function into the micromechanical feedback loop as shown in (b). The semi-difference pressure across the cochlear partition, p_d, the vertical velocity of the cochlear partition, v, and the linear pressure output of the outer hair cells (OHCs), p_{OHC}^{lin}, are all shown.

The quasilinear notation, *QL*, indicates that the nonlinearity is expected to produce distortion which can be treated as a small perturbation compared to the fundamental response. On this basis a new quasilinear impedance for the OHCs, $Z_{OHC}^{QL}(x,\omega)$, is defined as

$$Z_{OHC}^{QL}(x,\omega) \equiv \frac{p_{OHC}^{QL}(x,\omega)}{v(x,\omega)} \tag{2.32}$$

2.4.2 The fundamental response to a single tone stimulus

The principle of the quasilinear method is that the distortion which occurs in the system variables of a nonlinear model can be treated as a small perturbation compared to the fundamental component. On this basis, the system variables can be represented by their fundamental component and the harmonic components can be neglected in the calculation of the fundamental response. Kanis & de Boer justify neglecting these higher order components by demonstrating that the 3rd order harmonic is always more than 25 dB below the fundamental component, and that incorporating the 3rd order response produces no significant change in the estimated fundamental component (Kanis & de Boer, 1993).

An iterative method is used to determine the response of the quasilinear model, as detailed in appendix E.1. To summarise, an initial estimate of the quasilinear CP impedance is obtained by assuming that the model is fully active. The finite difference method is applied to estimate the fundamental velocity response of the CP which is then used, in conjunction with the linear OHC impedance, to determine the time domain input to the nonlinearity. The fundamental pressure output of the nonlinearity is then estimated and equation (2.32) is applied to determine a revised estimate of the quasilinear OHC impedance which provides a revised estimate of the CP impedance, taking into account the effect of the nonlinearity. The process is repeated iteratively until the estimated CP velocity distribution differs by less than 0.1% between iterative cycles. In general, the required number of iteration cycles increases with the stimulus level. For example, the response of the Kanis & de Boer quasilinear model to a 5 kHz stimulus tone can be estimated in only 7 iterations for a 20 dB SPL stimulus, but 30 iterations are required for a stimulus level of 100 dB SPL. These computations can be performed on a 2.4 GHz computer in less than 30 seconds.

The response of the Kanis & de Boer quasilinear model to a 6 kHz stimulus tone at various levels is shown in figure 2.13. These results are consistent with those presented by Kanis & de Boer (1993), and illustrate the compressive nonlinear growth of the response in the vicinity of the characteristic place. The input to the hyperbolic tangent nonlinearity shown in equation (2.31) is scaled so that the OHC gain is significantly reduced only when the stimulus level exceeds about 40 dB, as illustrated in the level curves of figure 2.13d. It is possible to simulate these results with the linear

model if the distribution of OHC gain, $\gamma(x)$, introduced in equation (2.20) is defined as $\gamma_{QL}(x,\omega)$, shown below.

$$\gamma_{QL}(x,\omega) \equiv \frac{Z_{OHC}^{QL}(x,\omega)}{Z_{OHC}^{lin}(x,\omega)} \tag{2.33}$$

Figure 2.14 shows the distribution of $\gamma_{QL}(x,\omega)$ for several different stimulus levels, for a stimulus frequency of 6 kHz. This demonstrates that the model becomes almost passive in the region just basal to the characteristic place, at high stimulus levels, since $\gamma_{QL}(x)$ is close to zero in this region.

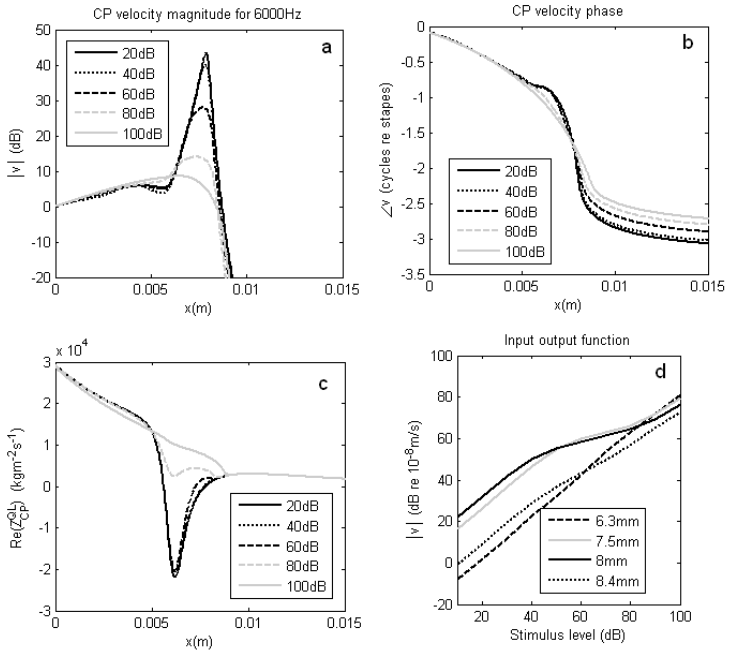

Figure 2.13 The response of the Kanis & de Boer quasilinear cochlear model
Plots (a) and (b) show the amplitude and phase of the CP velocity evoked by a 6 kHz stimulus, evaluated using N=1000. The corresponding distributions of the quasilinear OHC impedance are also shown in (c). The input output level functions at four locations along the CP are presented in (d), where x=8 mm corresponds to the characteristic place. Stimulus stapes velocities are given in units of dB re 10^{-8}m/s.

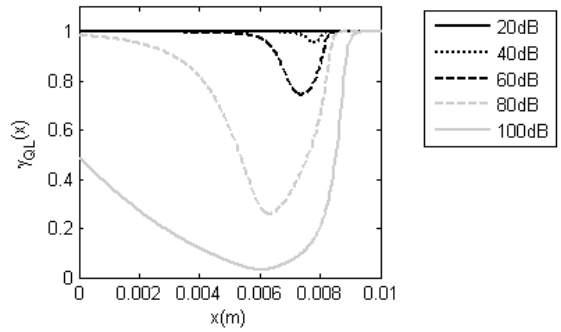

Figure 2.14 The influence of stimulus level on the quasilinear OHC gain distribution
The quasilinear OHC gain, γ_{QL}, is plotted for a 6 kHz stapes excitation at a variety of stimulus levels given in units of dB re 10^{-8}m/s. The response was evaluated using N=1000, and it should be noted that the 6 kHz characteristic place is approximately 8 mm from the stapes.

2.4.3 Estimating harmonic distortion products

The nonlinearity used by Kanis & de Boer to represent the action of the OHCs is a hyperbolic tangent function. As this nonlinear function is symmetrical its output will contain odd-order harmonic components in addition to the fundamental component (appendix G). These harmonics were neglected when estimating the fundamental component, as they have relatively small amplitude. However, once the fundamental response has been estimated, it is possible to apply the quasilinear method to predict the harmonic components as well.

The iterative process used by Kanis & de Boer for estimating the harmonic components is described in appendix E.2 − E.3. This also details the rearrangement made to the quasilinear process in order to achieve more consistent convergence of the iteration sequence. The results, such as those shown in figure 2.15 for a 6 kHz stimulus, are consistent with those obtained by Kanis & de Boer (1993) although slightly different stimulus levels are used to account for the difference in middle ear properties. The variation in the 3rd order harmonic response, with increasing stimulus level, is illustrated in figure 2.16. The source of this component is the 3rd harmonic of the OHC pressure output due to the presence of the fundamental component, given in (2.34). Figure 2.16a shows that this source pressure is greatest at the best place of the fundamental frequency as at this location the fundamental component of the CP velocity has the greatest amplitude. The source broadens, and spreads towards the characteristic place of the 3rd harmonic component, as the stimulus level increases. Figure 2.16b illustrates that, at low stimulus levels, the amplitude of the 3rd harmonic component in the resultant velocity is greatest in the vicinity of the characteristic place of the fundamental frequency. However, as the stimulus level increases, the 3rd order response spreads towards its own characteristic place. Although the harmonic response remains large at the best place of the fundamental component, at high stimulus levels (such as 100 dB re 10^{-8}m/s) its amplitude is greatest at its own characteristic place.

$$p_{OHC,A}^{QL}(x,m\omega) = \frac{1}{T}\int_0^T \tanh\left[2\,\mathrm{Re}\left(Z_{OHC}^{lin}(x,\omega)\cdot v(x,\omega)\cdot\exp(i\omega t)\right)\right]\cdot\exp\left(-im\omega t\right)dt \qquad (2.34)$$

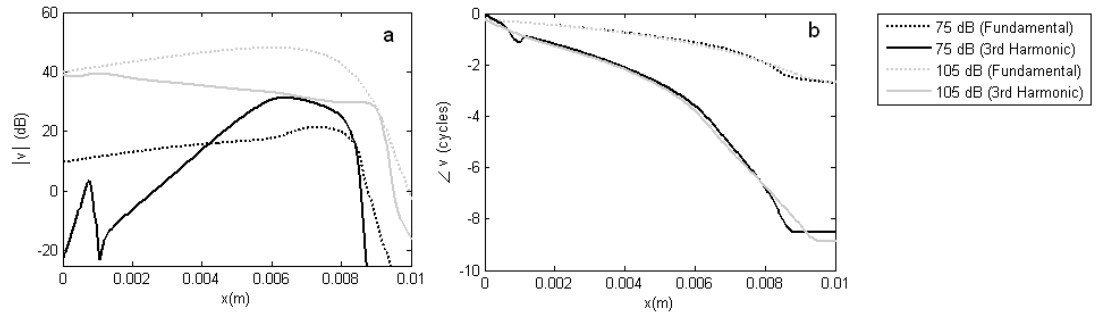

Figure 2.15 Comparison of the fundamental and 3rd harmonic response of the quasilinear model
Plots (a) and (b) show the amplitude and phase of the fundamental and 3rd order CP velocity components evoked by a 6 kHz stapes velocity at 75 dB re 10^{-8}m/s and 105 dB re 10^{-8}ms in the Kanis & de Boer quasilinear cochlear model. The fundamental and 3rd order responses are referenced to 10^{-5}m/s and 10^{-7}m/s respectively, in order to allow for comparison with chapter 2 of Kanis (1995).

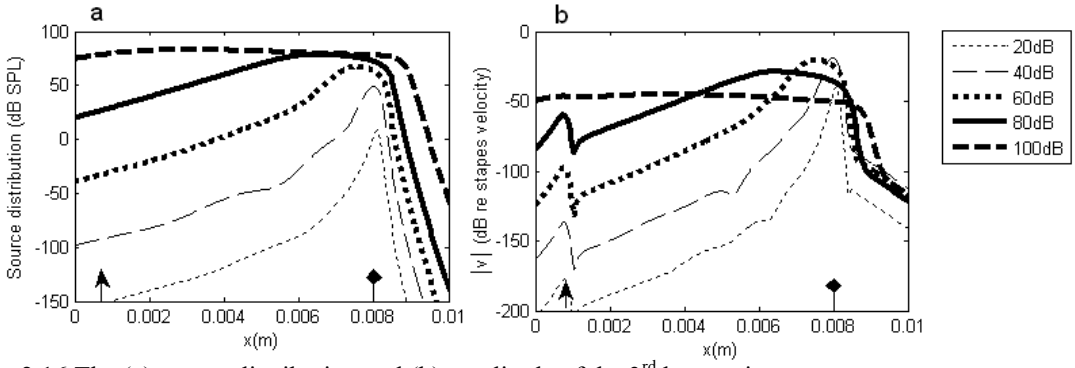

Figure 2.16 The (a) source distribution and (b) amplitude of the 3rd harmonic response
The quasilinear Kanis & de Boer cochlear model was stimulated at the stapes with a 6 kHz tone at a variety of stimulus levels and (a) the source distribution for the 3rd harmonic was estimated from $p_{OHC,A}^{QL}(x,3\omega)$, defined in (2.34). The amplitude of the 3rd harmonic component of the CP velocity is also shown in (b). Stimulus levels are given in dB re 10^{-8}m/s. In each graph the characteristic places for 6 and 18 kHz are indicated by the diamond and triangular arrows respectively. The results were obtained using a discrete model with N=1000.

For a 6 kHz stapes velocity presented at 0 to 100 dB re 10^{-8}m/s, the estimate of the fundamental component changes by less than 1% when the 3rd harmonic is included in the quasilinear calculations, instead of being neglected. In addition the predicted source distribution for the 3rd harmonic changes by less than 2% if the 3rd harmonic is used to improve the estimate of the fundamental response. This is consistent with Kanis & de Boer's finding that the inclusion of the 3rd harmonic changes the predicted fundamental component by less than 0.01 dB. Therefore we conclude that the principle of the quasilinear method is valid, at least for these stimulus conditions, and that the fundamental component of the response of the nonlinear cochlear model can be accurately estimated by neglecting the harmonic components.

The hyperbolic tangent nonlinear function will produce other odd-order harmonic components in addition to the 3rd harmonic. Of these higher order responses, the 5th harmonic has the largest amplitude. For a 6 kHz stimulus tone, the 5th harmonic component amplitude can reach within 10 dB of the 3rd harmonic component amplitude at high stimulus levels (e.g. a stapes velocity of 100 dB re 10^{-8}m/s). Despite this, the estimate of the 3rd harmonic component changes by less than 2% if the 5th harmonic is included in the quasilinear calculation, compared to the estimated 3rd harmonic response when is the 5th harmonic is neglected. For this reason, we conclude that it is appropriate to extend the quasilinear method to the estimation of harmonic components.

2.4.4 Two tone suppression

Two tone suppression is the reduction of the cochlear response to one tone (the 'probe' tone) due to the simultaneous presentation of another tone (the 'suppressor' tone) in the ear canal (Robles & Ruggero, 2001). This effect is maximised when the two tones have almost equal frequency. It is important for a cochlear model to replicate the phenomenon of two tone suppression, as it is often cited as evidence for the nonlinearity of the active process (Patuzzi, 1996).

The quasilinear method for estimating the response of the cochlear model to two tone stimulation reviewed in appendix E.4, based on the description given by Kanis & de Boer (1994). In summary, the primary responses to the stimulus frequencies f_1 and f_2 are first estimated individually using the quasilinear method for single tone stimuli. These estimates are then revised using a second iterative process in which the fundamental responses to each of these tones are combined to form the input to the OHC nonlinearity. An example of two tone suppression in the quasilinear Kanis & de Boer cochlear model is shown in figure 2.17. The simulation was performed using a 7 kHz probe tone and a 7.25 kHz suppressor tone. The plots illustrate that the probe tone frequency component of the BM velocity response is substantially reduced in amplitude in the vicinity of its best place by the introduction of the suppressor tone. In association with this, the OHC gain at the probe tone frequency is also considerably reduced in the region basal to the best place of the probe frequency.

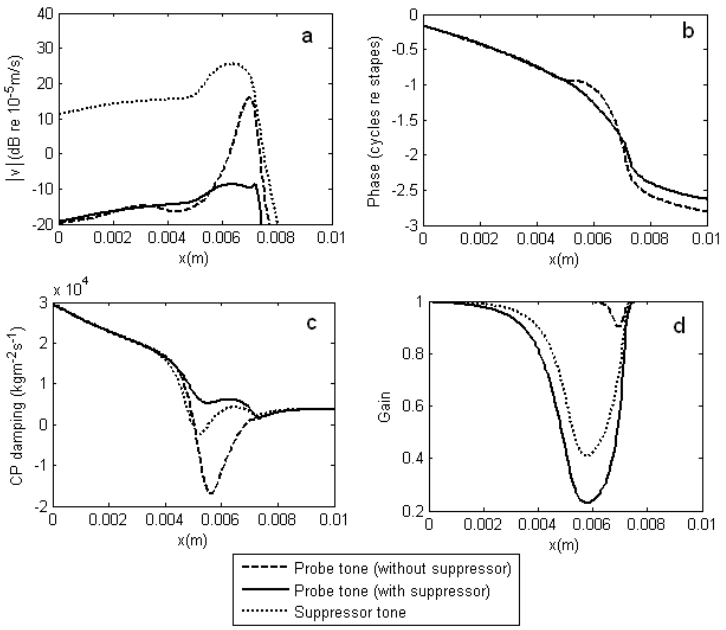

Figure 2.17 An example of two tone suppression in the Kanis & de Boer cochlear model.
The (a) amplitude and (b) phase of the response evoked by a 7 kHz probe tone and a 7.25 kHz suppressor tone, presented at levels of 50 and 80 dB re 10^{-8} m/s respectively. The amplitude is presented in units of dB re 10^{-5} m/s to correspond with the figures of Kanis (1995). The (c) damping of the cochlear partition, CP, and (d) the OHC gain at 7 kHz are also shown.

2.4.5 Two tone distortion products

The distortion products (DPs) evoked by two tone stimuli (f_1 and f_2, $f_2>f_1$) can be estimated with the quasilinear method, using a combination of the techniques discussed in sections 2.4.3 and 2.4.4. A sequence of three iterative procedures is used to predict the DPs. These evaluate the response of the model to each stimulus tone in isolation, the effect of two tone suppression and the DP component of the CP response. The third stage requires an iteration process similar to that used in the quasilinear evaluation of the harmonic response to a single tone stimulus. A full description of the method for predicting two tone DPs is given in appendix E.5.

An example of the $2f_1 - f_2$ DP predicted by the quasilinear method for the Kanis & de Boer cochlear model is given in figure 2.18. These results are consistent with those obtained by Kanis (1995). There is, however, a 10 dB difference in the DP component of the semi-difference pressure when using f_2/f_1=1.04. The origin of this discrepancy is unknown. It is unlikely to be associated with poor convergence of the original Kanis & de Boer iterative method, as that process is convergent for this stimulus paradigm. However, we have confidence in the validity of the result shown in figure 2.18c because it is consistent with the state space time domain estimate (section 2.5), at least in the vicinity of the f_2 and DP characteristic places.

We verified the quasilinear approximation for the case of two tone distortion products by considering the estimated DP evoked by two stimulus tones presented at levels of 70 dB SPL with f_1=1.8 kHz and f_2=2.2 kHz. The primary responses alter by less than 0.02 dB if the DP is incorporated into their evaluation.

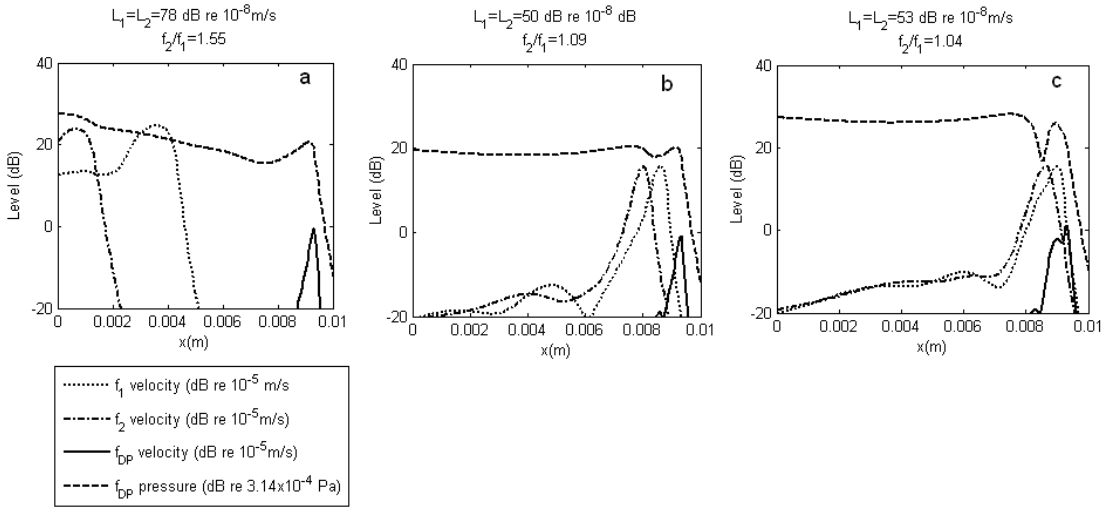

Figure 2.18 The predicted $2f_1 - f_2$ DP component in the quasilinear Kanis & de Boer model
Three different stimulus paradigms are shown: (a) f_2/f_1=1.55, (b) f_2/f_1=1.09 and (c) f_2/f_1=1.04. In each case the DP frequency (f_{dp}) is equal to 5 kHz and the level of the primary stimulus tones (L_1 and L_2) have been chosen so that the amplitude of the DP component of the CP velocity is approximately 0 dB re 10^{-5}m/s at its characteristic place. The CP velocity is given in units of dB re 10^{-5}m/s and the semi-difference pressure is in units of dB re 3.14×10^{-4}Pa. These results are comparable to those of Kanis (1995), chapter 5 (figures 1,2, and 3).

2.5 The state space model

The effect on DPOAEs of random perturbations in the cochlear gain is investigated below, and it is known that for some perturbations the linear cochlear model may not be stable (Elliott *et al.*, 2007; Ku *et al.*, 2008). In this section, the Kanis & de Boer cochlear model is cast into the state space framework, which is described by Elliott *et al.* (2007) for the Neely & Kim (1986) cochlear model. This can be used to assess the stability of the linear model (section 2.5.2), which is an implicit necessary condition for the validity of the quasilinear method, and also to evaluate the time domain solution of the nonlinear model for both single tone and two tone stimuli (sections 2.5.3 and 2.5.4).

2.5.1 Formulation of the state space model

In general, a state space time domain representation of a physical system takes the form shown below, where $\mathbf{w}(t)$ is the "state" vector, $\mathbf{u}(t)$ is the input vector and $\mathbf{y}(t)$ is the output vector.

$$\dot{\mathbf{w}}(t) = \mathbf{A}\mathbf{w}(t) + \mathbf{B}\mathbf{u}(t) \tag{2.35}$$

$$\mathbf{y}(t) = \mathbf{C}\mathbf{w}(t) + \mathbf{D}\mathbf{u}(t) \tag{2.36}$$

If $\mathbf{w}(t)$, $\mathbf{u}(t)$ and $\mathbf{y}(t)$ are $n-$, $m-$ and $p-$ dimensional vectors respectively then $\mathbf{A}$ is the $n-$by-n 'system' matrix, $\mathbf{B}$ is the $n-$by-m 'input' matrix, $\mathbf{C}$ is the $p-$by-n 'output' matrix, and $\mathbf{D}$ is the $p-$by-m 'direct feedthrough' matrix (Beale, 2006). The eigenvalues of the system matrix, **A,** are the poles of the system transfer function. The system is stable if the real parts of all these eigenvalues are negative, and therefore the stability of the system can be determined from the state space representation.

The state space representation can be constructed using either the equations of motion of the system (Elliott *et al.*, 2007; Ku, 2008), or the system transfer function (Furuta *et al.*, 1988). As the dynamic components of the active mechanics are not explicitly expressed in the Kanis & de Boer model, making it difficult to construct the equations of motion, the system transfer function is used to form a state space representation of the uncoupled linear active Kanis & de Boer model in appendices F.1 and F.2. The longitudinal fluid coupling is then incorporated to form the coupled linear active state space model in appendix F.3.

2.5.2 The stability of the linear active Kanis & de Boer cochlear model

The eigenvalues, λ, of the system matrix **A** correspond to the poles of the system and are complex such that $\lambda = \sigma + i\omega$. The system is known to be stable if the real part (σ) of all the poles are negative. The state space formulation can be used to show that all the poles of a single

micromechanical element in the uncoupled model remain negative provided that the OHC gain, γ, defined in (2.20), remains less than 1.07 (see appendix F.2.2). The coupled linear active model is also stable provided that a maximum limit is imposed on $\gamma(x)$, which reduces the value of γ below one for locations within 5 mm of the apex, as shown in figure F.6 of appendix F.3.4.

The use of the state space model to predict the stability of the coupled system can be illustrated by imposing a step-change in the OHC gain, $\gamma(x)$. Figure 2.19 shows the poles of the coupled linear active Kanis & de Boer cochlear model, where a step change has been introduced at the 6 kHz characteristic place. For small step sizes, such as a change in γ(x) of 0.01, σ is negative for all of the poles indicating that the model is stable. However as the step size increases, σ becomes positive for some of the poles at approximately 6 kHz. This indicates that the model becomes unstable if $\gamma(x)$ either steps-up by 0.05 or steps-down by 0.5.

In chapter 4, a non-uniform distribution of γ(x) is introduced into the model to generate reflections of travelling waves. Appendix F.3.4 explains how this random γ(x) distribution is implemented and demonstrates that gain variations of up to 7% can be accommodated in the linear active Kanis & de Boer model before it becomes unstable.

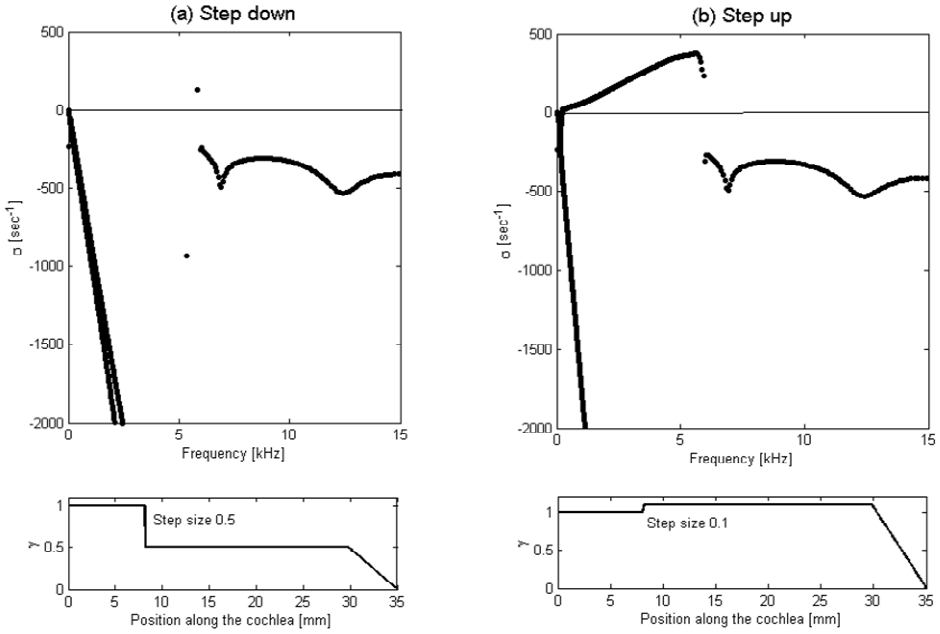

Figure 2.19 The poles of the coupled linear active Kanis & de Boer cochlear model
These results were obtained using the state space system matrix when an (a) step-down, and (b) step-up, change in the OHC gain distribution $\gamma(x)$ is introduced at the 6 kHz characteristic place. In both cases there are some poles whose real components are positive indicating instability.

2.5.3 Single tone stimulation of the coupled nonlinear state space model

A nonlinear state space model, solved in the time domain, is described in appendix F.5. A MATLAB implementation of this model was provided by Ku (2008), and the steady state time domain responses can be compared with those predicted by the quasilinear method.

Figure 2.20 compares the predicted quasilinear response of the model to a 6 kHz stimulus tone with the estimated steady state time domain solution. The time required to evaluate the response at all four stimulus levels on a 2.4 GHz computer was just 25 seconds for the quasilinear method, compared to 19 hours using the state space approach. The state space solution cannot be treated as a "gold standard" result, as the predicted amplitude of low level components, such as the 3rd harmonic response near the base of the cochlear model, is influenced by the length of the observation time as discussed in appendix F.5. However, it is useful to compare the state space and quasilinear predictions to determine if there are any discrepancies which cannot be attributed to weaknesses in the state space solution, as this may be indicative of errors in the quasilinear approach.

Figure 2.20 illustrates that the fundamental component predicted by the state space and quasilinear methods differ by less than 5 dB in the region between the base and the characteristic place. However, there are some significant discrepancies between the 3rd harmonic responses predicted by the state space and quasilinear method. For example, for a 0 dB stimulus, the state space method appears to suggest the 3rd harmonic can reach within 65 dB of the fundamental response. In contrast, the quasilinear method indicates that the 3rd harmonic response to the 0 dB stimulus is more than 100 dB below the fundamental. Similarly the 3rd harmonic response to a 60 dB stimulus is greater near the base in the state space estimate compared to the quasilinear prediction. These differences are attributed to the failure of the state space model to reach a steady state within the 30 ms observation period at all locations within the cochlear model, as illustrated in appendix F.5. For regions of the cochlear model where the state space model does reach steady state within 30 ms, such as the vicinity of the 6 kHz characteristic place, the state space and quasilinear estimates differ by less than 7 dB for stimulus levels $\geq$ 60 dB. Overall the quasilinear approach provides a better approximation to the steady state behaviour than the time domain solution, and provides a considerable saving of computational time by a factor of about 2500.

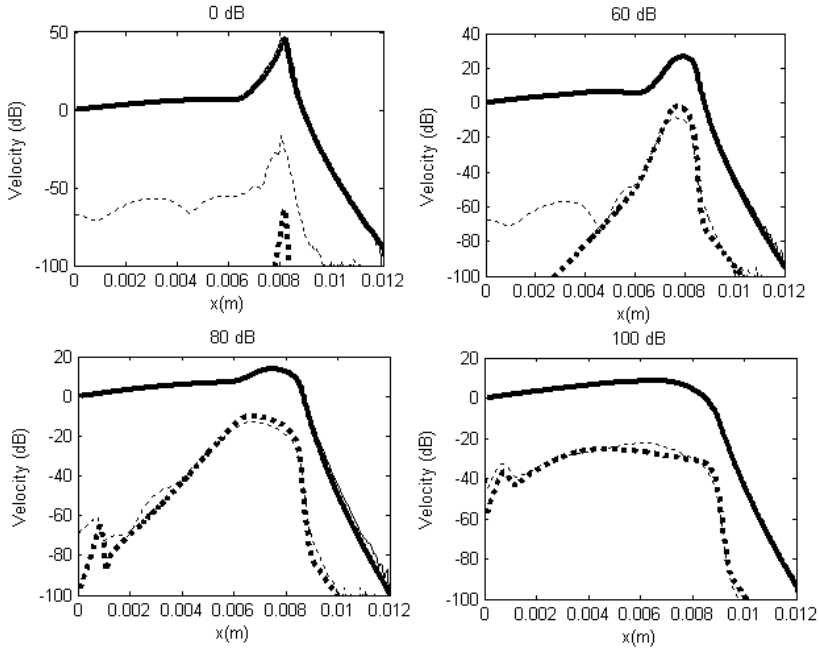

Figure 2.20 Comparison of the predicted quasilinear frequency domain and state space time domain responses to a single tone stimulus
The response of the Kanis & de Boer cochlear model to a 6 kHz stimulus tone presented at a variety of stimulus levels was estimated using the quasilinear frequency domain method (thick lines) and the state space time domain method (thin lines). The state space model was observed for 30 ms, and the steady state result was then determined from the final 20 ms of the predicted response in order to minimise transient effects. In each case a hyperbolic tangent function was used to represent the nonlinear action of the OHCs and the discrete model used N=500 element. The solid and dotted lines denote the fundamental and 3rd harmonic responses respectively. The stimulus levels are referenced to a volume velocity of 10^{-16} m^{-2}s^{-1} in the ear canal, and the CP velocity is referenced to the velocity of the fundamental response at the base of the model.

2.5.4 Two tone stimulation of the coupled nonlinear state space model

Kanis & de Boer (1996) used the quasilinear method to predict the DPs evoked in their cochlear model by two stimulus pure tones at frequencies f_1 and f_2. They compared the results with those obtained using a time domain method, as an alternative to the quasilinear approach. They observed good agreement between the steady state time domain solution and the quasilinear estimate for a range of lower side band DPs ($2f_1 - f_2$, $3f_1 - 2f_2$ and $4f_1 - 3f_2$) using a frequency ratio (f_2/f_1) of 1.2. In addition they found the $2f_1 - f_2$ DP amplitude predicted by the two approaches differed by less than 5 dB across the region of the model encompassing the f_2 best place and DP characteristic place. However, near the stapes, Kanis & de Boer note that for stimulus frequency ratios close to unity (f_2/f_1=1.04) the amplitude of the time domain result exceeds that of the quasilinear method by approximately 10 dB. For this reason, they conclude that the quasilinear approximation breaks down in the basal region of the cochlear model as the stimulus frequency ratio approaches unity. Yet although the quasilinear approximation is more likely to be compromised for small f_2/f_1 ratios, due to the increased spatial overlap of the two primary travelling waves and the evoked DP travelling waves, it is unclear why this effect should occur only in the basal region of the model whilst the approximation remains valid in the region encompassing the best places of f_2 and $2f_1 - f_2$.

For example, the travelling waves at frequencies f_2, f_1 and $2f_1 - f_2$ would be expected to exhibit little nonlinear behaviour close to the base, compared to the regions of the model that correspond to their respective best places. Therefore it is counter-intuitive that the quasilinear estimate should be valid between the characteristic places of f_2 and $2f_1 - f_2$, but not near the base of the model. In view of the discrepancy observed by Kanis & de Boer, and the difficulty interpreting it, we compare the DPs predicted by the quasilinear method with those obtained using the state space time domain model described in appendix F.5.

Figure 2.21 compares the predicted $2f_1 - f_2$ DP response of the cochlear model using the quasilinear method and time domain state space approach. The results for several stimulus frequency ratios are displayed. As mentioned in section 2.5.3, the state space result is not a "gold standard" to which the quasilinear estimate can be validated, since the effects of transients and time windowing in the analysis of the response limit its accuracy especially for low level components. However, it is useful to compare the state space and quasilinear predictions to determine if there are any discrepancies which cannot be attributed to weaknesses in the state space result, as this may be indicative of errors in the quasilinear approach. Figure 2.21 illustrates that in the vicinity of the $2f_1 - f_2$ characteristic place, the predicted amplitude of the DP component differs by less than 5 dB between the quasilinear and state space estimates. At more basal locations, there are discrepancies between the predictions, and the state space approach generally tends to suggest higher DP amplitudes than the quasilinear method estimate. Both of these observations are consistent with the findings of Kanis & de Boer (1996). However, we attribute the discrepancies between the state space time domain and quasilinear estimates of the DP amplitude near the base of the model to the limitations of the time domain approach rather than errors in the quasilinear method. This is because the state space solution is most likely to be influenced by transient and time windowing artefacts near the base, where the transient response of the model has a longer decay time (Ku, 2008) and the DP amplitude is small compared to its level at its characteristic place. For example, at a distance of 2 mm from the stapes, the time domain estimate of amplitude of the $2f_1 - f_2$ DP reduces by about 6 dB if the response is measured approximately 25 ms after the stimulus onset, compared to the response observed around 5 ms after the stimulus onset. The amplitude of the transient DP response in the basal region of the state space time domain model appears to increase as f_2/f_1 decreases, possibly due to the change in frequency of the DP component.

Figure 2.22 shows the DPs predicted by the quasilinear method and the state space time domain method for a stimulus frequency ratio of 1.2. The computational time required to establish all four DP components was approximately 4 minutes with the quasilinear approach and 10 hours for the state space method. For the larger amplitude DPs ($2f_1 - f_2$, $2f_2 - f_1$ and $3f_1 - 2f_2$) the quasilinear and state space estimates of the DP amplitude at the DP characteristic place differ by less than 5 dB. At locations where the DP amplitude is small, the state space time domain method tends to overestimate the level of the DP component due to the effects of transients and time windowing.

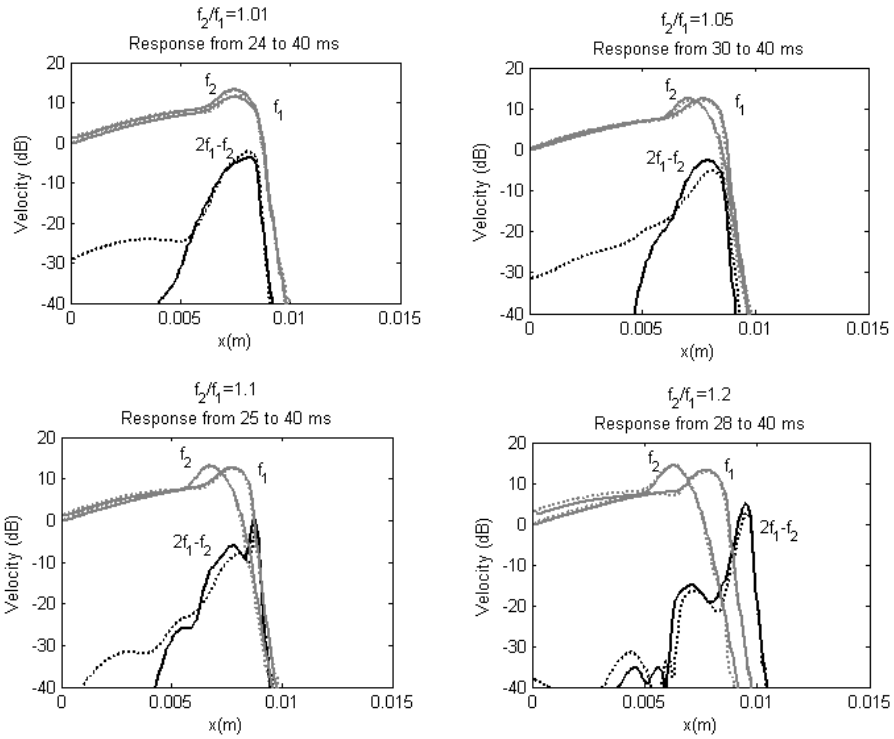

Figure 2.21 Comparison of the $2f_1 - f_2$ response to two tone stimulation predicted by the quasilinear frequency domain and state space time domain methods
The plots show the primary and $2f_1 - f_2$ DP CP velocity responses of the Kanis & de Boer cochlear model when two stimulus tones, f_1 and f_2, are applied at different stimulus ratios. The responses are estimated using the quasilinear (solid lines) and the time domain (dotted linear) state space method. In each case f_1 = 6 kHz and the stimulus levels were 81 dB re 10^{-16}m^{-2}s^{-1}. The state space model was observed for 40 ms, but only approximately the final 10 ms was used in this analysis in order to minimise the effects of transients. The CP velocity is referenced to the amplitude of the f_1 primary response at the base of the model.

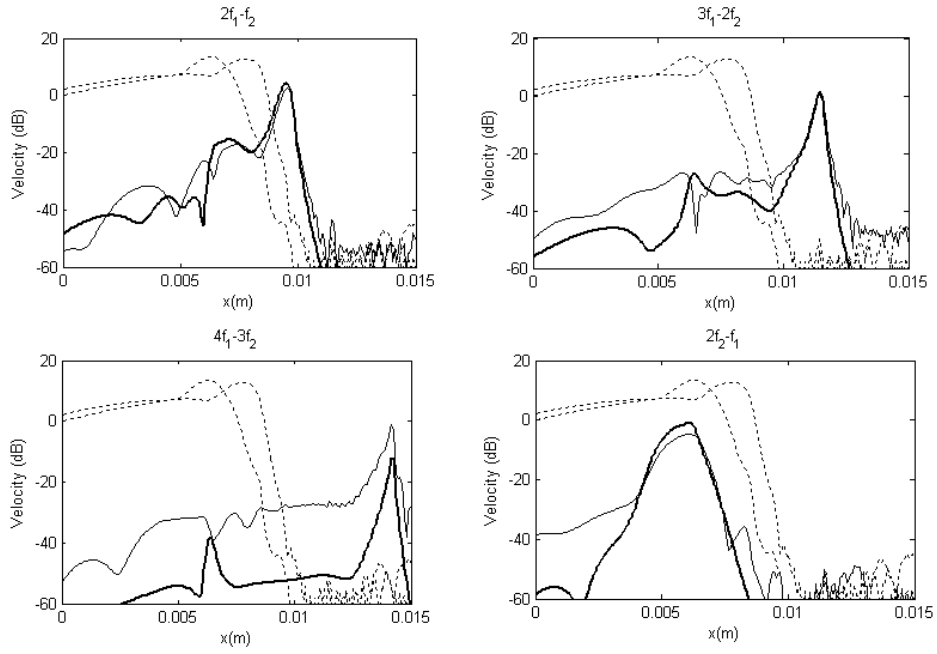

Figure 2.22 Comparison of the DP responses to two tone stimulation estimated using the quasilinear and state space methods
The plots show the predicted $2f_1 - f_2$, $3f_1 - 2f_2$, $4f_1 - 3f_2$ and $2f_2 - f_1$ DPs evoked by two stimulus tones at f_1=6 kHz and f_2=7.2 kHz (at 80 dB re 10^{-16}m^{-2}s^{-1}) in the Kanis & de Boer cochlear model. The responses were obtained using the quasilinear method (thick solid line) and the state space time domain method (thin solid line). The primary responses (dotted lines) are also shown for reference. The state space model was observed for 40 ms, but only the final 20 ms was used in this analysis to minimise the effect of transients.

In summary, we find no evidence that the quasilinear estimate of DPs evoked by two pure tone stimuli at frequencies f_1 and f_2 is invalid for any stimulus frequency ratio or DP frequency. For this reason, we proceed with the quasilinear method for predicting the response of the cochlear model.

2.5.5 Summary of state space comparison

The frequency domain state space Kanis & de Boer cochlear model allowed us to verify that the linear and quasilinear micromechanical model is stable for a broad range of stimulus frequencies when no perturbations are imposed on the active mechanics. If irregularities in the active impedance are introduced, the model remains stable and the quasilinear method is valid for small or smoothed changes.

The nonlinear time domain state space model also provided predicted responses for single tone and two tone stimulation. A comparison between these time domain results and the estimated quasilinear responses indicates that it is appropriate to use the quasilinear method across a broad range of stimulus parameters and that this allows a considerable reduction in computational time.

2.6 Conclusions regarding the Kanis & de Boer micromechanical model

In this chapter the one-dimensional cochlear model was described. We also reviewed the finite difference and WKB methods which are used to evaluate the response of the linear model, and the quasilinear method of Kanis & de Boer for estimating the response of the nonlinear model.

As summarised in section 1.9 (i), this chapter offers the following contributions:

- Development of a method to decompose the total semi-difference pressure into forward and backward travelling wave components for a linear cochlear model (section 2.3). This is in contrast to the well-used alternative approach whereby the WKB method is employed to determine the total solution from the predicted forward and backward travelling components (e.g. Talmadge *et al.*, 1998). The decomposition method appears to offer useful insight into the response evoked by internal sources within the cochlear model.
- A modification of the iterative procedure used in the quasilinear method which improves the rate of convergence of the method when evaluating harmonic responses (appendix E.3).
- Development of a state space model of the Kanis & de Boer micromechanical model, which has been implemented in both the frequency and time domains in MATLAB (section 2.5 and appendix F). A substantial portion of this development was achieved by extending the work of Ku (2008). However, this extension has only been possible due to the relationship which we were able to establish between the Kanis & de Boer micromechanical model and that used by Ku (appendix F.4).

3. Alternative micromechanical models

The response of a coupled cochlear model, such as that of Kanis & de Boer described in chapter 2, is dependent on several micromechanical properties. These include the nonlinear function used to represent the action of the outer hair cells (OHCs), the position of this nonlinearity within the micromechanical feedback loop, the nature of the displacement which acts as the input to the nonlinear function, and the spatial distributions of the micromechanical parameters. In this chapter we consider the influence of these factors on the predicted response of the model, and select the most appropriate micromechanical properties with which to proceed to investigate distortion product otoacoustic emissions.

3.1 The nonlinear function

The cochlear model developed by Kanis & de Boer is a dynamic nonlinear model (Harte *et al*., 2005) and is therefore suitable for replicating the nonlinear cochlear response to stimulation (section 1.2.3). However the hyperbolic tangent function which they use to represent the nonlinear behaviour of the OHCs is symmetric and so does not generate even-order harmonic distortion products (appendix G.1). As physiological measurements suggest that both even- and odd- order harmonic components are generated inside the cochlea in response to a single tone stimulus (Cooper, 1998; Parthasarathi *et al.*, 2003; Olsen, 2004), we consider an asymmetric alternative to the hyperbolic tangent nonlinearity: the first order Boltzmann function. Use of this nonlinear function in the cochlear model is in good agreement with the experimental observation that the response of the OHCs in frogs and mice can be well-matched by a first order Boltzmann function (Pickles, 1982; Dallos (1996); Kros *et al.*, 1996).

3.1.1 The first order Boltzmann function

Several different asymmetric nonlinear functions have been used in cochlear models to represent the nonlinear action of the OHCs in the past (Chertoff *et al.*, 2001; Bian *et al.*, 2002), but the first order Boltzmann function is the simplest choice. It has been successfully applied to cochlear models in the past, such as the uncoupled model of Cooper (1998) in which this nonlinear function was used to explain his observations of the odd and even harmonic components evoked by a single tone stimulus in the guinea pig cochlea.

The first order Boltzmann function is defined in (3.1). The value of α, which determines the maximum output of the nonlinearity and has the same dimensions as the input u, can be set so that the response of the model begins to saturate at a specified stimulus level. The dimensionless constant β controls the asymmetry of the function, and the first order Boltzmann function becomes identical to the hyperbolic tangent function for β=1. The dimensionless constant η is assigned a value of 1 when, as in this case, the input u has units of pressure[2].

$$F(u) = \frac{\alpha}{\eta}\left(\frac{1}{1+\beta e^{-\eta u/\gamma_B}} - \frac{1}{1+\beta}\right) \tag{3.1}$$

The value of γ_B, which has the same dimensions as the input, is constrained such that

[2] In section 3.3 the position of the nonlinearity within the micromechanical feedback loop moves, and so the value of η is changed to 2.5×10^{10} to compensate for the change in units of the input.

$$\left.\frac{dF(u)}{du}\right|_{u=0} = 1 \text{ so } \gamma_B = \frac{\alpha\beta}{(1+\beta)^2} \tag{3.2}$$

This ensures that the nonlinearity provides 0 dB gain to the fundamental component at low stimulus levels. The way in which the parameters α and β control the form of the first order Boltzmann function is illustrated in figure 3.1. This shows that the parameter α affects the input level at which saturation occurs, as well as controlling the maximum output of the nonlinear function. Therefore, for a given input level, increasing the value of α reduces the amplitude of both odd- and even- harmonic components in the output of the function. In addition, increasing α increases the compression threshold, which we shall define as the minimum input level at which the growth rate of the fundamental component of the nonlinear function output falls below 1 dB/dB. The value of the parameter β influences the relative amplitude of the odd and even harmonic components in the output of the nonlinear function. For example, the function becomes more asymmetric as β increases and therefore the amplitude of the even order harmonics, relative to the odd order harmonics, should increase as β increases. Throughout this section, these parameters are arbitrarily fixed such that α=2 and β=3 (so $\gamma_B = 0.38$) for simplicity. Discussion regarding the selection of suitable α and β values for the cochlea is deferred until section 3.5.

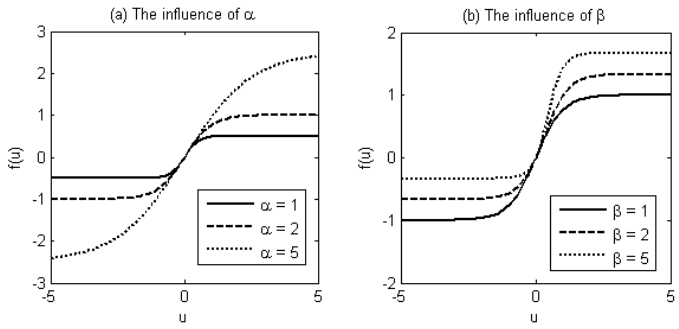

Figure 3.1 The first order Boltzmann function
The plots show the influence of the parameters α and β on the form of the first order Boltzmann function, defined in equation (3.1). (a) The influence of α, for β=1. (b) The influence of β for α=2. In each case γ_B is constrained so that the condition given in (3.2) is satisfied. Note that if α=2 and β=1, the first order Boltzmann function is identical to a hyperbolic tangent function.

3.1.2 The nonlinearity in isolation

Figure 3.2 shows the output of an isolated first order Boltzmann function when a sinusoidal input is applied at a variety of input levels. It demonstrates that both even- and odd- order harmonic components occur in the output, as anticipated. In contrast, the 2nd harmonic and DC components are absent in the output of the hyperbolic tangent function.

The spectrum of the distortion products (DPs) which arise in the output of the isolated first order Boltzmann function when two equal amplitude pure tones (f_1 and f_2) are applied at the input, is shown in Figure 3.3. Both odd- and even- order DPs are evident in the output of this nonlinear function. In contrast, only odd-order DPs are present in the output of an isolated hyperbolic tangent function.

(a)

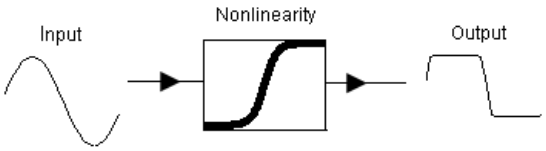

(b)

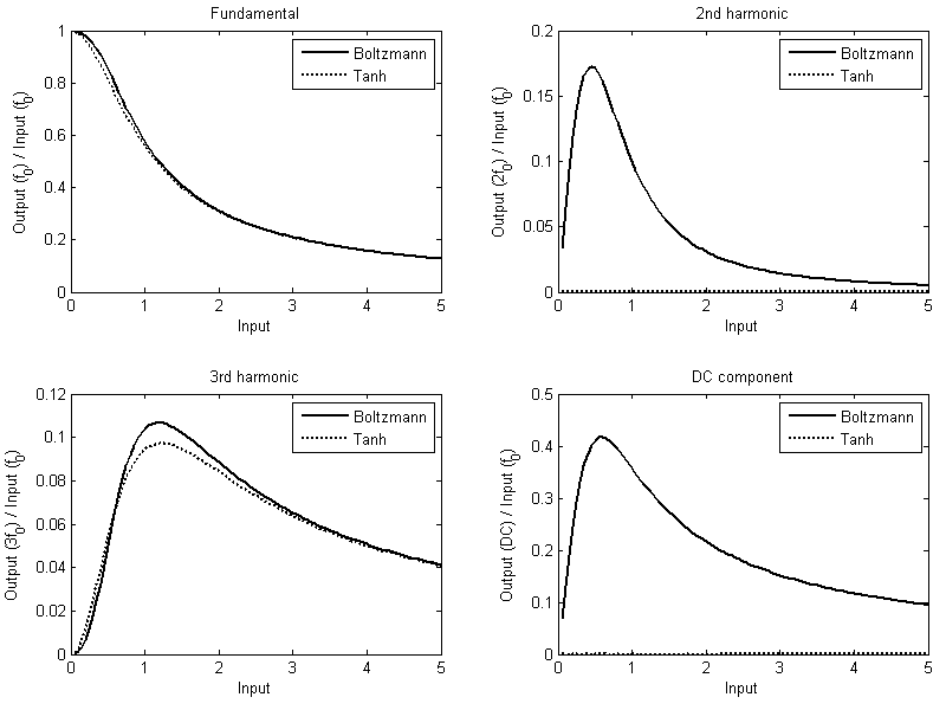

Figure 3.2 The response of the isolated nonlinear function to a single tone input
The plots show (a) an illustration of the nonlinear function in isolation driven by a sinusoid and (b) the transfer response (the amplitude of the output component per unit input amplitude) of the first order Boltzmann function (β=3) compared to that of the hyperbolic tangent function (Tanh) for a range of frequency components. Note that no even order harmonics are produced by the symmetric tanh function, including a DC component. The units of the input are arbitrary, and α=2 so γ_B=0.38.

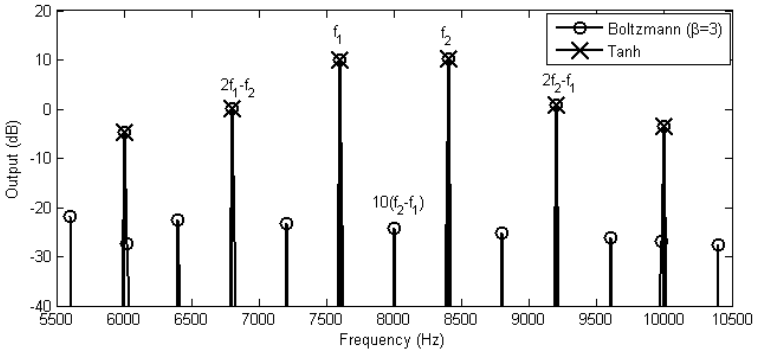

Figure 3.3 The response of the isolated nonlinear function to two tone stimulation
The DPs generated by the nonlinear function in isolation are shown. The input contains two equal amplitude tones at frequencies f_1=7.6 kHz and f_2=8.4 kHz. Results are given for the Tanh nonlinearity and the first order Boltzmann function (β=3). The units of the input and output are arbitrary, but equal stimulus levels are used for f_1 and f_2. In the Boltzmann function, α=2 so γ_B=0.38.

There are few physiological measurements of the harmonic response of the cochlear partition to single tone stimulation. However, both Cooper (1998) and Olsen (2004) have observed the 2nd harmonic component of the mechanical response of the mammalian cochlea to acoustic stimulation, and their results demonstrate that the amplitude of this component can reach within -20 to -10 dB of the level of the fundamental response. The coupled cochlear model will only be capable of simulating the generation of a 2nd harmonic component in response to single tone stimulation, or predicting even order DPs in response to two tone stimulation, if the Boltzmann function is used instead of the hyperbolic tangent function. For this reason, we proceed using a first order Boltzmann function to represent the nonlinear action of the OHCs. In the following sections of this chapter we demonstrate that several other features of the micromechanical model influence the amplitude of the harmonic and DP responses, in addition to the choice of the nonlinear function. For this reason we defer selecting values of the Boltzmann function parameters, α and β, for the cochlear model until these other factors have been considered.

3.2 The influence of the position of the nonlinearity within the micromechanical feedback loop

For a linear active cochlear model, each micromechanical element pictured in figure 2.2 can be represented by the feedback diagram shown in figure 3.4a (Neely, 1985). In this illustration the linear pressure output of the feedback loop which represents the action of the OHCs, p_{OHC}^{lin}, is assumed to act on the CP in the same way as the transmembrane pressure, p_d, as discussed in section 2.4.1. Filter 1 corresponds to the passive mechanical impedance of the BM. Filter 2 is a simplified representation of the impedance of the active OHC complex, incorporating the many factors that contribute to the action of the OHCs including linear components of the mechanoelectrical and electromechanical transduction processes associated with the cells. The nonlinearity can be positioned either before filter 2 (figure 3.4b) as suggested by Cooper (1998) or after filter 2 (figure 3.4c) as implicit in the model of Kanis & de Boer (1993) described in section 2.4.1. In this section we consider the influence of the position of the nonlinearity on the predicted response of a cochlear model.

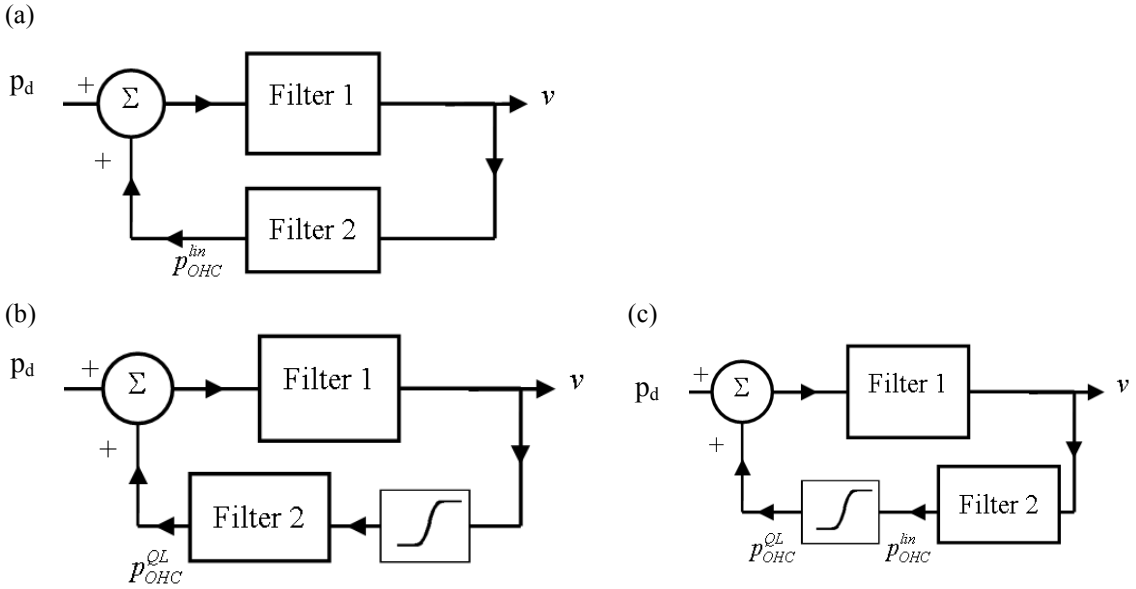

Figure 3.4 Block diagrams of different micromechanical feedback loop arrangements
An example of a linear active model (a) and two active nonlinear models (b & c) are shown. The semi-difference pressure across the cochlear partition, the velocity response of the basilar membrane, the linear pressure output of the outer hair cells and the quasilinear output of the outer hair cells are denoted by p_d, v, p_{OHC}^{lin}, and p_{OHC}^{QL} respectively. Filters 1 and 2 represent the admittance of the basilar membrane and the dynamics of the outer hair cells respectively.

A summary of the results of this investigation were presented in a letter to the editor of the Journal of The Acoustical Society of America, How *et al.* (2010), re-printed in appendix H. The simulated results presented in this section differ quantitatively from those of How *et al.*because of differences in the parameters of the nonlinear function. For example, in this section we use a value of β equal to 3 and a uniform value of α for the coupled cochlear model. In contrast, How *et al.*use a β value of 1.2 and a spatial distribution of α so that it increases from the base to the apex for reasons discussed which will be discussed in section 3.5.

3.2.1 The position of the nonlinearity in an uncoupled element

Figure 3.5 shows the predicted response of a single uncoupled micromechanical element, located at the 6 kHz characteristic place, to sinusoidal stimulation. This element has micromechanical properties identical to those described by Kanis & de Boer, in all but two aspects. First, a first order Boltzmann function is used to represent the nonlinear action of the OHCs rather than the hyperbolic tangent function employed by Kanis & de Boer. Secondly, the simulation is performed twice: once with the nonlinearity positioned *before* filter 2, and again with it positioned *after* filter 2. The Boltzmann function parameter β is set equal to 3 for both of these arrangements. The value of α is changed from 5 to 10 when the nonlinear function is moved from before to after filter 2 so that the amplitude of the fundamental component is the same in each case and the dimensions of α are the same as the input to the nonlinear function. It should also be noted that the dimensionless Boltzmann function parameter η is assigned a value of 2.5×10^{10} rather than 1, when the nonlinearity is positioned *befo*re, instead of aft*er*, filter 2 to compensate for the change in the units of the input to the nonlinearity. As a result of these Boltzmann parameter selections, the fundamental response of the element changes by less than 1 dB when the position of the nonlinearity within the micromechanical feedback loop is altered, as shown in figure 3.5.

Figure 3.5 also demonstrates that, for both micromechanical arrangements, local maxima occur in the simulated *harmonic* responses when either the fundamental frequency, or the harmonic frequency, is equal to the characteristic frequency of the element. Although the amplitude of the fundamental response is not significantly affected, the amplitude of the harmonic components is influenced by the position of the nonlinearity within the micromechanical feedback loop. For example, the local maximum in the 2nd harmonic response which occurs when the stimulus frequency is close to the characteristic frequency of the uncoupled element decreases in amplitude by 8 dB if the nonlinearity is moved from *before* to *after* filter 2 in the micromechanical feedback loop. Conversely the other local maximum in the 2nd harmonic response, which occurs when the 2nd harmonic frequency corresponds to the characteristic frequency of the element, increases in amplitude by 13 dB if the same change is made to the micromechanical feedback loop.

When considering the generation of the 2nd harmonic response within the micromechanical feedback loop we denote the stimulus frequency as f_0 and therefore the 2nd harmonic frequency is $2f_0$. Figure 3.6a illustrates the passage of the 2nd harmonic component through the micromechanical feedback loop. It shows that filter 2 will either operate on a signal at $2f_0$ or f_0 depending on whether the nonlinearity is positioned *before* or *after* filter 2 respectively. If the response of filter 2 were independent of frequency, then the position of the nonlinear function relative to this filter would have no influence on the amplitude of the 2nd harmonic component generated by the feedback loop. However, this is not the case. Figure 3.6b shows the normalised amplitudes of filters 1 and 2 for an uncoupled micromechanical element located at the 6 kHz characteristic place. This figure is similar to a graph presented in How *et al.* (2010), but it has been modified to emphasise the influence on the 2nd harmonic component of the position of the nonlinearity relative to filter 2. Figure 3.6b demonstrates that if f_0 = 6 kHz and $2f_0$ = 12 kHz, then the amplitude response of filter 2 is much smaller at $2f_0$ compared to f_0. Therefore, when a stimulus is present at f_0 = 6 kHz, the amplitude of the 2nd harmonic is reduced when the nonlinearity is positioned before, rather than after, filter 2. In contrast, if f_0 = 3 kHz and $2f_0$ = 6 kHz, then the amplitude response of filter 2 is approximately double at $2f_0$ compared to f_0. For this reason, when the stimulus is presented at f_0 = 3 kHz, the amplitude of the 2nd harmonic component increases when the nonlinearity is positioned before, rather than after, filter 2. In summary, the influence of the position of the nonlinearity within the micromechanical feedback loop on the simulated 2nd harmonic response shown in figure 3.5 is associated with the frequency dependence of filter 2 which represents the impedance of the OHC complex.

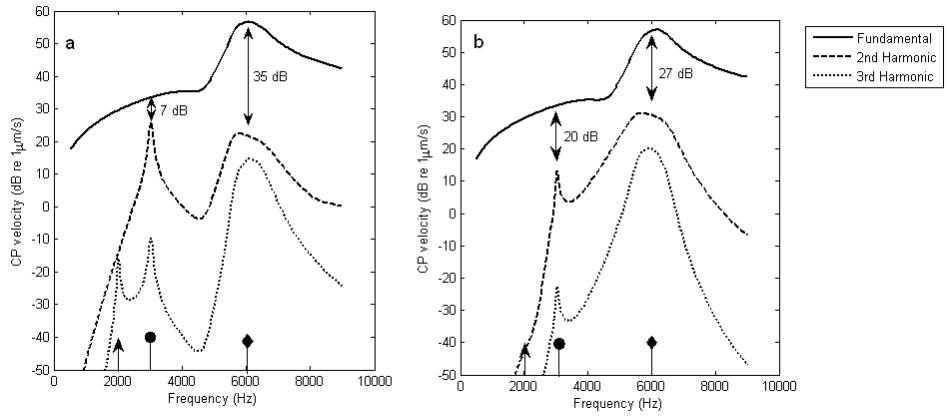

Figure 3.5 The frequency response of a single micromechanical element
A range of stimulus frequencies, at a level of 1 Pa, are presented to a single micromechanical element located at the 6 kHz characteristic place. The nonlinearity is positioned either (a) before or (b) after filter 2, as shown in Figure 3.4. A first order Boltzmann function, with β=3 and (a) α=5 or (b) α=10, is used to represent the nonlinear action of the OHCs. The value of α was selected so that the fundamental response is unaffected by the change in the position of the nonlinearity within the micromechanical feedback loop. The diamond, circular and triangular arrow heads indicate stimulus frequencies at which the fundamental, 2nd harmonic or 3rd harmonic frequency correspond to the characteristic frequency of the micromechanical element respectively.

(a)

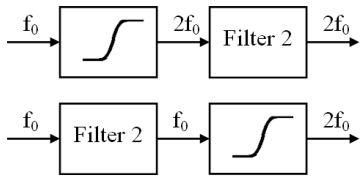

(b)

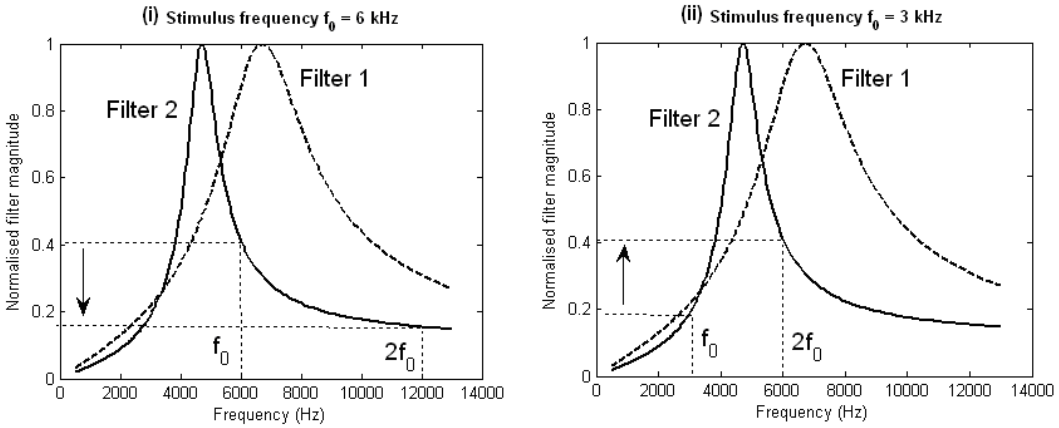

Figure 3.6 The frequency response of filters 1 and 2 in the Kanis & de Boer cochlear model
Plot (a) shows the frequency of the signal of interest when predicting the 2nd harmonic component of the response to a stimulus presented at frequency f_0. The output of the nonlinear function will also contain components at the fundamental and other harmonic frequencies, but these are neglected for simplicity. (b) illustrates the assumed frequency response functions for filters 1 (dashed line) and 2 (solid line), associated with the passive BM admittance and OHC impedance respectively, observed at the 6 kHz characteristic place in the Kanis & de Boer (1993) model of the human cochlea. Dotted lines indicate the difference in the amplitude of filter 2 at f_0 and $2f_0$ when the stimulus is presented at (i) f_0 = 6 kHz and (ii) f_0 = 3 kHz.

3.2.2 The position of the nonlinearity in a coupled model

In this section the influence of the position of the nonlinearity within the micromechanical feedback loop on the coupled cochlear model is described. The value of α is changed from 0.8 to 2 when the nonlinear function is moved from *before* to *after* filter 2 so that the fundamental component has the same saturation threshold in each case. As for an uncoupled element, the dimensionless Boltzmann function parameter η is assigned a value of 2.5×10^{10} rather than 1, when the nonlinearity is positioned *before,* instead of *after*, filter 2 to compensate for the change in the units of the input to the nonlinearity. In these simulations, all of the Boltzmann function parameters are uniformly distributed along the cochlear partition.

The effect on the harmonic response to a single tone stimulus

Figure 3.7(i) shows the response of the guinea pig cochlea to single tone stimulation at the 17 − 19 kHz characteristic place, observed by Cooper (1998). The fundamental, 2nd harmonic and 3rd harmonic components of the response are given for a range of stimulus frequencies between 6 and 21 kHz. This figure also presents the simulated response of the coupled cochlear model, observed at the 6 kHz characteristic place. The stimulation is performed twice, with the nonlinear function positioned either (ii) before or (iii) after filter 2 as illustrated in figure 3.4(b and c)**.** As a consequence of the selected Boltzmann function parameters, the *fundamental* response predicted by the model changes by less than 1.5 dB when the position of the nonlinearity within the micromechanical feedback loop is altered. The magnitude of this change is comparable to the scale of numerical errors that can arise in the computation process (appendix B.1), and so it is not considered significant. However, although the simulated fundamental response is unaffected, the position of the nonlinearity within the micromechanical feedback loop does influence the harmonic responses of the coupled model. For example, figure 3.7 shows that predicted the 2nd harmonic response observed at the 6 kHz characteristic place in the cochlear model has two local maxima which occur when the stimulus frequency is equal to either 6 or 3 kHz. For these stimuli either the fundamental or 2nd harmonic component frequencies correspond to the characteristic frequency of the observation location. If the nonlinearity is positioned *before*, rather than *after*, filter 2 in the micromechanical feedback loop then the predicted amplitude of the 2nd harmonic component of the response at a 3 kHz stimulus tone increases from − 10 to 3 dB relative to the fundamental component. In addition, the same change in the micromechanical model causes the predicted amplitude of the 2nd harmonic component to decrease from − 24 to − 35 dB relative to the fundamental response for a 6 kHz stimulus. Therefore, positioning the nonlinearity before rather than after filter 2 either enhances or reduces the amplitude of the 2nd harmonic response when either the 2nd harmonic or fundamental component frequency is equal to the characteristic frequency respectively. These effects are largely uninfluenced by other model parameters such as the Boltzmann function parameters α and β. The same effects were observed for the uncoupled model in section 3.2.1, and an explanation for the influence of the position of the nonlinear function within the micromechanical feedback loop was proposed.

Although the nature of the influence of the position of the nonlinear function is not generally affected by other model parameters, the amplitude of the predicted level of the 2nd harmonic response relative to the fundamental response is sensitive. For example, when the 2nd harmonic frequency is equal to the characteristic frequency of the observation location, the amplitude of the 2nd harmonic component relative to the fundamental response depends on the Boltzmann function parameters α and β, in addition to the position of the nonlinearity within the micromechanical feedback loop. For this reason, it is difficult to determine whether the nonlinearity should be positioned either before or after filter 2 in order to best replicate the results of Cooper (1998).

However, How *et al.* (2010) suggest that for suitable choices of α and β discussed in section 3.5, the results of Cooper (1998) are most accurately simulated by the model if the nonlinearity is positioned before rather than after filter 2.

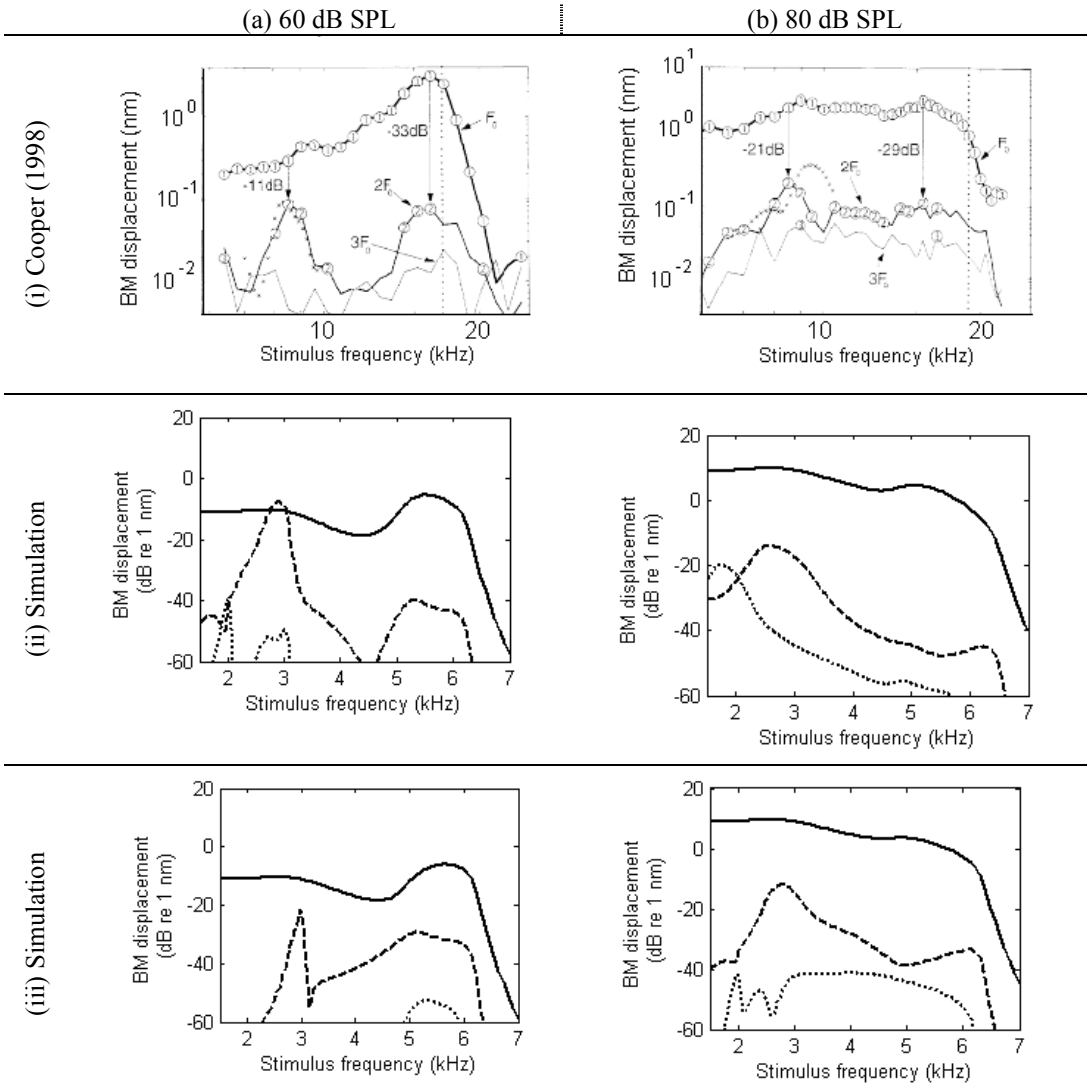

Figure 3.7 The influence of the position of the nonlinearity within the micromechanical feedback loop on the harmonic response of the coupled cochlear model
(i) The measured response of the BM to a single tone stimulus in the guinea pig cochlea, observed at the 17 − 19 kHz characteristic place [From figure 2 of Cooper (1998), with permission from John Wiley & Sons]. The stimulus was presented at (a) 60 dB SPL and (b) 80 dB SPL. The fundamental, 2nd harmonic, and 3rd harmonic components of the response are denoted by F_0, $2F_0$ and $3F_0$ respectively. (ii) & (iii) The simulated response of the coupled cochlear model to a single tone stimulus presented at (a) 60 dB SPL and (b) 80 dB SPL, observed at the 6 kHz characteristic place. The nonlinearity is positioned either (ii) *befo**re*** or (iii) aft***er*** filter 2, as shown in figure 3.4. A first order Boltzmann function, with β=3 and (ii) α =0.05 or (iii) α=0.13, is used to represent the nonlinear action of the OHCs. The predicted fundamental, 2nd harmonic and 3rd harmonic components of the BM displacement are denoted by the solid, dashed and dotted lines respectively.

The effect on the distortion products evoked by two tone stimulation

Figure 3.8a shows the predicted response of the coupled model evoked by two stimulus tones at frequencies f_1 and f_2. Only the largest amplitude DP components of the BM velocity are shown. Higher order components, such as the $3f_1 - 2f_2$ and $3f_2 - 2f_1$ DPs, were at least 60 dB below the primary responses. The amplitude of the primary responses (f_1 and f_2) vary by less than 1 dB if the position of the nonlinearity within the micromechanical feedback loop is moved. As this change is of comparable magnitude to the scale of numerical errors that can arise in the computation process (appendix B.1), it is not considered significant. Although the primary responses are unaffected, the DPs can be influenced by the position of the nonlinearity within the feedback loop. For example, the amplitude of the predicted $2f_1 - f_2$ and $3f_1 - 2f_2$ DPs decrease by 5 and 16 dB respectively when the nonlinearity is moved from *be*fo*re,* to af*ter,* filter 2.

Figure 3.8b shows the spectrum recorded from the BM of the chinchilla cochlea in response to two tone stimulation by Robles *et al.*(1997). The middle ear model and the micromechanical parameters of the cochlear model are designed to replicate the response of the human ear, rather than the chinchilla ear, and so it is not appropriate to compare the absolute levels of the spectral components observed experimentally with those predicted by the model. Comparison of the relative amplitudes of the spectral components between the simulation and physiological measures is more appropriate. It should be noted that a lower stimulation level was used in the model, compared to the experimental study, in order to achieve a broad agreement in the amplitude of the $2f_1 - f_2$ DP, relative to the f_1 component in both the simulated and experimental result. Robles *et al.*(1997) observe that the amplitudes of the $2f_1 - f_2$ and $3f_1 - 2f_2$ DPs are approximately 22 and 28 dB below that of the f_1 component of the BM velocity respectively. The model simulation predicts these values to be equal to 23 dB and 65 dB respectively, or 29 and 81 dB respectively, depending on whether the nonlinearity is positioned before, or after, filter 2 in the micromechanical feedback loop. Although both arrangements underestimate the amplitude of the 4^{th} order DP, the best agreement with the physiological measure is observed when the micromechanical feedback loop incorporates the nonlinear function positioned before filter 2.

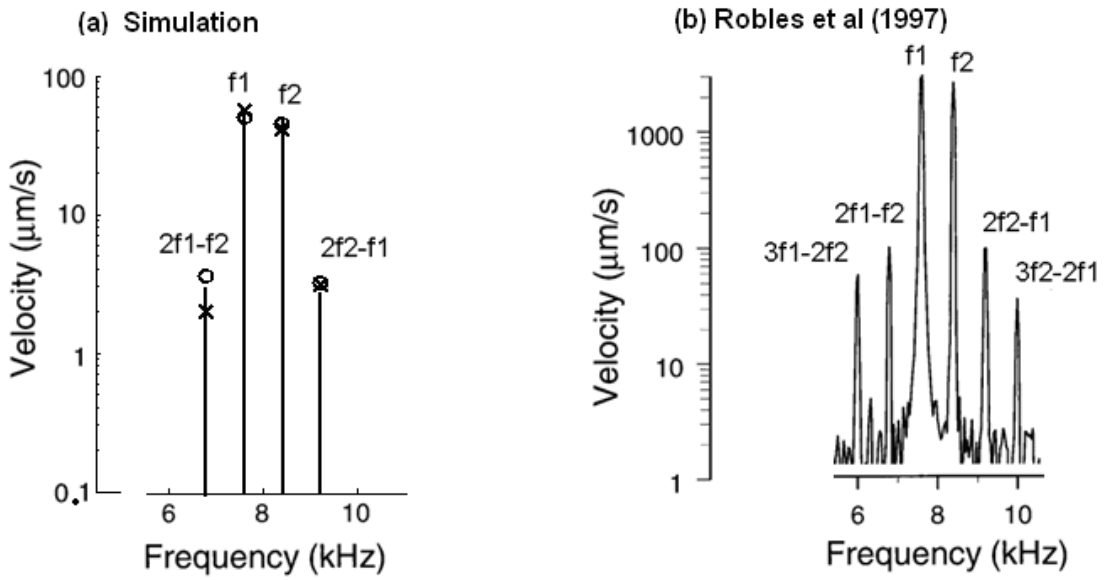

Figure 3.8 The influence of the position of the nonlinearity in the micromechanical feedback loop on the response of the model to two tone stimulation
(a) The predicted CP velocity components, evoked by two tones (L_1=L_2=60 dB re 10^{-8}m/s), at frequencies f_1, f_2, $2f_1 - f_2$, and $2f_2 - f_1$. The result is observed at the characteristic place of 8.1 kHz, as at this position in the cochlear model the f_1 and f_2 components have almost equal amplitude. The simulation is performed twice: with nonlinearity positioned either *before* (circles) or *after* (crosses) the OHC dynamics in the micromechanical feedback loop. The Boltzmann function uses β=3 and the parameter α is set so that the primary tones are equally saturated for both micromechanical arrangements so that α=0.8 and α=2 when the nonlinearity is positioned *befo*re and aft*er* filter 2 respectively. (b) The physiological measurement of Robles *et al.*at the 8 kHz characteristic place in the chinchilla cochlea (L_1=L_2=80 dB SPL), used with permission. In all cases stimuli were presented at f_1= 7.6 kHz, f_2=8.4 kHz (f_2/f_1=1.11). [From figure 1 of Robles *et al.* (1997), with permission from Am. Physiol. Soc]

In summary, the predicted harmonics and DPs in the cochlear model have higher amplitudes, relative to the fundamental response, if the nonlinearity is positioned *before*, rather than a*fter*, filter 2. The influence of the position of the nonlinear function within the micromechanical feedback loop may not be evident in the fundamental response, as the micromechanical parameters can be adjusted to compensate for any affect on the fundamental component. Therefore it is important to consider the harmonic response of the model when deciding where to position the nonlinear function within the micromechanical feedback loop of a simple cochlear model such as the one considered in this chapter. In section 3.5, we opt to position the nonlinearity before filter 2 for further work. However, it is feasible that either micromechanical arrangement could be used, provided that the parameters of the Boltzmann function (α and β) are appropriately set to provide sufficient levels of harmonic and DP components in each case.

3.3 Vertical or shear motion input to the nonlinear function

When the Kanis & de Boer cochlear model is modified so that the nonlinearity is positioned before filter 2 in the micromechanical feedback loop, the input to the nonlinear function is dependent on the vertical velocity of the BM, v. However the anatomical orientation of the OHCs within the organ of Corti, illustrated in figure 3.9, suggests that motion of the OHC stereocilia arises not from this vertical movement, but from the relative shear motion of the BM and TM (Lim, 1980; Gueta *et al.*, 2008). As the nonlinearity in the cochlear model is attributed with the action of the OHCs, it may therefore be more appropriate to use a *shear* motion, rather than a *vertical* motion, to determine the input to the nonlinear function.

Neely & Kim (1986) suggest a model in which the difference in shear displacement between the tectorial membrane (TM) and the organ of Corti (OC), ξ, provides the input to the OHCs. The shear displacement, ξ, is assumed to depend linearly on the BM velocity, v, as shown in (3.3), where Z_2 and Z_3 denote the impedances of the TM and the coupling between the TM and OC respectively and are defined in appendix E.6. The dimensionless constants b_w and g_{lever} have values of 0.4 and 1, and represent the ratio of the average displacement across the width of the CP to the maximum displacement over the width of the BM, and the BM to IHC lever gain respectively.

$$\xi(x,\omega) = \frac{g_{lever}}{b_w} \frac{Z_2(x,\omega)}{Z_2(x,\omega)+Z_3(x,\omega)} \frac{v(x,\omega)}{i\omega} \tag{3.3}$$

Figure 3.10 shows a block diagram representation of a single micromechanical feedback loop, and how it is modified when the input to the nonlinearity is switched from v to ξ. It illustrates that this change effectively introduces filter 3 into the micromechanical feedback loop, which represents the response of the TM and the coupling between the TM and OC.

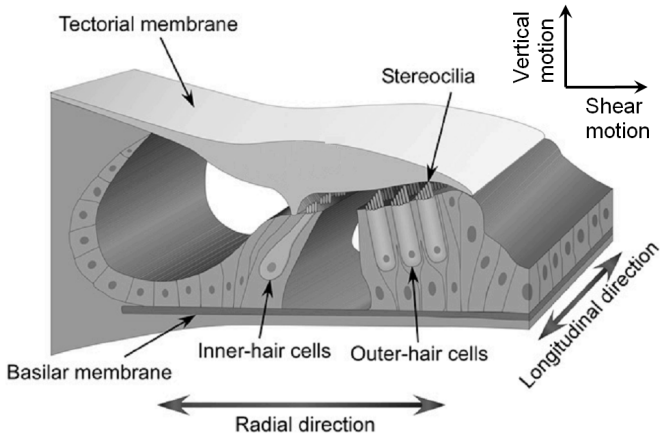

Figure 3.9 Illustration of the anatomy of the cochlear partition
This shows the position of the outer hair cells (OHCs) with respect to the Basilar membrane and Tectorial membrane. The orientation of the motion described in the text as "vertical" and "shear" is also shown for reference. [From figure 1 of Gueta *et al.* (2008), with permission from the author].

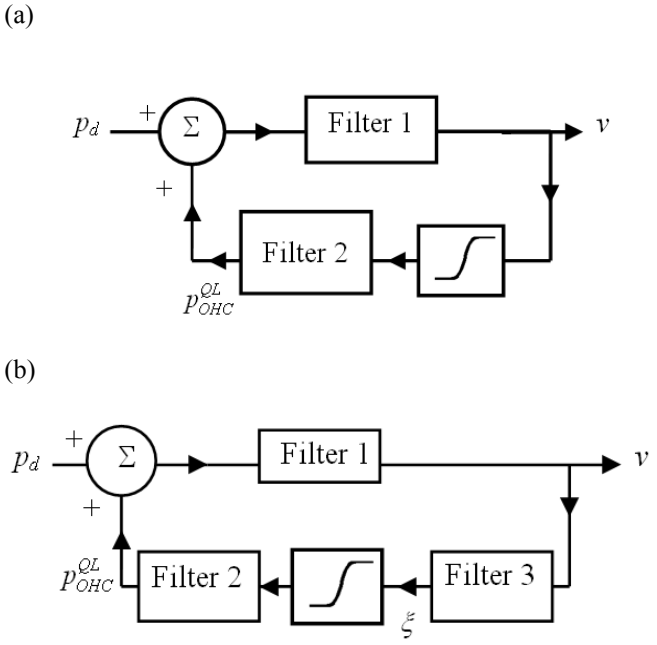

Figure 3.10. Block diagrams of micromechanical feedback loops which differ in the input to the nonlinear function.
The input to the nonlinear function is either (a) the vertical BM velocity v or (b) the difference in shear displacement of the TM and OC, ξ. Filters 1 and 2 represent the admittance of the basilar membrane and the dynamics of the outer hair cells respectively. The shear displacement, ξ, is assumed to have linear dependence on v, as shown in equation (3.3), so that filter 3 can be described by the impedance

$$\frac{g_{lever}}{i\omega b_w}\frac{Z_2}{Z_2+Z_3}$$

In this section, the influence of the orientation of the input to the nonlinear function is considered by comparing the response of the model when the input to the nonlinearity is switched from *vertical* BM velocity v (Figure 3.10a), to *shear* displacement ξ (figure 3.10b). In all simulations the nonlinearity is positioned before filter 2 in the micromechanical feedback loop, and a first order Boltzmann function (β=3) is used to represent the nonlinear action of the OHCs.

3.3.1 The influence on the uncoupled model

We start by considering the effect of changing the input to nonlinear function from *vertical* BM velocity v (figure 3.10a), to *shear* displacement ξ (figure 3.10b) on a single micromechanical element within the cochlear model. Figure 3.11 shows the response of an uncoupled element to a single tone stimulus presented at a range of frequencies. The simulation is performed twice with the input to the nonlinearity determined by either the vertical BM velocity, v, or the shear displacement. ξ. The result demonstrates that there is a range of stimulus frequencies, between about 4 and 6 kHz, at which the amplitude of the harmonic components *increase* when the input to the nonlinearity changes from v to ξ. For lower stimulus frequencies (≤ 3 kHz), the amplitude of the harmonic components tends to *decrease* if the nonlinearity input changes from v to ξ.

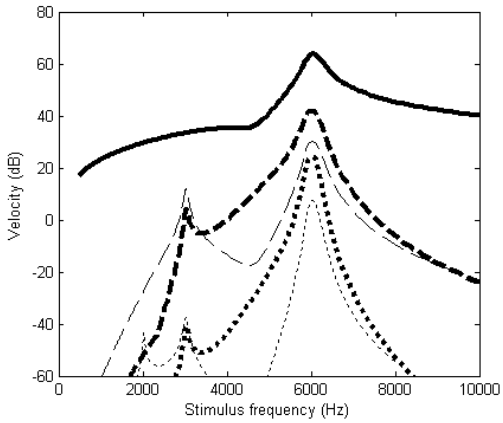

Figure 3.11 The influence of the input to the nonlinear function on the response of a single micromechanical element
The fundamental (solid line), 2nd harmonic (dashed line) and 3rd harmonic (dotted line) components of the cochlear partition velocity are shown for a micromechanical element at the 6 kHz characteristic place. The thin lines and thick lines correspond to the micromechanical models illustrated in figure 3.10(a) and (b) respectively. The nonlinear action of the OHCs is represented by a first order Boltzmann function with β=3 and α=24 (for figure 3.10a) or α=20 (figure 3.10b).

The frequency responses of the filters 1, 2 and 3 used in figure 3.10 for the micromechanical element located at the 6 kHz characteristic place are given in figure 3.12. The filter amplitudes in figure 3.12 are normalized with respect to the filter amplitude at 6 kHz because the Boltzmann function parameter α has been adjusted so that the fundamental component exhibits equal saturation at this stimulus frequency in both micromechanical arrangements. When the input to the nonlinearity is changed from v to ξ, there are two changes to the micromechanical feedback loop: filter 3 is introduced and the form of filter 2 changes to accommodate the change in the output of the nonlinear function from v to ξ.

If the vertical BM velocity, v, provides the input to the nonlinear function, the input is determined purely by filter 1 for a given stimulus frequency (figure 3.10a). If instead the shear displacement ξ acts as the input to the nonlinear function, then the input is determined by both filters 1 and 3 (figure 3.10b). Filter 1 has the same frequency response in both micromechanical arrangements. However, filter 3 has bandpass characteristics such that the input to the nonlinearity is enhanced relative to a 6 kHz signal, for stimulus frequencies between 4 and 6 kHz. In contrast, filter 3 attenuates the input to the nonlinearity, relative to a 6 kHz signal, for very low and very high stimulus frequencies. Therefore, when the input to the nonlinear function is changed from v to ξ, the introduction of filter 3 into the micromechanical feedback loop increases the input to the nonlinearity for stimulus frequencies at 4 − 6 kHz, and reduces the input for all other stimulus frequencies. For this reason, the amplitude of the harmonic components increase at stimulus frequencies between 4 and 6 kHz, and decreases at other frequencies, when the input to the nonlinearity is changed from v to ξ, as observed in figure 3.11.

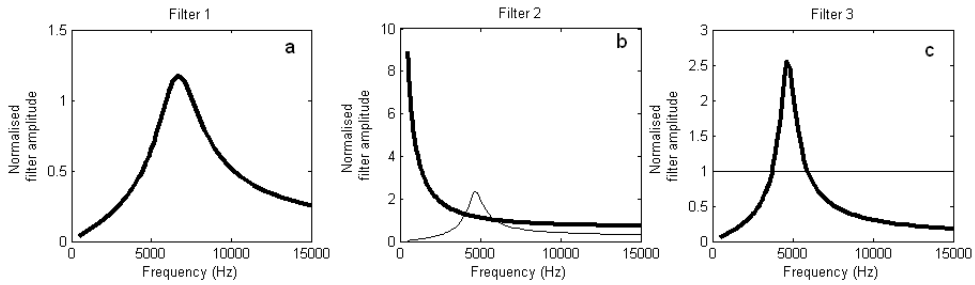

Figure 3.12 The form of the filters 1, 2 and 3 in the Kanis & de Boer cochlear model
Plots (a) to (c) show the responses of filter 1, 2 and 3 at the 6 kHz characteristic place. The filter amplitude is normalised relative to the filter amplitude at 6 kHz. The thin and thick lines correspond to the filters for the different micromechanical models shown in figure 3.10(a) and (b) respectively. In plot (a) the filter 1 responses are indistinguishable.

3.3.2 The influence on the coupled model

We now investigate the effect of changing the input to nonlinear function from *vertical* BM velocity v (figure 3.10a), to *shear* displacement ξ (figure 3.10b), on the coupled cochlear model.

The fundamental response to single tone stimulation

Figure 3.13 shows the fundamental response of the cochlear model to a range of stimulus frequencies, observed at the 6 kHz characteristic place. The simulation is performed twice, with the input to the nonlinear function either being determined by v or ξ. In both cases a Boltzmann function is used to represent the nonlinear action of the OHCs, and it is positioned before filter 2 in the micromechanical feedback loop. At low stimulus levels, such as a stapes velocity of 50 dB re 10^{-8} m/s, the change in the nature of the input to the nonlinear function has no substantial effect. However, at a higher stimulus level of 80 dB re 10^{-8} m/s a difference is observed: when the input to the nonlinearity is changed from the vertical BM velocity, v, to the shear displacement, ξ, the amplitude of the fundamental response decreases and the OHC gain reduces. These effects are most apparent for stimulus frequencies between 3.8 and 6 kHz, when the response is observed at the 6 kHz characteristic place in the cochlear model. Although a reduction in response amplitude and OHC gain are often associated with greater saturation of the nonlinear function, it has not proved possible to adjust the uniformly distributed parameters of the Boltzmann function to compensate for a change in the nature of the input to the nonlinear function from v to ξ. This is not surprising considering the gain distributions for the 80 dB response shown in figure 3.13, which illustrate that at low stimulus frequencies (<3.8 kHz) the nonlinear function is more saturated when the vertical BM velocity provides the input, whilst at higher stimulus frequencies (3.8 to 5.5 kHz) the nonlinear function is more saturated when the shear displacement acts as the input.

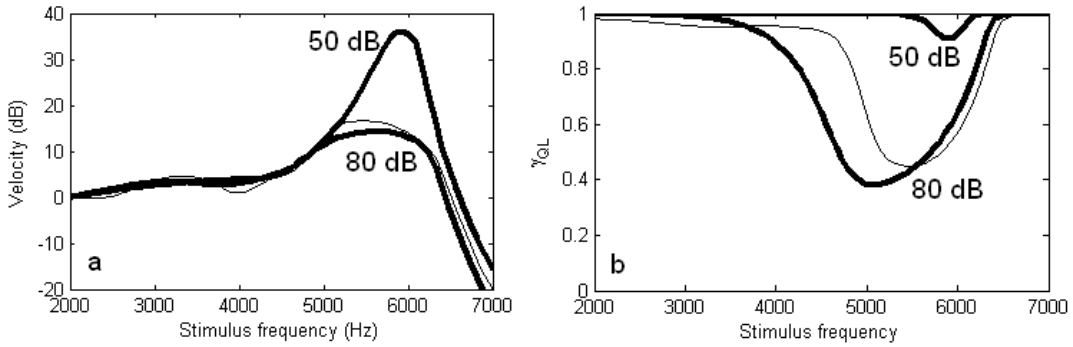

Figure 3.13 The influence of the input variable to the nonlinear function on the fundamental response of the coupled cochlear model
Plot (a) shows the fundamental response of the coupled model to a 6 kHz stimulus presented at 50 and 80 dB re 10^{-8}m/s. The amplitude is given in dB relative to the low frequency response at 2 kHz. Plot (b) gives the fundamental OHC gain (γ_{QL}), as defined in equation (2.30), for the same stimuli used in (a). The input to the nonlinear function is either the vertical BM velocity v (thin lines), or the shear displacement ξ (thick lines). In both cases, the nonlinearity is a Boltzmann function (β=3, α=0.8) and it is positioned before filter 2.

The harmonic response to single tone stimuli

Figure 3.14 shows the spatial distributions of the fundamental and harmonic responses of the model to a 6 kHz stimulus tone presented at the stapes at 60 dB re 10^{-8}m/s. There are two effects of changing the input to the nonlinear function from v to ξ on the harmonic components. Firstly, at the characteristic place of the fundamental frequency, the amplitude of the harmonic components increase relative to the fundamental component. For example, figure 3.14 demonstrates that the amplitude of the 2nd harmonic component at the 6 kHz characteristic place increases from -40 dB to -27 dB, relative to the fundamental response, when the input of the nonlinear function changes from v to ξ. Secondly, the amplitude of the harmonic components at their characteristic places decrease when the input to the nonlinearity switches from v to ξ. In Figure 3.14 the amplitude of the 2nd harmonic component at its characteristic place decreases from -4 dB to -35 dB relative to the fundamental response when the input to the nonlinear function changes from v to ξ.

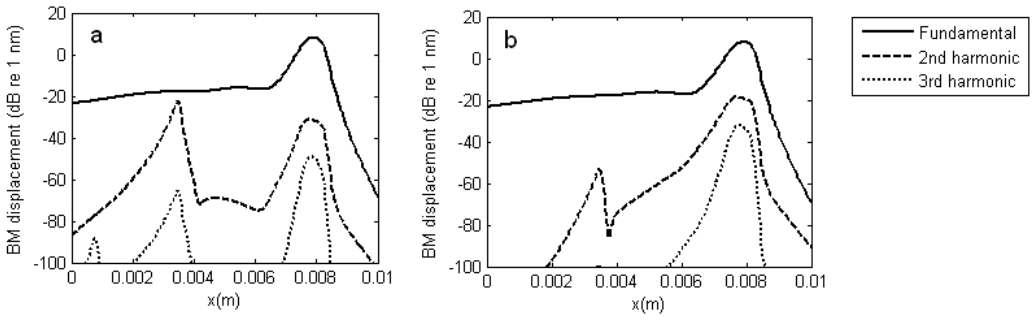

Figure 3.14 The influence of the input variable to the nonlinear function on the harmonic response of the coupled model
The plots show the fundamental and harmonic responses to a 6 kHz stimulus at 60 dB re 10^{-8}m/s in a model where the input to nonlinear function is either determined by (a) the vertical velocity of the CP, v, or (b) the difference in shear displacement between the tectorial membrane and the organ of Corti, ξ. A first order Boltzmann function (β=3 and α=0.8) is used in both models.

The measurement of Cooper (1998), in the guinea pig cochlea, suggests that the 2nd harmonic component should be approximately 11 dB below the fundamental component at the characteristic place of the 2nd harmonic frequency. Therefore, the model response is more in agreement with physiological observations if v, rather than ξ, is used to determine the input to the nonlinear function.

These observations of the model suggest that the nonlinear function is more readily saturated at the characteristic place, but less readily saturated at more basal locations, if the input to the nonlinearity changes from v to ξ. The quasilinear approximation assumes that, at all locations within the cochlear model, the harmonic components are small relative to the fundamental and so it is the amplitude of the fundamental response which determines the degree to which the nonlinear function is saturated. At a location immediately basal to the 6 kHz characteristic place, figure 3.12 suggests that the input to the nonlinearity at 6 kHz is increased by the introduction of filter 3 into the micromechanical feedback loop. Therefore the nonlinearity is more saturated at this location, and higher levels of harmonic components are generated within the cochlear model if the input to the nonlinear function is switched from v to ξ. However, at the characteristic place of the 2nd harmonic frequency, filter 3 acts to reduce the input to the nonlinear function at 6 kHz, and so the nonlinear function is less saturated at this location, and lower levels of harmonic components are generated when the input to the nonlinear function changes from v to ξ.

The distortion products evoked by two tone stimulation

Figure 3.15 shows the predicted DP spectrum evoked by two stimulus tones presented at 7.6 and 8.4 kHz. The simulation is performed twice, with the micromechanical feedback arranged so the input to the nonlinear function was either determined by the vertical BM velocity, v, or the difference in shear displacement between the tectorial membrane and the organ of Corti, ξ. The value of the Boltzmann function parameter α was adjusted between simulations so that the amplitude of the primary components at the 8 kHz characteristic place is changed by less than 1 dB by the alteration in the micromechanical feedback loop. The results demonstrate that changing the input of the nonlinear function from v to ξ has little effect on the predicted DPs. For example, the amplitude of the $2f_1 - f_2$ DP changes by less than 1 dB if the input to the nonlinear function is switched from v to ξ. The $3f_1 - 2f_2$ DP decreases by 7 dB, whilst the $2f_2 - f_1$ and $3f_2 - 2f_1$ DPs increase by 5 and 6 dB respectively, if the input to the nonlinearity is changed from v to ξ. Therefore the effect of altering the micromechanical feedback loop such that the input to the nonlinearity is changed from v to ξ, depends on the frequency of the DP component.

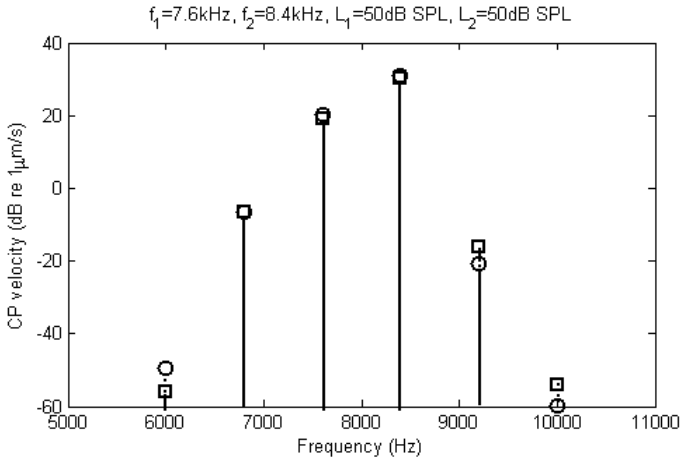

Figure 3.15. The influence of the input variable to the nonlinear function on the response to two tone stimulation
The plots shows CP velocity components evoked by two tones (L_1=L_2=50 dB re 10^{-8}m/s) at the 8 kHz place in the model, at frequencies f_1, f_1, $2f_1 - f_2$, $2f_2 - f_1$, $3f_1 - 2f_2$ and $3f_2 - 2f_1$ when it is stimulated by f_1=7.6 and f_2=8.4 kHz. The input to the OHCs is either determined by v (circles) or ξ (squares). Both simulations use a first order Boltzmann function (β=3) to represent the nonlinear action of the OHCs, and the parameter α is set equal to either 0.8 or 0.42 when using v or ξ respectively so that the level of the fundamental components is the same in each case.

In summary, the harmonic response and the spatial OHC gain distribution arising from single tone stimulation can be influenced by whether the vertical BM velocity, v, or shear displacement ξ, determines the input to the nonlinear function. For example, the amplitude of the harmonic response is more consistent with the physiological measurement of Cooper (1998) if v, rather than ξ, provides the input to the nonlinear function. There is also a change in the amplitude of the predicted DPs, which is generally small (<10 dB) and is dependent on the frequency of the DP. In section 3.5, we opt to proceed with a model in which the input to the nonlinear function is determined by the shear displacement, ξ. It should be noted, however, that this model tends to underestimate the amplitude of harmonic components in the vicinity of their characteristic place. This is a pragmatic choice which allows the estimated response of the quasilinear model to be compared with the results of the state space time domain model in which the input to the nonlinearity is determined by ξ.

3.4 Alternative micromechanical parameters

The micromechanical parameters suggested by Kanis & de Boer allow their cochlear model to exhibit features which are broadly consistent with physiological observations of the human cochlea. For example, the place-frequency map of the fully active linear Kanis & de Boer cochlear model differs by less than ¼ of an octave from the human Greenwood formula, up to distance of 0.025 m from the stapes. Also, at a given location within the model the characteristic frequency reduces by 0.46 octaves when local activity is removed, consistent with experimental observation (Robles & Ruggero, 2001). In addition the cochlear amplifier (CA) gain for the model is approximately 37 dB, for stimulus frequencies below 15 kHz, which is approaching the value of 40 − 60 dB observed in experimental studies of the basal region of the mammalian cochlea (Sellick *et al.*, 1982; Johnstone *et al.*, 1986; Robles & Ruggero, 2001). However, there are some features of their model which do not agree with experimental observations. For example, the response of the model to single tone stimulation does not exhibit reduced CA gain or broader sharpness of tuning as the stimulus frequency decreases and the characteristic place moves from the base to the apex.

The aim of this section is to present a set of adapted micromechanical parameters, for which the fundamental response to single tone stimulation exhibits reduced sharpness of tuning as stimulus frequency decreases, without compromising the qualities of the original micromechanical model such as the accuracy of the place frequency-map and the high CA gain near the base. The motivation for this is that the modified micromechanical parameters may allow the model to better predict the place-fixed component of distortion product otoacoustic emissions (DPOAEs), as the reflection of travelling waves within the cochlea is dependent on the tuning of the response (Zweig & Shera, 1995a).

3.4.1 The modified micromechanical parameters

The micromechanical parameters were altered by trial and error, inspired by the spatial variation of the micromechanical parameters in the cochlear model of Ku *et al.* (2008), which permits broader tuning of the response towards the apex of the model. The result is that the micromechanical parameters describing the active mechanics are modified as shown in table 3.1, to produce a model which exhibits the linear characteristics described in the following section. These characteristics are achieved by introducing the exponential distributions $Q_1(x)$ and $Q_2(x)$, defined in (3.4) and illustrated in figure 3.16, into the description of the parameters describing the active mechanics. The passive mechanics are unaffected by these changes.

$$Q_1(x) = \exp(-0.7x / L) \text{ and } Q_2(x) = 0.2(x / L)^{0.6} + 1.01 \tag{3.4}$$

The function $Q_1(x)$ is used to reduce both the sharpness of tuning and the CA gain towards the apex of the cochlea. Distribution $Q_2(x)$ is used to compensate for the reduction in CA gain introduced by $Q_1(x)$ so that gain does not become too small in the apical region of the model. The net result is a small shift in the active place-frequency map (figure 3.20), a slight decrease in gain as frequency decreases (figure 3.18), and a broadening of the response as stimulus frequency decreases (figure 3.17).

Micromechanical parameter	Interpretation	(i) Original Kanis & de Boer model	(ii) Modified model
δ_{sc}	A dimensionless damping parameter in the active mechanics	0.14	$0.14\times Q_1$
σ_0	A dimensionless parameter which describes the shift in resonance between the OHCs and BM.	0.7	$0.7\times\sqrt{Q_1}$
e_0	A factor which determines the maximum pressure output of the OHCs	4.28×10^{-5}	$4.28\times10^{-5}\times Q_2$

Table 3.1 The micromechanical parameters of the (i) original and (ii) modified cochlear models
The interpretation of the parameters is based on that given by Kanis & de Boer (1994), in terms of the Basilar membrane (BM) and outer hair cells (OHCs). The distributions $Q_1(x) = \exp(-0.7x / L)$ and $Q_2(x) = 0.2(x / L)^{0.6} + 1.01$ where obtained by trial and error for a model of length L. All other parameters for the modified model are the same as in the original description of Kanis & de Boer (see chapter 2).

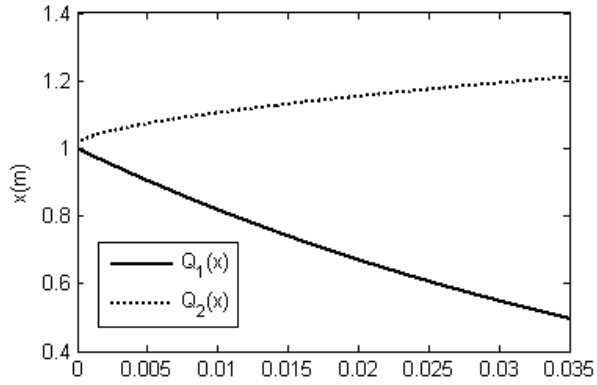

Figure 3.16 The distributions $Q_1(x)$ and $Q_2(x)$

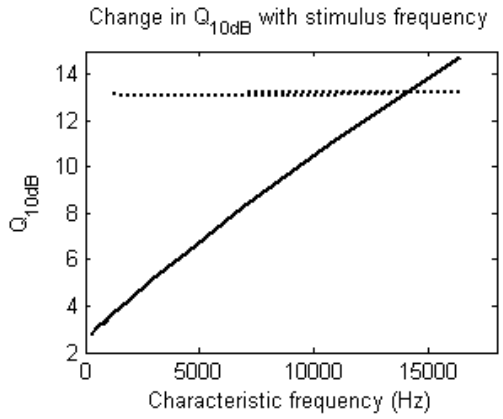

Figure 3.17 The predicted Q_{10dB}
The Q_{10dB} measure of sharpness of tuning is shown for a range of locations with different characteristic frequencies. Values are shown for the coupled cochlear model containing either the original Kanis & de Boer micromechanical parameters (dotted line), or the modified parameters (solid line).

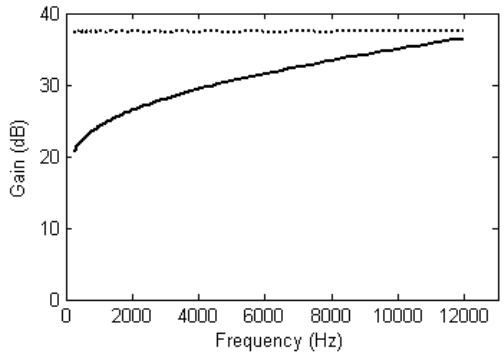

Figure 3.18 The predicted cochlear amplifier gain
The cochlear amplifier gain, defined as the difference in maximum velocity amplitude between the active and passive responses, is shown for the coupled cochlear model incorporating either the original Kanis & de Boer micromechanical parameters (dotted line) or the modified parameters (solid line).

3.4.2 Properties of the linear model with modified micromechanical parameters

Figure 3.17 shows the Q_{10dB} over a range of stimulus frequencies for the fully active linear cochlear model incorporating either the original, or modified, micromechanical parameters.

It demonstrates that there is little variation in sharpness of tuning with stimulus frequency in the original model, as the Q_{10dB} is approximately equal to 13 for all stimulus frequencies between 1 and 16 kHz. However, in the modified model the sharpness of tuning decreases as the stimulus frequency decreases, so that the Q_{10dB} of the response reduces from 11 for a 10 kHz stimulus to 3 for a 0.3 kHz tone. Therefore if the model incorporates the modified micromechanical parameters, rather than the original ones, it provides a better simulation of the physiological result shown in figure 1.12, where Q_{10dB} decreases from approximately 9 to 1 as the stimulus frequency reduces from 10 to 0.2 kHz.

Figure 3.18 shows the CA gain of the coupled model incorporating either the original or modified micromechanical parameters. For high stimulus frequencies the modification of the micromechanical parameters has no significant effect on the CA gain, as the gain of the 12 kHz response is 37 dB in both cases. However, the modified micromechanical parameters significantly reduce the CA gain for low frequency responses, compared to the original micromechanical parameters. For example, the gain of the 500 Hz response decreases from 37 dB to 22 dB when the original micromechanical parameters are modified. Therefore the model is more consistent with physiological measurements from chinchilla cochlea, in which the gain for low frequency stimuli

(0.5 − 0.8 kHz) is around 10 to 20 dB (Robles & Ruggero, 2001), when the modified, rather than original, micromechanical parameters are used.

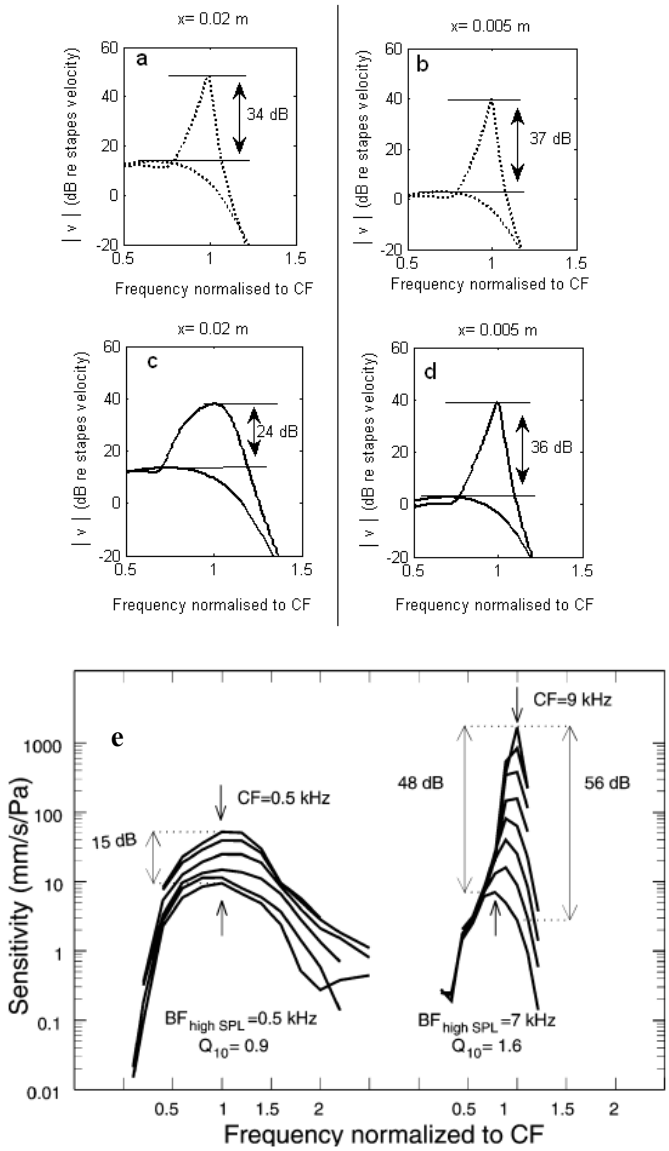

Figure 3.19 The estimated response in the basal and apical regions of the cochlear model
The plots show the velocity response of the cochlear partition in a model incorporating either the original micromechanical parameters of Kanis & de Boer (a and b), or the modified micromechanical parameters described in the text (c and d). In each case the coupled model contains N=1000 elements and the basal boundary condition minimises reflections. The stimulus frequency is normalised to the CF at each observation location which corresponds to (a) 0.59 Hz, (b) 9.8 kHz, (c) 0.54 kHz & (d) 9.6 kHz. In each case, both the active and passive linear responses are shown and the CA gain in given in dB. In (e), the measured sensitivity (ratio of BM velocity to stimulus pressure) at the base and apex of the chinchilla cochlea is given for reference. The apical and basal measurements were made using laser interferometry at the characteristic places for 0.5 and 9 kHz respectively. In each case the multiple curves correspond to different stimulus levels, and the up/down arrows indicate the best frequency for the highest/lowest levels respectively. [From figure 13 of Robles & Ruggero (2001), with permission from Am. Physiol. Soc]

In figure 3.19, the velocity response of the cochlear model at a basal and apical location is compared to an experimental measurement in the chinchilla cochlea (Robles & Ruggero, 2001). This demonstrates that at a basal location (5 mm from the stapes), the modification of the micromechanical parameters has little effect on the gain of the cochlear model, which is around 37 dB. This is less than the gain observed in the basal region of the chinchilla cochlea, approximately 48 dB, but cannot be increased without compromising the stability of the model (Kanis, 1995). At the apical location (20 mm from the stapes), the modified micromechanical parameters reduce the CA gain by 10 dB, but this remains greater than the 15 dB gain observed in the apical region of the chinchilla cochlea.

It is not possible to further manipulate the micromechanical parameters to achieve more accurate replication of the physiological measures of sharpness of tuning or CA gain due to adverse effects that this can introduce into the place-frequency map of the fully active cochlear model. For example, the modified micromechanical parameters introduce a small shift of the characteristic place towards the base for low frequency stimuli such that the characteristic place for a 0.25 kHz stimulus moves 1 mm closer to the base when the parameters are modified. This shift can be seen in figure 3.21, which shows the predicted velocity response of the model for several stimulus frequencies. If further modification of the parameters is introduced to further reduce the gain in the apex of the model, this shift is enhanced. Therefore the set of modified micromechanical parameters shown in table 3.1 are thought to represent a suitable compromise between the properties of CA gain and Q_{10dB} variation required to replicate experimental observations, without substantially altering the place-frequency map of the cochlear model.

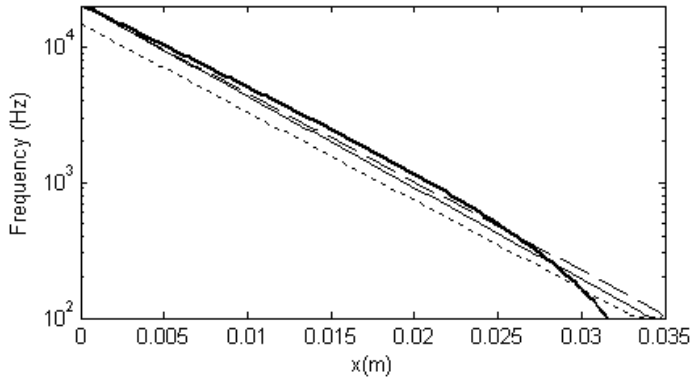

Figure 3.20 The estimated place-frequency map for the fully active cochlear model
The map is shown for a cochlear model incorporating the original Kanis & de Boer micromechanical parameters (dashed thin line) or the modified micromechanical parameters (solid thin line). The Greenwood function for the human cochlea (solid thick line) and the predicted response of the passive model (dotted line) are also shown for reference.

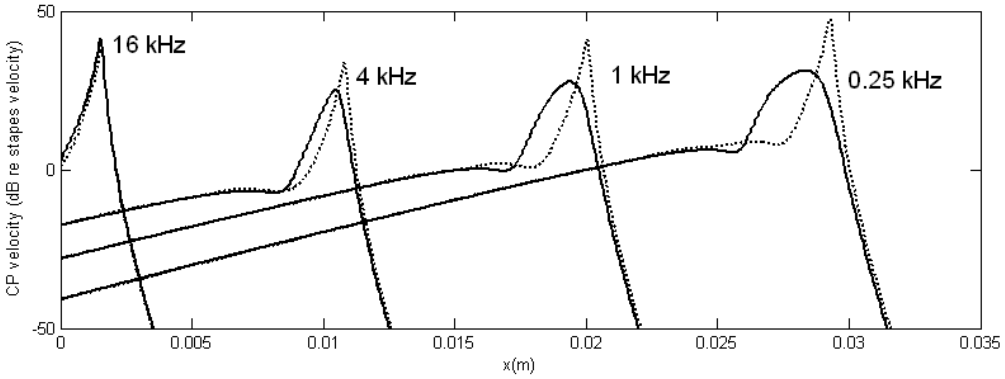

Figure 3.21 The velocity response of the cochlear partition to a range of stimulus frequencies
Results are shown for the coupled model incorporating the original Kanis & de Boer micromechanical parameters (dotted lines) and the model containing the modified parameters described in the test (solid lines).

3.5 Selecting a micromechanical model

In the previous sections, a variety of micromechanical properties have been considered. However, in the interest of simplicity it is necessary to select a single micromechanical model in order to proceed with investigating the properties of DPOAEs.

3.5.1 The micromechanical properties

The selected micromechanical properties, and the reasons for these choices, are given in table 3.2. To summarise, a micromechanical model is selected with the modified parameters described in section 3.4, in which a first order Boltzmann function (β=1.2) is used to represent the nonlinear action of the OHCs. This nonlinearity is positioned before filter 2, a simplified representation of the impedance of the active OHC complex, in the micromechanical feedback loop. In addition, the difference in shear displacement between the tectorial membrane and the organ of Corti is used as the input to the nonlinear function.

Selection	Reasoning
A set of *modified micromechanical parameters* are used, as described in section 3.4.	The new parameters allow the linear active response of the model to exhibit the trend that the cochlear response is more broadly tuned towards the apex than towards the base. This trend may be significant for estimating the place-fixed component of cochlear DPs for which the broadness of tuning is thought to be important (Zweig & Shera, 1995a).
A *first order Boltzmann function* is used to represent the nonlinear action of the OHCs.	The Boltzmann function allows the model to predict even order harmonic responses to single tone stimuli. It has not been possible to determine suitable values of the Boltzmann function parameters α and β from physiological measurements, as discussed in appendix G.2. For this reason, the values of α and β are chosen such that the model predicts saturation thresholds and levels of harmonic distortion in response to single- and two-tone stimuli that most closely match features of physiological measurements.
The nonlinearity is positioned *before* filter 2 in the micromechanical feedback loop, as described in section 3.2	It is feasible that either micromechanical arrangement could be used, provided that the parameters of the Boltzmann function (α and β) are appropriately set to provide sufficient levels of harmonic components in each case. However, figure 3.22 demonstrates that if the nonlinearity is positioned after filter 2 in the feedback loop then a value of β in excess of 7 is required to generate amplitudes of the 2nd harmonic component that are consistent with physiological measurement. In contrast, β=1.2 is sufficient when the nonlinearity is positioned before filter 2 in the micromechanical feedback loop. As experimental observations generally find that $\beta \leq 5$ (appendix G.2), we conclude that the most appropriate model is one where the Boltzmann function (β=1.2) is positioned before filter 2.
The *difference in shear displacement* between the tectorial membrane and organ of Corti, ξ, is used as the input to the nonlinear function.	This pragmatic selection allows the predictions of the quasilinear model to be compared with those of a state space time domain model, provided by Ku (2008), in which ξ is used as the input to the nonlinear function. This choice is consistent with anatomical considerations (Lim, 1980; Gueta *et al.*, 2008). However, a limitation of this selection is that the amplitude of the harmonic components at their characteristic place is underestimated if ξ, rather v, is used as the input to the nonlinear function.

Table 3.2 The selected micromechanical features and the reasons for these choices

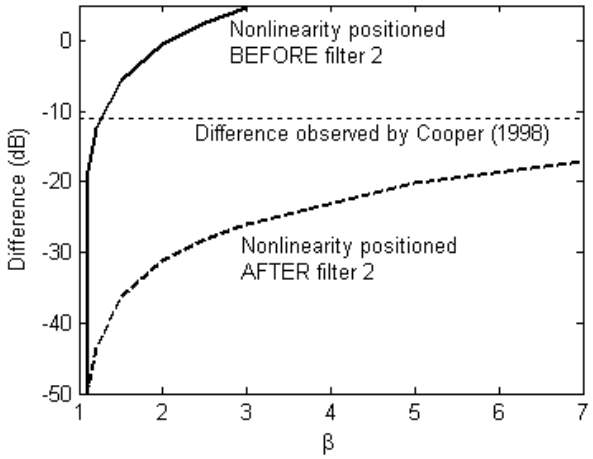

Figure 3.22 The influence of parameter β on the relative amplitude of the fundamental and harmonic responses to single tone stimulation
Results are shown for a 6 kHz stimulus tone applied to a model where the nonlinearity is either positioned *before* filter 2 (solid line) or *after* filter 2 (dashed line). The difference is observed at the characteristic place of the 2nd harmonic component. In this model a first order Boltzmann function is used to represent the nonlinear action of the OHCs, and the modified set of micromechanical parameters is used. The input to the OHCs is the CP velocity *v*. The saturation of the fundamental response is kept equal in both arrangements, using α=0.8 and α=2 when the nonlinearity is position *bef*o*re* and aft*er* the OHC dynamics respectively. The thin dotted line shows the difference of − 11 dB observed in the guinea pig cochlea by Cooper (1998), for reference.

The first order Boltzmann function is used to represent the nonlinear behaviour of the OHCs. The parameter β controls the asymmetry of the nonlinear function and is assigned a uniform value of 1.2 as described in table 3.2. It is possible that an alternative value may be more suitable, and it could be appropriate to use a distribution of β values which vary between the base and the apex. However, the value of β has little effect on the amplitude of the predicted $2f_1 - f_2$ or $2f_2 - f_1$ DPOAEs. For example, if the model is stimulated by two pure tones simultaneously (L_1= 65, L_2 = 55 dB SPL and f_1=1.8, f_2 = 2.2 kHz) then the amplitude of the simulated $2f_1 - f_2$ and $2f_2 - f_1$ DPOAEs change by less than 1 dB if β is increased from 1.2 to 3. For this reason, we simply proceed using β=1.2 without further investigation.

It is also necessary to specify the value of the Boltzmann function parameter α, which determines the saturation threshold and maximum output of the nonlinear function. One approach to this would be to assign a uniform distribution to α, such that the saturation threshold would occur for the same value of shear displacement ξ at all locations along the cochlear partition. However, there is little physiological data to support this assumption. Figure 3.23a shows the maximum predicted shear displacement at the characteristic place, evoked by a 0 dB SPL pure tone stimulus presented at a range of frequencies in the ear canal of the model. The predicted amplitude of the maximum shear displacement increases from the base of the apex as a consequence of the frequency dependence of the middle ear mechanics and linear cochlear micromechanics. If the parameter α was constant along the length of the model, then the ear canal pressure corresponding to the saturation threshold

would decrease as the stimulus frequency decreases. However, in contrast to this, there is experimental evidence to suggest the saturation threshold does not vary substantially for different stimulus frequencies. For example, the growth functions for different frequency components of a human TEOAE suggest that the saturation threshold corresponds to a level between 30 and 40 dB SPL in the ear canal (Grandori, 1985). Similarly, the saturation threshold deduced from human DPOAE growth functions varies by less than 10 dB when the f_2 frequency changes from 0.5 to 4 kHz (Lopez-Poveda *et al.*, 2003). For this reason, we opt to use an α distribution which gives a saturation threshold of approximately 30 dB SPL in the ear canal across a range of stimulus frequencies between 0.5 and 6 kHz. This distribution is illustrated in figure 3.23b, and the resulting BM displacement growth function is shown in figure 3.24 for three different stimulus frequencies. A plateau is imposed on the α distribution close to the base of the model, such that the value of α does not fall below 0.02, and as a result the saturation threshold increases above 30 dB SPL for stimulus frequencies greater than 6 kHz. The plateau is necessary because the amplitude of a response to a high frequency stimulus presented at 30 dB SPL, at its characteristic place in the cochlear model, can be exceeded by the amplitude of a response to a lower frequency stimulus, as shown in figure 3.25. Therefore the plateau in the distribution of α near the base of the model prevents the value of α becoming so small that all low frequency stimuli are suppressed in this region.

(a)

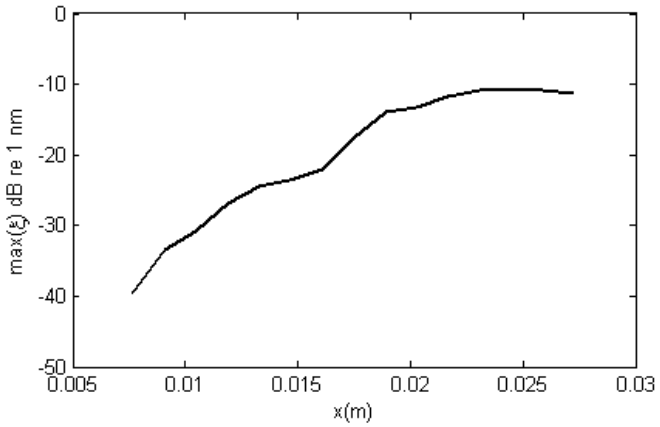

(b)

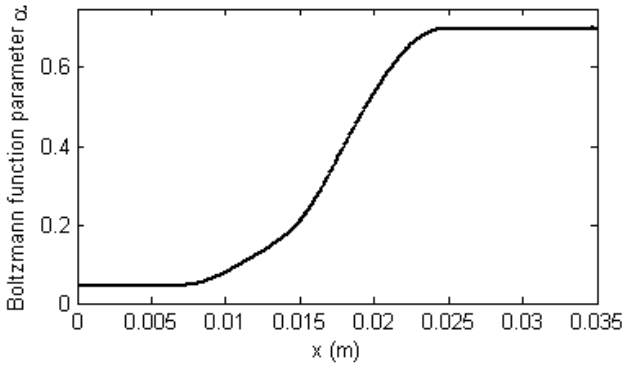

Figure 3.23 The spatial variation of the Boltzmann function parameter α
Plot (a) shows the maximum shear displacement ξ at the characteristic place predicted by the linear model for a 0 dB SPL pure tone stimulus presented in the ear canal at a variety of frequencies. The displacement tends

to increase as distance from the base increases. For this reason, the spatial variation shown in (b) is introduced into the Boltzmann function parameter α.

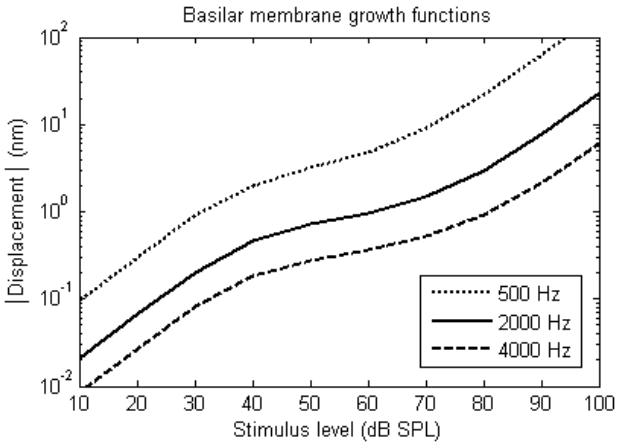

Figure 3.24 Nonlinear growth of the BM response at the characteristic place
The plot shows the predicted growth of BM displacement for stimuli presented at 0.5, 2, and 4 kHz observed at their respective characteristic places within the cochlear model

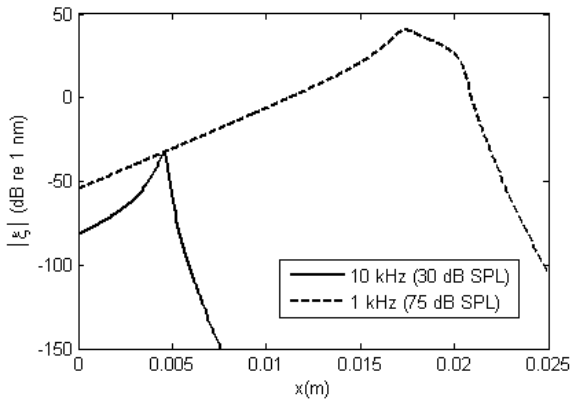

Figure 3.25 The comparison of the amplitude of the response evoked by different stimulus frequencies
The difference in shear displacement (ξ) between the tectorial membrane and the organ of Corti, predicted by the quasilinear cochlear model is shown for single tone stimuli applied at 1 and 10 kHz at levels of 75 and 30 dB SPL respectively. At the 10 kHz place, approximately 5mm from the base of the model, the magnitude of ξ is approximately the same for both stimulus frequencies.

3.5.2 The response of the selected model to single tone stimulation

It is worth briefly reviewing the response of the selected model to single tone stimulation before processing to estimate the DPs it predicts. Figure 3.24 shows the growth function of BM displacement with increasing stimulus levels in the cochlear model described in section 3.5.1. Between the stimulus levels of 40 and 70 dB SPL, the compressive nonlinear growth is rate is 0.3 − 0.4 dB/dB, consistent with the value of 0.12 − 0.5 dB/dB observed experimentally in the basal region of mammalian cochleae (Robles & Ruggero, 2001).

The harmonic responses of the model to single tone stimulation at two different stimulus frequencies are shown in figure 3.26. At the characteristic place, the level of the harmonic components are approximately 40 dB below the amplitude of the fundamental response. This is in broad agreement with the measurement experimental observations which indicate that harmonic components can reach up 20 dB of the fundamental response depending on the stimulus level (Cooper & Rhode, 1995; Khanna & Hao, 1999).

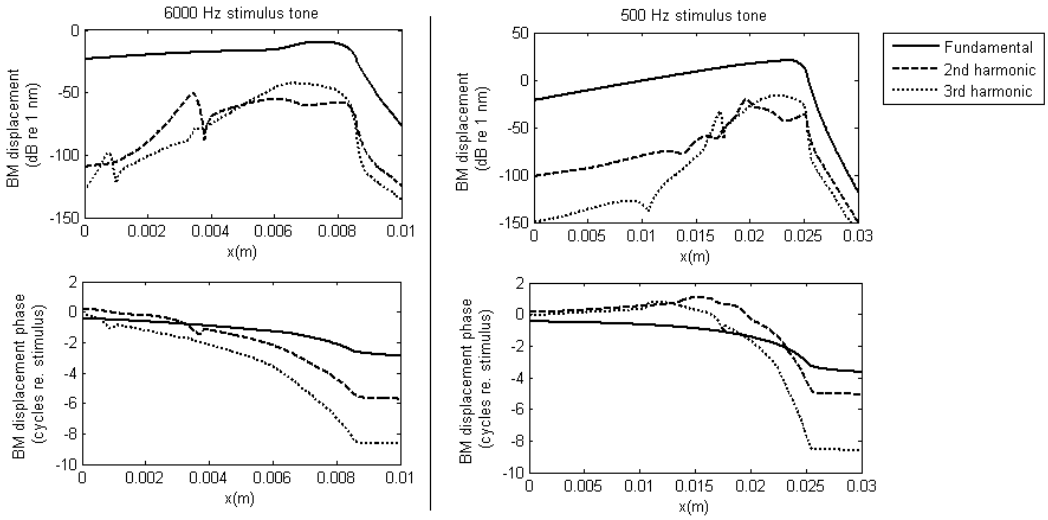

Figure 3.26 The predicted fundamental and harmonic responses to a single tone stimulus
The results are shown for both a 6 kHz and 0.5 kHz stimulus, presented at 60 dB SPL in the ear canal of the model

3.6 Conclusions regarding micromechanical parameters

We have investigated the effect that several different variations in the micromechanical model can have on the single tone harmonics and two tone DPs predicted by the quasilinear model. These variations included the degree of asymmetry in the nonlinear function used to represent the OHCs, the position of the nonlinear function within the micromechanical feedback loop, the shear or vertical orientation of the input to the nonlinear function, and the spatial distribution of the micromechanical parameters. Based on these results, we have selected an appropriate micromechanical model with which to proceed to investigate predicted DPOAEs.

As summarised in section 1.9 (ii), this chapter offers the following contributions:

- Fine tuning of the original Kanis & de Boer micromechanical parameters, so that the linear responses of the model to low frequency single tone stimuli appear more consistent with physiological observations (section 3.4).
- A description and explanation of the influence of the position of the nonlinear function within the micromechanical feedback loop (section 3.2)

4. Predicted $2f_1 - f_2$ DPOAE characteristics

In this chapter the simulated distortion product otoacoustic emissions (DPOAEs) predicted by the cochlear model are presented and special attention is paid to the $2f_1 - f_2$ distortion product (DP). The properties of this emission are extensively documented in the literature and this information is used to determine the successes and weaknesses of the model with regard to DPOAE prediction.

Details of the cochlear model used are given in section 3.5. The response of the model is estimated using the quasilinear method described in section 2.4, and transmission into and out of the cochlear model is described by the two-port model of the middle ear and ear canal detailed in appendix C.1. We start by considering the $2f_1 - f_2$ DPOAE characteristics predicted by a "baseline" model, in which no impedance irregularities have been introduced into the active micromechanics (section 4.1). We then introduce random irregularities into the active micromechanics of the model and present the $2f_1 - f_2$ DPOAE characteristics simulated with this "perturbed" model (section 4.2). This allows the place-fixed effects to be studied separately from the wave-fixed effects. Overall this chapter addresses the first four research questions posed in section 1.9 concerning the $2f_1 - f_2$ DPOAE.

4.1 Predictions of a baseline model

We start by considering the $2f_1 - f_2$ DPOAEs predicted by a baseline model, in which no irregularities have been deliberately imposed on the active micromechanics. As this emission is typically the largest emission detected in the human ear canal, its properties are well documented. In this section we present the simulated $2f_1 - f_2$ DPOAE characteristics and compare them to the physiological properties described in the literature. Having established the strengths and weaknesses of the baseline mode, we conclude that it is appropriate to use the model for further applications such as hypothesis testing and investigating the $2f_1 - f_2$ DPOAE source.

4.1.1 Amplitude of the $2f_1 - f_2$ DPOAE

Figure 4.1 shows the predicted pressure spectrum in the ear canal, evoked by the presentation of two stimulus pure tones at frequencies f_1 and f_2 ($f_2 > f_1$). The equivalent experimental result obtained by Lonsbury-Martin & Martin (2007) is given in figure 1.15d. The amplitude of the $2f_1 - f_2$, $3f_1 - 2f_2$ and $2f_2 - f_1$ emissions predicted by the model differ by less than ± 5 dB from the values measured by Lonsbury-Martin & Martin. As the amplitude of the $2f_1 - f_2$ DPOAE can vary by ± 5 dB between individuals for a given stimulus paradigm (Mills *et al.*, 2007), we conclude that the model prediction is consistent with the experimental result for these DPs. The $3f_2 - 2f_1$ DPOAE has an amplitude of − 41 dB SPL in the simulation, but is absent from the Lonsbury-Martin & Martin spectrum. This is not thought to be a significant discrepancy, as the noise floor of the experimental study was − 32 dB and would therefore conceal the presence of this distortion product in the physiological result.

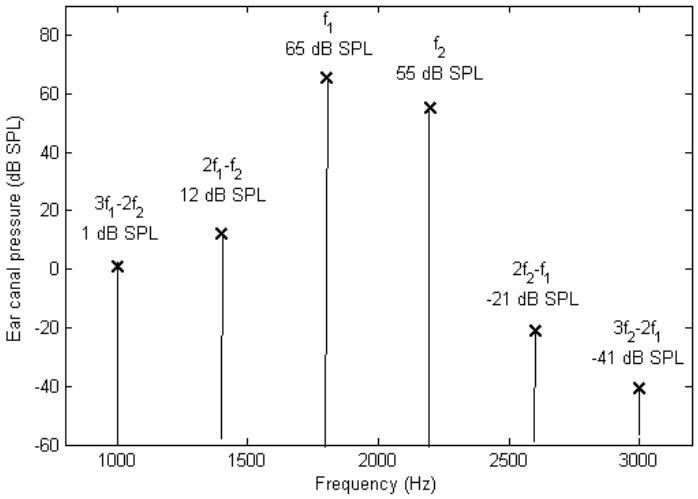

Figure 4.1 The simulated ear canal pressure spectrum
The response of the cochlear model was evaluated at frequencies of f_1, f_2, $3f_1 - 2f_2$, $2f_1 - f_2$, $2f_2 - f_1$ and $3f_2 - 2f_1$ when two simultaneous tones were presented in the ear canal at f_1=1.8 and f_2=2.2 kHz and L_1=65 and L_2=55 dB SPL.

Although we have seen that the model prediction for the $2f_1 - f_2$ DPOAE can be consistent with experimental measurement for a single stimulus paradigm, the amplitude and phase of this emission depends on the following four stimulus parameters: level (L_2), level difference ($L_1 - L_2$), frequency (f_2) and frequency ratio (f_2/f_1) of the primary tones (e.g. Harris *et al.*, 1989; Gaskill & Brown, 1990; Abdala, 1996). For this reason, the $2f_1 - f_2$ DPOAE amplitude can be conceptualised in a four-dimensional space described by the f_2 stimulus frequency, the ratio f_2/f_1, and the two primary tone levels L_1 and L_2. As this four-dimensional space is not easily visualised, many physiological studies choose to set two of the stimulus variables constant and report their results as contour plots of DPOAE amplitude or phase (Whitehead, 1995b, 1995a; Knight & Kemp, 2000; Mills, 2002). Alternatively, a conventional line graph can be obtained if three of the stimulus variables are fixed. In the following sections we use a combination of contour plots and line graphs to illustrate the $2f_1 - f_2$ DPOAE properties predicted by the model.

In addition to the above stimulus parameters, it is also possible that the amplitude and phase of the evoked $2f_1 - f_2$ DPOAE could be influenced by the relative phase of the stimulus tones. We do not investigate this explicitly, but endeavour to use appropriate relative phases in our simulations through the use of a middle ear model which approximates the physiological phase response of the middle ear (appendix C).

4.1.2 The $2f_1 - f_2$ DPOAE dependence on f_2 frequency

Figure 4.2 shows the amplitude of the predicted $2f_1 - f_2$ DPOAE for stimulus levels L_1 and L_2 equal to 60 and 50 dB SPL respectively and an f_2/f_1 value of 1.21. The simulation was performed using several different f_2 frequencies between 1 and 8 kHz. The measurements made by Mills *et al.* (2007), from the ears of 20 normal hearing subjects using the same stimulus parameters, are also shown for reference.

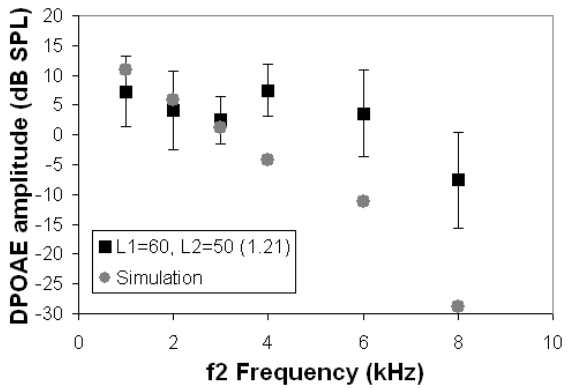

Figure 4.2 The amplitude of the $2f_1 - f_2$ DPOAE for a range of stimulus frequencies
The DPOAE predicted by the model (grey circles) can be compared to the amplitude of this emission measured in the ears of 20 normal hearing subjects by Mills *et al.* (2007). The mean values (black squares) and one standard deviation (error bars) are shown for the physiological results. In both cases the stimuli were presented at levels L_1=60 and L_2=50 dB SPL with f_2/f_1=1.21.

Comparison of the simulated and measured results shown in figure 4.2 reveals that, for f_2 stimulus frequencies between 1 and 3 kHz, the values of the predicted $2f_1 - f_2$ DPOAE amplitude are within one standard deviation of the mean physiological measurements. However, as the stimulus level increases above 3 kHz the amplitude of the predicted $2f_1 - f_2$ DPOAEs falls off. As f_2 increases from 1 to 8 kHz the model predicts a decline of 40 dB in the emission amplitude, which is much larger than the 15 dB decrease observed by Mills *et al*. This discrepancy between the frequency dependence of the predicted and measured $2f_1 - f_2$ DPOAE amplitudes is not thought to be associated with an error in the middle ear transfer function, which is believed to be reasonably accurate for the reasons given in appendix C.3. Therefore the weakness in the model which leads to an underestimation of the $2f_1 - f_2$ DPOAE amplitude at high f_2 frequencies (>4 kHz) is attributed to insufficiencies in either the amplitude of the BM response to stimulation at high frequencies, the saturation threshold of the nonlinear function in the basal region of the model, or some other aspect of the nonlinear cochlear model. Attempts to modify the model to address these possible insufficiencies have been unsuccessful as the modifications introduced other undesirable effects. For example, altering the micromechanical parameters to enhance the amplitude of the response could have a detrimental effect on the place-frequency map and stability of the model. We also found that reducing the saturation threshold near the base of the model, to enhance the DPs evoked by high frequency stimuli, can unfavourably affect the propagation of low frequency forward travelling waves through this region (section 3.5.1).

Overall, we conclude that the amplitude of the $2f_1 - f_2$ DPOAE is consistent with experimental measures when f_2 is less than 4 kHz. However, the model tends to underestimate the amplitude of the emission by more than 20 dB when f_2 exceeds 4 kHz. Therefore caution should be applied when comparing DPOAE amplitudes across a wide range of stimulus frequencies.

4.1.3 The dependence of the $2f_1 - f_2$ DPOAE on L_1 and L_2

Figure 4.3a shows simulated contour plots of the predicted $2f_1 - f_2$ DPOAE amplitude as a function of stimulus levels L_1 and L_2 for various f_2/f_1 ratios. In each case the results have been averaged across f_2 frequencies between 1 and 3 kHz. An experimental contour plot, measured by Meinke *et al.* (2005) using f_2/f_1 equal to 1.21, is reproduced in figure 4.3b for reference. Comparing the simulated and measured results shows similarities in the range of $2f_1 - f_2$ DPOAE amplitudes on the plots and the asymmetry in the dependence of the emission on L_1 and L_2. For example, when f_2/f_1 equal to 1.2, the maximum predicted DPOAE level of approximately 10 dB SPL differs by only 2 dB from the maximum level of 12 dB SPL observed in the physiological study, which is within ± 5 dB variation observed between individual subjects (Mills *et al.*, 2007). Also, for this frequency ratio, the predicted emission amplitude is maximised when L_1 and L_2 are set equal to 75

and 65 dB SPL respectively. This is in close agreement with the experimental result which reveals optimal stimulus levels of 75 and 70 dB SPL for L_1 and L_2 respectively for this stimulus frequency ratio.

The contour plots shown in figure 4.3 contain much information regarding the dependence of $2f_1 - f_2$ DPOAE amplitude on the stimulus level L_1 and the stimulus level difference ($L_1 - L_2$), and these aspects of the predicted emission are examined in more detail in the following two sections. We then progress onto a discussion of the influence of stimulus frequency ratio on the $2f_1 - f_2$ DPOAE amplitude, as this ratio affects the relative amplitude of the primary travelling waves at the distributed site where the $2f_1 - f_2$ DP is generated.

(a) Simulation

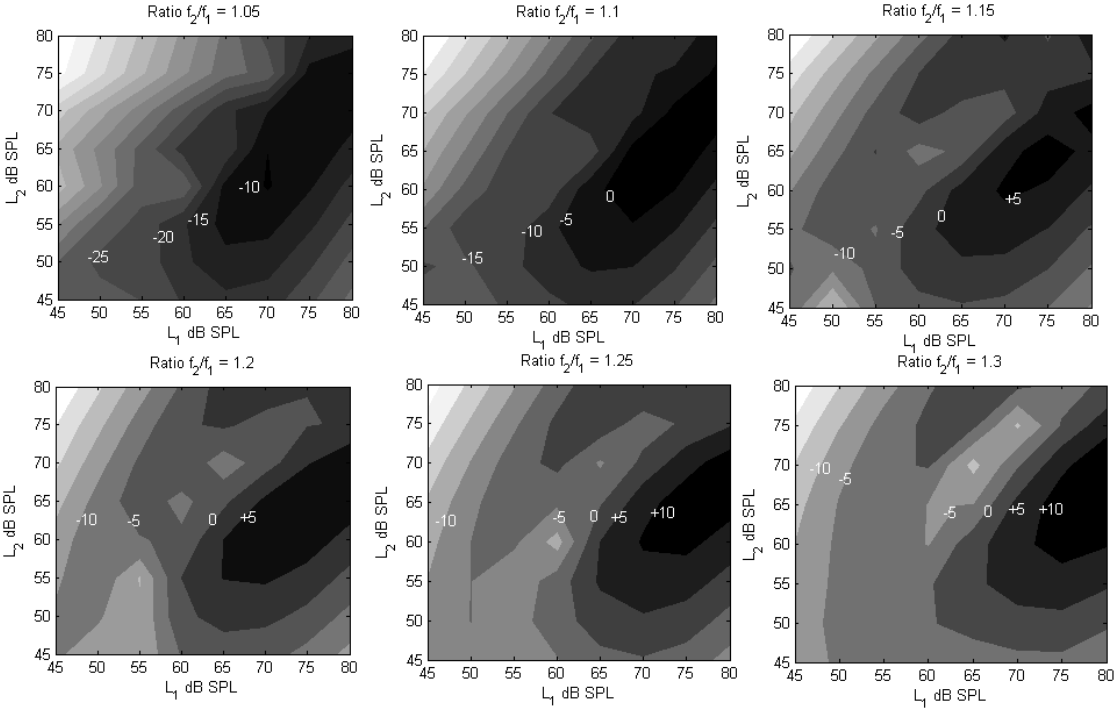

(b) Meinke *et al.* (2005)

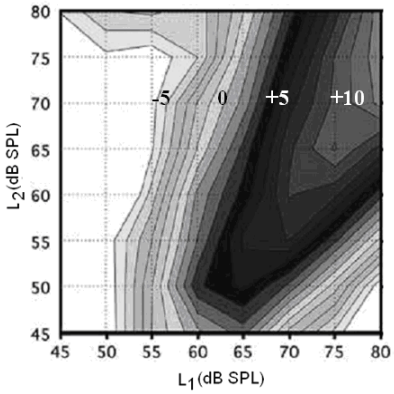

Figure 4.3 $2f_1 - f_2$ DPOAE level contour plots
(a) The predicted amplitude of the $2f_1 - f_2$ DPOAE in dB SPL, evoked by two stimulus tones at levels L_1 and L_2. The simulations for various f_2/f_1 ratios are shown. In each case the predicted DPOAE levels are averaged across f_2 values of 1, 1.5, 2, 2.5 & 3 kHz.
(b) The measured $2f_1 - f_2$ DPOAE amplitude (dB SPL) for various stimulus levels, averaged across 10 human ears and stimulus frequency f_2 values between 0.6 and 8.8 kHz (f_2/f_1 = 1.21). [From figure 3a of Meinke *et al.* (2005), with permission from Elsevier]

(a) Simulation (b) Data from Mills *et al.* (2007)

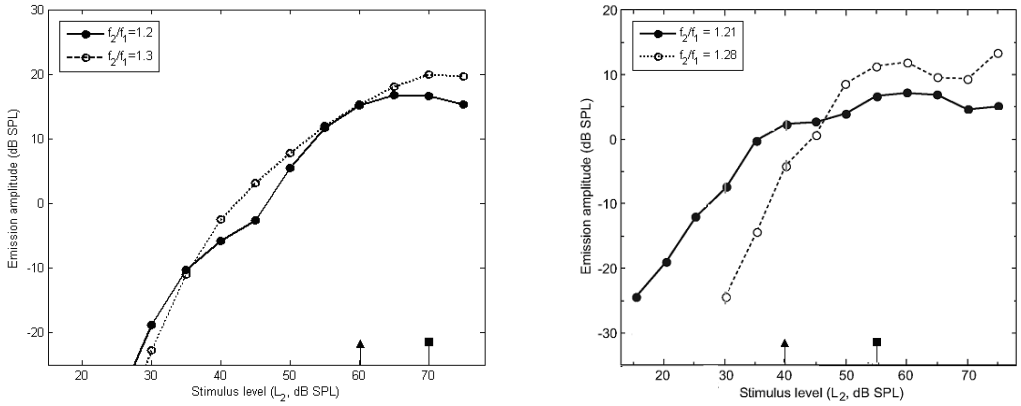

Figure 4.4 Growth functions for the $2f_1 - f_2$ DPOAE
(a) The amplitude of the $2f_1 - f_2$ DPOAE predicted by the model for f_2=2 kHz, L_1=L_2+10 dB and f_2/f_1=1.2 or 1.3. (b) The amplitude of the $2f_1 - f_2$ DPOAE recorded in the ear canal of one human subject by Mills *et al.* (2007) using f_2=4 kHz, L_1=L_2+10 dB and f_2/f_1 = 1.21 or 1.28. [From figure 1 of Mills *et al.* (2007), with permission from Wolters Kulver Health]. In both plots, the triangular and square arrows denote the compression threshold, based on the criteria used by Abdala (2000).

4.1.4 Growth of the $2f_1 - f_2$ DPOAE

A DPOAE growth function is recorded using a fixed relationship between L_1 and L_2, such as constant $L_1 - L_2$ or L_1=0.4L_2+39dB (the "scissor paradigm" described in section 1.5.2). The "growth rate" of the $2f_1 - f_2$ DPOAE refers to the increase in DPOAE amplitude for every dB increase in stimulus level, and is commonly quoted in units of dB/dB.

Growth rates and saturation thresholds

Comparing stimulated growth functions with those measured in experimental studies is not straight forward as the intersubject variation in both the saturation threshold and the gradient must be taken into account. Abdala (2000) defined saturation threshold, L_{sat}, as the stimulus level above which the amplitude of the DPOAE increased by no more than 2 dB with further stimulus level increases, and found that these thresholds varied by ± 10 dB between subjects. In addition, the gradient can vary by ± 0.4 dB/dB between individuals (Lind, 1998; Abdala, 2000).

Figure 4.4a shows the growth of the predicted $2f_1 - f_2$ DPOAE with stimulus level, when L_1=L_2+10 dB, f_2 = 2 kHz and f_2/f_1 is equal to either 1.2 or 1.3. Experimental results obtained by Mills *et al.* (2007) from normal human ears, for similar stimulus parameters, are given in figure 4.4b for reference. The simulation is performed at a lower f_2 frequency (2 kHz) compared to the experimental measurement (4 kHz) in order to avoid any affects associated with the model's tendency to underestimate the $2f_1 - f_2$ DPOAE amplitude at high frequencies (section 4.1.2). Figure 4.4a suggests that the predicted L_{sat}, as defined by Abdala (2000), occurs at approximately 60 or 70 dB SPL when f_2/f_1 equals 1.2 or 1.3 respectively. In comparison, the experimental measurement

exhibits a saturation threshold of 40 or 55 dB SPL, for f_2/f_1 values of 1.21 and 1.28 in that order. Although the difference between the simulated saturation thresholds and those measured by Mills *et al*. exceeds the ± 10 dB variation observed between human subjects, this discrepancy is not thought to be significant because other experimental studies using the same stimulus paradigm record higher saturation thresholds. An example is the work of Abdala (2000) who recorded saturation thresholds between 62 and 75 dB SPL for an f_2/f_1 value of 1.2. On average, for the two stimulus frequency ratios shown in figure 4.4a, the model predicts that the $2f_1 - f_2$ DPOAE growth rate will be 1.2 dB/dB for stimulus levels between L_{sat} − 20 dB and L_{sat}. The average growth rate observed by Mills *et al.* for the same stimulus level range is 0.9 dB/dB, which is within ± 0.4 dB/dB of the predicted value.

Influence of f_2/f_1 ratio

The model suggests the saturation threshold, L_{sat}, should increase as stimulus frequency ratio increases. This is demonstrated by figure 4.4a, in which the saturation threshold increases from 60 to 70 dB SPL as f_2/f_1 increases from 1.2 to 1.3. A similar trend is seen in the data of Mills *et al*, in figure 4.4b. However, this increase in L_{sat} with stimulus frequency ratio is not always evident in experimental data (Abdala, 2000), possibly as a consequence of large intersubject variation in DPOAE growth rates. The relationship between f_2/f_1 ratio and L_{sat} observed in the model is thought to originate from the change in spatial overlap of the primary travelling wave envelopes as the stimulus frequency ratio changes. The $2f_1 - f_2$ DPOAE is thought to be generated in the vicinity of the f_2 best place, and as f_2/f_1 increases the level of the f_1 travelling wave at this location reduces. Therefore a higher stimulus level would be required to saturate the nonlinear function representing the action of the OHCs at the f_2 best place.

Notches in the growth function

For some specific stimulus paradigms the baseline model predicts non-monotonic growth or "notches" in the $2f_1 - f_2$ DPOAE growth function. For example, figure 4.5a shows the growth of the $2f_1 - f_2$ DPOAE with increasing stimulus level (L_1=L_2) when f_2 is equal to 2 kHz and f_2/f_1 is 1.2. A notch can be seen in this growth function when L_1= L_2 = 57.5 dB SPL. Figure 4.5b illustrates that the notch is associated with a change in the phase of the $2f_1 - f_2$ DPOAE of around half a cycle. This notch was evident as a minima in the simulated DPOAE contour plots (figure 4.3a), for stimulus frequency ratios between 1.15 and 1.3, when L_1 and L_2 are equal at around 55 to 65 dB SPL. The contour plots suggest that notches in the simulated growth function will be not be observed if the L_1=L_2 + 10 dB paradigm is used, but that they will be detected using other linear stimulus relations such as L_1=L_2 or the "scissor" paradigm. The predicted notch is only evident in the model when f_2 is around 2 kHz, and is not present for all stimulus frequency ratios.

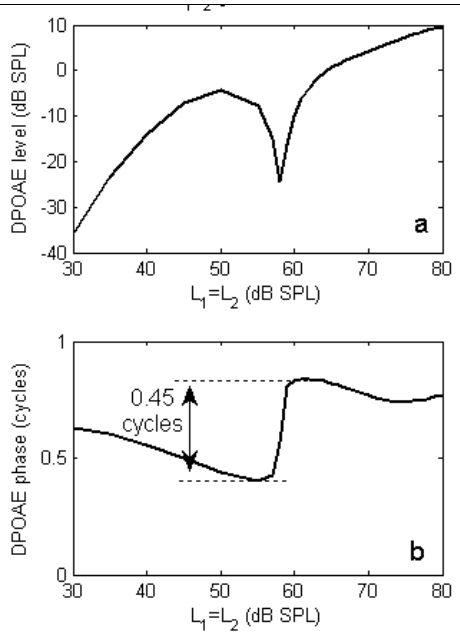

Figure 4.5 The notch in the predicted $2f_1 - f_2$ DPOAE growth

(a) Predicted growth of the $2f_1 - f_2$ DPOAE with increasing stimulus level ($L_1=L_2$) when $f_2/f_1=1.2$, and $f_2=2$ kHz. This simulation was performed in a model in which no impedance irregularities had been imposed on the active micromechanical impedance.

(b) The phase of the emission shown in (a), in cycles and referenced to $2\phi_1 - \phi_2$ where ϕ_1 and ϕ_2 correspond to the phase of the stapes velocity at frequencies f_1 and f_2.

These simulations are performed using a baseline model, in which no irregularities have been deliberately imposed on the micromechanics, and so the results predict only the behaviour of the wave-fixed DPOAE component as discussed in section 5.1. It has not been possible to determine if notches occur in the growth of the wave-fixed component of DPOAEs measured in experimental studies, as the process used to separate the wave-fixed and place-fixed components of the physiological emission usually average results over several f_2 frequencies.

Notches in the DPOAE growth functions observed from human ears are often attributed to shifts in the emission fine structure described in section 4.2.3 (He & Schmiedt, 1993). However, this cannot be the origin of the notch illustrated in figure 4.5a as the baseline model is unable to generate a place-fixed DPOAE component necessary for the production of fine structure. Instead, there are two possible explanations for its origin, both of which require only one source mechanism, such as the spatially distributed wave-fixed (distortion) source mechanism present in the baseline model described in section 5.1.1. Firstly, Lukashkin & Russell (2001) demonstrate that amplitude notches are evident in a contour plot of the $2f_1 - f_2$ DP output of a single isolated nonlinear function as a function of the level of the two input tones (A_1 and A_2), and that these notches are accompanied by a change in the DP phase of ½ a cycle. However, it is not possible to attribute the notch seen in figure 4.5a, to the behaviour of the nonlinear function as the predicted notch is not a robust feature observed for all stimulus level relationships and all stimulus frequencies. Secondly, Mills (2002) suggests that the notch could occur as a result of a change in the interaction between elements within the distributed wave-fixed $2f_1 - f_2$ DP source region as the increase in stimulus level alters the spatial overlap between the primary travelling waves. On this basis, a notch may be expected to occur in the growth of the $2f_1 - f_2$ DPOAE when the phase distribution of the source region changes so that neighbouring source elements change from a pattern of constructive interference to one of destructive interference. Mills bases this proposition on the results obtained from measurements of

notches in the growth functions of Mongolian gerbils, and observed that a phase change of up to half a cycle accompanies the notch. To test this explanation, figure 4.6 shows the accumulative $2f_1 - f_2$ DPOAE recorded in the ear canal as the distribution of the $2f_1 - f_2$ OHC pressure output is gradually "switched-on" from the base of the model. At low stimulus levels, such as 40 dB SPL, all of the elements within the source region appear to interact constructively to form the total $2f_1 - f_2$ DPOAE as gradually increasing the source length results in monotonic growth of the predicted emission. However, as the stimulus level approaches or exceeds the level at which the notch occurs, figure 4.6a demonstrates that the growth in the simulated DPOAE amplitude with increasing source length is no longer monotonic. This indicates the presence of destructive interference between neighbouring elements within the DP source distribution.

In summary, we conclude that notches in the growth of the wave-fixed (distortion) component of the $2f_1 - f_2$ DPOAE can occur in the model for some stimulus paradigms. This is thought to arise from relative changes in phase of neighbouring source elements as the stimulus level increases, such that the contributions from these source elements partially cancel each other at higher stimulus levels (Mills, 2002). It is possible that these notches are not observed for all stimulus paradigms because of the influence of the middle ear response on the relative phase of the primary tones.

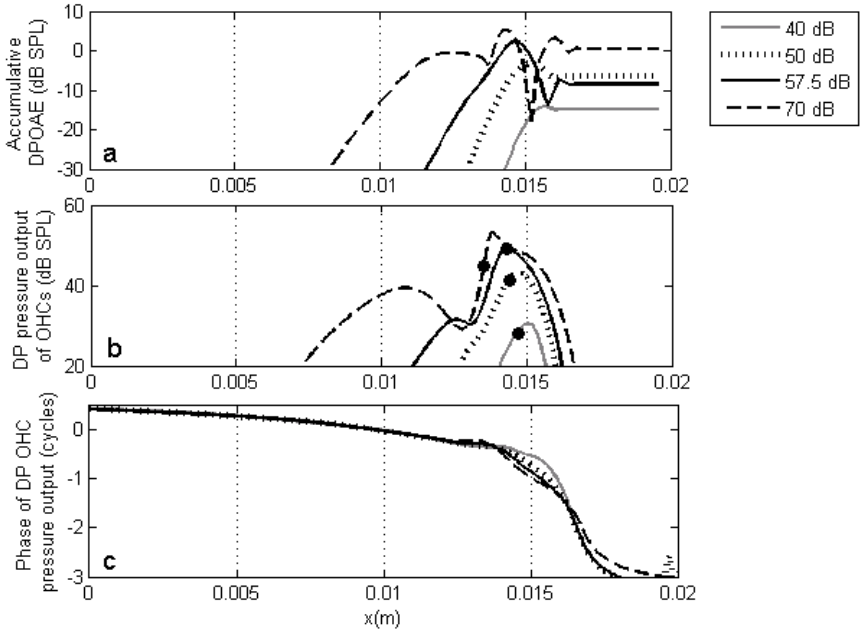

Figure 4.6 The influence of the DP source distribution on the predicted $2f_1 - f_2$ DPOAE
(a) The accumulative $2f_1 - f_2$ DPOAE amplitude predicted by the model is shown as the wave-fixed (distortion) source is gradually "switched-on" from the base of the model. In this case, f_2/f_1=1.2, f_2= 2kHz and L_1=L_2 (dB SPL). The stimulus level is given in dB SPL in the key. The amplitude and phase of the DP pressure output of the OHCs, for these primary tones, which forms the total distributed DP source distribution, is given in (b) and (c) respectively. The dots on plot (b) mark the f_2 best place for each stimulus level.

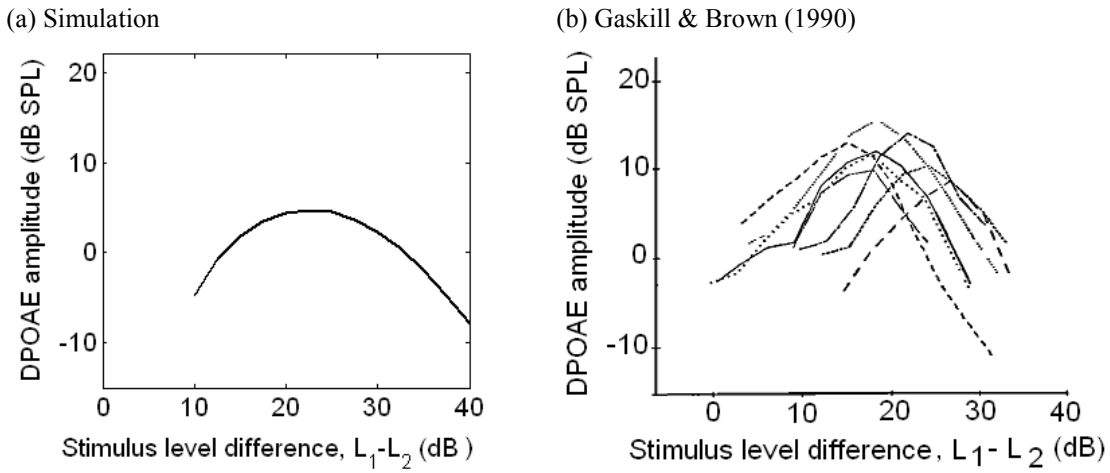

Figure 4.7 The influence of stimulus level difference on the $2f_1 - f_2$ DPOAE
(a) The predicted dependence of the $2f_1 - f_2$ DPOAE amplitude of the stimulus level difference $L_1 - L_2$, when L_2 is fixed at 40 dB SPL, f_2/f_1=1.2 and f_2=2 kHz. (b) The experimental $2f_1 - f_2$ DPOAE amplitude recorded by Gaskill & Brown (1990) from human ears using f_2/f_1=1.225 and L_2=40 dB SPL. The different lines correspond to different f_2 frequencies between 3 and 6 kHz. [From figure 7a of Gaskill & Brown (1990), with permission from ASA].

4.1.5 Optimal stimulus level difference

Figure 4.7a shows the simulated variation in $2f_1 - f_2$ DPOAE amplitude with stimulus level difference. A similar experimental measure by Gaskill & Brown (1990) is reproduced in Figure 4.7b for comparison. In both cases the stimulus level L_2 was fixed at 40 dB SPL. The model predicts that, at this L_2 level, the optimal stimulus level difference ($L_1 - L_2$) is approximately 20 to 25 dB. This is in broad agreement with the measurements of Gaskill & Brown who observe the optimal level difference to be between 15 and 25 dB. They also note that there is variation of at least 10 dB in the optimal level difference between subjects.

The optimal stimulus level difference ($L_1 - L_2$) depends on the stimulus level and the stimulus frequency ratio. Figure 4.8 shows the decrease in optimal level difference with increasing L_2 level predicted by the model and compares it with the experimental observations of Gaskill & Brown (1990) and Whitehead (1995a). The reduction in predicted optimal level difference from 25 to 5 dB as L_2 increases from 45 to 80 dB SPL is reasonably consistent with the change measured in the experimental studies, given the difference in stimulus frequencies and f_2/f_1 ratios. Figure 4.9 shows simulated increase in the optimal stimulus level difference with increasing f_2/f_1 ratio, along side the experimental results collected by Abdala (1996) are also shown in figure 4.9 for reference. Both the simulation and the physiological measurement suggest that the optimal stimulus level difference increases with increasing stimulus frequency ratio.

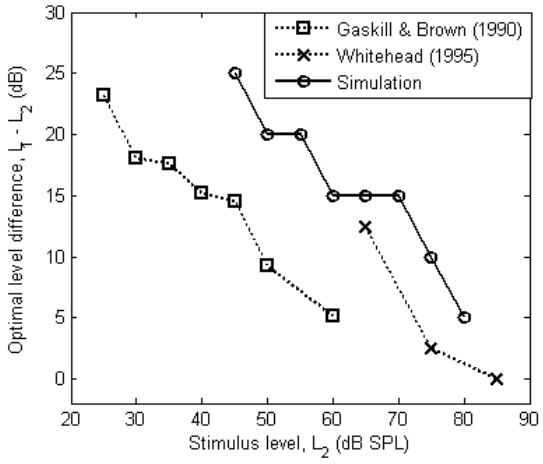

Figure 4.8 The influence of stimulus level on the optimal level difference
The plot shows the predicted dependence of the optimal stimulus level difference for $2f_1 - f_2$ DPOAE amplitude on stimulus level L_2, is compared to experimental data. The simulated results are averaged across f_2/f_1 ratios of 1.05 − 1.3 and f_2 frequencies 1 to 3 kHz, and the optimal level difference ($L_1 - L_2$) is estimated to the nearest 5 dB. The experimental data is taken from Whitehead (1995a) and Gaskill & Brown (1990) which used a variety of f_2/f_1 ratios between 1.1 and 1.3 and f_1 frequencies between 1 and 10 kHz.

Figure 4.9 The influence of f_2/f_1 ratio on the optimal level difference
The plot shows the predicted dependence of the optimal stimulus level difference for $2f_1 - f_2$ DPOAE amplitude on stimulus frequency ratio f_2/f_1 and it is compared to experimental data. The simulation was performed using L_2 = 50 dB SPL and f_2=1 kHz. The experimental results were estimated from figure 8 of Abdala (1996), which was obtained using L_2 = 50 dB SPL and f_2 = 1.5 kHz.

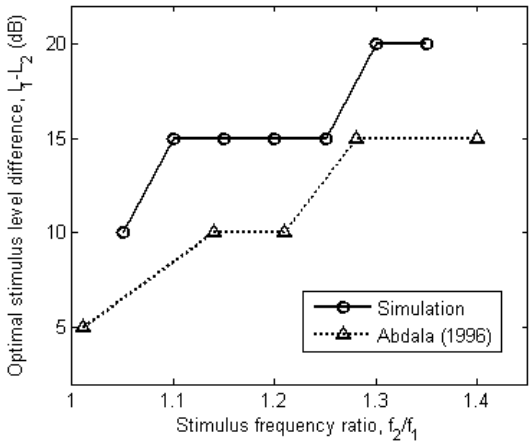

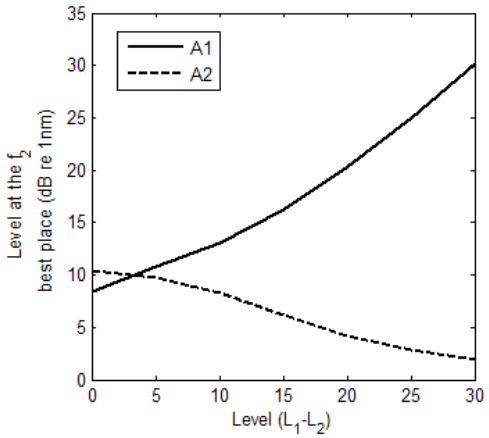

Figure 4.10 The level of input to the nonlinear function at the f_2 best place in the coupled model
The levels of the input to the nonlinear function, A_1 and A_2, are equated with the primary components of the shear displacement and are evaluated at the f_2 best place in the coupled model for a range of stimulus level differences. Levels L_1 and L_2 correspond to stimulus levels in the ear canal of the model and for this simulation L_2= 50 dB SPL, f_2= 2 kHz and f_2/f_1=1.1.

Explanations for the optimal stimulus level difference have been proposed by Gaskill & Brown (1990) and Lukashkin & Russell (2001). To summarise, the wave-fixed distortion source of the $2f_1 - f_2$ DP is thought to be generated in the region of the f_2 best place, where the amplitude of the travelling wave envelopes can be denoted by A_1 and A_2 for f_1 and f_2 respectively. Increasing the stimulus level difference such that L_1 exceeds L_2, increases A_1 relative to A_2 as shown in figure 4.10. For example, as L_1 increases from 0 to 30 dB above L_2, A_1 increases from about − 2 to 28 dB relative to A_2. The amplitude of the $2f_1 - f_2$ DP component of the output from an isolated nonlinear function for a variety of A_1 and A_2 levels is illustrated in figure 4.11.

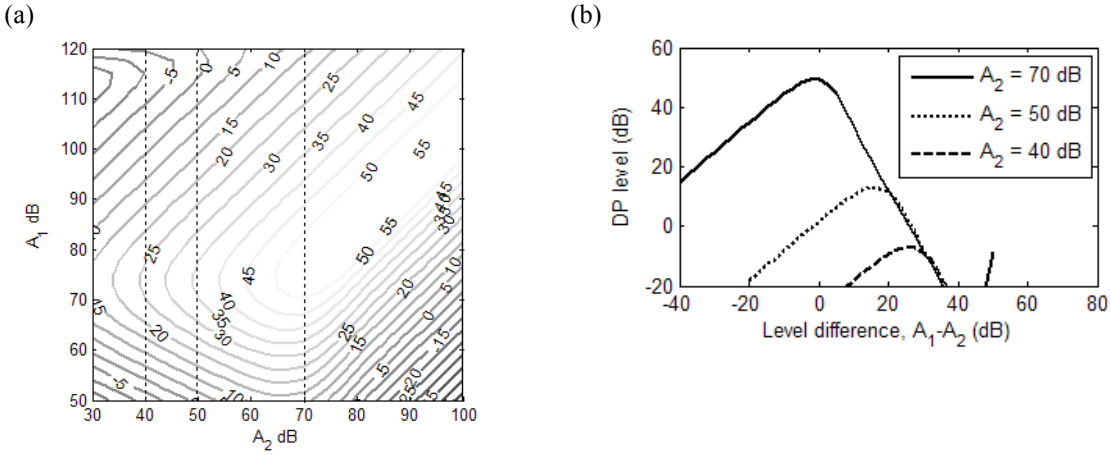

Figure 4.11 Simulated contour plot of the $2f_1 - f_2$ DP output of the isolated nonlinear function
(a) A single isolated first order Boltzmann function is stimulated by tones with frequencies f_1 and f_2 and corresponding levels A_1 and A_2 respectively, and the amplitude of resulting $2f_1 - f_2$ DP component of the output is plotted. (b) The estimated level of the DP component is also shown for fixed A_2 levels corresponding to the dotted lines in (a). In both cases, the dB scale reference is arbitrary, f_2 = 1 kHz and f_2/f_1=1.1.

Figure 4.11 demonstrates that as A_1 increases relative to A_2, the amplitude of the DP output increases until an optimal $A_1 - A_2$ difference is reached, and above this level the amplitude of the DP output decreases. The optimal $A_1 - A_2$ difference also decreases as A_2 increases. For this reason, the optimal stimulus level difference ($L_1 - L_2$) and its dependence on stimulus level can be attributed to the behaviour of the nonlinear function in isolation. This conclusion contradicts the suggestion of Whitehead (1995b) that it is the mutual suppression of the primary travelling waves which is responsible for the decline in the $2f_1 - f_2$ DPOAE amplitude as $L_1 - L_2$ exceeds the optimal value. However, figure 4.12 shows the dependence of the emission amplitude on $L_1 - L_2$ when the effect of mutual suppression is temporarily removed from the quasilinear model. This demonstrates that mutual suppression has no significant influence on the decline in the $2f_1 - f_2$ DPOAE amplitude at high stimulus level differences.

Figure 4.12 The simulated effect of suppression on the optimal level difference
The full quasilinear method requires three iterative stages to evaluate the predicted distortion product evoked by two stimulus pure tones: Self-suppression of the primary tones, mutual suppression of the primary tones and finally self-suppression of the distortion product component. The predicted amplitude of the $2f_1 - f_2$ DPOAE for a variety of stimulus level differences, estimated using the full model is shown as a solid line. The predicted response with the DP self-suppression stage neglected (dotted line) and DP self-suppression and mutual suppression of the primaries neglected (dashed line) are also shown to facilitate interpretation of the full quasilinear result. In each case L_2= 60 dB SPL, f_2=1 kHz and f_2/f_1=1.2.

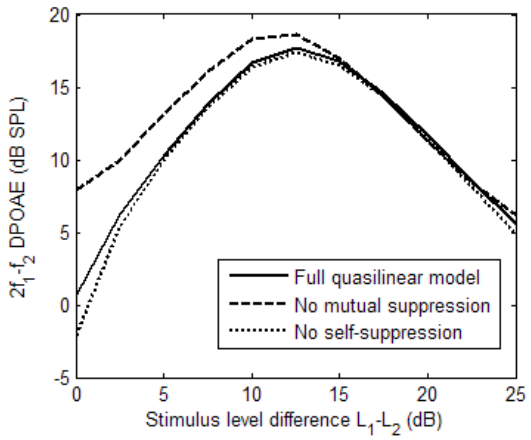

In summary, we conclude that the optimal level difference originates from the behaviour of the isolated nonlinear function and change in the value of A_1 relative to A_2 at the DP generation site as L_1 changes relative to L_2.

4.1.6 Optimal stimulus frequency ratio

The existence of a stimulus frequency ratio which maximises the $2f_1 - f_2$ DPOAE is a common feature of physiological measurements. The optimum ratio is usually between 1.1 and 1.35 for human subjects, depending on the individual ear and the stimulus parameters (Harris *et al.*, 1989; Abdala, 1996). For the same stimulus paradigm, the optimum stimulus frequency ratio can vary between individuals by up to ± 0.1 (Harris *et al.*, 1989).

Figure 4.13a shows the simulated $2f_1 - f_2$ DP amplitude as a function of stimulus frequency ratio. At low stimulus levels such as 40 or 50 dB SPL, the predicted optimum f_2/f_1 ratio is between 1.15 and 1.25. This is in agreement with the optimal ratio of 1.25 observed by Gaskill & Brown (1990) at low stimulus levels ($L_1 = 55$ and $L_2 = 40$ dB SPL). Figure 4.13b shows the change in the optimum f_2/f_1 ratio predicted by the model as stimulus level increases. Experimental results obtained by Harris *et al.* (1989) and Knight & Kemp (1999) are also shown for comparison. This figure illustrates that the model tends to over-estimate the rate at which the optimum f_2/f_1 ratio increases with stimulus level which causes the model to overestimate the optimal stimulus frequency at higher stimulus levels.

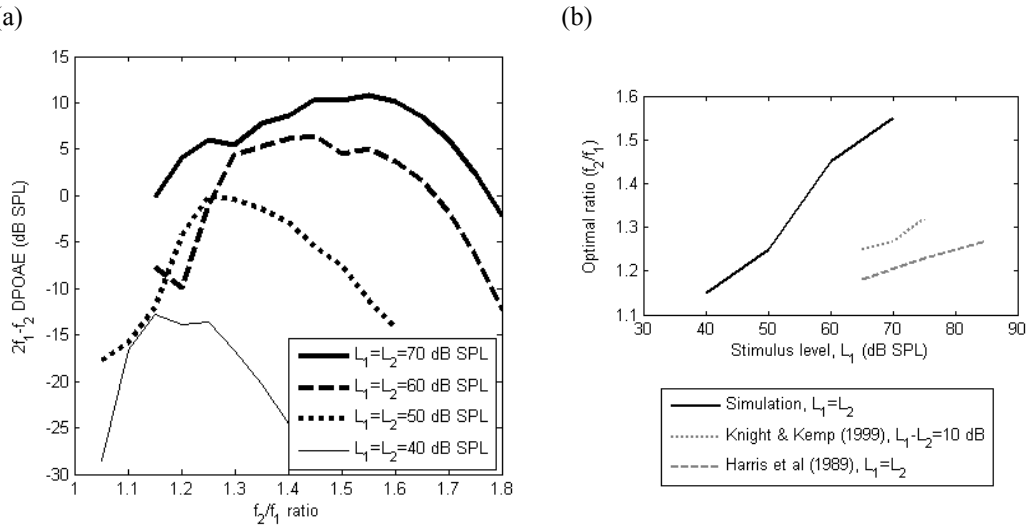

Figure 4.13 The influence of stimulus level on the optimal f_2/f_1 ratio
(a) The variation in the predicted $2f_1 - f_2$ DPOAE amplitude with stimulus frequency ratio f_2/f_1. The simulation was performed using f_2=2 kHz various L_1 levels (40, 50 60 & 70) and L_2=L_1. (b) The variation in the predicted optimum stimulus frequency ratio with stimulus level. Physiological data from Harris *et al.* (1989) and Knight & Kemp (1999) is also shown for reference. The results from Harris *et al.* are averaged across f_2 frequencies between 1 and 4 kHz. The level difference used for these experimental measures is indicated in the key.

(a) Knight & Kemp (2001) (b) Simulation

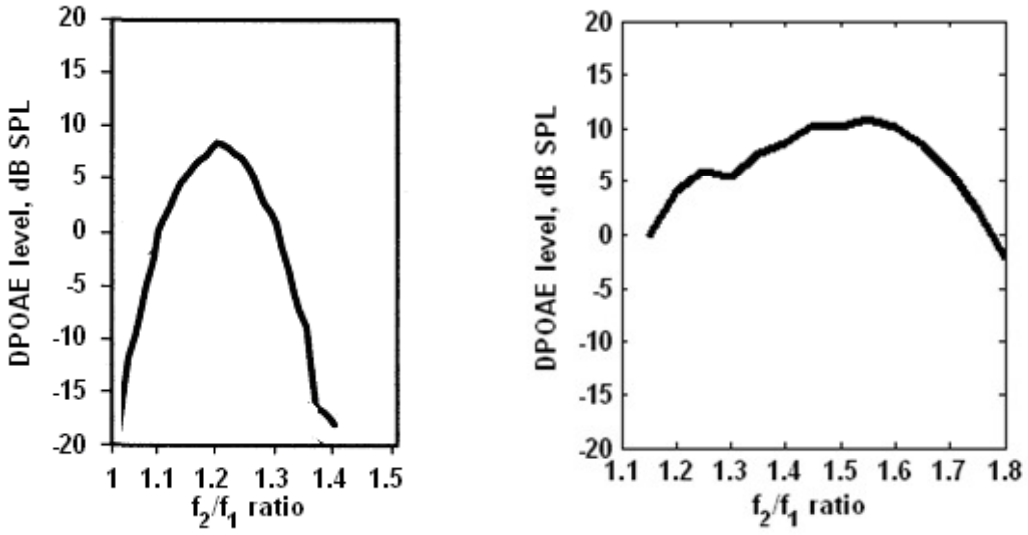

Figure 4.14 The dependence of $2f_1 - f_2$ DPOAE amplitude on f_2/f_1 ratio
(a) The wave-fixed (distortion) $2f_1 - f_2$ DPOAE amplitude measured from a human ear by Knight & Kemp (2001), using $L_1=L_2=$ 70 dB SPL. The result is averaged across recordings in which $2f_1 - f_2$ ranged between 1 and 4 kHz. [From Knight & Kemp (2001), figure 5a, with permission from ASA] (b) The simulated $2f_1 - f_2$ DPOAE amplitude when $L_1=L_2$=70 dB SPL and f_2=2 kHz, taken from figure 4.13a.

This tendency is demonstrated by figure 4.14 which shows the amplitude of the $2f_1 - f_2$ DPOAE as a function of stimulus frequency ratio for a higher stimulus level ($L_1=L_2$ = 70 dB SPL). This figure provides a comparison between the experimental result recorded by Knight & Kemp (1999) and the model simulation. The optimal f_2/f_1 of 1.55 predicted by the model is significantly greater than the stimulus frequency ratio of around 1.2 which maximises the $2f_1 - f_2$ emission in the Knight & Kemp study.

Figure 4.15 shows the influence of stimulus frequency on the optimal f_2/f_1 ratio predicted by the model. As the $2f_1 - f_2$ DP frequency is increased from 1.5 to 3 kHz, the simulated optimal f_2/f_1 ratio decreases from 1.3 to 1.18. This trend is consistent with the results of Harris *et al.* (1989) who found that the optimal f_2/f_1 ratio reduces from around 1.27 to 1.21 as the DP frequency increases from 1 to 4 kHz for stimulus levels between 65 and 85 dB SPL ($L_1=L_2$). However, the model appears to overestimate the rate at which the optimal f_2/f_1 ratio increases as stimulus frequency decreases.

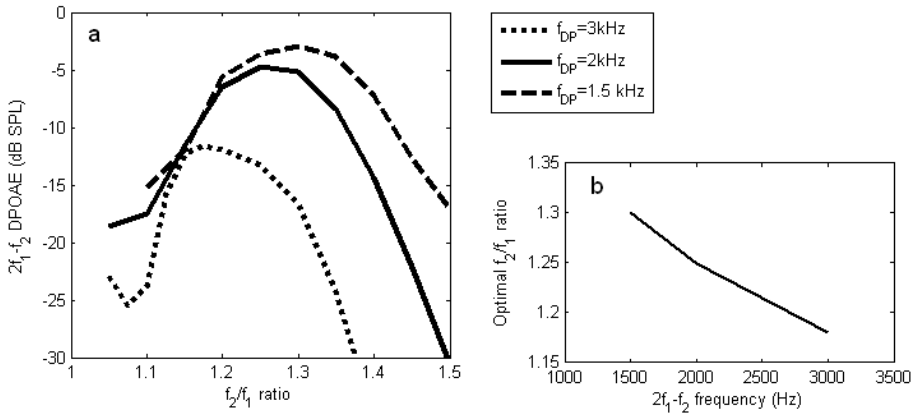

Figure 4.15 The influence of DP frequency on the optimal f_2/f_1 ratio
(a) The variation in the predicted $2f_1 - f_2$ DPOAE amplitude with stimulus frequency ratio f_2/f_1. The simulation was performed using various $2f_1 - f_2$ (f_{DP}) frequencies (1.5, 2 and 3 kHz) and L_1=L_2=50 dB SPL. (b) The dependence of the predicted optimal stimulus frequency ratio on DP frequency.

Origin of the optimal f_2/f_1 ratio

The bell-shaped dependence of the $2f_1 - f_2$ DPOAE on the f_2/f_1 ratio, exhibited by the model predictions (figure 4.13 and figure 4.15) and experimental measurements (figure 4.14a) is commonly attributed to changes in the amplitude of the primary travelling wave envelopes at the DP source region (Gaskill & Brown, 1990; Lukashkin & Russell, 2001). The stimulus frequency ratio can influence the levels A_1 and A_2 of the primary tones f_1 and f_2 respectively, near the f_2 best place which corresponds to the $2f_1 - f_2$ DP source region. Figure 4.16 illustrates that as f_2/f_1 increases from 1.05 to 1.6, the amplitude difference ($A_1 - A_2$) decreases from 0.7 dB to − 11.7 dB. This decrease in the level of A_1 relative A_2, as the spatial overlap of the primary travelling wave decreases, is thought to be responsible for the decline in the emission amplitude as the stimulus frequency ratio increases above the optimum f_2/f_1 value (Gaskill & Brown, 1990; Lukashkin & Russell, 2001; Mills, 2002). However, there is not an agreed explanation in the literature for the decline of the emission amplitude as the f_2/f_1 ratio falls below the optimum value. There are two predominant arguments for this effect. First, Lukashkin & Russell (2001) propose that the dependence of the $2f_1 - f_2$ DPOAE amplitude on the f_2/f_1 ratio is equivalent to the dependence on stimulus level difference ($L_1 - L_2$) and can therefore be entirely attributed to the behaviour of the nonlinear function in isolation (section 4.1.5). However, figure 4.11 suggests that, at low stimulus levels, it is necessary for A_1 to exceed A_2 by 20 to 25 dB in order $2f_1 - f_2$ DP component of the output of the nonlinear function to decline in amplitude. Considering that A_1 does not exceed A_2 by more than 1 or 2 dB for this stimulus paradigm, even at very low f_2/f_1 ratios (figure 4.16), it is not possible to attribute the decline in $2f_1 - f_2$ DPOAE amplitude below the optimum f_2/f_1 ratio to the behaviour of the isolated nonlinear function. The alternative explanation, suggested by Kanis & de Boer (1997), is that the decline of the DPOAE amplitude at low f_2/f_1 ratios occurs due to overloading, or saturation, of the nonlinear function leading to mutual suppression of the primary responses. They base this suggestion on the observation that a decline in DPOAE amplitude at very low f_2/f_1 ratios is not evident at low stimulus levels. Their explanation is tested in figure 4.17 which

shows the simulated dependence of the $2f_1 - f_2$ DPOAE amplitude on f_2/f_1 ratio. The result was evaluated for the full quasilinear model and for a manipulated model which neglects either the DP self-suppression or both the mutual suppression of the primary tones and the self-suppression of the DP. This figure demonstrates that when the effect of mutual suppression is neglected from the quasilinear model, the decline in emission amplitude at low stimulus frequency ratios is no longer apparent. Therefore we can confirm that mutual suppression seems predominantly responsible for the reduction in $2f_1 - f_2$ DPOAE amplitude at low f_2/f_1 ratios.

(a)

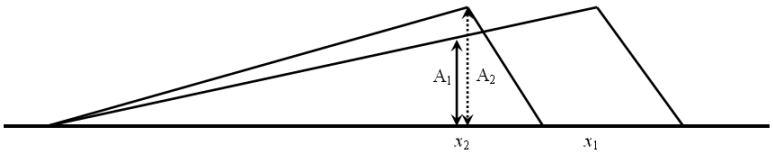

(b)

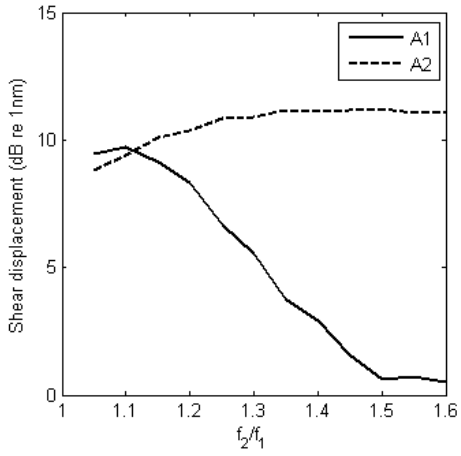

Figure 4.16. The influence of f_2/f_1 ratio on the amplitude to the input to the nonlinear function at the f_2 best place
(a) An illustration of the levels A_1 and A_2, which correspond to the amplitudes of the f_1 and f_2 primary travelling waves at the location of the f_2 best place. The labels x_1 and x_2 denote the best places for f_1 and f_2 respectively. [Redrawn from Lukashkin & Russell (2001), figure 1]. (b) The effective amplitudes A_1 and A_2, at the f_2 best place of the baseline cochlear model, when stimuli are presented at L_1=L_2=50 dB SPL with f_2 = 2 kHz. These amplitudes correspond to the f_1 and f_2 components of the difference in shear displacement between the BM and TM respectively, which serve as the input to the nonlinear function representing the action of the OHCs at this location.

Figure 4.17 Simulation of the influence of suppression on the optimal f_2/f_1 ratio
The amplitude of the $2f_1 - f_2$ DPOAE is simulated for a range of f_2/f_1 ratios in three different cochlear models, L_1=L_2=50 dB SPL and $2f_1 - f_2$=2 kHz. Results are shown for the full quasilinear model (solid line), a modified model excluding any self-suppression of the DP component (dotted line) and finally a modified model which excludes any mutual suppression of the primary frequency components, in addition to any self-suppression of the DP component (dashed line).

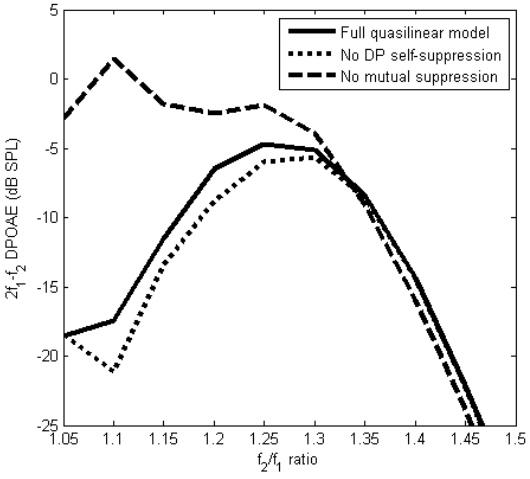

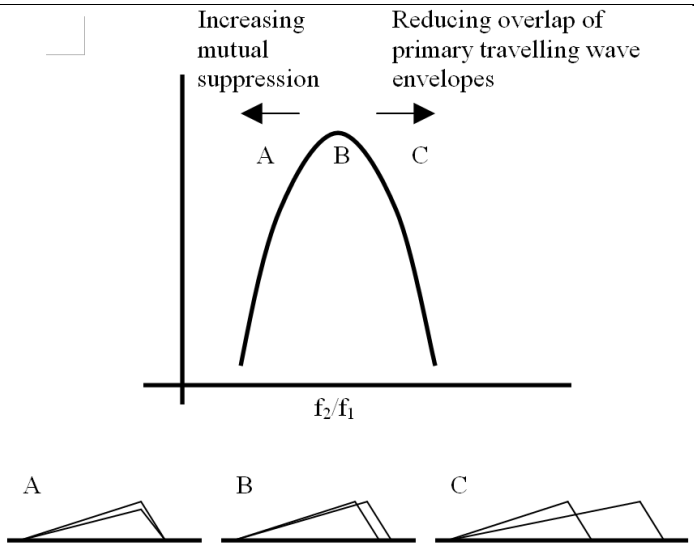

Figure 4.18 An illustration of the relationship between f_2/f_1 ratio and primary travelling wave overlap
Top: A representation of the $2f_1 - f_2$ DPOAE level as a function of f_2/f_1. Bottom: A picture of the change in overlap of the primary travelling wave envelopes corresponding to regions A, B, and C on the top graph.

In summary, figure 4.18 illustrates the origin of the influence of f_2/f_1 ratio on $2f_1 - f_2$ DPOAE amplitude. On this basis the value of the optimal f_2/f_1 ratio for a given stimulus level paradigm is determined in a rather complicated way by the sharpness of tuning of the primary travelling waves and the degree to which the nonlinear function, representing the action of the OHCs, becomes saturated when the primary travelling waves are almost superimposed. These factors are also expected to influence the rate at which the emission amplitude declines when the f_2/f_1 ratio deviates away from the optimal value.

4.1.7 Strengths and weaknesses of the model predictions

This section has reviewed the $2f_1 - f_2$ DPOAE properties which are predicted by the baseline cochlear model and revealed that the model has many strengths. For example, the amplitude of the predicted $2f_1 - f_2$ emission is consistent with experimental measures when f_2 is less than 4 kHz (section 4.1.2). The relative amplitude of the different order DPOAEs also appears to be in good agreement with that observed in physiological studies (section 4.1.1). The contour plots of $2f_1 - f_2$ DPOAE amplitude as a function of L_1 and L_2 are similar to those observed experimentally in terms of the range of amplitude values on the plot and the asymmetry in the dependence of the emission amplitude on L_1 and L_2 (section 4.1.3). The saturation threshold and growth rate of the emission with increasing stimulus level do not differ significantly from experimental results, at least for the stimulus paradigms considered in section 4.1.4. In addition the optimum level difference ($L_1 - L_2$) for the simulated $2f_1 - f_2$ DPOAE, and its dependence on stimulus level and stimulus frequency, are reasonably consistent with data from physiological studies (4.1.5). Finally we note that the optimum f_2/f_1 ratio for the predicted $2f_1 - f_2$ emission is consistent with experimental measures at low stimulus levels or high stimulus frequencies. The prediction that this optimum ratio will

increase with increasing stimulus level or decreasing stimulus frequency is qualitatively similar to trends observed in physiological studies (section 4.1.6).

The model made a few predictions regarding the behaviour of the $2f_1 - f_2$ DPOAE which were difficult to verify against experimental measurements. For example, the model suggests that the saturation threshold of the $2f_1 - f_2$ DPOAE should increase as stimulus frequency ratio increases. In section 4.1.4 we discuss that, although this tendency has been observed in some physiological studies it is not consistently evident at a statistically significant level, perhaps as a consequence of the large intersubject variation in DPOAE saturation thresholds. We also observe in section 4.1.4 that notches occur in the predicted emission growth function for some, but not all, stimulus level paradigms and stimulus frequencies. These notches are attributed to phase changes between the elements of the DP source region, but it has not been possible to verify their existence in the growth function of the wave-fixed (distortion) component recorded from human ear canals.

The greatest limitations of the model with regard to predicting $2f_1 - f_2$ DPOAE properties are as follows. Firstly, the model underestimates the amplitude of the $2f_1 - f_2$ DPOAE when f_2 is equal to or above 4 kHz. In chapter 6 we see that this is also true of the $2f_2 - f_1$ emission. The origin of this weakness, which we were unable to rectify, is discussed in section 4.1.2. The other limitations of the model were all associated with the prediction of the optimal f_2/f_1 ratio, which illustrates the sensitivity of this parameter to weaknesses in the model. For example, although the estimated optimal f_2/f_1 are consistent with physiological measures at low stimulus levels and high stimulus frequencies, the model tends to overestimate the optimal f_2/f_1 ratio at high stimulus levels (L_1 and $L_2 > 55$ dB SPL) and lower stimulus frequencies ($2f_1 - f_2$ less than 3 kHz). Also, at higher stimulus levels (e.g. 70 dB SPL) the level of the predicted emission does not decline sufficiently when f_2/f_1 is changed from the optimal value (figure 4.14). Section 4.1.6 identifies that the two factors which determine the optimal simulated f_2/f_1 ratio are the sharpness of tuning of the primary response and the degree to which the nonlinear function is saturated, but it is difficult to isolate these factors within the model to determine which may be at fault. However we can make some informed suggestions by comparing the dependence of DPOAE amplitude on f_2/f_1 ratio between our model and the original Kanis & de Boer model, as the models differ in terms of the change in sharpness of tuning with stimulus level and stimulus frequency. This comparison suggests that our model overestimates the optimal f_2/f_1 ratio at high stimulus levels due to the form of the nonlinear function, but that the insufficient fall-off in emission amplitude at non-optimal ratio values could be an indication that the passive response of the model is too broadly tuned. The comparison also implies that the optimal f_2/f_1 ratio predicted by our model is over sensitive to changes in stimulus frequency because the primary tone responses are too broad at low stimulus frequencies. Overall, the model limitations suggest that some improvements in $2f_1 - f_2$ DPOAE prediction could be made by reconsidering the sharpness of tuning of the BM travelling wave at low stimulus frequencies and the form of the nonlinear function in the future development of the model discussed in chapter 7.

In summary, we conclude that the baseline model makes appropriate predictions for a broad range of $2f_1 - f_2$ DPOAE properties and so it is valid to extend the application of the model to hypothesis testing and to investigate the source mechanisms for this emission. The weaknesses of the model suggest that caution should be used when analysing results of simulations which extend over a broad range of stimulus frequencies or stimulus levels.

4.2 Predictions of a perturbed model

There is considerable evidence from experimental and modelling studies that the $2f_1 - f_2$ DP is generated by two different mechanisms within the cochlea: A wave-fixed (distortion) source distributed over a region close to the f_2 best place, and a place-fixed (reflection) source located at the $2f_1 - f_2$ characteristic place. So far, only the wave-fixed component has been included in our predictions of the $2f_1 - f_2$ DPOAE as we have been using a baseline model in which no irregularities have been imposed on the cochlear partition impedance to act as place-fixed sites of reflection.

In this section we introduce random irregularities into the active mechanics of the cochlear partition, to act as sites of reflection. We refer to the model as "perturbed", rather than "baseline", when it incorporates such irregularities. We find that the incorporation of these irregularities allows the model to replicate some of the DPOAE fine structure characteristics which are observed experimentally.

4.2.1 The impedance irregularities

Zweig & Shera (1995b) propose that random irregularities in the impedance of the cochlear model can be used to generate OAE fine structure, similar to that observed in physiological measurement. They explain that, in a system in which Bragg scattering can occur, distributed irregularities in the impedance generate coherent reflection of forward travelling waves with wavelength λ when the spatial separation between the perturbations is equal to an integer multiple of λ/2. This coherent reflection process is illustrated in figure 4.19. If the forward travelling signal is composed of many different wavelengths, rather than one, then only the component with a wavelength equal to twice the spatial separation of the impedance irregularities will be coherently reflected. If the system contains randomly distributed irregularities then a forward travelling wave with wavelength λ will be coherently reflected from only those irregularities which are spatially separated by distances which are integer multiples of λ/2.

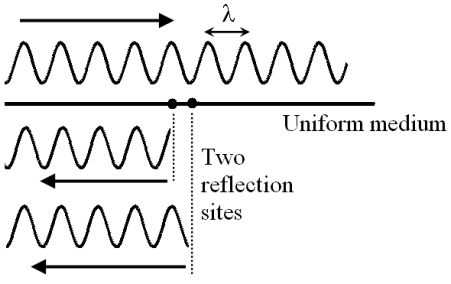

Figure 4.19 An illustration of coherent reflection in a uniform system
In this case the impedance irregularities as spatially separated by a distance λ/2, where λ is the wave length of the forward travelling wave.

The situation in the cochlea is more complicated as the impedance changes with longitudinal position and consequentially the wavelength of the travelling wave reduces as it propagates. Assuming for simplicity that the amplitude of the forward travelling wave within the cochlea has a constant amplitude and a wavelength which varies slowly with distance from the stapes, then it is theoretically possible for small amounts of coherent reflection to occur at any location within the cochlea given that the randomly distributed impedance irregularities are likely to contain some components with a spatial separation equal to half of the instantaneous wavelength. However, because the instantaneous wavelength changes as the forward travelling wave propagates, the reflected waves originating from different regions of the cochlea will have different wavelengths and the net result is an incoherent jumble of small reflected waves. For this reason, coherent reflections are mainly thought to occur within the cochlea because the amplitude of the travelling wave is *not* constant. The amplitude of the forward travelling wave is greatest in the vicinity of the characteristic place and so the reflected waves from this region dominate the total backward travelling wave. As the dominant backward travelling waves originate from a small region of the cochlea, and the wavelength of the travelling wave is assumed to vary slowly with distance, these reflections will be coherent and form a substantial backward travelling wave. Talmadge *et al.* (1998) note that coherent reflection of forward travelling waves will only occur in a cochlear model if two conditions are met. Firstly, the amplitude of the forward travelling wave at the site of reflection must exceed the amplitude of the incident wave at other locations and be sufficient to generate a reflection given the small scale of the impedance irregularities. Secondly, the peak of the travelling wave must be wide enough to incorporate 1 or 2 wavelengths of the travelling wave. It is helpful to recall this theory when considering the generation of the place-fixed component of DPOAEs in sections 4.2.2 and 6.3. For example, the conditions for coherent reflection outlined by Talmadge *et al.* may not be satisfied if the peak of the travelling wave envelope becomes too low or broad at high stimulus levels, as then the amplitude of the reflected waves from the best place of the forward travelling wave may fail to dominate those originating from other locations within the cochlear model. Similarly the amplitude of the reflected waves could be compromised if the scale of the impedance irregularities reduces with stimulus level in the quasilinear model.

The random irregularities which act as sites of reflection for forward travelling waves could be associated with impedance irregularities in either the active mechanics, perhaps from differences in the force exerted by neighbouring OHCs (Zweig & Shera, 1995a), or the passive mechanics, possibly from spatial variations in the BM radial fibres (Shera & Guinan, 2008). Talmadge *et al.* (1998) introduce random irregularities into the stiffness component of the CP impedance in their cochlear model in order to simulate spontaneous OAEs and DPOAE fine structure. Similarly Ku *et al.* (2009) introduced random irregularities into the active component of the CP impedance in order to simulate SOAEs. Following the work of Ku *et al*, we introduce random irregularities into the active component of the CP impedance in order to generate the place-fixed (reflection) component

of the $2f_1 - f_2$ DP. This is implemented using the OHC gain parameter, $\gamma(x)$, which was introduced in equation (2.20) and takes a value between 0 and 1 (Elliott *et al.*, 2007; Ku *et al.*, 2008). When an irregularity is introduced into the cochlear model, we can apply the decomposition process described in section 2.3, to estimate the forward and backward components of the total semi-difference pressure, which we label $p_d^+(x)$ and $p_d^-(x)$ respectively. Although this method was developed for the linear model, we invoke the quasilinear approximation in order to apply to the primary or DP components which arise in response to two tone stimulation of the nonlinear cochlear model.

Given that the CA gain of the cochlear model decreases with distance from the stapes, the amplitude of the impedance irregularities distributed along the CP will have to increase in order for the model to be capable of generating equal amplitude reflections from basal and apical regions. The size of a single step-increase in $\gamma(x)$ that would be necessary to evoke equal reflections at different locations in the model is shown in figure 4.20. When random irregularities are imposed on the $\gamma(x)$ distribution of the quasilinear model, the amplitude of the irregularities is scaled using the distribution shown in figure 4.20. This allows sufficient reflection of low frequency travelling waves (<4 kHz), such that the place-fixed component of the DP is detectable in the ear canal, without causing the model to become unstable when higher frequency stimuli are present. Figure 4.21 shows the distribution of random irregularities imposed on the OHC gain distribution throughout this chapter. The root-mean-square of the variation in the maximum value of $\gamma(x)$ between the 1 and 2 kHz characteristic places is 5%.

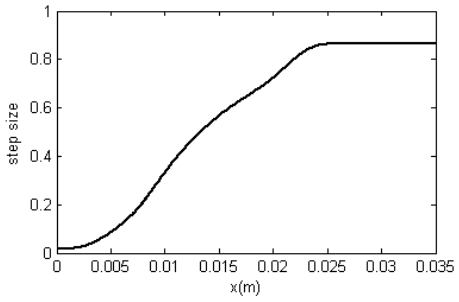

Figure 4.20 The gain step size required for a constant reflection ratio throughout the model
The plot shows the step-increase in OHC gain $\gamma(x)$ required at position x, to achieve a reflection ratio of $\left|p_d^- / p_d^+\right|_{x=0} = 1.3$ when the stapes is stimulated at the characteristic frequency. The value of $\gamma(x)$ between the base and the step-change is set equal to 1, and the stapes boundary condition is set to minimise reflections of the backward travelling wave. The reflection ratio 1.3 is chosen for this example as it is the highest reflection ratio that can be achieved with out introducing instability.

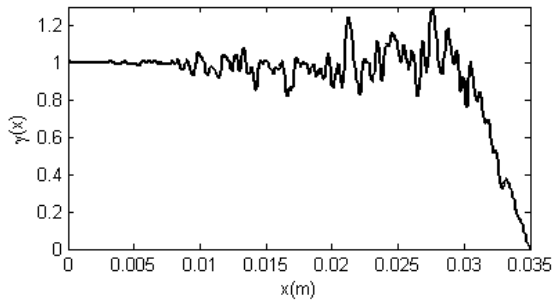

Figure 4.21 The $\gamma(x)$ distribution used in the perturbed cochlear model
This distribution results from imposing random irregularities on the active $\gamma(x)$ distribution.

The physiological origin of the impedance irregularities could be associated with differences in the orientation or force exerted by neighbouring OHCs (Shera & Guinan, 2008). The irregularities are thought to occur even in healthy human cochleae, as some disorganisation is evident in the spatial distribution of human OHCs in fresh tissue samples, and some OHCs may be missing completely (Glueckert *et al.*, 2005). We have not been able to establish from the literature whether or not the increased amplitude of the impedance variations between the base and the apex, used in the model, are evident in the human cochlea. This is because it is unusual to find descriptions of invasive observations within the human cochlea, and those observations of human OHCs which are available in the literature do not compare spatially separated sites. It is also possible that impedance irregularities may not be visible in the anatomy (Withnell *et al.*, 2003), as they could be associated with differences in force exerted by neighbouring OHCs, rather than differences in their spatial orientation, and it would not be evident from visual inspection of tissue samples if these variations in OHC performance were more exaggerated in the apical region compared to the basal region of the cochlea.

4.2.2 Estimating the place-fixed component

In this investigation, the place-fixed (reflection) component of the DP is estimated by comparing two separate simulations. The first uses a baseline cochlear model to determine the wave-fixed (distortion) component of the DPOAE, and the second uses a perturbed model in which the irregularities described in section 4.2.1 are imposed on the active cochlear partition impedance to estimate the total DPOAE. It is then assumed that the place-fixed (reflection) component corresponds to the difference between these simulations such that

$$\text{Place-fixed DP} = \text{Total DP} - \text{Wave-fixed DP} \tag{4.1}$$

This approach has limitations in a nonlinear model. For example, it is possible that the introduction of impedance irregularities into the model may not only introduce a place-fixed reflection of the DP travelling waves, but could also alter the wave-fixed DP source via reflections which could occur in the primary travelling waves. However, in section 5.1.4 we show that the largest contribution to the place-fixed DPOAE component originates from impedance irregularities at the $2f_1 - f_2$ characteristic place. For this reason we proceed with this simple approach to estimating the place-fixed DPOAE component.

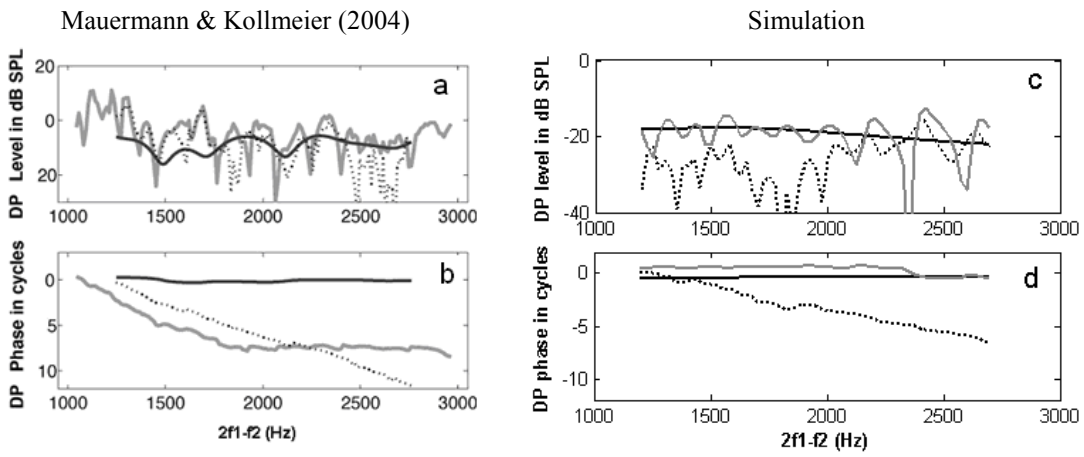

Figure 4.22 $2f_1 - f_2$ DPOAE fine structure
The (a) amplitude and (b) phase of the $2f_1 - f_2$ DPOAE recorded from one ear by Mauermann & Kollmeier (2004), using L_1=51 and L_2=30 dB SPL with f_2/f_1=1.2. A time windowing procedure was used to separate the total DPOAE (grey line) into component with difference phase behaviours: A component with essentially constant phase (black solid line) and a component with phase which varies rapidly with $2f1 - f2$ frequency (black dotted line). [From Mauermann & Kollmeier (2004), figure 1 b and c, with permission from ASA]. The (c) amplitude and (d) phase of the predicted $2f_1 - f_2$ DPOAE simulated in the cochlear model, using L_1=50 and L_2=30 dB SPL with f_2/f_1=1.25. The total emission, the wave-fixed component and the place-fixed component are again denoted by the solid grey, the solid black, the dotted black lines respectively.

4.2.3 The $2f_1 - f_2$ DPOAE fine structure

In experimental studies, peaks and troughs in the $2f_1 - f_2$ DPOAE amplitude are observed as f_2 is varied for a fixed stimulus frequency ratio. This amplitude fluctuation is known as 'fine structure'. Figure 4.22 shows the $2f_1 - f_2$ DPOAE fine structure recorded from a human ear canal by Mauermann & Kollmeier (2004). The simulated $2f_1 - f_2$ DPOAE fine structure predicted by the model is also shown for comparison. The stimulus frequency ratio used in the simulation is higher than that used in the experimental study in order maximise the amplitude of the simulated emission at this stimulus level. The figure demonstrates that both the physiological measurement and the simulation exhibit peaks and troughs in the $2f_1 - f_2$ DPOAE amplitude. These amplitude fluctuations exceed 10 dB. This is consistent with the observation of Dhar & Abdala (2007), who found that the fine structure trough-to-peak amplitude in their 10 adult subjects was approximately 16 dB ± 8 dB.

Mauermann & Kollmeier (2004) use a time windowing technique to separate the total DPOAE into two components with different phase behaviours: one component has essentially constant phase, whilst the phase of the other component varies rapidly with stimulus frequency. Figure 4.22 shows that the wave-fixed component estimated by the model has similar phase behaviour to the component with constant phase observed by Mauermann & Kollmeier. These wave-fixed components exhibit little amplitude variation as the stimulus frequency changes. In contrast, the phase of the predicted place-fixed component varies rapidly as the stimulus frequency changes, in a comparable manner to the second component extracted by Mauermann & Kollmeier. Also, unlike

the wave-fixed components, the place-fixed components fluctuate in amplitude as the stimulus frequency changes in both the model simulation and the experimental measure.

In many experimental studies of $2f_1 - f_2$ DPOAE fine structure, the spacing between two minima occurring at adjacent frequencies of f_a and f_b has been quantified using the ratio $\Delta f/f_{mean}$, where $f_{mean} = \sqrt{f_a f_b}$ and Δf is given by $f_b - f_a$. Smaller values of this ratio indicate narrower fine structure. The ratio typically takes a value of around 1/15 for human subjects (Zweig & Shera, 1995b; Dhar & Abdala, 2007), but tends to increase as the stimulus frequency decreases. For example, Dhar & Abdala (2007) found that if the $2f_1 - f_2$ DP frequency reduced from 2000 to around 750 Hz, the $\Delta f/f_{mean}$ ratio increases from 0.06 ± 0.02 to 0.15 ± 0.02. The fine structure predicted by the model for DP frequencies of 2000 and 750 Hz exhibit $\Delta f/f_{mean}$ ratio values of 0.08 and 0.13 respectively, which is consistent with the results of Dhar & Abdala.

Origin of the fine structure

Fine structure in the amplitude of the $2f_1 - f_2$ DPOAE was first reported by Gaskill & Brown (1990) and He & Schmiedt (1993). It is thought to arise because the total $2f_1 - f_2$ is formed of a vector sum of two components (Brown *et al.*, 1996) which have different phase characteristics (Shera & Guinan, 1999). These two components have been identified in various experimental and modelling studies (Shaffer *et al.* (2003),Talmadge *et al.* (1998) etc) and are evident in the perturbed cochlear model (figure 4.22).

There are two ways in which the wave-fixed and place-fixed DPOAE components could combine to form $2f_1 - f_2$ DPOAE fine structure evident in the cochlear model. Firstly, amplitude fluctuations in the place-fixed component could directly result in amplitude variations for the total DPOAE. Secondly, amplitude fluctuations in the total $2f_1 - f_2$ DPOAE could arise from alternating constructive and destructive summation between the wave-fixed and place-fixed components, which is expected to occur as a consequence of their different phase characteristics. Figure 4.22 suggests that both of these effects can influence the formation of $2f_1 - f_2$ DPOAE fine structure at different stimulus frequencies. For example there are DP frequencies, in both the model simulation (near 2500 Hz) and the physiological measurement (around 1500 Hz), at which the amplitude of the place-fixed component approaches that of the wave-fixed component and under these conditions the fine structure of the total DPOAE appears to exhibit peaks and troughs at frequencies which correspond to fluctuations in the amplitude of the place-fixed component. This indicates that at these DP frequencies, the DPOAE fine structure arises predominantly from amplitude fluctuations in the place-fixed component. The model simulation suggests that the level of the place-fixed component must exceed that of the wave-fixed component by at least 5 to 10 dB if this effect is to be the primary cause of the fine structure.

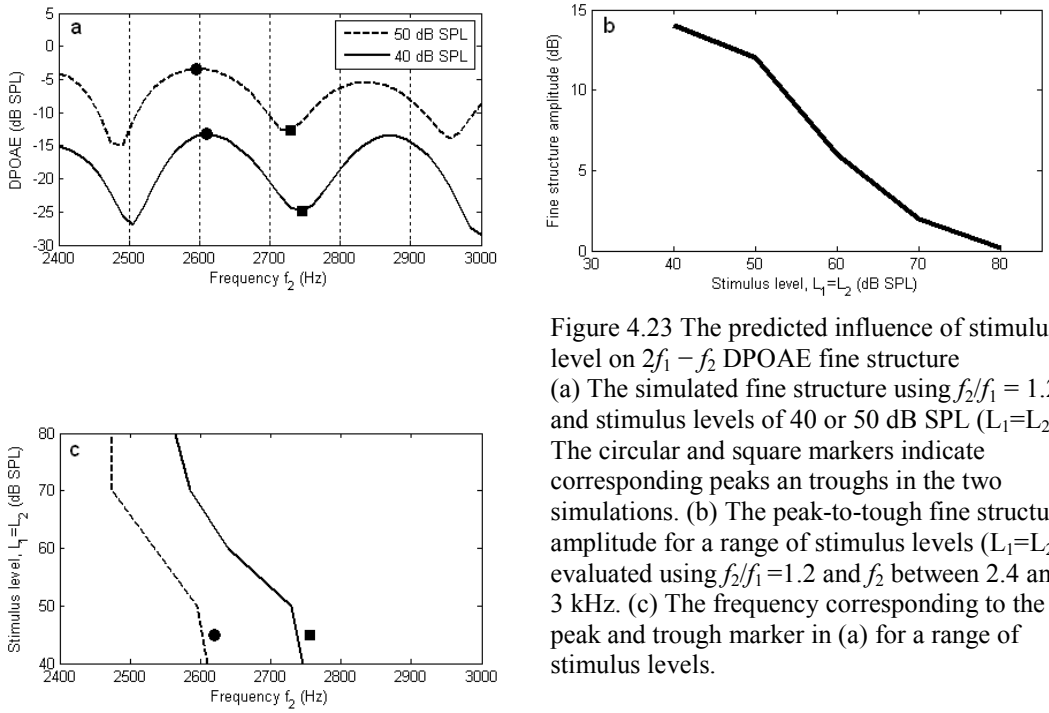

Figure 4.23 The predicted influence of stimulus level on $2f_1 - f_2$ DPOAE fine structure (a) The simulated fine structure using f_2/f_1 = 1.2 and stimulus levels of 40 or 50 dB SPL (L_1=L_2). The circular and square markers indicate corresponding peaks an troughs in the two simulations. (b) The peak-to-tough fine structure amplitude for a range of stimulus levels (L_1=L_2) evaluated using f_2/f_1 =1.2 and f_2 between 2.4 and 3 kHz. (c) The frequency corresponding to the peak and trough marker in (a) for a range of stimulus levels.

At other DP frequencies, the fine structure is thought to be formed mainly from the constructive and destructive summation of the two components. For example, the predicted peak and trough observed in the total emission amplitude at DP frequencies of 1.6 and 2.4 kHz respectively correspond to relative phase differences between the place-fixed and wave-fixed components of 2.04 and 5.52 cycles in that order.

The influence of stimulus parameters on predicted fine structure

Figure 4.23 shows how the properties of the simulated $2f_1 - f_2$ DPOAE fine structure vary with stimulus level. The model predicts that the stimulus level will affect the fine structure in two ways. Firstly, the amplitude of the fine structure will reduce as the stimulus level increases. Figure 4.23b estimates that the peak-to-trough amplitude will decrease from approximately 13 to 4 dB as the stimulus level increases from 45 to 65 dB SPL for these stimulus frequencies (f_2/f_1=1.2 and f_2= 2.4 to 3 kHz). The cause of this effect within the cochlear model is likely to be associated with the change in the relative amplitude of the wave-fixed and place-fixed DPOAE components discussed in section 4.2.5. Secondly, the f_2 stimulus frequencies at which the peaks and troughs occur will shift towards lower frequencies as the stimulus level increases. Figure 4.23c suggests that the peaks and troughs can shift by 100 − 150 Hz as the stimulus level increases from 40 to 60 dB SPL. This may be due to the basal shift in the best places for f_1 and f_2 as the stimulus level increases. These two trends are also evident in experiment measures. For example, figure 4.24 shows the $2f_1 - f_2$ DPOAE fine structure recorded by He & Schmiedt (1993). This illustrates that the peak-to-trough amplitude of the fine structure decreases from around 15 to 5 dB as the stimulus level increases from 45 to 65 dB SPL.

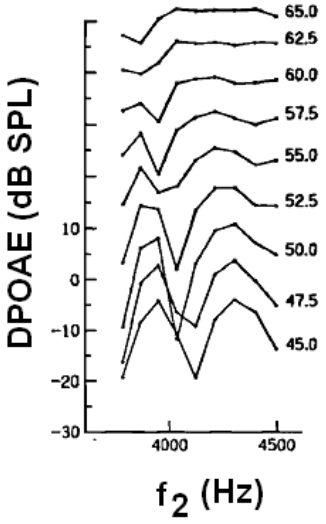

Figure 4.24 Measured influence of stimulus level on $2f_1 - f_2$ DPOAE fine structure
The results were observed from one ear by He & Schmiedt (1993), using $L_1=L_2$ and $f_2/f_1=1.2$.
[From figure 4 of He & Schmiedt (1993), with permission from ASA]

He & Schmiedt also observe that the f_2 frequencies at which peaks and troughs occur shift towards lower frequencies as the stimulus level increases. In this example, the shift is approximately 200 Hz for a 20 dB increase in stimulus level. Therefore the influence of stimulus level on the fine structure predicted by the model is also observed, on a similar scale, in experimental measurements.

4.2.4 Notches in the $2f_1 - f_2$ DPOAE growth function

In section 4.1.4 we observed that notches can occur in the growth function of the $2f_1 - f_2$ DPOAE predicted by a baseline model. These notches occurred for some, but not all, stimulus paradigms when the stimulus level was around 50 to 60 dB SPL. They were attributed to changes in the relative phase of elements within the source region of the wave-fixed $2f_1 - f_2$ DP as the stimulus level increased. However, He & Schmiedt (1993) suggest that notches should also occur as a consequence of shifts in fine structure associated with the mixing of the wave-fixed and place-fixed components of the DPOAE in the ear canal.

Figure 4.25a shows the growth of the simulated $2f_1 - f_2$ DPOAE with increasing stimulus level, using a paradigm in which $L_1=L_2$, $f_2/f_1=1.1$ and $f_2=2.5$ kHz. In this case the predicted wave-fixed component, evaluated using the baseline model, exhibits no significant notch. There is a change in the growth rate of the simulated wave-fixed component when the stimulus level reaches 60 dB, associated with the phase changes between elements within the DP source region, but no substantial reduction in the amplitude of this component is observed. In contrast, when the growth of the total DPOAE is predicted by the perturbed model, a notch appears in the simulated growth function at a stimulus level of 60 dB SPL. The total DPOAE predicted by the perturbed model is made up of a wave-fixed and a place-fixed component, and the phase difference between these components as the stimulus level increases is shown in figure 4.25b.

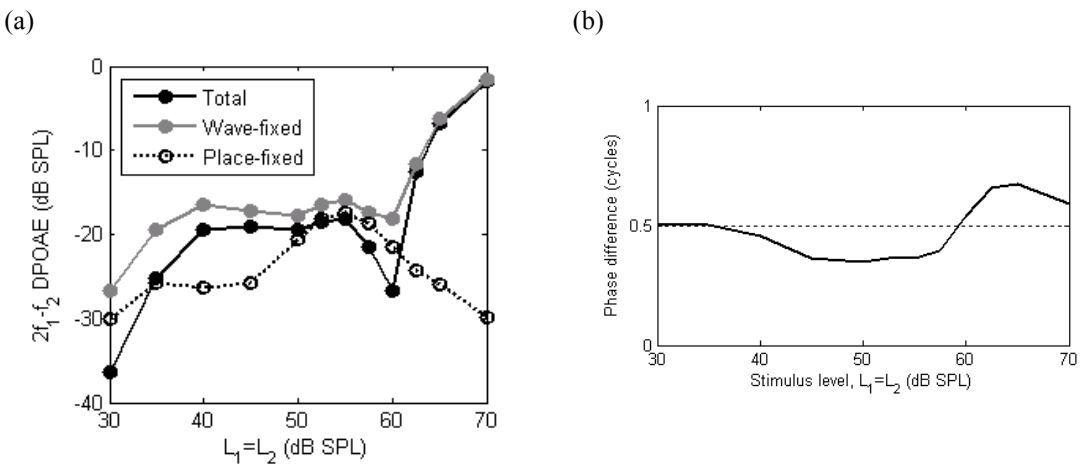

Figure 4.25 The predicted growth of the wave-fixed and place-fixed components
(a) The simulated amplitude of the predicted $2f_1 - f_2$ DPOAE and the wave-fixed and place-fixed components for increasing stimulus level (L_1=L_2 and f_2/f_1=1.1 and f_2=2500 Hz). (b) The phase difference between the place-fixed and wave-fixed components shown in (a).

The notch in the growth function of the total emission, at a stimulus level of 60 dB SPL, is thought to arise from destructive summation between the place-fixed and wave-fixed components of the DPOAE, as the phase difference between the two components is almost exactly ½ a cycle at this stimulus level. It is also interesting to note that the two components are again almost ½ a cycle out of phase at a stimulus level of 30 dB SPL, where the predicted amplitude of the total $2f_1 - f_2$ emission is less than the amplitude of either the wave-fixed or place-fixed components.

4.2.5 The influence of stimulus parameters on the place-fixed component

The influence of stimulus level

Figure 4.25a shows that the amplitude of the predicted $2f_1 - f_2$ DPOAE place-fixed component relative to the wave-fixed component decreases as stimulus level increases above 55 dB SPL. This is consistent with the experimental observation of Mauermann & Kollmeier (2004), who found that the amplitude of the place-fixed component decreased relative to the wave-fixed component at L_2 levels above 50 dB SPL in all of their 6 subjects using a 'scissor' stimulus paradigm (section 1.5.2). Figure 4.25a suggests that the relative amplitude difference between the DP components which occurs from stimulus levels in excess of 60 dB SPL arises because the considerable predicted increase in the wave-fixed component amplitude is accompanied by a decrease in the amplitude of the simulated place-fixed component. There are several factors which could be responsible for this including changes in source directionality, reduced influence of the irregularities in the active micromechanics as the model becomes more passive, and the broadening of the BM response to stimulation at higher stimulus levels.

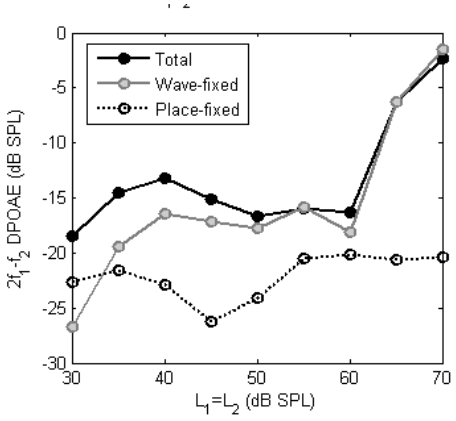

Figure 4.26 Simulated growth of the wave-fixed and place-fixed components in an alternative perturbed model
The plot shows the predicted amplitudes of the $2f_1 - f_2$ DPOAE and the wave-fixed and place-fixed components with increasing stimulus level (L_1=L_2 and f_2/f_1=1.1 and f_2=2500 Hz). In this case a different perturbed model was used, compared to that used throughout the rest of this thesis. The impedance irregularities were introduced into the passive, rather than the active, micromechanical impedance.

The first two explanations are unlikely to be primarily responsible for the predicted relative decline in the amplitude of the place-fixed component at high stimulus levels. Section 5.1.3 explains that any change in source directionality with stimulus level is expected promote forward travelling waves propagating towards the place-fixed reflection site at higher levels, not diminish them. In addition, figure 4.26 shows the simulated growth of the emission evaluated using a modified perturbed cochlear model in which the impedance irregularities were introduced into the passive, not the active, micromechanics. This demonstrates that the predicted increase in the wave-fixed component amplitude relative to the place-fixed component does not seem to be directly related to the reduced influence of irregularities in the active micromechanics at high stimulus levels. However, the broadening of the BM response could explain the relative amplitude difference between the two DP components as the stimulus level increases. To illustrate this, figure 4.27 shows the influence of the suppression of the DP travelling wave on the growth of the total predicted $2f_1 - f_2$ DPOAE and its wave-fixed and place-fixed components. The CA supplies energy to the DP travelling wave over a distributed region of the cochlea, but is most active at a distance of 13 mm from the stapes for this simulation. Figure 4.27a demonstrates that the CA gain at this location reduces from about 1 to less than 0.2 as the stimulus levels (L_1=L_2) increase from 30 to 70 dB SPL. Figure 4.27b shows the spatial distribution of the BM response at the DP frequency and illustrates that the CA gain reduction is associated with a broadening of the DP travelling wave which could lead to a reduction in coherent reflection from the DP characteristic place. Given the low amplitude of the DP travelling wave, the origin of the extensive CA suppression at the DP frequency at high stimulus levels is likely to result from the primary travelling waves rather than self-suppression of the DP component. The influence of DP suppression on the relative amplitude of the wave-fixed and place-fixed components of the DPOAE is confirmed by figure 4.27c, which shows the growth of the $2f_1 - f_2$ emission predicted by a modified cochlear model in which the DP travelling wave is not influenced by suppression. In this modified simulation the amplitude of both the wave-fixed and place-fixed DPOAE components increase with the stimulus level and so no substantial relative amplitude different arises.

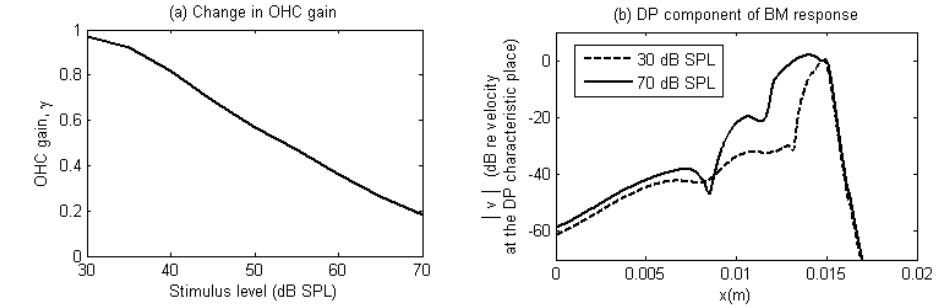

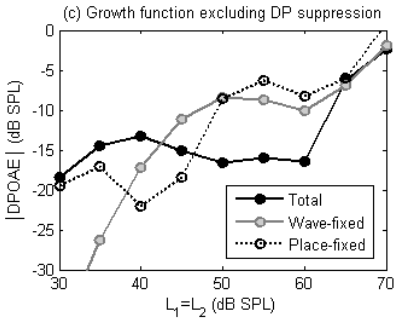

Figure 4.27 The influence of self-suppression on the growth of the $2f_1 - f_2$ DP
(a) The predicted OHC gain, observed in the quasilinear model at a location corresponding the point of maximum CA activity at the DP frequency in a fully active linear model (a distance of 13 mm from the stapes in this case). (b) The simulated DP component of the BM velocity response to stimulation by two tones, f_1 and f_2. The response is shown for stimulus levels (L_1=L_2) of 30 and 70 dB SPL. (c) The predicted growth function for the $2f_1 - f_2$ DPOAE in a quasilinear model which has been modified so that the DP travelling wave is not suppressed by the primary tones or influenced by self-suppression. In all plots, f_2= 2 kHz and f_2/f_1 =1.2.

The influence of stimulus frequency

The $2f_1 - f_2$ DPOAE fine structure simulation shown in figure 4.22b demonstrates that the absolute amplitude of the predicted place-fixed component varies with stimulus frequency, and that the relative amplitude of the place-fixed and wave-fixed components can also vary with stimulus frequency. The fluctuations in the absolute amplitude of the predicted place-fixed component are expected to arise due to the random size variations in the impedance irregularities imposed on the active micromechanics of the cochlear model. Substantial changes in the relative amplitudes of the wave-fixed and place-fixed components with stimulus frequency could be associated with several different properties of the model, all of which may contribute to a certain degree. Firstly, the properties of the middle ear result in changes in the effective level of the stimuli reaching the cochlea as the stimulus frequency varies, even when the stimulus levels in the ear canal are kept constant. This could be significant because, as discussed above, the stimulus level can affect the amplitude of the place-fixed component relative to the wave-fixed component of the DPOAE. Secondly, the extent of spatial overlap between the primary travelling waves in the cochlear model is likely to change with stimulus frequency, even if the f_2/f_1 ratio is fixed, due to the change in the sharpness of tuning of the BM response with stimulus frequency (section 3.4.2). Changes in spatial overlap can influence the relative phase of the elements with the wave-fixed DP source distribution and impact on the directionality of the source (section 5.1.3). These alterations in source

directionality could lead to changes in the relative amplitude of the wave-fixed and place-fixed DPOAE components as a consequence of stimulus frequency variation.

The influence of stimulus frequency ratio

Figure 4.28 shows the variation in amplitude of the predicted place-fixed $2f_1 - f_2$ DPOAE component with stimulus frequency ratio. This plot contains a simulation, and the experimental result of Knight & Kemp (2001) for comparison. The simulation predicts that the amplitude of the wave-fixed component will exceed that of the place-fixed component when the stimulus frequency ratio is close to the optimal value, between 1.2 and 1.6 for the cochlear model. When f_2/f_1 exceeds 1.15, the amplitude of the predicted place-fixed component decreases as the stimulus frequency ratio increases. The origin of this effect within the cochlear model is likely to be a change in the directionality of the spatially distributed wave-fixed DP source. In section 5.1.1, the source length is shown to change as the f_2/f_1 ratio changes which can impact on the source directionality (section 5.1.3). This decrease in the amplitude of the predicted place-fixed DPOAE component with increasing stimulus frequency ratio is in agreement with the experimental measurement, in which the wave-fixed component dominates the place-fixed component for f_2/f_1 ratios between 1.1 and 1.35. At very high stimulus frequency ratios, the amplitude of both components declines in the simulation and the physiological result. However, at very low f_2/f_1 values (<1.15) the model predicts that the amplitude of the place-fixed DPOAE component should decline as the stimulus frequency ratio approaches unity. This is in contrast to the experimental outcome, which suggests that the amplitude of this component continues to rise as f_2/f_1 approaches unity.

(a) Knight & Kemp (2001)

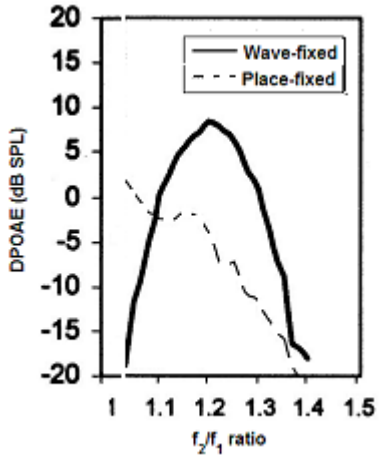

(b) Simulation

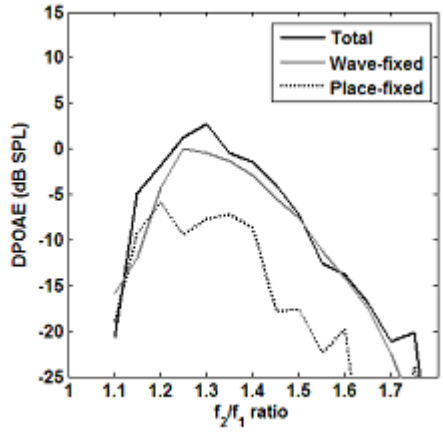

Figure 4.28 The influence of f_2/f_1 ratio on the wave-fixed and place-fixed DPOAE components
(a) The amplitude of the wave-fixed and place-fixed components of the $2f_1 - f_2$ DPOAE measured by Knight & Kemp using a time windowing technique. The DP frequencies are averaged between 1.1 and 4 kHz, and $L_1=L_2=70$ dB SPL. [From Knight & Kemp (2001), figure 5, with permission from ASA] (b) The predicted amplitude of the total $2f_1 - f_2$ DPOAE and the wave-fixed and place-fixed components. The simulation was performed using $L_1=L_2=50$ dB SPL and f_2=2kHz.

Other studies, such as that of Wilson & Lutman (2006), have also observed that at low f_2/f_1 ratios that amplitude of the place-fixed component exceeds that of the wave-fixed component by around 15 dB. Therefore the model tends to underestimate the amplitude of the place-fixed component, relative to the wave-fixed component, at low stimulus frequency ratios below approximately 1.15. There could be several explanations for this. For example, it is possible that if the tuning of the BM response is too broad in the cochlear model then the wave-fixed DP source region may extend too close to the DP characteristic place at low f_2/f_1 and adversely affect the generation of the place-fixed component at this location. This suggested weakness of the model would be consistent with some of the limitations noted previously in section 4.1.7 regarding the dependence of the wave-fixed $2f_1 - f_2$ DPOAE on stimulus frequency ratio. It is also possible that self-suppression of the DP response may be occurring in the model at low f_2/f_1 ratios, which would impact the sharpness of tuning of the BM response and the CA gain at the DP characteristic place and could therefore reduce the amplitude of the place-fixed component.

4.3 Conclusions regarding $2f_1 - f_2$ DPOAE prediction

This chapter provides a response to the following research questions posed in section 1.9 concerning the predicted $2f_1 - f_2$ DPOAE:

- What are the strengths and weaknesses of the model regarding $2f_1 - f_2$ DPOAE prediction?
- What explanation does the model provide for the dependence of the $2f_1 - f_2$ DPOAE amplitude on the stimulus parameters?
- What causes notches in the growth of the $2f_1 - f_2$ DPOAE predicted by the model?
- What is the origin of DPOAE fine structure in our model?

From sections 4.1 and 4.2 we identify the strengths and weaknesses of the model regarding $2f_1 - f_2$ DPOAE predictions. Overall we conclude that the model makes appropriate predictions for a broad range of $2f_1 - f_2$ emission properties and that it is valid to extend the application of the model to investigate source mechanisms for this emission, and to test experimental hypotheses. The limitations of the model suggest improvements that could be made in future development which are discussed in chapter 7. Sections 4.1.5 and 4.1.6 provide evidence which is used to either verify or challenge existing theories concerning the basis of stimulus effects on DPOAE level. Sections 4.1.4 and 4.2.4 identify notches in the growth of the predicted $2f_1 - f_2$ DPOAE, including a notch in the growth of the estimated wave-fixed DPOAE component for a small range of stimulus paradigms. A possible explanation for this notch is suggested, based on the work of Mills (2002). Finally, section 4.2.3 illustrates the predicted $2f_1 - f_2$ DPOAE fine structure and discusses the two ways in which this fine structure could be formed in the model from combination of the wave-fixed and place-fixed components.

The main contributions of this chapter are listed below and correspond to the summary given in section 1.9(iii-v).

- A comprehensive prediction of $2f_1 - f_2$ DPOAE characteristics for a broad range of stimulus parameters, using a model which can estimate both the wave-fixed and place-fixed components of the emission
- Confirmation that the Lukashkin & Russell (2001) explanation for the reduction in the $2f_1 - f_2$ DPOAE amplitude when $L_1 >> L_2$, which leads to the occurrence of an optimal stimulus level difference for this DP, can be extended to a coupled cochlear model (section 4.1.5)
- New evidence for attributing the reduction of $2f_1 - f_2$ DPOAE amplitude at low f_2/f_1 ratios to the effect of mutual suppression of the primary tones (section 4.1.6)
- Identification and explanation of predicted notches in the growth of the estimated wave-fixed $2f_1 - f_2$ DPOAE component for a small range of stimulus paradigms (section 4.1.4)

5. Predicted $2f_1 - f_2$ DPOAE source and transmission mechanisms

Having gained an understanding of the strengths and weaknesses of the model with regarding $2f_1 - f_2$ DPOAE prediction, in this chapter the model is applied to address the remaining research questions posed in section 1.9 concerning the $2f_1 - f_2$ DPOAE. This includes an investigation of the mechanism and location of the $2f_1 - f_2$ DP source within the cochlear model. As the cochlear origin of the $2f_1 - f_2$ DPOAE has been studied extensively in human subjects, these results provide useful verification of the generation mechanisms within the model.

We also apply the model to hypothesis testing in section 5.2. Two particular hypotheses are considered: those relating to the Allen & Fahey (1998) and the He *et al.* (2008) experiments. These studies were chosen as illustrations of cases in which the model either challenges or supports the experimental hypothesis. These experimental studies are also interesting because they have been used in the literature to inform on the transmission mechanism by which the $2f_1 - f_2$ DP propagates out of the cochlea from its generation site.

5.1 Investigation of source mechanism and location

The source mechanism for the $2f_1 - f_2$ DP has been detailed extensively in the literature. Figure 5.1 illustrates this generation mechanism, which consists of two components: a wave-fixed source positioned in the vicinity of the f_2 best place, and a place-fixed source located at the DP characteristic place. This simple picture is likely to be complicated in reality by multiple reflections between the base and the DP characteristic place (Stover *et al.*, 1996).

In this section we determine the source of the $2f_1 - f_2$ distortion product in the model, and confirm that it is consistent with the two source illustration given in figure 5.1. We assume that the wave-fixed component corresponds to the $2f_1 - f_2$ DPOAE which is predicted by the baseline model, and that the place-fixed component can be estimated by comparing the emission simulated by the perturbed model with that simulated by the baseline model (section 4.2.2). We start by considering the location and distribution of the wave-fixed component, and its directional properties. We then investigate the location of the place-fixed source in the perturbed cochlear model. This approach allows us to develop analysis tools which will be useful for investigating the source of the $2f_2 - f_1$ DPOAE, which is less well understood, in chapter 6.

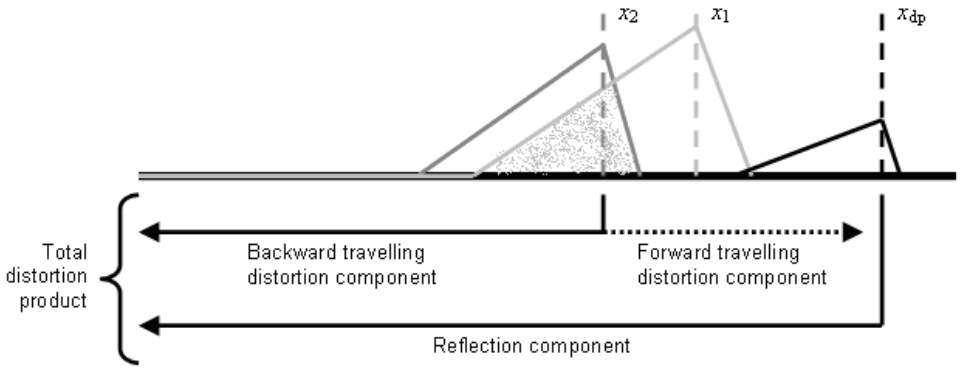

Figure 5.1 Illustration of the two source components for a lower side band emission
This picture is based on figure 1 of Shaffer *et al.* (2003) and refers only to lower side band emissions, such as the $2f_1 - f_2$ DPOAE. The grey triangles represent the travelling wave envelopes evoked by the stimulus tones f_1 and f_2. The black triangle denotes the distortion product (f_{dp}) travelling wave, and the grey shaded region shows the predicted region of origin for the distortion source. Distortion products at other frequencies (not $2f_1 - f_2$) have been neglected for clarity.

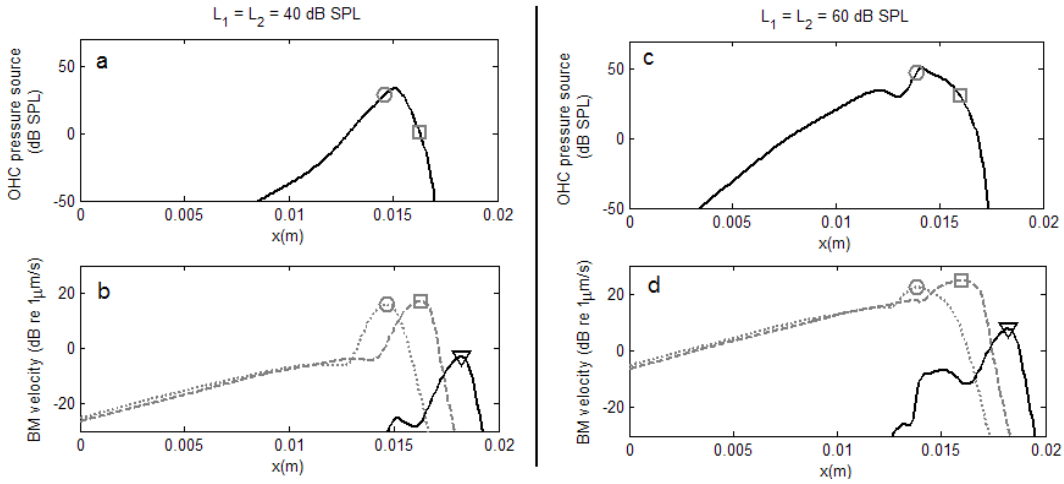

Figure 5.2 The $2f_1 - f_2$ DP component of the OHC pressure output
Plots (a) and (c) show the DP component of the OHC pressure output. The BM velocity response is also shown in (b) and (d) where the frequency components f_2, f_1, and $2f_1 - f_2$ are represented by the grey dotted, grey dashed, and solid black lines respectively. In each case f_2 = 2 kHz, f_2/f_1 = 1.25 and the stimulus levels are either (a and b) L_1=L_2=40 dB SPL or (c and d) L_1=L_2=60 dB SPL. The best places for f_2, f_1, and the $2f_2 - f_1$ characteristic place are indicated by the circle, square, and triangle markers respectively.

5.1.1 The $2f_1 - f_2$ wave-fixed source distribution

We assume that the wave-fixed distortion mechanism is entirely responsible for generating the $2f_1 - f_2$ DPOAE in a baseline cochlear model. However, in principle, there could also be a wave-fixed reflection component generated by impedance irregularities introduced by the nonlinearity. Appendix D.2 demonstrates that these wave-fixed impedance irregularities are most prominent at moderate stimulus levels, but negligible at low or high stimulus levels. It is difficult to distinguish between the distortion and nonlinear reflection components of the wave-fixed DP in the cochlear model, as both are expected to exhibit the same phase behaviour when the stimulus frequency is varied. We assume, however, that the distortion source contribution dominates the wave-fixed emission, which is essentially sourced by the distribution of the OHC pressure output at the DP frequency.

The $2f_1 - f_2$ component of the OHC pressure output

Figure 5.2 shows the simulated distribution of the $2f_1 - f_2$ component of the OHC pressure output, and the corresponding BM velocity response, for two different stimulus levels. It is helpful to recall the distinction between 'characteristic' and 'best' place when inspecting this figure. For a given stimulus frequency presented at the stapes we define the 'characteristic' and 'best' places as the locations on the cochlear partition corresponding to the peak in the travelling wave envelope predicted by either a linear active or quasilinear cochlear model respectively. Therefore the 'characteristic' place is independent of stimulus level whilst the 'best' place is not. The best places for the f_1 and f_2 stimulus tones are easily identified from the primary travelling wave responses in

the quasilinear cochlear model. However, as the DP travelling wave is evoked by internal distributed source rather than a stapes stimulus, the best place for this frequency may not correspond to the peak of the DP travelling wave envelope. For this reason the DP characteristic place, rather than the DP best place, is indicated on the figures. Figure 5.2(a and c) illustrates that there is a peak in the amplitude of the $2f_1 - f_2$ OHC pressure output near the f_2 best place, and that the distribution is broader for the higher stimulus level compared to the lower levels. It also demonstrates that the distribution of the $2f_1 - f_2$ component of the BM velocity, exhibits two peaks: One at the f_2 best place where the source amplitude is greatest, and one at the DP characteristic place. This simulation result is consistent with the source illustration shown in figure 5.1, as it indicates that the DP pressure output of the OHCs generates a forward travelling wave which propagates to the $2f_1 - f_2$ characteristic place.

The effective wave-fixed (distortion) source distribution

Although figure 5.2 (a and c) illustrates the distribution of the $2f_1 - f_2$ OHC pressure output, it does not inform us as to whether this distribution is capable of generating DP backward travelling waves which would be able to propagate out of the cochlea and be detectable in the ear canal. For this reason, the *effective* source region for the wave-fixed component of the $2f_1 - f_2$ DPOAE is estimated by taking each individual element of the OHC pressure source distribution described in figure 5.2, and evaluating the level of the DPOAE which is evoked by that element in isolation. We then identify the dominant source region as the area of the model over which the individual source elements evoke a DPOAE level which is within 10 dB of the maximum level evoked by any single element. This approach finds the most influential source elements, but collectively their performance will depend on the phase relationships which determine the interactions between them. The dark grey shaded area in Figure 5.3a shows the estimated effective source region for the wave-fixed $2f_1 - f_2$ DPOAE component generated by 50 dB SPL stimuli (L_1=L_2) using a variety of f_2/f_1 ratios and fixed f_2 (2 kHz). This region increases in length from 1.5 to 2.5 mm as the stimulus frequency ratio reduces from 1.4 to 1.01. The figure also shows that the location of the distributed source region straddles the f_2 best place and considerable contributions to the amplitude of the wave-fixed DPOAE are generated on either side of this location. The exact width of the source region depends on the boundary definition used, but the estimate of 1.5 to 2.5 mm for a stimulus level of 50 dB SPL equates to 0.04L to 0.07L, where L is the cochlear model length. This estimate is in good agreement with that of Zhang & Mountain (2008), who found that that the length of the source region in their model grew from <0.05L to 0.1L as the stimulus frequency ratio reduced from 1.4 to less than 1.1 (figure 1.22a).

The light grey shaded region in figure 5.3a corresponds to the area of the model over which the $2f_1 - f_2$ DP component of the OHC pressure output is within 10 dB of the maximum value. For the

$2f_1 - f_2$ DP, this region is expected to essentially coincide with the dark grey shaded effective source area as the travelling waves at $2f_1 - f_2$ are able to propagate throughout this area of the model. However, when we consider the $2f_2 - f_1$ DPOAE in chapter 6, we anticipate that some differences between the dark and light shaded regions will emerge.

Figure 5.3b shows that the estimated length of the effective $2f_1 - f_2$ DP source region increases from about 1 to 2 mm as the stimulus level (L_1=L_2) increases from 30 to 80 dB SPL for a stimulus frequency ratio of 1.2. This equates to an increase from 0.03L to 0.06L, and is associated with the broadening of the travelling wave envelope for higher stimulus levels which increases the spatial overlap between the f_1 and f_2 travelling waves. In summary, figure 5.3 demonstrates that the width of the source region tends to increase if either the stimulus level is increased, or the stimulus frequency ratio is decreased.

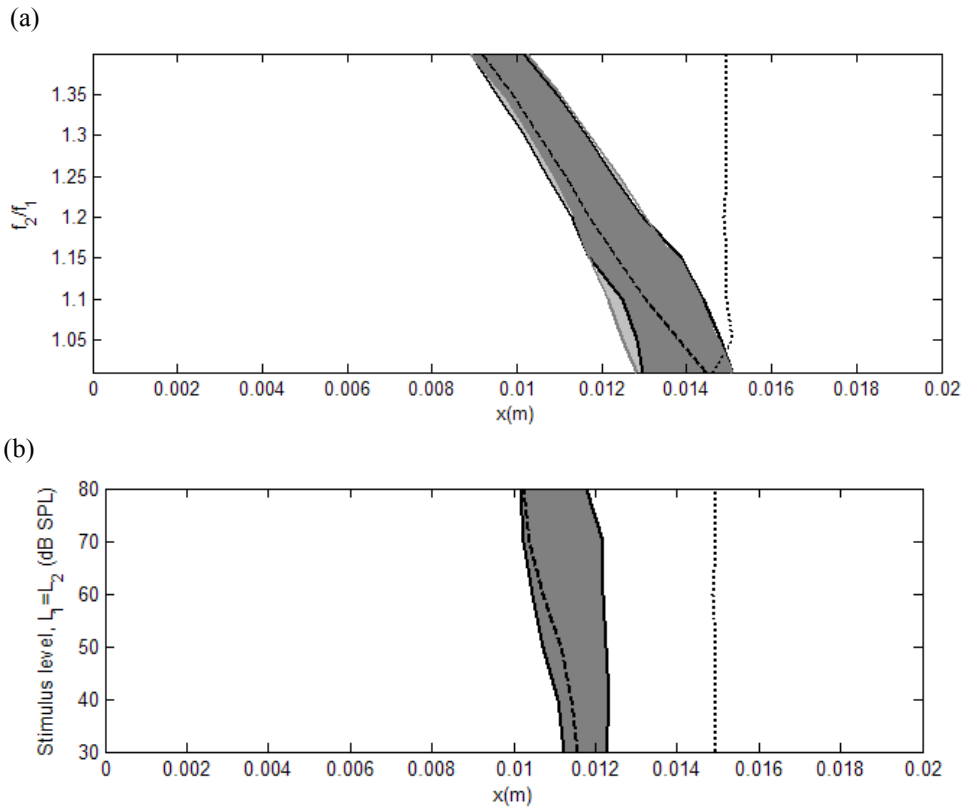

Figure 5.3 The predicted location and length of the $2f_1 - f_2$ DP source region
(a) The simulated length and location of the $2f_1 - f_2$ wave-fixed DPOAE source for a variety of the f_2/f_1 ratios using L_1=L_2= 50 dB SPL and $2f_1 - f_2$ = 2 kHz. The dark grey shaded region highlights this source region, which is bounded by the solid black lines. The light grey shaded region illustrates the source region estimated from the DP component of the OHC pressure output only. (b) The simulated length and location of the $2f_1 - f_2$ wave-fixed DPOAE source region for a variety of stimulus levels, using f_2/f_1=1.2 and $2f_1 - f_2$ = 2 kHz. In both plots, the black dashed and dotted lines correspond to the f_2 best place and $2f_1 - f_2$ characteristic place respectively.

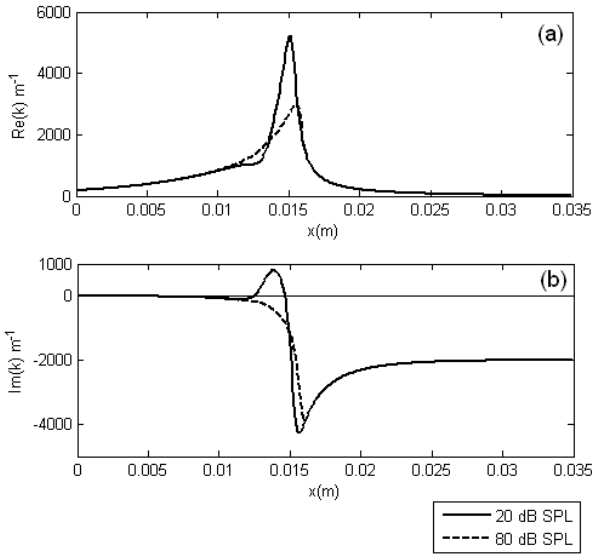

Figure 5.4 The wave number of the travelling wave
The (a) real and (b) imaginary components of the wavenumber of the travelling wave in the quasilinear model, when it is stimulated by a single 2 kHz tone at a level of either 20 or 80 dB SPL.

The effective $2f_1 - f_2$ DP source region shown in figure 5.3 suggests that significant contribution to the wave-fixed DPOAE can be generated from a location that is apical of the f_2 best place. This can occur in the model because the f_2 travelling wave does not convert from a propagating travelling wave to an evanescent wave immediately upon reaching its best place. Instead of a discrete change from travelling wave to evanescent behaviour, there is a finite region of the model over which the amplitude of the real component of the wavenumber falls off towards zero (corresponding to a decline in the amplitude of the f_2 travelling wave) and the negative imaginary part of the wavenumber builds up (signifying the transfer to an evanescent wave). This is illustrated in figure 5.4 which shows the real and imaginary parts of the wavenumber of a travelling wave evoked by a 2 kHz single tone stimulus in the quasilinear model. Therefore, beyond the f_2 best place, it is still possible for the residual f_2 travelling wave to interact with the f_1 travelling wave and contribute to the wave-fixed DPOAE source.

Interactions between individual source elements

Figure 5.3 indicates the effective amplitude of individual elements within the DP source region, but does not offer insight into whether these elements are likely to sum together constructively or destructively to form the total $2f_1 - f_2$ DPOAE. Instead we investigate whether any substantial destructive summation is occurring within the source region by modifying the model such that the length of the $2f_1 - f_2$ OHC pressure source is gradually extended from the base of the model whilst monitoring the level of the DPOAE predicted by the model. This technique is illustrated in figure 5.5 and, for this stimulus paradigm, the predicted $2f_1 - f_2$ DPOAE amplitude increases monotonically with the length of the source region. The monotonic increase suggests that there is no significant destructive interference occurring between the distributed elements of the source

region. However we observed in figure 4.6 that, at higher stimulus levels, this approach can detect destructive summation occurring between different elements within the source distribution.

5.1.2 Relative amplitude of different DPOAE frequency components

The $2f_1 - f_2$ DP is the largest DPOAE observed in humans. Figure 4.1 shows the amplitude of various frequency components recorded in the human ear canal during the presentation of two simultaneous pure tones. In this section we discuss the origin of the relative amplitudes of these DPOAEs. As part of this investigation we mention the source of the $2f_2 - f_1$ DP, which is described in much more detail in chapter 6.

The difference in amplitude between DPs of different orders appears to originate from differences in the amplitude of the wave-fixed DP pressure source, and will therefore by influenced by the choice of nonlinear function. For example, figure 5.6 shows the simulated internal pressure source distribution which generates the wave-fixed components of the 3rd and 5th order DPs in the cochlear model. The maximum amplitude of the pressure source, which occurs in the vicinity of the f_2 best place, is greater for the lower order DPs, compared to the higher order DPs.

(a)

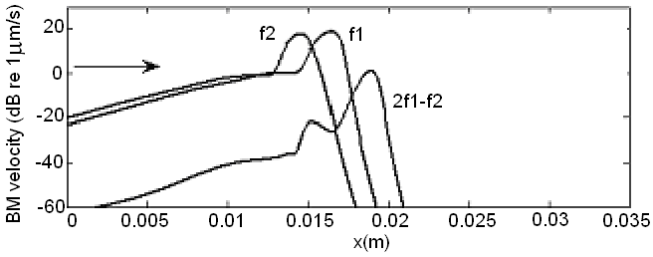

(b)

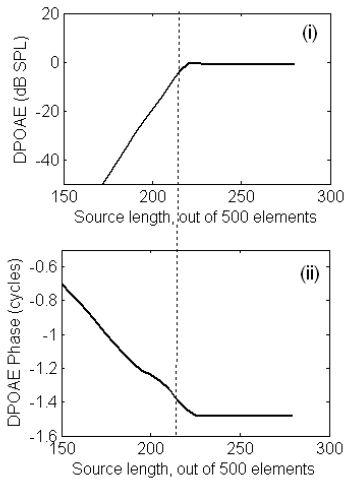

Figure 5.5 The influence of source length on the predicted DPOAE amplitude
At each location the predicted amplitude and phase of the $2f_1 - f_2$ DP wave-fixed source is described by the pressure output of the OHCs at the DP frequency. In this simulation the source is "switched-off" throughout most of the model, and then it is gradually switched on from the base of the model as illustrated in (a). As the source length increases, the total predicted wave-fixed DPOAE is estimated and shown in (b). The source length at which the source region first incorporates the f_2 best place is indicated by the dotted line in (b). For this simulation $L_1=L_2=50$ dB SPL and f_2= 2kHz.

The difference in amplitude between upper and lower side band emissions of the same order is likely to arise as a consequence of the difference in the breadth of the wave-fixed pressure source distribution. This difference can be seen in the spatial distributions of the $2f_1 - f_2$ and $2f_2 - f_1$ DP wave-fixed pressure sources in figure 5.6. On the apical side of the f_2 best place the amplitude of the pressure source falls-off over a shorter distance for the upper- compared to the lower- side band emission. In addition figure 5.7 shows the predicted contributions to the total DPOAE from each component of the DP source term, which takes into account not only the pressure source distribution but also the propagation of DP from the source region to the base of the cochlea. This figure should be interpreted with caution, as any interference between neighbouring source elements is neglected. However, it confirms that the source elements which contribute most significantly to the DPOAE observed in the ear canal are positioned across a broader region for the $2f_1 - f_2$ DP compared to the $2f_2 - f_1$ DP.

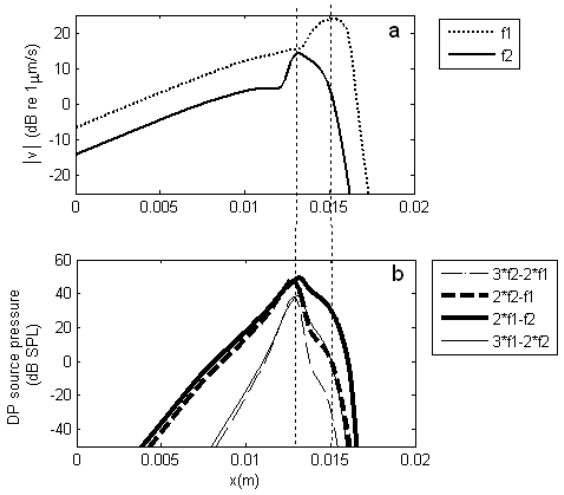

Figure 5.6 The source distribution for different DP frequencies
(a) The f_1 and f_2 components of the predicted BM velocity response evoked by two stimulus pure tones at frequencies f_1 and f_2, in the baseline model The stimulus levels L_1 and L_2 were set equal to 65 and 55 dB SPL respectively and f_2=2200 Hz and f_1=1800 Hz. (b) The predicted quasilinear OHC output pressure at various DP frequencies, generated by the stimulus tones described in (a). This pressure acts as the internal pressure source distribution for travelling waves at the DP frequencies. Other DP frequencies are also expected to occur in the OHC output pressure, but these have been neglected for simplicity. In (a) and (b) the thin dotted lines indicate the location at which the BM velocity amplitude is greatest for each stimulus tone.

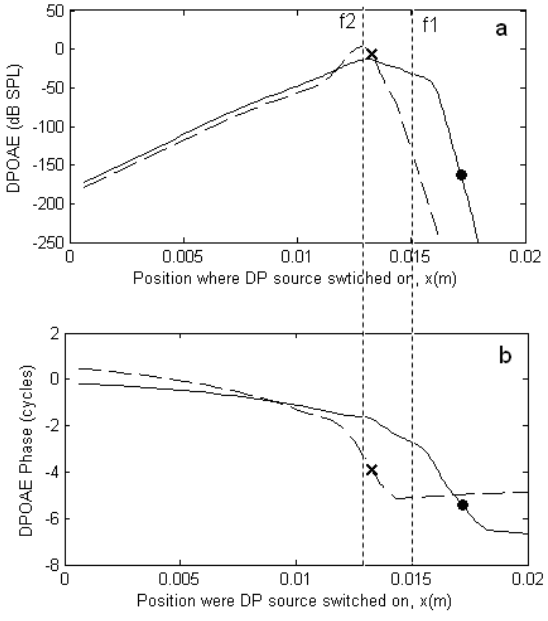

Figure 5.7 The contribution to the total DPOAE from individual wave-fixed source elements
The (a) amplitude and (b) of the predicted DPOAE detected in the ear canal of the model when the DP source from one element only is "switched on". The stimulus parameters are the same as those described in figure 5.6. The plot shows the amplitude of the resulting simulated DPOAE as a function of the location of the DP source element. Results shows shown for the $2f_1 - f_2$ (solid line) and the $2f_2 - f_1$ (dashed line) DPOAEs. The characteristic place of $2f_1 - f_2$ and $2f_2 - f_1$ are denoted by the circle and cross markers respectively. The vertical dotted lines indicate the best places of the f_2 and f_1 primary travelling waves.

5.1.3 Directionality of the $2f_1 - f_2$ wave-fixed component

Shera & Guinan (2008) explain that if the source elements comprising a distributed source have a phase distribution typical of a forward travelling wave in the cochlea, then the source will be highly directional. We investigate the directionality of the DP source region using two approaches. First, the amplitude of the travelling wave on the basal and apical sides of the distributed source region is compared to the amplitudes observed for a point source. Secondly, the forward-backward decomposition method (section 2.3) is used to support our conclusions.

The influence of source length

Figure 5.8 shows the amplitude of the travelling wave evoked by an internal source, observed at the base and at the characteristic place in the active linear cochlear model. The source is positioned between the base and the characteristic place, and the length of the source is gradually increased. The amplitude of the evoked travelling wave at the base and characteristic place is given in units of dB relative to the amplitude of the travelling wave evoked by a point source in the centre of the extending region. Figure 5.8a demonstrates that if the source has uniform amplitude and phase, then the source exhibits no directionality. In this case, the amplitude of both the forward and backward travelling waves evoked by the internal source increase equally as the source length extends. However, figure 5.8b shows that if the internal source is given the phase distribution of a forward travelling wave then the source becomes directional as the source length increases. In this case the amplitude of the forward travelling wave exceeds that of the backward travelling wave, relative to the waves generated by a point source.

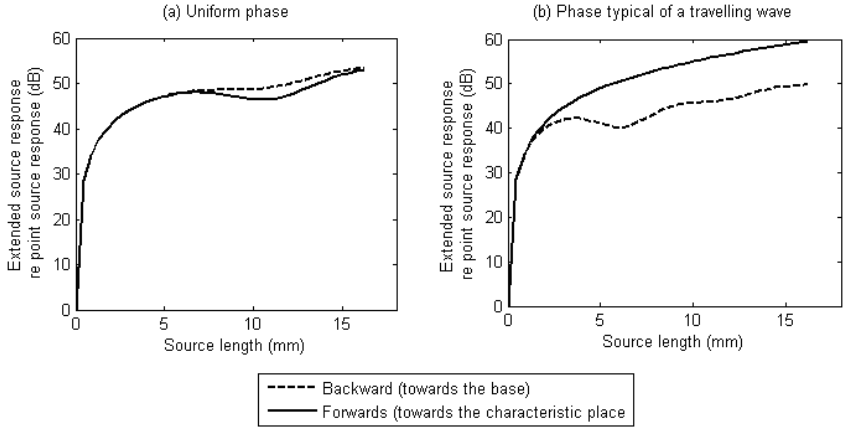

Figure 5.8 The directionality of an extended source
These plots show the predicted BM velocity at the base (dashed lines) and at the characteristic place (solid lines) in an active linear model, evoked by an internal 1.3 kHz velocity source distribution of increasing length. The source starts as a 10nm/s velocity source presented to one micromechanical element, at a distance halfway between the stapes and the characteristic place. The source is gradually extended by increasing the number of elements to which the 10 nm/s velocity stimulus is presented. The phase of the source along its length is either (a) uniform or (b) consistent with the phase of a travelling wave, so that the source phase at an element located at x_i, is given by $\phi(x_s) = \int_0^{x_s} k(x')dx'$

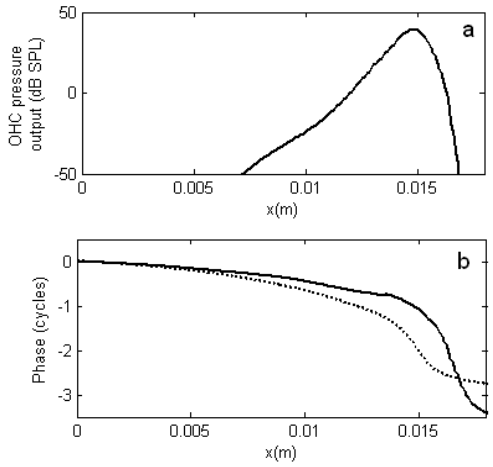

Figure 5.9 The (a) amplitude and (b) phase of the predicted $2f_1 - f_2$ component of the OHC pressure output
This simulation was performed using L_1=L_2=50 dB SPL, f_2=2 kHz and f_2/f_1= 1.2. The phase is referenced to the phase at the base. The dotted line denotes the phase of a forward travelling wave initiated by a 2 kHz single tone stimulus at the stapes, for comparison.

Figure 5.9 shows the amplitude and phase of the $2f_1 - f_2$ component of the OHC pressure output, which forms the basis of the wave-fixed source within the baseline cochlear model. It illustrates that the phase behaviour of this pressure is similar to that of a forward travelling wave. For this reason, as the source length increases, we would expect the wave-fixed DP source to become more directional such that it preferentially evokes forward travelling waves rather than backward travelling waves. Given the effective $2f_1 - f_2$ source distributions shown in figure 5.3, we anticipate that the changing source directionality will act to enhance forward travelling waves relative to backward travelling waves as the stimulus level increases or the f_2/f_1 ratio decreases.

Using forward-backward travelling wave decomposition

Figure 5.10 shows the estimated forward and backward travelling components of the DP travelling wave that are evoked by two different stimulus levels, using the forward-backward decomposition method (section 2.3). Although both forward and backward travelling waves are evident in the region between the base and the f_2 best place, the amplitude of the forward travelling wave in this region falls below the error floor of the decomposition method if the stapes boundary condition is adjusted to minimise reflections of backward travelling waves. On the apical side of the f_2 best place, only a forward travelling DP wave is evident as the amplitude of the backward travelling wave decreases below the error floor. If the amplitude of the forward travelling DP wave, p_d^+, near the DP characteristic place is compared to the amplitude of the backward travelling DP wave, p_d^-, on the basal side of the f_2 best place then the ratio p_d^+ / p_d^- is approximately equal to 1.3 for the 50 dB SPL stimulus level. However, the ratio increases so that p_d^+ / p_d^- is around 1.6 for the 60 dB SPL stimulus level, indicating that the wave-fixed source has become more directional as the stimulus level has increased.

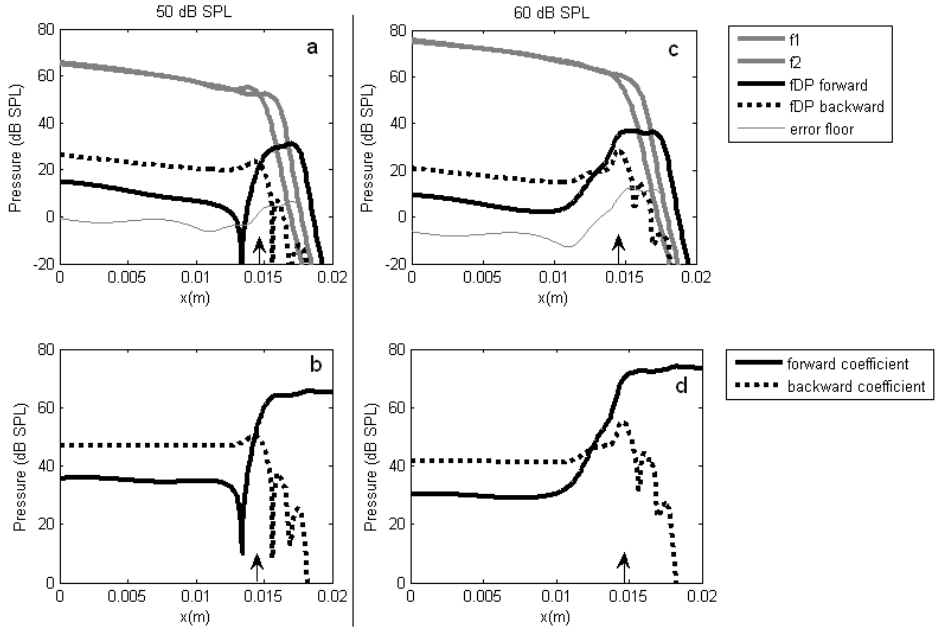

Figure 5.10 The forward and backward travelling components of the $2f_1 - f_2$ DP
(a) The amplitude of the forward and backward travelling waves at the DP frequency. The amplitude of the f_1 and f_2 travelling waves are also shown (grey lines) for reference. (b) The coefficients of the DP forward and backward travelling wave. The simulations are performed using L_1=L_2=50 dB SPL, f_2=2 kHz and f_2/f_1=1.2. In (c and d) the same responses are obtained except that a stimulus level of L_1=L_2=60 dB SPL was used. The arrow marks the f_2 best place in each of the plots.

The use of forward-backward travelling wave decomposition to investigate changes in source directionality has its limitations, and the most significant is that the amplitude growth of the DP forward travelling is nonlinear and this may prevent significant changes in directionality from being detected at higher stimulus levels. However, the result is consistent with the previous assessment of directionality based on source length, which suggests that the directionality of the wave-fixed source should increase with stimulus level due to an increased source length.

5.1.4 Origin of the $2f_1 - f_2$ DPOAE place-fixed component

The predicted place-fixed DP component is evaluated by introducing random irregularities into the active component of the CP impedance, to form a perturbed cochlear model, as described in section 4.2. This should allow the forward travelling wave evoked by the wave-fixed DP source in the region of the f_2 best place, to be reflected when it reaches the $2f_1 - f_2$ characteristic place. However, the introduction of the irregularities could also modify the DP component of the OHC pressure output, through reflections of the $f_1$and f_2 primary travelling waves at their best places. Therefore it is important to determine the dominant mechanism behind what we have classified as the place-fixed DP component.

The solid line in figure 5.11 shows the amplitude of the place-fixed DPOAE component, evoked by imposing a single step increase in the active OHC impedance so that $\gamma(x)$ increases by 0.1 at a

single location in the cochlear model. This has been obtained by substituting the results of the baseline model from those of the model incorporating the irregularity. The location of the impedance step is moved progressively from the base to the apex of the model, and the amplitude of the place-fixed DPOAE is evaluated for each position as described in section 4.2.2. The figure reveals that although a small place-fixed component is measured when the step-up is located near the f_1 or f_2 best places, the place-fixed component from the $2f_1 - f_2$ characteristic place is about 17 dB larger. The small place-fixed component which is evoked by an irregularity positioned near the f_2 or f_1 best places results from reflections in the primary travelling waves which then modify the input to the nonlinear function. This is evidenced by the dotted line in figure 5.11 which demonstrates that irregularities at the f_1 or f_2 best places do not significantly influence the predicted DP if reflection of the primary travelling waves is neglected from the simulation. Overall we conclude that the place-fixed component of the $2f_1 - f_2$ DPOAE estimated by the perturbed model, originates primarily from a linear reflection mechanism located at the $2f_1 - f_2$ characteristic place.

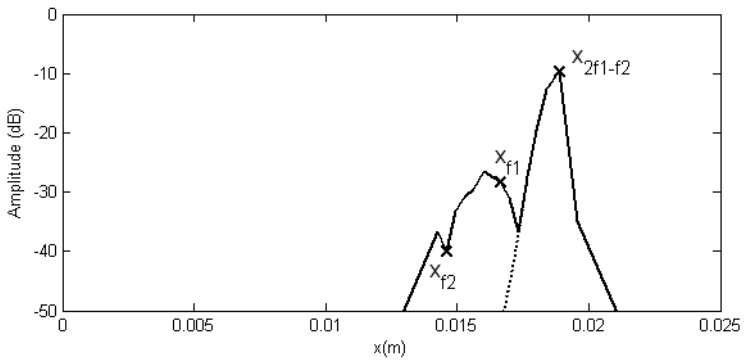

Figure 5.11 The location of the place-fixed (reflection) $2f_1 - \mathbf{f}_2$ DP source mechanism
This plot shows the predicted amplitude of the place-fixed component of the $2f_1 - f_2$ DPOAE generated by imposing a single step into the active impedance of the cochlear model at various locations, x(m). The stimulus parameters were L_1=L_2=50 dB SPL, f_2= 2 kHz and f_2/f_1=1.3. The best places for f_1, f_2 and the $2f_1 - f_2$ characteristic place are indicated by x_{f1}, x_{f2} and x_{2f1-f2} respectively. The solid line corresponds to the result from a model in which the irregularity affects the primary and DP travelling waves. In contrast the dotted line corresponds to a model in which the irregularity affects only the DP, not the primary, travelling waves.

5.2 Application of the model to hypothesis testing

In this section we consider how the model can be applied to hypothesis testing in order to gain a better understanding of the implications of some experimental results. Two examples are given: The Allen & Fahey (1998) experiment and the He *et al.* (2008) experiment. These studies were chosen as illustrations of cases in which the model either challenges or supports the experimental hypothesis respectively. This application also provides further verification of the model predictions as they are in good agreement with simulations performed in other studies, at least as far as those other models have been taken. In this section we also seek to explore the results of these experiments in more depth.

5.2.1 The Allen-Fahey experiment

The Allen-Fahey experiment, described in section 1.7.3 was originally designed to quantify the gain of the CA, but was unsuccessful. Several explanations for the null result of this experiment have been proposed in the literature:

(i) There is no cochlear amplifier (Allen & Fahey, 1992)

(ii) Distortion products travel out of the cochlea via fluid compression waves, not reverse travelling waves, and therefore the principle of the method is flawed (Ren & Nuttal, 2006)

(iii) The contribution of the reflection source (place-fixed) mechanism is neglected

(iv) There may be some suppression of the DP for small f_2/f_1 ratios (Shera & Guinan, 2007)

(v) There may be wave interference occurring between the DP and the primaries, or between DPs of different frequencies (de Boer *et al.*, 2005)

(vi) The directionality of the distortion source (wave-fixed) mechanism may change with f_2/f_1 ratio (Shera & Guinan, 2007), as a result of the distributed nature of the source region (Neely & Liu, 2008), which would invalidate the underlying assumptions of the method

In the past, the cochlear models of Kanis (1995) and Neely & Liu (2008) have been used to discount explanation (i) on the basis that the null result of the Allen-Fahey experiment can be replicated using a cochlear model which incorporates an amplifier mechanism. Explanation (ii) has also been rebuffed because, so far, cochlear models have only been able to replicate the Allen-Fahey experiment result if the reverse propagation of DPs towards the stapes is dominated by the travelling wave mechanism rather than a compression wave or a hybrid mechanism (Shera *et al.*, 2007). Further objections to the backward propagation of DPs out of the cochlea via fluid compression waves were discussed in section 1.4.4. The other explanations (iii) − (iv) are more

difficult to assess based on the literature, and for this reason we apply our cochlear model to simulate the Allen-Fahey experiment in order to determine which of these suggestions is likely to be most influential.

We start by replicating the Allen-Fahey experiment in the baseline cochlear model. Figure 5.12a shows the result that Allen & Fahey anticipated in their 1992 experiment, based on the assumption that the cochlear amplifier enhances the travelling wave amplitude by a factor G. As explained in section 1.7.3, the experiment involves presenting two tones (f_1 and f_2) in the ear canal, and adjusting the stimulus levels (L_1=L_2) such that a pre-specified response level occurs at the characteristic place corresponding to the $2f_1 - f_2$ DP frequency. During the experiment, the $2f_1 - f_2$ DP frequency is fixed and the level of the DPOAE in the ear canal is monitored for a range of f_1 values. Allen and Fahey argue that the shift in the relative position of the DP source and the region over which the CA amplifies the BM travelling wave at the DP frequency as the f_2/f_1 reduces towards unity, should result in a G^2 increase in the DPOAE amplitude detected in the ear canal where G is the gain of the CA. Therefore figure 5.12a illustrates that the DP amplitude was anticipated to increase as f_1 is moved towards the DP frequency. It should also be noted that the stimulus level L_1 is expected to decrease as f_1 approaches the DP frequency as the spatial overlap between the f_1 and f_2 primary travelling waves increases, enhancing the DP source pressure and reducing the stimulus levels required.

Figure 5.12b shows the result of the original Allen-Fahey experiment. In contrast to the anticipated result, the level of the DPOAE in the ear canal remains essentially constant for all f_1 frequencies. Therefore Allen & Fahey concluded that G was close to 1, or in other words, there is no cochlear amplifier. Kanis (1995) demonstrated that the original Allen & Fahey experiment may not have included values of f_1 sufficiently close to $2f_1 - f_2$ to detect the value of G correctly. However replications of the experiment, which included smaller f_2/f_1 ratios, were consistent with the null result of Allen & Fahey (de Boer *et al.*, 2005; Shera & Guinan, 2007). The results of the simulated experiment performed by Neely & Liu (2008), using a cochlear model in which the CA provides a gain of 47 dB to the BM displacement, is shown in figure 5.12c. This demonstrates that, contrary to the expected result (figure 5.12a), the predicted DPOAE amplitude declines as f_1 approaches the DP frequency. Neely & Liu conclude that the Allen-Fahey experiment does not provide an accurate method for quantifying the gain of the CA.

Our simulation of the Allen-Fahey experiment is shown in figure 5.12d. It differs from that of Neely & Liu mainly in the behaviour of the f_1 pressure amplitude. This difference arises because, in our simulation, it is the DP component of the response rather than the total response at the DP characteristic place which is kept constant throughout the simulation. For this reason, the f_1 pressure component does not follow the iso-displacement curve as f_1 approaches the DP frequency

in our simulation. The conclusion from our model simulation, that the DPOAE amplitude should fall off as f_1 tends towards the DP frequency, is the same as that of Neely & Liu.

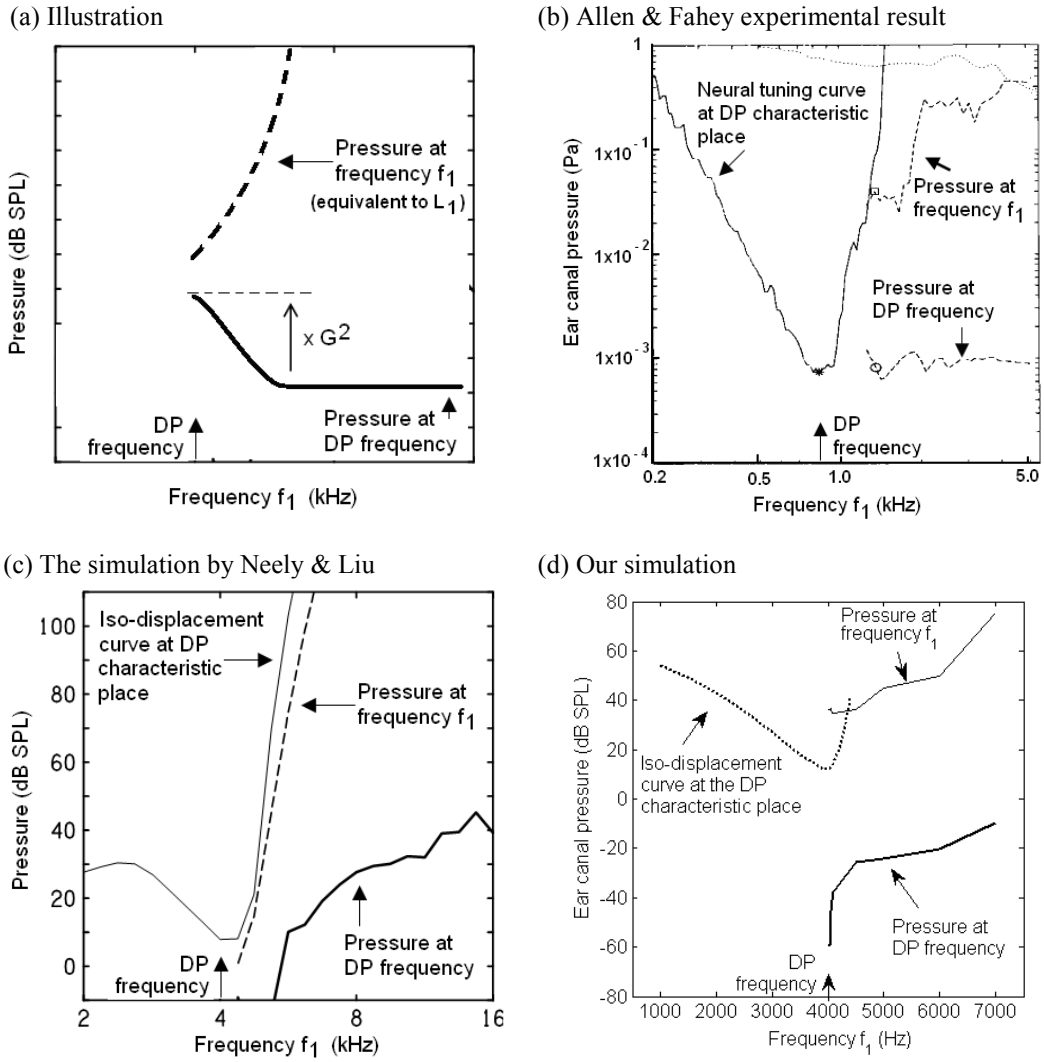

Figure 5.12 The result of the Allen-Fahey experiment
(a) Illustration of the anticipated result of the Allen-Fahey experiment, based on the explanation given in section 1.7.3. As the stimulus frequency ratio f_2/f_1 decreases, and f_1 tends towards the DP frequency, the DP pressure in the ear canal is expected to increase by either a factor of G or G^2 where G is the gain of the cochlear amplifier. (b) The experimental results recorded in cats by Allen & Fahey. [From Allen & Fahey (1992), figure 5, with permission from ASA]. (c) The simulation performed by Neely & Liu, using a model of the cat cochlea [From Neely & Liu (2008), figure 4 with permission of the authors and World Scientific]. (d) Our simulation. The stimulus levels (L_1=L_2) were adjusted for each f_1 frequency, such that the $2f_1 - f_2$ DP component of the shear displacement was fixed at − 25 dB re 1 nm, at the 4 kHz characteristic place. Throughout the simulation the DP frequency ($2f_1 - f_2$) was equal to 4 kHz, and the f_1 frequency was varied from 4020 to 7000 Hz.

Explanations for the null Allen-Fahey result

As we simulated the Allen-Fahey result in the baseline cochlear model, in which there are no place-fixed sites of reflection for forward travelling waves, we can conclude that explanation (iii) is not important: The null result of the Allen-Fahey experiment is not associated with neglecting the place-fixed component of the $2f_1 - f_2$ DP from the experimental design.

To eliminate explanation (iv) the cochlear model was manipulated to neglect self-suppression of the DP travelling wave and mutual suppression of the primary responses. Figure 5.13 shows the simulation of the Allen-Fahey experiment using this manipulated model. It demonstrates that although these suppression effects can alter the amplitude of the $2f_1 - f_2$ DPOAE by up to approximately 5 dB, this change is not sufficient to explain the decline in DPOAE amplitude of over 50 dB which is observed as the f_1 frequency is reduced from 7000 to 4000 Hz in the full quasilinear model. For this reason, suppression can be excluded as the dominant cause of the null Allen-Fahey experiment result in the cochlear model. This is similar to the conclusion of de Boer *et al.* (2005) who verified experimentally that there was little change in the degree of mutual suppression between the primary tones as the stimulus frequency ratio decreased in their replication of Allen-Fahey experiment in the guinea pig cochlea.

Our simulation, and the earlier work of Kanis (1995), allows explanation (v) to also be dismissed. This is because it was not necessary to incorporate other DP components, such as the $2f_2 - f_1$ or the $3f_1 - 2f_1$, in order to replicate the null result of the Allen-Fahey experiment. The interaction between the $2f_1 - f_2$ DP and the primary tones is also negligible as the result of the simulation is altered by less than 1 dB if the $2f_1 - f_2$ DP component is permitted to modify the estimation of the primary responses in the quasilinear iterative process.

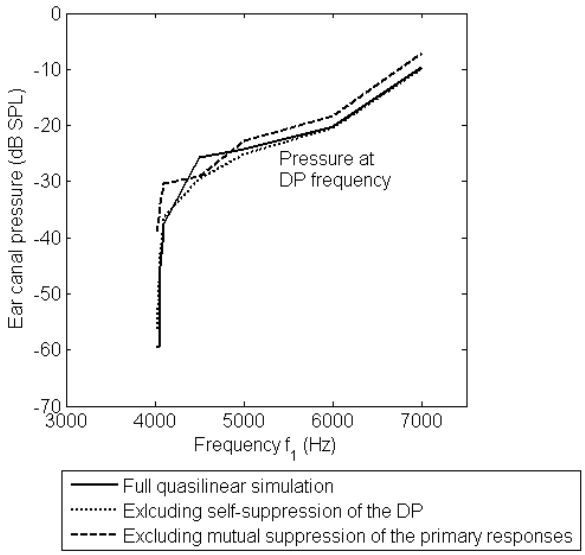

Figure 5.13 The influence of suppression on the Allen-Fahey result
The plot shows the simulated Allen-Fahey experiment performed in the full quasilinear model (solid line), and in the model when it is manipulated to exclude self-suppression of the DP component (dotted line) and to exclude mutual suppression of the primary responses in addition to self-suppression of the DP component (dashed line). Both of these plots are equivalent to that shown in figure 5.12d, except that the iso-displacement and f_1 pressure variations have been neglected for simplicity.

As all other explanations have been rebuffed, this leaves only explanation (vi) which suggests that the directionality of the source region changes as the stimulus frequency ratio reduces. It is, however, not possible to alter the directionality of the source region in the model to confirm this finding since it is such an intrinsic part of the nonlinear distortion generation and longitudinal coupling within the model. Instead, some support for this explanation can be derived from the evidence presented in section 5.1.3, that the length of the distributed wave-fixed source region tends to increase as the stimulus frequency ratio reduces towards unity, and that this is expected to change the directionality of the source region. For example, as the f_2/f_1 ratio reduces and the source length increases, the DP travelling waves it evokes tend to be emitted preferentially towards the apex rather than towards the base. Allen & Fahey, anticipating no change in source directionality as f_2/f_1 decreases, expected the level of the $2f_1 - f_2$ DPOAE recorded in the ear canal to increase by a factor of G^2 as f_2/f_1 reduced to unity. However, the model predicts that the extending source region will increasingly tend to emit DP travelling waves preferentially towards the DP characteristic place, rather than the base, as the stimulus frequency ratio reduces towards unity. This would lower the level of the $2f_1 - f_2$ DPOAE, compared to the expectation of Allen & Fahey, because the amplitude of the backward travelling wave is reduced and lower stimulus levels are needed to evoke the required response at the DP characteristic place. For this reason, the Allen & Fahey experiment may underestimate the gain of the CA as a consequence of changes in source directionality with changes in the stimulus frequency ratio.

5.2.2 Fluid compression waves and the He *et al.* experiment

The He *et al.* (2008) study is one of several recent experiments which measure the phase behaviour of the BM motion at the $2f_1 - f_2$ DP frequency between the base and the f_2 best place, in an attempt to detect the phase pattern expected for a backward travelling wave. Along with other studies (Ren, 2004; de Boer *et al.*, 2008) this experiment detects phase behaviour which is typical of a forward (not a backward) travelling wave in this region, and therefore casts doubt on the theory that DPs propagate out of the cochlea via backward travelling waves. We have simulated the He *et al.* experiment in our cochlear model, in which the only mechanism for reverse propagation of DPs out of the cochlear is via reverse travelling waves. We find, in agreement with the model of de Boer *et al.* (2008), that the phase behaviour observed by He *et al.* is indeed at odds with the theory of reverse DP propagation via backward travelling waves.

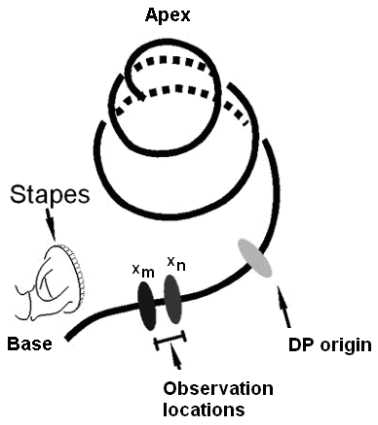

Figure 5.14 Illustration of the observation locations used by He *et al.*
In their experiment, the gerbil cochlea is stimulated by two tones which generate a $2f_1 - f_2$ distortion product in the grey region indicated. Observations of the BM at then made at locations x_m and x_n which have characteristic frequencies of 15 kHz and 12 kHz respectively.
[From figure 1 of He *et al.* (2008), with universal permission].

Overview of the He *et al.* (2008) experiment

He *et al.* (2008) observed the amplitude and phase of the BM velocity at two different locations (x_m and x_n) in the gerbil cochlea, as illustrated in figure 5.14. The cochlea was stimulated by two pure tones (f_1 and f_2) and $2f_1 - f_2$ DP travelling waves are generated in the vicinity of the f_2 best place. The value of f_2 is selected so that the source region of the $2f_1 - f_2$ DP lies between x_n and the DP characteristic place. The principle of the experiment is that the direction of the $2f_1 - f_2$ travelling wave emitted from the DP source region can be identified from the phase measurements at x_m and x_n. The analysis exploits the observation that the travelling wave accumulates phase lag as it propagates. On this basis, He *et al.* hypothesise that the $2f_1 - f_2$ backward travelling wave, should exhibit the following properties:

- The phase lag at x_m should be greater than the phase lag at x_n
- If the source location moves closer to x_n as the f_2 frequency increases, then the phase lag should decrease at both x_m and x_n

The reasoning behind these hypotheses is illustrated in figure 5.15 which shows the phase of a travelling wave evoked by an internal 2 kHz source. The source is placed at different locations within the linear active cochlear model and the phase of the resulting travelling wave is observed at x_m and x_n. This demonstrates that a backward travelling wave evoked by an internal point source of fixed frequency exhibits the phase characteristics anticipated by He *et al.* in a linear cochlear model: the phase lag of the travelling wave is greater at x_m compared to x_n. In addition, when the source location is moved further away from x_n, the phase lag observed at both x_m and x_n increases. Similar results are obtained in a quasilinear model, and in a scenario in which the source frequency is related to the source location such that the frequency increases as the location moves closer to the base.

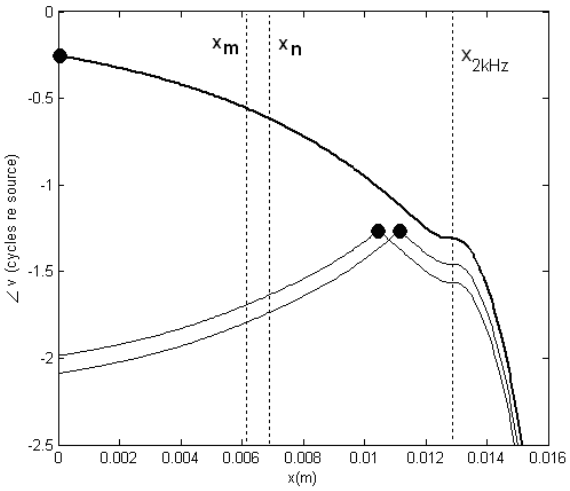

Figure 5.15 The phase of the BM velocity response to an internal 2 kHz source in the linear active cochlear model
The locations x_m, x_n and x_{2kHz} correspond to the observation points in figure 5.14 and the 2 kHz characteristic place respectively. Each solid line corresponds to a different source location, as indicated by the black dotes. When the source is located at the base of the model, the travelling propagates from the base to the apex, accumulating increasing phase lag in this direction. When an internal source is located between x_n and x_{2kHz}, the phase of the travelling wave is greater at x_m compared to x_n. If the internal source location is moved closer to x_n, then the phase lag observed at either x_m or x_n increases.

The results of the experiment

He *et al.* perform two experiments. The first uses a single tone stimulus at frequency f_0 presented in the ear canal. This generates the expected forward travelling wave on the cochlear partition, and the phase of this wave is detected at the observation points x_m and x_n. To summarise, the results demonstrate a greater phase lag at x_n compared to x_m and greater phase lag at both sites as the stimulus frequency increases. These results are consistent with those anticipated for a forward travelling wave, and were used by He *et al.* to verify their observation techniques. This experiment was simulated in the model to demonstrate that the predicted response was qualitatively similar to that observed by He *et al,* as shown in appendix I.

In the second experiment, two tones were presented in the ear canal at frequencies f_1 and f_2 such that a $2f_1 - f_2$ DP would be generated within the cochlea. Other DPs would also be expected to arise, but are neglected from this discussion for simplicity. The wave-fixed (distortion) component of the $2f_1 - f_2$ DP is thought to arise from a distributed region in the vicinity of the f_2 best place (section 5.1.1). As sites x_m and x_n correspond to locations with characteristic frequencies of 15 kHz and 12 kHz respectively in the gerbil cochlea, the $2f_1 - f_2$ DP generation region is expected to be between x_n and the DP characteristic place provided that $2f_1 - f_2$ is less than 10.9 kHz. For this reason, the DP phase measurements observed at locations x_m and x_n are expected to correspond to a backward travelling wave when $2f_1 - f_2$ is less than 10.9 kHz. The results observed by He *et al.* are displayed in figure 5.16. These plots do not show the phase behaviour expected of a backward travelling wave when $2f_1 - f_2$ is less than 10.9 kHz. Instead the phase behaviour of the DP travelling wave observed at the two sites appears to be consistent with a forward travelling wave.

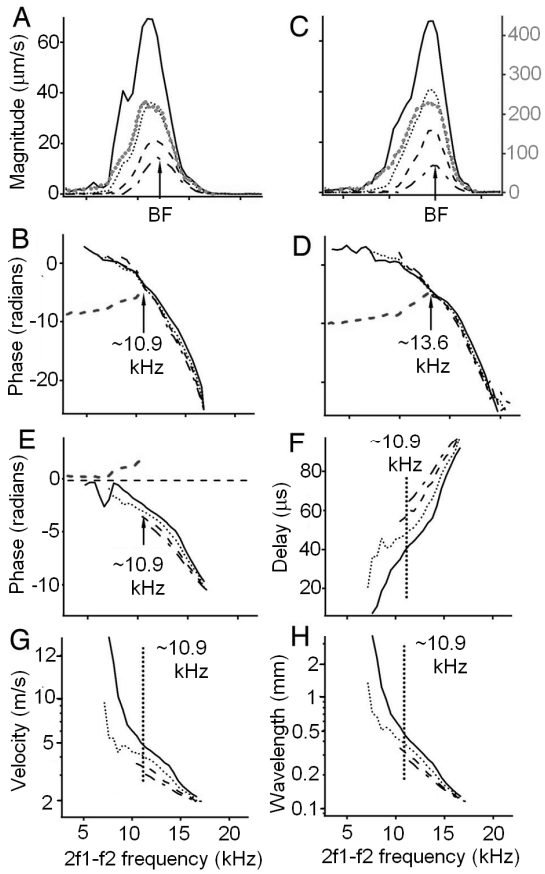

Figure 5.16 The result of the He *et al*. (2008) experiment
The magnitude (A and B) and phase (C and D) of the $2f_1 - f_2$ distortion component of the BM response to two stimulation of the gerbil cochlea, observed at two spatially separated locations. The observation locations x_m and x_n are located at the 15 kHz and 12 kHz characteristic places respectively, which are spatially separated by approximately 0.6 mm. Responses to stimulus levels (L_1=L_2) of 40, 50, 60, and 70 dB SPL are denoted by dash-dot, dashed, dotted and solid black lines in that order. The stimulus frequency ratio f_2/f_1 =1.05 is held constant throughout the experiment. The grey dotted lines in A and B show the amplitude of the response to a 60 dB SPL single pure tone stimulus (scale on the right hand side) for reference. Plots A and C correspond to the more apical site whilst B and D were observed the basal location. C and D show the phase of the responses given in A and B relative to $2\phi_1 - \phi_2$ where ϕ_1 and ϕ_1 correspond to the phase of the stapes motion at f_1 and f_2 in that order. E gives the phase of BM velocity at site 2, relative to site 1. The dashed lines in C,D and E indicate the results that are anticipated for a backward DP travelling wave. *F* shows the delay ($\Delta\phi$) in propagation of the DP travelling wave, at each DP frequency, between sites 1 and 2, calculated using the phase data in E and the stimulus frequency (e.g. delay= $-\Delta\phi/f_{dp}$ where $\Delta\phi$ is the phase change and $f_{dp}=2f_1 - f_2$). G and H give the group velocity and wavelength of the travelling wave respectively, which are estimated from the delay (*F*) and the known distance between the observation sites. [figure 2 of He *et al.* (2008), with universal permission]

The baseline model simulation of the two tone He *et al.* experiment is shown in figure 5.17. The simulation is not expected to be quantitatively comparable to the physiological result of He *et al.* because of animal differences and differences in observation location. The observation sites for the simulation were positioned distances of 10.5 and 11.3 mm from the stapes which correspond to locations with characteristic frequencies of 4 and 3.5 kHz respectively. These sites were selected so that it would be possible to detect a backward travelling wave in the two tone experiment using the range of frequencies over which the model predictions of distortion products appears to be strongest (f_2 between 1 and 4 kHz and f_2/f_1 = 1.2). Although only one stimulus level (40 dB SPL) is

shown in the simulation for simplicity, similar results were obtained using higher levels. As the x_n site is located at the 3.5 kHz characteristic place, then the wave-fixed (distortion) DP source is expected to be on the apical side of the two observation points provided that $2f_1 - f_2$ is less than 2.3 kHz. Plots C and D, in figure 5.17, show that as the DP frequency decreases below 2.3 kHz the simulated phase lag on the DP travelling wave observed at x_m and x_n increases. Also, plot E suggests that when $2f_1 - f_2$ is below 2.3 kHz, the phase of the simulated DP travelling wave observed at x_n slightly leads that observed at x_m. These model predictions are consistent with the hypotheses of He *et al*, but at odds with their experimental results shown in figure 5.16.

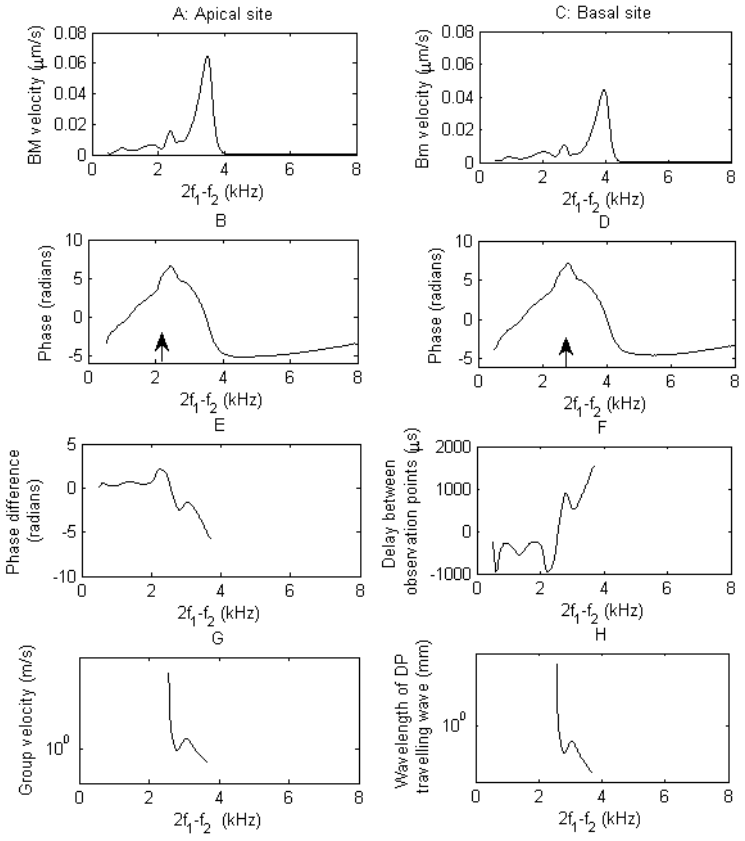

Figure 5.17 The simulated He *et al.* (2008) experiment
The model simulation of the $2f_1 - f_2$ distortion component of the BM velocity response to two tone stimulation, observed at two spatially separated locations. The observation locations x_m and x_n are located at the 4 kHz and 3.5 kHz characteristic places respectively, which are spatially separated by approximately 0.8 mm. The stimulus levels, L_1=L_2, were set to 40 dB SPL and f_2/f_1=1.2. A and B show the magnitude of the DP response at sites x_n and x_m respectively. C and D show the phase of the responses shown in A and B relative to $2\phi_1 - \phi_2$ where ϕ_1 and ϕ_1 correspond to the phase of the stapes motion at f_1 and f_2 in that order. The black arrows indicate the frequency below which the $2f_1 - f_2$ wave-fixed generation site is expected to be further from the base than the observation site. E gives the phase of BM velocity at site x_n, relative to site x_m. *F* shows the delay ($\Delta\phi$) in propagation of the DP travelling wave, at each DP frequency, between sites 1 and 2, calculated using the phase data in E and the stimulus frequency (e.g. delay= $-\Delta\phi/f_{dp}$ where $\Delta\phi$ is the phase change and $f_{dp}=2f_1 - f_2$). G and H give the group velocity and wavelength of the travelling wave respectively, which are estimated from the delay (*F*) and the known distance between the observation sites.

(a) The output of the DP source is predominantly a backward travelling wave (black arrows) which passes through x_n before reaching x_m.

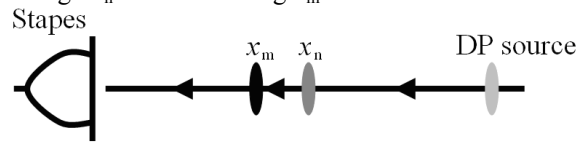

(b) The output of the DP source is predominantly a fluid compression wave (grey arrows), which vibrates the stapes and initiates a forward travelling wave (black arrows) which passes through x_m before reaching x_n.

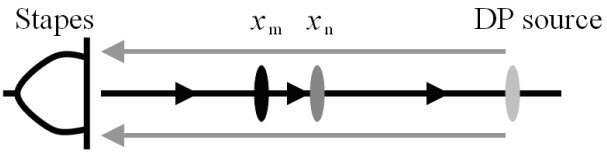

Figure 5.18 Possible reverse DP propagation mechanisms in the He *et al.* experiment
In these illustrations, the cochlea is stimulated by two pure tones simultaneously to generate a distortion product (DP) at the location indicated by the light grey marker. The phase of the BM velocity at the DP frequency is observed at locations x_m and x_n, corresponding to the black and dark grey markers respectively. The phase lag of the BM velocity component at the DP frequency is expected to be either (a) smaller at x_n compared to x_m or (b) greater at x_n compared to x_m. If f_2 is increased, and f_2/f_1 is fixed, then the DP source moves closer to x_n and the $2f_1 - f_2$ characteristic place moves towards the base. This is would lead to either a (a) decreased or (b) increased phase lag at x_m and x_n as f_2 increases.

He *et al.* conclude that, as their experiment failed to detect a DP backward travelling wave between the DP source region and the base of the cochlear model, the $2f_1 - f_2$ DP must primarily propagate out of the cochlea fast via fluid compression waves rather than slow backward travelling waves. They propose that the fast fluid compression wave results in motion of the stapes which, in turn, gives rise to a DP forward travelling wave which propagates from the base to the DP characteristic place. Figure 5.18 illustrates the He *et al.* fast compression wave theory, and compares it to the alternative backward travelling wave mechanism.

The unresolved problem

Attempts to reconcile the phase measurements of He *et al.* (figure 5.16) and others (Ren, 2004; de Boer *et al.*, 2008) with the predictions of conventional 'local' cochlear models (figure 5.17) like ours have, so far, been unsuccessful. These models only support BM travelling waves, not fluid compression waves, and the velocity of the BM is determined only by the local pressure difference across it (de Boer & Nuttal, 2008). De Boer *et al.* (2008) implemented a similar experiment to that of He *et al*. and made several modifications to their conventional cochlear model in an attempt to better simulate the observed phase behaviour. This included introducing impedance irregularities into their baseline model in order to generate both place-fixed and wave-fixed DP travelling waves, and investigating the effect of broadening the region over which the CA acts to enhance CA motion. They found that introducing impedance irregularities had no significant impact on the phase behaviour predicted by the model. We can confirm that there is also no notable difference in the nature of the predicted DP phase behaviour between the baseline and perturbed versions of our model. In addition, de Boer *et al.* (2008) concluded that broadening the CA region did not

adequately explain the discrepancy between the model prediction and the experimental outcome, because this adaptation was not consistent with the original physiological single tone measurements from the guinea pig cochlea on which their model was based.

We investigated whether reflection of backward travelling waves at the stapes, or errors in phase unwrapping of the physiological recordings could explain the absence of a backward travelling wave in the results of He *et al.* We found that maximising the stapes reflection of backward travelling waves in our baseline cochlear model did not substantially alter the DP phase behaviour simulated by the model. The unwrapping algorithm, used to ensure that the phases recorded in the experiment formed a continuous curve, is sensitive to noise which can obscure the 2π radian jumps in phase that need to be detected in order to stitch together the continuous phase curve. Although in simulations the phase results are subject to very little noise, making the unwrapping reliable, it is not known how reliable the unwrapping is for the noisier experimental results. For this reason we sampled the simulated phase results at intervals of approximately 400 Hz, similar to the interval used by He *et al.*, and superimposed random fluctuations on the predicted phase to act as noise. The amplitude of the noise was gradually increased and we found that the nature of the predicted phase behaviour was not influenced by errors in the unwrapping algorithm until the phase noise exceeded $\pm\pi/2$ radians. When these high noise fluctuations are superimposed on the predicted $2f_1 - f_2$ DP phase behaviour, the results become erratic and do not lead to a better replication of the He *et al.* results. Therefore, we have found no evidence that the phase behaviour observed by He *et al.* is influenced by errors in the unwrapping algorithm.

The failure of conventional local cochlear models to replicate the phase behaviour of the $2f_1 - f_2$ DP observed experimentally by He *et al.* and others presents a considerable challenge to our type of model. On the other hand, these conventional travelling wave models appear to explain features of the $2f_1 - f_2$ DPOAE characteristics which cannot be accounted for by a fluid compression wave model or a hybrid model supporting both backward travelling waves and fluid compression waves, such as predicting the results of the Allen-Fahey experiment (Shera *et al.*, 2007). De Boer *et al.*(2008) suggest that it may be possible to address this challenge by pursuing a travelling wave model with 'non-local' micromechanical properties. For example, de Boer & Nuttal (2008) successfully replicate the phase behaviour observed by He *et al.* using a 'feedforward' cochlear model, in which travelling waves propagate more readily in the forward direction compared to the backward direction. However, a side-effect of the feedforward mechanism is that backward travelling waves can be strongly attenuated, compromising both the predicted amplitude of the DPOAEs and the influence of coherent reflection within the cochlear model (de Boer & Nuttal, 2008; de Boer *et al.*, 2008). For this reason, the application of cochlear modelling to explain the $2f_1 - f_2$ DP phase behaviour observed by He *et al.* and others remains an active area of research.

5.3 Conclusions regarding the predicted $2f_1 - f_2$ DPOAE source and transmission mechanisms

In this chapter the source mechanism for the $2f_1 - f_2$ DPOAE within the cochlear model studied, and we find results consistent with the theory summarised in sections 1.4.3. The model predicts that there is a distributed source of the $2f_1 - f_2$ wave-fixed component occupying an area which includes the f_2 characteristic place. The length of this estimated region increases as the stimulus level increases or stimulus frequency ratio decreases towards unity. This wave-fixed source is directional relative to a point source, and its tendency to emit forward travelling waves in preference to backward travelling waves is greater for increased source lengths. The place-fixed component of the $2f_1 - f_2$ DPOAE is found to originate primarily from impedance perturbations located in the vicinity of the DP characteristic place within the model. These results serve to verify the generation mechanisms of the $2f_1 - f_2$ DP in the cochlear model, and suggest that it could provide useful insight into the generation of the $2f_2 - f_1$ DP which is less well understood.

This chapter also addresses the following research questions posed in section 1.9 concerning the $2f_1 - f_2$ DPOAE:

- What forward and backward DP travelling waves are generated within the model in response to two tone stimulation?
- What explanation does our cochlear model, which contains a cochlear amplifier, offer for the null result of the Allen & Fahey experiment?
- Can the model provide insight into the results of Ren and colleagues who are unable to detect backward travelling waves on the BM at DP frequencies?

Consideration of these questions produced the main contributions of this chapter, listed below, which correspond to those summarised in section 1.9 (vi-vii).

- The development of analysis tools for probing the source mechanism for the $2f_1 - f_2$ DPOAE within the model. This includes the use of the decomposition method to estimate the predicted forward and backward DP travelling wave components, the results of which provide supporting evidence for the directionality of the DP source region (section 5.1.3).
- An analysis of the explanations cited in the literature for the outcome of the Allen-Fahey experiment. The results confirm that the null result observed in this physiological study is likely to be a consequence of changes in the directionality of the wave-fixed DP source as the stimulus paradigm is varied (section 5.2.1).
- Verification of the challenge to conventional cochlear models presented by the phase measurements of He *et al.* (2008), in which DPs propagate out of the cochlea via backward travelling waves (section 5.2.2)

6. Predicted $2f_2 - f_1$ DPOAE characteristics

Distortion product otoacoustic emissions (DPOAEs) can be classified as 'upper' or 'lower' side-band emissions according to their frequency relative to the stimulus tones f_1 and f_2 ($f_2 > f_1$). The $2f_1 - f_2$ DP is an example of a lower side-band emission, and its measured characteristics and simulated properties are discussed in chapters 4 and 5. The $2f_2 - f_1$ DPOAE is the largest upper side band emission detected in human ears. As upper and lower side-band emissions are thought to arise from generation mechanisms at different locations within the cochlea, it could prove insightful to investigate the source of the $2f_2 - f_1$ DP within the cochlear model.

In this chapter we address the research questions posed in section 1.9 which relate to the $2f_2 - f_1$ DPOAE. The outcome is a summary of the $2f_2 - f_1$ DPOAE characteristics predicted by the model compared to physiological results, and a description of the emission source within the cochlear model. The generation mechanism for the $2f_2 - f_1$ DP is interesting because the wave-fixed source of the upper side band DP is very close to its own characteristic place (figure 1.21b). This differs from the $2f_1 - f_2$ DP wave-fixed source region which is spatially separated from its own characteristic place (figure 1.21a). However, the close proximity of the $2f_2 - f_1$ characteristic place and the wave-fixed source makes it more difficult to interpret simulated results for this emission

6.1 The measured and predicted characteristics of the $2f_2 - f_1$ distortion product

In this section we summarise the measured characteristics of the $2f_2 - f_1$ DPOAE described in the literature, and also demonstrate the strengths and weaknesses of the model with regard to predicting these properties. We consider the properties of the wave-fixed and place-fixed components of the predicted emission, as well as the behaviour of the total $2f_2 - f_1$ DP. We conclude that, although it has some limitations, the model adequately predicts a range of $2f_2 - f_1$ DPOAE characteristics and is therefore useful for gaining further insight into the mechanisms underlying the generation of this emission within the cochlea.

6.1.1 Detection

The $2f_2 - f_1$ DPOAE can be observed in up to 90% of human ears (Horn *et al.*, 2008), but this is dependent on the stimulus paradigm and this emission is not as prevalent as the $2f_1 - f_2$ DPOAE (Moulin *et al.*, 1993; Erminy *et al.*, 1998; Lasky, 1998a, 1998b; Moulin, 2000; Fitzgerald & Prieve, 2005). In addition, Fitzgerald & Prieve (2005) found that the intra-subject variation in emission amplitude was greater for the $2f_2 - f_1$ compared to the $2f_1 - f_2$ DPOAE

The $2f_2 - f_1$ DPOAE has also been observed in a variety of mammals such as the rabbit (Lonsbury-Martin *et al.*, 1987) and the gerbil (Brown & Kemp, 1985; Dong & Olsen, 2008). Intracochlear measures of the $2f_2 - f_1$ distortion product in the basilar membrane velocity of the chinchilla cochlea, and the cochlear fluid pressure of the gerbil have also been obtained (Robles *et al.*, 1997; Dong & Olson, 2005; Dong & Olsen, 2008).

6.1.2 Amplitude

The absolute amplitude of the $2f_2 - f_1$ DPOAE

The amplitude of the $2f_2 - f_1$ DPOAE depends on the level, level difference, frequency and frequency ratio of the primary tones (Erminy *et al.*, 1998). As an example, figure 6.1a shows the average $2f_2 - f_1$ emission amplitude recorded from 108 human ears by Martin *et al.* (1998). This demonstrates that for moderate stimulus levels and an f_2/f_1 ratio of 1.21, the $2f_2 - f_1$ DPOAE level varies between − 10 and 5 dB SPL across a range of stimulus frequencies. Figure 6.1b shows the simulated amplitude of the $2f_2 - f_1$ DPOAE predicted by the perturbed cochlear model.

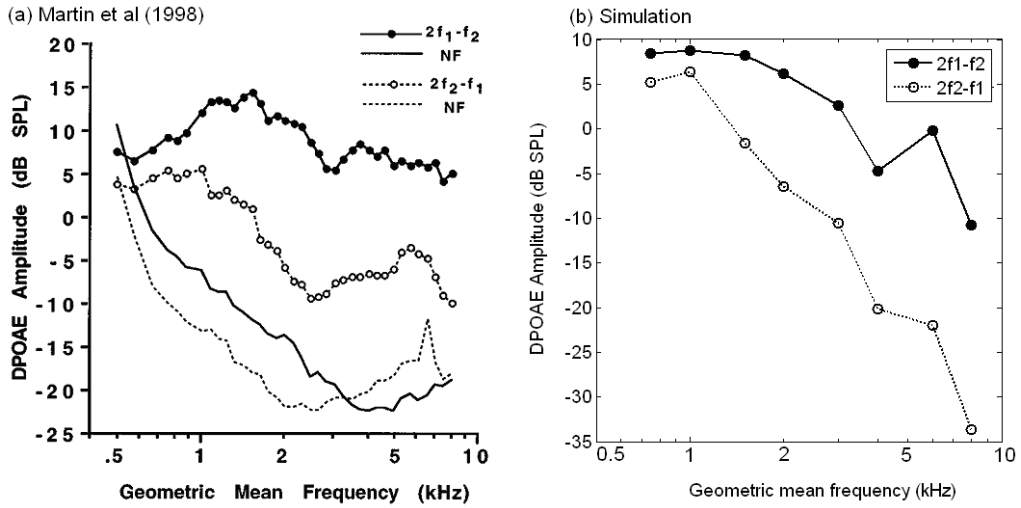

Figure 6.1 Amplitude of the $2f_2 - f_1$ DPOAE for a range of DP frequencies
(a) The physiological measurement of the average DPOAE amplitude in 108 human ears, using f_2/f_1=1.21 [from figure 7 of Martin *et al.* (1998), with permission from ASA]. (b) The predicted amplitude of the $2f_2 - f_1$ and $2f_1 - f_2$ DPOAEs evoked by stimulus tones f_2/f_1=1.2. The simulation was performed using a perturbed model incorporating random irregularities in the active BM impedance, as described in section 4.2.1. In both plots, the amplitudes of the $2f_1 - f_2$ and $2f_2 - f_1$ emissions are denoted by the solid and dotted lines respectively. Stimulus levels of $L_1 = L_2$=75 dB SPL were used. The geometric mean frequency corresponds to the square root of $f_1 f_2$.

Comparing figure 6.1a and b, establishes that the $2f_2 - f_1$ DPOAE amplitude predicted by the model is within ± 5 dB of the amplitude observed in the experimental study at low stimulus frequencies ($\sqrt{f_1 f_2} \leq 1$ kHz or $f_2 < 1.1$ kHz). However, the model tends to underestimate the amplitude of the $2f_2 - f_1$ DPOAE at high stimulus frequencies. For example, when f_2 exceeds 4.4 kHz, the predicted $2f_2 - f_1$ emission level is at least 10 dB smaller than that observed experimentally. The model has a similar tendency to underestimate the amplitude of the $2f_1 - f_2$ DPOAE for high stimulus frequencies, and the possible reasons for this were discussed in section 4.1.2.

Intracochlear distortion product measurements

In contrast to measurements in the ear canal, where the amplitude of the $2f_1 - f_2$ emission exceeds that of the $2f_2 - f_1$ DPOAE, intracochlear measures of BM velocity in the chinchilla suggest that the $2f_1 - f_2$ and $2f_2 - f_1$ DPs have similar magnitude when observed at a location near the characteristic places of the primary tones (Robles *et al.*, 1997). For example, figure 6.2 shows the predicted BM velocity at the f_2 best place in the perturbed cochlear mode, and a Robles *et al.* (1997) measurement from the chinchilla cochlea for comparison. The model is not expected to replicate the absolute levels of the DP components observed in the experimental study, due to animal differences in both the cochlea and middle ear. However, it is possible to compare the relative amplitudes of the DPs between the simulation and the physiological study. Robles *et al.* observed that the 3rd order DPs were approximately equal amplitude and around 20 dB below the level of the primary responses. The model simulation is in agreement with this, as the levels of the 3rd order DPs differ by only 2 dB, and fall approximately 20 dB below the level of the primary responses.

(a) Robles *et al.* (1997) (b) Simulation

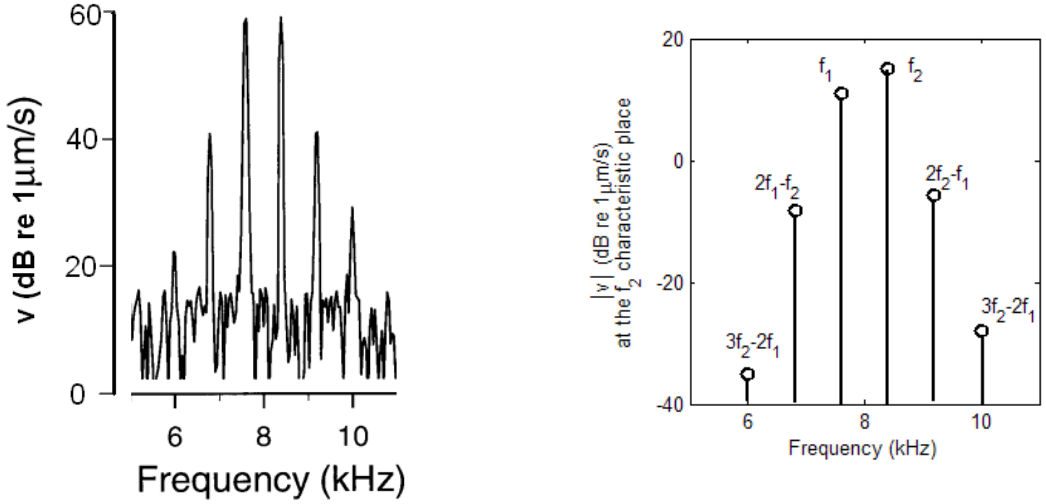

Figure 6.2 The spectrum of the BM velocity response to two tone stimulation
(a) The measured BM velocity of the chinchilla cochlea in response to two tone stimulation, observed at the 8 kHz characteristic place by Robles *et al.* (1997). [From figure 1b of Robles *et al.* (1997), with permission from Am. Physiol. Soc]. In both cases, the stimuli were presented at L_1=L_2=70 dB SPL and frequencies f_1=7.6 kHz and f_2=8.4 kHz. (b) The predicted BM velocity evoked by two stimulus tones presented to the ear canal of the cochlear model, evaluated for the frequency components $3f_2 - 2f_1$, $2f_2 - f_1$, f_2, f_1, $2f_1 - f_2$ and $3f_1 - 2f_2$. The perturbed model incorporates random irregularities as described in section 4.2.1

(a) Moulin (2000) (b) Simulation

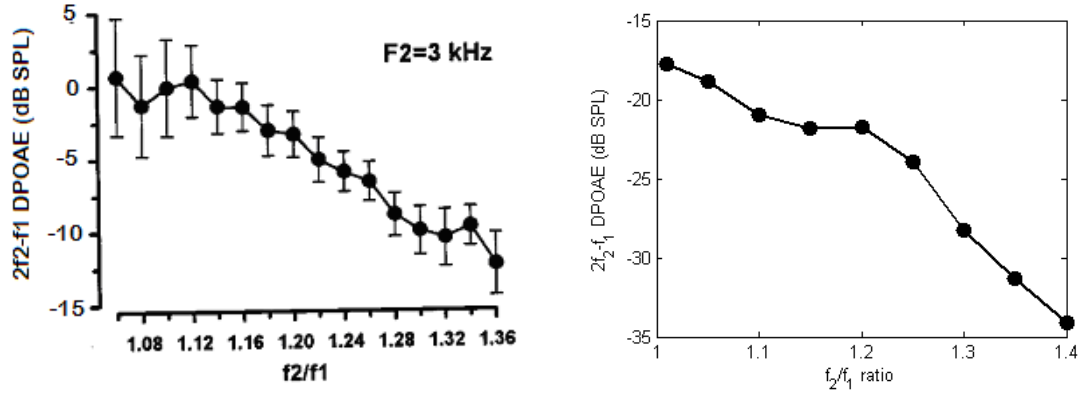

Figure 6.3 The dependence of $2f_2 - f_1$ DPOAE amplitude on f_2/f_1 ratio
(a) Variation measured of $2f_2 - f_1$ DPOAE amplitude with stimulus frequency ratio, averaged across 18 human ears. The stimulus levels were L_1=65 and L_2=60 dB SPL, f_2=3 kHz. [Adapted from Moulin (2000), figure 3]. (b) The amplitude of the $2f_2 - f_1$ DPOAE predicted by the model incorporating random irregularities as described in section 4.2.1. The stimulus levels were set to L_1=L_2=50 dB SPL and f_2= 3 kHz.

6.1.3 Influence of stimulus frequency ratio

General features of the dependence of $2f_2 - f_1$ DPOAE amplitude on f_2/f_1 ratio

Figure 6.3 shows the measured and predicted influence of f_2/f_1 ratio on the $2f_2 - f_1$ DPOAE amplitude. The measurement of Moulin (2000) demonstrates that the emission amplitude tends to increase as the f_2/f_1 ratio decreases towards 1. In contrast to the behaviour of the $2f_1 - f_2$ DPOAE, there is no substantial decline in the amplitude of the $2f_2 - f_1$ emission as f_2/f_1 approaches unity in the experimental study. This physiological result is consistent with other recordings from humans

and chinchilla (Robles *et al.*, 1997; Knight & Kemp, 1999, 2001; Fitzgerald & Prieve, 2005; Horn *et al.*, 2008), but the dependence of the $2f_2 - f_1$ DPOAE on stimulus frequency ratio is known to vary significantly between individual subjects (Moulin, 2000). The simulation was performed at a lower stimulus level compared to the experimental measurement, because section 4.1.6 revealed that the model tends to over estimate the optimal f_2/f_1 ratio at higher stimulus levels for upper side band emissions. The predicted amplitude of the $2f_2 - f_1$ DPOAE decreases by about 9 dB as the f_2/f_1 ratio increases from 1.05 to 1.3. This is similar behaviour to that observed in the experimental study, which shows a decrease in emission amplitude of approximately 12 dB as the f_2/f_1 ratio increases from 1.05 to 1.32. The high intersubject variation in the dependence of $2f_2 - f_1$ DPOAE amplitude on f_2/f_1 ratio is illustrated by the results of Moulin (2000), reproduced in figure 6.4. In this study, the optimal f_2/f_1 values ranged from ≤1.06 to 1.16.

In section 4.1.6 the decline in the $2f_1 - f_2$ DPOAE amplitude as the f_2/f_1 approached unity was attributed to the influence of mutual suppression of the primary tones. The absence of this effect on the $2f_2 - f_1$ DPOAE in figure 6.3 suggests that the wave-fixed DP sources for the two emissions occur at different locations within the cochlea.

The effect of stimulus level on the influence of the f_2/f_1 ratio

Figure 6.5 and figure 6.6 show the predicted and measured dependence of the $2f_2 - f_1$ DPOAE amplitude on stimulus frequency ratio for different stimulus levels. The model simulation predicts that the optimum f_2/f_1 ratio for the $2f_2 - f_1$ emission should increase from around 1.01 to 1.1 as the stimulus level (L_1=L_2) increases from 50 to 70 dB SPL.

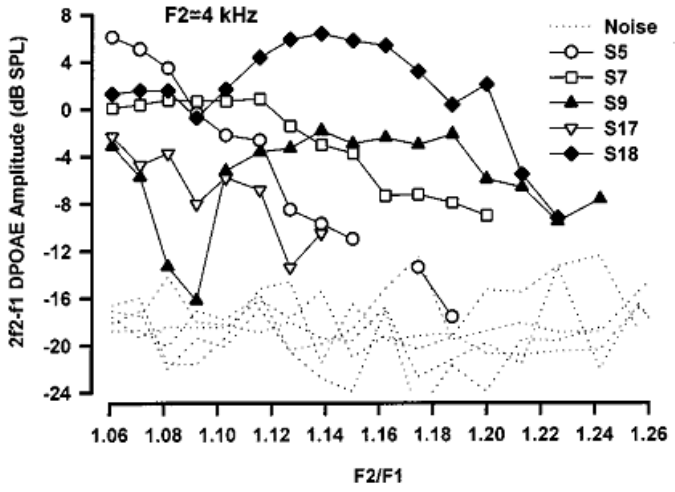

Figure 6.4 The intersubject variation in the influence of f_2/f_1 on the $2f_2 - f_1$ DPOAE amplitude
The plot shows the amplitude of the $2f_2 - f_1$ DPOAE measured in 5 different individuals by Moulin (2000) for a range of f_2/f_1 ratios. The key refers to the different subjects. Measurements were made using L_1=65, L_2=60 dB SPL and f_2 = 4 kHz. [From figure 5 of Moulin (2000), with permission from ASA].

It is difficult to determine if this trend is consistent with physiological results, in view of the large intersubject variation in the optimal f_2/f_1 ratio. For example, although the measurements of Knight & Kemp (1999) shown in figure 6.6 were only recorded for 4 different f_2/f_1 ratios (1.05, 1.20, 1.27 and 1.32), the results suggest that increasing the L_1 stimulus level (L_1=L_2+10dB) from 65 dB SPL to 75 dB SPL shifts the optimal stimulus frequency ratio from 1.2 to 1.27. However, such a shift is not observed in the Knight & Kemp (1999) results for other stimulus paradigms such as L_1=L_2 or L_1=L_2 + 5dB. In addition, Fitzgerald & Prieve (2005) comment that they observe an increase in the measured optimal f_2/f_1 ratio as stimulus level increases, although they do not quantify the scale of this change. Therefore, the increase in optimal f_2/f_1 ratio with increasing stimulus level predicted by the model for the $2f_2 - f_1$ emission could be consistent with experimental measurements.

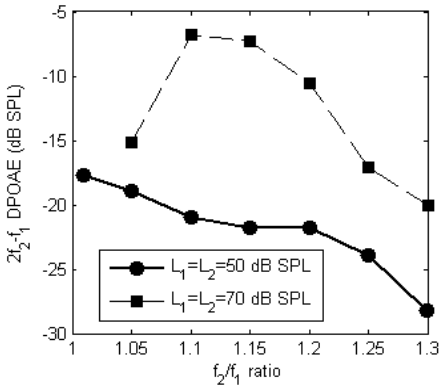

Figure 6.5 The predicted influence of stimulus level on the optimal f_2/f_1 ratio
The plot shows $2f_2 - f_1$ DPOAE amplitude as a function of f_2/f_1 ratio for two different stimulus levels, using f_2= 3 kHz. The model incorporates random irregularities as described in section 4.2.1.

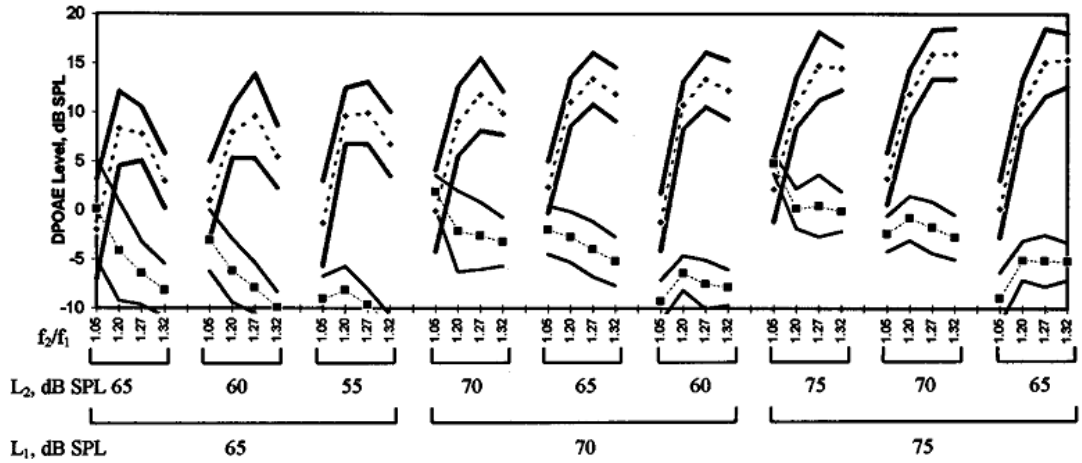

Figure 6.6. The influence of stimulus level on the $2f_1 - f_2$ and $2f_2 - f_1$ DPOAEs
The plot shows the average 3rd order DPOAEs recorded from 9 human ears at a range of stimulus levels and f_2/f_1 ratios by Knight & Kemp (1999). The results are averaged across measurements using f_2 values between 1.7 and 2.4 kHz. The average amplitudes of the $2f_1 - f_2$ (dotted line) and $2f_2 - f_1$ (squares) are shown, along with the solid lines which represent ±1 standard error from the mean values. [From figure 2 of Knight & Kemp (1999), with permission from ASA].

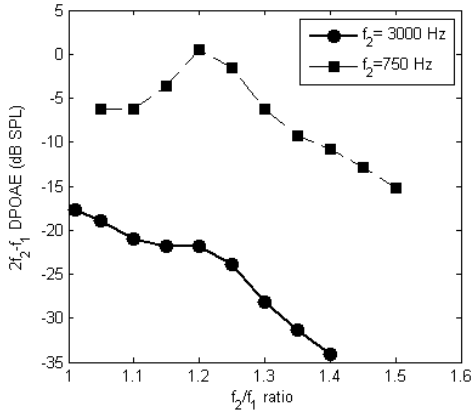

Figure 6.7 The predicted influence of stimulus frequency on the optimal f_2/f_1 ratio
The plot shows the predicted $2f_2 - f_1$ DPOAE amplitude, as a function of f_2/f_1 ratio for stimulus levels L_1=L_2=50 dB SPL using either f_2 = 3 kHz (solid line & circles) or f_2 = 0.75 kHz (dashed line & squares). The perturbed model incorporates random irregularities as described in section 4.2.1.

The effect of stimulus frequency on the f_2/f_1 ratio

Figure 6.7 shows the dependence of the simulated $2f_2 - f_1$ amplitude on f_2/f_1 ratio for two different stimulus frequencies. The model predicts that the optimal f_2/f_1 ratio for the $2f_2 - f_1$ emission will increase from ≤1.01 to 1.2 when the f_2 frequency is reduced from 3 to 0.75 kHz. This is in good qualitative agreement with the trend observed by Fitzgerald & Prieve (2005) who found that the optimal f_2/f_1 ratio for the $2f_2 - f_1$ DPOAE increases from 1.05 to 1.1 when f_2 is decreased from 2 to 0.7 kHz. However, the scale of the 0.2 increase in the optimal f_2/f_1 ratio predicted by the model is greater than the increases of 0.05 (Fitzgerald & Prieve, 2005) and 0.08 (Moulin, 2000) observed for similar stimulus frequency changes in experimental studies. For this reason, the model appears to overestimate the influence of stimulus frequency on the optimal f_2/f_1 ratio compared to experimental studies. Fitzgerald & Prieve (2005) suggest that the change in optimal f_2/f_1 ratio with stimulus frequency arises from the sharper tuning of the BM response to higher stimulus frequencies which influences the degree of overlap between primary travelling waves. On this basis, the tendency of the model to overestimate the influence of stimulus frequency on the optimal f_2/f_1 ratio could suggest that the change in sharpness of tuning between the base and apex of the model is too great. This is consistent with the conclusion drawn in section 4.3 regarding the models tendency to overestimate the influence of stimulus frequency on the optimal f_2/f_1 ratio for the $2f_1 - f_2$ DPOAE.

(a) Knight & Kemp (2001) (b) Model simulation

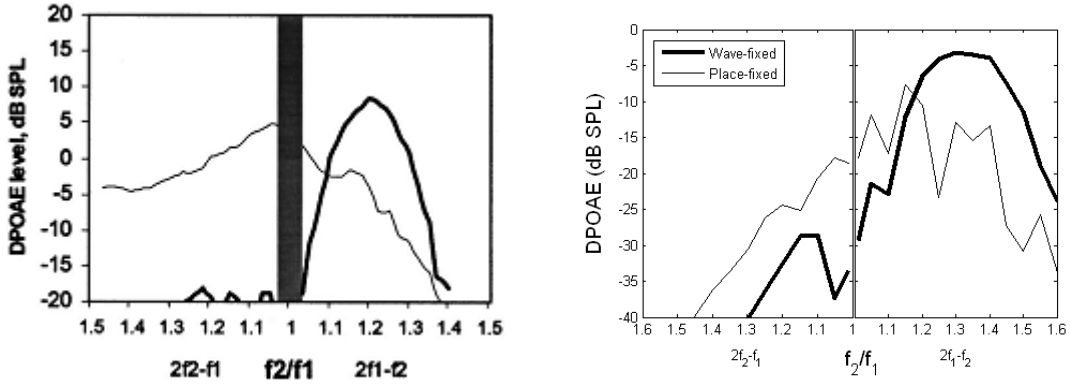

Figure 6.8 The influence of f_2/f_1 on the components of the $2f_1 - f_2$ and $2f_2 - f_1$ DPOAEs
(a) The amplitude of the wave-fixed (thick line) and place-fixed (line thin) for the $2f_1 - f_2$ and $2f_2 - f_1$ DPOAEs, measured in the human ear canal by Knight & Kemp (2001) using L_1=L_2=70 dB SPL and DP frequencies averaged across 1 to 4 kHz. [From figure 5 of Knight & Kemp (2001), with permission from ASA]. (b) The simulated wave-fixed and place-fixed components of the $2f_1 - f_2$ and $2f_2 - f_1$ DPOAEs, using f_2=3 kHz, and L_1=L_2=50 dB SPL.

The wave-fixed and place-fixed components

Figure 6.8 shows the estimated amplitude of the wave-fixed and place-fixed components of the simulated $2f_2 - f_1$ DPOAE across a wide range of stimulus frequency ratios (1.01 to 1.60). The experimental measurement made by Knight & Kemp (2001) is also shown for reference. For f_2/f_1 values between 1.01 and 1.3, the amplitude of the place-fixed $2f_2 - f_1$ varies by about 10 dB, which is comparable to the change of approximately 7 dB in the Knight & Kemp study. However, at higher stimulus frequency ratios in excess of 1.3, the amplitude of the place-fixed component falls off rapidly in the cochlear model which is not evident in the Knight & Kemp measurement. It is difficult to determine if this discrepancy constitutes a significant limitation of the cochlear model, as there is little other experimental data available for the components of the $2f_2 - f_1$ emission at high stimulus frequency ratios and it is often averaged over several stimulus paradigms (such as different level differences or f_2 stimulus frequencies).

6.1.4 Influence of stimulus level difference

Figure 6.9 shows the dependence of the simulated $2f_2 - f_1$ DPOAE amplitude on the stimulus level difference ($L_1 - L_2$) predicted by the perturbed model. It suggests that the amplitude of the predicted $2f_2 - f_1$ emission amplitude will be maximised for small level differences, between -5 and 5 dB, at moderate stimulus levels (50 to 70 dB SPL). This simulated result is consistent with physiological measurements, which demonstrate that the level of the human $2f_2 - f_1$ DPOAE is greatest when the level difference is equal to zero (Knight & Kemp, 1999; Fitzgerald & Prieve, 2005; Horn *et al.*, 2008). This is in contrast to the behaviour of the $2f_1 - f_2$ emission, which is enhanced by a stimulus level difference such that $L_1 > L_2$ (section 4.1.5).

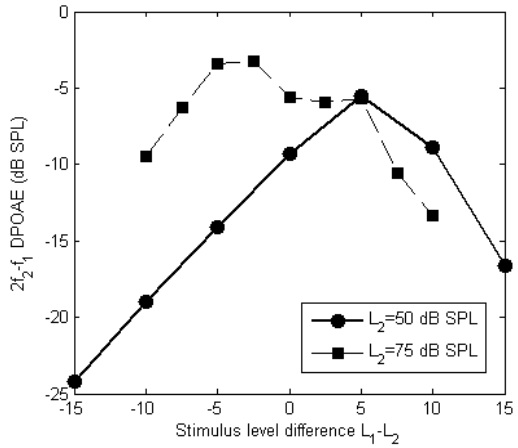

Figure 6.9 The predicted dependence of the $2f_2 - f_1$ DPOAE on stimulus level difference
The simulation was performed using f_2/f_1=1.2 and L_2 equal to either 50 or 70 dB SPL

The optimal stimulus level difference for the $2f_1 - f_2$ DPOAE is attributable to the behaviour of the nonlinear function (section 4.1.5) and the same is true of the optimal level difference for the $2f_2 - f_1$ DPOAE. For example, figure 6.10 shows the levels of the f_1 and f_2 components of the shear displacement at the $2f_2 - f_1$ characteristic place, which serve as the inputs to the nonlinear function. The levels of the input to the nonlinear function are labelled A_1 and A_2 and this location was chosen as it corresponds to a site within the $2f_2 - f_1$ DP wave-fixed source region in the cochlear model, as shown in section 6.2. The figure illustrates that when the level difference between the tones presented in the ear canal ($L_1 - L_2$) is 5 dB, which optimises the $2f_2 - f_1$ DPOAE at this L_2 level, then the level difference in the input to the nonlinear function ($A_1 - A_2$) is around 0 to 5 dB at the DP characteristic place.

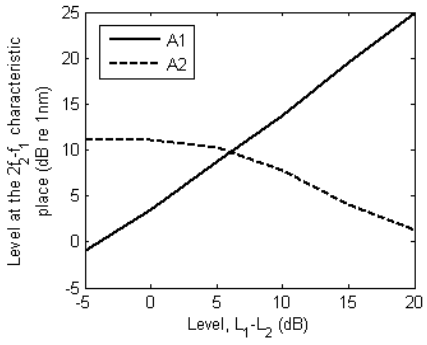

Figure 6.10 The predicted level of input to the nonlinear function at the DP characteristic place
The plot shows the f_1 and f_2 inputs to the nonlinear function, denoted by A_1 and A_2, that are evoked at the $2f_2 - f_1$ characteristic place in the coupled cochlear model by stimulus tones presented in the ear canal at levels L_1 and L_2. The simulation was performed by setting L_2 equal to 50 dB SPL and varying L_1 such that the level difference ($L_1 - L_2$) increased from − 5 to +20 dB.

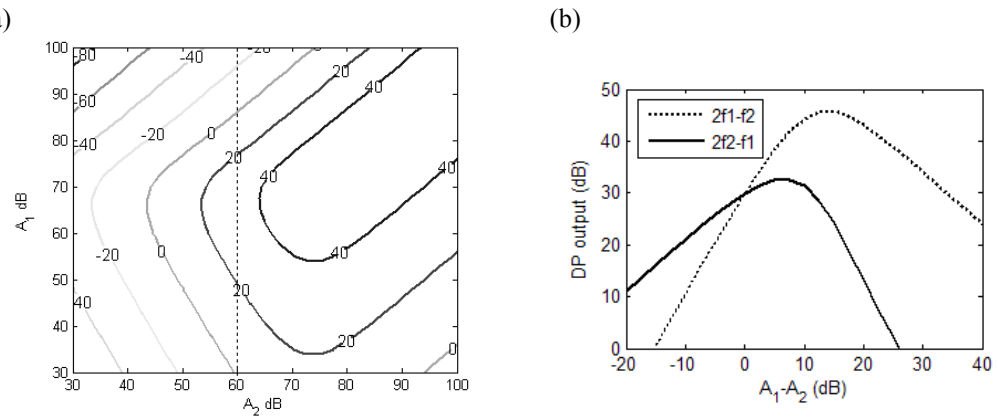

Figure 6.11 The level of the $2f_2 - f_1$ DP component output of an isolated nonlinear function
(a) A contour plot of the $2f_2 - f_1$ DP component output from a single isolated first order Boltzmann function stimulated at frequencies f_1 and f_2 with levels of A_1 and A_2 respectively. (b) The variation in the DP output as $A_1 - A_2$ varies for a fixed A_2 value of 60 dB. The results are shown for both the $2f_2 - f_1$ (solid line) and $2f_1 - f_2$ (dotted line) DPs.

Figure 6.11 shows the simulated amplitude of the $2f_2 - f_1$ DP in the output of a single isolated first order Boltzmann function when two tones at frequencies f_1 and f_2, with levels of A_1 and A_2 respectively, are presented at the input. Figure 6.11b demonstrates that the $2f_2 - f_1$ DP component of the output is maximised when $A_1 - A_2$ is 5 dB, which corresponds to a stimulus level difference ($L_1 - L_2$) of about 5 dB in the coupled cochlear model. It also shows that the level difference ($A_1 - A_2$) required to maximise the $2f_2 - f_1$ DP component of the output for an isolated nonlinearity is less than the level difference needed to optimise the $2f_1 - f_2$ DP component. This suggests that the difference in the optimal level difference for the $2f_2 - f_1$ and $2f_1 - f_2$ DPOAEs observed for the coupled model could also arise simply from the properties of the nonlinear function in isolation.

6.1.5 Growth functions

The predicted growth of the total $2f_2 - f_1$ DPOAE in a perturbed cochlear model, including both the wave-fixed and place-fixed components, is shown in figure 6.12. This demonstrates that the simulated place-fixed component dominates the total emission at low stimulus levels, but decreases in amplitude at higher levels. The introduction of the place-fixed component to the simulation reduces the growth rate from 1.1 dB/dB to 0.3 dB/dB, as a consequence of the contribution from the place-fixed component at low stimulus levels. This is in good agreement with the $2f_2 - f_1$ DPOAE growth rate of around 0.6 − 0.9 dB/dB measured by Horn *et al.* (2008) using f_2/f_1 ratios between 1.04 and 1.12, given that the growth rate is likely to differ by at least ± 0.4 dB/dB between individuals (section 4.1.4).

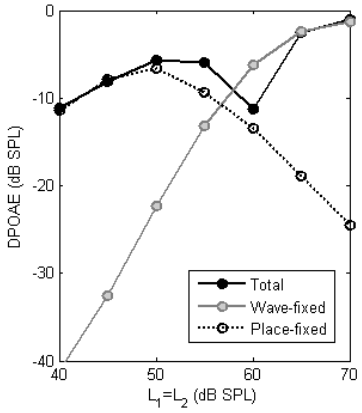

Figure 6.12 The predicted growth of the $2f_2 - f_1$ DPOAE
The simulation was performed using f_2 = 2 kHz, L_1=L_2, and f_2/f_1 = 1.10

The decline in the amplitude of the $2f_2 - f_1$ place-fixed component at high stimulus levels indicates a limitation of the model because it requires that simulations of the $2f_2 - f_1$ emission have to be performed at a lower stimulus levels than experimental measures to achieve similar results (e.g. fine structure simulations). The same decline was observed in section 4.2.5 for the place-fixed component of the $2f_1 - f_2$ emission, but it was not thought indicative of a weakness in the model as it has less impact on the simulated fine structure of the lower- compared to the upper- side band emission. In section 4.2.5, the decline of the place-fixed $2f_1 - f_2$ emission at high stimulus levels was attributed to suppression of the DP travelling in the vicinity of the DP characteristic place by the primary travelling waves. This is also likely to be responsible for the underestimation of the place-fixed component of the $2f_2 - f_1$ emission because, if the effect of DP suppression by the primary tones is neglected from the model, the amplitude of the place-fixed component increases by 37 dB whilst the wave-fixed component changes by less than 2 dB when L_1=L_2=70 dB SPL. As the suppression of the DP travelling wave by the primary responses has a more substantial influence on the upper- rather than the lower- side band emission at high stimulus levels, this suggests that there is less spatial separation between the DP characteristic place and the best places for the primary tones for the $2f_2 - f_1$ DP compared to the $2f_1 - f_2$ DP. Overall the predicted growth of the upper side band emission indicates that the source of the $2f_2 - f_1$ DP within the cochlear model may be more representative of the human ear at low stimulus levels.

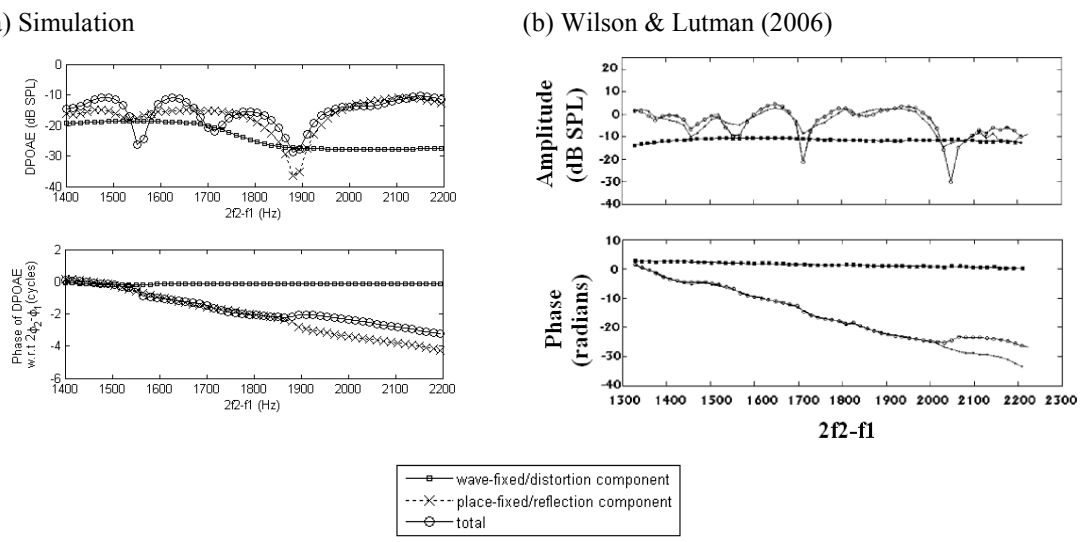

Figure 6.13 The $2f_2 - f_1$ DPOAE fine structure
(a) The predicted level and phase of the $2f_2 - f_1$ DPOAE in the ear canal, using L_1=L_2=50 dB SPL and f_2/f_1=1.2. The perturbed model incorporates irregularities in the active mechanics, as described in section 4.2.1. (b) Level and phase of the measured $2f_2 - f_1$ DPOAE observed in a human ear canal by Wilson & Lutman (2006), using L_1=65, L_2=60 dB SPL and f_2/f_1 between 1.05 and 1.32. The wave-fixed and place-fixed components were separated using a time-windowing technique. [From figure 2 of Wilson & Lutman (2006), with permission of ASA]. In both plots, the open circles correspond to the total DPOAE, and the wave-fixed (distortion) and place-fixed (reflection) components are denoted by filled squares and crosses respectively.

6.1.6 Fine structure

Figure 6.13 shows the fine structure for the $2f_2 - f_1$ DPOAE predicted by the perturbed cochlear model and the experimental measure of Wilson & Lutman (2006) for comparison. The amplitude and phase of the wave-fixed and place-fixed components are shown in addition to the total emission. In both cases the amplitude of the total predicted $2f_2 - f_1$ DPOAE is seen to fluctuate by 10 to 20 dB as the DP frequency is swept from 1.4 to 2.2 kHz. The amplitude and phase of the wave-fixed component is essentially constant across this frequency range, apart from the decrease in the predicted result at 1700 − 1800 Hz which is thought to arise from the properties of the middle ear transfer function. In contrast, the place-fixed component of both the simulation and the measurement has fluctuating amplitude and phase which varies rapidly as the stimulus frequency changes.

As for the $2f_1 - f_2$ DPOAE fine structure discussed in section 4.2.3, the fine structure illustrated in figure 6.13 could arise in two different ways. Firstly, the amplitude fluctuations in the place-fixed component could directly give rise to amplitude fluctuations in the total $2f_2 - f_1$ DPOAE. Secondly, the difference in phase behaviour could lead to alternating constructive and destructive summation between the two components. Both of these mechanisms appear to be evident in the simulated fine structure (figure 6.13a). For example, when the emission frequency is close to 1450 or 1900 Hz, the peaks and troughs of the predicted fine structure correspond to fluctuations in the place-fixed

component. At these frequencies, the simulated fine structure thought to arise predominantly from the amplitude fluctuations in the estimated $2f_2 - f_1$ place-fixed component. Only fine structure of this origin is evident in the physiological measurement of Wilson & Lutman (2006). However, at other emission frequencies peaks and troughs occur in the predicted DPOAE amplitude which do not correspond to variations in either the level of either place-fixed or wave-fixed components (such as 1550 − 1800 Hz). At these frequencies, fine structure is attributed to the alternating constructive and destructive summation of the wave-fixed and place-fixed components. This is consistent with the relative phase of the two components predicted by the model. For example, the total simulated $2f_2 - f_1$ DPOAE exhibits a peak and a trough at 1625 and 1715 Hz respectively. At these locations, the phase difference between the place-fixed and wave-fixed components corresponds to 0.99 and 1.52 cycles in that order, which confirms that peaks and troughs can occur in the $2f_2 - f_1$ fine structure when the wave-fixed and place-fixed components are either entirely in phase or out of phase respectively. Although fine structure of this origin is not evident in the Wilson & Lutman (2006) measurement, the analysis of other experimental measures discussed below suggests that fine structure of this nature can be recorded in the human ear canal.

Similarities in fine structure between the $2f_2 - f_1$ and $2f_1 - f_2$ DPOAEs

Figure 6.14 compares the fine structure of the $2f_2 - f_1$ and $2f_1 - f_2$ DPOAEs. The experimental measure of Knight & Kemp (1999) is also shown for reference. The simulated and measured results agree that for some but not all, emission frequencies, fine structure peaks and troughs can coincide for the $2f_2 - f_1$ and $2f_1 - f_2$ DPOAEs. When they do coincide, the peaks and troughs may not have the same amplitude. At DP frequencies which correspond to peaks and troughs in the fine structure of both the $2f_2 - f_1$ and $2f_1 - f_2$ emission, analysis of the simulated wave-fixed and place-fixed components verifies that the two components are almost either entirely in phase or out of phase respectively. For example, a peak is predicted when the DP frequency is equal to 1.25 kHz in the simulated fine structure of both emissions. At this DP frequency, the predicted phase difference in cycles between the wave-fixed and place-fixed components is 6.05 and 7.06 for the $2f_2 - f_1$ and $2f_1 - f_2$ emissions respectively, which indicates that the components are essentially in phase at this DP frequency. Inspection of other peaks and troughs that occur coincidently in the simulated fine structure for both emissions suggests that the fine structure for the two emissions will coincide only when the origin of the fine structure is the alternating destructive and constructive summation of the wave-fixed and place-fixed component. If instead, the simulated fine structure of one or both of the emissions is dominated by amplitude fluctuations in the place-fixed component, the peaks and troughs of the predicted fine structure should not occur at the same DP frequencies for both DPOAEs. This final suggestion is supported by the measurements of Wilson (2005), who observed $2f_2 - f_1$ and $2f_1 - f_2$ DPOAE fine structure in cases where the amplitude of the estimated place-fixed component dominated that of the wave-fixed component. In these measurements there are very few

DP frequencies at which peaks and troughs occur coincidently in the fine structure of both emissions.

The similarity that occurs in the $2f_2 - f_1$ and $2f_1 - f_2$ fine structure has some theoretical implications for the origin of the place-fixed component of the $2f_2 - f_1$ DP. For example, it will be shown in section 6.2.2 that for a given DP frequency the wave-fixed source will have a phase distribution that is essentially the same for both the $2f_1 - f_2$ and $2f_2 - f_1$ DPs. For this reason, coincidences in the $2f_1 - f_2$ and $2f_2 - f_1$ emission fine structure suggest that the phase lag accumulated by the DP travelling wave between the wave-fixed generation site and the reflection site should differ by an integer number of cycles between the two emissions.

(a)

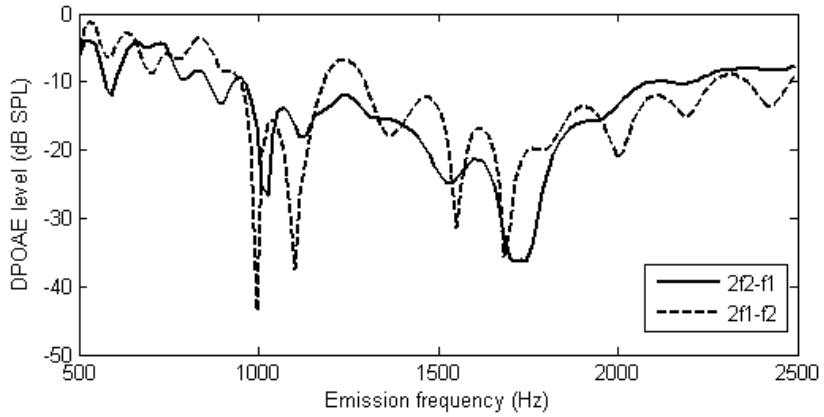

(b)

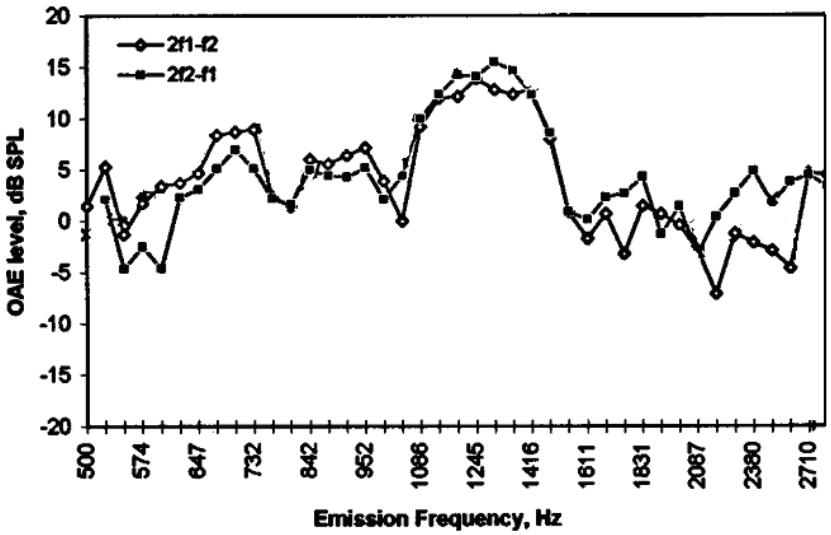

Figure 6.14 Comparison of the $2f_2 - f_1$ and $2f_1 - f_2$ DPOAE fine structure
(a) The predicted amplitude of the $2f_2 - f_1$ and $2f_1 - f_2$ DPOAEs in a perturbed model incorporating irregularities in the active micromechanics, as described in chapter 4.2.1. Stimulus levels L_1=L_2= 50 dB SPL are used, with f_2/f_1=1.05. (b) Level of the measured $2f_1 - f_2$ and $2f_2 - f_1$ DPOAE observed in a human ear canal by Knight & Kemp (1999). Measurements were made using L_1=L_2=70 dB SPL and f_2/f_1=1.05. [From figure 6 of Knight & Kemp (1999), with permission from ASA].

The simplest, but not the only, interpretation of this result is that the ratio of f_{Source}/f_{dp} is the same for both emissions, where f_{Source} is the best frequency of the wave-fixed source location for the DP frequency, f_{dp}. For example, if a 2 kHz DP is measured with a stimulus frequency ratio of 1.05 and $L_1=L_2=50$ dB SPL, we know from the $2f_1 - f_2$ emission that the f_{Source}/f_{dp} ratio is approximately 1.105 as it originates from the vicinity of the f_2 best place. Assuming that this ratio is also true of the $2f_2 - f_1$ DP, we could tentatively suggest that the wave-fixed source of the upper-side band emission originates from the vicinity of the 2210 Hz characteristic place when the DP frequency is equal to 2 kHz. This would correspond to a distance of 14.3 mm from the stapes which is 0.6 mm closer to the base that the $2f_2 - f_1$ characteristic place. Although this deduction is highly speculative, it is consistent with the finding in section 6.2.2 which shows that the centre of the distributed $2f_2 - f_1$ wave-fixed source is located between 14 and 14.5 mm from the base of the cochlear model when the DP frequency is 2 kHz and the f_2/f_1 ratio is set equal to 1.05.

6.1.7 Strengths and weaknesses of $2f_2 - f_1$ DPOAE predictions

There are many characteristics of the $2f_2 - f_1$ DPOAE simulated by the model which agree well with experimental measures. These predicted properties include the amplitude of the emission for f_2 stimulus frequencies less than around 4.4 kHz (section 6.1.2), the optimal stimulus frequency ratio across a range of stimulus levels (section 6.1.3), the optimal stimulus level difference (section 6.1.4), the rate of growth (section 6.1.5), and the amplitude of the fine structure at low stimulus levels (section 6.1.6).

The model also has some significant weaknesses. As for the $2f_1 - f_2$ DPOAE, the model tends to underestimate the amplitude of the $2f_2 - f_1$ emission when the f_2 stimulus frequency exceeds 4.4 kHz (section 6.1.2) and possible explanations for this are discussed in section 4.1.2.The model also underestimates the amplitude of the place-fixed $2f_2 - f_1$ DPOAE component, relative to the wave-fixed component, at high stimulus levels. A consequence of this limitation is that simulations have to be performed at lower stimulus levels than those employed in experimental studies in order to observe effects such as the $2f_2 - f_1$ DPOAE fine structure (section 6.1.6). Section 4.2.5 explains that excessive suppression of the DP travelling wave in the vicinity of the DP characteristic place at high stimulus levels may be responsible for this weakness, which could indicate that the peak of the primary travelling wave envelope broadens too much as the stimulus increases in the cochlear model.

6.2 The wave-fixed $2f_2 - f_1$ DPOAE source

In this section, the origin of the wave-fixed $2f_2 - f_1$ DPOAE within the cochlear model is investigated. A summary of the literature regarding the source of the $2f_2 - f_1$ DPOAE is given in section 1.4.2. Analysis of group delay, component separation using time-windowing techniques, and the results of suppressor tone experiments suggest that this emission has two sources: A wave-fixed source mechanism, distributed over a region basal of the $2f_2 - f_1$ characteristic place where the primary travelling waves overlap, and a place-fixed source located at the $2f_2 - f_1$ characteristic place. These two source mechanisms are illustrated for the $2f_2 - f_1$ DPOAE in figure 6.15.

As the model generally makes valid predictions of the $2f_2 - f_1$ DPOAE characteristics, especially at low stimulus levels, we apply the model to provide insight into the generation mechanism underlying the wave-fixed component of this emission. We assume that the baseline model generates a wave-fixed component which is dominated by a distortion mechanism and that any wave-fixed nonlinear reflection that may occur at moderate stimulus levels can be neglected. We start by considering the region of the model over which the quasilinear OHC pressure output contains a significant DP component. We then evaluate the effective $2f_2 - f_1$ DP source region, taking into account the mechanical properties of the cochlear partition which limit the propagation of DP travelling waves on the apical side of the DP characteristic place. Finally, in section 6.2.3 we use the forward-backward decomposition method to verify the location of the source region for the $2f_2 - f_1$ DP travelling wave, and find the results to be consistent with those presented in the previous sections.

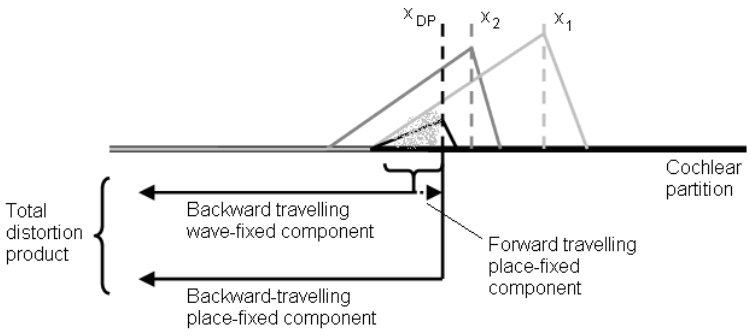

Figure 6.15 Illustration of the two source components for an upper side band emission
The grey and black triangles represent travelling waves corresponding to the primary and distortion product frequencies respectively. The grey shaded area indicates the likely generation region for the wave-fixed component.

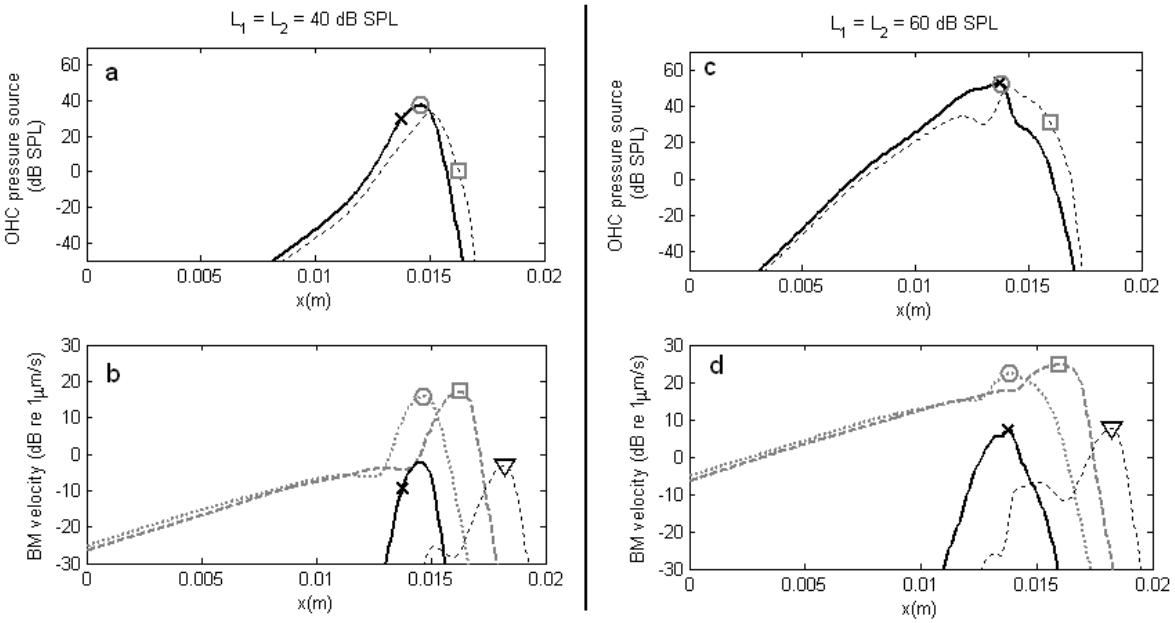

Figure 6.16 The DP component of the OHC pressure output
Plots (a and c) show the DP component of the OHC pressure output where the thick solid line and thin dotted line correspond to the $2f_2 - f_1$ and $2f_1 - f_2$ DP respectively. The BM velocity response (b and d) where the frequency components f_2, f_1, $2f_2 - f_1$ and $2f_1 - f_2$ are represented by the grey dotted, grey dashed, solid black, and thin black dotted lines in that order. In each case f_2 = 2 kHz, f_2/f_1 = 1.25 and the stimulus levels are either (a and b) L_1=L_2=40 dB SPL or (c and d) L_1=L_2=60 dB SPL. The best places for f_2, f_1, and the characteristic places for $2f_2 - f_1$ and $2f_2 - f_1$ are indicated by the circle, square, cross and triangle markers respectively.

6.2.1 The $2f_2 - f_1$ OHC pressure source distribution

Figure 6.16 shows the predicted $2f_2 - f_1$ and $2f_1 - f_2$ DP components of the pressure output of the OHCs, and the BM velocity response, for two different stimulus levels. At low stimulus levels (L_1 = L_2 = 40 dB SPL) the $2f_2 - f_1$ component of the OHC pressure is greatest at the f_2 best place. At higher stimulus levels (L_1=L_2=60 dB SPL) this is still the case, but the f_2 best place has shifted closer to the $2f_2 - f_1$ characteristic place such that the two locations overlap. The distribution of the OHC pressure output differs for the $2f_2 - f_1$ DP compared to the $2f_1 - f_2$ DP. For example, the $2f_2 - f_1$ component of the OHC pressure output has greater amplitude on the basal side of the f_2 best place, and smaller amplitude of the apical side of this location, compared to the $2f_1 - f_2$ component. There is also a difference in the simulated DP components of the BM velocity response which is most apparent for the 60 dB SPL stimuli. The $2f_2 - f_1$ component of the BM velocity exhibits only one peak, in the vicinity of the f_2 best place, whilst the $2f_1 - f_2$ component shows peaks at both the f_2 best place and the $2f_1 - f_2$ characteristic place. This is consistent with the pressure response of the gerbil cochlea made by Dong & Olsen (2008), who observed a single peak response for the $2f_2 - f_1$ DP component compared to a double peaked response for the $2f_1 - f_2$ DP component (figure 1.21). Two peaks are expected to occur in the $2f_1 - f_2$ DP component of the BM velocity in association with the location of the maximum pressure source near the f_2 best place and the large amplitude of the DP forward travelling at the $2f_1 - f_2$ characteristic place (Kim *et al.*, 1980). The absence of a

two peaks in the $2f_2 - f_1$ BM velocity component suggests that the $2f_2 - f_1$ wave-fixed DP source is not spatially separated from the $2f_2 - f_1$ DP characteristic place.

6.2.2 The wave-fixed pressure source distribution

It is not possible for the DP pressure output of the OHCs at every location within the cochlear model to influence the DPOAE in the ear canal. This is particularly relevant for the $2f_2 - f_1$ DP as the maximum $2f_2 - f_1$ component of the OHC pressure output arises at a location which is further from the base than the DP characteristic place. However, DP pressure sources on the apical side of the DP characteristic place should not simply be dismissed because we have seen that there is not a discrete change from travelling wave to evanescent wave at the characteristic place in the model (section 5.1.1). For this reason, large $2f_2 - f_1$ pressure sources may be able to contribute significantly to the emission detected in the ear canal, even if they are located on the apical side of the DP characteristic place. In this section we evaluate the effective wave-fixed $2f_2 - f_1$ DPOAE source distribution which can influence the level of the emission in the ear canal using the technique described in section 5.1.1.

Source length and location

The dark grey shaded area in figure 6.17 shows the predicted effective source length (defined in 5.1.1) for the wave-fixed component of the $2f_2 - f_1$ DPOAE. The figure also illustrates how the length and position of this region changes as the stimulus frequency ratio is increased from 1.01 to 1.4. The light grey area corresponds to the region over which the simulated $2f_2 - f_1$ component of the OHC pressure output is within 10 dB of its maximum value. At f_2/f_1 values close to 1, the dark and light grey regions essentially coincide. However, as f_2/f_1 increases, the effective source regions shifts closer to the base than the region of the maximum OHC pressure output.

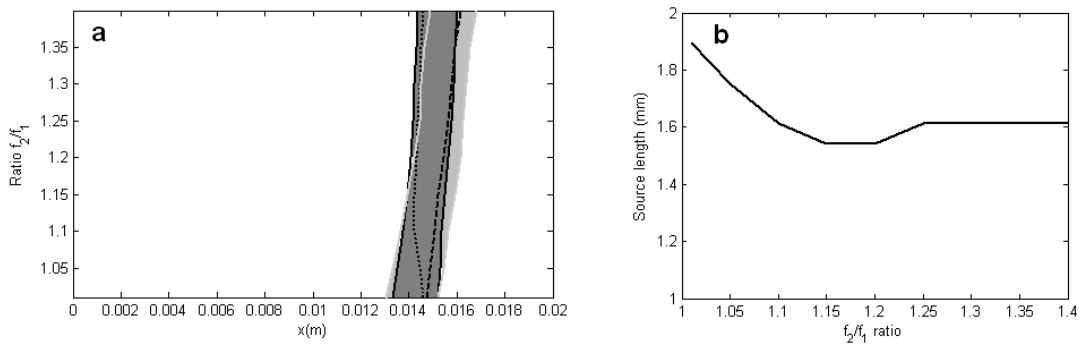

Figure 6.17 The location and length of the wave-fixed $2f_2 - f_1$ DP source
The plots show the simulated length of the $2f_2 - f_1$ DPOAE source with varying f_2/f_1 ratio using $L_1=L_2=50$ dB SPL and $2f_2 - f_1 = 2$ kHz. (a) The solid black lines indicate the boundaries of the source region, and the dotted and dashed lines denote the locations at which the maximum BM velocity occurs at frequencies $2f_2 - f_1$ and f_2 respectively. The dark grey shaded area represents the effective source region, whilst the light grey region corresponds to the area of maximal OHC pressure output at the DP frequency. (b) The length of the dark grey region, shown in (a), for various stimulus frequency ratios.

The length of the effective $2f_2 - f_1$ DP source region predicted by the model, changes by less than 0.5 mm as the f_2/f_1 ratio increases from 1.01 to 1.4. A comparison between the predicted effective wave-fixed DP source region and the distribution of the DP component of the OHC pressure output, for a single stimulus frequency ratio, is shown in figure 6.18.

Figure 6.17a shows that the effective source region for the $2f_2 - f_1$ DP within the cochlear model is distributed between the f_2 best place and a location just basal of the $2f_2 - f_1$ characteristic place. This is consistent with the observation of Martin *et al.* (1998), who found that the $2f_2 - f_1$ DPOAE was most effectively suppressed by a tone that was higher in frequency than f_2. As the apical boundary of this dominant source area is close to the f_2 best place, this means that a significant contribution to the simulated $2f_2 - f_1$ wave-fixed DPOAE originates from a region extending up to approximately 1.6 mm further from the base than the $2f_2 - f_1$ characteristic place. This can occur because there is a finite region beyond the $2f_2 - f_1$ characteristic place over which the travelling wave amplitude is decaying and motion is becoming evanescent. It is also possible that evanescent wave coupling may allow the DP component of the OHC pressure output on the apical side of the $2f_2 - f_1$ characteristic place to contribute to the DPOAE observed in the ear canal of the model. Figure 6.19 shows the predicted $2f_2 - f_1$ component of the semi-difference pressure evoked by a single element of the source distribution described in figure 6.17a. The location of the source element is 1.6 mm further from the base than the $2f_2 - f_1$ characteristic place, and so the amplitude of the semi-difference pressure in the immediate vicinity of the source element decays exponentially with distance from the source. However, between the $2f_2 - f_1$ characteristic place and the base of the model, there is a $2f_2 - f_1$ travelling wave with phase behaviour consistent with that of backward propagation towards the stapes.

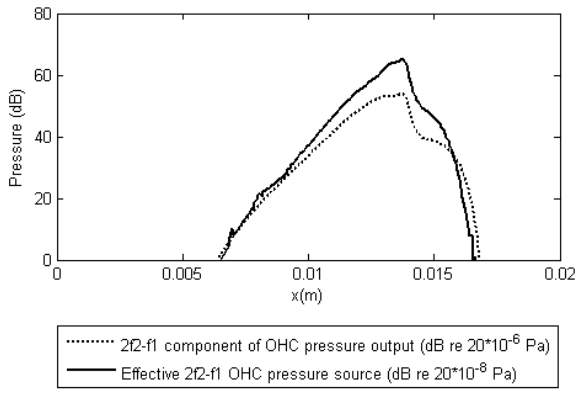

Figure 6.18 Comparison of the effective wave-fixed source distribution and the OHC pressure output for the $2f_2 - f_1$ DP
In this plot the effective source distribution and OHC pressure output are denoted by solid and dotted lines respectively. The two different distributions are given in dB referenced to different pressure levels for ease of comparison, as the absolute level of the estimated effective source distribution is arbitrary and depends on the number of elements used to represent the length of the cochlear partition (500 in this example). For these simulations L_1=L_2= 70 dB SPL, f_2=2 kHz and f_2/f_1=1.1.

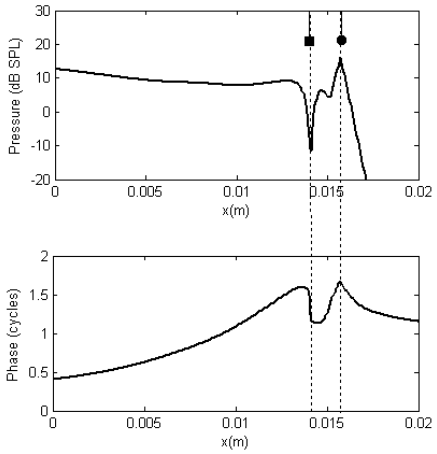

Figure 6.19 The predicted $2f_2 - f_1$ component of the semi-difference pressure evoked by a single element pressure source
The pressure source is located at a distance of 15.7mm from the stapes, on the apical side of the DP characteristic place. The amplitude and phase of the source was determined by the DP component of the OHC pressure output at this location, when the model is stimulated by two pure tones L_1=L_2=50 dB SPL, $2f_2 - f_1$=2 kHz and f_2/f_1=1.2. The characteristic place for the $2f_1 - f_2$ frequency, and the source location, are indicated by the square and circular markers respectively. The basal boundary condition of the model was modified to minimise reflections.

Figure 6.20 shows the simulated length of the $2f_2 - f_1$ wave-fixed DPOAE source for a variety of the stimulus levels (L_1=L_2), using f_2/f_1 equal to 1.1. At low stimulus levels, where the model predictions most accurately reflect the measured properties of the $2f_2 - f_1$ emission, the effective wave-fixed DP source region spans the area between the $2f_2 - f_1$ characteristic place and the f_2 best place. As stimulus level increases, the effective wave-fixed DP source region broadens out towards the base of the model. The model also suggests that the effective wave-fixed source length increases from 1 to 4.5 mm as the stimulus level increases from 30 to 80 dB SPL.

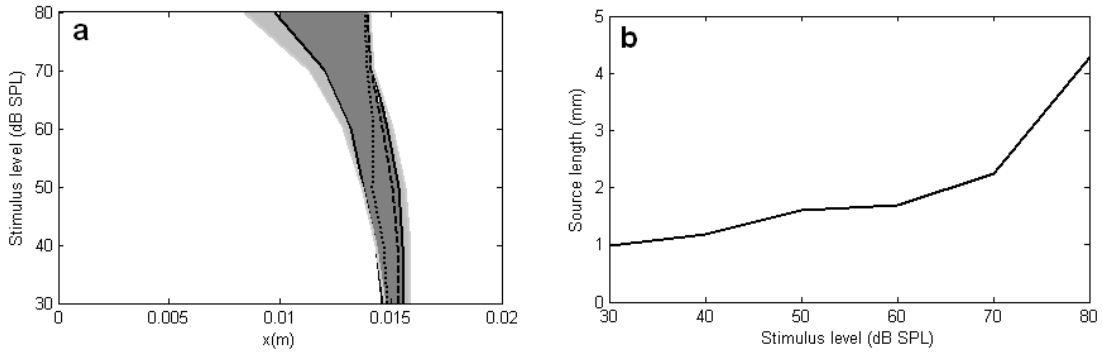

Figure 6.20 The predicted length and location of the wave-fixed $2f_2 - f_1$ DPOAE source
The length of the $2f_2 - f_1$ DPOAE source is predicted for various stimulus levels, using f_2/f_1=1.1 and $2f_2 - f_1$ = 2 kHz. (a) The solid black lines indicate the boundaries of the source region, and the dotted and dashed lines denote the locations at which the maximum BM velocity occurs at frequencies $2f_2 - f_1$ and f_2 respectively. The dark grey shaded area represented the source region, whilst the light grey shading indicates the distribution that the source region would be expected to occupy if the source was restricted by the limitation imposed by the propagation region for the $2f_2 - f_1$ frequency. (b) The length of the dark grey zone shown in (a) for difference stimulus levels (L_1=L_2).

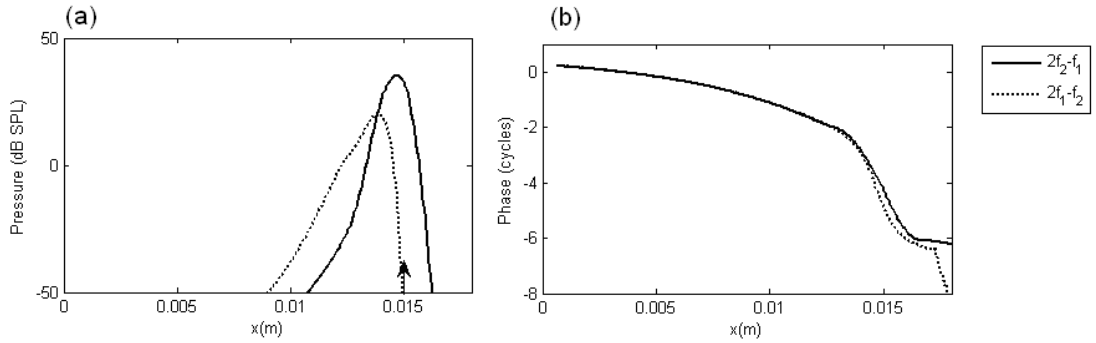

Figure 6.21 The influence of individual elements within the wave-fixed source distribution
The plots show the predicted (a) amplitude and (b) phase of the wave-fixed DPOAE component evoked by single pressure source elements at position x. At each position, the source element has the amplitude and phase described by the distribution of the DP component of the OHC pressure output evoked by two stimulus tones at levels L_1=L_2= 50 dB SPL, f_2/f_1=1.1 and DP frequency of 2 kHz. Results are shown for both the $2f_2 - f_1$ (solid lines) and $2f_1 - f_2$ (dotted lines) DPs, and the arrow indicates the characteristic place of the DP frequency.

Source directionality & forward travelling waves

The directionality of the effective wave-fixed $2f_2 - f_1$ DPOAE source region in the model is likely to change with source length in view of its phase distribution, illustrated in figure 6.21, for the reasons discussed in section 5.1.3. The length of the effective source region extends as the stimulus level increases (figure 6.20) and so the source is expected to preferentially enhance forward travelling DP waves, with respect to backward travelling DP waves, as the stimulus level increases.

So far, we have only considered the effective DP source for backward travelling waves which give rise to the wave-fixed component of the $2f_2 - f_1$ DPOAE. However, it is also important to consider the effective source region for forward DP travelling waves, given that the place-fixed component of the $2f_2 - f_1$ DPOAE tends to dominate the wave-fixed component in experimental studies. Wilson & Lutman (2006) suggest that the $2f_2 - f_1$ DPOAE could arise predominantly from $2f_2 - f_1$ forward travelling waves generated between the base and the DP characteristic place, which are then reflected at the characteristic place and propagate out of the cochlea. It is possible that wave-fixed forward travelling waves at the $2f_2 - f_1$ DP frequency could be generated in two different areas of the model at low stimulus levels. Firstly the forward travelling waves could originate within the same region as the $2f_2 - f_1$ wave-fixed backward travelling waves, and travel only short distances between their generation site and the $2f_2 - f_1$ characteristic place where they are reflected. Beyond the DP characteristic place the forward travelling waves should gradually decay away and become evanescent waves. Secondly, the DP forward travelling waves could be generated by a highly directional source with a preference for emitting forward travelling waves, which is distributed over an extended region between the base and the $2f_2 - f_1$ characteristic place. This source would have to be highly directional or it would have been detected in the previous investigation of the wave-fixed source of backward travelling waves (figure 6.17, for example). To

achieve this high degree of directionality it would be expected to be distributed over an extensive region of the cochlea.

In section 6.3.1, we discover that the place-fixed component of the $2f_2 - f_1$ DPOAE originates primarily from reflection sites in the vicinity of the DP characteristic place in the model. In order to determine the source of the forward travelling wave which gives rise to these reflections, we manipulate the model so that the $2f_2 - f_1$ DP component of the OHC pressure output is "switched off" over a controlled region of the model and monitor the DP component of the BM velocity at the $2f_2 - f_1$ characteristic place. When this $2f_2 - f_1$ DP source is switched off between the base and a location only 0.7 mm closer to the base than the $2f_2 - f_1$ characteristic place, we observe that there is no significant change (< 2 dB) in the amplitude of the $2f_2 - f_1$ component of the BM velocity in the region apical to the manipulated zone. This suggests that substantial forward travelling waves are not generated by an extensively distributed wave-fixed (distortion) mechanism located between the base and the characteristic place. Therefore we conclude that the wave-fixed forward travelling waves are generated in the immediate vicinity of the $2f_2 - f_1$ characteristic place and are likely to travel only a short distance.

6.2.3 Forward and backward travelling wave decomposition

Figure 6.22a shows the estimated forward and backward travelling waves, at the $2f_2 - f_1$ frequency, evoked by two stimulus tones at levels L_1=L_2=50 dB SPL. The basal boundary condition of the model was set to minimise reflections from the stapes (appendix C.2). The $p_0^{\pm}$ coefficients of the forward and backward travelling waves are shown in figure 6.22b. Although fluctuation in the amplitude of just one of the $p_0^{\pm}$ coefficients is an indicator that one of the travelling waves estimated by the decomposition method is dominated by errors associated with numerical inaccuracies or the WKB approximation, fluctuation in the amplitude of both coefficients over a region of the cochlear model is suggestive of a internal DP pressure operating in that vicinity (appendix B.2.4). The vertical dotted lines in figure 6.22 illustrate the boundaries of the source region that could explain the variations in the amplitude of both p_0^{+} and p_0^{-} in the vicinity of the $2f_2 - f_1$ characteristic place. Between the stapes and the basal boundary of this estimated source region, only a backward travelling DP wave is evident. The apical boundary of the estimated DP source region is further from the stapes than the $2f_2 - f_1$ characteristic place, and so the amplitude of the travelling waves fall off rapidly beyond this point. Within the estimated DP pressure source region, the amplitudes of both the predicted forward and backward travelling waves exceed the error floor of the decomposition process. The decomposition method suggests that significant forward travelling $2f_2 - f_1$ waves will only arise within the DP source region bounded by the vertical dotted lines on figure 6.22, which is consistent with the conclusion of section 6.2.2.

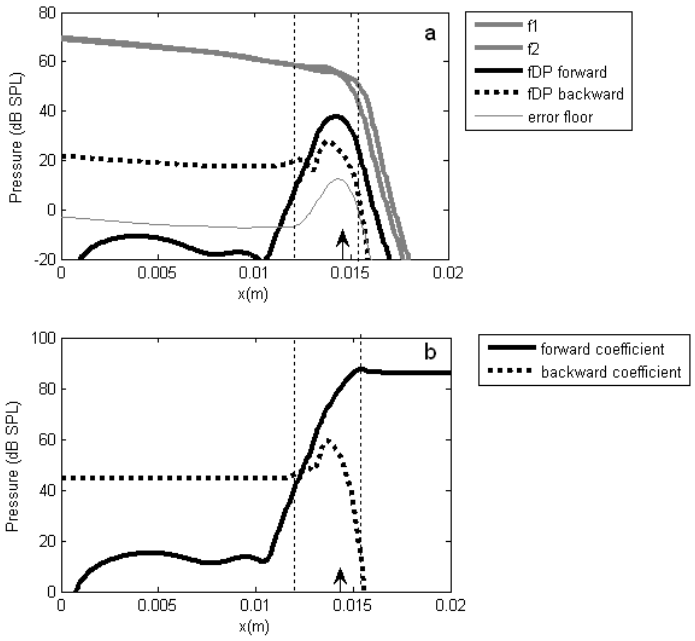

Figure 6.22 The estimated forward and backward travelling $2f_2 - f_1$ DP waves
(a) The estimated forward and backward travelling components of the DP frequency (fDP) semi-difference pressure for the $2f_2 - f_1$ distortion product. The f_2 and f_1 components of the simulated semi-difference pressure are also shown for reference. (b) The $p_0^{\pm}$ coefficients of estimated forward and backward travelling waves shown in (a). In both cases, L_1=L_2= 50 dB SPL, f_2=2 kHz, f_2/f_1=1.1 and the basal boundary condition was set to minimise reflections from the stapes. The vertical dotted lines indicate the region of the cochlear model over which the coefficients $p_0^{\pm}$ both vary suggesting the presence of an internal pressure source distribution. The arrow denotes the $2f_2 - f_1$ characteristic place, which also happens to correspond to the location of the f_2 best place for this stimulus paradigm.

6.3 The place-fixed component of the $2f_2 - f_1$ DPOAE

We have simulated the place-fixed component of the $2f_2 - f_1$ DPOAE by introducing irregularities into the active micromechanics of the cochlear model. These irregularities could give rise to DP backward travelling waves by either of two mechanisms: Reflection of DP forward travelling waves, or alterations in the DP component of the OHC pressure output due to reflection of the primary travelling waves. As the irregularities are at fixed locations, the phase of the reflected waves will change as the phase of the incident wave varies with stimulus frequency. This is true of reflections in either the primary or DP travelling waves and therefore the phase behaviour of the place-fixed $2f_2 - f_1$ observed in section 6.1.6 cannot be used to differentiate between these two possible generation mechanisms. In this section we investigate the location and mechanism behind the place-fixed source of the $2f_2 - f_1$ DP in the cochlear model.

6.3.1 The location and mechanism of the place-fixed source

To identify the location of the dominant mechanism underlying the place-fixed $2f_2 - f_1$ DPOAE within the model, we manipulate the model such that a single 10% impedance irregularity is introduced into the active micromechanics at varying distances from the stapes. At each location, we check the model for stability and examine the amplitude of the place-fixed DPOAE component generated by the inclusion of the single impedance irregularity. Figure 6.23 shows the predicted amplitude of the place-fixed $2f_2 - f_1$ DPOAE generated by a single impedance irregularity positioned at distance x from the base. We also repeat the simulation with a modified quasilinear method in which the impedance irregularity is only introduced to the $2f_2 - f_1$ DP component of the model response, and the primary responses are evaluated in a baseline model containing no impedance irregularity.

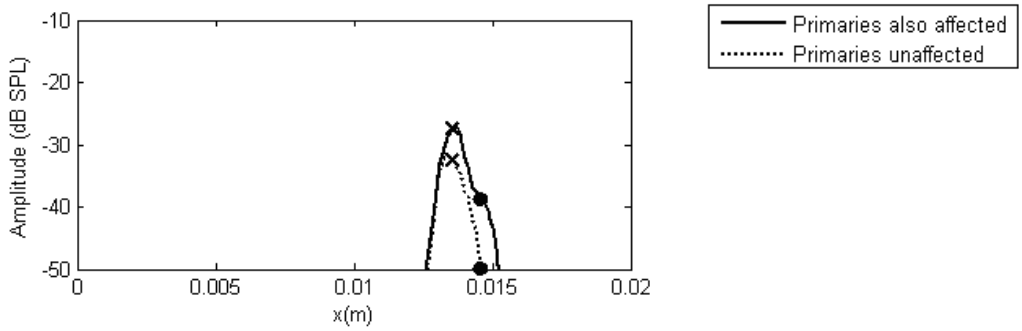

Figure 6.23 The location of the $2f_2 - f_1$ DPOAE place-fixed source
The plot shows the predicted amplitude of the place-fixed (reflection) $2f_2 - f_1$ DPOAE generated by a single impedance irregularity at position x(m) which enhances the OHC gain by 0.1 relative to a baseline cochlear model at that location. Stimulus parameters L_1=L_2=50 dB SPL, f_2=2 kHz and f_2/f_1=1.3 are used. The solid line shows the place-fixed component which arises when the impedance irregularity affects the primary and DP travelling waves. The dotted line indicates the place-fixed component which arises when the impedance irregularity only affects the DP travelling wave and the primary responses are evaluated for a baseline cochlear model. The characteristic place for $2f_2 - f_1$, and the best places for f_2 are indicated by the cross, and circle markers respectively.

Figure 6.23 demonstrates that when the irregularities are only introduced for the DP component of the model response, the predominant source of the place-fixed $2f_2 - f_1$ DPOAE is located at the $2f_2 - f_1$ characteristic place. It also shows that when the irregularity positioned at the DP characteristic place is applied to the primary responses, as well as the $2f_2 - f_1$ DP response, the amplitude of the place-fixed component increases by up to 5 dB. In addition, it is possible for irregularities positioned at the f_2 and f_1 best places to generate low level place-fixed $2f_2 - f_1$ DPOAE components but these are at least 10 dB smaller than the maximum place-fixed emission component which originates from the $2f_2 - f_1$ characteristic place for this stimulus frequency ratio.

Overall we conclude that place-fixed mechanism for the $2f_2 - f_1$ DP involves reflection of both the primary and the $2f_2 - f_1$ travelling waves in the model. The location of this place-fixed source is distributed but it predominantly originates from the $2f_2 - f_1$ characteristic place at high f_2/f_1 ratios.

6.3.2 The place-fixed component and $2f_2 - f_1$ fine structure

In section 6.1.6 we observed the predicted $2f_2 - f_1$ DPOAE fine structure simulated in the perturbed model. We discussed the origin of the fine structure and concluded that, depending on the frequency, it could arise either directly from amplitude fluctuations in the place-fixed component or as a consequence of alternative constructive and destructive summation between the wave-fixed and place-fixed components. However, section 6.3.1 revealed that there are two contributions to the place-fixed component of the $2f_2 - f_1$ DPOAE predicted by the model. Which of these is most important to the simulation of the $2f_2 - f_1$ emission fine structure?

We assess this by manipulating the quasilinear method so that the fine structure can be simulated in a version of the perturbed model in which the impedance irregularities only influence the DP, not the primary, travelling waves. The results are then compared with those obtained using a fully perturbed model in which the primary travelling waves, in addition to the DP travelling waves, are influenced by the impedance irregularities. The outcome is shown in figure 6.24. This demonstrates that neglecting reflections of the primary travelling waves reduces the amplitude of the place-fixed DP component, and therefore it also reduces the amplitude of the total $2f_2 - f_1$ DPOAE. Figure 6.24 shows that the residual place-fixed component, arising solely from reflections of the DP travelling wave, exhibits relatively slow and small amplitude fluctuations as the emission frequency changes, relative to the behaviour of the total $2f_2 - f_1$ emission. Therefore substantial amplitude fluctuations in the simulated place-fixed component are associated with reflection of the primary travelling waves, not the DP travelling wave. For example, the trough in the amplitude of the place-fixed component which occurs when $2f_2 - f_1$ is approximately 1850 − 1900 Hz is associated with reflection of the primary travelling waves, as it is not present in a model in which these reflections are neglected. For this reason, in cases where the fine structure coincides with amplitude

fluctuations in the place-fixed component, reflection of the primary travelling waves appears to be predominantly responsible for the fine structure. However, at most of the $2f_2 - f_1$ DP frequencies shown in figure 6.24 the fine structure of the total emission does not coincide with amplitude fluctuations in the place-fixed component, and so the predicted fine structure is attributed to interference between the place-fixed and wave-fixed components. In this case, the fine structure is not disrupted when reflection of the primary travelling waves is neglected from the model. Although the amplitude of the predicted total DPOAE reduces in the modified model, the fine-structure retains the same peak-to-trough amplitude. We also observe that the frequencies at which the peaks and troughs in the predicted $2f_2 - f_1$ fine structure occur shift to lower frequencies by 15 to 30 Hz when the reflection of primary travelling waves is removed from the model. This frequency shift is attributed to a change in the phase behaviour of the simulated place-fixed DP response when the reflection of the primary travelling waves is neglected. For example, figure 6.24 shows that if the place-fixed component originates purely from reflection of the DP travelling wave, then the phase lag of this component increases uniformly as the DP frequency increases. However, if the place-fixed component is made up of contributions from mechanisms involving reflections of both the primary travelling waves and the DP travelling wave, then the phase lag of the estimated place-fixed component increases rapidly, but not uniformly, as the DP frequency increases.

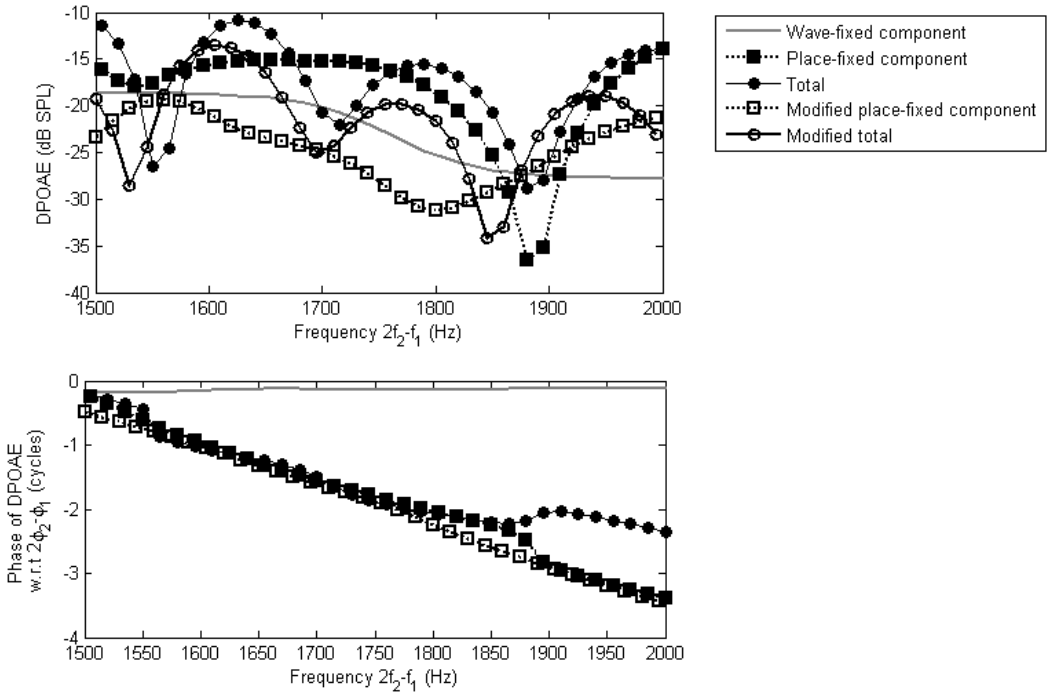

Figure 6.24 The influence of the place-fixed component on the $2f_2 - f_1$ DPOAE fine structure
The plot shows the wave-fixed, place-fixed and total predicted $2f_2 - f_1$ DPOAE evoked by stimulus tones L_1=L_2 = 50 dB SPL and f_2/f_1=1.2. These components were evaluated using a fully perturbed model. In addition, the model was modified so that the impedance irregularities only influenced the DP travelling wave, and this manipulated model was used to estimate the modified total DPOAE and the modified place-fixed component.

Overall, figure 6.24 suggests that when the predicted DPOAE fine structure predominantly arises from interference between the wave-fixed and place-fixed components, then the reflection of DP travelling waves is sufficient for this. Fine structure of this type, originating from interference, can be simulated without significant reflections of the primary travelling waves contributing to the place-fixed component. In contrast, the contribution of primary travelling wave reflection to the place-fixed component of the DPOAE is important in simulating fine structure for stimulus paradigms where the amplitude of the place-fixed component dominates that of the wave-fixed component, and fine structure of the DPOAE coincides with amplitude fluctuations of the place-fixed component.

6.4 Conclusions regarding the predicted $2f_2 - f_1$ DPOAE

This chapter provides a response to the following research questions posed in section 1.9 concerning the $2f_2 - f_1$ upper side band emission:

- What are the strengths and weaknesses of the model regarding $2f_2 - f_1$ DPOAE prediction?
- What explanation does the model provide for the dependence of the $2f_2 - f_1$ DPOAE amplitudes on the stimulus parameters?
- What is the origin of $2f_2 - f_1$ DPOAE fine structure in our model?
- What is the source mechanism for the $2f_2 - f_1$ DPOAE suggested our model? Can these upper sideband emissions be simulated by a cochlear model that does not incorporate fluid compression waves?

The most significant outcomes of this chapter arising from consideration of these research questions are listed below. The main contribution is the discussion of the predicted source mechanism for the $2f_2 - f_1$ DPOAE in sections 6.2 and 6.3, as listed in section 1.9(viii).

- Confirmation that the properties of the $2f_2 - f_1$ DPOAE can be simulated in a model in which DPs propagate out of the cochlea via backward travelling waves. From section 6.1 we conclude that the model makes appropriate predictions for a broad range of $2f_2 - f_1$ emission properties, especially at low stimulus levels, and that it is valid to extend the application of the model to investigate source mechanisms for this emission. Some of the limitations of the model were the same as those observed for the $2f_2 - f_1$ DPOAE described in chapter 4, and can be used to suggest improvements that could be made in future development of the model discussed in chapter 7.
- Plots of the location of the dominant source region for the wave-fixed component of the $2f_2 - f_1$ DPOAE within the model, which suggest that the source is distributed over the region between the DP characteristic place and the f_2 best place for most stimulus paradigms.
- Description of the location of the dominant place-fixed $2f_2 - f_1$ DPOAE component within the model and the different mechanisms by which travelling wave reflection can impact the $2f_2 - f_1$ DPOAE detected in the ear canal.

7. Conclusions and suggestions for future work

This chapter summarises the strengths and weaknesses of the model and the conclusions that can be drawn from the simulations. The most important contributions of the thesis, may be summarised as follows:

(i) Reformulation of the Kanis & de Boer (1993) quasilinear model of the cochlea to ensure computational convergence of the iterative process and verify stability of the model. The solution is also decomposed into forward and backward travelling wave components to facilitate interpretation of the results.

(ii) The fine tuning of the micromechanical parameters in the cochlear model is extended to improve the agreement between experimental responses of the cochlea to single and two tone stimuli and those predicted by the model. The effect of the position of the nonlinearity within the micromechanical feedback loop has also been clarified (How *et al.*, 2010).

(iii) A comprehensive comparison of experimental results and the simulated properties of the $2f_1 - f_2$ and $2f_2 - f_1$ DPOAEs predicted by the baseline and perturbed model. This allows many of the DPOAE characteristics to be explained but also determines which features of these emissions cannot be understood in such a simple model. This review also serves to establish which characteristics of the emissions are most sensitive to flaws in the tuning of the cochlear micromechanical model and could therefore be useful in tuning the parameters further.

(iv) Confirmation of the origin of the optimal stimulus level difference characteristic exhibited by both $2f_1 - f_2$ and $2f_2 - f_1$ using a coupled cochlear model.

(v) The identification and explanation of predicted notches in the wave-fixed component of the $2f_1 - f_2$ DPOAE growth function in the cochlear model.

(vi) Clarification of the limitations of the Allen-Fahey experiment.

(vii) Development of tools for assessing the directionality of wave-fixed DP sources within the cochlear model.

(viii) Suggestions regarding the source mechanism for the $2f_2 - f_1$ DPOAE.

The work also suggests some future research directions, which are outlined in section 7.3.

7.1 Strengths of the model

The strength of this study lies primarily in the simplicity of the model and the breadth of its application. The coupled model, incorporating a nonlinearity and micromechanical impedance perturbations, has been applied to predict a broad range of responses to single- and two- tone stimulation. The results include predicted effects such as self-suppression of the fundamental response and the harmonic responses evoked by single tone stimuli as well as mutual suppression and DPOAEs arising from two tone stimulation.

7.1.1 The properties of the quasilinear model

The model is based on the Kanis & de Boer (1993) simulation of the human cochlea, although the micromechanical parameters have been tuned so that the response better replicates the sharpness of tuning and CA gain exhibited by the mammalian cochlea in response to single tone stimulation across a range of frequencies. We also developed a state space formulation of the model, based on that devised by Elliott *et al.* (2007), which required construction of the state space matrix equations using the system transfer function rather than the equations of motion as these were not explicit for the Kanis & de Boer cochlear model. The application of the state space formulation provided a method of establishing the stability of the model, which is a prerequisite for the quasilinear method to be valid. Kanis & de Boer devised the quasilinear iterative approach for estimating the response of the model in the frequency domain. We found that this approach was very time efficient, especially when we modified the iterative process to improve the reliability of its convergence. The quasilinear responses of the model were compared to state space time domain simulations, and we found no evidence of significant discrepancies between the two approaches. Therefore the considerable time saving offered by the quasilinear approach, over a time domain approach such as the state space time domain method, does not appear to compromise the validity of the estimated response. The further advantage of the frequency domain approach is that it allows the model to be manipulated to gain insight into the mechanisms underlying DP generation. For example, it was possible to apply the impedance irregularities to only the DP travelling wave rather than the DP and the primary travelling waves simultaneously.

Simulations were performed using both the baseline model and a perturbed model, in which random irregularities were imposed on the active impedance of the model. This allowed it to be used for predicting reflection of forward travelling waves within the cochlear model and the place-fixed component of DPOAEs. Such impedance perturbations have been applied in other cochlear models, but these models have either been limited in other ways, such as neglecting the effect of suppression of the primary tones (Talmadge *et al.*, 1998), or they have not yet been applied to the simulation of DPOAEs (Ku, 2008).

In order to investigate the origin of DPs within the cochlear model we also developed some analysis tools, particularly the method for decomposing the travelling wave describing the semi-difference pressure into forward and backward travelling components. The novel aspects of this particular tool include its application to decompose the travelling wave solution, and the identification of cases where the method is not accurate. This decomposition method formed part of a battery of investigatory strategies which were applied to indicate the directionality of a wave-fixed DP source. The other strategies included evaluation of changes in source length as the stimulus parameters varied and the detection of constructive or destructive summation between neighbouring elements within the wave-fixed source distribution.

7.1.2 The predicted responses to single tone stimulation

The micromechanical parameters of the cochlear model were tuned to improve the agreement between the predicted responses to single tone stimulation, and experimental observations from the mammalian cochlea. In addition the parameters of the nonlinear function were selected to achieve appropriate levels of 2^{nd} and 3^{rd} order harmonics, relative to the fundamental component, in response to a single tone stimulus. The amplitude of the first order Boltzmann function was set to increase with distance from the base of the model, so that the saturation threshold of the fundamental response to single tone stimulation occurs at 30 dB SPL for a frequencies between 0.5 and 6 kHz. The resulting active model has a place-frequency map consistent with that of Greenwood (1990) throughout most of its length. The model also exhibits nonlinear growth in the fundamental component of 0.3 − 0.4 dB/dB between stimulus levels of 40 and 70 dB SPL which is in good agreement with the growth rates observed over a similar stimulus range in experimental studies which tend to be in the range of 0.12 − 0.5 dB/dB (Robles & Ruggero, 2001). In addition the predicted amplitude of the CP displacement at the characteristic place (such as 0.1 to 1 nm for a 50 dB SPL stimulus) is within the range of physiological measurements in mammalian cochleae (e.g. 0.05 to 10 nm) for the same stimulus level (Robles & Ruggero, 2001).

7.1.3 The predicted responses to two tone stimulation

The model has been used to simulate a broad range of $2f_1 - f_2$ and $2f_2 - f_1$ DPOAE properties which provides a useful basis on which to judge the validity of the model and any explanations which are drawn from it.

The predicted amplitude of the $2f_1 - f_2$ and $2f_2 - f_1$ DPOAEs agrees well with experimental measures provided that f_2 is below 4 kHz, and the relative amplitude of the two DPs seems to be appropriate across a broader stimulus frequency range. The model also replicates well the growth rate, optimal stimulus level difference, and fine structure of both DPOAEs. In addition, it estimates

appropriate optimal stimulus frequency ratios at low stimulus levels. In view of these successes, the model has provided useful insight into the origin of the optimal stimulus parameters (such as level difference and frequency ratio). It has also improved our understanding of the null result seen by Allen and Fahey in their attempt to use the $2f_1 - f_2$ DPOAE to estimate the gain of the cochlear amplifier. The model also makes some predictions regarding the source mechanism and location for the $2f_2 - f_1$ DPOAE, although these are difficult to verify against experimental evidence.

7.2 Limitations of the model

This section provides a summary of the weaknesses of the model with regard to simulating the cochlear response to single and two tone stimuli. It should be noted that despite all of the limitations listed below, the model predicts a variety of cochlear responses to single and two tone stimulation that show good agreement with experimental measurements. A cochlear model will always be a simplified version of a complex system, and so the model should not be disregarded on the basis of these weaknesses. Rather, the limitations indicate areas in which the model could be improved or developed.

7.2.1 The properties of the quasilinear model

The micromechanical model used was based on that of Kanis & de Boer (1993) and represents an empirical fit to the expected cochlear partition impedance, rather than a direct model of the mechanics of the organ of Corti. This may be the cause of some of the difficulties in tuning the model. In addition to this, our model incorporates the "long-wave" approximation, which assumes that the wavelength of the travelling wave is greater than the height of the model. This approximation is not valid near the peak of the travelling wave envelope, close to the characteristic place of the stimulus frequency, and therefore it may be possible to improve the model by increasing the dimensions. It is also worth noting that our model neglects any structural longitudinal coupling along the cochlear partition, as longitudinal coupling is assumed to occur entirely through the incompressible cochlear fluids. This is a controversial assumption and one that could be addressed in future models. We also assume that DPs propagate out of the cochlea via backward travelling waves and so fluid compression waves are neglected. Although this has been useful for investigating whether the travelling wave mechanism of reverse propagation of DPs out of the cochlea is sufficient for replicating the behaviour of DPOAEs, it may prove to be a significant limitation of the model in view of recent experimental evidence such as the He *et al.* (2008) experiment described in section 5.2.2.

The quasilinear approach, which assumes that the primary responses are unaffected by the presence of distortion in the cochlear model, may not be valid for all stimulus paradigms. For example, Kanis & de Boer (1996) find that the quasilinear estimate of the $2f_1 - f_2$ DP near the base of their cochlear model exceeds the time domain estimate by 10 dB when the stimulus frequency ratio is close to unity (e.g. f_2/f_1=1.04). Therefore more extensive comparison between the quasilinear frequency domain predictions of the model and those of a time domain approach such as the state space method is desirable.

7.2.2 The predicted responses to single tone stimulation

The amplitude of the first order Boltzmann function was set so that the fundamental response to single tone stimulation has a saturation threshold of 30 dB SPL for stimulus frequencies between 0.5 and 6 kHz. It was not possible to extend this to higher frequencies, as this resulted in adverse effects such as the saturation in the basal region of travelling waves evoked by low frequency stimuli. This approach seemed sensible, on the basis that saturation thresholds for TEOAEs and DPOAEs vary by less than 10 dB across a range of stimulus frequencies (section 3.5). However, other approaches may be more appropriate. For example, it would be possible to set the Boltzmann function amplitude such that saturation commences at some defined CP displacement amplitude.

The active micromechanical parameters of the cochlear model were also tuned so that the gain of the CA reduced from 37 dB to 20 dB from the basal to the apical end of the model. However, this gain variation is less than that observed in studies of laboratory animals such as the chinchilla where the gain reduces from 48 dB to 15 dB for high- and low- frequency stimuli respectively. It was not possible to further modify the gain variation in our model without compromising stability of the basal region of the cochlea or underestimating the amplitude of low frequency DPOAEs. In addition the micromechanical parameters were adjusted so that the Q_{10dB} of the cochlear frequency response to low stimulus levels decreased from 11 to 3 between the characteristic places for 10 and 0.3 kHz respectively. This compares well to the physiological data from mammalian cochleae in which the Q_{10dB} values decreases from 8 to 1 between the characteristic places corresponding to 10 and 0.2 kHz. However, there is some evidence from the DPOAE studies that the tuning of the model may be too broad at high stimulus levels and therefore further comparison between the tuning of the model and higher level single tone stimuli could be fruitful.

7.2.3 The predicted responses to two tone stimulation

Although the amplitude of the $2f_1 - f_2$ and $2f_2 - f_1$ DPOAEs are in good agreement with experimental measures when f_2 is below 4 kHz, the amplitudes of both emissions are underestimated by the model at higher stimulus frequencies. It is unclear where this weakness originates within the model, but it is likely to be associated with insufficiencies in the amplitude of the BM response to high frequency stimulation, or some aspect of the nonlinear function in the basal region of the model such as the amplitude which influences the saturation threshold of the BM response.

There are some discrepancies between the DPOAE properties predicted by the model, and those observed in physiological studies, which may indicate that the frequency response of the model at high stimulus levels is too broadly tuned. These discrepancies are evident in the dependence of the

$2f_1 - f_2$ and $2f_2 - f_1$ DPOAEs on stimulus frequency ratio at moderate and high stimulus levels, but this limitation of the model could also be responsible for the fall off in the level of the place-fixed $2f_1 - f_2$ DPOAE place-fixed component at low stimulus frequency ratios, and in the decline in the amplitude of the place-fixed $2f_2 - f_1$ DPOAE component relative to the wave-fixed component at high stimulus levels.

7.3 The assumed micromechanical model

The model used for predicting human DPOAEs in chapters 4, 5 and 6 consists of a first order Boltzmann function positioned before the filter representing the dynamics of the OHC within the micromechanical feedback loop. The input to the nonlinear function is determined by the difference in shear displacement between the tectorial membrane and the organ of Corti. In addition, the micromechanical parameters were selected so that that the gain of cochlear amplifier and sharpness of the BM tuning reduced between the base and the apex of the model. The reasons for these choices are discussed in chapter 3, but in this section we consider whether any of these assumptions could influence the conclusions that have been drawn from the model predictions.

7.3.1 The nonlinear function

The nonlinearity associated with the OHC mechanoelectrical transduction process is thought to be primarily responsible for the nonlinear behaviour of the cochlea (Ashmore, 2008). This nonlinearity is most accurately described by either a 3rd order polynomial function (Chertoff *et al.*., 1996) or a second order Boltzmann function (Bian *et al*.., 2002). However it is common to use a more basic sigmoidal nonlinear function, such as the first order Boltzmann function, when constructing a cochlear model to simulate DPOAE generation in the interest of simplicity (Kanis & de Boer, 1997; Vetesnik et al., 2006; Liu & Neely, 2010). In this section we consider whether the conclusions drawn from the model would have been different if a more physiological nonlinear function, such as a second order Boltzmann function, had been employed instead of the first order Boltzmann function.

Several properties of the model are sensitive to the choice of the nonlinear function: The relative amplitude of different order DPs, the relative amplitude of the two third order DPs, the shape of contour lines showing the dependence of the DP amplitude on the input level for an isolated nonlinear function, the length of the wave-fixed DP source region, the phase distribution of the wave-fixed distortion source, the growth of the DPOAE with stimulus level, and the influence of stimulus level on both the optimal $L_1 - L_2$ difference and the optimal f_2/f_1 ratio. However, few of these sensitivities are thought to impact the conclusions drawn in this thesis. For example, none of our conclusions are based on the value of the relative amplitude of the various DP frequency components. In addition, mutual suppression of the primary responses if not unique to the first order Boltzmann nonlinearity and this suppression is expected to increase with either increasing stimulus level, or decreasing f_2/f_1 ratio, no matter which nonlinear function used in the micromechanical feedback. In association with this, although the estimated length of the wave-fixed DP source region is likely to depend on the choice of the nonlinear function, this length should *increase* with decreasing f_2/f_1 irrespective of the form of the nonlinearity. For these reasons

the conclusions regarding the origin of the optimal $L_1 - L_2$ difference, optimal f_2/f_1 ratio and the limitations of the Allen & Fahey experiment are not thought to be dependent on the choice of the nonlinear function.

It is worth noting that as the form of the nonlinearity influences the dependence of DPOAE amplitude on stimulus level, the shape of the contour lines shown in figures 4.3, 4.11 and 6.11 are contingent upon the choice of the nonlinear function. Despite the fact that these plots were simulated using a first order Boltzmann function, the predictions of the coupled model are in reasonably good agreement with experimental measures (figure 4.3) and therefore unlikely to have been substantially adversely affected by the choice of the nonlinear function. However, the dependence of the contour plots on the form of the nonlinearity does suggest that the notches observed in the wave-fixed DP growth function may be dependent on the form of the nonlinearity. For this reason the simulated notches should not be used to infer the exact depth of notch that could be observed from a human ear, or the specific stimulus paradigm at which it may be observed.

Finally, it has already been suggested that the tendency of the model to overestimate the dependence of the optimal f_2/f_1 ratio on stimulus level may be associated with the use of the first order Boltzmann function (sections 4.1.7 and 6.1.7). This weakness indicates that the model may saturate too rapidly as the stimulus level increases and implies that the model may be improved by use of an alternative nonlinear function.

Sections 4.1.7 and 6.1.7 demonstrate that the cochlear model makes appropriate predictions for many properties of human DPOAEs, which illustrates the usefulness of the first order Boltzmann function in the model despite its simplicity. Overall there is no evidence to suggest that the conclusions of the thesis can not be extended qualitatively to cochlear models incorporating a physiological nonlinearity, such as a second order Boltzmann function, in the micromechanical feedback loop or to the human cochlea itself.

7.3.2 Other aspects of the micromechanical feedback loop

In the model, nonlinear function was positioned before the filter representing the dynamics of the OHC within the micromechanical feedback loop and the input to the nonlinear function was determined by the difference in shear displacement between the tectorial membrane and the organ of Corti. These choices were made for a variety of reasons including anatomical considerations and physiological OHCs measurements (section 3.5.1). It is unlikely that the chosen position of the nonlinear function within the micromechanical feedback loop should have a considerable impact on the conclusions drawn from the model. This because, although the position of the nonlinear function within the micromechanical feedback loop can have a substantial influence on the amplitude of harmonic distortion within the cochlear model, this has essentially been compensated

for in the selection of the nonlinear function parameters (table 3.1). Similarly the use of the shear displacement between the tectorial membrane and organ of Corti to determine the input to the nonlinear function is not thought to significantly influence the conclusions. The predicted amplitude of the both the $2f_1 - f_2$ and $2f_2 - f_1$ DPs are not sensitive to the vertical or shear nature of this input (section 3.3) and an alternative input would be difficult to justify anatomically.

7.3.3 The tuning of the micromechanical parameters

The micromechanical parameters used in the model are based on those proposed by Kanis & de Boer (1993) which allow the model to replicate several aspects of the response of the human cochlea to single tone stimulation (section 3.4). These parameters were modified so that the response of the model was more consistent with physiological measurements across a broader range of stimulus frequencies (section 3.4.2). The model is profoundly influenced by the tuning of the micromechanical parameters, which could affect all aspects of the predicted response from the place-frequency map of the fully active model, to the sourcing and propagation of the DPs. For this reason, sections 7.2 and 7.4 discuss some changes to the micromechanical parameters which could be used in future development of the model. However, we do not expect the conclusions of the thesis to be dependent on the choice of micromechanical parameters so long as they have been selected to appropriately simulate the response of the human cochlea to single- and two- tone stimulation at a variety of intensity levels and frequencies.

7.4 Suggestions for future work

The strengths and weaknesses observed in the model, and the resulting predictions regarding the properties of DPOAEs, suggest some directions for future work which are discussed in this section.

7.4.1 Development of the model

The micromechanical parameters of any cochlear model are subject to review in the light of discrepancies that arise between simulated and experimental data. Therefore it may be possible to adjust the parameters further to address some of the observed limitations. For example, the sharpness of tuning of the BM response, and the parameters of the nonlinear function, were selected for the model to ensure that the simulated response to single tone stimulation produces responses that were consistent with invasive measures from within animal cochleae. However, in future it may be more appropriate to choose micromechanical parameters for a cochlear model which attempt to compromise between optimising accuracy of both single tone and two tone simulations. We would recommend that the predicted behaviour of the optimum f_2/f_1 ratio for the $2f_1 - f_2$ DP be used when determining the micromechanical parameters for a cochlear model on the basis of the response to two stimulus tones, as these simulations are very sensitive to both the sharpness of tuning the BM response and the rate at which the nonlinear function becomes saturated with increasing stimulus level.

We have used a local coupled cochlear model, in which the velocity of the BM is determined only by the local pressure difference across it, however there could be benefits in using an alternative 'feedforward' model in which forward travelling waves are amplified and backward travelling waves attenuated (de Boer *et al.*, 2008). A feedforward mechanism is suggested by the oblique orientation of OHCs in the organ of Corti (Geisler & Sang, 1995), and has been used in cochlear modelling by de Boer & Nuttal (2008) to simulate the DP phase behaviour observed by He *et al.* (2008) which cannot be replicated by a local cochlear model. However, a side-effect of the feedforward mechanism is that backward travelling waves can be strongly attenuated and this can compromise both the predicted amplitude of the DPOAEs and the influence of coherent reflection within the cochlear model (de Boer & Nuttal, 2008; de Boer *et al.*, 2008). For this reason, considerable work would be required to investigate the usefulness of cochlear models which incorporate a feedforward mechanism.

Our model is based on that of Kanis & de Boer (1993), which was derived from the earlier model of Neely & Kim (1986). The earlier model was linear, but was amongst the first to incorporate a locally active region on the basal side of the travelling wave peak. Models of this type represent an empirical fit to the expected cochlear partition impedance rather than directly epitomizing the

mechanics of the organ of Corti. Our model has inherited some of the limitations of this original model in addition to its many attributes. For example, a common criticism of the Neely & Kim model is that the OHCs have nothing to react off. For example, Fukazawa (1997) comments that in a model of this type the force of the OHCs should not able to change the movement of the cochlear partition, because the force is an 'internal' one. Another limitation raised by Ku (2008) is that models of the Neely & Kim variety achieve the desired half octave shift in the characteristic frequency between the passive and active response through a change in the micromechanical tuning by altering the stiffness, but that this shift is more likely to occur as a direct consequence of the amplification. In addition, the model reduces the complex behaviour of the OHCs to that of a simplistic micromechanical feedback loop consisting of two linear filters and a single nonlinear function. This is unlikely to do sufficient justice to the many processes associated with these cells such as hair bundle motility (Martin & Hudspeth, 1999; Jia & He, 2005), resonance differences between the tectorial membrane (TM) and stereocilia (Kanis & de Boer, 1993), frequency-dependent phase shifts between the OHC pressure output and the radial displacement of the BM and TM (Neely & Kim, 1986) as well as processes within the OHC (Santos-Sacchi, 1989). In addition, there are multiple nonlinearities within the physiological OHC feedback loop, as both the mechanoelectrical and electromechanical transduction processes exhibit nonlinear behaviour (Dallos, 1985; Kros *et al.*, 1992; Kakehata & Santos-Sacchi, 1996), which are reduced to a single nonlinear function in the model. In order to address these limitations and criticisms in future cochlear modelling work, it may be necessary to take a more direct approach to modelling the mechanics of the organ of Corti rather than developing an empirical fit to the expected impedance of cochlear partition.

7.4.2 Simulations

So far, the application of the model has been limited to the simulation of experiments in which only two stimulus tones are presented to the ear canal of the model. However, interest has been growing in the use of DPOAE suppression techniques to estimate cochlear amplifier gain (e.g. Neely *et al.*, 2003b) or to investigate the source of the $2f_2 - f_1$ DPOAE (e.g. Martin *et al.*, 1998). It would be useful to modify the MATLAB code in order to simulate these three tone experiments to determine which experimental methods may be the most fruitful. However, it would be particularly important to validate any predictions made by the quasilinear process under these circumstances as the amplitude of the third tone may be comparable to the primary or DP amplitude so that the quasilinear approximation may not be appropriate.

In addition, if the application of the model were extended to accommodate a third stimulus tone, it would be possible to investigate the experimental observation that $2f_1 - f_2$ DPOAEs can be

suppressed or enhanced by third stimulus tone which has a frequency higher than f_2 (Lonsbury-Martin & Martin, 2008) .

7.4.3 Experiments

The model predicts notches in the growth function of the $2f_1 - f_2$ DPOAE wave-fixed component at moderate stimulus levels. In the model, these notches originate from a change in the phase relationship between neighbouring elements of the wave-fixed source distribution which result in an alteration of source directionality as the stimulus level increases. However, it has not been possible to verify this result by comparison with experimental data as DPOAE component separation is usually performed with a time windowing techniques across a range of f_2 frequencies in physiological studies. Unfortunately the stimulus level and amplitude of the notch predicted by the model is highly sensitive to stimulus frequency, possibly because it is related to the relative phase of the primary travelling waves, and so wave-fixed growth functions that have been obtained using time-windowing techniques and averaged across many f_2 frequencies cannot be expected to exhibit the notch. It may prove interesting to measure the $2f_1 - f_2$ DPOAE growth function in human subjects using an alternative component separation technique, such as a suppressor tone to reduce the place-fixed component. The presence of notches in the $2f_1 - f_2$ DPOAE wave-fixed component could have implications for the application of DPOAE growth functions which are occasionally proposed as a tool for estimating psychoacoustic hearing threshold level or loudness growth.

7.4.4 Longer term uses of the model

If some of the limitations of the current model can be resolved, it may be possible to use the model to design novel stimulus paradigms that, for example, generate specific excitation patterns on the cochlea. Novel methods may thus be computationally developed for achieving the long-term goal of using OAEs to accurately measure the frequency variation of cochlear amplifier gain or even hearing loss. One of the significant advantages to using OAEs to investigate the properties of the cochlea, instead of direct measurements of BM velocity for example, is that they are non-invasive and the physiological health of the cochlear is not compromised. The work of this thesis has demonstrated the complexity of the interactions that generate DPOAEs, such as those between the distributed nonlinearity and the propagation of the various wave components. In many cases simple explanations of specific effects, which take into account one part of this complex interaction but not another, are not adequate to explain the experimental results. It has been shown that a model can be used to tease apart some of these interactions. Continued development of models that can be used to test various theories of cochlear function is thus an important goal.

Appendices

A. Derivation of the one-dimensional wave equation

In this section the approximations, boundary conditions and equations of motion for the cochlear model are described, so that the one-dimensional wave equation can be derived.

A.1 Approximations of the two-dimensional box model

The simple three dimensional 'box' model of the cochlea, illustrated in Figure A.1, incorporates the following approximations:

(i) The cochlear walls are immobile (Shera & Zweig, 1992)

(ii) The effect of "fluid ducts" can be neglected (Shera & Zweig, 1992; Voss *et al.*, 1996)

(iii) The spiral shape of the cochlea is straightened out. This may introduce some errors in the apical region of the model (Viergever, 1978; Cai *et al.*, 2005), where the cochlea curvature is greatest, but this is neglected as there is limited physiological data available for the apical region

(iv) Reissner's membrane is neglected as it is acoustically transparent (Dallos, 1992; Gelfand, 1998)

(v) The two cochlear channels have equal cross-sectional area and shape (de Boer, 1996)

(vi) The cross-sectional area of the channels in the human cochlea actually differs in the region very close to the base, as shown in Figure A.2, but this is neglected for simplicity

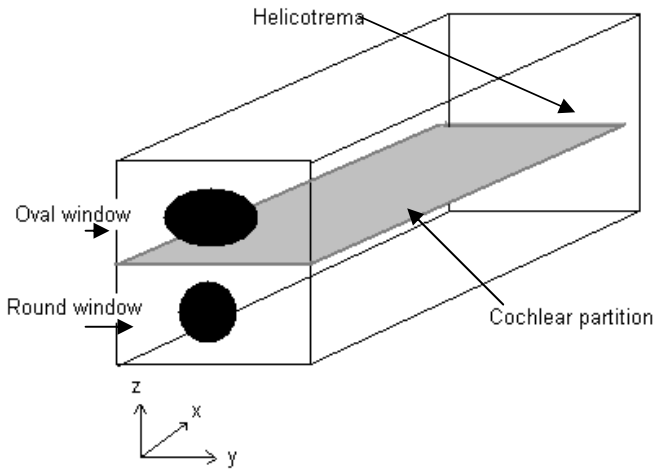

Figure A.1 A three-dimensional 'box' model of the cochlea

(vii) The effective height of the channels (the ratio of the cross-sectional area to the width of the channel) is assumed to be constant, neglecting any variation with distance from the base

Figure A.2 shows that the height of the lower channel is about 1mm throughout most of the cochlea (Rebscher *et al.*, 1996)

(viii) The cochlear fluids have negligible viscosity, so that only the cochlear partition (CP) motion dissipates energy (de Boer, 1996). Cochlear input impedance is not significantly affected by the introduction of the fluid viscosity for frequencies > 500 Hz (Koshigo *et al.*, 1983; Puria & Allen, 1991)

(ix) The cochlear fluids and CP are incompressible (de Boer, 1996)

(x) There is no structural longitudinal coupling along the CP, and elements along the CP interact through fluid coupling only (de Boer, 1996). This is a controversial assumption based on the work of Voldrich (1978) who observed that, in guinea pig cochleae, displacement of the BM did not spread along the membrane in the longitudinal direction (Naidu & Mountain, 2001). Other studies have observed significant longitudinal coupling which acts to increase the stiffness of the cochlear partition and broadens the peak of the travelling wave envelope in the region of the characteristic place in cochlear models (von Békésy, 1960; Naidu & Mountain, 2001). However, the space constant for the longitudinal coupling of the cochlear partition has a measured value between 20 and 44μm (Naidu & Mountain, 2001; Emadi *et al.*, 2004), which is small compared to the width of the individual micromechanical elements in our model (approximately 70μm, corresponding to about 10 outer hair cells). Therefore coupling is neglected and the micromechanical elements are assumed to interact only through the fluid

In order to reduce a the three-dimensional box model into a two-dimensional model, any radial motion (across the width of the CP) is neglected and parameters of the CP (such as mass) are averaged across its width (de Boer, 1996).

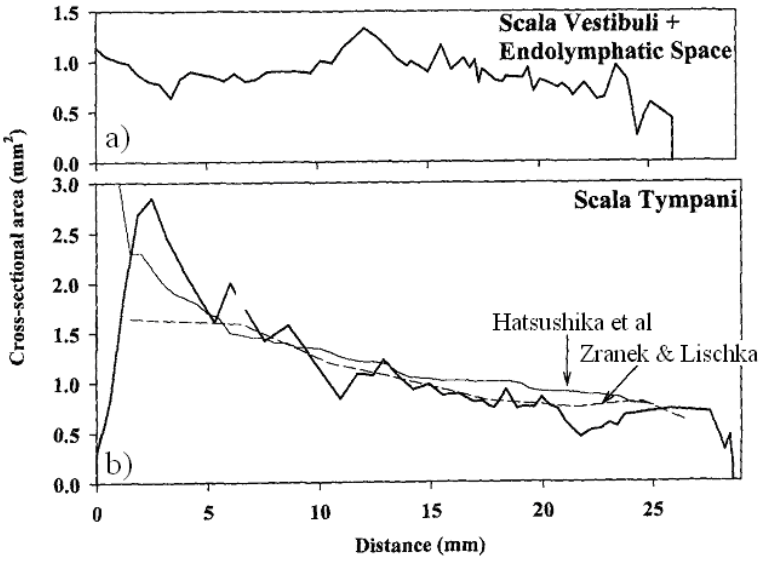

Figure A.2 The cross sectional area of the (a) upper and (b) lower channels of the human cochlea
The areas were estimated from MRI imagines [From Thorne *et al.* (1999) figure 6, with permission from John Wiley & Sons]

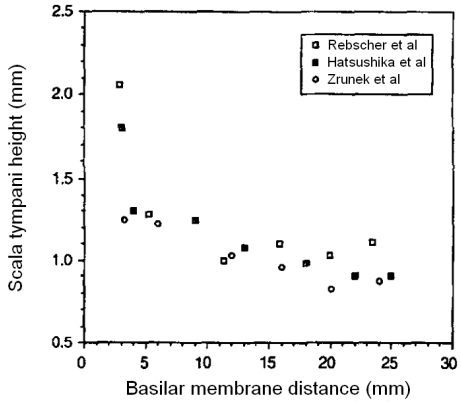

Figure A.3 The height of the human scala tympani
The measurements are collated from three different studies [From figure 4 of Rebscher *et al.* (1996), with permission from Inform Healthcare]

A.2 The variables

In the two-dimensional box model of the cochlea, shown in figure 2.1, the fluid velocities in the $x-$ and $z-$ directions are denoted by $u_f(x,z,t)$ and $v_f(x,z,t)$ respectively. The vertical velocity of the cochlear partition (CP) is given by $v(x,t)$ and the fluid pressure, $p_f(x,z,t)$, is also shown.

The fluid pressure within the cochlear channels can be represented as a superposition of two different states, which differ in the relative forces applied to the cochlear windows in each case.

(i) **The symmetric mode**: Identical forces are applied to both the oval and round windows, so that a symmetrical fast compression wave travels along both the upper and the lower channel simultaneously (Lineton, 2001). As this mode does not result in any pressure difference across the CP, it does not induce a travelling wave (Patuzzi, 1996).

(ii) **The asymmetric mode**: Equal and opposite forces are applied to the oval and round windows (Lineton, 2001). This asymmetry exerts a pressure difference across the CP and induces a travelling wave.

As it is only the second state that induces a travelling wave, only the pressure difference across the CP is important for deriving the wave equation. As a consequence of this, the notation can be simplified by defining the semi-difference pressure, $p_{d,}$ as shown below.

$$p_d(x,z,t) = \tfrac{1}{2}\left(p_f(x,z,t) - p_f(x,-z,t)\right) \tag{A.1}$$

In the asymmetrical state, the forces applied to the cochlear windows are equal and opposite. Therefore the expression for p_d becomes

$$p_d(x,z,t) = p_f(x,z,t) \tag{A.2}$$

A.3 The long-wave approximation

The "long-wave" approximation states that the wavelength of the travelling wave, λ_{TW}, is much greater than the height of the cochlear channel, so that $H/\lambda_{TW} < 2\pi$ (de Boer, 1996). Using this approximation, the fluid velocity can be related to the CP velocity as shown in (A.3). This effectively reduces the two-dimensional model into a one- dimensional model as the variable $\partial v_f / \partial z$, used in the wave equation derivation (appendix A.5) is dependent on only one spatial co-ordinate, x.

$$v_f(x,z,t) = \left(1 - \tfrac{z}{H}\right)v(x,t) \tag{A.3}$$

The travelling wave slows down, and its wavelength decreases, as it approaches its characteristic place (Nobili *et al.*, 1998), so the long-wave approximation is not expected to be valid in the immediate vicinity of the peak of the travelling wave envelope. It is worth noting that the finite difference method, used to numerically evaluate the wave equation solution for a discrete cochlear model (section 2.1.2), is also limited in this region as the wavelength of the travelling wave may become shorter than the width of a discrete element (0.07 mm). However despite these limitations, the responses of the one-dimensional model successfully replicate the responses of more complex models which do not assume the long-wave approximation, provided that observations are made at

a location where the approximation is valid (Shera *et al.*, 2004). Therefore we proceed with the one-dimensional model for simplicity.

A.4 Model boundary conditions

The boundary conditions of the cochlear model are listed below:

- The velocity across the area of the stapes footplate is assumed to be uniform
- The stapes footplate velocity is equal, and opposite, to the round window velocity
- Only vertical fluid flow is permitted through the Helicotrema
- The semi-difference pressure at the Helicotrema is zero

$$p_d(L,t) = 0 \tag{A.4}$$

- Continuity at the CP requires that $v_f(x,0,t) = v(x,t)$
- Continuity at the ceiling of the cochlear channel requires that $u_f(x,H,t)=0$
- Conservation of momentum at the stapes requires that

$$\left.\frac{\partial p_d(x,t)}{\partial x}\right|_{x=0} = -\rho \frac{\partial u_{st}(t)}{\partial t} \tag{A.5}$$

A.5 The wave equation

The principles of conservation of mass (A.6) and momentum (A.7) are used to derive the wave equation, as described by de Boer (1996).

$$\frac{\partial u_f(x,z,t)}{\partial x} + \frac{\partial v_f(x,z,t)}{\partial z} = 0 \Rightarrow \frac{\partial u_f(x,t)}{\partial x} = \frac{v(x,t)}{H} \tag{A.6}$$

$$\frac{\partial p_d(x,z,t)}{\partial x} = -\rho \frac{\partial u_f(x,z,t)}{\partial t} \tag{A.7}$$

Differentiating (A.6) with respect to t and (A.7) with respect to x, allows these two equations to be combined such that

$$\frac{\partial^2 p_d(x,t)}{\partial x^2} = -\frac{\rho}{H}\frac{\partial v(x,t)}{\partial t} \tag{A.8}$$

For a linear model, this can be re-written in the frequency domain by substituting $\partial v/\partial t = i\omega v$ for harmonic oscillations with angular frequency ω.

$$\frac{\partial^2 p_d(x,\omega)}{\partial x^2} = -\frac{i\omega\rho}{H} v(x,\omega) \tag{A.9}$$

An impedance for the CP, $Z_{CP}(x,\omega)$, can also be defined for a linear model to relate the CP velocity to the semi-difference pressure as shown below

$$Z_{CP}(x,\omega) \equiv \frac{-2p_d(x,\omega)}{v(x,\omega)} \tag{A.10}$$

Substituting (A.10), into (A.9), produces the following one-dimensional wave equation for a linear cochlear model in the frequency domain. The physical interpretation of $k(x,\omega)$, based on the WKB solution to the wave equation (section 2.1.2), is that Re(k) corresponds to the wavenumber of the travelling wave whilst Im(k) describes the exponential growth rate of the travelling wave amplitude. On this basis c_{TW} can be interpreted as the travelling wave velocity.

$$\frac{\partial^2 p_d(x,\omega)}{dx^2} + k^2(x,\omega)\cdot p_d(x,\omega) = 0 \tag{A.11}$$

where

$$k^2(x,\omega) = -\frac{2i\omega\rho}{H\cdot Z_{CP}(x,\omega)} = \frac{\omega^2}{c_{TW}^2} \tag{A.12}$$

and

$$c_{TW}^2 = \frac{i\omega H Z_{CP}}{2\rho} \tag{A.13}$$

Provided there is no internal pressure source, equation (A.11) applies everywhere in the cochlea apart from the basal and apical boundaries. For harmonic oscillation these boundary conditions become…

At the stapes:

$$\left.\frac{\partial p_d(x,\omega)}{\partial x}\right|_{x=0} = -i\rho\omega u_{st} \tag{A.14}$$

At the Helicotrema:

$$p_d(L,\omega) = 0 \tag{A.15}$$

A.6 The source term

If there is a distributed pressure source $S(x,\omega)$ acting on the cochlear partition then, in a linear model, the vertical velocity of the cochlear partition has two components: One arising from the semi-difference pressure caused by the stapes vibration (v_0), and another that results directly from the distributed pressure source (v_s). They combine such that

$$v(x,\omega) = v_0(x,\omega) + v_s(x,\omega) \tag{A.16}$$

where

$$v_0(x,\omega) = \frac{-2p_d}{Z_{CP}(x,\omega)} \text{ and } v_s(x,\omega) = \frac{S(x,\omega)}{Z_{CP}(x,\omega)}$$

Substitution of (A.16) into (A.9) gives the wave equation in the presence of a distributed pressure source …

$$\frac{\partial^2 p_d(x,\omega)}{dx^2} + k^2(x,\omega)\cdot p_d(x,\omega) = -\frac{1}{2}\cdot k^2(x,\omega)\cdot S(x,\omega) \tag{A.17}$$

B Solution methods

B.1 The finite difference method

This technique, devised by Neely (1981), discretizes the cochlear model in order to solve the linear wave equation (A.11) numerically. This is achieved by converting the differential equations (A.11), (A.14) and (A.15) into a single matrix equation which can be solved by computer software such as MATLAB.

To apply the finite difference method, the length of the cochlea is divided into N-1 elements, so that N points compose the cochlea in the *x*-direction. The first point is the oval window (or stapes footplate), and the final point is the Helicotrema. The length of a single element, Δ, is given by Δ=L/(N-1). The matrix equation is formed by using Taylor series expansion to replace the $\partial^2 p_d / \partial x^2$ term by its finite difference approximation in (A.11), so that equation of motion for the q^{th} element becomes…

$$\frac{1}{\Delta^2}\{p_d(q+1)-2p_d(q)+p_d(q-1)\}+k^2(q,\omega)\cdot p_d(q,\omega)=0 \tag{B.1}$$

The boundary conditions can also be re-written for first and last elements as shown in (B.2) and (B.3). In (B.2) the stapes velocity, u_{st}, is written as a linear combination of two components (Elliott *et al.*, 2007): The velocity arising from external excitation (u_{st}^{in}) such as the pressure stimulus in the ear canal, and the component resulting from the internal pressure response of the cochlea at the base (u_{st}^{out}).

$$\frac{1}{\Delta}\{p_d(2)-p_d(1)\}=-i\omega\rho\cdot u_{st}=-i\omega\rho\cdot\left(u_{st}^{in}+u_{st}^{out}\right) \tag{B.2}$$

$$p_d(N)=0 \tag{B.3}$$

By considering the pressure at the stapes also as a linear combination of the two components arising from the external excitation (p_{st}^{in}) and the internal pressure response of the cochlea at the base (p_{st}^{out}), the specific acoustic impedance of the stapes, Z_{st}, can be defined as shown in (B.4) (Lineton, 2001). Assuming the round window impedance is very small so that $p_{st}^{out}=-2p_d(1)$, the finite difference basal boundary condition can be re-written as shown in (B.5).

$$Z_{st}(\omega)\equiv-\frac{p_{st}}{u_{st}} \tag{B.4}$$

$$\frac{1}{\Delta}\{p_d(2)-p_d(1)\}-\frac{2i\omega\rho}{Z_{st}}p_d(1)=-i\omega\rho u_{st}^{in} \tag{B.5}$$

Equations (B.1), (B.3), and (B.5) can be combined to give the following matrix equation, where C and M denote the fluid coupling and mobility matrices respectively. In this expression the specific acoustic admittances are defined as $Y_{st}= 1/Z_{st}$ and $Y_{CP}=1/Z_{CP}$.

(B.6)

$$\left[\underbrace{\frac{1}{\Delta^2}\begin{pmatrix}-\Delta & \Delta & 0 & 0 & 0 & 0\\ 1 & -2 & 1 & 0 & 0 & 0\\ 0 & \dots & \dots & \dots & 0 & 0\\ 0 & 0 & \dots & \dots & \dots & 0\\ 0 & 0 & 0 & 1 & -2 & 1\\ 0 & 0 & 0 & 0 & 0 & \Delta^2\end{pmatrix}}_{=C}-\underbrace{\frac{i2\omega\rho}{H}\begin{pmatrix}H\cdot Y_{st} & 0 & 0 & 0 & 0 & 0\\ 0 & Y_{CP}(2) & 0 & 0 & 0 & 0\\ 0 & 0 & \dots & 0 & 0 & 0\\ 0 & 0 & 0 & \dots & 0 & 0\\ 0 & 0 & 0 & 0 & Y_{CP}(N-1) & 0\\ 0 & 0 & 0 & 0 & 0 & 0\end{pmatrix}}_{=M}\right]\begin{pmatrix}p_d(1)\\ \dots\\ \dots\\ \dots\\ \dots\\ p_d(N)\end{pmatrix}=\begin{pmatrix}-i\omega\rho u_{st}^{in}\\ 0\\ 0\\ 0\\ 0\\ 0\end{pmatrix}$$

The finite difference method is expected to produce an erroneous solution to the wave equation if an insufficient number of elements is used to represent the length of the cochlea (N). For example, Kanis & de Boer (1993) comment that discretization errors become apparent in their model when the number of elements falls below 15 per mm. This would equate to a minimum N of 525 in a full length cochlear model. Figure B.1 and Figure B.2 illustrate that N > 500 is required to minimise discretization errors in our implementation of the linear active Kanis & de Boer cochlear model. Since the minimum wavelength of the model is about 0.5 mm, this corresponds to approximately 7 elements when N = 500.

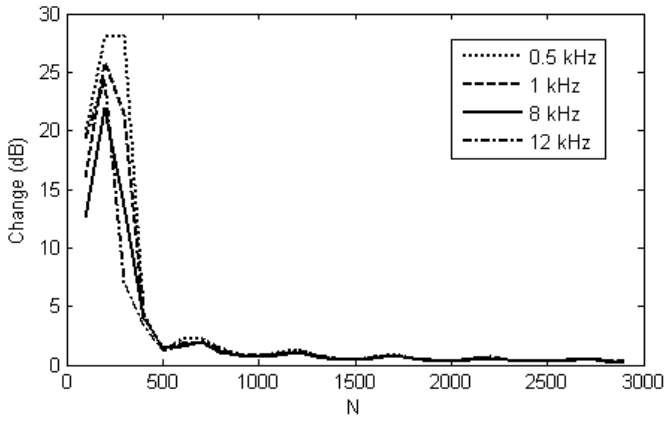

Figure B.1 The influence of the number of elements (N) used in the finite difference method
The plot shows the maximum change in amplitude of the $p_d(x,\omega)$ distribution predicted by the finite difference method using N elements compared to N+100 elements

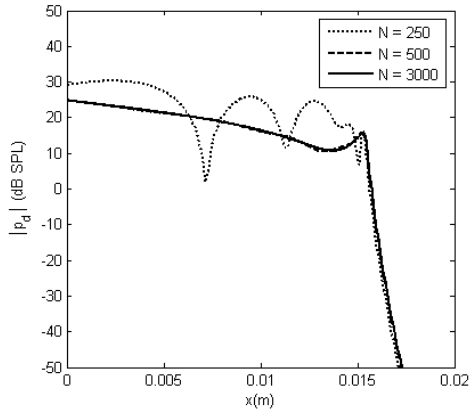

Figure B.2 The influence of N of the predicted semi-difference pressure distribution
The plot shows the magnitude of the semi-difference pressure evoked by a 2 kHz stimulus in the linear active Kanis & de Boer (1993) cochlear model for a variety of N values, where N indicates the number of elements used to represent the length of the cochlear partition

B.2 The Wentzel, Kramers and Brillouin (WKB) method

The WKB method is a mathematical technique for obtaining an approximate solution to linear second order differential equations, of the form shown in (B.7), which arise in many fields of physics (Quantum mechanics, diffusion theory etc). It is described by many authors (e.g. Bellman, 1972; Bender & Orszag, 1999), but the summary presented here is based on the synopsis of Matthews & Walker (1970).

$$\frac{d^2y(x)}{dx^2} + F(x)y(x) = 0 \tag{B.7}$$

In this section the WKB solution is derived and the validity of applying the WKB technique to cochlear models is discussed, with respect to the one-dimensional cochlear model.

B.2.1 Derivation of the WKB solution

The WKB method provides an approximate solution to (B.7), where y(x) is a system variable, x is a spatial coordinate and $F(x)$ is a variable which is positive for $x \geq 0$ and must have the dimensions of (length)$^{-1}$ (Bellman, 1972). The estimated solution is derived by considering a trial solution of the form shown in (B.8), which is suggested by the result that would be expected if $F(x)$ was constant.

$$y = \exp\{i\phi(x)\} \tag{B.8}$$

For this trial solution, the differential equation becomes

$$-(\phi'(x))^2 + i\phi''(x) + F(x) = 0 \tag{B.9}$$

where the apostrophe indicates differentiation with respect to *x*.

Assuming that $\phi''(x)$ is small, (B.9) can be approximated by

$$\phi'(x) \approx \pm\sqrt{F(x)} \tag{B.10}$$

Therefore, to a first approximation, the trial solution is given by

$$y(x) \approx \exp\{i\phi(x)\} \text{ where } \phi(x) \approx \pm\int_0^x \sqrt{F(\tilde{x})}\, d\tilde{x} \tag{B.11}$$

Iteration can be used to determine a second approximation as (B.11) indicates that

$$\phi''(x) \approx \frac{1}{2\sqrt{F}} F'(x) \tag{B.12}$$

and substituting (B.12) into (B.9), gives

$$(\phi'(x))^2 \approx F(x) \pm \frac{i}{2} \frac{F'(x)}{\sqrt{F(x)}} \tag{B.13}$$

so that

$$y(x) \approx \frac{1}{F^{1/4}} \left\{ c^+ e^{i\int_0^x \sqrt{F(\tilde{x})}d\tilde{x}} + c^- e^{-i\int_0^x \sqrt{F(\tilde{x})}d\tilde{x}} \right\} \tag{B.14}$$

where c^+ and c- are constants.

Considering (B.9) and (B.12), the earlier assumption that $\phi''(x)$ is "small" can be expressed as

$$\left|\phi''(x)\right| \approx \frac{1}{2}\left|\frac{F'(x)}{\sqrt{F(x)}}\right| << \left|F(x)\right| \tag{B.15}$$

Equation (B.11) indicates that $1/\sqrt{F}$ is approximately 2π "wavelengths" or one "exponential length" of the trial solution. Therefore the approximation that $\phi''(x)$ is small is valid if $F(x)$ is either constant or slowly varying, such that the change in $F(x)$ over one wavelength is small compared to $|F|$.

In summary the solution to a second order differential equation, such as (B.7), can be approximated by the sum of two independent solutions, or 'basis' functions, which can be added together with arbitrary constants to form the general solution. The basis functions for (B.7) are given in (B.16).

$$\begin{aligned} \varphi^+(x) &= \frac{\varphi_0^+}{F^{1/4}(x)} \exp\left(-i\int_0^x \sqrt{F(\tilde{x})}d\tilde{x}\right) \\ \varphi^-(x) &= \frac{\varphi_0^-}{F^{1/4}(x)} \exp\left(+i\int_0^x \sqrt{F(\tilde{x})}d\tilde{x}\right) \end{aligned} \tag{B.16}$$

These basis functions can be used to form the general solution (B.17), where $\varphi_0^{\pm}$ are constants chosen to normalise the basis functions as shown in (B.18).

$$y(x) \approx c^{+}\varphi^{+}(x) + c^{-}\varphi^{-}(x) \tag{B.17}$$

$$\int_0^{\infty} \left|\varphi^{+}(x)\right|^2 dx = 1 \text{ and } \int_0^{\infty} \left|\varphi^{-}(x)\right|^2 dx = 1 \tag{B.18}$$

The WKB solution, (B.17), will not be valid if $F(x)$ changes too rapidly such that (B.15) is not valid. In addition, if $F(x)$ passes through zero at some location (e.g. x_0), then care must be taken to ensure that the approximate solutions either side of x_0 are consistent[3].

B.2.2 Physical interpretation of the WKB solution for cochlear models

For a cochlear model, the WKB solution to the wave equation (A.11) can be written as shown in (B.19), where $p_0^{\pm}$ are constants, with normalised basis functions (B.20). It should be noted that a common convention in cochlear applications of the WKB solution is for the basis functions to be normalised using (B.21) (Talmadge *et al.*, 1998).

$$p_d(x) = p_0^{+}\sqrt{\frac{k_0}{k(x)}}\exp\left(-i\int_0^x k(\tilde{x})d\tilde{x}\right) + p_0^{-}\sqrt{\frac{k_0}{k(x)}}\exp\left(+i\int_0^x k(\tilde{x})d\tilde{x}\right) \tag{B.19}$$

$$\varphi^{+}(x) = \frac{\varphi_0^{+}}{\sqrt{k(x)}}\exp\left(-i\int_0^x k(\tilde{x})d\tilde{x}\right) \text{ and } \varphi^{-}(x) = \frac{\varphi_0^{-}}{\sqrt{k(x)}}\exp\left(+i\int_0^x k(\tilde{x})d\tilde{x}\right) \tag{B.20}$$

$$\begin{aligned} &\left|\frac{\varphi_0^{\pm}}{\sqrt{k(x)}}\exp\left(\mp i\int_0^x k(\tilde{x})d\tilde{x}\right)\right|_{x=0} = 1 \\ &\Rightarrow \varphi_0^{+} = \varphi_0^{-} = \sqrt{k(x=0)} \equiv \sqrt{k_0} \end{aligned} \tag{B.21}$$

To determine the physical interpretation of the basis functions, a model incorporating a uniform CP impedance is considered. In this scenario $k(x)$ would be a complex constant with real and imaginary parts η_k and χ_k respectively (B.22), and so the basis functions could be re-written in the form of (B.23).

$$k = \eta_k + i\chi_k \tag{B.22}$$

$$\varphi^{+}(x) \propto e^{\chi_k x}e^{-i\eta_k x} \text{ and } \varphi^{-}(x) \propto e^{-\chi_k x}\,\mathrm{e}^{+i\eta_k x} \tag{B.23}$$

[3] This is because $F(x)$ was defined as greater than zero for x>0 in the derivation, and so a change in sign of $F(x)$ can be problematic

There are two components to the basis functions shown in (B.23): One part which oscillates along the $x-$ axis, with a spatial wavelength of $2\pi/\eta_k$, and another component which varies in amplitude along the $x-$ axis with an exponential growth rate of $1/\chi_k$. Therefore the basis functions correspond to travelling waves with wavenumber η_k. As η_k is positive the basis functions, φ^+ and φ^-, correspond to forward and backward travelling waves respectively.

In a realistic cochlear model, $k(x)$ is a complex function of x. As this complex function can still be broken down into real and imaginary components, then the basis functions continue to be interpreted as forward and backward travelling waves. In this case the wavenumber is given by the real part of $k(x)$, and varies with x.

Shera *et al.* (2004) note that there is long-standing controversy in cochlear mechanics regarding whether the forward and backward travelling waves discussed above actually occur in the cochlea. For example, it may be possible to find alternative basis functions to form a solution to the cochlear wave equation (2.1). In addition other approaches avoid the wave equation completely, such as that of Nobili *et al.* (2003) who interpret the response of the cochlea as a weighted sum of motions of individual BM oscillators which interact with each other via the incompressible cochlear fluid. Shera *et al.* (2004) argue that these different interpretations represent alternative conceptual frameworks for the same underlying physics and that the travelling wave concept is no less physically appropriate than other interpretations whilst being easier to visualise. For this reason we continue to represent the physics of the cochlear model with a wave equation, the solutions to which are interpreted as travelling waves.

B.2.3 The validity of the WKB method

The WKB is an approximation method and equation (B.19) is actually a truncation of an exponential power series which forms the full WKB approximate solution to the cochlear wave equation. Bender & Orszag (1999) explain that the full WKB approximate solution can be written as

$$p_d(x) \approx \exp\left[\sum_{m=0}^{\infty} S_m(x)\right] \tag{B.24}$$

The first three terms in the series are given by

$$S_0(x) = \pm\int_0^x k(\tilde{x})d\tilde{x}$$

$$S_1(x) = -\frac{1}{2}\ln k(x) \qquad \text{(B.25)}$$

$$S_2 = \int_0^x \left\{ \frac{1}{8k^3(\tilde{x})}\frac{d^2}{d\tilde{x}^2}\left(k^2(\tilde{x})\right) - \frac{5}{32k^5(\tilde{x})}\left(\frac{d}{d\tilde{x}}k^2(\tilde{x})\right)^2 \right\} d\tilde{x}$$

It can be seen that equation (B.19) corresponds to sum of the first two terms in the WKB series. In order for this series to provide an asymptotic solution for $p_d(x)$, the magnitude of the successive terms must decrease. Applying this condition to the first two terms in the series, $S_1(x) << S_0(x)$, produces an expression equivalent to that given in (B.15). In addition, Bender & Orszag (1999) note that it is only appropriate to truncate the full WKB series approximation after $S_1(x)$ if

$$\left|S_2(x)\right| << 1 \qquad \text{(B.26)}$$

In this section we assess the validity of the WKB method in two ways. First the conditions for the use of the WKB approximation, equations (B.15) and (B.26), are evaluated. Then we compare the estimated WKB solution with that obtained using the finite difference technique.

The WKB condition

The condition of the WKB approximation (B.15), can be re-written for a cochlear model as shown below (de Boer, 1996). This condition is equivalent to stating that there is no significant reflection of travelling waves in the cochlear model.

$$\left|\frac{1}{k^2}\frac{dk(x)}{dx}\right| << 1 \qquad \text{(B.27)}$$

Figure B.3a shows examples of the magnitude of this WKB condition parameter, for two different micromechanical cochlear models. This illustrates that for a single stimulus tone, the WKB solution is likely to be least accurate near the base, and in the vicinity of the characteristic place. At the base, both the real and imaginary parts of $k(x)$ are small and so the term $1/k^2$ in (B.27) becomes large, as illustrated in Figure B.4a, and causes the condition to be violated. In contrast, at the characteristic place it is the dk/dx term which becomes large (Figure B.4b) and threatens the validity of (B.27). In addition, the WKB condition can be violated for low frequency stimuli (<500 Hz) at basal locations within the cochlear model, as illustrated in Figure B.3b. Despite this violation, the WKB results appear to be perfectly reasonable in this region, as illustrated in Figure B.6.

(a) Spatial distributions of the WKB condition for a 2kHz stimulus

(b) Frequency distributions of the WKB condition at two different locations along the cochlear partition

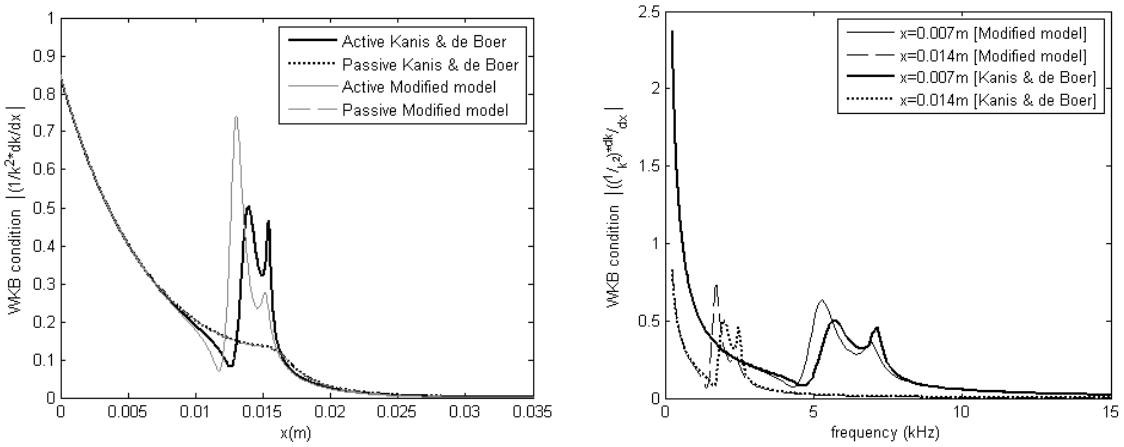

Figure B.3 The WKB approximation condition given in equation (B.27)
The plots show the amplitude of the WKB approximation condition for (a) a 2kHz stimulus and (b) a range of stimulus frequencies observed at two different locations along the cochlear partition. The results are shown for two different linear micromechanical models: The Kanis & de Boer (1993) model and a modified model described in section 3.5. In (a) the results for both passive and active variants of the models are shown, but in (b) the passive distributions are neglected for simplicity.

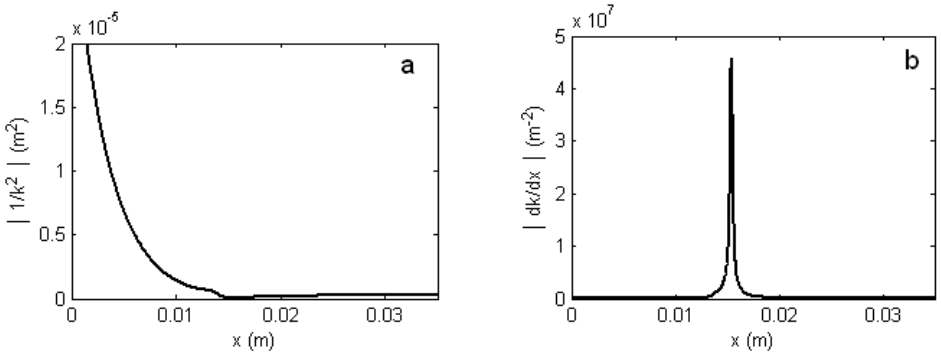

Figure B.4 The distributions of (a) $\left|1/k^2\right|$ and (b) $\left|dk/dx\right|$,
These distributions are plotted for a 2 kHz stimulus tone in the original Kanis & de Boer linear active cochlear model with N=1000.

The other condition which should be satisfied in order for the WKB approximation to be truncated after the first two terms, (B.26), is satisfied within the linear active cochlear model. This is demonstrated by Figure B.5, which shows the spatial distribution of $\left|S_2(x)\right|$, for a 2 kHz stimulus. It also illustrates that variation in $\left|S_2(x)\right|$ for a variety of stimulus frequencies at two different locations within the cochlear model. The results suggest that $\left|S_2(x)\right|$ is consistently less than 1 throughout the cochlear model, and so it is appropriate to truncate the approximate WKB solution after the first two terms of the series.

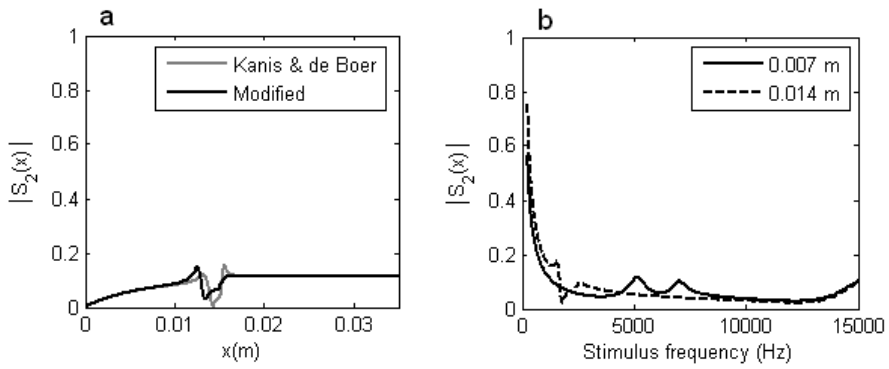

Figure B.5 The WKB approximation condition (B.26)
The WKB approximation is evaluated for (a) a 2kHz stimulus and (b) a range of stimulus frequencies observed at two different locations along the cochlear partition. The results in (a) are shown for two different linear micromechanical models: The Kanis & de Boer (1993) model and a modified model described in section 3.5. In (b) the results for only the Kanis & de Boer model are shown for simplicity.

Overall, the nature of the inequalities in the WKB conditions is such that there is no objectively defined level at which the term on the left hand side of (B.26) or (B.27) become "*much* less" than 1. However, as the left hand side remains less than 1 for a broad range of stimulus frequencies (0.25 to 15 kHz) throughout most of the cochlear model, we conclude that the WKB solution can be used reliably provided that it is verified against another approach, such as the finite difference method.

Comparison the finite difference solution

The validity of the WKB solution can also be investigated by comparing predictions with those of the finite difference method. However, both approaches are subject to discretization errors when the WKB solution is evaluated numerically. To minimise these errors, the two solutions are compared using a high value of N (N=3000), as shown in Figure B.6.

For stimulus frequencies >1 kHz, the two solutions differ by less than 1.3 dB. Below this frequency, the difference increases to around 2 dB. The discretization errors, shown in Figure B.1, could account for up to 0.5 dB of this difference, leaving a small error which may be associated with the WKB approximation. However, as this residual error is of the same order as the discretization error, it is not thought to be significant. This result is consistent with the extensive validation of the application of the WKB solution to cochlear models in the literature. For example, Zweig *et al.* (1976) and Steele & Taber (1979) confirm that the WKB solution agrees with accurate numerical solutions for one- and two-dimensional cochlear models respectively. De Boer & Viergever (1982) also confirm that there is "generally" good agreement between the WKB and 'exact' solutions for two- and three-dimensional cochlear models, even in cases where the condition of absent reflections is violated.

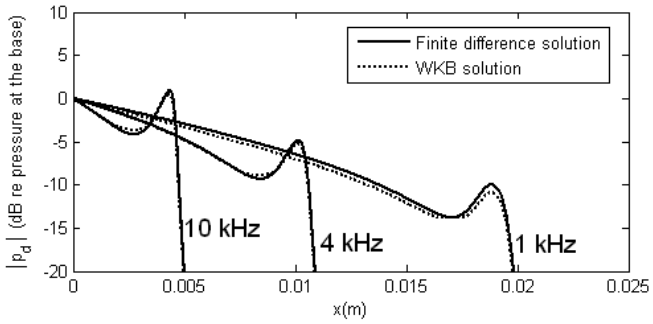

Figure B.6 Comparison of the finite difference and WKB approximation estimated results
The plot shows the response of the modified cochlear model estimated using the discrete method (solid lines) and WKB approximation (dotted lines) for sinusoidal stapes stimulation at a various frequencies. Details of the model can be found in section 3.5.

B.2.4 Internal sources

It is important to consider the application of the WKB method to linear models containing internal sources or sites of reflection, as this is important when studying the cochlear origins of otoacoustic emissions and the generation of distortion in the cochlea. The approach described in this section is based on the explanation given by Talmadge *et al.* (1998).

When an internal source distribution $S(x,\omega)$ is present, the cochlear wave equation can be written as shown in (A.17). The source distribution is complex, with dimensions of pressure. The solution can be estimated by a linear sum of the two basis functions given in (B.20). However, the coefficients of the basis functions, p_0^+ and p_0^-, are no longer constants. Instead they become function of x over the source region. Therefore the WKB solution for a cochlear model with an internal source distribution is of the form given in (B.28). In these expressions k_0 is the wavenumber at the base of the cochlear model, and is introduced to normalise the basis functions (see appendix B.2.2). The coefficients $p_0^+(x)$ and $p_0^-(x)$ should only vary with x in regions where there are sources, and are, in principle, constant elsewhere.

$$p_d(x) = \frac{\sqrt{k_0}}{\sqrt{k(x)}}\left\{p_0^+(x)\cdot\exp\left(-i\int_0^x k(x')dx'\right) + p_0^-(x)\cdot\exp\left(+i\int_0^x k(x')dx'\right)\right\} \qquad \text{(B.28)}$$

The WKB solution can also be applied to a model containing impedance perturbations, as well as internal sources. On the face of it, a model containing impedance irregularities is likely to violate the WKB condition requiring no significant reflections (B.27). However, provided that the distribution of impedance perturbations is known, then these irregularities can be viewed as distribution of internal sources in a "smooth" cochlear model so that the WKB approximation remains valid (Talmadge *et al.*, 1998). For example the complex wavenumber for the model containing the impedance perturbations, $k(x)$ can be written as a sum of the wavenumber for the

"smooth" model and a perturbation parameter $\delta k(x)$ which characterises the effect of the impedance irregularities, as shown below.

$$k^2(x) = k_{smooth}^2(x) + \delta k^2(x) \tag{B.29}$$

This allows the wave equation to be arranged such that the impedance perturbations appear as a source term, as demonstrated in (B.30).

$$\frac{\partial^2 p(x)}{\partial x^2} + k_{smooth}^2(x)\,p(x) = \underbrace{-\delta k(x)\,p(x)}_{\text{Source term}} \tag{B.30}$$

C The middle ear and ear canal

In this section the basal boundary condition of the cochlear model, and the transmission of sound through the middle ear are considered.

C.1 The ear canal and middle ear

The ear canal and middle ear influence the transmission of sound in and out of the cochlea. Therefore, in order to predict DPOAEs, recorded in the ear canal, a model of these two components is needed. The model used is essentially a replica of that described by Ku (2008), which is based on the middle ear model of Kringlebotn (1988). It involves a sequence of two-port networks: one representing the ear canal and the second corresponding to the middle ear. Details of these models are given by Ku (2008). In summary, illustrations of these two port networks are shown in

Figure C.1. The ear canal is modelled as tube, of diameter 0.007m and 3.85×10^{-5} m^2 cross-sectional area, in which sound propagates as plane waves. A foam earplug, with damping R_{plug}, can also be incorporated into the ear canal model. The middle ear representation is formed by a collection of mass-spring-damper models corresponding to the atrium and mastoid cells, the tympanic cavity, the eardrum, the eardrum suspension, the eardrum rim, the malleus and the incus, the coupling between the ossicles, the stapes, the stapedial tendon and the oval window. The impedances used to constructed the matrix elements of the middle ear two-port network are formed from these constituent mass-spring-damper models and some additional transformer ratios which arise from the difference in the cross-sectional area between the eardrum and stapes footplate and the difference in lengths of the malleus and the incus. All of the parameters are listed in Table C.1.

(a)

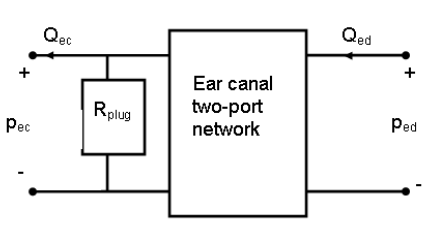

$$\begin{bmatrix} p_{ec} \\ Q_{ec} \end{bmatrix} = \begin{bmatrix} 1 & 0 \\ 1/R_{plug} & 1 \end{bmatrix} \begin{bmatrix} T_{eced11} & T_{eced12} \\ T_{eced21} & T_{eced22} \end{bmatrix} \begin{bmatrix} p_{ed} \\ Q_{ed} \end{bmatrix}$$

(b)

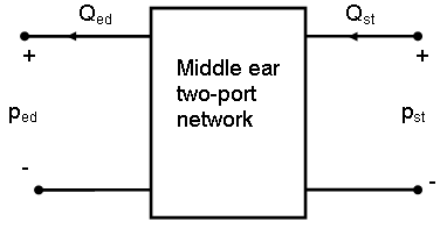

$$\begin{bmatrix} p_{ed} \\ Q_{ed} \end{bmatrix} = \begin{bmatrix} T_{edst11} & T_{edst12} \\ T_{edst21} & T_{edst22} \end{bmatrix} \begin{bmatrix} p_{st} \\ Q_{st} \end{bmatrix}$$

Figure C.1 Two-port models of (a) the ear canal and (b) the middle ear
In this plots, p and Q denote the pressure and volume velocity respectively. The parameters associated with the earcanal, eardrum and stapes are labelled *ec*, *ed*, and *st* respectively. R_{plug} represents the damping effect introduced by a foam plug into the ear canal. [From Ku (2008), figure A5]. In (a) the matrix elements T_{eced} are formed by considering a tubular model of ear canal, in which sound propagates as plane waves. In (b) the matrix elements T_{edst} are determine from an array of mass-spring-damper models representing the different mechanisms in the middle ear, and the transformer ratios arising from area and lever arm ratios.

The transfer function for the ear canal and middle ear model is shown in Figure C.2. It should be noted that the inertial mass of the stapes and the resistance of the coupling between the malleus and the incus have both been reduced by a factor of 10, compared to the values used by Ku (2008), in order to better match the measured values for the backward transfer function.

Mechanical quantity being modelled	Inertia (Ns^2/m^5)	Compliance (m^5/N)	Resistance (Ns/m^5)
Antrum and mastoid cells	1×10^{2}	3.9×10^{-11}	6×10^{6}
Tympanic cavity	0	4×10^{-12}	0
Eardrum	7.5×10^{2}	0	0
Suspension of the eardrum	6.6×10^{3}	3×10^{-12}	2×10^{6}
Rim of the eardrum	0	1.3×10^{-11}	1.2×10^{7}
Coupling between the malleus and the incus	0	3.8×10^{-12}	1.2×10^{6}
Ossicles (the malleus and incus)	2.2×10^{3}	∞	2×10^{7}
Coupling between the incus and the stapes	0	5.6×10^{-12}	6×10^{8}
Stapes, stapedius tendon and oval window	4.6×10^{2}	5.6×10^{-12}	0

Table C.1 The parameters of the middle ear
These impedance, compliance and resistance terms used to form the multiple mass-spring-damper models which collective constitute the middle ear model. [Adapted from Table A.4, Ku, 2008).

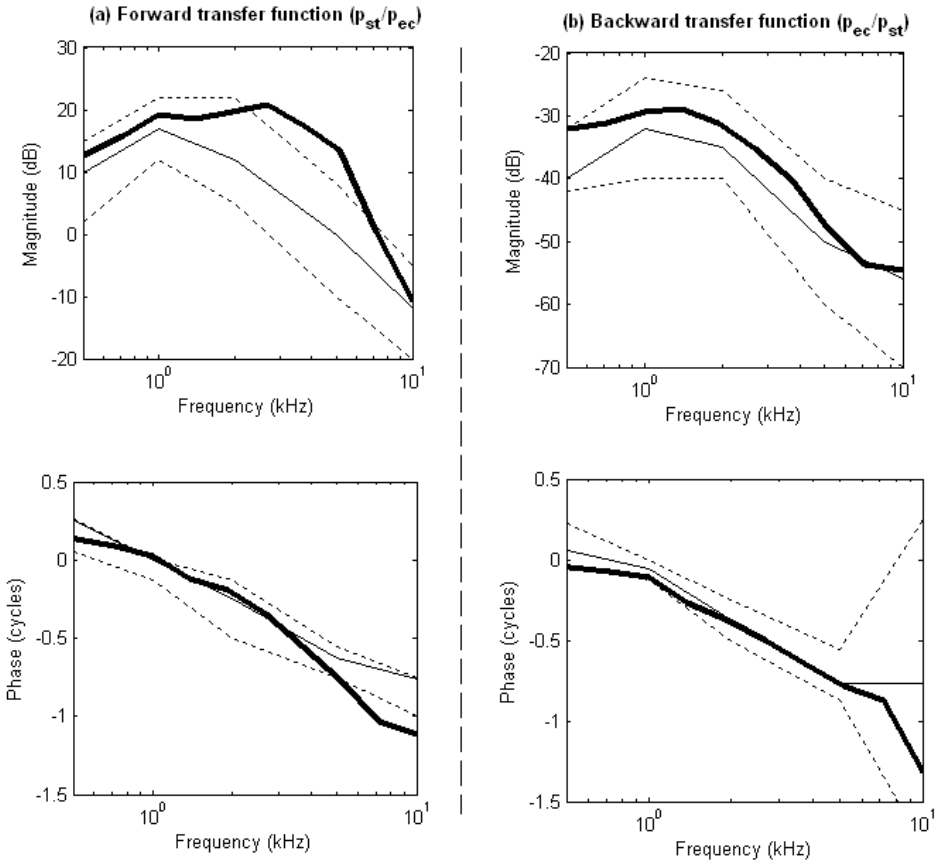

Figure C.2 Comparison of the middle ear and ear canal model with experimental measures
The (a) forward and (b) backward transfer functions for the ear canal and middle ear models (thick black line) ar shown along with the experimental measurements from human cadavers [Puria, 2003). Thin black lines show the average (solid line) and min/max values (dotted lines) for the experimental data. The transfer functions are defined as ratios of the pressure at the stapes (p_{st}) and ear canal pressure (p_{ec}) are shown above.

C.2 The basal boundary condition

In order to implement the basal boundary condition of the cochlear model, it is necessary to form an expression for the specific acoustic impedance of the stapes, Z_{st}, defined in (B.4). This impedance is equivalent to the 'reverse middle ear impedance' used by Ku (2008) in his formulation of the state space cochlear model. As it was not possible to formulate the state space basal boundary condition from the two-port network discussed above, Ku used a simple mass-spring-damper model to represent the stapes impedance Z_{st}. In order to allow comparison between the predictions of the quasilinear and state space models, we also choose to use a mass-spring-damper model to characterise the stapes impedance. Although this mass-spring-damper model of the stapes is generally used throughout this thesis, an alternative expression is occasionally used to minimise reflections at the basal boundary. This "reflectionless" condition is not intended to be realistic, but is used to limit the number of sources of backward travelling waves in the model (Kanis & de Boer, 1994; de Boer *et al.*, 2008) and to aid the interpretation of distortion product generation in some circumstances. The implementation of the mass-spring-damper and "reflectionless" stapes models are described below.

(i) A mass-spring-damper model

In general, a simple mass-spring-damper model is used to represent the stapes impedance (Neely & Kim, 1986), so that Z_{st} takes the form shown below, where $m_{st} = 1.4$ kgm^{-2} , $c_{st} = 32000$ kgm^{-2}s^{-2} and $s_{st} = 2.6\times10^{8}$ kgm^{-2}s^{-1}. These values are based on those measured in human cadavers by Puria (2003), and assuming a stapes surface area of 3.2 mm^2 (Ku, 2008).

$$Z_{st}(\omega) = im_{st}\omega + c_{st} + \frac{s_{st}}{i\omega} \tag{C.1}$$

This expression for the impedance of the stapes results in a reflection of backward travelling waves generated within the cochlear model, as shown in Figure C.3

(ii) An expression to minimise reflections

To minimise reflections at the base of the cochlear model, the stapes impedance is set equal to the impedance encountered by a backward travelling wave as it approaches the base (Lineton, 2001). Using the WKB approximation, the semi-difference pressure of a backward travelling wave, can be written as shown below (see appendix B.2 for further details). The dependence on ω has been neglected for simplicity.

$$p_d^-(x) = \frac{p_0^-}{\sqrt{k(x)}} \exp\left(+i\int k(x')dx'\right) \tag{C.2}$$

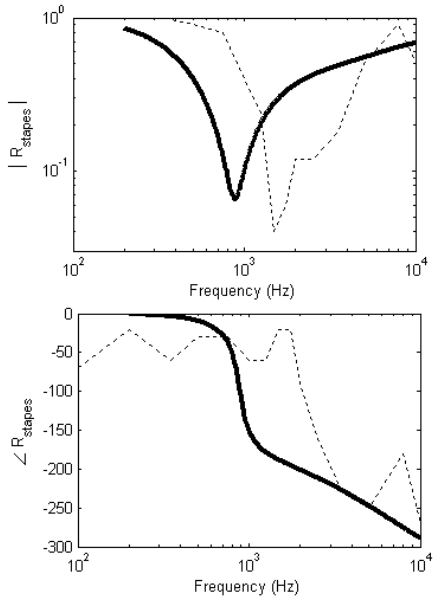

Figure C.3 The reflection coefficient for backward travelling waves at the stapes
The reflection coefficient (R_{stapes}) for travelling waves propagating towards the stapes, at the basal boundary was evaluated using $R_{stapes} = \dfrac{2Z^-_{x=0} - Z_{st}}{2Z^-_{x=0} + Z_{st}}$, where Z_{st} is the stapes impedance defined in equation (C.1), and $Z^-_{x=0}$ is the characteristic impedance for backward travelling waves such that

$$Z^-_{x=0} \equiv -\frac{p^-_d(x=0)}{u^-_f(x=0)}$$

The reflection coefficient for the cochlear model (thick line) and that calculated by Puria (2000) from measurements of human ears (thin dotted line) are both shown

An expression for the longitudinal fluid velocity towards the base, $u^-_f(x)$, can be obtained from (C.2) using conversation of momentum (A.7), so that

$$\begin{aligned} u^-_f(x) &= \frac{i}{\rho\omega}\frac{dp^-_d(x)}{dx} \\ &= -\frac{ip^-_d(x)}{\rho\omega}\cdot\left\{\frac{1}{2k(x)}\cdot\frac{dk(x)}{dx} + ik(x)\right\} \end{aligned} \qquad \text{(C.3)}$$

The impedance for the backward travelling wave is then given by

$$Z^-(x) \equiv -\frac{p^-_d(x)}{u^-_f(x)} = i\rho\omega\left(\frac{1}{2k(x)}\frac{dk(x)}{dx} + ik(x)\right)^{-1} \qquad \text{(C.4)}$$

So for a reflectionless boundary condition, $Z_{st} = 2Z^-(x=0)$ where $Z^-(x)$ is given in (C.4). It should be noted that (C.4) can also be rearranged as shown below (Viergever & de Boer, 1987). If the WKB condition (B.27) were to strictly hold and k was real and equal to ω/c_{TW}, where c_{TW} is the travelling wave velocity, then the expression for the impedance of the backward travelling wave reduces to the characteristic impedance $Z^-(x) = \rho c_{TW}(x)$ (Kinsler & Frey, 1962).

$$Z^-(x) = \frac{\rho\omega}{k(x)}\left(1 - \frac{i}{2k^2(x)}\frac{dk^2(x)}{dx^2}\right)^{-1} \qquad \text{(C.5)}$$

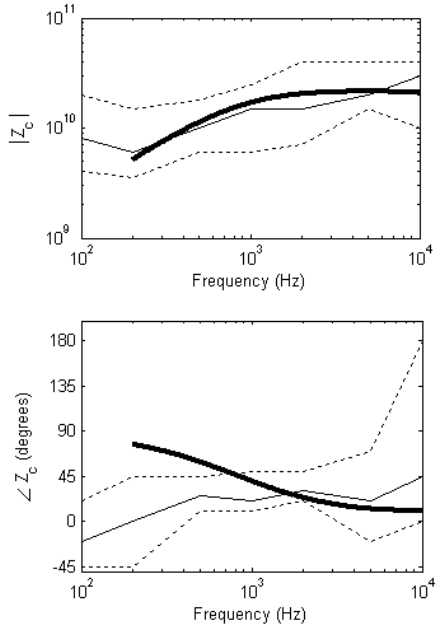

Figure C.4 The cochlear input impedance
The plots show the cochlear input impedance Z_c for the model (thick line), evaluated using the impedance for a forward travelling wave at the base of the model

$$Z_c = Z^+(x=0) \equiv \left.\frac{p_d^+(x)}{u_f^+(x)}\right|_{x=0}$$

$$= \left.\frac{\rho\omega}{k(x)}\left(1+\frac{i}{2k^2(x)}\frac{dk^2(x)}{dx^2}\right)^{-1}\right|_{x=0}$$

The human cochlear input impedance measurements of Puria (2000) are also shown. Thin black lines show the average (solid line) and min/max values (dotted lines) for the experimental data.

In general, the mass-spring-damper representation of the stapes is used throughout this thesis. However, on specified occasions the impedance of the stapes is set to minimise reflections at the basal boundary to aid interpretation.

It should be noted that the input impedance of the cochlear model can be deduced using similar expressions to those shown above. This input impedance for the model is shown in Figure C.4, and experimental results are also shown for comparison.

C.3 Impact of the middle ear on predicted otoacoustic emissions

Puria (2003) studied the effect of the middle ear on otoacoustic emissions, using measurements obtained from the temporal bones of 5 human cadaver temporal bones. His results are summarised in Figure C.5a, which shows the dependence on stimulus frequency of the middle ear "round-trip" pressure gain, $2f_1 - f_2$ DPOAE amplitude and CEOAE amplitude. The band pass nature of the middle ear pressure gain was calculated by Puria from the previous results shown in Figure C.2, and demonstrates that the middle ear round-trip gain falls off as the stimulus frequency increases above 1 kHz. Figure C.5 demonstrates that the CEOAE amplitude also falls off with increasing stimulus frequency above 1 kHz, suggesting that this could be associated with the reduction in the middle ear transfer function. However, the DPOAE amplitude is not substantially influenced by the stimulus frequency, compared to the behaviour of the middle ear gain or CEOAE amplitude. There are several factors that could have influenced this result, such as the comparison between DPOAEs from young living ears with the middle ear gain of older cadaver ears and the difference in frequency between the input and output for DPOAEs. However Puria (2003) comments that there is little evidence to suggest that aging or death significantly affects the behaviour of the middle ear

response at any frequencies other than 4 − 5 kHz. In addition, there is reportedly little change in the round-trip middle ear gain if the frequency difference between the input and output signal for DPOAEs is taken into account. Therefore, the origin of the difference between the frequency dependence of the middle ear round-trip gain and the level of the DPOAE measurement remains unclear.

Figure C.5b shows the round-trip pressure gain for the middle ear model and the level of the $2f_1 - f_2$ DPOAE predicted by the model. In contrast to the experimental observation of Puria (2003), the model predicts that the DPOAE amplitude will fall off with increasing frequency above 1 kHz, in a manner similar to the fall off exhibited by the middle ear round-trip gain. Figure C.5b also shows the $2f_1 - f_2$ component of the BM velocity at the base of the model, which demonstrates a relatively constant amplitude as the distortion product frequency increases. Overall the predicted frequency dependence of the $2f_1 - f_2$ DPOAE amplitude differs from that observed experimentally. This difference could arise from errors either in the middle ear model, or in the nonlinear properties of the micromechanical model near the base. As Figure C.3, Figure C.4 and

Figure **C.1** indicate that the responses of the middle ear model are a good replication of experimental measures, and any further reasonable attempts to improve the middle ear model (such as adjusting the reflection of backward travelling waves at the stapes) has no significant effect on the levels of the high frequency DPOAEs. For this reason we conclude that the nonlinear properties of the micromechanical model near the base are responsible for the discrepancy.

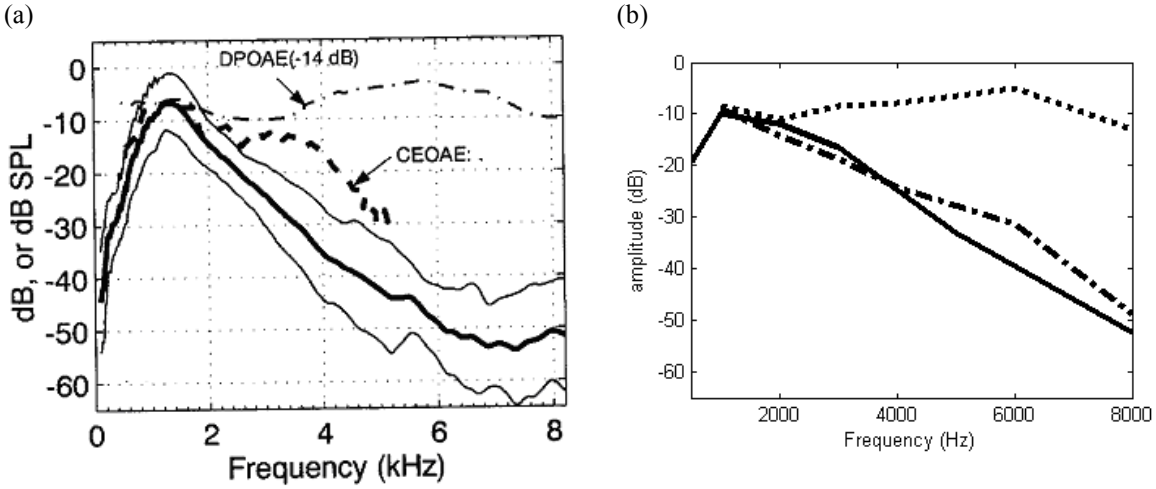

Figure C.5 The round-trip middle ear pressure gain and OAE amplitudes
(a) The "round-trip" pressure gain of the human middle ear measured by Puria (2003). The thick line indicates the average measurement from the 5 subjects, and the thin lines denote the range of measured values. The dash-dot and dashed lines show the levels of DPOAEs and CEOAEs recorded from healthy human subjects by Smurzynski and Kim (1992). The level of the DPOAE measures has been reduced by 14 dB for display purposes. [From Puria (2003), figure 5, with permission from ASA]. (b) The middle ear round-trip pressure gain for the model (solid line), the predicted $2f_1 - f_2$ DPOAE amplitude (dash-dot line), and the $2f_1 - f_2$ components of the BM velocity at the base of the model (dotted line). The units of the DPOAE and BM distortion product are dB SPL − 25dB and dB re 1μm/s + 40 dB respectively.

D Testing for reflections

We have assumed that the baseline cochlear model, in no irregularities have been deliberately introduced into the impedance distribution, contains no significant sources of reflection. As this influences our interpretation of the wave decomposition results in section 2.3.2, and our interpretation of the DP wave-fixed source mechanism in section 5.1 and 6.2, this assumption should be checked.

In a cochlear model with uniform CP impedance, travelling waves initiated at the stapes would not be reflected along the CP. However in a cochlear model, the CP impedance is a function of position from the base, and therefore it is feasible that reflections may occur. The amplitude of these reflections is expected to depend on the rate and magnitude of the impedance changes. In addition, it is conceivable that the changes in impedance between adjacent elements in a discrete cochlear model may be sufficient to generate significant reflections. In this section a battery of tests, rather than a single test, is applied to determine the significance of reflections in the baseline cochlear model. This approach is taken because each of the tests has limitations and is subjective to some degree.

D.1 Reflections in a linear active cochlear model

In this section, the discrete linear active Kanis & de Boer cochlear model is tested to determine if it contains significant sources of reflection. Unfortunately it is not possible to cite the accuracy of the WKB solution in a discrete cochlear model as evidence of a lack of reflections, as the WKB result can be accurate even if the condition for no reflections is violated (de Boer & Viergever, 1984). Instead, the following evidence is presented to demonstrate that no substantial reflections occur in the model.

(i) The WKB approximation condition is satisfied

In appendix B.2.3, the validity of the WKB approximation, (B.22), is investigated. The conclusion is that the approximation is appropriate for a broad range of stimulus frequencies. As the WKB approximation is equivalent to the condition for absent reflections, this suggests that there should be no substantial reflections in the linear Kanis & de Boer cochlear model. However, further evidence is needed to demonstrate an absence of significant reflections in the model due to the ambiguous nature of the inequality in the WKB condition discussed in appendix B.2.3.

(ii) The wavenumber spectrum of the model response is one-sided

In a homogenous system the inverse Fourier transform of the BM velocity, $V(k)$, has a narrow peak around k_0 where k_0 is the constant real wavenumber of the travelling wave. De Boer & Viergever (1984) explain that as inhomogeneity is introduced and increases, the distribution of *V(k)* widens, eventually to the extent that it crosses the k=0 axis indicating that reflections are present. When analysing the inverse Fourier transform, it is appropriate to neglect wavenumbers for which $|V(k)|$ is more than 50dB below the peak $|V(k)|$ value, as these low magnitude components are comparable with the artefacts introduced by spatial windowing as a finite sample of length L is used. Figure D.1 shows the magnitude of $|V(k)|$ obtained by numerically taking the Fourier transform of the BM velocity, $v(x)$, predicted by the linear active Kanis & de Boer cochlear model in response to a stimulus presented at the stapes. This demonstrates that the magnitude of $|V(k)|$ for negative k is negligible compared to its amplitude for positive k values. The figure also illustrates that if a step decrease in the active impedance of 5% is introduced at the characteristic place, then reflections do occur as the amplitude of the $|V(k)|$ components corresponding to negative k values increases.

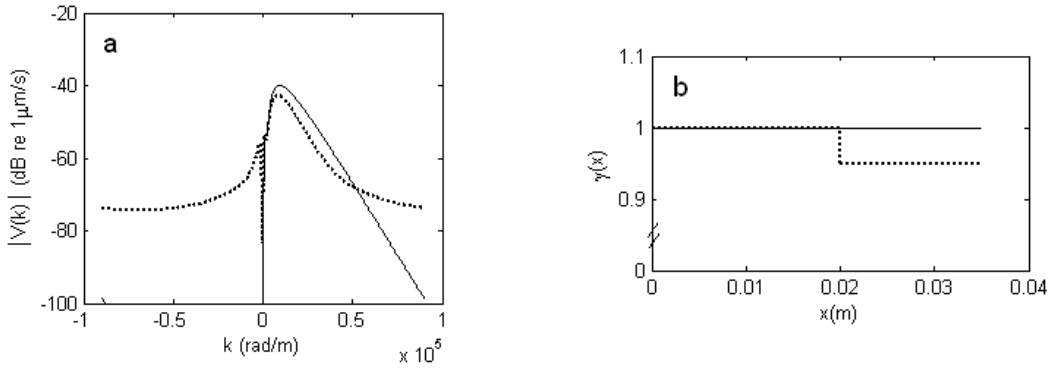

Figure D.1 Negative components in the wavenumber spectrum
(a) The wavenumber spectrum of the response of the original Kanis & de Boer linear active model, found by taking the inverse Fourier transform of the estimated CP velocity response to a 1 kHz stapes stimulation obtained using the finite difference method (N=1000). Two spectra are shown: One for a "smooth" model, in which no impedance perturbations have been introduced (solid line), and the other (dotted line) for the same model containing a step-down change in the OHC gain, γ(x), as illustrated in (b).

(iii) The input impedance of the model is a smooth function of stimulus frequency

The cochlear input impedance, Z_c, is defined in terms of the semi-difference pressure, p_d, and longitudinal fluid velocity, u_f, as shown below (Shera & Zweig, 1993). Any reflections arising in the model influence the pressure and the fluid velocity near the stapes, and therefore influence the cochlear input impedance.

$$Z_c(\omega) \equiv \left. \frac{p_d(x,\omega)}{u_f(x,\omega)} \right|_{x=0} \tag{D.1}$$

In a model with no reflections, Z_c is expected to be a smooth function of frequency. Figure D.2 demonstrates that this is the case for the discrete linear active Kanis & de Boer cochlear model. In contrast, variations of up to 10 dB can be observed in the magnitude of Z_c when irregularities in the active impedance are introduced to the model to act as sources of reflection.

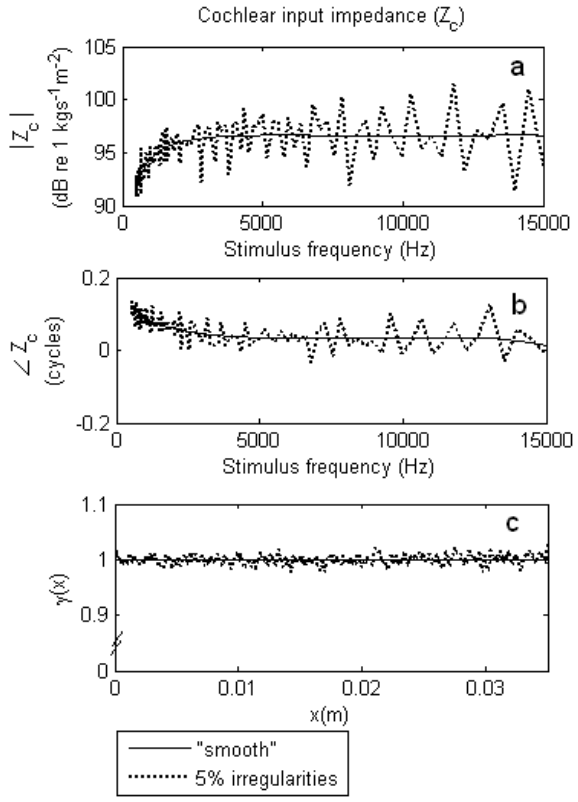

Figure D.2 Ripples in the cochlear model input impedance
The (a) magnitude and (b) phase of the cochlear input impedance, Z_c, for a range of stimulus frequencies presented to the linear active Kanis & de Boer cochlear model. The solid lines are results for a model where no impedance irregularities are introduced. The dotted line denotes a model where a random 5% variation in the OHC gain, γ(x), has been imposed along the CP to act as sources of reflection. The distribution γ(x) for each case is shown in (c).

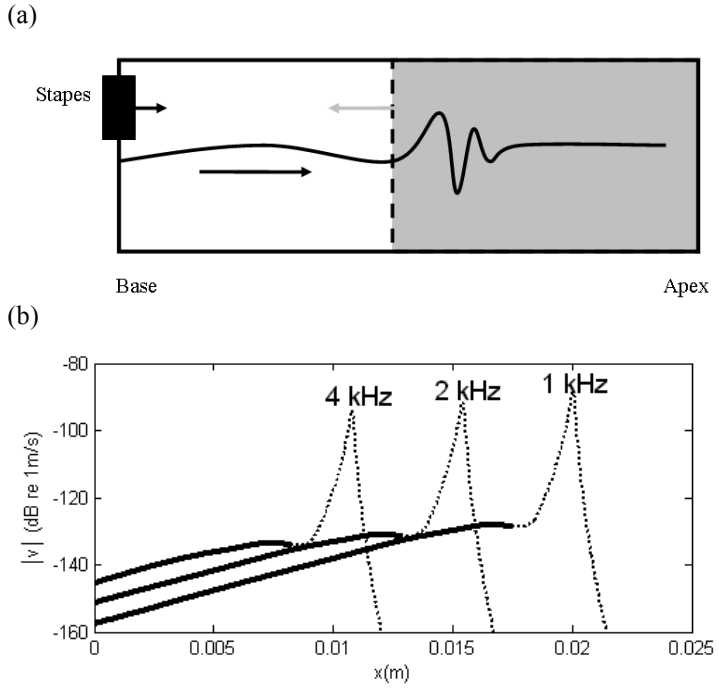

Figure D.3 The effect of truncating the cochlear model (a) An illustration of the truncation of the cochlear model at the location of the black dashed line. Stimulation is applied at the stapes, initiating a travelling wave in the direction of the black arrow. If a source of reflection is present in the vicinity of the characteristic place, this may result in a backward travelling reflected wave, denoted by the grey arrow. However, this reflected wave should be eliminated by introducing a reflectionless truncation at the black dashed line. (b) The responses of the full (dotted lines) and truncated (solid lines) linear active Kanis & de Boer model, calculated with the finite difference method and N=1000.

(iv) Truncating the model does not significantly alter the basal response

Reflections are most likely to occur from the vicinity of the characteristic place, as this is the region where the spatial variation in the wavenumber is the greatest. This can be investigated by truncating the model, with a 'reflectionless' boundary condition basal to the characteristic place. If no significant reflections are propagating between the characteristic place and the base in the full model, then the response should be unaffected by the truncation. The process is illustrated in Figure D.3a. This approach would fail to detect local reflections from the characteristic place, which do not propagate basally as far as the un-shaded region. However, local reflections are neglected in this analysis on the basis that reflections which are unable to propagate a substantial distance are unlikely to be significant.

When a truncation is imposed at location x_{trun}, the number of elements used to represent the length of the discrete model reduces from N to N_{trun}. Conservation of momentum at the truncation leads to the boundary condition (D.2) in the finite difference method notation. This boundary should minimise reflections if the CP impedance immediately adjacent to the truncation, $Z_{CP}(N_{trun}-1)$, is set equal to the impedance of the forward travelling wave at this location $Z^{+}(N_{trun}-1)$ defined in (D.3).

$$\frac{p_d(N_{trun})-p_d(N_{trun}-1)}{\Delta}=-i\omega\rho u_f(N_{trun}-1)=-\frac{i\omega\rho p_d(N_{trun}-1)}{Z_{CP}(N_{trun}-1)} \qquad \text{(D.2)}$$

$$Z^{+}\left(N_{trun}-1\right)=\frac{Z_{char}(N_{trun}-1)}{1-\frac{1}{2i\omega\rho}\left(\frac{Z_{char}(N_{trun})-Z_{char}(N_{trun}-2)}{2\Delta}\right)} \tag{D.3}$$

where for the j[th] element,

$$Z_{char}(N_j)=\frac{\rho\omega}{k(N_j)}=\sqrt{½\,i\omega\rho HZ_{CP}(N_j)} \tag{D.4}$$

This method can be used to impose a reflectionless boundary condition at any point along the CP. Introducing the truncation 2.5 mm basal of the characteristic place, elicits a change of less than ¼ dB in the velocity response of the cochlear partition across a range of stimulus frequencies (Figure D.3b). This implies that there are no sites of significant reflection in the vicinity of the characteristic place, as the response in the basal region is not affected by the truncation.

It should be noted that at locations very close to the characteristic place, numerical errors can occur in the implementation of the finite difference equations as a consequence of the rapid spatial variation in parameters such as the characteristic impedance Z_{char}. These errors can be substantially reduced by increasing N, the number of elements in the discrete model.

In conclusion, there are no substantial reflections occurring within the discrete linear active Kanis & de Boer cochlear model, for N=1000. As the impedance variations are greater in the active model, compared to the passive model, we can infer that significant reflections are also absent in the discrete linear passive Kanis & de Boer model.

D.2 Quasilinear cochlear models

We have established that, for a linear cochlear model, reflections can be neglected in both the passive and active case. In contrast, Figure D.4 and Figure D.5 illustrate that backward travelling waves arise in a baseline quasilinear cochlear model, in which no impedance irregularities have been deliberated introduced, at moderate stimulus levels (40 − 80 dB SPL). This is due to the spatial variations in the active impedance which are introduced by the effects of self-suppression. For example, Figure D.4 shows the inverse Fourier transform of the velocity distribution obtained by allowing the quasilinear method to converge for a single frequency excitation at 2 kHz. This graph demonstrates that some of the $k<0$ components of the $V(k)$ spectrum have amplitudes within 40 dB of the optimal $k>0$ components for stimuli at 60 and 80 dB SPL, indicating that negative wavenumbers cannot be neglected. In addition the input impedance of the Kanis & de Boer model, shown in Figure D.5, exhibits peaks and troughs for the 60 dB SPL stimulus. These results indicate the presence of backward travelling waves, which may arise as a consequence of impedance

perturbations due to self-suppression acting as sites of reflection. Figure D.6 demonstrates that the nonlinearity causes the amplitude of the WKB condition parameter $\left|\frac{1}{k^2}\frac{dk}{dx}\right|$ to increase in the region basal to the characteristic place, relative to a linear model with comparable CA gain. Despite this behaviour at moderate stimulus levels, it should be noted at for low levels (< 40 dB SPL) and very high levels (> 80 dB SPL) no significant reflections occurring within the cochlear model are evident in either the wavenumber spectrum (Figure D.4) or the input impedance (Figure D.5).

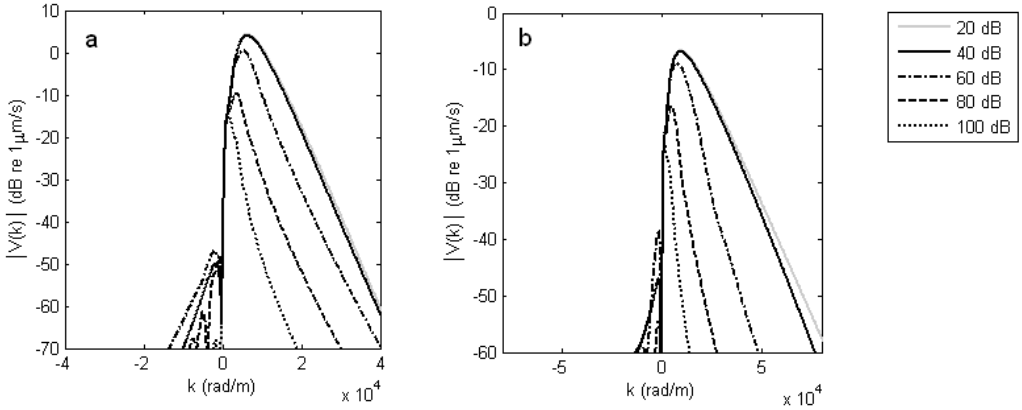

Figure D.4 The inverse Fourier transform of the quasilinear fundamental velocity distribution
The plots show the inverse Fourier transform, $V(k)$, of the fundamental velocity distribution $v(x)$ evoked by a 2 kHz tone in the (a) modified Neely & Kim model and (b) the Kanis & de Boer model. The result is obtained using the quasilinear method, and a discrete model with N=1000.

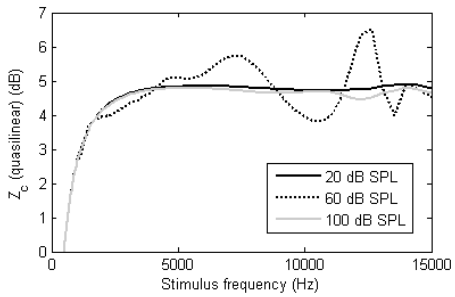

Figure D.5 The estimated input impedance for the quasilinear cochlear model
The input impedance, Z_c, of the quasilinear Kanis & de Boer cochlear model is shown for a range of stimulus levels, evaluated using the finite difference method with N=1000.

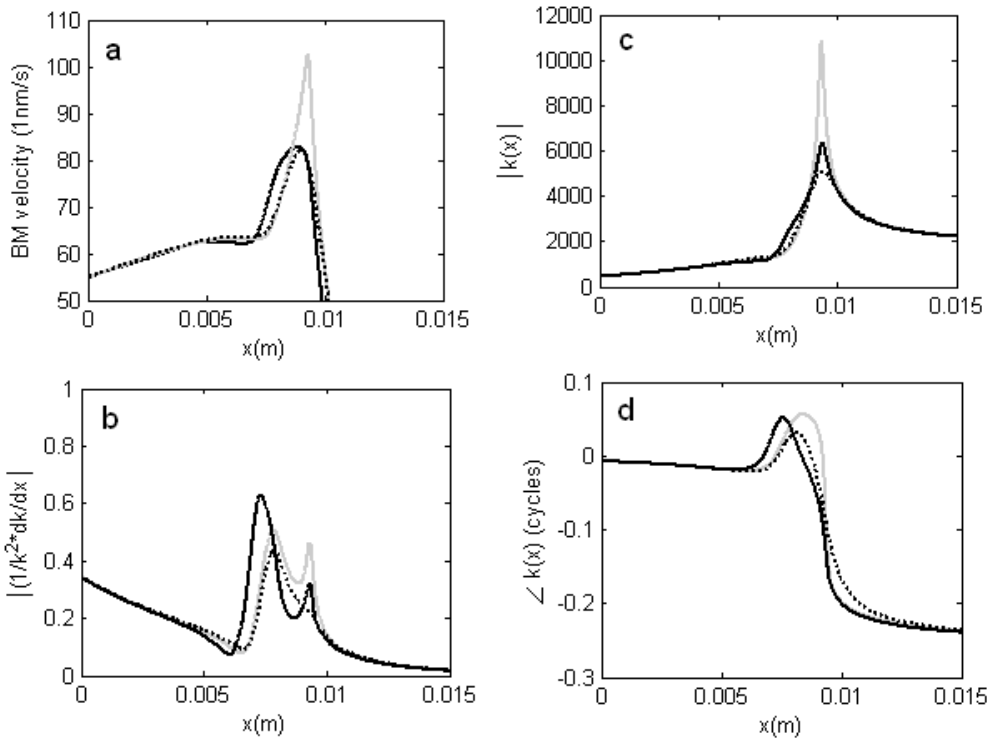

Figure D.6 The WKB approximation condition for the quasilinear model
(a) The velocity response and (b) amplitude of the WKB condition parameter for the Kanis & de Boer model stimulated at 5 kHz. Results are shown for a 60 dB SPL stimulus in the QL model (solid black line) and linear model using $\gamma = 0.74$ (dotted black line) and $\gamma = 1$ (solid grey line). The (c) magnitude and (d) phase of the complex wavenumber, $k(x)$, are also shown. The calculations were performed using N=1000.

E Quasilinear iterative procedures

In this appendix, the details of the quasilinear iteration used in this thesis are presented. This is partly for completion and partly because it differs in some details from the method described by Kanis & de Boer. These differences were introduced to make the process more consistent and were found to significantly improve the convergence properties of the iterative procedure.

In appendix E.1 − E.5, the quasilinear method is discussed with reference to the original micromechanical model of Kanis & de Boer. Appendix E.6 discusses the application of this method to a different micromechanical model, that of Neely & Kim (1986).

E.1 Fundamental component of the response to a single tone stimulus

An illustration of the Kanis & de Boer (1993) iterative process used to estimate the fundamental response of the quasilinear model to a stimulus with angular frequency ω is shown in Figure E.1. The process stops when the estimate of $v(x,\omega)$ varies by less than 0.1% between iterative cycles. When implementing this procedure in MATLAB it is necessary to construct a time vector t, ranging between 0 and $2\pi/\omega$, with N_t samples per period. Kanis & de Boer recommend using N_t equal to 24, but as numerical integration errors can occur at high stimulus levels we use a t of variable sample length. This is achieved by evaluating step 2 of the process several times with increasing values of N_t in a single iterative cycle. Step 2 is considered complete only when a value of N_t is found for which further increases in N_t produce no significant change in the estimated pressure output of the OHCs. For example, when evaluating the response of the Kanis & de Boer quasilinear model to a 5 kHz stimulus, we find that N_t equal to 24 is sufficient for stimulus levels up to 60 dB SPL, but that higher values of N_t are required for greater stimulus levels.

As the position of the nonlinearity within the feedback loop influences the calculation of $p_{OHC}^{QL}(x,\omega,n)$ in step 2, either equation (E.1) or (E.2) should be used depending on whether the nonlinearity (F) is placed *before* or *after* or filter 2 respectively (see section 3.2).

$$p_{OHC}^{QL}(x,\omega) = \frac{1}{T}\int_0^T Z_{OHC}^{lin}(x,\omega)\cdot F\left(v(x,\omega)\cdot\exp(i\omega t)\right)\cdot\exp\left(-i\omega t\right)dt \qquad \text{(E.1)}$$

$$p_{OHC}^{QL}(x,\omega) = \frac{1}{T}\int_0^T F\left(Z_{OHC}^{lin}(x,\omega)\cdot v(x,\omega)\cdot\exp(i\omega t)\right)\cdot\exp\left(-i\omega t\right)dt \qquad \text{(E.2)}$$

Kanis & de Boer employ averaging between iterative cycles to improve the rate of the convergence of the procedure. We observed by trial and error indicated that using an averaging ratio of 0.3×new + 0.7×old, appeared to produce consistently rapid convergence across a range of stimulus levels.

Step 0: An initial estimate of the CP impedance is made by assuming the model is fully active

$$Z_{CP}^{QL}(x,\omega,n=1) = Z_{CP}^{pass}(x,\omega) - Z_{OHC}^{lin}(x,\omega)$$

Step 1: The finite difference method is used to determine $p_d(x,\omega,n)$ and, $v(x,\omega,n)$ given $Z_{CP}^{QL}(x,\omega,n)$

Step 2: The response of the OHCs is calculated in the following stages…

(i) A time domain input to the nonlinearity is constructed from the fundamental component of the CP velocity

$$p_{OHC}^{lin}(x,t,n) = 2\,\mathrm{Re}\left(Z_{OHC}^{lin}(x,\omega)\cdot v(x,\omega,n)\cdot\exp(i\omega t)\right)$$

(ii) The time domain signal is passed through the hyperbolic tangent nonlinear function and the fundamental component of the output extracted…

$$p_{OHC}^{QL}(x,\omega,n) = \frac{1}{T}\int_0^T p_{ref}\,\tanh\left\{p_{OHC}^{lin}(x,t,n)\,/\,p_{ref}\right\}\cdot e^{i\omega t}dt$$

Step 3: A new estimate of the CP impedance is formed

$$Z_{CP}^{QL}(x,\omega,n+1) = Z_{CP}^{pass} - \frac{p_{OHC}^{QL}(x,\omega,n)}{v(x,\omega,n)}$$

Step 4: Stop iteration when, at every location, either

$$\frac{\left|v(x,\omega,n)-v(x,\omega,n-1)\right|}{\left|v(x,\omega,n)\right|} < 0.001 \text{ or}$$

$$20\cdot\log_{10}\left(\frac{\left|v(x,\omega,n)\right|}{\max\left|v(x,\omega,n)\right|}\right) < -100\text{dB}$$

Figure E.1 The quasilinear iterative process for evaluating the fundamental response

The scaling parameter p_{ref}, which has dimensions of pressure, is set equal to 2 by Kanis & de Boer (1993). Steps 1 to 3 are repeated until the estimate of v varies by less than 0.1%. The parameter n denoted the n^{th} iterative cycles

E.2 The harmonic response to a single tone stimulus

Given the predicted fundamental response to a single tone stimulus, it is possible to extend the quasilinear method to estimate the harmonic responses as described below.

The m^{th} harmonic component of p_{OHC}^{QL} can be regarded theoretically in two different ways. First, there is the harmonic component generated by the BM motion at the fundamental frequency which acts as an internal source for the harmonic response. This component of p_{OHC}^{QL} is labelled $p_{OHC,A}^{QL}$ and is calculated using (E.3) and (E.4), where the time period T is equal to $2\pi/\omega$ and $F[]$ corresponds to the nonlinearity.

$$p_{OHC,A}^{QL}(x,m\omega) = \frac{1}{T}\int_0^T F\left(p_{OHC,A}^{lin}(x,t)\right)\cdot\exp\left(-im\omega t\right)dt \tag{E.3}$$

where

$$p_{OHC,A}^{lin}(x,t) = 2\,\mathrm{Re}\left(Z_{OHC}^{lin}(x,\omega)\cdot v(x,\omega)\cdot\exp(i\omega t)\right) \tag{E.4}$$

Second, it is useful to calculate the total quasilinear pressure output of the OHCs at harmonic frequency $m\omega$, including the effects of any self-suppression of the harmonic response. This total quasilinear pressure is labelled $p_{OHC,B}^{QL}$, and is evaluated using (E.5) and (E.6). The extent of the self-suppression of the harmonic response can be estimated from the difference between $p_{OHC,B}^{QL}$ and $p_{OHC,A}^{QL}$, denoted by Δp_{OHC}^{QL}, and is used to define the harmonic quasilinear impedance of the OHC complex, as shown in (E.7).

$$p_{OHC,B}^{QL}(x,m\omega) = \frac{1}{T}\int_0^T F\left(p_{OHC,B}^{lin}(x,t)\right)\cdot\exp\left(-im\omega t\right)dt \tag{E.5}$$

where

$$p_{OHC,B}^{lin}(x,t) = 2\,\mathrm{Re}\begin{pmatrix} Z_{OHC}^{lin}(x,\omega)\cdot v(x,\omega)\cdot\exp(i\omega t) \\ +Z_{OHC}^{lin}(x,m\omega)\cdot v(x,m\omega)\cdot\exp(im\omega t)\end{pmatrix} \tag{E.6}$$

and

$$Z_{OHC}^{QL}(x,m\omega) \equiv \frac{\Delta p_{OHC}^{QL}(x,m\omega)}{v(x,m\omega)} = \frac{p_{OHC,B}^{QL} - p_{OHC,A}^{QL}}{v(x,m\omega)} \tag{E.7}$$

The Kanis & de Boer (1993) iterative process for evaluating the harmonic response is illustrated in Figure E.2. It uses the wave equation for the harmonic component shown in (E.8). This is analogous to the fundamental wave equation given in (A.17), but in this case the distributed source is the harmonic component of $p_{OHC,B}^{QL}$.

$$\frac{\partial^2 p_d(x,m\omega)}{\partial x^2} - \frac{2im\omega\rho}{HZ_{CP}^{pass}(x,m\omega)} \cdot p_d(x,m\omega) = \frac{1}{2}\frac{2im\omega\rho}{HZ_{CP}^{pass}(x,m\omega)} \cdot p_{OHC,B}^{QL}(x,m\omega) \qquad \text{(E.8)}$$

Alternatively the wave equation for the harmonic response can be re-arranged into the form shown in (E.9). If this wave equation is used, instead of (E.8), the iterative process then requires an additional step within each cycle, compared to the original Kanis & de Boer approach, as shown in Figure E.2 The convergence of this modified iterative procedure is more rapid than the original, as illustrated in Figure E.3. A possible explanation for this improvement is discussed in appendix E.3.

$$\frac{\partial^2 p_d(x,m\omega)}{\partial x^2} - \frac{2im\omega\rho}{HZ_{CP}^{QL}(x,m\omega)} \cdot p_d(x,m\omega) = \frac{1}{2}\frac{2im\omega\rho}{HZ_{CP}^{QL}(x,m\omega)} \cdot p_{OHC,A}^{QL}(x,m\omega) \qquad \text{(E.9)}$$

In summary, our approach to evaluating the harmonic components is identical to that of the quasilinear method proposed by Kanis & de Boer, apart from the rearrangement of (E.8) into (E.9). In our investigation the iteration process continues until the estimated fundamental, harmonic and DP responses vary by less than 1% between cycles. The process also stops after 50 iterations, even if this condition is not met, provided that the harmonic response is 100 dB below that of the fundamental component. For the stimulus frequencies considered in this investigation, up to 63 iterations were required to establish the fundamental, 2nd, and 3rd order components of the BM displacement evoked by a single tone stimulus in a cochlear model incorporating a Boltzmann nonlinearity. This calculation is achieved on a 2.4 GHz computer in less than 60 seconds which is significantly less than the computational time of 2 to 4 hours required to allow a time domain simulation to reach steady state Ku (2008).

Step 0: Estimate the fundamental response $v(x,\omega,n)$, make an initial estimate of the CP impedance for $m\omega$ by assuming the model is fully active at this frequency

$$Z_{CP}^{QL}(x,m\omega,n=1) = Z_{CP}^{pass}(x,m\omega) - Z_{OHC}^{lin}(x,m\omega)$$

then evaluate

$$p_{OHC,A}^{QL}(x,m\omega,n=1) = \frac{1}{T}\int_0^T \tanh\left\{2\,\mathrm{Re}\left(Z_{OHC}^{lin}(x,\omega)\cdot v(x,\omega,n)\cdot\exp(i\omega t)\right)\right\}\cdot e^{im\omega t}dt$$

Step 1: Equations (A.11) and (A.10) are used to re-estimate $p_d(x,\omega,n)$ and $v(x,\omega,n)$, given $Z_{CP}^{QL}(x,\omega,n)$. In addition, equations (E.9) and (A.10) are used to determine $p_d(x,m\omega,n)$ and $v(x,m\omega,n)$, given $Z_{CP}^{QL}(x,m\omega,n)$.

Step 2: The OHC response is calculated

$$p_{OHC}^{QL}(x,\omega,n+1) = \frac{1}{T}\int_0^T p_{ref}\tanh\left\{\frac{1}{p_{ref}}\begin{pmatrix}2\,\mathrm{Re}\left(Z_{OHC}^{lin}(x,\omega)\cdot v(x,\omega,n)\cdot\exp(i\omega t)\right)\\+2\,\mathrm{Re}\left(Z_{OHC}^{lin}(x,m\omega)\cdot v(x,m\omega,n)\cdot\exp(im\omega t)\right)\end{pmatrix}\right\}\cdot e^{i\omega t}dt$$

$$p_{OHC,B}^{QL}(x,m\omega,n+1) = \frac{1}{T}\int_0^T p_{ref}\tanh\left\{\frac{1}{p_{ref}}\begin{pmatrix}2\,\mathrm{Re}\left(Z_{OHC}^{lin}(x,\omega)\cdot v(x,\omega,n)\cdot\exp(i\omega t)\right)\\+2\,\mathrm{Re}\left(Z_{OHC}^{lin}(x,m\omega)\cdot v(x,m\omega,n)\cdot\exp(im\omega t)\right)\end{pmatrix}\right\}\cdot e^{im\omega t}dt$$

$$p_{OHC,A}^{QL}(x,m\omega,n+1) = \frac{1}{T}\int_0^T p_{ref}\tanh\left\{\frac{2}{p_{ref}}\mathrm{Re}\left(Z_{OHC}^{lin}(x,\omega)\cdot v(x,\omega,n)\cdot\exp(i\omega t)\right)\right\}\cdot e^{im\omega t}dt$$

Step 3: A new estimate of the CP impedance at the fundamental frequency is formed

$$Z_{CP}^{QL}(x,\omega,n+1) = Z_{CP}^{pass} - \frac{p_{OHC}^{QL}(x,\omega,n+1)}{v(x,\omega,n)}$$

Step 4: In the *original* Kanis & de Boer method $p_{OHC,B}^{QL}(x,m\omega,n)$ is used to solve (E.8) to obtain $p_d(x,m\omega,n+1)$ and

$$v(x,m\omega,n+1) = \frac{\begin{Bmatrix}-2\,p_d(x,m\omega,n+1)\\+p_{OHC,B}^{QL}(x,m\omega,n+1)\end{Bmatrix}}{Z_{CP}^{pass}(x,m\omega)}$$

Step 4: In the *modified* method

$$Z_{OHC}^{QL}(x,m\omega n+1) = \frac{\begin{Bmatrix}p_{OHC,B}^{QL}(x,m\omega,n+1)\\-p_{OHC,A}^{QL}(x,m\omega,n+1)\end{Bmatrix}}{v(x,m\omega,n)}$$

so that

$$Z_{CP}^{QL}(x,m\omega,n+1) = \begin{Bmatrix}Z_{CP}^{pass}(x,m\omega)\\-Z_{OHC}^{QL}(x,m\omega,n+1)\end{Bmatrix}$$

Step 5: Stop iteration when, at every location, either

$$\frac{\left|v(x,m\omega,n)-v(x,m\omega,n-1)\right|}{\left|v(x,m\omega,n)\right|} < 0.01 \text{ or } 20\cdot\log_{10}\left(\frac{\left|v(x,m\omega,n)\right|}{\max\left|v(x,\omega,n)\right|}\right) < -100\text{dB for n>50}$$

Figure E.2 The quasilinear iterative process for estimating the m[th] order harmonic component of the response to a single tone stimulus

The nonlinearity scaling parameter p_{ref}, which has dimensions of pressure, is set equal to 2 by Kanis & de Boer (1993). It is necessary to employ boundary conditions for the harmonic component and so we assume that $p_d(x=L,m\omega,n)=0$ at the helicotrema and that the stapes velocity associated with the external stimulus, introduced in (B.2), is zero: $u_{st}^{in}(m\omega)=0$

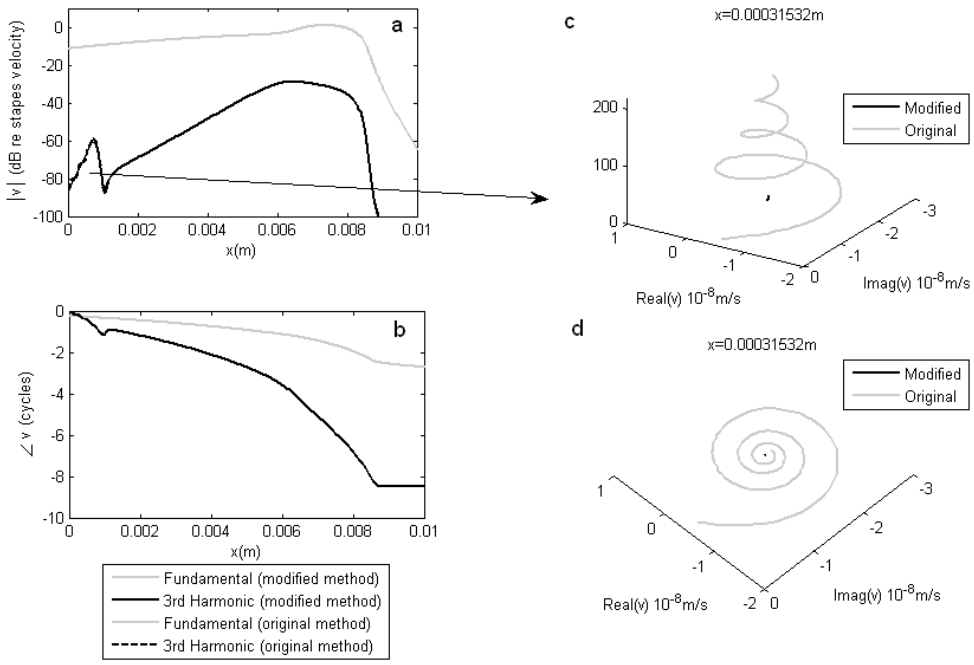

Figure E.3 The convergence of the quasilinear iterative estimate of the harmonic response
The (a) amplitude and (b) phase of the response of the Kanis & de Boer micromechanical model after convergence to a stimulus stapes velocity of 80 dB re 10^{-8}m/s at 6 kHz. The fundamental (black lines) and 3rd order (grey lines) components were estimated using either the original (dotted lines) or modified (solid lines) iterative methods. (c) & (d) The rate of convergence of the 3rd harmonic estimate, at a location 0.0003 m from the stapes, is illustrated. The total number of iterations required for the whole distribution to converge was 218 for the original method, and 11 for the modified method.

E.3 Improved convergence of the iterative process

The modified iteration procedure, for estimating the harmonic components of the response to a single tone stimulus with the quasilinear method, exhibits more rapid convergence that the original iteration scheme. The quasilinear method uses a fixed-point iteration process, which is described in simple terms by (E.10). This process will converge, as shown in Figure E.4, provided that condition (E.11) is satisfied, and the convergence is more rapid for smaller gradients (Bostock & Chandler, 1990).

$$z_{n+1} = g\{z_n\} \tag{E.10}$$

$$\left|\frac{dg(z)}{dz}\right| < 1 \tag{E.11}$$

The analogy between this simple convergence formula and the quasilinear method is not obvious because of the complex and coupled nature of the cochlear model solution. If z_n corresponds to the CP velocity at location x_i, where i takes a value between 1 and N, then $g(z_n)$ corresponds to the CP velocity $v(x_i)$ predicted by the following iterative cycle, using the equations shown in Figure E.2.

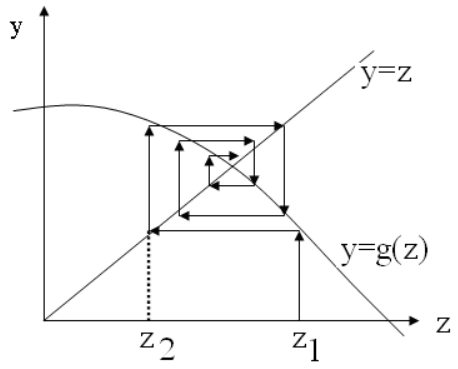

Figure E.4 An illustration of a fixed-point iteration scheme
This iterative method finds the solution to z=g(z). An initial estimate of the solution, z_1, is gradually improved by repeatedly settings z_{n+1} equal to $g(z_n)$. The process will convergence provided that condition (E.11) is satisfied.

For a problem with complex variables we can apply (E.10) and (E.11) to the real and imaginary components separately, to generate the following convergence condition

$$\left|\frac{\partial \mathrm{Re}[g(z)]}{\partial \mathrm{Re}[z]}\right| < 1 \text{ and } \left|\frac{\partial \mathrm{Im}[g(z)]}{\partial \mathrm{Im}[z]}\right| < 1 \qquad \text{(E.12)}$$

As the cochlear model consists of coupled micromechanical elements, the rate of convergence for the solution at one location along the CP may be influenced by the value of the solution at all the other N-1 locations which also change every iterative cycle. Therefore we have been unable to prove whether the fixed-point iteration method is guaranteed to converge to a solution at a given location, without prior knowledge of the solution at all other locations. However, when the solution at all locations has been estimated, it is possible to evaluate the partial derivates in (E.12) to determine if one application of the fixed-point iteration method can be expected to converge more rapidly than the other. For example, when the predicted solution $v(x)$ has been obtained, the function $g[v(x_i)]$ can be estimated by repeatedly calculating $g[v(x_i)]$ for a range of $v(x_i)$ values close to the known $v(x_i)$ solution. The resulting $g[v(x_i)]$ functions at a location 0.0075 m from the base, for the two alternative iteration schemes, are shown in Figure E.5. The gradient values shown in this figure indicate that although the convergence condition (E.12) is satisfied for both the original and modified iterative processes, the gradient for the modified scheme is much smaller suggesting this process should converge more rapidly. This is consistent with the observation that in practice, the original method requires more iterative cycles to reach an estimated solution compared to the modified process.

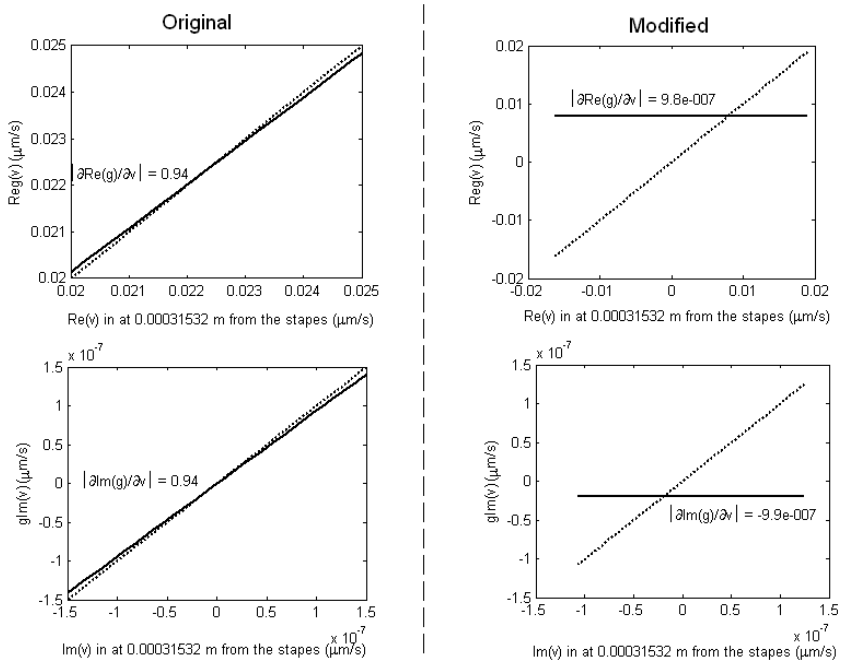

Figure E.5 The convergence properties of the iterative procedure
Plots of $y=g[v(x_i)]$ are shown for the original (a & b) and modified (c & d) fixed-point iteration schemes, for the location 0.0003 m from the stapes, when the Kanis & de Boer model is stimulated with a stapes velocity of 80 dB re 10^{-8} m/s at 6 kHz. This is the same location as featured in Figure E.3. The dotted line shows $y=v(x_i)$ for reference.

E.4 Two tone suppression

The iterative process used to establish the quasilinear response of a cochlear model to two tone stimulation (ω_1 and ω_2) is shown in Figure E.6. Only the primary responses, at frequencies ω_1 and ω_2 are estimated at this stage. However, distortion components can also be determined using the quasilinear method as shown in appendix E.5.

E.5 Estimating distortion products

The quasilinear procedure for estimating distortion products, arising when the cochlear model is stimulated by two tones (f_1 and f_2) simultaneously, is illustrated in Figure E.7. The estimation of distortion products involves a sequence of three iterative procedures: the two single tone responses, the two tone suppression and finally the distortion product response. The third stage is analogous to the iterative process used to predict the harmonic response to a single tone stimulus.

Step 0: A time period, T, is selected which will contain an integer number of cycles of both stimuli (f_1 and f_2). The fundamental response of cochlear model to each tone individually is then established using the quasilinear method (appendix E.1). This provides estimates of $Z_{CP}^{QL}(x,\omega_1,n=1)$ and $Z_{CP}^{QL}(x,\omega_2,n=1)$

Step 1: The finite difference method is used to determine $p_d(x,\omega_{1\text{ and }2},n)$ and, $v(x,\omega_{1\text{ and }2},n)$ given $Z_{CP}^{QL}(x,\omega_{1\text{ and }2},n)$

Step 2: The response of the OHCs is calculated in the following stages…
(i) A time domain input to the nonlinearity is constructed from the ω_1 and ω_2 components of the CP velocity

$$p_{OHC}^{lin}(x,t,n)=\sum_{l=1,2} 2\,\mathrm{Re}\left(Z_{OHC}^{lin}(x,\omega_l)\cdot v(x,\omega_l,n)\cdot\exp(i\omega_l t)\right)$$

(ii) The time domain signal is passed through the hyperbolic tangent nonlinear function and the fundamental component of the output extracted…

$$p_{OHC}^{QL}(x,\omega_l,n)=\frac{1}{T}\int_0^T p_{ref}\,\tanh\left\{p_{OHC}^{lin}(x,t,n)/\,p_{ref}\right\}\cdot e^{i\omega_l t}dt \quad \text{for } l=1 \text{ or } 2$$

Step 3: A new estimate of the CP impedance is formed

$$Z_{CP}^{QL}(x,\omega_l,n+1)=Z_{pass}(x,\omega_l)-\frac{p_{OHC}^{QL}(x,\omega_l,n)}{v(x,\omega_l,n)} \quad \textit{for } l=1 \textit{ or } 2$$

Step 4: Stop iteration when, at every location, either

$$\frac{\left|v(x,\omega_l,n)-v(x,\omega_l,n-1)\right|}{\left|v(x,\omega_l,n)\right|}<0.001 \quad \text{for } l=1 \text{ or } 2$$

$$\text{or } 20\cdot\log_{10}\left(\frac{\left|v(x,\omega_l,n)\right|}{\max\left|v(x,\omega_l,n)\right|}\right)<-100 \text{ dB}$$

Figure E.6 The quasilinear iterative process for estimating the primary quasilinear responses to two tone stimulation
The two stimulus tones have angular frequencies ω_1 and ω_2. The scaling parameter p_{ref}, which has dimensions of pressure, is set equal to 2 by Kanis & de Boer (1993).

Step 0: A time period, T, is selected which will contain an integer number of cycles of both stimuli (f_1 and f_2). The fundamental response of cochlear model to each tone individually is then established using the quasilinear method (appendix E.1). Then the two tone quasilinear iteration is performed (appendix E.4) to provide estimates of

$$Z_{CP}^{QL}(x,\omega_1,n=1) \text{ and } Z_{CP}^{QL}(x,\omega_2,n=1)$$

The estimated primary velocity responses $v(x,\omega_l,n)$, where l = 1 or 2, can be used to make an initial estimate of the CP impedance at the distortion product frequency ω_{dp} by assuming the model is fully active at this frequency

$$Z_{CP}^{QL}(x,\omega_{dp},n=1) = Z_{CP}^{pass}(x,\omega_{dp}) - Z_{OHC}^{lin}(x,\omega_{dp})$$

The distributed pressure source for the distortion product can then be estimated

$$p_{OHC,A}^{QL}(x,\omega_{dp},n=1) = \frac{1}{T}\int_0^T \tanh\left\{\sum_{l=1,2} 2\,\mathrm{Re}\left(Z_{OHC}^{lin}(x,\omega_l)\cdot v(x,\omega_l,n)\cdot\exp(i\omega_l t)\right)\right\}\cdot e^{i\omega_{dp}t}\,dt$$

Step 1: Equations **(A.11)** and **(A.10)** are used to re-estimate $p_d(x,\omega_l,n)$ and $v(x,\omega_l,n)$, given $Z_{CP}^{QL}(x,\omega_l,n)$, for l =1 and 2 In addition, equations **(E.9)** and **(A.10)** are used to determine $p_d(x,\omega_{dp},n)$ and $v(x,\omega_{dp},n)$, given $Z_{CP}^{QL}(x,\omega_{dp},n)$.

Step 2: The OHC response is calculated

$$p_{OHC}^{QL}(x,\omega_j,n+1) = \frac{1}{T}\int_0^T p_{ref}\tanh\left\{\frac{1}{p_{ref}}\left(\begin{array}{l}\sum_{l=1,2} 2\,\mathrm{Re}\left(Z_{OHC}^{lin}(x,\omega_l)\cdot v(x,\omega_l,n)\cdot\exp(i\omega_l t)\right)\\ +2\,\mathrm{Re}\left(Z_{OHC}^{lin}(x,\omega_{dp})\cdot v(x,\omega_{dp},n)\cdot\exp(i\omega_{dp}t)\right)\end{array}\right)\right\}\cdot e^{i\omega_j t}\,dt \quad \text{for j=1 or 2}$$

$$p_{OHC,B}^{QL}(x,\omega_{dp},n+1) = \frac{1}{T}\int_0^T p_{ref}\tanh\left\{\frac{1}{p_{ref}}\left(\begin{array}{l}\sum_{l=1,2} 2\,\mathrm{Re}\left(Z_{OHC}^{lin}(x,\omega_l)\cdot v(x,\omega_l,n)\cdot\exp(i\omega_l t)\right)\\ +2\,\mathrm{Re}\left(Z_{OHC}^{lin}(x,m\omega)\cdot v(x,m\omega,n)\cdot\exp(im\omega t)\right)\end{array}\right)\right\}\cdot e^{i\omega_{dp}t}\,dt$$

$$p_{OHC,A}^{QL}(x,\omega_{dp},n+1) = \frac{1}{T}\int_0^T p_{ref}\tanh\left\{\frac{1}{p_{ref}}\sum_{l=1,2} 2\,\mathrm{Re}\left(Z_{OHC}^{lin}(x,\omega_l)\cdot v(x,\omega_l,n)\cdot\exp(i\omega_l t)\right)\right\}\cdot e^{i\omega_{dp}t}\,dt$$

Step 3: A new estimates of the CP impedance are formed …

$$Z_{CP}^{QL}(x,\omega_l,n+1) = Z_{CP}^{pass}(x,\omega_l) - \frac{p_{OHC}^{QL}(x,\omega_l,n+1)}{v(x,\omega_l,n)} \quad \text{for } l = 1 \text{ or } 2$$

$$Z_{OHC}^{QL}(x,\omega_{dp},n+1) = \frac{p_{OHC,B}^{QL}(x,\omega_{dp},n+1) - p_{OHC,A}^{QL}(x,\omega_{dp},n+1)}{v(x,\omega_{dp},n)}$$

so that

$$Z_{CP}^{QL}(x,\omega_{dp},n+1) = Z_{CP}^{pass}(x,\omega_{dp}) - Z_{OHC}^{QL}(x,\omega_{dp},n+1)$$

Step 4: Stop iteration when, at every location, either

$$\frac{\left|v(x,\omega_{dp},n) - v(x,\omega_{dp},n-1)\right|}{\left|v(x,\omega_{dp},n)\right|} < 0.01$$

or $20\cdot\log_{10}\left(\dfrac{\left|v(x,\omega_{dp},n)\right|}{\max\left|v(x,\omega_{1\text{ or }2},n)\right|}\right) < -100\text{dB}$ for n>50

Figure E.7 the quasilinear iterative process for estimating the distortion product evoked by two tone stimulation

The stimulus tones (ω_1 and ω_2), evoke the DP, ω_{dp}. The scaling parameter p_{ref}, which has dimensions of pressure, is set equal to 2 by Kanis & de Boer (1993).

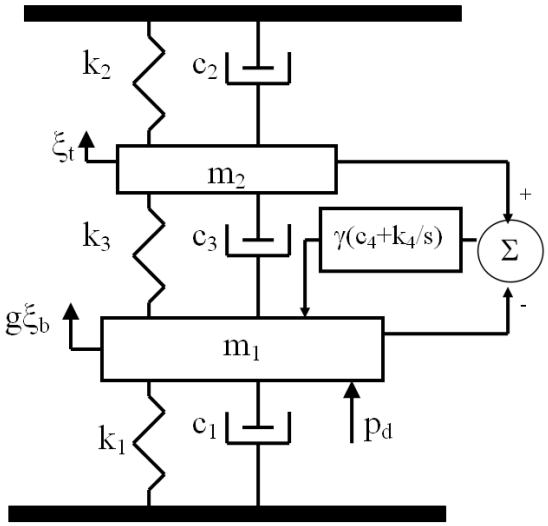

Figure E.8 The micromechanical model of Neely & Kim
This plot is based on figure 2.1 of Ku (2008). The micromechanical parameters (k_1, c_1, m_1, m_2, k_3, c_3, k_4, c_4) are defined in Table E.1(i). The vertical displacement of the BM and the radial displacement of the tectorial membrane are denoted by ξ_b and ξ_t respectively. The gain between the organ of Corti and the reticular laminar, g, is set equal to 1 (Neely & Kim, 1986). In addition, $s=i\omega$, where ω is the angular frequency of the stimulus. Neely & Kim define four impedances in their model: The passive impedance of the OC ($Z_1 = sm_1+c_1+k_1/s$), the passive impedance of the TM ($Z_2 = sm_2 + c_2 + k_2/s$), the coupling between the TM and OC ($Z_3 = c_3 + k_3/s$), and the phase shift between the shear displacement input to the OHCs and the active pressure output ($Z_4 = c_4 + k_4/s$).

E.6 The quasilinear Neely & Kim model

A single micromechanical element in the Neely & Kim (1986) model can be represented as shown in Figure E.8, where the parameters are defined in Table E.1. The micromechanical feedback loop for the linear active Neely & Kim model can also be illustrated by the block diagram given in Figure E.9a. In this diagram the filters are defined in terms of the impedances given in the caption to Figure E.8.

Micromechanical parameter	Interpretation	(i) Original Neely & Kim model	(ii) Original Kanis & de Boer model	(iii) Modified model
b	The ratio of the average displacement across the width of the CP to the maximum displacement over the width of the BM	*0.4*	*0.4*	*0.4*
g	The BM to IHC lever gain	1	1	1
m_1	The mass of the OC	$3\times10^{-2}\,kgm^{-2}$	bm_{KB}	bm_{KB}
k_1	The compliance of the OC	$1.1\times10^{10}e^{-400x}\,Nm^{-3}$	bk_{KB}	bk_{KB}
c_1	The damping of the OC	$200+1.5\times10^{4}e^{-200x}Nsm^{-3}$	bc_{KB}	bc_{KB}
k_2	The compliance of the TM	$7\times10^{7}e^{-440x}Nm^{-3}$	*0*	*0*
c_2	The damping of the TM	$100e^{-220x}Nsm^{-3}$	*0*	*0*
m_2	Mass of the TM	$5\times10^{-3}kgm^{-2}$	-	-
k_3/m_2	The ratio of the compliance in the coupling between the OC and TM to the mass of the TM	-	$\sigma^2\omega_n^2$	$\sigma^2\omega_n^2Q_1$
c_3/m_2	The ratio of the damping in the coupling between the OC and TM to the mass of the TM	-	$\delta_{sc}\omega_n$	$\delta_{sc}\omega_nQ_1$
c_4	The damping associated with the action of the OHCs	$100e^{-80x}Nsm^{-3}$	$be_0d_0\omega_n$	$be_0d_0\omega_nQ_2$
k_4	The compliance associated with the action of the OHCs	$6.15\times10^{9}e^{-400x}Nsm^{-3}$	$be_0d_0\omega_n^2$	$be_0d_0\omega_n^2Q_2$

Table E.1 The micromechanical parameters of Neely & Kim (1986) model related to other cochlear models (i) Neely & Kim model of the cat cochlea in S.I units (Elliott *et al.*, 2007), (ii) the original Kanis & de Boer model as formulated in appendix F.4, and (iii) the parameters of the modified model presented in section 3.4. The interpretation of the parameters is based on that given by Neely & Kim (1986), in terms of the cochlear partition (CP), organ of Corti (OC), tectorial membrane (TM), and outer hair cells (OHCs). The factors m_{KB}, c_{KB}, k_{KB}, σ, δ_{sc}, e_0, d_0 and ω_n are defined in section 2.2.1. The distributions Q_1 andQ_2 are defined in section 3.4.

A nonlinear model can be developed from the linear active Neely & Kim model by inserting a nonlinear function into the micromechanical feedback loop as shown in Figure E.9 b and c. Such a model can be solved using the quasilinear method described in the previous sections, given the following modification. In step 1 of the quasilinear iterative process described in E.1, it is necessary to evaluate the difference in shear displacement between the tectorial membrane (TM) and organ of Corti (OC), ξ, in addition to the variables p_d and v, using (E.13) (Neely & Kim, 1986).

$$\xi(x,\omega,n)=\frac{g_{lever}}{b_w}\frac{Z_2(x,\omega)}{Z_2(x,\omega)+Z_3(x,\omega)}\frac{v(x,\omega,n)}{i\omega} \tag{E.13}$$

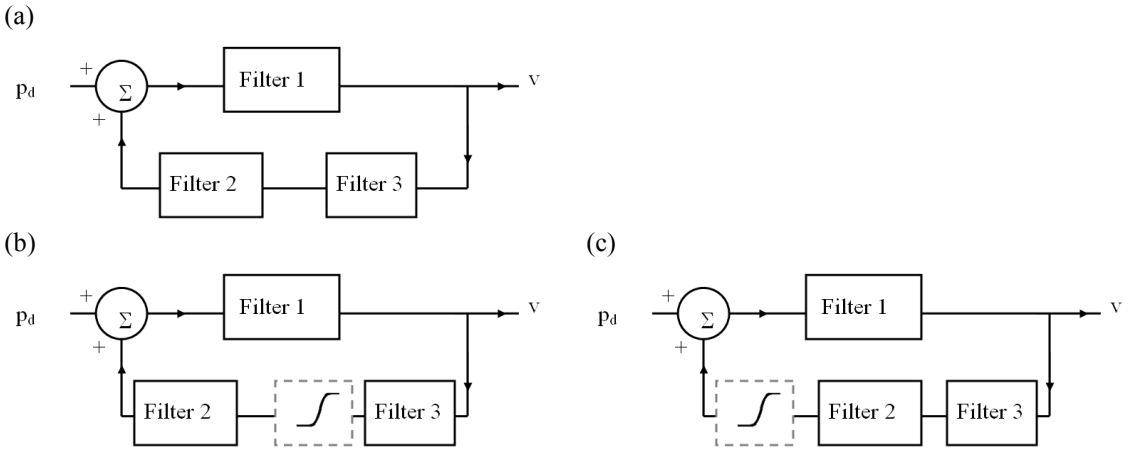

Figure E.9 Representations of single micromechanical element in the Neely & Kim (1986) model
The block diagrams represent (a) linear active model of Neely & Kim. Filter 1 denotes the passive admittance of the organ of Corti ($1/Z_1$), filter 2 describes the dynamics of the OHC (Z_4) and filter 3 arises from the interaction between the TM and OC ($gZ_2/(b(Z_2+Z_3))$). Impedances Z_1, Z_2, Z_3 and Z_4 are defined in the caption of Figure E.8. A nonlinear model can be developed by inserting a nonlinear function either (b) before or (c) after filter 2.

This shear displacement then acts as the input to the OHCs, so that the quasilinear pressure output $p_{OHC}^{QL}(x,\omega,n)$ in step 2, can be calculated using either equation (E.14) or (E.15) depending on whether the nonlinearity is placed *before* or *after* or filter 2 respectively

$$p_{OHC}^{QL}(x,\omega,n)=\frac{1}{T}\int_0^T Z_4(x,\omega)\cdot F\left(\xi(x,\omega,n)\cdot\exp(i\omega t)\right)\cdot\exp\left(-i\omega t\right)dt \qquad \text{(E.14)}$$

$$p_{OHC}^{QL}(x,\omega,n)=\frac{1}{T}\int_0^T F\left(Z_4(x,\omega)\cdot\xi(x,\omega,n)\cdot\exp(i\omega t)\right)\cdot\exp\left(-i\omega t\right)dt \qquad \text{(E.15)}$$

Finally, in step 3 of the iterative process the quasilinear impedance of the CP can be estimated using

$$Z_{CP}^{QL}(x,\omega,n+1)=Z_{CP}^{pass}-\frac{g_{lever}}{b_w}\frac{Z_2}{Z_2+Z_3}\frac{p_{OHC}^{QL}(x,\omega,n)}{i\omega\xi(x,\omega,n)} \qquad \text{(E. 16)}$$

In summary, the quasilinear method can be used to estimate the response of the nonlinear Neely & Kim coupled cochlear model. However, the process must be adapted to account for the fact that in the Neely & Kim formulation the input to the OHCs is the difference in the shear displacement between the TM and OC. This is in contrast to the Kanis & de Boer formulation, where the input to the OHCs is associated with the vertical displacement of the cochlear partition. The use of different variables to stimulate the OHCs means that the quasilinear response of the model will be different in each formulation even if equivalent micromechanical parameters are used.

F. State space representation of the Kanis & de Boer cochlear model

In this section the state space model of the Kanis & de Boer micromechanical cochlear model is described. First a general method for obtaining the frequency domain state space framework for a linear system, from the system transfer function, is reviewed. This is then applied to the uncoupled, linear, active Kanis & de Boer micromechanical model. This state space model is used as the basis of the coupled linear active state space model in appendix F.3. Finally, the state space representation of the uncoupled linear active model is used to determine a relationship between two different micromechanical models considered in appendix F.4.

F.1 A frequency domain state space representation of a linear system

Furuta *et al.* (1988) describe a method for constructing a frequency domain state space representation of a linear system from its transfer function. In this section the approach is summarised for a general system and it is applied to the Kanis & de Boer linear active cochlear model.

If a system is stimulated by a sinusoidal pressure input p, at an angular frequency ω, and generates an output velocity v, then the system transfer function (H_{ss}) is defined below. In this case, $s = i\omega$, but in general s may contain real and imaginary components to allow unstable systems to be characterised.

$$\frac{v(s)}{p(s)} \equiv H_{ss}(s) \tag{F.1}$$

The state space model for a system can be written in the time domain as

$$\begin{aligned} \dot{\mathbf{w}}(t) &= \mathbf{A}\mathbf{w}(t) + \mathbf{B}p(t) \\ v(t) &= \mathbf{C}\mathbf{w}(t) + \mathbf{D}p(t) \end{aligned} \tag{F.2}$$

where $\mathbf{w}$ is the state vector, incorporating the displacement of one of the system components, w, and several orders of its time derivative such that

$$\mathbf{w}^T = [w_1 \quad \dot{w}_1 \quad \ddot{w}_1 \quad \dddot{w}_1] \tag{F.3}$$

In the present case $v(t)$ is not directly proportional to $p(t)$, so the "feed through" matrix $\mathbf{D}$ is zero.

If each element of the state vector $\mathbf{w}(t)$ is now proportional to e^{st}, the state space equations written as

$$s\mathbf{w}(s) = \mathbf{A}\mathbf{w}(s) + \mathbf{B}p(s)$$
$$\text{and} \qquad v(s) = \mathbf{C}\mathbf{w}(s) \tag{F.4}$$

Equation (F.4) can be rearranged to give an expression for $H_{ss}(s)$ in terms of the state space matrices **A**, **B**, **C** and **D** as shown below. In this equation 'adj' and 'det' refer to the adjoint and determinant matrix functions respectively and **I** denotes the identity matrix.

$$H_{ss}(s) = \mathbf{C}\left(s\mathbf{I} - \mathbf{A}\right)^{-1}\mathbf{B} = \frac{\mathbf{C}\ \mathrm{adj}\left(s\mathbf{I} - \mathbf{A}\right)\mathbf{B}}{\det\left(s\mathbf{I} - \mathbf{A}\right)} \tag{F.5}$$

The determinant of ($s\mathbf{I} - \mathbf{A}$] gives a denominator polynomial of order q in s, while every element of the adjoint matrix of ($s\mathbf{I} - \mathbf{A}$] gives a numerator polynomial of order $\leq q-1$ in s (Furuta *et al.*, 1988). Therefore equation (F.5) can be re-written as (F.6), where $\phi_{ss}(s)$ is a lower order polynomial than $\chi_{ss}(s)$.

$$H_{ss}(s) = \frac{\phi_{ss}(s)}{\chi_{ss}(s)} \tag{F.6}$$

Equations (F.5) and (F.6) can be used to determine the elements of the state space matrices **A**, **B**, **C** and **D** using the following procedure. First, note that the variables $G(s)$ is Figure F.1 such that

$$\frac{G_{ss}(s)}{p(s)} = \frac{1}{\chi_{ss}(s)} = \frac{1}{s^n + \alpha_{n-1}s^{n-1} + \cdots + \alpha_1 s + \alpha_0} \tag{F.7}$$

and

$$\frac{v(s)}{G_{ss}(s)} = \phi_{ss}(s) = \beta_{n-1}s^{n-1} + \beta_{n-2}s^{n-2} + \cdots \beta_1 s + \beta_0 \tag{F.8}$$

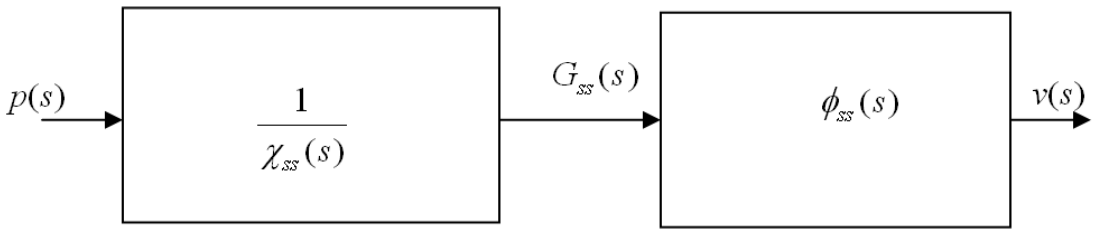

Figure F.1 Representation of the transfer function given in equation (F.6) for a single micromechanical element of a cochlear model.

Cross multiplying (F.7), and multiplying both sides by e^{st}, we can define $w(s)e^{st}$ as $w(t)$ so that $sw(s)e^{st}$ is equal to $dw(t)/dt$ etc. Therefore (F.7) can be written in the time domain as

$$\begin{aligned} &\alpha_0 w(t) + \alpha_1 \frac{dw(t)}{dt} + \cdots + \alpha_{q-1} \frac{d^{q-1}w}{dt^{q-1}} + \frac{d^q w}{dt^q} = p(t) \\ &\Rightarrow \frac{d^q w}{dt^q} = -\alpha_0 w(t) - \alpha_1 \frac{dw(t)}{dt} - \cdots - \alpha_{q-1} \frac{d^{q-1}w}{dt^{q-1}} + p(t) \end{aligned} \tag{F.9}$$

Secondly, Figure F.1 also shows that

$$v(s) = \phi_{ss}(s) w(s) \tag{F.10}$$

which, using a similar method to that described above, can also be represented in the time domain as

$$v(t) = \beta_{q-1} \frac{d^{q-1}w(t)}{dt^{q-1}} + \cdots + \beta_1 \frac{dw(t)}{dt} + \beta_0 \tag{F.11}$$

If a state vector $\mathbf{w}^T = \left[w_1, w_2, w_3, \ldots w_q \right]$ is now selected, such that $w_2 = \dot{w}_1$, $w_3 = \dot{w}_2 = \ddot{w}_1$ etc, then (F.9) and (F.11) can be written in the matrix forms

$$\frac{d}{dt}\begin{bmatrix} w_1 \\ w_2 \\ w_3 \\ \vdots \\ w_{q-1} \end{bmatrix} = \begin{bmatrix} 0 & 1 & 0 & \cdots & 0 \\ 0 & 0 & 1 & & 0 \\ \vdots & & & \ddots & 0 \\ 0 & & & & 1 \\ -\alpha_0 & -\alpha_1 & \cdots & \cdots & -\alpha_{q-1} \end{bmatrix} \begin{bmatrix} w_1 \\ w_2 \\ w_3 \\ \vdots \\ w_{q-1} \end{bmatrix} - \begin{bmatrix} 0 \\ 0 \\ \vdots \\ 0 \\ 1 \end{bmatrix} p(t) \tag{F.12}$$

and

$$v(t) = \begin{bmatrix} \beta_0 & \beta_1 & \cdots & \cdots & \beta_{q-1} \end{bmatrix} \begin{bmatrix} w_1 \\ w_2 \\ w_3 \\ \vdots \\ w_{q-1} \end{bmatrix} \tag{F.13}$$

Therefore the state space matrices are given by

$$\mathbf{A} = \begin{bmatrix} 0 & 1 & 0 & \cdots & 0 \\ 0 & 0 & 1 & & 0 \\ \vdots & & & \ddots & 0 \\ \vdots & & & & 1 \\ -\alpha_0 & -\alpha_1 & \cdots & \cdots & -\alpha_{q-1} \end{bmatrix}, \mathbf{B} = \begin{bmatrix} 0 \\ 0 \\ \vdots \\ 0 \\ 1 \end{bmatrix}, \tag{F.14}$$

$$\text{and } \mathbf{C} = \begin{bmatrix} \beta_0 & \beta_1 & \cdots & \cdots & \beta_{q-1} \end{bmatrix}$$

The general method described in the previous section can be applied to a single micromechanical element of the linear Kanis & de Boer cochlear model in order to assess the stability of the uncoupled model and contribute to the construction of a coupled state space model.

F.2 The uncoupled linear active Kanis & de Boer micromechanical model

The general technique for formulating a state space model of a linear system in the frequency domain, given in appendix F.1. In this section, the technique is applied to obtain a state space model of a single micromechanical element in the linear active Kanis & de Boer cochlear model. This is then used to evaluate the response to of the uncoupled model to sinusoidal stimulation and to determine the stability of the system.

F.2.1 The state space representation

The linear active Kanis & de Boer cochlear model is described by two impedances $Z_{CP}^{pass}(x,s)$ and $Z_{OHC}^{lin}(x,s)$, where $s=i\omega$ in this case, defined in (F.15) and (F.16). The variables $m_{KB}(x)$, $c_{KB}(x)$, and $k_{KB}(x)$ represent the mass, resistance and stiffness per unit area of the basilar membrane (BM) respectively, and details of the other parameters can be found in section 2.2.1.

$$Z_{CP}^{pass}(x,s) = sm_{KB}(x) + c_{KB}(x) + \frac{k_{KB}(x)}{s} \tag{F.15}$$

$$Z_{OHC}^{lin}(x,s) = e_o\omega_n(x)\cdot d_0\left\{\frac{1+ib(x,s)}{\delta_{SC}+i\left[b(x,s)-\dfrac{\sigma^2}{b(x,s)}\right]}\right\} \tag{F.16}$$

where

$$ib(x,s) = \frac{s}{\omega_n}$$

The overall system transfer function (F.17) is a function of these two impedances. The input to the overall micromechanical element is the transmembrane pressure, $p(s)$, and the output is the vertical velocity of the CP, $v(s)$. The parameter $\gamma(x)$ controls the gain of the activity in the model so that $\gamma(x)=0$ and $\gamma(x)=1$ for a passive and an active model respectively (Neely & Kim, 1986).

$$\frac{v(x,s)}{p(x,s)} \equiv H_{ss}(x,s) = \frac{1}{Z_{CP}^{pass}(x,s) - \gamma(x)Z_{OHC}^{lin}(x,s)} \tag{F.17}$$

In order to construct the state space matrices for a single micromechanical element of the Kanis & de Boer model, the polynomials $\chi_{ss}(s)$ and $\phi_{ss}(s)$ (defined in appendix F.1) must be formed. This is achieved by expanding (F.17) in powers of s and comparing the result to (F.6), to give

$$\begin{aligned}\chi_{ss}(s) &= s^4 + s^3\left[\delta_{sc}\omega_n m_{KB} + c_{KB} - \gamma e_0 d_0 \omega_n\right]/m_{KB} \\ &+ s^2\left[m_{KB}\sigma^2\omega_n^2 + c_{KB}\delta_{sc}\omega_n + k_{KB} - \gamma e_0 d_0 \omega_n^2\right]/m_{KB} \\ &+ s\left[c_{KB}\sigma^2\omega_n^2 + k_{KB}\delta_{sc}\omega_n\right]/m_{KB} + k_{KB}\sigma^2\omega_n^2/m_{KB}\end{aligned} \tag{F.18}$$

and

$$\phi(s) = s^3/m_{KB} + s^2\delta_{sc}\omega_n/m_{KB} + s\sigma^2\omega_n^2/m_{KB} \tag{F.19}$$

The coefficients of these polynomials are listed below by comparison with (F.9) and (F.11), and these parameters can be used to construct the state space matrices **A**, **B**, **C** and **D** as shown in (F.14).

$$\begin{aligned} \alpha_0 &= \frac{\sigma^2\omega_n^2 k_{KB}}{m_{KB}} & \beta_0 &= 0 \\ \alpha_1 &= \frac{\left(k\delta_{sc}\omega_n + \sigma^2\omega_n^2 c_{KB}\right)}{m_{KB}} & \beta_1 &= \frac{\sigma^2\omega_n^2}{m_{KB}} \\ \alpha_2 &= \frac{\left(k_{KB} + \delta_{sc}\omega_n c_{KB} + \sigma^2\omega_n^2 m_{KB} - \gamma e_0 d_0 \omega_n^2\right)}{m_{KB}} & \beta_2 &= \frac{\delta_{sc}\omega_n}{m_{KB}} \\ \alpha_3 &= \frac{\left(c_{KB} + \delta_{sc} m_{KB}\omega_n - \gamma e_0 d_0 \omega_n\right)}{m_{KB}} & \beta_3 &= \frac{1}{m_{KB}} \end{aligned} \tag{F.20}$$

The vertical velocity of the BM, $v(s)$, can be calculated from the state space representation using

$$v(s) = \mathbf{C}\left(s\mathbf{I} - \mathbf{A}\right)^{-1}\mathbf{B}p(s) \tag{F.21}$$

The state space representation for the uncoupled Kanis & de Boer cochlear model is validated by comparing the resulting velocity response, with $s=i\omega$, to that obtain by direct application of the transfer function as shown in Figure F.2. The responses differ by less than 3×10^{-14}dB across a range of stimulus frequencies.

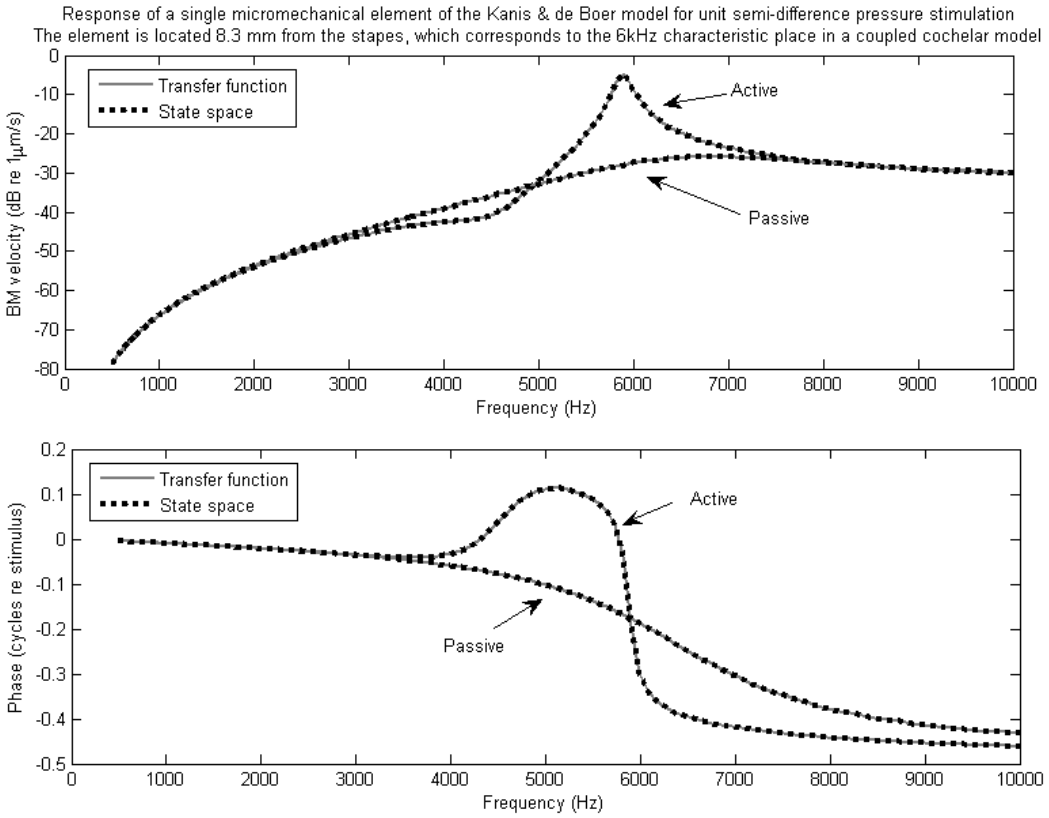

Figure F.2 The response of a single micromechanical element in the Kanis & de Boer cochlear model
The responses is calculated using the conventional method (grey line) and the state space approach (black dotted line).

F.2.2 The stability of the uncoupled Kanis & de Boer model

The eigenvalues, λ, of the system matrix **A** correspond to the poles of the system. The poles are complex such that $\lambda = \sigma + i\omega$, and the system is known to be stable if the real part (σ) of all the poles are negative. Figure F.3 shows the poles for a single micromechanical element in the uncoupled linear active Kanis & de Boer cochlear model, located 8.3 mm from the stapes where the characteristic frequency is 6 kHz. The poles are shown for a variety of gains, γ, as defined in (2.20). Provided that $\gamma \leq 1$, the real parts of these poles are negative which indicates the system is stable. However, when $\gamma > 1.07$ the micromechanical element becomes unstable when stimulated at a frequency close to its characteristic frequency. For example, an unstable pole arises at a frequency of 5.9 kHz when $\gamma = 1.2$ for this single element located at the 6 kHz characteristic place.

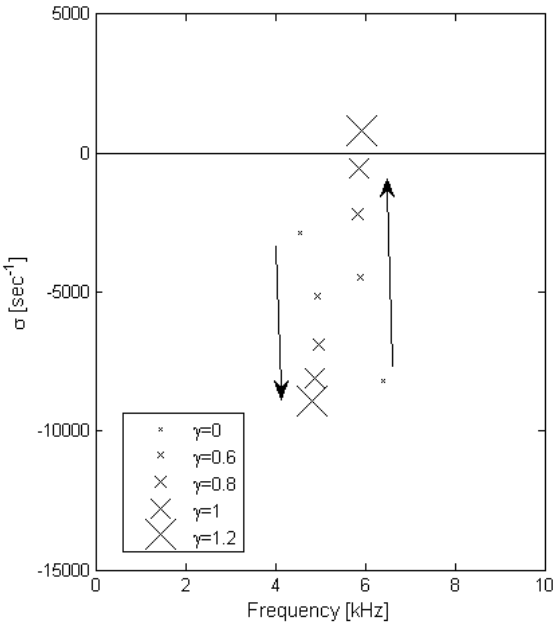

Figure F.3 The poles (×) for a single micromechanical element in the Kanis & de Boer cochlear model
The element is located 8.3mm from the stapes (the 6 kHz characteristic place), for a variety of γ values. The arrows indicate the motion of the poles as γ increases.

F.3 The coupled linear active Kanis & de Boer cochlear model

In this section a state space representation of the linear coupled Kanis & de Boer cochlear model is constructed using the formulation for the uncoupled micromechanical elements (appendix F.2), and the longitudinal fluid coupling method of Elliott *et al.* (2007).

F.3.1 Defining the state space vectors and matrices

For the j^{th} micromechanical element, the state vector for that individual element is shown below, where w_j is the vertical displacement of the BM.

$$\mathbf{w}_j^T = \begin{bmatrix} w_j & \dot{w}_j & \ddot{w}_j & \dddot{w}_j \end{bmatrix} \tag{F.22}$$

The state vector for the complete coupled model is now defined as

$$\mathbf{w}^T(t) = \begin{bmatrix} \mathbf{w}_1^T(t) & \mathbf{w}_2^T(t) & \cdots & \mathbf{w}_N^T(t) \end{bmatrix} \tag{F.23}$$

Each micromechanical element is stimulated by the input to that element $p_j(t)$ and generates a vertical velocity $v_j(t)$. The input and output vectors for the complete model are now defined as

$$\mathbf{p}^T(t) = \begin{bmatrix} p_1(t) & p_2(t) & \cdots & p_N(t) \end{bmatrix} \tag{F.24}$$

$$\mathbf{v}^T(t) = \begin{bmatrix} v_1(t) & v_2(t) & \cdots & v_N(t) \end{bmatrix} \tag{F.25}$$

Elliott *et al.* (2007) explain that, for each micromechanical element, the dynamics can be expressed in state space as

$$\dot{\mathbf{x}}_j(t) = \mathbf{A}_j \mathbf{w}_j(t) + \mathbf{B}_j p_j(t) \tag{F.26}$$

$$v_j(t) = \mathbf{C}_j \mathbf{w}_j(t) \tag{F.27}$$

So that all of the elemental uncoupled state space models can be gathered together in the following matrix equation

$$\dot{\mathbf{w}}(t) = \mathbf{A}_E \mathbf{w}(t) + \mathbf{B}_E \mathbf{p}(t) \tag{F.28}$$

$$\mathbf{v}(t) = \mathbf{C}_E \mathbf{w}(t) \tag{F.29}$$

where

$$\mathbf{A}_E = \begin{bmatrix} \mathbf{A}_1 & 0 & & \vdots \\ 0 & \mathbf{A}_2 & & \vdots \\ \vdots & & \ddots & 0 \\ & \cdots & 0 & \mathbf{A}_N \end{bmatrix}, \mathbf{B}_E = \begin{bmatrix} \mathbf{B}_1 & 0 & & \vdots \\ 0 & \mathbf{B}_2 & & \vdots \\ \vdots & & \ddots & 0 \\ & \cdots & 0 & \mathbf{B}_N \end{bmatrix}, \mathbf{C}_E = \begin{bmatrix} \mathbf{C}_1 & 0 & & \vdots \\ 0 & \mathbf{C}_2 & & \vdots \\ \vdots & & \ddots & 0 \\ & \cdots & 0 & \mathbf{C}_N \end{bmatrix} \tag{F.30}$$

F.3.2 The basal and apical boundaries

Each micromechanical element 1<j< N-1 describes the behaviour of the CP, but j=1 and j=N correspond to the systems representing the stapes footplate and helicotrema fluid respectively. At the stapes,

$$\frac{v_1(s)}{p_1(s)} = H_{ME}(s) = \frac{1}{Z_{ME}(s)} = \frac{s}{s^2 m_{ME} + s c_{ME} + k_{ME}} \tag{F.31}$$

where $u_{st}(s)$ is the stapes velocity, $p_1(s)$ is the pressure difference across the BM at the base of the cochlea, $H_{ME}(s)$ is the middle ear transfer function, Z_{ME}(s) is the middle ear impedance and $m_{ME,}$ c_{ME}, and k_{ME} denote the middle ear mass damping and stiffness respectively.

A state space model for the stapes can be formed from (F.31), as shown below.

$$\dot{\mathbf{w}}_1 = \mathbf{A}_1 \mathbf{w}_1 + \mathbf{B}_1 p_1 \text{ and } v_1 = \mathbf{C}_1 \mathbf{w}_1 \tag{F.32}$$

where

$$\mathbf{A}_1 = \begin{bmatrix} 0 & 1 \\ -k_{ME}/m_{ME} & -c_{ME}/m_{ME} \end{bmatrix}, \mathbf{B}_1 = \begin{bmatrix} 0 \\ 1 \end{bmatrix} \text{ and } \mathbf{C}_1 = \begin{bmatrix} 0 & 1/m_{ME} \end{bmatrix} \tag{F.33}$$

At the helicotrema, the semi-difference pressure is set to zero. Therefore, for simplicity, all the elements of $\mathbf{A}_N$, $\mathbf{B}_N$ and $\mathbf{C}_N$ are set to zero.

F.3.3 The longitudinal fluid coupling

The longitudinal fluid coupling and boundary conditions can be described by the differential equations described in appendix A in finite difference form.

$$\frac{\partial^2 p}{\partial x^2} + \frac{2\rho}{H}\dot{v}(t) = 0 \Rightarrow \frac{p_{n-1}(t) - 2p_n(t) + p_{n+1}(t)}{\Delta^2} + \frac{2\rho}{H}\dot{v}(t) = 0 \tag{F.34}$$

At the base

$$\left.\frac{\partial p(t)}{\partial x}\right|_{x=0} + 2\rho\dot{v}_{out}(t) = -2\rho\dot{v}_{in}(t) \Rightarrow \frac{p_2(t) - p_1(t)}{\Delta} + 2\rho\dot{v}_{out}(t) = -2\rho\dot{v}_{in}(t) \tag{F.35}$$

At the helicotrema

$$p(t)\big|_{x=L} = 0 \Rightarrow p_N(t) = 0 \tag{F.36}$$

These equations can be written in matrix form, in a similar way to that described in appendix B.

$$\mathbf{F}\mathbf{p}(t) - \dot{\mathbf{v}}(t) = \mathbf{q}(t) \tag{F.37}$$

where

$$\mathbf{F} = \frac{H}{2\rho\Delta^2}\begin{bmatrix} \frac{\Delta}{H} & \frac{\Delta}{H} & & & & \\ 1 & -2 & 1 & 0 & & \\ 0 & 1 & -2 & 1 & & \\ & \ddots & \ddots & \ddots & \ddots & 0 \\ & & 0 & 1 & -2 & 1 \\ & & & & 0 & \frac{-2\rho\Delta^2}{H} \end{bmatrix} \text{ and } \mathbf{q} = \begin{bmatrix} \dot{v}_{in}(t) \\ 0 \\ 0 \\ \vdots \\ \vdots \\ 0 \end{bmatrix} \tag{F.38}$$

Assuming matrix **F** is invertible, then (F.37) can be re-written as shown below, where (F.29) has been used to eliminate $\dot{v}(t)$.

$$\mathbf{p}(t) = \mathbf{F}^{-1}\mathbf{q}(t) + \mathbf{F}^{-1}\dot{\mathbf{v}}(t) = \mathbf{F}^{-1}\mathbf{q}(t) + \mathbf{F}^{-1}\mathbf{C}_E\dot{\mathbf{x}}(t) \tag{F.39}$$

Substituting (F.39) into (F.28) now gives

$$\begin{aligned} &\dot{\mathbf{w}}(t) = \mathbf{A}_E\mathbf{w}(t) + \mathbf{B}_E\left(\mathbf{F}^{-1}\mathbf{q}(t) + \mathbf{F}^{-1}\mathbf{C}_E\dot{\mathbf{w}}(t)\right) \\ &\Rightarrow \left(\mathbf{I} - \mathbf{B}_E\mathbf{F}^{-1}\mathbf{C}_E\right)\dot{\mathbf{w}}(t) = \mathbf{A}_E\mathbf{w}(t) + \mathbf{B}_E\mathbf{F}^{-1}\mathbf{q}(t) \\ &\Rightarrow \dot{\mathbf{w}}(t) = \left(\mathbf{I} - \mathbf{B}_E\mathbf{F}^{-1}\mathbf{C}_E\right)^{-1}\mathbf{A}_E\mathbf{w}(t) + \left(\mathbf{I} - \mathbf{B}_E\mathbf{F}^{-1}\mathbf{C}_E\right)^{-1}\mathbf{B}_E\mathbf{F}^{-1}\mathbf{q}(t) \end{aligned} \tag{F.40}$$

Therefore

$$\dot{\mathbf{w}}(t) = \mathbf{A}_{full}\mathbf{w}(t) + \mathbf{B}_{full}\mathbf{u}(t) \tag{F.41}$$

where

$$\mathbf{A}_{full} = \left(\mathbf{I} - \mathbf{B}_E \mathbf{F}^{-1} \mathbf{C}_E\right)^{-1} \mathbf{A}_E \quad \mathbf{B}_{full} = \left(\mathbf{I} - \mathbf{B}_E \mathbf{F}^{-1} \mathbf{C}_E\right)^{-1} \mathbf{B}_E \text{ and } \mathbf{u}(t) = \mathbf{F}^{-1}\mathbf{q}(t) \tag{F.42}$$

The frequency response of the state space system can be obtained by assuming that each element of $\mathbf{w}(t)$ is proportional to $e^{i\omega t}$, so that $\mathbf{w}(t)$ can be written as $\mathbf{w}(\omega)e^{i\omega t}$. It is then possible to solve (F.42) and (F.29) to obtain an estimate of $\mathbf{v}(\omega)$.

$$\begin{aligned} & i\omega\mathbf{w}(\omega) = \mathbf{A}_{full}\mathbf{w}(\omega) + \mathbf{B}_{full}\mathbf{u}(\omega) \\ & \Rightarrow \left(i\omega\mathbf{I} - \mathbf{A}_{full}\right)\mathbf{w}(\omega) = \mathbf{B}_{full}\mathbf{u}(\omega) \\ & \therefore \mathbf{v}(\omega) = \mathbf{C}_E\mathbf{x}(\omega) = \mathbf{C}_E\left(i\omega\mathbf{I} - \mathbf{A}_{full}\right)^{-1}\mathbf{B}_{full}\mathbf{u}(\omega) \end{aligned} \tag{F.43}$$

In practice, the matrices inverted in (F.42) and (F.43) can be *ill-conditioned*, making the calculations susceptible to computational errors. The MATLAB function 'balance' can improve the condition of a matrix. For example, an ill-conditioned matrix $\mathbf{Q}_c$ can be reconstructed by two matrices $\mathbf{Q}_a$ and $\mathbf{Q}_b$ which are better conditioned than $\mathbf{Q}_c$ using the command…

$$\left[\mathbf{Q}_a, \mathbf{Q}_b\right] = \text{balance}\left(\mathbf{Q}_c\right) \tag{F.44}$$

The matrices are related according to $\mathbf{Q}_c = \mathbf{Q}_a\mathbf{Q}_b\mathbf{Q}_a^{-1}$, so that is it possible to use $\mathbf{Q}_a\mathbf{Q}_b^{-1}\mathbf{Q}_a^{-1}$ instead of $\mathbf{Q}_c^{-1}$ to reduce computational error in calculations.

The frequency domain response computed from the state space model is compared to that calculated with the finite difference solution for the coupled linear active Kanis & de Boer model, in Figure F.4. The accuracy of the state space solution is limited in the apical region of the cochlear model for higher frequencies. Numerical errors in the computation process involved in estimating the state space response appear to introduce an effective 'noise floor' approximately 300 dB below the peak BM velocity amplitude. Excluding this region, the responses predicted by the two alternative approaches differ by less than 0.02 dB for these example responses.

F.3.4 The stability of the coupled Kanis & de Boer cochlear model

The stability of the coupled Kanis & de Boer cochlear model can be assessed using the state space formulation. The eigenvalues of the system matrix $\mathbf{A}_{\text{full}}$, correspond to the poles of the system, and the system is known to be stable if the real part of every eigenvalue is negative. In this section we consider the stability of the model for a variety of OHC gain distributions, $\gamma(x)$; A uniform $\gamma(x)$ distribution, a distribution of $\gamma(x)$ resulting from self-suppression in the quasilinear model, and a non-uniform $\gamma(x)$ distribution in which irregularities have been introduced to act as sources of reflection.

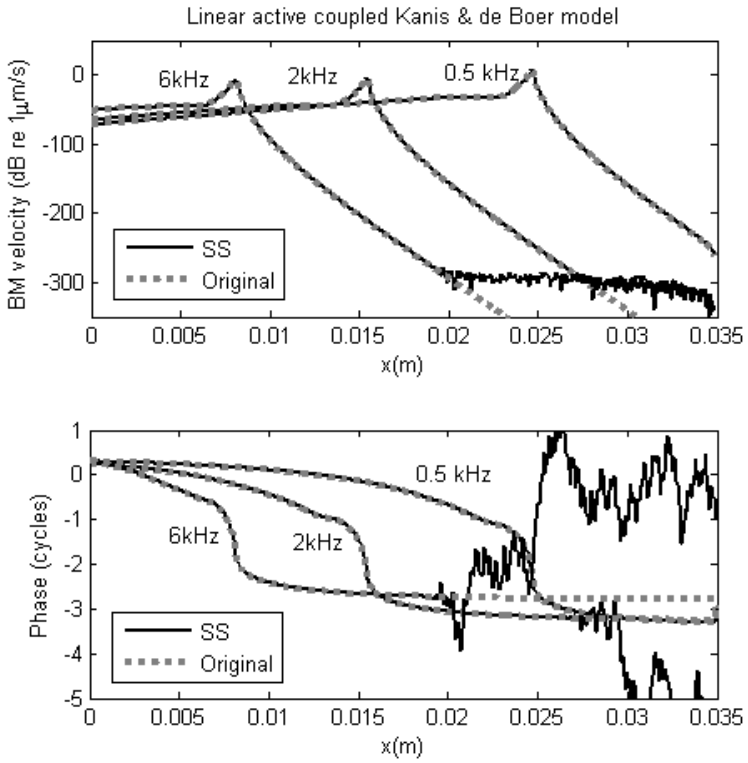

Figure F.4 Comparison of the state space and finite different solutions for the linear active model
The plots show the state space (solid black line) and finite difference (dotted grey line) solutions for the coupled linear active Kanis & de Boer cochlear model

The coupled linear active model

Figure F.5 shows the poles of the coupled model for a variety of uniform OHC gain distributions, γ. The real parts of the poles are plotted as a function of the characteristic frequency, which is proportional to the imaginary component of the pole. Although the results for each γ appear to be a continuous line, they are actually composed of 500 discrete pole positions. In general, the real parts of the all poles are negative for $\gamma \leq 1$. The exceptions to this are two low frequency poles whose real parts become positive when γ exceeds 0.7. This low frequency instability can be eliminated by imposing a maximum $\gamma(x)$ distribution on the model, such as that shown in Figure F.6. In contrast, for values of $\gamma > 1$, the real part of a large number of the poles becomes positive which indicates that the model is unstable.

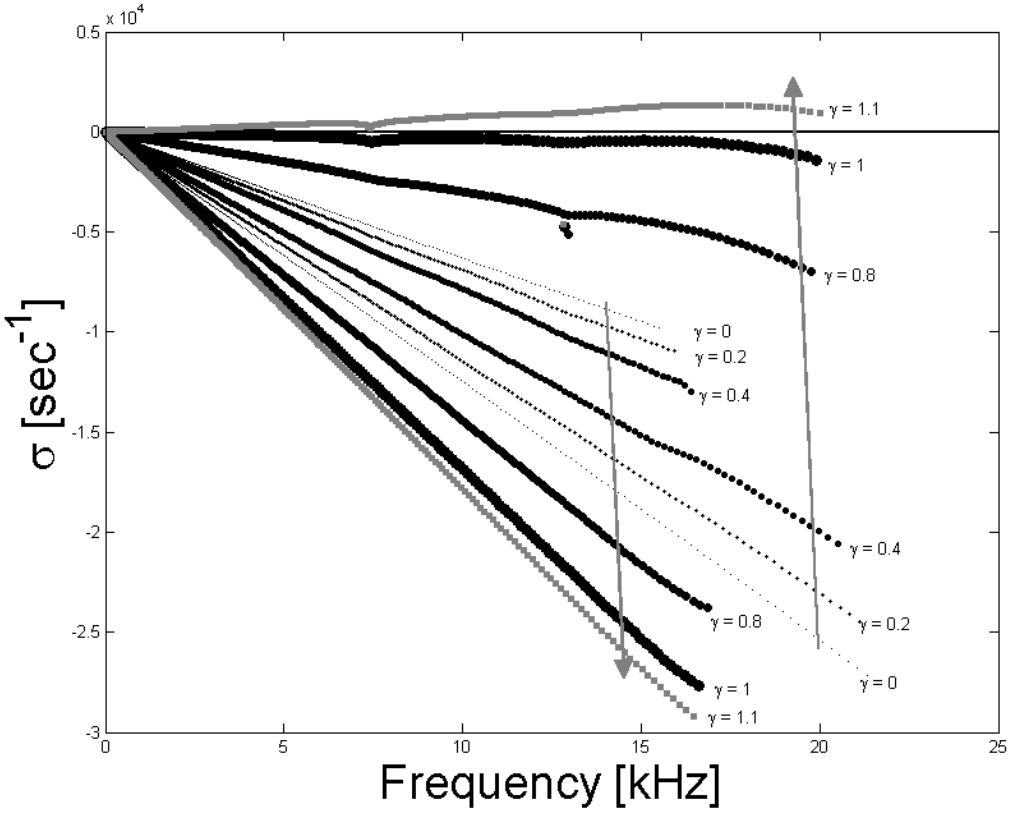

Figure F.5 The influence of OHC gain on the poles of the Kanis & de Boer cochlear model
The poles of the coupled linear active Kanis & de Boer cochlear model are shown for various values of γ(x), where γ(x) is constant along the length of the model. For each γ value, 1000 poles depict the behaviour of the model. The grey arrows indicate the movement of the poles as the value of γ increases.

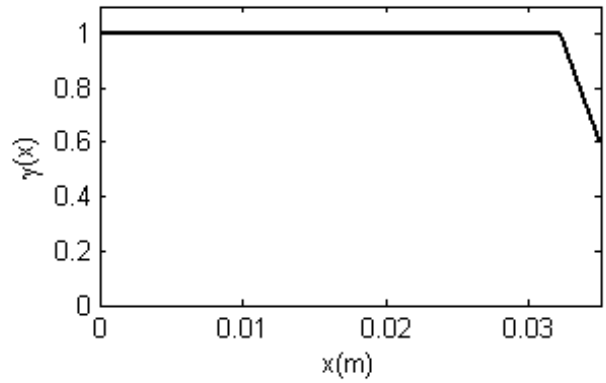

Figure F.6 The baseline distribution of OHC gain
The plot shows a distribution of γ(x) which eliminates instability in the Kanis & de Boer coupled cochlear model at extremely low stimulus frequencies (e.g. 97 and 107 Hz).

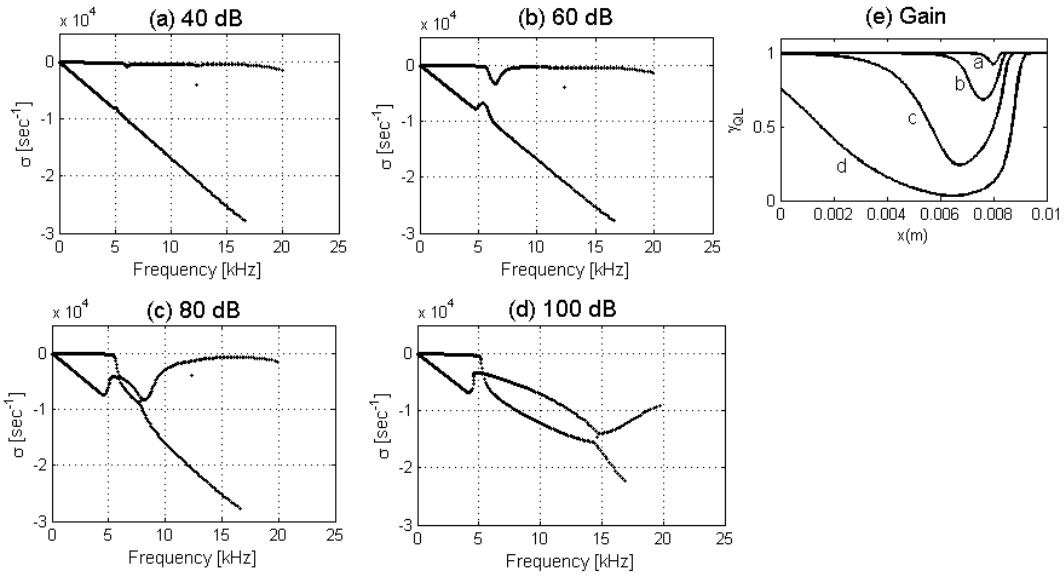

Figure F.7 The poles of the quasilinear Kanis & de Boer cochlear model
(a) to (d): The poles of the coupled linear active Kanis & de Boer state space system matrix, for different $\gamma_{QL}(x)$ distributions evoked by a 6 kHz stimulus applied at different stimulus levels (in units of dB re 10^{-8}m/s). The $\gamma_{QL}(x)$ distributions were obtained using the quasilinear method described in appendix E, and are shown in (e).

The coupled quasilinear model

The state space model can be used to predict the stability of the quasilinear coupled system, in which variations in OHC gain, $\gamma_{QL}(x)$, arise due to self-suppression. For example, Figure F.7 shows the poles of the linear active Kanis & de Boer state space model, for a variety of $\gamma_{QL}(x)$ distributions which correspond to a range of stimulus levels. These graphs illustrate that the real part of the pole (σ) varies as the stimulus level increases, but that the model remains stable as σ remains negative for all of the poles provided that the maximum gain distribution shown in Figure F.6 is imposed.

The coupled linear model with random gain irregularities

The state space model can be used to predict the stability of the linear coupled system, where variations in OHC gain, $\gamma(x)$, are deliberately introduced to act as sources of reflection. For example, in section 2.5.2, the linear active Kanis & de Boer cochlear model was found to become unstable if $\gamma(x)$ either steps-up by 0.5 or steps-down by 0.05. Non-uniform variation in $\gamma(x)$ can be introduced using the MATLAB formula

$$\gamma(x) = 1 + \frac{\nu}{2} - \nu \cdot \text{smooth}[\varepsilon(x)] \tag{F.45}$$

where $\varepsilon(x)$ is a distribution of numbers with values between 0 and 1 produced by the MATLAB random number generator and ν is the magnitude of the gain variations. The average value of $\gamma(x)$, along the length of the cochlear partition, remains unchanged by the introduction of random variations. However, the local value of $\gamma(x)$ does exceed 1 at some locations. The poles for the

coupled model containing this non-uniform distribution of $\gamma(x)$ are shown in Figure F.8. Random variations in the gain of up to 7% can be accommodated before the model becomes unstable.

F.4 Comparing two micromechanical models

Kanis & de Boer (1993) comment that their micromechanical cochlear model is similar to, but simplier than, the micromechanical model of Neely & Kim (1986). However, it is difficult to determine the relationship between the two models, as the dynamic components of the active impedance are not explicitly expressed in the Kanis & de Boer model. By casting both *uncoupled* models into the frequency domain state space framework, however, it is possible to compare the matrix elements and establish a relationship between the micromechanical parameters.

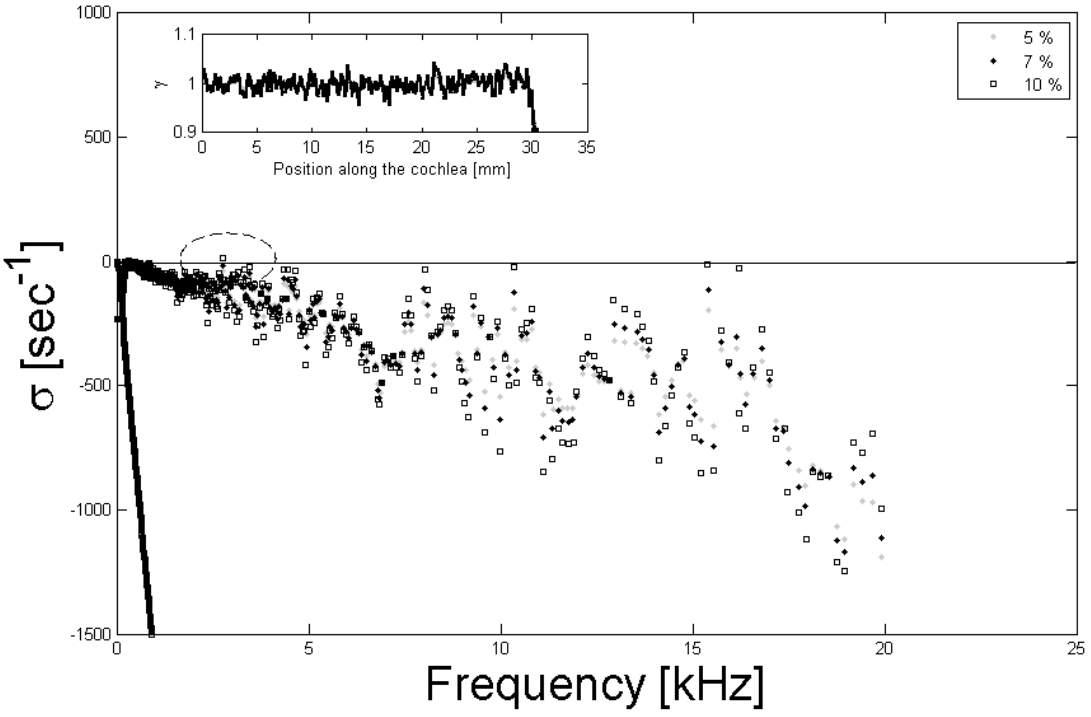

Figure F.8 The poles of the perturbed linear active Kanis & de Boer cochlear model
The plot shows the poles of the linear active Kanis & de Boer model, with a non-uniform distribution of the OHC gain γ. The dashed circle indicates a pole for which the real part is positive.

The state space representation of the Neely & Kim micromechanical model was developed by Elliott *et al.* (2007) from the equations of motion. If the Neely & Kim micromechanical model is re-cast into state space formulation using the system transfer function, so that the results are comparable with those previously obtained for the Kanis & de Boer cochlear model (appendix F.2), then the state space vector takes the form $\mathbf{x}^T = \begin{bmatrix} z_1 & \dot{z}_1 & \ddot{z}_1 & \dddot{z}_1 \end{bmatrix}$ and the state space matrices are given by

$$A = \begin{bmatrix} 0 & 1 & 0 & \cdots & 0 \\ 0 & 0 & 1 & & 0 \\ \vdots & & & \ddots & 0 \\ \vdots & & & & 1 \\ -\alpha_0 & -\alpha_1 & \cdots & \cdots & -\alpha_{n-1} \end{bmatrix}, B = \begin{bmatrix} 0 \\ 0 \\ \vdots \\ 0 \\ 1 \end{bmatrix}, \; C = \begin{bmatrix} \beta_0 & \beta_1 & \cdots & \cdots & \beta_{n-1} \end{bmatrix}, \text{and } D = 0 \tag{F.46}$$

where, in this case,

$$\begin{aligned} \alpha_0 &= \frac{k_1\left(k_2+k_3\right)+k_2k_3-\gamma k_2k_4}{m_1m_2} & \beta_0 &= 0 \\ \alpha_1 &= \frac{c_1\left(k_2+k_3\right)+k_1\left(c_2+c_3\right)+k_2c_3+c_2k_3-\gamma\left(k_2c_4+c_2k_4\right)}{m_1m_2} & \beta_1 &= \frac{b\left(k_2+k_3\right)}{m_1m_2} \\ \alpha_2 &= \frac{m_1\left(k_2+k_3\right)+c_1\left(c_2+c_3\right)+m_2\left(k_1+k_3\right)+c_2c_3-\gamma\left(m_2k_4+c_2c_4\right)}{m_1m_2} & \beta_2 &= \frac{b\left(c_2+c_3\right)}{m_1m_2} \\ \alpha_3 &= \frac{m_1\left(c_2+c_3\right)+m_2\left(c_1+c_3\right)-\gamma m_2c_4}{m_1m_2} & \beta_3 &= \frac{b}{m_1} \end{aligned} \tag{F.47}$$

Comparing the α and β coefficients in (F.20) with those given in (F.47), allows the Kanis & de Boer cochlear model to be re-written in the formulation used by Neely & Kim using the relationships given in Table F.1.

Origin of relationship	Relationship
In order to balance the γ terms when equating the α_0 and α_1 coefficients, it is assumed that…	$k_2 = 0 \;\&\; c_2 = 0$
Equating β_3 coefficients:	$m_1 = bm_{KB}$
Equating β_1 coefficients:	$\frac{k_3}{m_2} = \sigma^2\omega_n^2$
Equating β_2 coefficients:	$\frac{c_3}{m_2} = \delta_{sc}\omega_n$
Equating α_0 coefficients:	$k_1 = bk_{KB}$
Equating α_1 coefficients:	$c_1 = bc_{KB}$
Equating α_3 coefficient γ terms:	$c_4 = be_0d_0\omega_n$
Equating α_2 coefficient γ terms:	$k_4 = e_0d_0b\omega_n^2$

Table F.1 The relationship between the micromechanical parameters or Kanis & de Boer and Neely & Kim models

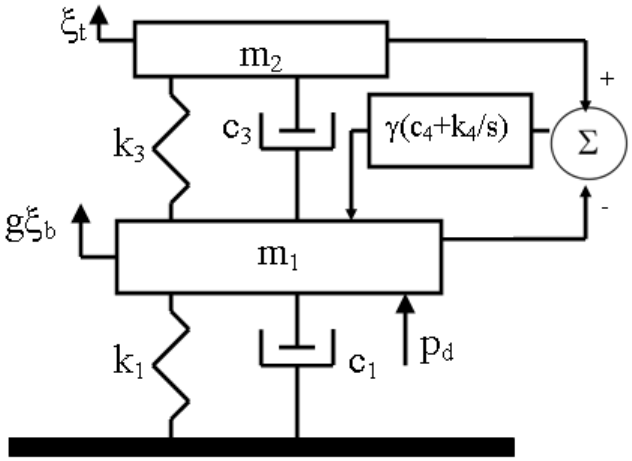

Figure F.9 The micromechanical model of Kanis & de Boer
The plot is based on figure 2.1 of Ku (2008) and the micromechanical parameters (k_1, c_1, m_1, m_2, k_3, c_3, k_4, c_4) are defined in terms of the original Kanis & de Boer parameters in Table F.1. The vertical displacement of the BM and the radial displacement of the tectorial membrane are denoted by ξ_b and ξ_t respectively. The gain between the organ of Corti and the reticular laminar, g, is set equal to 1 (Neely & Kim, 1986). In addition, $s=i\omega$, where ω is the angular frequency of the stimulus.

Using these relationships, the Kanis & de Boer micromechanical model could be represented by a block diagram as shown in Figure F.9. It is not possible to explicitly specify the parameters m_2, c_3 and k_3 in terms of the Kanis & de Boer micromechanical quanities. Therefore we assign $m_2(x)$ a small, constant value throughout the length of the CP (1×10^{-5} kgm-^{2}) and use the equations in Table F.1 to calculate the resultant values of c_3 and k_3.

The response of a linear active cochlear model, using the micromechanics of Kanis & de Boer, is not dependent on which formulation is used. For example, the predicted response is the same for the original Kanis & de Boer model as it is when for the Neely & Kim model modified to incorporate the micromechanics of Kanis & de Boer. However, care must be taken when considering nonlinear models, as the input to the nonlinearity representing the action of the OHCs differs between the formulations as described in appendix E.5.

F.5 A time domain solution for a nonlinear model

Elliott *et al.* (2007) describe a state space formulation of the Neely & Kim (1986) cochlear model. They illustrate how the model can be adapted to incorporate a nonlinear function to represent the action of the OHCs, and use a MATLAB ordinary differential equation solver, ode45, to obtain the time domain response of the system using an iterative method. The steady state response predicted by this time domain state space method, can be compared with the estimated response obtained used the quasilinear method.

The MATLAB program used to obtain the time domain state space solution for the nonlinear cochlear model was provided by Ku (2008). It was modified so that the micromechanical parameters equated to those used by Kanis & de Boer, using the relationships given in Table F.1. A hyperbolic tangent function was used to represent the nonlinear action of the OHCs. The micromechanical feedback loop was arranged so that the nonlinearity is positioned before the filter describing the dynamics of the OHCs, and the input to the OHCs is determined by the difference in shear displacement between the tectorial membrane and the BM.

The steady state response of the state space model is compared to the estimated quasilinear response in section 2.5. Discrepancies may occur between the two predictions if the quasilinear approximation is invalid. However, differences may also arise due to errors in the state space response. These inaccuracies predominantly arise due to the failure of the model to reach a steady state at all locations with the observation time, and the effect of time windowing in the analysis of the response. Use of longer observation times allows both of these errors to be minimised, but requires significantly longer computational time.

For example, when the state space model is stimulated by a 6 kHz stimulus tone, a 2.4 GHz computer requires approximately 4 to 7 hours to evaluate the first 30 ms of the response depending on the stimulus level. We assume that the response has reached steady state within the 30 ms observation period. However, this is not necessarily true at all locations for all components. For example, Figure F.10 shows the amplitude of the fundamental and 3rd harmonic components of the state space response to a 6 kHz stimulus presented at 60 dB at two different locations within the cochlear model. The characteristic place, 8 mm from the stapes, both the fundamental and 3rd harmonic components appear to have reached a steady state within 30 ms. However at a more basal location, 2 mm from the stapes, the amplitude of the 3rd harmonic component does not reach a steady state within the 30 ms observation time. Therefore the harmonic response predicted by the state space model is likely to be erroneous at the basal location unless a longer observation period is employed. However, at the locations where steady state is not achieved within the observation period, the amplitude of the harmonic components is very small (< -100 dB) relative to the fundamental component. For this reason, despite the limitations, the observation time is not generally extended beyond 30 or 40 ms.

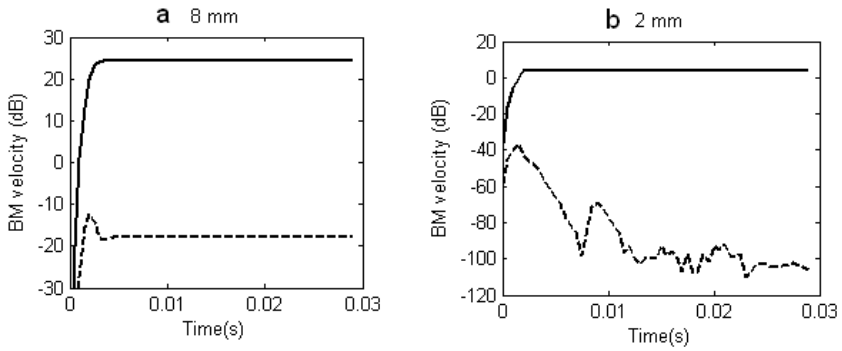

Figure F.10 The change over time of the fundamental and harmonic components of the state space time domain model

The plot shows the fundamental (solid line) and 3rd harmonic (dashed line) components of the response of state space model to a 6 kHz stimulus tone presented at 60 dB re 10^{-16} $m^{-2}s^{-1}$ in the ear canal. The amplitude of the components is observed at two different locations (a) the characteristic place for 6 kHz (8 mm from the stapes) and (b) a location basal to the characteristic place (2 mm from the stapes).

G Asymmetric and symmetric nonlinear functions

G.1 The harmonic components predicted by a nonlinear function

The hyperbolic tangent function is symmetric so that, for an input *u*, it satisfies the relation (G.1) as illustrated in Figure G.1. The first order Boltzmann function is not symmetric as it does not satisfy this relation.

$$\tanh(-u) = -\tanh(u) \tag{G.1}$$

To demonstrate that no even-order harmonics are produced by a symmetric nonlinear function acting on a sinusoidal input, consider the input $x(t) = A\cos(\omega t)$ The nonlinear function *F*, acts on this input to produce the Fourier components X_k defined in (G.2).

$$\begin{aligned} X_k &= \frac{1}{T}\int_{-T/2}^{T/2} F\left[x(t)\right]\cdot\exp(-i2\pi kt/T)dt \\ &= \frac{1}{T}\int_{-T/2}^{0} F\left[x(t)\right]\exp(-i2\pi kt/T)\ \mathrm{dt} + \frac{1}{T}\int_{0}^{T/2} F[x(t)]\exp(-i2\pi kt/T)\ \mathrm{dt} \end{aligned} \tag{G.2}$$

Substituting $t' = t + T/2$ into the first term gives

$$\begin{aligned} X_k &= \frac{1}{T}\int_{0}^{T/2} F\left[x(t'-T/2)\right]\exp(-i2\pi kt/T)\exp\left(i\pi k\right)\ \mathrm{dt}' \\ &\quad + \frac{1}{T}\int_{0}^{T/2} F[x(t)]\exp(-i2\pi kt/T)\ \mathrm{dt} \end{aligned} \tag{G.3}$$

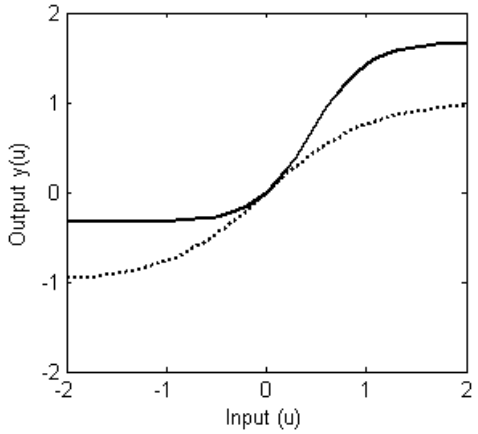

Figure G.1 Illustrations of a first order Boltzmann function
The two lines denote β=5 (solid line), and a hyperbolic tangent function (dotted line).

The cosine nature of $x(t)$ means that $x(t+T/2)=-x(t)$ (Bostock & Chandler, 1990), and so the output of the symmetric nonlinearity becomes $F[x(t-T/2)]=F[-x(t)]=-F[x(t)]$. Therefore

$$X_k=\frac{1}{T}\left(1-\exp\left(i\pi k\right)\right)\int_0^{T/2}F\left[x(t)\right]\exp(-i2\pi kt/T)\ \mathrm{dt} \qquad \text{(G. 4)}$$

This indicates that whenever k=2n, where n is an integer, X_k will equal zero and so no even-order harmonic components can be generated.

G.2 Parameters for the first order Boltzmann function

Figure G.2 shows examples of the OHC response functions measured in the ear of a Bullfrog, a mouse, and another mammal (Pickles, 1982; Dallos, 1996) together with a first order Boltzmann function. In each case, the α and β parameters of the Boltzmann function have been adjusted to match the physiological measurements using trial an error. The use of the first order Boltzmann function should be treated with caution in these cases, because the input and output variables shown in Figure G.2 have different units, but the Boltzmann function was defined in section 3.1.1 in such a manner that the input and output variables are expected to have the same dimensions. For this reason we do not attempt to estimate the value of α, the parameter which determines the amplitude of the Boltzmann function, from these graphs. However, it is interesting to note that the dimensionless Boltzmann function parameter β takes a value between 4 and 5 in each of the cases shown in Figure G.2. Overall, it is likely that β could assume any value from 1 up to about 5, as the smaller value of 1.7 used by Cooper (1998) was useful in modelling the uncoupled response of the guinea pig cochlea.

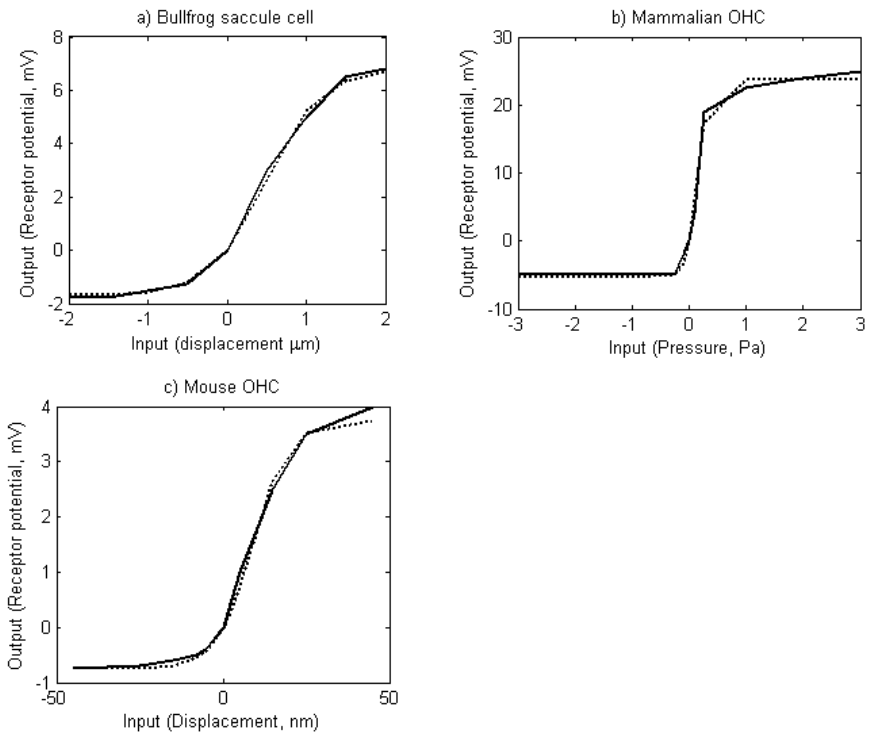

Figure G.2 OHC input-output functions
The plots show Boltzmann functions (dotted lines) fitted subjectively to experimental transfer functions (solid lines) for outer hair cells (OHCs) of a) A Bullfrog (Data from Hudspeth & Corey 1977, cited in Pickles, 1982) using Boltzmann constants α=8.5, β=4 and γ=0.35, b) A Mammalian OHC (Dallos, 1996) using Boltzmann constants α=29,β=4.5 and γ=0.09, c) A Mouse OHC (Data from ~Russell, Cody & Richardson (1986), cited in Dallos, 1996) using α=4.5, β=5 and γ=5.5.

H How *et al.* (2010)

The text, figures and simulations presented in this journal letter were developed by myself.

Guidance and editorial assistance were provided by S J Elliott and B Lineton

The influence on predicted harmonic and distortion product generation of the position of the nonlinearity within cochlear micromechanical models (L)

Jacqueline A. How,[a] Stephen J. Elliott, and Ben Lineton
Institute of Sound and Vibration Research, University of Southampton, Southampton, Hampshire SO17 1BJ, United Kingdom

(Received 8 October 2009; revised 27 November 2009; accepted 7 December 2009)

Numerical techniques are used to explore the influence on the predicted basilar membrane (BM) response of the position of the nonlinearity within the micromechanical feedback loop of an active nonlinear cochlear model. This position is found to influence both the harmonic and distortion product spectra of the predicted BM response. The BM motion at the fundamental or primary frequencies is not significantly altered by the position of the nonlinearity, however, provided that the gain is appropriately adjusted. The observed effects are explained in terms of the frequency responses of the elements within the micromechanical feedback loop.
 [DOI: 10.1121/1.3279812]

PACS number(s): 43.64.Kc, 43.64.Bt, 43.64.Jb [BLM] Pages: 652–655

I. INTRODUCTION

Discrete models of the cochlea have been used extensively to describe and investigate the mechanics of the cochlea (Neely and Kim, 1986; Viergever and de Boer, 1987; Kanis and de Boer, 1993; Ku, 2008). In a linear active variant of this model, each micromechanical element can be described by a feedback diagram, as shown in Fig. 1(a) (Neely, 1985), where p_{OHC}^{in} is the pressure arising from the active outer hair cells (OHCs) and is assumed to act in the same way on the basilar membrane (BM) as the transmembrane pressure difference p.

Filter 1 corresponds to the passive mechanical admittance of the BM. Filter 2 is a simplified representation of the impedance of the active OHC complex, incorporating the many factors that contribute to the action of the OHCs, including linear components of the mechanoelectrical and electromechanical transduction processes associated with the cells. For example, filter 2 may encompass contributions from hair bundle motility (Martin and Hudspeth, 1999), processes within the OHC (Santos-Sacchi, 1989), extra-cellular processes, such as resonance of the tectorial membrane (TM) and stereocilia (Kanis and de Boer, 1993), and frequency-dependent phase shifts between the OHC pressure output and the radial displacement of the BM and TM (Neely and Kim, 1986). A nonlinearity, attributed to the OHC transduction process, can be positioned either *before* (Cooper, 1998) or *after* (Kanis and de Boer 1993) filter 2, as shown in Figs. 1(b) and 1(c), respectively. In other physical systems, such as chemical and thermodynamic processes, the position of the nonlinearity within a model is known to influence the predicted results (Aguirre *et al.*, 2005). As this effect has yet to be examined for cochlear models, we use numerical modeling to investigate the effect on the predicted BM response of changing the position of the nonlinearity within the micromechanical feedback loop. This is initially achieved by predicting the fundamental and low order harmonic components of the BM displacement evoked by single tone stimulation of the model. In addition, the influence on distortion products (DPs) arising from two tone excitation of the alternative micromechanical arrangements is also quantified.

II. MODEL AND METHOD

A discrete long-wave cochlear model is used, where the longitudinal coupling is mediated by the cochlear fluid and 1000 micromechanical elements are used to represent the 35 mm length of the human cochlea. The assumed passive admittance of the BM (filter 1) and the dynamics of the OHC complex (filter 2) correspond to those suggested by Kanis and de Boer (1993) for a human cochlear model. The frequency response functions for the filters, observed at the 4 kHz characteristic place in the cochlear model, are shown in Fig. 2. Details of the boundary conditions and the two port model used to represent the ear canal and middle ear are described by Elliott *et al.* (2007) and Ku (2008).

The nonlinearity within each micromechanical element is assumed to be a first order Boltzmann function (Cooper, 1998), defined as follows:

$$f(u) = \frac{\alpha}{\eta}\left(\frac{1}{1+\beta e^{-\eta u/\gamma}} - \frac{1}{1+\beta}\right). \quad (1)$$

The value of α, which determines the maximum output of the nonlinearity and has the same dimensions as the input u, increases from base to apex so that the coupled model exhibits a compression knee-point at 30 dB sound pressure level (SPL) for frequencies between 0.5 and 6 kHz. The spatial distribution of α differs between the two alternative micromechanical arrangements to ensure that this assumed condition is satisfied in both cases. The dimensionless constant η is assigned a value of either 2.5×10^{10} or 1, when the nonlinearity is positioned either before or after filter 2, respec-

[a]Author to whom correspondence should be addressed. Electronic mail: jh@isvr.soton.ac.uk

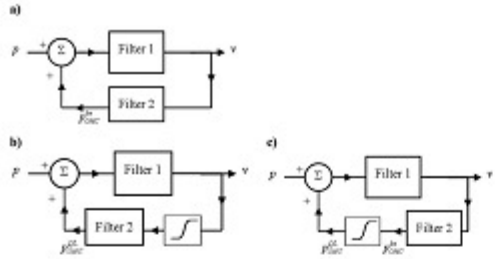

FIG. 1. Block diagrams representing the micromechanical feedback loop within each element of the discrete cochlear model. Examples of (a) a linear active model and [(b) and (c)] two alternative active nonlinear models are shown. The pressure difference across the BM and the BM velocity are denoted by p and v in each diagram. The linear pressure output and the quasilinear pressure output of the OHCs are represented by p_{OHC}^{lin} and p_{OHC}^{qu}, respectively. Filters 1 and 2 represent the passive admittance of the basilar membrane and the impedance of the OHC complex, respectively.

tively, to compensate for the change in the units of the input to the nonlinearity. The dimensionless constant β controls the asymmetry of the function and is set equal to 1.2. The value of γ, which has the same dimensions as the input, is selected so that the nonlinearity provides 0 dB gain to the fundamental component at low stimulus levels. The parameters β and γ influence the amplitude of even- and odd-order

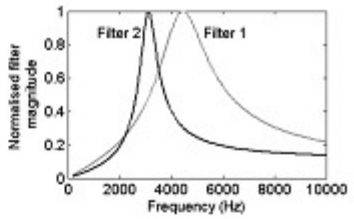

FIG. 2. Assumed frequency response functions for filters 1 and 2, associated with the passive BM admittance and the impedance of OHC complex, respectively, observed at the 4 kHz characteristic place in the cochlear model.

harmonic components of the nonlinear output, respectively (Cooper, 1998).

The fundamental response of the model is estimated using an iterative, quasilinear method devised by Kanis and de Boer (1993). This approach, with modifications described in the online appendix to improve the convergence, was also applied to estimate harmonic components and DPs.

III. RESULTS

A. Single tone excitation

For single tone stimulus levels of 60 and 80 dB SPL between 1 and 7 kHz, the fundamental component of the

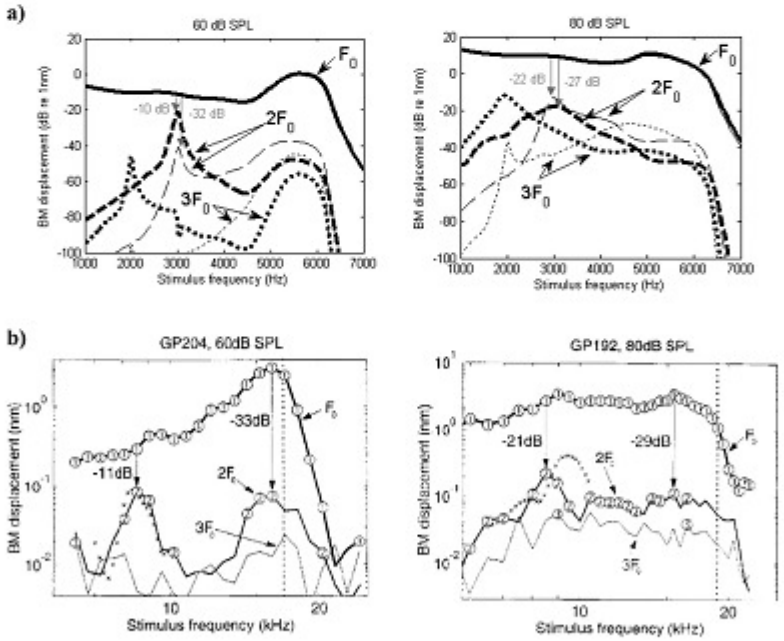

FIG. 3. (a) The predicted spectra of BM displacement evoked by single stimulus tones at the fundamental (solid line), second harmonic (dashed line), and third harmonic (dotted line) frequencies, observed at a distance of 81 mm from the stapes, which corresponds to the 6 kHz characteristic place. The results are shown for two cochlear models: one where the nonlinear is positioned before filter 2 (thick lines), and one where the nonlinearity is positioned after filter 2 (thin lines). Stimulus levels of 60 and 80 dB SPL have been used. (b) The observations of Cooper (1998) of the BM displacement response to single tone stimuli in the guinea pig cochlea at the 17–19 kHz characteristic place, used with permission. The crosses indicate the fundamental responses to low level stimuli and can be neglected when comparing (a) and (b).

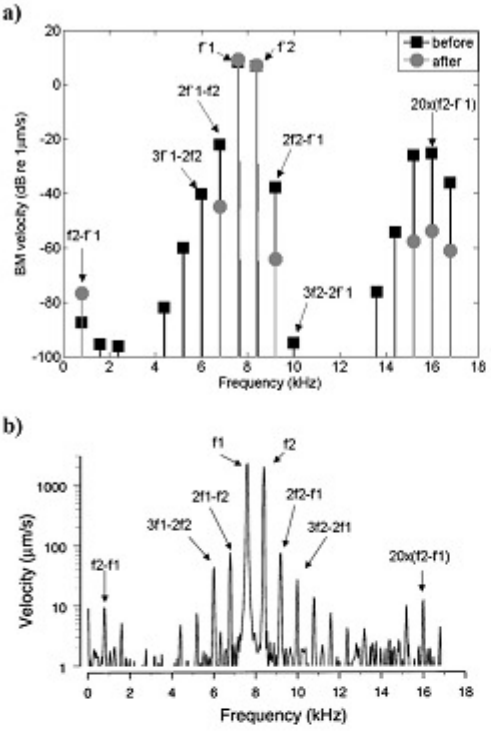

FIG. 4. (a) The predicted spectrum of the BM velocity at the f_2 characteristic place in the cochlear model ($L_1=L_2=70$ dB SPL) with the nonlinearity positioned before (squares) or after (circles) filter 2, and (b) the physiological measurement of Robles *et al.* (1997) at the 8 kHz characteristic place in the chinchilla cochlea ($L_1=L_2=80$ dB SPL), used with permission. In both cases, stimuli were presented at $f_1=7.6$ kHz and $f_2=8.4$ kHz.

predicted BM displacement differs by less than 5 dB between the two micromechanical arrangements [Fig. 3(a)]. However, the amplitude of the estimated harmonic components is significantly influenced by the position of the nonlinearity within the micromechanical feedback loop. For example, the relative amplitude of the predicted fundamental and second harmonic responses to a 3 kHz tone at 60 dB SPL decreases by 22 dB, from −10 to −32 dB relative to the fundamental response, when the nonlinearity is moved from before to after filter 2.

B. Two tone stimulation

When two tones with frequencies f_1 and f_2 are presented simultaneously to the model, DPs are predicted in the BM response, as shown in Fig. 4(a). The amplitude of the predicted $2f_1-f_2$ and $2f_2-f_1$ DPs is decreased by 23 and 26 dB, respectively, when the nonlinearity is moved from before to after filter 2. In contrast, the predicted BM velocity at the primary frequencies does not change by more than 2 dB for the same change in position.

IV. DISCUSSION AND CONCLUSIONS

The simulations of pure tone responses are compared to the experimental results obtained by Cooper (1998) from a guinea pig cochlea shown in Fig. 3(b). There are amplitude differences between the simulations and the physiological observations. These differences may arise because the assumed middle ear response of the model differs from that of the guinea pig, resulting in different effective stimulus levels, or because the parameters of the model are primarily adjusted to replicate the response of the human cochlea. However, it is interesting to note that the relative difference between the amplitude of the fundamental and second harmonic responses to a 60 dB stimulus observed by Cooper (1998) is 11 dB when the second harmonic frequency is approximately equal to the best frequency of the observation location, and that this is best replicated by the model when the nonlinearity is positioned before, rather than after, filter 2. The position of the nonlinearity within the micromechanical feedback loop does not have a substantial effect on the fundamental response. The micromechanical arrangement affects the harmonic response because the impedance of the OHC complex, represented by filter 2 in Fig. 1, is frequency dependent (Fig. 2). For example, when considering the effect of the feedback loop on the second harmonic response, the signal of most interest is at the fundamental frequency f_0 before the nonlinearity, but changes to $2f_0$ in the nonlinearity's output. Therefore if the nonlinearity is positioned before filter 2, filter 2 operates on a signal at frequency $2f_0$, but if the nonlinearity is positioned after filter 2, then filter 2 acts on a signal at frequency f_0. The extent to which the position of the nonlinearity influences the harmonic responses is thus expected to depend on the nature of the impedance used in the model to represent the OHC complex.

The frequency dependence of filter 2 is also responsible for the influence of the position of the nonlinearity on the predicted DP amplitudes since it acts on either the DP frequency, or the primary frequencies individually, when the nonlinearity is placed either before or after filter 2, respectively. For example, Robles *et al.* (1997) found that the amplitude of the $2f_1-f_2$ DP is approximately 28 dB below the amplitude of the primary frequencies in their observation of the chinchilla cochlea shown in Fig. 4(b). The simulation uses a lower stimulus level than the physiological measurement in order to achieve a similar degree of saturation, as a consequence of the middle ear differences. The relative amplitude of the predicted $2f_1-f_2$ DP to the primaries decreases from −31 to −54 dB when the nonlinearity is moved from before to after filter 2, and so the former model again appears to be most consistent with the measured data. Despite the considerable effect on the DPs, the amplitudes of the primary responses are not altered significantly by the placement of the nonlinearity.

In summary, the position of the nonlinearity within the micromechanical feedback loop can substantially affect simulations of harmonic responses and distortion products, without significantly influencing the fundamental response if the gain is adjusted appropriately. The extent of this effect will depend on the form of the cochlear model used in the

simulations, as it is attributed to the assumed frequency dependence of the impedance attributed to the OHC complex.

Aguirre, L. A., Coelho, M. C. S., and Correa, M. V. (**2005**). "On the interpretation and practice of dynamical differences between Hammerstein and Wiener models," IEE Proc.: Control Theory Appl. **152**, 349–356.

Cooper, N. P. (**1998**). "Harmonic distortion on the basilar membrane in the basal turn of the guinea-pig cochlea," J. Physiol. (London) **509**, 277–288.

Elliott, S. J., Ku, E. M., and Lineton, B. (**2007**). "A state space model for cochlear mechanics," J. Acoust. Soc. Am. **122**, 2759–2771.

Kanis, L., and de Boer, E. (**1993**). "Self-suppression in a locally active nonlinear model of the cochlea: A quasilinear approach," J. Acoust. Soc. Am. **94**, 3199–3206.

Ku, E. M. (**2008**). "Modelling the human cochlea," Ph.D. thesis, University of Southampton, United Kingdom.

Martin, P., and Hudspeth, A. J. (**1999**). "Active hair-bundle movements can amplify a hair cell's response to oscillatory mechanical stimuli," Proc. Natl. Acad. Sci. U.S.A. **96**, 14306–14311.

Neely, S. T. (**1985**). "Mathematical modelling of cochlear mechanics," J. Acoust. Soc. Am. **78**, 345–352.

Neely, S. T., and Kim, D. O. (**1986**). "A model for active elements in cochlear biomechanics," J. Acoust. Soc. Am. **79**, 1472–1480.

Robles, L., Ruggero, M. A., and Rich, N. C. (**1997**). "Two-tone distortion on the basilar membrane of the chinchilla cochlea," J. Neurophysiol. **77**, 2385–2399.

Santos-Sacchi, J. (**1989**). "Asymmetry in voltage-dependent movements of isolated outer hair cells from the organ of Corti," J. Neurosci. **9**, 2954–2962.

Viergever, M. A., and de Boer, E. (**1987**). "Matching impedance of a non-uniform transmission line: Application to cochlear modelling," J. Acoust. Soc. Am. **81**, 184–186.

I The He *et al.* experiment

The He *et al*. experiment is described in section 5.2.2, and was designed to determine the direction of the $2f_1 - f_2$ DP travelling wave evoked by two tone stimulation of the gerbil cochlea.

The first stage of the experiment recorded measurements at two internal locations, following single tone stimulation of the cochlea via a tone presented in the ear canal. The results are shown in Figure I.1. The experiment was simulated on the cochlear model, and the predicted results are displayed in Figure I.2. Although only one stimulus level (40 dB SPL) is shown in the simulation for simplicity, similar results were obtained using higher levels. The simulation and physiological result of He *et al.* are not quantitatively similar because of animal differences and differences in observation location. The observation sites for the simulation were positioned distances of 10.5 and 11.3 mm from the stapes. The characteristic frequencies of these sites are 4 and 3.5 kHz respectively. They were selected so that it would be possible to detect a backward travelling wave in the two tone experiment using the range of frequencies over which the model predictions of distortion products appears to be strongest (f_2 between 1 and 4 kHz).

The results of the simulation and experimental study, using a single tone stimulus, are qualitatively similar in several ways. For example, both the model simulation and physiological study exhibit peaks in the frequency response of the two locations (A and C) at the “best” frequency. Both cases also demonstrate that the response amplitude reduces as the stimulus frequency deviates from the best frequency, but the effect is asymmetric and the fall-off in amplitude is more rapid when the stimulus frequency increases above the best frequency compared to decreases in stimulus frequency. In Figure I.1.and Figure I.2, the phase lag at the observation sites increases as the stimulus frequency increases (B and D). In the model, the phase lag at each site is essentially the same other than at frequencies close to the best frequency of each place and so the estimates of phase difference, delay, group velocity at travelling wave wavelength (E, F, G and H) are only meaningful for stimulus frequencies between approximately 2.5 and 4 kHz. For this frequency range, increases in stimulus frequency tend to increase the phase difference, delay and travelling wave wavelength between the observation sites calculated for both the model simulation and the experimental results. In addition, the travelling wave velocity between the observation sites increases with stimulus frequency in both cases. These qualitative similarities between the model predictions and experimental outcomes of the single tone He *et al.* experiment lead us to conclude that the model could provide useful insight into the two tone He *et al.* experiment.

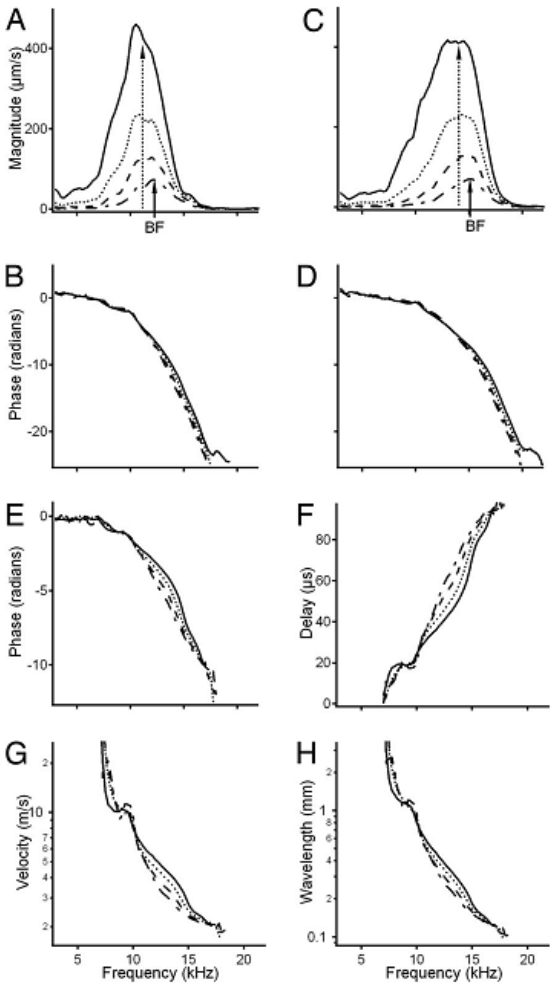

Figure I.1 The He *et al.* single tone stimulus experimental measurements

The BM velocity at locations 1 and 2 following presentation of single tones (at frequency f_0) in the ear canal at levels of 40, 50, 60 and 70 dB SPL indicated by dash-dot, dashed, dotted and solid lines respectively.

A and B show the amplitude and phase of the BM velocity at site 2 which has a 'best frequency' (BF) of ~12kHz. C and D show the amplitude and phase of the BM velocity at site 1, which has a BF of ~15kHz.

The phase of BM velocity at site 2, relative to site 1, is given in E. The delay in propagation of the travelling wave, at each stimulus frequency, between sites 1 and 2 is shown in F and is calculated using the phase data in E and the stimulus frequency (e.g. delay= $-\Delta\phi/f$ where $\Delta\phi$ is the phase change and f the stimulus frequency). The group velocity and wavelength of the travelling wave (G and H respectively) is calculated from the delay (F) and the known distance between the observation sites.

[From He *et al.* (2008), figure 3, with universal permission]

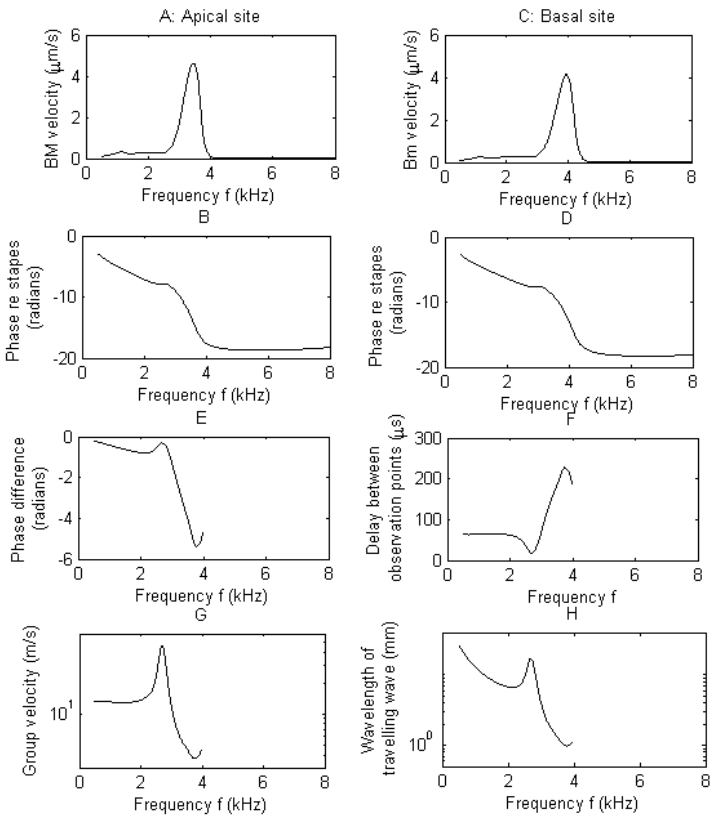

Figure I.2 The simulated He *et al* single tone stimulus experiment

Model simulation of the He *et al*. experiment. A single pure tone was presented to the ear canal of the model at 40 dB SPL and observed at sites 1 and 2 located at distances of 10.5 and 11.3 mm from the stapes respectively. A and C show the amplitude of the response observed at sites 2 and 1 respectively. B and D show the phase of the response corresponding to responses shown in A and B relative to the stapes motion. E gives the phase of BM velocity at site 2, relative to site 1. F shows the delay in propagation of the travelling wave, at each stimulus frequency, between sites 1 and 2, calculated using the phase data in E and the stimulus frequency (e.g. delay= $-\Delta\phi/f$ where $\Delta\phi$ is the phase change and f the stimulus frequency). G and H give the group velocity and wavelength of the travelling wave respectively, calculated from the delay (F) and the known distance between the observation sites.

References

Abdala, C. (1996). 'Distortion product otoacoustic emission (2f1 − f2) amplitude as a function of f2/f1 frequency ratio and primary tone level separation in human adults and neonates', J. Acoust. Soc. Am., 100(6), 3726 − 3740.

Abdala, C. (2000). 'Distortion product otoacoustic emission (2f10f2) amplitude growth in human adults and neonates', J. Acoust. Soc. Am., 107(1), 446 − 456.

Aibara, R., Welsh, T., Puria, S. and Goode, R.L. (2001). 'Human middle-ear sound transfer function and cochlear input impedance', Hearing Res. 152, 100 − 109.

Allen, J. and Neely, S.T. (1992). 'Micromechanical models of the cochlea', Phys. Today 45(7), 40 − 47.

Allen, J. B. (1980). 'Cochlear micromechanics − A Physical model of transduction', J. Acoust. Soc. Am., 68(6), 1660 − 1670.

Allen, J. B. and Fahey, P.F (1992). 'Using acoustic distortion products to measure the cochlear amplifier gain on the basilar membrane', J. Acoust. Soc. Am., 92(1), 178 − 188.

Ashmore, J. (2008). 'Cochlear Outer Hair Cell Motility', Physiol. Rev. 88, 173 − 210.

Ashmore, J., Chambard, J-M. and Richmond, S. (2002). 'Cochlear Transduction, From models to molecules and back again', Audiol. Neuro-Otol., 7, 6 − 9.

Baumgart, J., Chiaradia, C., Fleischer, M., Yarin, Y., Grundmann, R. and Gummer, A.W. (2008). 'Fluid mechanics in the subtectorial space', Concepts and Challenges in The Biophysics of Hearing, Proceedings of the 10th International Workshop on the Mechanics of Hearing, edited by Cooper, N.P. and Kemp, D.T., (World Scientific), Singapore.

Beale, G. (2006). http//teal.gmu.edu/~gbeale/ece_220/state_space_01.html. Retrieved October 19th 2009.

Bellman, R. (1972). 'The Liouville-WKB approximation and Asymptotic Series. Perturbation Techniques in Mathematics, Engineering and Physics', (Dover Publications), New York, pp.80 − 111.

Bender, C. M. and Orszag, S.A. (1999). 'WKB theory. Advanced Mathematical Methods of Scientists and Engineers. Asymptotic Methods and Perturbation Theory', (Springer), New York, pp. 484 − 543.

Bian, L., Chertoff, M.E. and Miller, M.A. (2002). ‘Deriving a cochlear transducer function from low-frequency modulation of distortion product otoacoustic emissions’, J. Acoust. Soc. Am., 112(1), 198 − 210.

Boege, P. and Janssen, T. (2002). ‘Pure-tone threshold estimation from extrapolated distortion product otoacoustic emission I/O-functions in normal and cochlear hearing loss ears’, J. Acoust. Soc. Am., 111(4), 1810 − 1818.

Bostock, L. and Chandler, S. (1990). ‘Core Maths for A-level’, (StanleyThornes), Cheltenham.

Brown, A. M., Harris, F.P. and Beveridge, H.A. (1996). ‘Two sources of acoustic distortion products from the human cochlea’, J. Acoust. Soc. Am., 100(5), 3260 − 3267.

Brown, A. M. and Kemp, D.T. (1985). ‘Intermodulation distortion in the cochlea, could basal vibration be the major cause of round window CM distortion?’ Hearing Res., 19, 191 − 198.

Brownell, W. E., Bader, C.R., Bertrand, D. and Ribaupierre, Y.D. (1985). ‘Evoked Mechanical Responses of Isolated Cochlear Outer Hair Cells’, Science, 227(4683), 194 − 196.

Cai, H., Manoussaki, D. and Chadwick, R.S. (2005). ‘Effects of coiling on the micromechanics of the mammalian cochlea’, J. R. Soc. Interface, 2, 341 − 348.

Chadwick, R. S. (1998). ‘Compression, gain, and nonlinear distortion in an active cochlear model with subpartitions’, Proc. Nat. Acad. Sci. U.S.A., 95, 14594 − 14599.

Chertoff, M. E., Steele, T., Ator, G. A. and Bian, L. (1996). 'Characterising cochlear mechano-electric transduction using a nonlinear systems identification procedure', Journal of the Acoustical Society of America, 100(6), 3741 − 3753.

Chertoff, M. E., Miller, M.A. and Bian, L. (2001). ‘Properties and Quantification of Linear and Nonlinear Systems’, Semin. Hear., 22(4), 325 − 338.

Chittka, L. and Brockmann, A. (2005). ‘Perception space − The final frontier’, PLoS Biology, 3(4), e137.

Cooper, N. P. (1998). ‘Harmonic distortion on the basilar membrane in the basal turn of the guinea-pig cochlea’, J. Physiol., 509(1), 277 − 288.

Cooper, N. P. and Rhode, W.S. (1995). ‘Nonlinear mechanics at the apex of the guinea-pig cochlea’, Hearing Res., 82, 225 − 243.

Dallos, P. (1985). ‘Response Characteristics of Mammalian Cochlear Hair Cells’, The AuJ. Neurosci., 5(6), 1591 − 1608.

Dallos, P. (1992). ‘The active cochlea’, The J. Neurosci. 12(12), 4575 − 4585.

Dallos, P. (1996). ‘Overview, Cochlear Neurobiology,’ The Cochlea, edited by Dallos, P., Popper, A.N. and Fay, R.R.., (Springer-Verlag), New York, pp.1 − 36.

Davis, H. (1953). ‘Acoustic Trauma in the Guinea Pig’, J. Acoust. Soc. Am, 25(6), 1180 − 1189.

Davis, H. (1983). ‘An active process in cochlear mechanics’, Hearing Res. 9, 79 − 90.

De Boer, E. (1980). ‘Auditory Physics. Principles in Hearing Theory I’, Phys. Rep., 62(2), 87 − 174.

De Boer, E. (1983). ‘No sharpening? A challenge for cochlear mechanics’, J. Acoust. Soc. Am., 73(2), 567 − 573.

De Boer, E. (1995a). ‘The ‘inverse problem’ solved for a three-dimensional modelof the cochlea. I. Analysis’, J. Acoust. Soc. Am., 98(2), 896 − 903.

De Boer, E. (1995b). ‘On equivalence of locally active models of the cochlea’, J. Acoust. Soc. Am., 98 (3), 1400 − 1409.

De Boer, E. (1996). ‘Mechanics of the Cochlea, Modelling efforts’, The Cochlea, edited by Dallos, P., Popper, A.N. and Fay, R.R., (Springer), New York, pp. 258 − 317.

De Boer, E. and Nuttal, A.L. (1999). ‘The ‘inverse problem’ solved for a three-dimensional model of the cochlea. III. Brushing-up the method’, J. Acoust. Soc. Am., 105(6), 3410 − 3420.

De Boer, E. and Nuttal, A.L (2008). ‘Obvious and 'hidden' waves in the cochlea’, Proceedings of the 10th International Workshop on the Mechanics of Hearing, edited by Cooper, N.P. and Kemp, D.T., (World Scientific), Singapore, pp. 34 − 40.

De Boer, E., Nuttal, A.L., Hu, N., Zou, Y. and Zheng, J. (2005). ‘The Allen-Fahey experiment extended’, J. Acoust. Soc. Am., 117(3), 1260 − 1266.

De Boer, E. and Viergever, M.A. (1982). ‘Validity of the Liouville-Green (or WKB) method for cochlear mechanics’, Hearing Res., 8, 131 − 155.

De Boer, E. and Viergever, M.A. (1984). ‘Wave propagation and dispersion in the cochlea’, Hearing Res., 13, 101 − 112.

De Boer, E., Zheng, J.F., Porsov, E., and Nuttall (2008), A.L. 'Inverted direction of wave propagation (IDWP) in the cochlea', J. Acoust. Soc. Am., 123(3), 1513 − 1521.

Dhar, S. and Abdala, C. (2007). 'A comparative study of distortion-product-otoacoustic-emission fine structure in human newborns and adults with normal hearing', J. Acoust. Soc. Am., 122, 2191 − 2202.

Dillon, H. (2001). 'Assessing candidacy for hearing aids', Hearing Aids, (Thieme), New York, pp. 209 − 233.

Dong, W. and Olsen, E.S (2008). 'Supporting evidence for reverse cochlear travelling waves', J. Acoust. Soc. Am., 123(1), 222 − 240.

Dong, W. and Olson, E.S (2005). 'Two-tone distortion in intracochlear pressure', J. Acoust. Soc. Am., 117(5), 2999 − 3015.

Dorn, P. A., Konrad-Martin, D., Neely, S.T., Keefe, D.H, Cyr, E. and Gorga, M.P. (2001). 'Distortion product otoacoustic emission input/output functions in normal-hearing and hearing-impaired human ears', J. Acoust. Soc. Am., 110(6), 3119 − 3131.

Elliott, S. J., Ku, E. and Lineton, B. (2007). 'A state space model for cochlear mechanics', J. Acoust. Soc. Am., 122(5), 2759 − 2771.

Emadi, G., Richter, C-P. and Dallos, P. (2004). 'Stiffness of the Gerbil Basilar Membrane, Radial and Longitudinal Variations', J. Neurophysiol., 91, 474 − 488.

Erminy, M., P. Avan and P. Bonfils (1998). 'Characteristics of the Acoustic Distortion Product 2f2 − f1 from the Normal Human Ear', Acta Oto-Laryngol., 118(1), 32 − 36.

Evans, E. F. (1975). 'The Sharpening of Cochlear Frequency Selectivity in the Normal and Abnormal Cochlea', Audiology, 14, 419 − 442.

Evans, E. F., Wilson, J.P. and Borerwe, T.A. (1981). 'Animal models of tinnitus', Symposium on Tinnitus, (Pitman books), London.

Fitzgerald, T. S. and Prieve, B.A (2005). 'Detection of Hearing Loss Using 2f2 − f1 and 2f1 − f2 Distortion Product Otoacoustic Emissions', J. Speech. Lang. Hear. R., 48, 1165 − 1186.

Forge, A. and Schacht, J. (2000). 'Aminoglycoside Antibiotics', Audiol. Neuro-Otol., 5, 3 − 22.

Franklin, D. J., McCoy, M.J., Martin, G.K. and Lonsbury-Martin, B.L. (1992). 'Test/Retest Reliability of Distortion-Product and Transient Evoked otoacoustic emissions', Ear Hear, 13(6), 417 − 429.

Fukazawa, T. (1997). 'A model of cochlear micromechanics', Hearing Res., 113, 182 − 190.

Furuta, K., Sano, A. and Atherton, D. (1988). Chapter 1. Mathematical Description of Linear Systems. State Variable Methods in Automatic Control. New York, Wiley.

Gan, R.Z., Reeves, B.P. and Wang, X. (2007). 'Modelling of Sound Transmission from Ear Canal to Cochlea', Ann. Biomed. Eng., 35(12), 2108 − 2195.

Gaskill, S.A. and Brown, A.M. (1990). 'The behaviour of the acoustic distortion product, 2f1 − f2, from the human ear and its relation to auditory sensitivity', J. Acoust. Soc. Am., 88(2), 821 − 839.

Gaskill, S.A. and Brown, A.M. (1993). 'Comparing the level of the acoustic distortion product 2f2 − f1 with behavioural threshold audiograms from normal-hearing and hearing-impaired ears', Brit. J. Audiol., 6, 397 − 407.

Geisler, C.D. and Sang, C. (1995). 'A cochlear model using feed-forward outer-hair-cell forces', Hearing Res., 86(1,2), 132 − 146.

Gelfand, S.A. (1998). 'Hearing, An introduction to psychological and physiological acoustics', (Marcel Dekker), New York.

Glueckert, R., Pfaller, K., Kinnefors, S-F. and Rask-Anderson, H. (2005). 'High resolution scanning electron microscopy of the human organ of Corti. A study using freshly fixed surgical specimens', Hearing Res., 199, 40 − 56.

Gold, T. (1948). 'Hearing II. The Physical Basis of the Action of the Cochlea', Proc. Roy. Soc. Lond. B. Bio.135(881), 492.

Goldstein, J.L. (1967). 'Auditory Nonlinearity', J. Acoust. Soc. Am., 41(3), 676 − 689.

Goodman, S.S., Withnell, R.H. and Shera, C.A (2003). 'The origin of SFOAE microstructure in the guinea pig', Hearing Res., 183, 7 − 17.

Gorga, M.P., Neely, S.T., Bergman, B.M., Beauchaine, K.L., Kaminski, J.R. and Liu, Z. (1994). 'Towards understanding the limits of distortion product otoacoustic emission measurements', J. Acoust. Soc. Am., 96(3), 1494 − 1500.

Gorga, M.P., Neely, S.T., Dierking, D.M. and Dorn, P.A. (2003). ‘Distortion product otoacoustic emission suppression tuning curves in normal-hearing and hearing-impaired human ears’, J. Acoust. Soc. Am., 114(1), 263 − 278.

Gorga, M.P., Neely, S.T., Dierking, D.M., Kopun, J., Jolkowski, K., Groenenboom, K., Tan, H. and Stiegemann, B. (2007). ‘Low frequency and high-frequency cochlear nonlinearity in humans’, J. Acoust. Soc. Am., 112(3), 1671 − 1691.

Grandori, F. (1985). ‘Nonlinear phenomena in click- and tone-burst- evoked otoacoustic emissions from human ears’, Audiology, 24(1), 71 − 80.

Greenwood, D.D. (1990). ‘A cochlear frequency-position function for several species-29 years later’, J. Acoust. Soc. Am., 87(6), 2592 − 2605.

Greenwood, D.D. (1996). ‘Comparing octaves, frequency ranges, and cochlear map-curvature across species’, Hearing Res., 94, 157 − 162.

Gueta, R., Barlam,D., Shneck, R.Z., and Rousso, I. (2008). ‘Sound-Evoked Deflections of Outer Hair Cell Stereocilia Arise from Tectorial Membrane Anisotropy’, Biophys. J., 94, 4570 − 4576.

Guinan, J.J. and McCue, M.P. (1987). ‘Asymmetries in the acoustic reflexes of the cat stapedius muscle’, Hearing Res., 33, 97 − 114.

Hall, A.J. (2005). ‘Otoacoustic emissions and hearing threshold’, Faculty of Engineering, Science and Mathematics. Southampton, University of Southampton. Doctor of Philosophy.

Hall, J.L. (1974). ‘Two-tone distortion products in a nonlinear model of the basilar membrane’, J. Acoust. Soc. Am., 56(6), 1818 − 1828.

Hall, J.W. (2000). ‘Distortion product and transient evoked OAEs,Measurement and Analysis’, Handbook of Otoacoustic Emissions, edited by Danhauer, J.L., (Singular), San Diego, pp. 95 − 162.

Harris, F.P., Lonsbury-Martin, B.L., Stagner, B.B., Coats, A.C., and Martin, G.K. (1989). ‘Acoustic distortion products in humans, Systematic changes in amplitude as a function of f2/f1 ratio’, J. Acoust. Soc. Am., 85(1), 220 − 229.

Harte, J. M., Elliott, S. J., Kapadia, S. and Lutman, M. E. (2005). 'Dynamic nonlinear cochlear model predictions of click-evoked otoacoustic emission suppression', Hearing Research, 207, 99 − 109.

Harte, J. M., Pigasse, G. and Dau, T. (2009). 'Comparison of cochlear delay estimates using otoacoustic emissions and auditory brainstem responses', J. Acoust. Soc. Am., 126(3), 1291 − 1301.

Hatzopoulos, S., Pelosi, G., Peteruccelli, J., Rossi, M., Vigi, V., Chierici, R. and Martini (2001), A. 'Efficient Otoacoustic Emission Protocols Employed in a Hospital-based Neonatal Screening Program', Acta Oto-Laryngol., 121, 269 − 273.

He, N. and Schmiedt, R.A. (1993). 'Fine structure of the 2f 1 − f2 acoustic distortion product, Changes with primary level ' J. Acoust. Soc. Am., 94(5), 2659 − 2669.

He, W.X., Fridberger, A., Porsov, E., Grosh, K. and Ren, T.Y (2008). 'Reverse wave propagation in the cochlea', P. Natl. Acad. Sci. USA, 105(7), 2729 − 2733.

Helmholtz, H. (1877). 'On the Analysis of Musical Tones by the Ear', On the Sensations of Tone, edited by Ellis, A.J., (Dover), New York, pp. 49 − 65.

Hofstetter, P., Ding, D., Powers, N. and Salvi, R.J. (1997). 'Quantitive relationship of carboplatin dose to magnitude of inner and outer hair cell loss and the reduction in distortion product otoacoustic emission amplitude in chinchillas', Hearing Res., 112, 199 − 215.

Horn, J.H., Pratt, S.R. and Durrant, J.D. (2008). 'Parameters to Maximize 2f2 − f1 Distortion Product Otoacoustic Emission Levels', J. Speech. Lang. Hear. R., 51, 1620 − 1629.

How, J.A., Elliott, S.J. and Lineton, B. (2010). 'The influence on predicted harmonic and distortion produce generation of the position of the nonlinearity within cochlear micromechanical models (L)', J. Acoust. Soc. Am., 127(2), 652 − 655.

Janssen, T. and Muller, J. (2008). 'Otoacoustic Emissions as a Diagnostic Tool in a Clinical Context', Active Processes and Otoacoustic Emissions, edited by Manley, G.A., Fay, R.R. and Popper, A.N., (Spinger), New York, pp. 421 − 460.

Jia, A. and He, D.Z.Z. (2005). 'Motility-associated hair-bundle motion in mammalian outer hair cells', Nat. Neurosci., 8(8), 1028 − 1034.

Johnstone, B.M., Patuzzi, R. and Yates, G.K. (1986). 'Basilar membrane measurements and the travelling wave', Hearing Res., 22, 147 − 153.

Kakehata, S. and Santos-Sacchi, J. (1996). 'Effects of Salicylate and Lanthanides on Outer Hair Cell Motility and Associated Gating Charge', J. Neurosci., 16(16), 4881 − 4889.

Kalluri, R. and Shera, C.A. (2001). 'Distortion-product source unmixing, A test of the two-mechanism model for DPOAE generation', J. Acoust. Soc. Am., 109(2), 622 − 637.

Kanis, L. (1995). ‘Cochlear nonlinearity. A computational model of the cochlea solved in the frequency domain’, Doctor of Philosphy, University of Amsterdam.

Kanis, L. and de Boer, E. (1993). ‘Self-suppression in a locally active nonlinear model of the cochlea, A quasilinear approach’, J. Acoust. Soc. Am., 94(6), 3199 − 3206.

Kanis, L. and de Boer, E. (1994). ‘Two-tone suppression in a locally active nonlinear model cochlea’, J. Acoust. Soc. Am., 96(4), 2156 − 2165.

Kanis, L. and de Boer, E. (1996). ‘Comparing frequency-domain with time-domain solutions for a locally active nonlinear model of the cochlea’, J. Acoust. Soc. Am., 100(4), 2543 − 2546.

Kanis, L. and de Boer, E. (1997). ‘Frequency dependence of acoustic distortion products in a locally active model of the cochlea’, J. Acoust. Soc. Am., 101(3), 1527 − 1531.

Kapadia, S. and Lutman, M.E. (1997). ‘Are normal hearing thresholds a sufficient condition for click evoked otoacoustic emissions?’ J. Acoust. Soc. Am., 101, 3566 − 3578.

Kemp, D.T. (1978). ‘Stimulated Acoustic Emissions from within Human Auditory-System’, J. Acoust. Soc. Am., 64(5), 1386 − 1391.

Kemp, D.T. (1980). ‘Towards a model for the origin of cochlear echos’, Hearing Res., 2, 533 − 548.

Kemp, D.T. (1986). ‘Otoacoustic emissions, travelling waves and cochlear mechanisms’, Hearing Res. 22, 95 − 104.

Khanna, S.M. and Hao, S.M. (1999). ‘Nonlinearity in the apical turn of a living guinea pig cochlea’, Hearing Res. 135, 89 − 104.

Khanna, S.M. and Leonard, D.G.B. (1982). ‘Basilar membrane tuning in the cat cochlea’, Science 215, 305 − 306.

Kiang, N.Y.S. and Moxon, E.C. (1974). ‘Tails of tuning curves of auditory-nerve fibres’, J. Acoust. Soc. Am., 55(3), 620 − 630.

Kim, D.O. (1980). ‘Cochlear mechanics, Implications of electromotility and acoustic observations’, Hearing Res. 2, 297 − 317.

Kim, D.O., Molnar, F. and Matthews, J.W. (1980). ‘Cochlear mechanics, Nonlinear behaviour in two-tone responses as reflected in cochlear-nerve-fibre responses and ear-canal sound pressure’, J. Acoust. Soc. Am., 67(5), 1704 − 1721.

Kinsler, L.E. and Frey, A.R. (1962). ‘Chapter 5, Acoustic Plane Waves. Fundamentals of Acoustics’, (Wiley & Sons), New York, pp.108 − 127.

Knight, R.D. and Kemp, D.T. (1999). ‘Relationships between DPOAE and TEOAE amplitude and phase characteristics’, J. Acoust. Soc. Am., 106(3), 1420 − 1435.

Knight, R.D. and Kemp, D.T. (2000). ‘Indications of different distortion product otoacoustic emission mechanisms from a detailed f1, f2 area study’, J. Acoust. Soc. Am., 107(1), 457 − 473.

Knight, R.D. and Kemp, D.T. (2001). ‘Wave and place fixed DPOAE maps of the human ear’, J. Acoust. Soc. Am., 109(4), 1513 − 1525.

Kolston, P.J. and Ashmore, J. (1996). ‘Finite element micromechanical modelling of the cochlea in three dimensions’, J. Acoust. Soc. Am., 99(1), 455 − 467.

Koshigo, S., Kwok, W-K. and Tubis, A. (1983). ‘Effects of periplymph viscosity on low frequency intracochlear pressures and the cochlear impedance of the cat’, J. Acoust. Soc. Am., 74(2), 486 − 492.

Kringlebotn, M. (1988). ‘Network model for the human’, Scand. Audiol. 17, 75 − 85.

Kros, C. F., Dallos, P., Popper, A.N., and Fay, R.R. (1996). ‘Physiology of mammalian cochlear hair cells’, The Cochlea, edited by Dallos, P., Popper, A.N. and Fay, R.R., (Springer), New York, pp 318 − 387.

Kros, C. J., Rusch, A and Richardson, G.P. (1992). ‘Mechano-Electrical Transducer Currents in Hair Cells of the Cultured Neonatal Mouse Cochlea’, P. Roy. Soc. B − Bio. Sci. 249(1325), 185 − 193.

Krössl, M. and Vater, M. (2000). ‘Consequences of Outer Hair Cell Damage for Otoacoustic Emissions and Audio-vocal Feedback in the Mustached Bat’,, J. Assoc. Res. Otol., 1, 300 − 314.

Ku, E. (2008). ‘Modelling the Human Cochlea’. Faculty of Engineering, Science and Mathematics, Institute of Sound and Vibration Research. Southampton, University of Southampton. Doctor of Philosophy.

Ku, E., Elliott, S.J. and Lineton, B. (2008). ‘Statistics of instabilities in a state space model of the human cochlea’, J. Acoust. Soc. Am., 124(2), 1068 − 1079.

Ku, E., Elliott, S.J. and Lineton, B. (2009). ‘Limit cycle oscillations in a nonlinear state space model of the human cochlea’, J. Acoust. Soc. Am., 126(2), 739 − 750.

Kummer, P., Janssen, T. and Arnold, W. (1995). 'Suppression tuning characteristics of the 2f1 − f2 distortion product otoacoustic emission in humans', J. Acoust. Soc. Am., 98(1), 197 − 210.

Kummer, P., Janssen, T. and Arnold, W. (1998). 'The level and growth behaviour of the 2f1 − f2 distortion product otoacoustic emission and its relationship to auditory sensitivity in normal hearing and cochlear loss', J. Acoust. Soc. Am., 103(6), 3431 − 3444.

Lasky, R.E. (1998a). 'Distortion product otoacoustic emissions in human newborns and adults. I. Frequency effects', J. Acoust. Soc. Am., 103(2), 981 − 991.

Lasky, R.E. (1998b). 'Distortion product otoacoustic emissions in human newborns and adults. II. Level effects', J. Acoust. Soc. Am., 103(2), 992 − 1000.

Le Page, E.L. (2003). 'The mammalian cochlear map is optimally warped', J. Acoust. Soc. Am., 114 (2), 896 − 906.

Liberman, M.C., Zuo, J. and Guinan, J.J. (2004). 'Otoacoustic emissions without somatic mobility, Can stereocilia drive the mammalian cochlea?' J. Acoust. Soc. Am., 116(3), 1649 − 1655.

Lim, D.J. (1980). 'Cochlear anatomy related to cochlear micromechanics. A review', J. Acoust. Soc. Am., 67(5), 1686 − 1695.

Lim, K-M. and Steele, C.R. (2002). 'A three-dimensional nonlinear active cochlear model analyzed by the WKB-numeric method', Hearing Res. 170, 190 − 205.

Lind, O. (1998). 'A Clinical Study on the Growth of Distortion Product Otoacoustic Emissions and Hearing Loss at 2 kHz in Humans', Scand. Audiol. 27(4), 207 − 212.

Lind, O. and Randa, S.J (1992). 'Spontaneous otoacoustic emissions, Short time stability', Acta Oto-Laryngol. 112(s492), 79 − 81.

Lineton, B. (2001). 'Testing a model of stimulus frequency otoacoustic emissions in humans'. Faculty of Engineering, Science and Mathematics, Institute of Sound and Vibration Research. Southampton, University of Southampton. Doctor of Philosophy.

Long, G.R. and Tubis, A. (1988). 'Modification of spontaneous and evoked otoacoustic emissions and associated psychoacoustic microstructure by aspirin consumption', J. Acoust. Soc. Am., 84(4), 1343 − 1353.

Lonsbury-Martin, B.L. and Martin, G.K. (2007). 'Distortion-Product Otoacoustic Emissions in Populations with Normal Hearing Sensitivity, Otoacoustic Emissions. Clinical Applications, edited by Robinette, M.S. and Glattke, T.J., (Thieme), New York, pp. 107 − 130.

Lonsbury-Martin, B.L. and Martin, G.K. (2008). ‘Mammalian Models of Otoacoustic Emissions’, Active Processes and Otoacoustic Emissions, edited by Manley, G.A., Fay, R.R., and Popper, A.N., (Springer), New York, pp. 261 − 305.

Lonsbury-Martin, B.L., Martin, G.K., Probst, R. and Coats, A.C. (1987). ‘Acoustic distortion products in rabbit ear canals, I. Basic features and physiological vulnerability’, Hearing Res. 28, 173 − 189.

Lopez-Poveda, E.A., C. J. Plack and R. Meddis (2003). ‘Cochlear nonlinearity between 500 and 8000 Hz in listeners with normal hearing’, J. Acoust. Soc. Am., 113(2), 951 − 960.

Lukashkin, A.N. and Russell, I.J. (2001). ‘Origin of the bell-like dependence of the DPOAE amplitude on primary frequency ratio’, J. Acoust. Soc. Am., 110(6), 3097 − 3106.

Lukashkin, A.N. and Russell, I.J. (2005). ‘Dependence of the DPOAE amplitude pattern on acoustical biasing of the cochlear partition’, Hearing Res. 203, 45 − 53.

Mammano, F. and Nobili, R. (1993). ‘Biophysics of the cochlea, Linear approximation’, J. Acoust. Soc. Am., 93(6), 3320 − 3332.

Martin, G.K., Jassir, D., Stagner, B.B., Whitehead, M.L. and Lonsbury-Martin, B.L. (1998). ‘Locus of generation for the 2f(1) − f(2) vs 2f(2) − f(1) distortion-product otoacoustic emissions in normal-hearing humans revealed by suppression tuning, onset latencies, and amplitude correlations’, J. Acoust. Soc. Am., 103(4), 1957 − 1971.

Martin, G. K., Probst, R. and Lonsbury-Martin, B.L. (1990). ‘Otoacoustic Emissions in Human Ears, Normative Findings’, Ear Hear 11(2), 106 − 120.

Martin, P. and Hudspeth, A.J. (1999). ‘Active hair-bundle movements can amplify a hair cell's response to oscillatory mechanical stimuli’, P. Natl. Acad. Sci. USA96(25), 14306 − 14311.

Matthews, J. and Walker, R.L. (1970). ‘The WKB Method’, Mathematical Methods of Physics, (Addison-Wesley), California, pp. 27 − 38.

Mauermann, M. and Kollmeier, B. (2004). ‘Distortion product otoacoustic emissions (DPOAE) input/output functions and the influence of the second DPOAE source’, J. Acoust. Soc. Am., 116(4), 2199 − 2212.

Mauermann, M., Uppenkamp, S., van Hengel, P.W.J. and Kollmeier, B. (1999). ‘Evidence for the distortion product frequency place as a source of distortion product otoacoustic emission (DPOAE) fine structure in humans. I. Fine structure and high-order DPOAE as a function of the frequency ratio f 2/f1 ‘ J. Acoust. Soc. Am., 106(6), 3473 − 3483.

McFadden, D. and Plattsmier, H.S. (1984). 'Aspirin abolishes spontaneous oto-acoustic emissions', J. Acoust. Soc. Am., 76(2), 443 − 448.

Meinke, D.K., Stagner, B.B., Martin, G.K. and Lonsbury-Martin, B.L. (2005). 'Human efferent adaptation of DPOAEs in the L1,L2 space', Hearing Res. 208, 89 − 100.

Mills, D.M. (1998). 'Interpretation of distortion product otoacoustic emission measurements. II. Estimating tuning characteristics using three stimulus tones', J. Acoust. Soc. Am., 103(1), 507 − 523.

Mills, D.M. (2002). 'Interpretation of standard distortion product otoacoustic emission measurements in light of the complete parametric response', J. Acoust. Soc. Am., 112(4), 1545 − 1560.

Mills, D.M., Feeney, M.P. and Gates, G.A. (2007). 'Evaluation of Cochlear Hearing Disorders, Normative Distortion Product Otoacoustic Emission Measurements', Ear Hear 28(6), 778 − 792.

Moleti, A., Patemoster, N., Bertaccini, D., Sisto, R., and Sanjust, F. (2009). 'Otoacoustic emissions in time-domain solutions of nonlinear non-local cochlear models', J. Acoust. Soc. Am., 126(5), 2425 − 2438.

Moleti, A. and Sisto, R. (2008). 'Comparison between otoacoustic and auditory brainstem response latencies supports slow backward propagation of otoacoustic emissions', J. Acoust. Soc. Am., 123(3), 1495 − 1503.

Moulin, A. (2000). 'Influence of primary frequencies ratio on distortion product otoacoustic emissions amplitude II. Interrelations between multicomponent DPOAEs, tone-burst-evoked OAEs, and spontaneous OAEs', J. Acoust. Soc. Am., 107(3), 1471 − 1486.

Moulin, A., Collet, L., Veuillet, E. and Morgon, A. (1993). 'Interrelations between transiently evoked otoacoustic emissions, spontaneous otoacoustic emissions, and acoustic distortion products in normally hearing subjects', Hearing Res. 65, 216 − 233.

Naidu, R.C. and Mountain, D.C. (2001). 'Longitudinal Coupling in the Basilar Membrane', J. Assoc. Res. Otol. 2, 257 − 267.

Neely, S.T. (1981). 'Finite difference solution of a two dimensional mathematical model of the cochlea', J. Acoust. Soc. Am., 69(5), 1386 − 1393.

Neely, S.T. (1985). 'Mathematical modelling of cochlear mechanics', J. Acoust. Soc. Am., 78(1), 345 − 352.

Neely, S.T., Gorga, M.P. and Dorn, P.A. (2003a). 'Cochlear compression estimates from measurements of distortion-product otoacoustic emissions', J. Acoust. Soc. Am., 114(3), 1499 − 1507.

Neely, S. T., Gorga, M.P. and Dorn, P.A. (2003b). 'Cochlear compression estimates from measurements of distortion-product otoacoustic emissions', J. Acoust. Soc. Am., 114(3), 1489 − 1507.

Neely, S.T. and Kim, D.O. (1986). 'A model for active elements in cochlear biomechanics', J. Acoust. Soc. Am., 79(5), 1472 − 1480.

Neely, S.T. and Liu, Y-W. (2008). 'Retrograde propagation of cochlear distortion', Concepts and Challenges in The Biophysics of Hearing, Proceedings of the 10th International Workshop on the Mechanics of Hearing, edited by Cooper, N.P. and Kemp, D.T., (World Scientific), Singapore.

Nobili, R., Mammano, F. and Ashmore, J. (1998). 'How well do we understand the cochlea?' Trends Neurosci. 21, 159 − 167.

Nobili, R., Vetesnik, A., Turicchia, L. and Mammano, F. (2003). 'Otoacoustic Emissions from Residual Oscillations of the Cochlear Basilar Membrane in a Human Ear Model', J. Assoc. Res. Otol. 4, 478 − 494.

Norton, S.J., Gorga, M.P., Widen, J.E., Folsom, R.C., Sininger, Y., Cone-Wesson, B., Vohr, B.R. and Fletcher, K.A. (2000). 'Identification of Neonatal Hearing Impairment, Summary and Recommendations', Ear Hear 21(5), 529 − 535.

Olsen, E.S. (2004). 'Harmonic Distortion in intracochlear pressure and its analysis to explore the cochlear amplifier', J. Acoust. Soc. Am., 115(3), 1230 − 1241.

Parthasarathi, A., Grosh, A.K., Zheng, J. and Nuttal, A.L. (2003). 'Effect of current stimulus on in vivo cochlear mechanics', J. Acoust. Soc. Am., 113(1), 442 − 452.

Parthasarathy, T. K. and Klostermann, B. (2001). 'Similarities and differences in distortion-product otoacoustic emissions among four FDA-approved devices', J Am Acad Audiol 12(8), 397 − 405.

Pascal, J., Bourgeade, A., Lagier, M. and Legros, C. (1998). 'Linear and nonlinear model of the human middle ear', J. Acoust. Soc. Am., 104(3), 1509 − 1516.

Patuzzi, R. (1996). Cochlear Micromechanics and Macromechanics. Dallos, P., Popper, A.N. and Fay, R.R. New York, Springer, 186 − 257.

Peterson, L.C. and Bogert, B.P. (1950). ‘A dynamical theory of the Cochlea’, J. Acoust. Soc. Am., 22(3), 369 − 381.

Pickles, J.O. (1982). ‘An introduction to the physiology of Hearing’. London, Academic Press.

Prijs, V.F., Schneider, S. and Schoonhoven, R. (2000). ‘Group delays of distortion product otoacoustic emissions, Relating delays measured with f1 − and f2 − sweep paradigms’, J. Acoust. Soc. Am., 107(6), 3298 − 3307.

Probst, R., Lonsbury-Martin, B.L. and Martin, G.K. (1991). ‘A review of otoacoustic emissions’, J. Acoust. Soc. Am., 89(2027 − 2064), 2027.

Puria, S. (2003). ‘Measurements of human middle ear forward and reverse acoustics, Implications for otoacoustic emissions’, J. Acoust. Soc. Am., 113(5), 2773 − 2789.

Puria, S. and Allen, J. (1991). ‘A parametric study of cochlear input impedance’, J. Acoust. Soc. Am., 89(1), 287 − 309.

Rebscher, S. J., Talbot, N., Bruszewski, W., Heilmann, M., Brasell, J. and Merzenich, M.M (1996). ‘A transparent model of the human scala tympani cavity’, J. Neurosci. Meth. 64, 105 − 114.

Relkin, E.M. (1988). ‘Introduction to the Analysis of Middle-Ear Function’. Physiology of the Ear. Jahn, A.F. and Santos-Sacchi, J. New York, Raven Press, 103 − 123.

Ren, T. and Nuttal, A.L. (2006). ‘Cochlear compression wave, An implication of the Allen-Fahey experiment (L)’, J. Acoust. Soc. Am., 119(4), 1940 − 1942.

Ren, T.Y. (2004). ‘Reverse propagation of sound in the gerbil cochlea’, Nat. Neurosci. 7(4), 333 − 334.

Rhode, W.S. (2007). ‘Distortion product otoacoustic emissions and basilar membrane vibration in the 6 − 9 kHz region of sensitive chinchilla cochleae’, J. Acoust. Soc. Am., 122, 2725 − 2737.

Robles, L. and M. A. Ruggero, M.A. (2001). ‘Mechanics of Mammalian Cochlea’, Physiol. Rev. 81(3), 1305 − 1352.

Robles, L., Ruggero, M.A. and Rich, N.C. (1986). ‘Basilar membrane mechanics at the base of the chinchilla cochlea. I. Input-output functions, tuning curves, and response phases’, J. Acoust. Soc. Am., 80(5), 1364 − 1374.

Robles, L., Ruggero, M.A. and Rich, N.C (1997). 'Two-tone Distortion on the Basilar Membrane of the Chinchilla Cochlea', J. Neurophysiol. 77, 2385 − 2399.

Roede, J., Harris, F.P., Probst, R. and Xu, L. (1993). 'Repeatability of Distortion Product Otoacoustic Emissions in Normally Hearing Humans', Audiology 32, 273 − 281.

Ruggero, M.A., Rich, N.C., Recio, A., Narayan, S.S. and Robles, L. (1997). 'Basilar-membrane response to tones at the base of the chinchilla cochlea', J. Acoust. Soc. Am., 101(4), 2151 − 2163.

Ruggero, M.A. and Temchin, A.N. (2005). 'Unexceptional sharpness of frequency tuning in the human cochlea', P. Natl. Acad. Sci. USA102(51), 18614 − 18619.

Santos-Sacchi, J. (1989). 'Asymmetry in Voltage-Dependent Movements of Isolated Outer Hair Cells from the Organ of Corti', J. Neurosci. 9(8), 2954 − 2962.

Schoohoven, R., Prijs, V.F. and Schneider, S. (2001). 'DPOAE group delays verses electrophysiological measures of cochlear delay in normal hearing ears', J. Acoust. Soc. Am., 190(4), 1503 − 1512.

Schroeder, M.R. (1973). 'An integrable model for the basiliar membrane', J. Acoust. Soc. Am., 53(2), 429 − 434.

Sellick, P.M., Patuzzi, R. and Johnstone, B.M. (1982). 'Measurement of basiliar membrane motion in the guinea pig using the Mossbauer technique', J. Acoust. Soc. Am., 71 (1), 131 − 141.

Shaffer, L.A., Withnell, R.H., Dhar, S., Lilly, D.J., Goodman, S.S. and Harmon, K.M. (2003). 'Sources and mechanisms of DPOAE generation, Implications for the prediction of auditory sensitivity', Ear Hear 24(5), 367 − 379.

Shera, C. and Guinan, J.J. (2007). 'Cochlear travelling-wave amplification, suppression, and beamforming probed using noninvasive calibration of intracochlear distortion sources', J. Acoust. Soc. Am., 121(2), 1003 − 1016.

Shera, C., Tubis, A. and Talmadge, C.L. (2004). 'Do Foward- and Backward-Travelling Waves Occur Within the Cochlea? Countering the Critique of Nobili et al', J. ASSOC. RES. OTOL. 5, 349 − 359.

Shera, C., Tubis, A., Talmadge, C.L., de Boer, E., Fahey, P.F., and Guinan, J.J. (2007). 'Allen-Fahey and related experiments support the predominance of cochlear slow-wave otoacoustic emissions', J. Acoust. Soc. Am., 121(3), 1564 − 1575.

Shera, C. and Zweig, G. (1992). ‘An emperical bound on the compressibility of the cochlea’, J. Acoust. Soc. Am., 92(3), 1382 − 1388.

Shera, C.A. (2004). ‘Mechanisms of Mammalian Otoacoustic Emission and their Implications for the Clinical Utility of Otoacoustic Emissions’, Ear Hear 25(2), 86 − 97.

Shera, C.A. and Guinan, J.J. (1999). ‘Evoked otoacoustic emissions arise by two fundamentally different mechanisms, A taxonomy for mammalian OAEs’, J. Acoust. Soc. Am., 105(2), 782 − 798.

Shera, C.A. and Guinan, J.J. (2008). Mechanisms of Otoacoustic Emissions. Active Processes and Otoacoustic Emissions. G. A. Manley, R. R. Fay and A. N. Popper. New York, Springer. 30, 305 − 342.

Shera, C.A., Guinan, J.J. and Oxenham, A.J. (2002). ‘Revised Estimates of Human Cochlear Tuning from Otoacoustic and Behavioural Measurements’, P. Natl. Acad. Sci. USA99(5), 3318 − 3323.

Shera, C.A., Talmadge, C.L. and Tubis, A. (2000). ‘Interrelations among distortion-product phase-gradient delays, Their connection to scaling symmetry and its breaking’, J. Acoust. Soc. Am., 108(6), 2933 − 2948.

Shera, C.A., Tubis, A. and Talmadge, C.L (2005). ‘Coherent reflection in a 2 − dimensional cochlea, Short-wave and long-wave scattering in the generation of relfection-source otoacoustic emissions’, J. Acoust. Soc. Am., 118(1), 287 − 313.

Shera, C.A. and Zweig, G. (1993). ‘Noninvasive measurement of the cochlear travelling-wave ratio’, J. Acoust. Soc. Am., 93(6), 3333 − 3352.

Siegel, J.H., Cerka, A.J., Recio-Spinoso, A., Temchin, A.N., van Dijk, P. and Ruggero, M.A. (2005). ‘Delays of stimulus-frequency otoacoustic emissions and cochlear vibrations contradict the theory of coherent reflection filtering’, J. Acoust. Soc. Am., 118(4), 2434 − 2443.

Stavroulaki, P., Apostolopoulos, N., Dinopoulou, D., Vossinakis, I., Tsakanikos, M. and Douniadakis, D. (1999). ‘Otoacoustic emissions − an approach for monitoring aminoglycoside induced ototoxicity in children’, Int. J. Pediatr. Otorhi. 50, 177 − 184.

Steele, C.R., Baker, G.J., Tolomeo, J.A., Zetes-Tolomeo, D.E. and Bronzino, J.D. (2000). ‘Cochlear mechanics’, CRC Press & Springer-Verlag. Second edition, 35 − 33.

Steele, C.R., Baker, G.J., Tolomeo, J.A., Zetes-Tolomeo, D.E. and Bronzino, J.D. (2006). Cochlear mechanics. Biomedical engineering fundamentals, Taylor Francis CRC Press. Third edition.

Steele, C.R. and Taber, L.A. (1979). 'Comparison of WKB and finite difference calculations for a two dimensional cochlea model', J. Acoust. Soc. Am., 65(4), 1001 − 1006.

Stover, L.J., Neely, S.T and Gorga, M.P. (1996). 'Latency and multiple sources of distortion product otoacoustic emissions', J. Acoust. Soc. Am., 99(2), 1016 − 1024.

Talmadge, C. L., G. R. Long, A. Tubis and S. Dhar (2004). 'Experimental confirmation of the two-source interference model for the fine structure of distortion product otoacoustic emissions', J. Acoust. Soc. Am., 105(1), 275 − 292.

Talmadge, C.L., Tubis, A., Long, G.R. and Piskorski, P. (1998). 'Modelling otoacoustic emissions and hearing threshold fine structures', J. Acoust. Soc. Am., 104(3), 1517 − 1543.

Thorne, M., Salt, A.N., DeMott, J.E., Henson, M.M., Henson, O.W. and Gewallt, S.L. (1999). 'Cochlear Fluid Space Dimensions for Six Species Derived From Reconstructions of Three-Dimensional Magnetic Resonance Images', Laryngoscope 109, 1661 − 1668.

Van Der Heijden, M. (2005). 'Cochlear gain control', Journal of the Acoustical Society of America, 117(3), 1223 − 1233.

Van Der Heijden, M. and Joris, P.X. (2006). 'Panoramic Measurements of the Apex of the Cochlea', J. Neurosci. 26(44), 11462 − 11473.

Van Hengel, P.W.J. and Duifhuis, H. (1999). 'The generation of distortion products in a nonlinear transmission line model of the cochlea'. Recent Developments in Auditory Mechanics, Sendi, Japan, World Scientific.

Vetesnik, A., Nobili, R. and Gummer, A.W. (2006). 'How Does the Inner Ear Generate Distortion Product Otoacoustic Emissions?' J Otorhinolaryngol Relat Spec. 68, 347 − 352.

Viergever, M.A. (1978). 'Basilar membrane motion in a spiral-shaped cochlea', J. Acoust. Soc. Am., 64(4), 1048 − 1053.

Viergever, M. A. and de Boer, E. (1987). 'Matching impedance of a nonuniform transmission line, Application to cochlear modelling', J. Acoust. Soc. Am., 81(1), 184 − 186.

von Békésy, G. (1960). Experiments in Hearing, Acoustic Society of America.

von Békésy, G. (1970). ‘Travelling waves as frequency analysers in the cochlea’, Nature 225, 1207 − 1209.

Voss, S.E., Rosowski, J.J. and Peak, W.Y. (1996). ‘Is the pressure difference between the oval and round windows the effective acoustic stimulus for the cochlea?’ J. Acoust. Soc. Am., 100(3), 1602 − 1616.

Wagner, W., Heppelmann, G., Vonthein, R. and Zenner, H. (2008). ‘Test-Retest repeatability of Distortion Product Otoacoustic Emissions’, Ear Hear 29(3).

Wake, M., Anderson, J., Takeno, S., Mount, R.J., and Harrison, R.V. (1996). ‘Otoacoustic Emission Amplification After Inner Hair Cell Damage’, Acta Oto-Laryngol. 116, 374 − 381.

White, R.D. and Grosh, K (2005). ‘Microengineered hydromechanical cochlear model’, P. Natl. Acad. Sci. USA102(5), 1296 − 1301.

Whitehead, M.L. (1995a). ‘Dependence of distortion-product otoacoustic emissions on primary levels in normal and impaired ears. I. Effects of decreasing L2 below L1’, J. Acoust. Soc. Am., 97(4), 2346 − 2358.

Whitehead, M.L. (1995b). ‘Dependence of distortion-product otoacoustic emissions on primary levels in normal and impaired ears. II. Asymmetry in L1, L2 space’, J. Acoust. Soc. Am., 97(4), 2359 − 2377.

Whitehead, M.L. (1998). ‘Species differences of distortion-product otoacoustic emissions, Comment on ‘Interpretation of distortion product otoacoustic emission measurements. I. Two stimulus tones’’, J. Acoust. Soc. Am., 103(5), 2740 − 2742.

Wilson, H. (2005). ‘Wave-fixed and place-fixed sources of Distortion Product Otoacoustic emissions’, Faculty of Engineering, Science and Mathematics, Institute of Sound and Vibration Research. Southampton, University of Southampton. MSc dissertation.

Wilson, H. and Lutman, M.E. (2006). ‘Mechanisms of generation of the 2f2 − f1 distortion product otoacoustic emission’, J. Acoust. Soc. Am., 120(4), 2108 − 2115.

Wit, H.P. and Ritsma, R.J. (1979). ‘Stimulated acoustic emissions from the human ear’, J. Acoust. Soc. Am., 66, 911 − 913.

Withnell, R. H., Shaffer, L.A. and Talmadge, C.L. (2003). ‘Generation of DPOAEs in the guinea pig’, Hearing Res. 178, 106 − 117.

Wittbrodt, M.J., Steele, C.R. and Puria, S (2006). ‘Developing a Physical Model of the Human Cochlea Using Microfabrication Methods’, Audiol. Neuro-Otol. 11, 104 − 112.

Wright, A. (1984). ‘Dimensions of the cochlear stereocilia in man and the guinea pig’, Hearing Res. 13, 89 − 98.

Zhang, X. and Mountain, D.C. (2008). ‘Distortion Product Emissions, Where do they come from?’ Concepts and Challenges in The Biophysics of Hearing. Proceedings of the 10th International Workshop on the Mechanics of Hearing, Keele, UK, World Scientific.

Zhao, F. and Stephens, D. (1999). ‘Test-retest variability of distortion-product otoacoustic emissions in human ears with normal hearing’, Scand. Audiol. 28, 171 − 178.

Zureck, P.M. and Sachs, R.M. (1979). ‘Combination Tones at Frequencies Greater Than the Primary Tones’, Science 205, 600 − 603.

Zweig, G. (1991). ‘Finding the impedance of the organ of Corti’, J. Acoust. Soc. Am., 89(3), 1229 − 1254.

Zweig, G., Lipes, R. and Pierce, J.R. (1976). ‘The cochlear compromise’, J. Acoust. Soc. Am., 59(4), 975 − 982.

Zweig, G. and Shera, C. (1995a). ‘The origin of periodicity in the spectrum of evoked otoacoustic emissions’, J. Acoust. Soc. Am., 98(4), 2018 − 2047.

Zweig, G. and Shera, C.A. (1995b). ‘The Origin of Periodicity in the Spectrum of Evoked Otoacoustic Emissions’, J. Acoust. Soc. Am., 98(4), 2018 − 2047.

Zwicker, E. (1986). ‘A hardware cochlear nonlinear preprocessing model with active feedback’, J. Acoust. Soc. Am., 80(1), 146 − 153.

Zwislocki, J. (1950). ‘Theory of the Acoustical Action of the Cochlea’, J. Acoust. Soc. Am., 22(6), 778 − 784.